



Вол. 72, бр. 3

2024



ISSN 0042-8469
e-ISSN 2217-4753
УДК 623 + 355/359

НАУЧНИ ЧАСОПИС МИНИСТАРСТВА ОДБРАНЕ И ВОЈСКЕ СРБИЈЕ

ВОЈНОТЕХНИЧКИ ГЛАСНИК





Том 72, № 3

2024



ISSN 0042-8469
e-ISSN 2217-4753
УДК 623 + 355/359

НАУЧНЫЙ ЖУРНАЛ МИНИСТЕРСТВА ОБОРОНЫ
И ВООРУЖЕННЫХ СИЛ РЕСПУБЛИКИ СЕРБИЯ

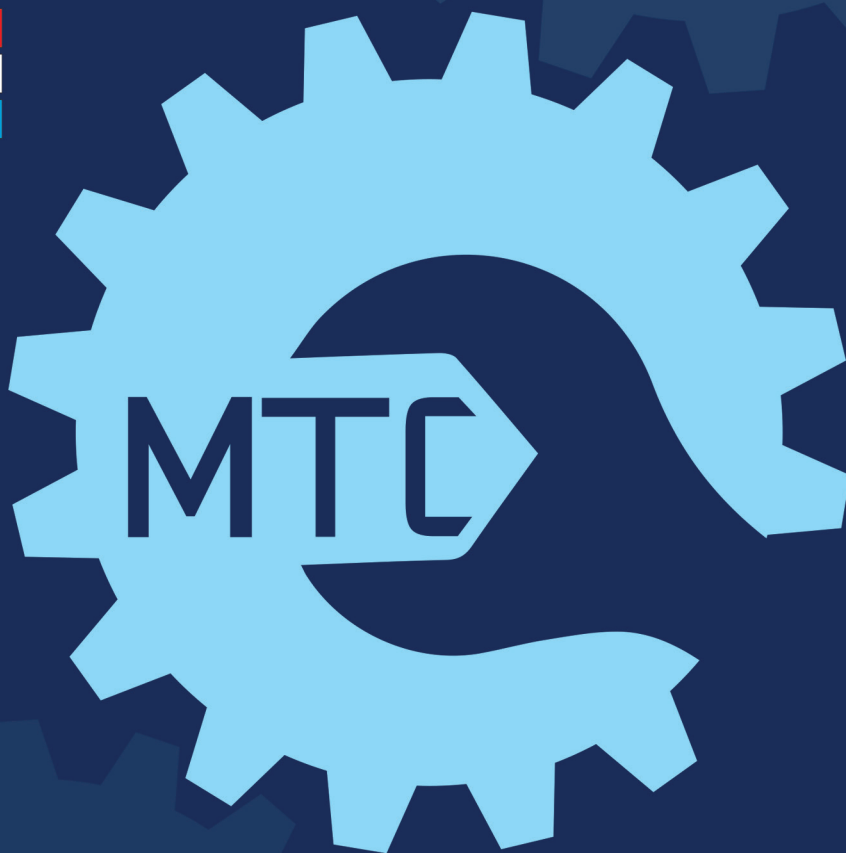
ВОЕННО-ТЕХНИЧЕСКИЙ ВЕСТНИК



ISSN 0042-8469
e-ISSN 2217-4753
UDC 623 + 355/359

Vol. 72, Issue 3

2024



MILITARY TECHNICAL COURIER

2024

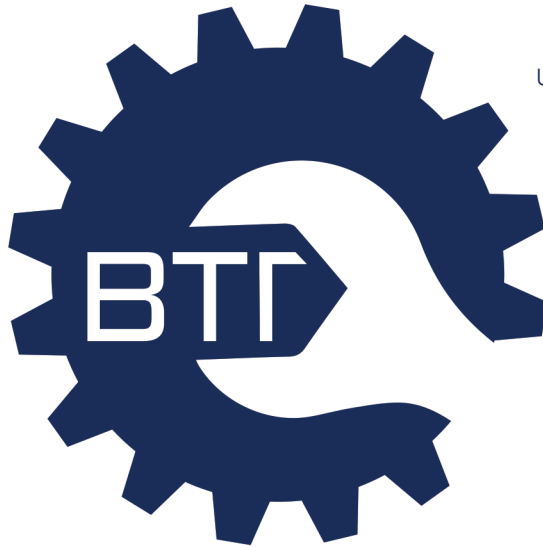
3

SCIENTIFIC JOURNAL OF THE MINISTRY OF DEFENCE AND THE SERBIAN ARMED FORCES

MILITARY TECHNICAL COURIER



ISSN 0042-8469
e-ISSN 2217-4753
UDC 623 + 355/359



НАУЧНИ ЧАСОПИС МИНИСТАРСТВА ОДБРАНЕ И ВОЈСКЕ СРБИЈЕ
ВОЈНОТЕХНИЧКИ ГЛАСНИК
ВОЛУМЕН 72 • БРОЈ 3 • ЈУЛ – СЕПТЕМБАР 2024.



NAUČNI ČASOPIS MINISTARSTVA ODBRANE I VOJSKE SRBIJE
VOJNOTEHNIČKI GLASNIK
VOLUMEN 72 • BROJ 3 • JUL – SEPTEMBAR 2024.

BTG.MO.YNP.CP6
www.vtg.mod.gov.rs
COBISS.SR-ID 4423938
DOI: 10.5937/VojnotehnickiGlasnik

ISSN 0042-8469
e-ISSN 2217-4753
UDC 623 + 355/359



НАУЧНЫЙ ЖУРНАЛ МИНИСТЕРСТВА ОБОРОНЫ И ВООРУЖЁННЫХ СИЛ РЕСПУБЛИКИ СЕРБИЯ

ВОЕННО-ТЕХНИЧЕСКИЙ ВЕСТНИК
ТОМ 72 • НОМЕР ВЫПУСКА 3 • ИЮЛЬ – СЕНТЯБРЬ 2024.



SCIENTIFIC JOURNAL OF THE MINISTRY OF DEFENCE AND SERBIAN ARMED FORCES

MILITARY TECHNICAL COURIER
VOLUME 72 • ISSUE 3 • JULY – SEPTEMBER 2024

ВТГ.МО.УПР.СРБ
www.vtg.mod.gov.rs
COBISS.SR-ID 4423938
DOI: 10.5937/VojnotehnickiGlasnik

ВЛАСНИЦИ:

Министарство одбране и Војска Србије

ИЗДАВАЧ:

Универзитет одбране у Београду, Војна академија

УРЕДНИШТВО (странице чланова уредништва у ORCID iD-у, Google Scholar-у, Web of Science ResearcherID-у, Scopus Author ID-у и РИНЦ-у доступни су на <http://www.vtg.mod.gov.rs/urednistvo.html>):

ГЛАВНИ И ОДГОВОРНИ УРЕДНИЦИ:

Др Драган Памучар, Универзитет у Београду, Факултет организационих наука, Београд, Србија, e-mail: dragan.pamucar@fon.bg.ac.rs,

Мр Небојша Гаћеша, Универзитет одбране у Београду, Војна академија, Београд, Србија, e-mail: nebojsa.gacesa@mod.gov.rs, tel. 011/3603-260, 066/87-00-123

Уредник за област математике и механике

Др Драган Трифковић, Универзитет одбране у Београду, Војна академија, Београд, Србија

Уредник за област електронике, телекомуникација и информационих технологија

Др Бобан Бонџулић, Универзитет одбране у Београду, Војна академија, Београд, Србија

Уредник за област машинства

Др Бранимир Крстић, Универзитет одбране у Београду, Војна академија, Београд, Србија

Уредник за област материјала и хемијских технологија

Др Михае Бучко, Универзитет одбране у Београду, Војна академија, Београд, Србија

УРЕЂИВАЧКИ ОДБОР:

Др Градимир Миловановић, Српска академија наука и уметности, Београд, Србија,

Др Ђи-Хуан Хи, Универзитет Суџоу, Факултет за текстилну и одевну технику, Суџоу, Кина,

Др Мајид Тафана, Универзитет Ла Сал, Одељење за пословне системе и аналитику, Филадельфија, САД,

Др Шанкар Чакраборти, Универзитет Јадавпур, Одељење за производно машинство, Калкута, Индија,

Др Раду-Емил Прекуп, Универзитет Политехника у Темишвару, Темишвар, Румунија,

Др Јургита Антуцхевичи, Технички универзитет Гедиминас у Вилњусу, Грађевински факултет, Вилњус, Литванија,

Др Срећко Јоксимовић, Универзитет у Јужној Аустралији, Аделејд, Аустралија,

Др Мортеза Јаздани, Факултет за бизнис и маркетинг ESIC, Мадрид, Шпанија,

Др Прасенџит Чатерџи, Институт за инжењерство MCKV, Одељење за машинство, Ховрах, Индија,

Др Жељко Стевић, Универзитет у Источном Сарајеву, Саобраћајни факултет, Добој, Република Српска, БиХ,

Др Хамед Фазлолахтабар, Универзитет Дамган, Одељење за индустријско инжењерство, Дамган, Иран,

Др Јарослав Ватробски, Универзитет у Шчећину, Факултет за економију, финансије и менаџмент, Шчећин, Пољска,

Др Кристиано Фрагаса, Универзитет у Болоњи, Одељење за индустријско инжењерство, Болоња, Италија,

Др Војчех Салабун, Западнопомерански технолошки универзитет у Шчећину, Факултет рачунарских наука и информационих технологија, Шчећин, Пољска,

Др Иева Меидуте-Кавалиаускиене, Војна академија Литваније „Генерал Јонас Жемаитис“, Вилњус, Литванија,

Др Шарка Мајерова, Универзитет одбране у Брну, Одељење за математику и физику, Брно, Чешка Република,

Др Фатих Еџер, Универзитет Афион Коџателе, Факултет за економију и административне науке, Афионкарахисар, Турска,

Др Ернесто Д.Р. Сантибанез Гонзалез, Универзитет у Талки, Одељење за индустријско инжењерство, Талка, Чиле,

Др Драган Маринковић, Технички универзитет у Берлину, Факултет за машинске и транспортне системе, Берлин, Немачка,

Др Стефано Валвано, Универзитет Коре у Ени, Одељење за ваздухопловни инжењеринг, Ена, Италија,

Др Рафал Мадонски, Универзитет Ђинан, Центар за истраживање електричне енергије, Гуанџоу, Кина,

Др Миленко Андрић, Универзитет одбране у Београду, Војна академија, Београд, Србија,

Др Самарџит Кар, Национални институт за технологију, Одељење за математику, Дургапур, Индија,

Др Росен Митрев, Технички универзитет у Софији, Софија, Бугарска,

Др Бојан Милановић, Универзитет одбране у Београду, Војна академија, Београд, Србија,

Др Ирик Мухамедџанов, Државни нафтни технолошки универзитет у Уфи, Уфа, Руска Федерација,

Др Павел Отрисал, Универзитет Палацки, Оломоуц, Чешка Република,

Др Радован Радвановић, Криминалистичко-полицијски универзитет, Београд, Србија,

Др Милица Петровић, Универзитет у Београду, Машински факултет, Београд, Србија,

Др Бошко Рашуо, Универзитет у Београду, Машински факултет, Београд, Србија,

Др Саад Аслам, Универзитет Сунваи, Куала Лумпур, Малезија,

Др Насрин Каусар, Технички универзитет Јилдиз, Факултет уметности и науке, Турска

СОБСТВЕННИКИ: Министерство обороны и Вооружённые силы Республики Сербия

ИЗДАТЕЛЬСТВО: Университет обороны в г. Белград, Военная академия

РЕДАКЦИЯ (со страницами членов редакции в ORCID iD, Google Scholar, Web of Science ResearcherID, Scopus Author ID и РИНЦ можно ознакомиться на сайте <http://www.vtg.mod.gov.rs/redakcia.html>):

ГЛАВНЫЕ И ОТВЕТСТВЕННЫЕ РЕДАКТОРЫ:

Д-р Драган Памучар, Белградский университет, факультет организационных наук, г. Белград, Сербия, e-mail: dragan.pamucar@fon.bg.ac.rs

Кандидат технических наук Небойша Гачеша, Университет обороны в г. Белград, Военная академия, г. Белград, Сербия,

e-mail: nebojsa.gacesa@mod.gov.rs, тел. +381 11 3603 260, +381 66 87 00 123

Редактор в областях: математика и механика

Д-р Драган Трифкович, Университет обороны в г. Белград, Военная академия, г. Белград, Сербия

Редактор в областях: электроника, телекоммуникации и информационные технологии

Д-р Бобан Бонджулич, Университет обороны в г. Белград, Военная академия, г. Белград, Сербия

Редактор в области: машиностроение

Д-р Бранимир Крстич, Университет обороны в г. Белград, Военная академия, г. Белград, Сербия

Редактор в областях: материаловедение и химические технологии

Д-р Михаел Бучко, Университет обороны в г. Белград, Военная академия, г. Белград, Сербия

РЕДАКЦИОННАЯ КОЛЛЕГИЯ:

Д-р Градимир Милованович, Сербская академия наук и искусств, г. Белград, Сербия,

Д-р Джи-Хуан Хи, Университет Сучжоу, факультет текстиля и производства одежды, г. Сучжоу, Китай,

Д-р Маджид Тафана, Университет Ла Саль, департамент бизнес-систем и аналитики, г. Филадельфия, США,

Д-р Шанкар Чакраборти, Университет Джадавпур, департамент производственных машин, г. Калькутта, Индия,

Д-р Радун-Емил Прекуп, Политехнический университет Тимишоары, г. Темишуара, Румыния,

Д-р Юргита Антучевичиене, Вильнюсский технический университет имени Гедиминаса, строительный факультет, г. Вильнюс, Литва,

Д-р Мартаз Иаздан, Школа бизнеса и маркетинга ESIC, г. Мадрид, Испания,

Д-р Прасенджит Чатерджи, Институт инженерии MCKV, департамент машиностроения, г. Хаора, Индия,

Д-р Желько Стевич, Восточно-Сараевский университет, транспортный факультет, г. Добой, Республика Сербская, БиГ,

Д-р Хамед Фазлолахтабар, Университет Дамгана, департамент промышленной инженерии, г. Дамган, Иран,

Д-р Ярослав Ватробски, Щецинский университет, факультет экономики, финансов и менеджмента, г. Щецин, Польша,

Д-р Кристиано Фрагаса, Болонский университет, департамент промышленной инженерии, г. Болонья, Италия,

Д-р Войчех Салабун, Западно-Померанский технологический университет в г. Щецин, факультет компьютерных наук и информационных технологий, г. Щецин, Польша,

Д-р Иева Меидуте-Кавалиаускиене, Литовская Военная академия им. генерала Йонаса Жемайтиса, г. Вильнюс, Литва,

Д-р Шарка Маерова, Университет обороны в г. Брно, физико-математический департамент, г. Брно, Чешская Республика,

Д-р Фатих Ецер, Университет Афьон Коджатеппе, Факультет делового администрирования, г. Афьонкарахисар, Турция,

Д-р Эрнесто Д.Р. Сантибанез Гонзалез, Университет Тальки, департамент промышленной инженерии, г. Талька, Чили,

Д-р Драган Маринкович, Берлинский технический университет, факультет машиностроительных и транспортных систем, г. Берлин, Германия,

Д-р Стефано Валвано, Университет Коре Энна, департамент авиационной инженерии, г. Энна, Италия,

Д-р Рафал Мадонски, Университет Цзинань, Центр энергетических исследований, г. Гуанчжоу, Китай,

Д-р Миленко Андрич, Университет обороны в г. Белград, Военная академия, г. Белград, Сербия,

Д-р Самарджит Кар, Национальный технологический институт, департамент математики, г. Дургапур, Индия,

Д-р Росен Митрев, Софийский технический университет, г. София, Болгария,

Д-р Боян Миланович, Университет обороны в г. Белград, г. Белград, Сербия,

Д-р Ирик Мухаметзянов, Уфимский государственный нефтяной технический университет, г. Уфа, Российская Федерация,

Д-р Павел Отрисал, Университет Палацкого, Оломоуц, Чешская Республика,

Д-р Радован Радованович, Университет криминалистики и полицейской подготовки, г. Белград, Сербия,

Д-р Милица Петрович, Белградский университет, машиностроительный факультет, г. Белград, Сербия,

Д-р Бошко Рашуо, Белградский университет, машиностроительный факультет, г. Белград, Сербия,

Д-р Саад Аслам, Университет Санвэй, Куала-Лумпур, Малайзия,

Д-р Насрин Каусар, Технический университет Иылдыз, Стамбул, Турция

OWNERS:

Ministry of Defence and Serbian Armed Forces

PUBLISHER:

University of Defence in Belgrade, Military Academy

EDITORIAL TEAM (the pages of the Editorial Team's members in ORCID iD, Google Scholar, Web of Science ResearcherID, Scopus Author ID, and PIHLJ can be accessed at

<http://www.vtg.mod.gov.rs/editorial-team.html>):

EDITORS IN CHIEF:

Dr. Dragan Pamučar, University of Belgrade, Faculty of Organizational Sciences, Belgrade, Serbia,
e-mail: dragan.pamucar@fon.bg.ac.rs

Nebojša Gaćeša, MSc, University of Defence in Belgrade, Military Academy, Belgrade, Serbia,
e-mail: nebojsa.gacesa@mod.gov.rs, tel. +381 11 3603 260, +381 66 87 00 123

Editor for Mathematics and Mechanics

Dr. Dragan Trifković, University of Defence in Belgrade, Military Academy, Belgrade, Serbia

Editor for Electronics, Telecommunications and Information Technology

Dr. Boban Bondžulić, University of Defence in Belgrade, Military Academy, Belgrade, Serbia

Editor for Mechanical Engineering

Dr. Branimir Krstić, University of Defence in Belgrade, Military Academy, Belgrade, Serbia

Editor for Materials and Chemical Technologies

Dr. Mihael Bučko, University of Defence in Belgrade, Military Academy, Belgrade, Serbia

EDITORIAL BOARD:

Dr. Gradimir Milovanović, Serbian Academy of Sciences and Arts, Belgrade, Serbia,

Dr. Ji-Huan He, Soochow University, College of Textile and Clothing Engineering, Soochow, China,

Dr. Madjid Tavana, La Salle University, Business Systems and Analytics Department, Philadelphia, USA,

Dr. Shankar Chakraborty, Jadavpur University, Department of Production Engineering, Kolkata, India,

Dr. Radu-Emil Precup, Politehnica University of Timisoara, Department of Automation and Applied Informatics, Timisoara, Romania,

Dr. Jurgita Antuchevičienė, Vilnius Gediminas Technical University, Faculty of Civil Engineering, Vilnius, Lithuania,

Dr. Morteza Yazdani, ESIC Business and Marketing School, Madrid, Spain,

Dr. Prasenjit Chatterjee, MCKV Institute of Engineering, Department of Mechanical Engineering, Howrah, India,

Dr. Željko Stević, University of East Sarajevo, Faculty of Transportation, Doboj, Republic of Srpska, Bosnia and Herzegovina,

Dr. Hamed Fazlollahtabar, Damghan University, Department of Industrial Engineering, Damghan, Iran,

Dr. Jarosław Wątróbski, University of Szczecin, Faculty of Economics, Finance and Management, Szczecin, Poland,

Dr. Cristiano Fragassa, University of Bologna, Department of Industrial Engineering, Bologna, Italy,

Dr. Wojciech Sałabun, West Pomeranian University of Technology in Szczecin, Faculty of Computer Science and Information Technology, Szczecin, Poland,

Dr. Ieva Meidutė-Kavaliauskienė, General Jonas Žemaitis Military Academy of Lithuania, Research Group on Logistics and Defense Technology Management, Vilnius, Lithuania,

Dr. Šárka Mayerová, University of Defence in Brno, Department of Mathematics and Physics, Brno, Czech Republic,

Dr. Fatih Ecer, Afyon Kocatepe University, Faculty of Economics and Administrative Sciences, Afyonkarahisar, Turkey,

Dr. Ernesto D.R. Santibanez Gonzalez, Universidad de Talca, Department of Industrial Engineering, Talca, Chile,

Dr. Dragan Marinković, Technical University Berlin, Faculty of Mechanical and Transport Systems, Berlin, Germany,

Dr. Stefano Valvano, Kore University of Enna, Department of Aerospace Engineering, Enna, Italy,

Dr. Rafal Madonski, Jinan University, Energy Electricity Research Center, Guangzhou, China,

Dr. Milenko Andrić, University of Defence in Belgrade, Military Academy, Belgrade, Serbia,

Dr. Samarjit Kar, National Institute of Technology, Department of Mathematics, Durgapur, India,

Dr. Rosen Mitrev, Technical University of Sofia, Sofia, Bulgaria,

Dr. Bojan Milanović, University of Defence in Belgrade, Military Academy, Belgrade, Serbia,

Dr. Irik Mukhametzyanov, Ufa State Petroleum Technological University, Ufa, Russian Federation,

Dr. Pavel Otrisal, Palacký University, Olomouc, Czech Republic,

Dr. Radovan Radovanović, University of Criminal Investigation and Police Studies, Belgrade, Serbia,

Dr. Milica Petrović, University of Belgrade, Faculty of Mechanical Engineering, Belgrade, Serbia,

Dr. Boško Rašuo, University of Belgrade, Faculty of Mechanical Engineering, Belgrade, Serbia,

Dr. Saad Aslam, Sunway University, Kuala Lumpur, Malaysia,

Dr. Nasreen Kausar, Yıldız Technical University, Istanbul, Turkey

САДРЖАЈ

ОРИГИНАЛНИ НАУЧНИ РАДОВИ

- Шивакумар Картик, Апасами Сарасвати, Сајед Ахмад Едалатпанах*
Проблем фази линеарног фракционог програмирања
помоћу лексикографског метода965-979
- Коти Н. В. В. Вара Прасад, Винај Мишра, Стојан Раденовић*
Теореме постојања за јединствену интерполативну Кананову контракцију
са применама код нелинеарних матричних једначина980-1003
- Нора Фетучи, Стојан Раденовић*
О неким резултатима фиксне тачке за експанзивна пресликавања
у S-метричким просторима1004-1018
- Никола Фабиано, Никола Мирков, Стојан Раденовић*
Нека разматрања о укупном времену заустављања за Колацов проблем ...1019-1028
- Равичандиран Тангатамиж, Ангамуту Муралираџ,
Перијасами Шанмугавил*
Нови приступ Лебеговом интегралу у прерађеним фази конусним
метричким просторима помоћу теорема јединствене спрегнуте
непокретне тачке1029-1045
- Пракасам Мураликришна, Перумал Хемавати, Раџа Винодкумар,
Перумал Чантини, Калијаперумал Паланивел, Сејед Ахмад Едалатпанах*
Изразите одлике и валидација δ^* -алгебри: аналитичко истраживање1046-1065
- Фу М. Нуен, Биен В. Во, Зоан В. Цао, Зунг В. Нуен*
Проучавање динамичких карактеристика пушака које функционишу по
принципу позајмице барутних гасова помоћу софтвера Solidworks Motion ..1066-1092
- Иван Б. Петровић, Милан Ж. Миленковић*
Унапређење процеса оперативног планирања применом хибридног
фази-вишекритеријумског приступа одлучивању1093-1119
- Душко З. Тешић, Дарко И. Божанић, Адис Пушка*
Примена вишекритеријумског одлучивања за избор локације за
савлађавање водене препреке газом у одбрамбеној операцији1120-1146
- Александар Р. Алексић, Борис В. Делибашић,
Жељко М. Јокић, Марко Р. Радовановић*
Примена АНР и VIKOR метода индивидуалног одлучивања и
Borda метода групног одлучивања при избору најефикаснијег
начина извршења припремног гађања на редном броју 1
далекометном пушком М-93 калибра 12,7 mm1147-1170
- Хауда Бегдад, Насер Рахал, Абделаиз Соици,
Сара Затар, Калед Бенмахди, Халима Авед*
Утицај прслине на нелинеарно понашање ојачаног композитног панела1171-1187
- Ајша Метери, Куидер Мадани, Белаид Мехаџ,
Мухамад Муктери, Илиас М. А. Гермауи*
Испитивање затезања прогресивног оштећења и лома у порозним
керамичким композитним материјалима помоћу проширеног метода
коначних елемената (XFEM)1188-1213
- Бобан П. Боњулић, Ненад М. Стојановић,
Владимир В. Лукин, Сергеј С. Кривенко*
Компресија JPEG и BPG без губитка визуелних информација
на примеру базе KonJND-1k1214-1241

<p><i>Тахир Газул, Мухамед Атиф Бената, Абделвахаб Катир, Јусуф Белџелили, Багдад Кроур, Мухамед Башир Бујаџера</i></p> <p>Аналитичко испитивање порозних ламинираних плоча од функционално градираних композита ојачаних угљеничним наноцевима (FG-CNTRC) на извијање и слободне вибрације.....</p>	1242-1271
<p><i>Амин Земри, Исмаил Мехаб</i></p> <p>Анализа изазваног динамичког понашања функционално степенованих греда под хармоничним покретним оптерећењем на еластичној основи помоћу методе коначних елемената</p>	1272-1305
<p><i>Јусуф Мулаи Арби, Нуредин Мамуди, Мухамад Бентахар</i></p> <p>Процењивање понашања структуре зидова од цигли од рециклиране пластике под монотоним и цикличним оптерећењем</p>	1306-1344
<p><i>Горан В. Павловић, Миле М. Савковић, Небојша Б. Здравковић, Горан Ђ. Марковић, Предраг З. Младеновић</i></p> <p>Оптимално решење носача једногредне мосне дизалице применом алгоритма Мољца.....</p>	1345-1368
<p><i>Бенамар Бали, Хамид Селаф, Ада Хаџ Мустифа, Дрис Џафари, Али Мекси</i></p> <p>Побољшавање физичких и хемијских карактеристика оцедних вода депонија путем филтрационог система који садржи отпад од гранита, опилџака гвожђа и рециклиране гуме</p>	1369-1394
<p><i>Милан Ђокић, Зоран Ј. Бајић, Владимир Игњатовић</i></p> <p>Пристап поузданом начину одређивања хемијске стабилности једнобазних барута применом методе микрокалориметрије</p>	1395-1413
<p><i>Абделкрим Бенахмед, Отби Бугенина, Али Мекси, Халед Бенмади, Халед Бендахане, Мохамед Садоун</i></p> <p>Динамичка анализа лучне бране</p>	1414-1440
ПРЕГЛЕДНИ РАДОВИ	
<p><i>Санела З. Вељковић, Милица Т. Ђурчић, Илија П. Гавриловић</i></p> <p>Тамне стране дипфејк технологије</p>	1441-1463
<p>САВРЕМЕНО НАОРУЖАЊЕ И ВОЈНА ОПРЕМА</p> <p><i>Драган М. Вучковић</i></p>	1464-1475
<p>ПОЗИВ И УПУТСТВО АУТОРИМА.....</p>	1476-1492

СОДЕРЖАНИЕ

ОРИГИНАЛЬНЫЕ НАУЧНЫЕ СТАТЬИ

<i>Сивакумар Картик, Аппасами Сарасвати, Сейед Ахмад Эдалатпанах</i> Задача нечеткого дробно-линейного программирования с использованием лексикографического метода	965-979
<i>Коти Н. В. В. Вара Прасад, Винай Мишра, Стоян Раденович</i> Теоремы существования унифицированного интерполяционного сокращения Каннана с применением нелинейных матричных уравнений.....	980-1003
<i>Нора Фетучи, Стоян Раденович</i> О некоторых результатах с неподвижной точкой в расширенных отображениях.....	1004-1018
<i>Никола Фабиано, Никола Мирков, Стоян Раденович</i> Некоторые соображения относительно общего времени о станочки для задачи Коллатца.....	1019-1028
<i>Равичандиран Тангатамиж, Ангамуту Муралираджд, Периясами Шанмугавил</i> Новый подход к интегралу Лебега в пересмотренных нечетких конусообразных метрических пространствах с помощью единой связанной неподвижной точки.....	1029-1045
<i>Пракасам Мураликришна, Перумал Хемавати, Раджа Винодкumar, Перумалр Чантини, Калияперумал Паланивел, Сейед Ахмад Эдалатпанах</i> Отличительные особенности и валидация δ^* -алгебры: аналитическое исследование.....	1046-1065
<i>Фу М. Нуиен, Биен В. Во, Зоан В. Цао, Зунг В. Нуиен</i> Изучение динамических характеристик газового огнестрельного оружия с использованием программного обеспечения Solidworks Motion	1066-1092
<i>Иван Б. Петрович, Милан Ж. Миленкович</i> Совершенствование процесса планирования операций с использованием гибридного нечетко-многокритериального подхода к принятию решений	1093-1119
<i>Душко З. Тешич, Дарко И. Божанич, Адис Пушка</i> Применение многокритериального принятия решений для выбора места преодоления водного препятствия вброд в ходе оборонительной операции.....	1120-1146
<i>Александр Р. Алексич, Борис В. Делибашич, Желько М. Йокич, Марко Р. Радованович</i> Применение методов индивидуального принятия решений АНР и VIKOR и метода группового принятия решений Vorda при выборе наиболее эффективного способа выполнения подготовительных упражнений №1 по стрельбе из дальнобойной винтовки М-93 калибра 12,7-мм	1147-1170
<i>Хауда Бегдад, Насер Рахал, Абдулазиз Соици, Сара Заттар, Халед Бенмахди, Халима Авед</i> Влияние трещин на нелинейное поведение упрочненной композитной панели	1171-1187
<i>Айша Метери, Куидер Мадани, Белаид Мехаб, Мухаммед Муктери, Илиас М. А. Гермауи</i> Исследование растяжений при прогрессирующих деформациях и разрушении пористых керамических композиционных материалов с метода конечных элементов (МКЭ)	1188-1213

<i>Бобан П. Бонджулич, Ненад М. Стоянович, Владимир В. Лукин, Сергей С. Кривенко</i>	
Сжатие изображений JPEG и BPG без визуальных потерь с помощью базы данных KopJND-1k	1214-1241
<i>Тахир Газул, Мухаммед Атиф Бената, Абделвахаб Катир, Йусуф Белджелили, Багдад Кроур, Мухаммед Башир Буажера</i>	
Аналитическое исследование изгиба и свободной вибрации пористых слоистых пластин FG-CNTRC	1242-1271
<i>Амине Земри, Исмаил Мечаб</i>	
Анализ вынужденного динамического поведения функционально-градиентных балок при гармонической подвижной нагрузке на упругом основании методом конечных элементов.....	1272-1305
<i>Юсуф Мулаи Арби, Нуредин Мамуди, Мухаммед Бентахар</i>	
Оценка структурных характеристик кладки кирпича из переработанного пластика при монотонной и циклической нагрузке	1306-1344
<i>Горан В. Павлович, Миле М. Савкович, Небойша Б. Здравкович, Горан Д. Маркович, Предраг З. Младенович</i>	
Оптимальное решение для однобалочной подкрановой балки моста с использованием алгоритма Moth-Flame	1345-1368
<i>Бенамар Балех, Хамид Селлаф, Адда Хадж Мостефа, Дрисс Джафари, Али Мекси</i>	
Улучшение физических и химических свойств фильтрата, образующегося на свалках, благодаря системе фильтрации, включающей гранитную пыль, металлическую стружку и переработанные резиновые отходы	1369-1394
<i>Милан Джокич, Зоран Й. Баич, Владимир Игнятович</i>	
Подход к надежному способу определения химической стойкости одноосновных порохов методом микрокалориметрии	1395-1413
<i>Абдельkrim Бенахмед, Отби Бугенина, Али Мекси, Халед Бенмади, Халед Бендахане, Мухаммед Садоун</i>	
Динамический анализ арочной плотины	1414-1440
ОБЗОРНЫЕ СТАТЬИ	
<i>Санела З. Велькович, Милица Т. Чурчич, Илья П. Гаврилович</i>	
Темные стороны дипфейк технологии	1441-1463
СОВРЕМЕННОЕ ВООРУЖЕНИЕ И ВОЕННОЕ ОБОРУДОВАНИЕ	
<i>Драган М. Вучкович</i>	
ПРИГЛАШЕНИЕ И ИНСТРУКЦИИ ДЛЯ АВТОРОВ РАБОТ	1476-1492

CONTENTS

ORIGINAL SCIENTIFIC PAPERS

- Sivakumar Karthick, Appasamy Saraswathi, Seyyed Ahmad Edalatpanah*
Fuzzy linear fractional programming problem using the lexicography method965-979
- Koti N. V. V. Vara Prasad, Vinay Mishra, Stojan Radenović*
Existence theorems for a unified interpolative Kannan contraction with
an application on nonlinear matrix equations.....980-1003
- Nora Fetouci, Stojan Radenović*
On some fixed point results for expansive mappings in S-metric spaces1004-1018
- Nicola Fabiano, Nikola Mirkov, Stojan Radenović*
Some considerations on the total stopping time for the Collatz problem1019-1028
- Ravichandhiran Thangathamizh, Angamuthu Muraliraj,
Periyasamy Shanmugavel*
New approach of Lebesgue integral in revised fuzzy cone metric spaces
via unique coupled fixed point theorems1029-1045
- Prakasam Muralikrishna, Perumal Hemavathi, Raja Vinodkumar,
Perumal Chanthini, Kaliyaperumal Palanivel, Seyyed Ahmad Edalatpanah*
Distinct features and validation of δ^* -algebras: an analytical exploration1046-1065
- Phu M. Nguyen, Bien V. Vo, Doan V. Dao, Dung V. Nguyen*
Studying the dynamic characteristics of gas-operated guns using
Solidworks Motion software1066-1092
- Ivan B. Petrović, Milan Ž. Milenković*
Improvement of the operations planning process using a hybridized
fuzzy-multi-criteria decision-making approach1093-1119
- Duško Z. Tešić, Darko I. Božanić, Adis Puška*
Application of multi-criteria decision making for the selection of a location
for crossing a water obstacle by fording in a defense operation1120-1146
- Aleksandar R. Aleksić, Boris V. Delibašić,
Željko M. Jokić, Marko R. Radovanović*
Application of the AHP and VIKOR methods of individual decision making
and the Borda method of group decision making when choosing the most
efficient way of performing preparatory shooting at serial number one from
a 12.7 mm long range rifle M-931147-1170
- Houda Beghdad, Nacer Rahal, Abdelaziz Souici,
Sara Zatir, Khaled Benmahdi, Halima Aouad*
Effect of a crack on the nonlinear behavior of a stiffened composite panel1171-1187
- Aicha Metehri, Kouider Madani, Belaïd Mechab,
Mohammed Mokhtari, Ilias M.A. Ghermaoui*
Tensile examination of progressive damage and failure in porous
ceramic composite materials using the XFEM1188-1213
- Boban P. Bondžulić, Nenad M. Stojanović,
Vladimir V. Lukin, Sergii S. Kryvenko*
JPEG and BPG visually lossless image compression via KonJND-1k database.1214-1241
- Tahir Ghazoul, Mohamed Atif Benatta, Abdelwahhab Khatir,
Youcef Beldjelili, Baghdad Krour, Mohamed Bachir Bouiadjra*
Analytical investigation on the buckling and free vibration of
porous laminated FG-CNTRC plates1242-1271

<i>Amine Zemri, Ismail Mechab</i>	
Forced dynamic analysis of functionally graded beams under harmonic moving loads on elastic foundation with the finite element method	1272-1305
<i>Youcef Moulai Arbi, Nouredine Mahmoudi, Mohammed Bentahar</i>	
Evaluating the structural performance of masonry walls incorporating recycled plastic bricks under monotonic and cyclic loading	1306-1344
<i>Goran V. Pavlović, Mile M. Savković, Nebojša B. Zdravković, Goran Đ. Marković, Predrag Z. Mladenović</i>	
Optimal solution for the single-beam bridge crane girder using the Moth-Flame algorithm.....	1345-1368
<i>Benamar Balegh, Hamid Sellaf, Adda Hadj Mostefa, Driss Djafari, Ali Meksi</i>	
Enhancing the physical and chemical characteristics of landfill leachate through a filtration system incorporating granite, iron filings, and recycled rubber waste	1369-1394
<i>Milan M. Djokić, Zoran J. Bajić, Vladimir D. Ignjatović</i>	
Towards the reliable chemical stability testing of the single base gunpowder using a microcalorimetry method	1395-1413
<i>Abdelkrim Benahmed, Otbi Bouguenina, Ali Meksi, Khaled Benmahdi, Khaled Bendahane, Mohamed Sadoun</i>	
Dynamic analysis of a vaulted dam.....	1414-1440
REVIEW PAPERS	
<i>Sanela Z. Veljković, Milica T. Ćurčić, Ilija P. Gavrilović</i>	
Dark sides of deepfake technology	1441-1463
MODERN WEAPONS AND MILITARY EQUIPMENT	1464-1475
<i>Dragan M. Vučković</i>	
CALL FOR PAPERS AND INSTRUCTIONS FOR AUTHORS.....	1476-1492

ORIGINAL SCIENTIFIC PAPERS


Fuzzy linear fractional programming problem using the lexicography method

Sivakumar Karthick^a, Appasamy Saraswathi^b,
Seyyed Ahmad Edalatpanah^c

^a SRM Institute of Science and Technology,
College of Engineering and Technology, Department of Mathematics,
Kattankulathur, Chengalpattu, Tamilnadu, Republic of India,
e-mail: ks9762@srmist.edu.in,
ORCID iD: <https://orcid.org/0000-0001-9176-4628>

^b SRM Institute of Science and Technology,
College of Engineering and Technology, Department of Mathematics,
Kattankulathur, Chengalpattu, Tamilnadu, Republic of India,
e-mail: saraswaa@srmist.edu.in, **corresponding author**,
ORCID iD: <https://orcid.org/0000-0003-0529-4346>

^c Ayandegan Institute of Higher Education,
Applied Mathematics Department,
Tonekabon, Islamic Republic of Iran,
e-mail: s.a.edalatpanah@aihe.ac.ir,
ORCID iD: <https://orcid.org/0000-0001-9349-5695>

 <https://doi.org/10.5937/vojtehg72-50429>

FIELD: mathematics, computer sciences

ARTICLE TYPE: original scientific paper

Abstract:

Introduction/purpose: In solving real-life fractional programming problems, uncertainty and hesitation are often encountered due to various uncontrollable factors. To overcome these limitations, the fuzzy logic approach is applied to these problems.

Methods: The discussion focused on solving the fuzzy linear fractional programming problem (FLFPP). First, the FLFP problem was converted into a lexicographic optimization problem, which was then solved to obtain the solution.

Results : A numerical example was presented to simplify the explanation of the algorithm. While most researchers solve FLFPPs using the ranking function method, this approach reduces the efficiency of the fuzzy problem.

Conclusion: This research contributes a comprehensive methodology for addressing fuzzy linear fractional programming problems using the lexicography method. The findings offer valuable insights for researchers,

practitioners, and decision-makers grappling with optimization challenges in settings where imprecise information significantly influences the decision landscape.

Key words: linear fractional programming, lexicography method, triangular fuzzy number.

Nomenclature: FLFP – Fuzzy Linear Fractional Programming
FFLP – Full Fuzzy Linear Programming
MOLFP – Multi Objective Linear Fractional Programming

Introduction

Linear fractional programming is an extension of linear programming where the objective function is a ratio of two linear functions. The goal is still to optimize this ratio subject to linear constraints. Fuzzy linear programming is an extension that incorporates the concept of fuzzy set theory into linear programming. In traditional linear programming, all parameters are assumed to be precise and deterministic. In fuzzy linear programming, some or all of the parameters, including coefficients and constants, are allowed to be fuzzy numbers, representing uncertainty.

The objective function and constraints are formulated with fuzzy coefficients and decision variables. The solution to a fuzzy linear programming problem yields a fuzzy decision variable, providing a range of possible values rather than a single precise value.

Zadeh (1965) has contributed to decision making in fuzzy environment. Specifically, to the concept of decision making in uncertainty and vagueness. This gives to FLFPP all parameters denoted as fuzzy numbers. This technique aims at uncertainty and vagueness in the problem, substituting crisp numbers with fuzzy ones. Consequently, LFP transforms into FLFPP. A pivotal development in FLFPP was introduced by Charnes & Cooper (1962). They successfully transformed LFPP to LPP and got solutions using the Simplex method.

Li (2008) implemented a lexicographic method to solve the matrix game with pay-offs represented by triangular fuzzy numbers. Ebrahimnejad (2017) solved fuzzy transportation problems with triangular fuzzy numbers using lexicographic ordering. Nan et al. (2010) defined the ranking order relations of TIFNs, which are applied to matrix games with payoffs of TIFNs. Prakash & Appasamy (2023) studied fully fuzzy spherical linear programming problems, where spherical fuzzy numbers are utilized as parameters. Hosseinzadeh Lotfi et al. (2009) discussed full fuzzy linear programming (FFLP) problems of which all parameters and variable are triangular fuzzy numbers and the concept of the symmetric triangular fuzzy

number and introduced an approach to defuzzify a general fuzzy quantity. Sharma (2015) introduced a new ranking method proposed for L-R flat fuzzy numbers which is based on the lexicographical ordering approach. Pérez-Cañedo et al. (2019) reviewed the established models and methods in FLP, focusing on lexicographic methods for ranking fuzzy numbers (FNs) in single and multi-objective LP, particularly within the context of fuzzy linear assignment problems due to their significance. Demir (2023) investigated the fabric dyeing process in a towel manufacturing factory using the lexicography method. Safaei (2014) approached a new method for solving fully FLFP problems. Dharmaraj & Appasamy (2023) applied a modified Gauss elimination technique for separable fuzzy nonlinear programming. Sivakumar & Appasamy (2024) solved LFPP by a mathematical approach. Abdel-Basset et al. (2019) and Karthick et al. (2024) proposed to solve the neutrosophic linear fractional programming problem with triangular neutrosophic numbers.

Aim: The aim of this research is to propose a novel approach, termed Fuzzy Linear Fractional Programming (FLFP), to address real-life fractional programming problems characterized by uncertainty and imprecision. The primary objective is to develop a robust methodology for decision support in complex decision-making scenarios where parameters exhibit fuzziness.

Novelty: This study introduces a hybrid framework that combines the fuzzy set theory and linear fractional programming, offering a unique solution approach to handle uncertainties in decision-making processes. Unlike conventional methods that may reduce efficiency, the proposed FLFP method aims to provide a more effective solution by incorporating fuzzy coefficients within the objective function and constraints.

Contribution: The research contributes a comprehensive methodology for addressing fuzzy linear fractional programming problems using the lexicography method. By presenting a systematic approach to navigating the complex landscape of fuzzy decision variables, this study offers valuable insights for researchers, practitioners, and decision-makers facing optimization challenges in settings where imprecise information significantly influences decision-making processes. The presented numerical example demonstrates the applicability and effectiveness of the proposed approach, highlighting its potential to overcome limitations associated with uncertainty and hesitation in real-life fractional programming problems.

Here, the NLFP problem is transformed into an equivalent crisp multi-objective linear fractional programming (MOLFP) problem which can be solved by the linear programming technique.

This research article is organized as follows: Section 2 is the discussion about fundamental definitions; Section 3 introduces the mathematical model and demonstrates the proposed method; Section 4 illustrates a suitable numerical example for the proposed method; and in Section 5, some conclusion is pointed out at the end of this paper.

Preliminary concepts

Definition 1 (Zadeh, 1965)

If X is a universal set and $x \in X$, then a fuzzy set \tilde{A} defined as, $\tilde{A} = \{(x, \mu_{\tilde{A}}(x)), x \in X\}$ where $\mu_{\tilde{A}}$ = membership function.

Definition 2 (Zadeh, 1965)

A fuzzy set \tilde{A} is called a fuzzy number if its membership function $\tilde{A}: R \rightarrow [0,1]$ satisfies the following conditions:

- \tilde{A} is convex,
- \tilde{A} is normal, and
- \tilde{A} is piecewise continuous.

Definition 3 (Ebrahimnejad, 2017)

A fuzzy number \tilde{A} on R is said to be a triangular fuzzy number(TFN) if its membership function $\tilde{A}: R \rightarrow [0,1]$ has the following criteria, and this TFN graphical representation is presented in Figure:1:

$$\tilde{A}(x) = \begin{cases} \frac{x-a_1}{a_2-a_1}, & a_1 \leq x \leq a_2 \\ \frac{a_1-x}{a_3-a_2}, & a_2 < x \leq a_3 \\ 0, & \text{otherwise.} \end{cases}$$

The TFN is denoted as notationally by $\tilde{A} = (a_1, a_2, a_3)$. and $F(R)$ is used for the set of all TFNs.

Definition 4 (Demir, 2023)

Let \leq_{lex} be the lexicographic order relation in R^3 and $\tilde{v}_1 = (v_1^l, v_1^c, v_1^u)$ and $\tilde{v}_2 = (v_2^l, v_2^c, v_2^u)$ two TFNs. We say that \tilde{v}_1 is relatively smaller than \tilde{v}_2 , which is denoted by $\tilde{v}_1 < \tilde{v}_2$ iff $(v_1^c, v_1^l - v_1^u, v_1^l + v_1^u) <_{lex} (v_2^c, v_2^l - v_2^u, v_2^l + v_2^u)$. We say that \tilde{v}_1 is relatively smaller than or equal to \tilde{v}_2 , which is denoted by $\tilde{v}_1 \leq \tilde{v}_2$ iff $(v_1^c, v_1^l - v_1^u, v_1^l + v_1^u) \leq_{lex} (v_2^c, v_2^l - v_2^u, v_2^l + v_2^u)$ and $\tilde{v}_1 = \tilde{v}_2$ iff $v_1^c = v_2^c, v_1^l - v_1^u = v_2^l - v_2^u, v_1^l + v_1^u = v_2^l + v_2^u$

Mathematical model

Linear fractional programming problem

The linear fractional programming problem is a mathematical optimization problem that involves maximizing or minimizing a ratio of two linear functions. It can be formulated as follows:

$$\text{Max}Q(x) = \frac{P(x)}{D(x)} = \frac{\sum_{j=1}^n p_j x_j + p_0}{\sum_{j=1}^n d_j x_j + d_0} \tag{1}$$

subject to

$$\sum_{j=1}^n a_{ij} x_j \leq \text{or} \geq \text{or} = b_i, i = 1, 2, 3, \dots, m$$

and $x_j \geq 0$. Here, x is the vector of variables to be determined, $P(x)$ and $D(x)$ are vectors of known coefficients, and a_{ij} is a known matrix of coefficients.

Proposed method

The formulation of the FLFP problem with triangular fuzzy parameters is articulated as follows: maximize the sum of products of \tilde{c}_j and \tilde{x}_j divided by \tilde{d}_j and \tilde{x}_j over n , subject to constraints involving the sum of products of \tilde{a}_{ij} and \tilde{x}_j , with \tilde{x}_j representing non-negative triangular fuzzy numbers (TFNs) for $j = 1, 2, \dots, n$.

Step 1: Define $\tilde{c}_j = (c_j^l, c_j^c, c_j^u)$, $\tilde{d}_j = (d_j^l, d_j^c, d_j^u)$, $\tilde{a}_{ij} = (a_{ij}^l, a_{ij}^c, a_{ij}^u)$, $\tilde{b}_i = (b_i^l, b_i^c, b_i^u)$, and $\tilde{x}_j = (x_j^l, x_j^c, x_j^u)$, transforming the FFLP problem into an expression maximizing the sum of $(c_j^l, c_j^c, c_j^u)(x_j^l, x_j^c, x_j^u)$, with constraints on $(a_{ij}^l, a_{ij}^c, a_{ij}^u)(x_j^l, x_j^c, x_j^u)$ and conditions on (x_j^l, x_j^c, x_j^u) being non-negative TFNs.

Step 2: Rewrite the FFLP problem by expressing the objective and constraints in terms of new symbols (s_j^l, s_j^c, s_j^u) and $(m_{ij}^l, m_{ij}^c, m_{ij}^u)$, maintaining the relationship with (b_i^l, b_i^c, b_i^u) and the non-negativity of TFNs for each j .

Step 3: Convert the FFLP problem into a lexicographic optimization problem by setting lex max criteria based on the central values, the difference, and the sum of the lower and upper bounds of the sums

involved, aligning with the conditions set for equality, and inequality constraints represented by the index sets l_e, l_{le}, l_{ge} .

Step 4: Further articulate the lexicographic maximization with additional constraints represented through the variables y_{i1}, y_{i2}, y_{i3} , introducing the parameters ϵ and L to delineate the ranges for the constraints, adhering to the specifications for l_{le} and l_{ge} .

Step 5: Address the multi-level lexicographic fuzzy linear programming (MLLFP) problem using classical methods for multi-objective optimization to pinpoint an optimal solution.

Step 6: Assess $\sum_{j=1}^n \frac{\tilde{c}_j \tilde{x}_j}{\tilde{a}_j \tilde{x}_j}$ with the derived optimal solution to determine the optimal fuzzy value of the FFLP problem, thus concluding the methodological approach for solving FFLP problems with triangular fuzzy parameters.

Numerical example: 1

The given problem involves FLFP, where the coefficients and constraints are represented by fuzzy numbers. Fuzzy numbers here are given in the form of triplets, which could represent, for example, the lower limit, the most probable value, and the upper limit of an estimation. This problem involves maximizing a fuzzy objective function subject to fuzzy constraints. Let us construct a potential application problem that could be represented by this mathematical formulation.

Application Scenario: Production Planning

Imagine a small manufacturing company that produces two types of products: Product 1 and Product 2. The company is operating in an uncertain environment where the profit margins, production costs, and available resources (like raw materials, labor, and machinery time) fluctuate within known ranges. These fluctuations are due to varying market conditions, supplier reliability, and labor availability. The company aims to maximize its profit margin while ensuring that production does not exceed its fuzzy constraints, which represent the uncertain availability of resources.

Variables: - \tilde{x}_1 = Quantity of Product 1 to produce. - \tilde{x}_2 = Quantity of Product 2 to produce.

Objective Function: Maximize the fuzzy profit ratio \tilde{Z} :

$$\tilde{Z} = \frac{(2,4,7)\tilde{x}_1 + (1,3,4)\tilde{x}_2}{(1,2,3)\tilde{x}_1 + (3,5,8)\tilde{x}_2}$$

This represents the goal of maximizing the ratio of total profit (numerator, with uncertain profit margins for products 1 and 2) to total

production costs (denominator, with uncertain costs for producing products 1 and 2).

Constraints: 1. Resource Constraint for Resource A (e.g., raw materials):

$$(0,1,2)\tilde{x}_1 + (1,2,3)\tilde{x}_2 \leq (1,10,27)$$

This constraint represents the fuzzy limitation of Resource A available for production, where the availability is uncertain.

2. Resource Constraint for Resource B (e.g., labor hours):

$$(1,2,3)\tilde{x}_1 + (0,1,2)\tilde{x}_2 \leq (2,11,28)$$

This represents the fuzzy limitation of Resource B, reflecting the uncertain availability of labor hours for production.

Application Problem Statement: A small manufacturing company is looking to determine the optimal production levels of two products under uncertain market conditions and resource availabilities. The company wants to maximize its profit ratio, taking into account the uncertain profit margins and production costs for both products, while also ensuring that the production does not exceed the uncertain availability of raw materials and labor hours. How should the company allocate its resources to the production of these two products to achieve its goal?

This problem encapsulates the challenge of making strategic decisions in an uncertain environment, typical of real-world situations faced by businesses. The use of fuzzy numbers allows for a more flexible and realistic modeling of uncertainties compared to traditional deterministic models.

$$Max\tilde{Z} = \frac{(2,4,7)\tilde{x}_1 + (1,3,4)\tilde{x}_2}{(1,2,3)\tilde{x}_1 + (3,5,8)\tilde{x}_2} \tag{2}$$

Subject to

$$(0,1,2)\tilde{x}_1 + (1,2,3)\tilde{x}_2 \leq (1,10,27)$$

$$(1,2,3)\tilde{x}_1 + (0,1,2)\tilde{x}_2 \leq (2,11,28)$$

From step 3 and step 4, we obtained the simplified form as

$$lexMax\tilde{Z} = \left(\frac{4x_1^c + 3x_2^c}{2x_1^c + 5x_2^c}, \frac{2x_1^l - 7x_1^u + x_2^l - 4x_2^c}{x_1^l - 3x_1^u + 3x_2^l - 8x_2^c}, \frac{2x_1^l + 7x_1^u + x_2^l + 4x_2^c}{x_1^l + 3x_1^u + 3x_2^l + 8x_2^c} \right) \tag{3}$$

subject to

$$\epsilon y_{11} \leq 10 - x_1^c - x_2^c \leq Ly_{11}$$

$$\begin{aligned}
-Ly_{11} + \epsilon y_{12} &\leq -26 + 2x_1^c - x_2^l + 3x_{12}^u \leq Ly_{12} \\
-L(y_{11} + y_{12}) + \epsilon y_{13} &\leq 28 - 2x_1^u - x_2^l - 3x_{12}^u \leq Ly_{13} \\
\epsilon y_{21} &\leq 11 - 2x_1^c - x_2^c \leq Ly_{21} \\
-Ly_{21} + \epsilon y_{22} &\leq -26 - x_1^l + 3x_1^u + 2x_2^u \leq Ly_{22} \\
-L(y_{21} + y_{22}) + \epsilon y_{23} &\leq 30 - x_1^l - 3x_1^l - 2x_2^u \leq Ly_{33}
\end{aligned}$$

Steps 5 and 6 yield : $\tilde{x}_1 = (1.23, 2.11, 1.23)$ $\tilde{x}_2 = (0, 0, 0)$ and $\tilde{Z} = (2, 2, 2.33)$. But for the same problem, Safaei obtained the solution $\tilde{Z} = (1.34, 2, 2.31)$.

Result analysis

Comparing two fuzzy solutions involves analyzing their ranges, central values, and the overall spread of the outcomes. Our solution is $\tilde{Z} = (2, 2, 2.33)$ and Safaei's solution is $\tilde{Z} = (1.34, 2, 2.31)$.

Central Value - Both solutions have a central value of 2, indicating that at the most probable estimation, the outcomes are considered equal. This central value suggests that both approaches agree on the most likely efficiency or performance measure under the given conditions.

Upper Limit - The upper limit of this research's solution is 2.33, slightly higher than Safaei's 2.31. Although the difference is minor, it indicates that these authors' solution allows for a slightly more optimistic outcome in the most favorable conditions.

Spread and Uncertainty - Safaei's solution demonstrates a wider spread (1.34 to 2.31) compared to these authors' solution (2 to 2.33). This wider spread suggests a higher level of uncertainty or variability in the outcomes considered by Safaei. A broader spread in the fuzzy solution can indicate that the model accounts for a wider range of factors or uncertainties affecting the optimization problem.

The graphical representation would illustrate the overlap between the two solutions, highlighting their agreement at the central value but differing in their consideration of possible variability and outcomes at the lower and upper bounds.

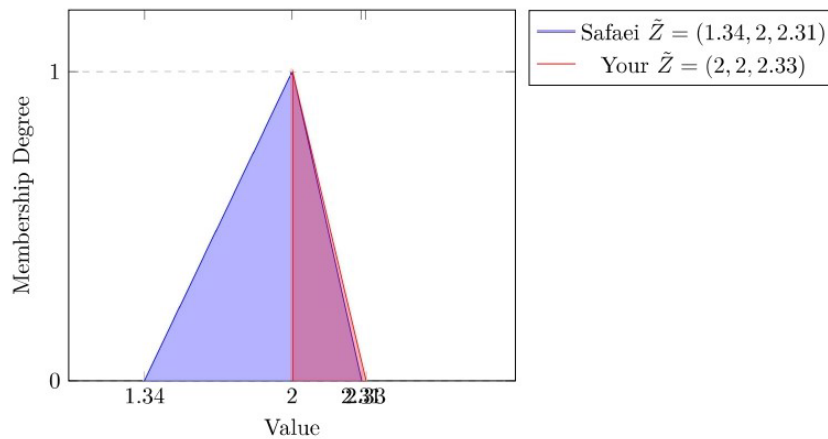


Figure 1 – Comparison of the fuzzy solutions

Future scope

- Extension to Non-linear Problems: One potential avenue for future research is to extend the FLFP problem to handle non-linear optimization problems. Incorporating fuzzy logic into non-linear fractional programming could broaden the applicability of the proposed methodology to a wider range of real-world decision-making scenarios.

- Multi-objective Optimization: Another direction for future research is to extend FLFP to multi-objective optimization problems. Developing methodologies to efficiently handle multiple conflicting objectives under uncertainty could provide decision makers with more comprehensive and informed decision support.

Advantages

- Improved Decision Support: The FLFP framework offers improved decision support by incorporating the fuzzy set theory into linear fractional programming. Decision makers can make more informed decisions in environments characterized by uncertainty and imprecision.

- Adaptability: The FLFP model demonstrates adaptability and versatility in handling diverse optimization challenges. Its ability to capture the intricacies of real-world scenarios makes it well-suited for addressing a wide range of decision-making problems.

- Efficiency: The application of the lexicography method provides a systematic and efficient approach to navigate the complex space of fuzzy

decision variables. This structured approach enhances the efficiency of the decision-making process, particularly in multi-criteria environments.

Limitations

- Computational Complexity: One potential limitation of the FLFP problem is its computational complexity, especially when dealing with large-scale optimization problems. Future research may need to explore techniques to enhance computational efficiency without compromising solution quality.

- Data Dependency: The effectiveness of the FLFP problem may be highly dependent on the availability and quality of data. Decision makers should exercise caution when applying the model in contexts where data availability is limited or uncertain.

Overall, the FLFP problem presents a promising approach for addressing decision-making problems in uncertain environments, but further research is needed to address its limitations and extend its applicability to a wider range of optimization scenarios.

Conclusion

In this article, we proposed the fuzzy linear fractional programming (FLFP) problem utilizing the lexicography method which presents a promising solution for addressing decision-making problems characterized by uncertainty and imprecision. By integrating the fuzzy set theory into linear fractional programming, the model captures the real-world scenarios where parameters exhibit inherent fuzziness.

The application of the lexicography method provides a systematic and efficient approach to navigate the complex space of fuzzy decision variables, offering a structured means of decision support in multi-criteria environments. The mathematical formulation of the FLFP problem demonstrates its adaptability and versatility in handling diverse optimization challenges.

Through illustrative examples and case studies, the research highlights the practical applicability of the proposed methodology, showcasing its effectiveness in comparison to traditional linear programming and linear fractional programming approaches. The findings underscore the advantages of FLFP in providing more realistic and nuanced solutions in the face of uncertainty.

This study contributes not only a novel methodology but also valuable insights for researchers and decision makers dealing with optimization problems in contexts where imprecise information significantly influences decision outcomes. The proposed FLFP framework, with its integration of

fuzzy logic and fractional programming principles, stands as a robust tool for addressing real-world complexities and advancing the field of decision support in uncertain environments.

References

- Abdel-Basset, M., Mohamed, M. & Smarandache, F. 2019. Linear fractional programming based on triangular neutrosophic numbers. *International Journal of Applied Management Science*, 11(1), pp.1-20. Available at: <https://doi.org/10.1504/ijams.2019.10017144>.
- Charnes, A. & Cooper, W.W. 1962. Programming with linear fractional functionals. *Naval Research Logistics Quarterly*, 9(3-4), pp.181-186. Available at: <https://doi.org/10.1002/nav.3800090303>.
- Demir, Y. 2023. An efficient lexicographic approach to solve multi-objective multi-port fabric dyeing machine planning problem. *Applied Soft Computing*, 144, art.number:110541. Available at: <https://doi.org/10.1016/j.asoc.2023.110541>.
- Dharmaraj, B. & Appasamy, S. 2023. Application of a Modified Gauss Elimination Technique for Separable Fuzzy Nonlinear Programming Problems. *Mathematical Modelling of Engineering Problems*, 10(4), pp.1481-1486. Available at: <https://doi.org/10.18280/mmep.100445>.
- Ebrahimnejad, A. 2017. A lexicographic ordering-based approach for solving fuzzy transportation problems with triangular fuzzy numbers. *International Journal of Management and Decision Making*, 16(4), pp.346-374. Available at: <https://doi.org/10.1504/ijmdm.2017.086997>.
- Hosseinzadeh Lotfi, F., Allahviranloo, T., Alimardani Jondabeh, M. & Alizadeh, L. 2009. Solving a full fuzzy linear programming using lexicography method and fuzzy approximate solution. *Applied Mathematical Modelling*, 33(7), pp.3151-3156. Available at: <https://doi.org/10.1016/j.apm.2008.10.020>.
- Karthick, S., Saraswathi, A. & Baranidharan, B. 2024. Neutrosophic Linear Fractional Programming Problem using Denominator Objective Restriction Method. *Dynamics of Continuous, Discrete and Impulsive Systems Series B: Applications and Algorithms*, 31(2), pp.89-101.
- Li, D.-F. 2008. Lexicographic method for matrix games with payoffs of triangular fuzzy numbers. *International Journal of Uncertainty, Fuzziness and Knowledge-Based Systems*, 16(3), pp.371-389. Available at: <https://doi.org/10.1142/s0218488508005327>.
- Nan, J.-X., Li, D.-F. & Zhang, M.-J., 2010. A Lexicographic Method for Matrix Games with Payoffs of Triangular Intuitionistic Fuzzy Numbers. *International Journal of Computational Intelligence Systems*, 3(3), pp.280-289. Available at: <https://doi.org/10.1080/18756891.2010.9727699>.
- Pérez-Cañedo, B., Concepción-Morales, E.R. & Edalatpanah, S.A. 2019. A Revised Version of a Lexicographical-based Method for Solving Fully Fuzzy Linear Programming Problems with Inequality Constraints. *Fuzzy Information and Engineering*, 11(4), pp.474-493. Available at: <https://doi.org/10.1080/16168658.2020.1761511>.

Prakash, Y. & Appasamy, S. 2023. Optimal Solution for Fully Spherical Fuzzy Linear Programming Problem. *Mathematical Modelling of Engineering Problems*, 10(5), pp.1611-1618. Available at: <https://doi.org/10.18280/mmep.100511>.

Safaei, N. 2014. A new method for solving fully fuzzy linear fractional programming with a triangular fuzzy numbers. *Applied Mathematics and Computational Intelligence (AMCI)*, 3(1), pp.273-281 [online]. Available at: <https://ejournal.unimap.edu.my/index.php/amci/article/view/80> [Accessed: 11 April 2024].

Sharma, U.A. 2015. A new lexicographical approach for ranking fuzzy numbers. *Mathematical Theory and Modeling*, 5(2), pp.143-153 [online]. Available at: <https://www.iiste.org/Journals/index.php/MTM/article/view/19713> [Accessed: 11 April 2024].

Sivakumar, K. & Appasamy, S. 2024. Fuzzy Mathematical Approach for Solving Multi-Objective Fuzzy Linear Fractional Programming Problem with Trapezoidal Fuzzy Numbers. *Mathematical Modelling of Engineering Problems*, 11(1), pp.255-262. Available at: <https://doi.org/10.18280/mmep.110128>.

Zadeh, L.A. 1965. Fuzzy sets. *Information and Control*, 8(3), pp.338-353. Available at: [https://doi.org/10.1016/s0019-9958\(65\)90241-x](https://doi.org/10.1016/s0019-9958(65)90241-x).

Problema de programación fraccionaria lineal difusa utilizando el método lexicográfico

Sivakumar Karthick^a, Appasamy Saraswathi^a, **autor de correspondencia**, Seyed Ahmad Edalatpanah^b

^a Instituto de Ciencia y Tecnología SRM, Facultad de Ingeniería y Tecnología, Departamento de Matemáticas, Kattankulathur, Chengalpattu, Tamil Nadu, República de la India,

^b Instituto de Educación Superior Ayandegan, Departamento de Matemáticas Aplicadas, Tonekabon, República Islámica de Irán

CAMPO: matemáticas, ciencias de computación

TIPO DE ARTÍCULO: artículo científico original

Resumen:

Introducción/objetivo: Al resolver problemas de programación fraccionaria de la vida real, a menudo se encuentra la incertidumbre y vacilación debido a varios factores incontrolables. Para superar estas limitaciones, se aplica el enfoque de lógica difusa a estos problemas.

Métodos: La discusión se centró en la solución del problema de programación fraccionaria lineal difusa (FLFPP). Primero, el problema FLFP se convirtió en un problema de optimización lexicográfica, que luego se resolvió para obtener la solución.

Resultados: Se presentó un ejemplo numérico para simplificar la explicación del algoritmo. Si bien la mayoría de los investigadores

resuelven los FLFPP utilizando el método de la función de clasificación, este enfoque reduce la eficiencia del problema difuso.

Conclusión: Esta investigación aporta una metodología integral para abordar problemas de programación fraccionaria lineal difusa utilizando el método de lexicografía. Los hallazgos ofrecen información valiosa para investigadores, profesionales y tomadores de decisiones que enfrentan desafíos de optimización en entornos donde la información imprecisa influye significativamente en el panorama de decisiones.

Palabras claves: programación fraccionaria lineal, método lexicográfico, número difuso triangular.

Задача нечеткого дробно-линейного программирования с использованием лексикографического метода

Сивакумар Картик^а, Аппасами Сарасвати^а, **корреспондент**,
Сейед Ахмад Эдалатпанах^б

^а SRM Институт науки и технологий,
Инженерно-технологический колледж, математический факультет,
Каттанколатур, Ченгалпатту, Тамилнад, Республика Индия

^б Айандеганский институт высшего образования,
Факультет прикладной математики,
Тонекабон, Исламская Республика Иран

РУБРИКА ГРНТИ: 27.47.00 Математическая кибернетика,
27.47.19 Исследование операций,
28.17.31 Моделирование процессов управления

ВИД СТАТЬИ: оригинальная научная статья

Резюме:

Введение/цель: При решении реальных задач дробного программирования часто возникают неуверенность и сомнения из-за различных неконтролируемых факторов. Для того чтобы преодолеть эти ограничения, к таким задачам применяется подход нечеткой логики.

Методы: Обсуждение было сосредоточено на решении задачи нечеткого дробно-линейного программирования (LP). Сначала задача FLFP была преобразована в задачу лексикографической оптимизации, которая таким образом была решена.

Результаты: Для упрощения объяснения алгоритма был представлен арифметический пример. Несмотря на то что большинство исследователей решают FLFPPS, используя метод ранжирующей функции, этот подход снижает эффективность нечеткой задачи.

Выводы: Данное исследование представляет собой комплексный метод решения задач нечеткого дробно-линейного

программирования с использованием лексикографического метода. Полученные результаты предоставляют ценную информацию исследователям, практикам и лицам, принимающим решения, которые сталкиваются с проблемами оптимизации в условиях, когда неточная информация существенно влияет на процесс принятия решений.

Ключевые слова: *дробно-линейное программирование, лексикографический метод, треугольное нечеткое число.*

Проблем фази линеарног фракционог програмирања помоћу лексикографског метода

Шивакумар Картик^а, Аласами Сарасвати^а, аутор за преписку, Сајед Ахмад Едалатпанах^б

^а CRM Институт за науку и технологију,
Висока школа технике и технологије, Одсек математике,
Катанкулатур, Ченгалпату, Тамилнаду, Република Индија

^б Ајандеган институт за високо образовање,
Катедра за примењену математику,
Тонекабон, Исламска Република Иран

ОБЛАСТ: математика, рачунарске науке
КАТЕГОРИЈА (ТИП) ЧЛАНКА: оригинални научни рад

Сажетак:

Увод/циљ: При решавању проблема фракционог програмирања у реалном животу често долази до несигурности и оклевања због различитих фактора које није могуће контролисати. Како би се превазишла ова ограничења, за овакве проблеме примењује се приступ заснован на фази логици.

Метод: Дискусија се фокусира на решавање проблема фази линеарног фракционог програмирања (FLFP). Прво је FLFP проблем пребачен у проблем лексикографске оптимизације и као такав је решен.

Резултати: Представљен је нумерички пример који поједностављује објашњење алгоритма. Док већина истраживача решава FLFP проблеме користећи метод рангирања функција, овај приступ редукује ефикасност фази проблема.

Закључак: Ово истраживање даје допринос путем свеобухватне методологије за решавање проблема фази линеарног фракционог програмирања помоћу лексикографског метода. Налази нуде драгоцене увиде за истраживаче, практичаре и доносиоце одлука који се сусрећу са проблемима оптимизације где непрецизне информације имају велики утицај при одлучивању.

Кључне речи: *линеарно фракционо програмирање, лексикографски метод, триангуларни фази број.*

Paper received on: 13.04.2024.
Manuscript corrections submitted on: 20.09.2024.
Paper accepted for publishing on: 22.09.2024.

© 2024 The Authors. Published by Vojnotehnički glasnik / Military Technical Courier (www.vtg.mod.gov.rs, втг.мо.унп.срб). This article is an open access article distributed under the terms and conditions of the Creative Commons Attribution license (<http://creativecommons.org/licenses/by/3.0/rs/>).



Existence theorems for a unified interpolative Kannan contraction with an application on nonlinear matrix equations

Koti N. V. V. Vara Prasad^a, Vinay Mishra^b, Stojan Radenović^c

^a Guru Ghasidas Vishwavidyalaya, Department of Mathematics, Bilaspur, Republic of India, e-mail: kvaraprasad71@gmail.com, ORCID ID: <https://orcid.org/0000-0002-2606-7292>

^b Guru Ghasidas Vishwavidyalaya, Department of Mathematics, Bilaspur, Republic of India, e-mail: vmishra9w@gmail.com, **corresponding author**, ORCID ID: <https://orcid.org/0000-0002-4223-3924>

^c University of Belgrade, Faculty of Mechanical Engineering, Belgrade, Republic of Serbia, e-mail: radens@beotel.rs, ORCID ID: <https://orcid.org/0000-0001-8254-6688>

 <https://doi.org/10.5937/vojtehg72-50753>

FIELD: mathematics

ARTICLE TYPE: original scientific paper

Abstract:

Introduction/purpose: This paper established a new mathematical framework by uncovering the relationships between Kannan contractions and interpolative Kannan contractions. The concept of unified interpolative Kannan contractions was introduced in the framework of a relational metric space. Additionally, the study aimed to broaden the concept of alpha admissibility by incorporating specific relational metric ideas.

Methods: A detailed exploration of the properties and characteristics of Kannan contractions and interpolative Kannan contractions was conducted. The research introduced the concept of unified interpolative Kannan contractions and formulated new fixed point results for these mappings.

Result: The study successfully established fixed point results for unified interpolative Kannan contractions within the framework of relational metric spaces. Additionally, an application of these results to solve a problem concerning nonlinear matrix equations was provided, further emphasizing their significance.

Conclusion: The findings of this study significantly advanced the understanding of Kannan contractions and interpolative Kannan contractions, offering a unified framework for their analysis. The introduction of unified

interpolative Kannan contractions and the expansion of alpha admissibility have broad implications for the field of mathematics.

Key words: unified interpolative Kannan contraction, \mathcal{R} -admissible, relational metric space.

Introduction

Kannan made a significant contribution to metric fixed point theory after Banach's influential fixed point theorem. While mappings satisfying the Banach contraction inequality are necessarily continuous, Kannan introduced a novel class of contractions in 1968, addressing the intriguing question of whether discontinuous mappings defined in a complete metric space and satisfying specific contractive conditions could possess a fixed point.

Kannan stated the following result.

THEOREM 1. *Let (X, ∂) be a complete metric space, and S be a self-map defined on X . If S is a Kannan contraction (KC, for brief), meaning that there exists a λ in the interval $[0, \frac{1}{2})$ such that,*

$$\partial(S\nu, S\mu) \leq \lambda[\partial(\nu, S\nu) + \partial(\mu, S\mu)], \quad \text{for all } \nu, \mu \in X, \quad (1)$$

then, S possesses a unique fixed point $\gamma \in X$, and for each $\nu \in X$, the sequence of iterates $\{S^n\nu\}$ converges to γ .

Kannan's fixed-point theorem represents a notable extension of Banach's remarkable work (Banach, 1922), leading to several generalizations, see (Debnath et al., 2021). Among these, a recent variant introduced by Karapinar, termed as interpolative Kannan-type contraction (or Kannan interpolative contraction), was demonstrated in Karapinar (2018). To guarantee the existence of a fixed point in a complete metric space, this contraction condition allows more flexibility in choosing the constants that control the contraction rate and can also incorporate the distance between points in the contractive condition. Additionally, it is worth mentioning that many classical and advanced contraction concepts have been recently re-examined through interpolation, see (Debnath et al., 2020; Hammad et al., 2023; Jain & Radenović, 2023; Jain et al., 2022; Karapinar, 2021; Karapinar et al., 2018a,b, 2021).

In his work, Karapinar (2018) presents an example that falls outside the scope of Kannan contractions but aligns with interpolative Kannan contractions. This highlights an additional advantage of interpolative Kannan

contractions over Kannan contractions. Despite existing research on the subject, there is a notable gap in the literature concerning the converse relationship, i.e., whether Kannan contractions imply interpolative Kannan contractions.

Recent studies [Nazam et al. \(2023a,b\)](#) have suggested that Kannan contractions do indeed imply interpolative Kannan contractions. However, this paper diverges from this perspective and, through illustrative examples, establishes that not every Kannan contraction implies an interpolative Kannan contraction. Consequently, this paper asserts that these two classes of contractions are independent from each other. This comprehensive understanding emphasizes the significance of both contraction types, providing valuable insights into their practical applications.

[Karapinar \(2018\)](#) introduced the concept of an interpolative Kannan contraction as follows:

DEFINITION 1. *A self-mapping S defined on a metric space (X, ∂) is considered as an interpolative Kannan type contraction (IKC, for brief) if there exists a pair of constant $\alpha, \lambda \in [0, 1)$ with $\alpha \neq 0$, satisfying*

$$\partial(S\nu, S\mu) \leq \lambda[\partial(\nu, S\nu)^\alpha \cdot \partial(\mu, S\mu)^{1-\alpha}], \text{ for all } \nu, \mu \in X, \text{ and } \nu \neq S\nu. \quad (2)$$

By employing the interpolative Kannan contraction, [Karapinar \(2018\)](#) established a unique fixed point theorem. Subsequently, [Karapinar et al. \(2018a\)](#) identified a limitation in the aforementioned result, highlighting that fixed points obtained from the contractive condition (2) may not necessarily be unique. To illustrate that not every Kannan contraction implies an interpolative Kannan contraction, these authors examine the following example.

EXAMPLE 1. Let $X = [0, 1]$ and consider the mapping $S : X \rightarrow X$ defined by $S\nu = \frac{\nu}{5}$. Let ∂ denote the usual metric.

Then, one can observe that, $\partial(S\nu, S\mu) = \frac{1}{5}|\nu - \mu|$, $\partial(\nu, S\nu) = \frac{4\nu}{5}$, and $\partial(\mu, S\mu) = \frac{4\mu}{5}$.

For $\lambda = \frac{2}{5} \in [0, \frac{1}{2})$, one can verify that:

$$\partial(S\nu, S\mu) = \frac{1}{5}|\nu - \mu| \leq \frac{2}{5} \cdot \frac{4}{5}(\nu + \mu) = \lambda \cdot [\partial(\nu, S\nu) + \partial(\mu, S\mu)].$$

This confirms that S fulfills condition (1). Now, the next task is to demonstrate that S does not satisfy (2). Suppose if possible S satisfies (2),

then, two points are chosen, $\frac{1}{100}$ and $\frac{99}{100}$, from the interval $[0, 1]$. Clearly, $\frac{1}{100} \neq \mathcal{S}(\frac{1}{100})$ and $\frac{99}{100} \neq \mathcal{S}(\frac{99}{100})$.

Case I: When $\nu = \frac{1}{100}$ and $\mu = \frac{99}{100}$, there have,

$$\frac{49}{250} = \partial(\mathcal{S}\nu, \mathcal{S}\mu) \leq \lambda [\partial(\nu, \mathcal{S}\nu)^\alpha \cdot \partial(\mu, \mathcal{S}\mu)^{1-\alpha}] = \frac{\lambda \cdot 99^{1-\alpha}}{125}. \quad (3)$$

Case II: When $\nu = \frac{99}{100}$ and $\mu = \frac{1}{100}$, there exists,

$$\frac{49}{250} = \partial(\mathcal{S}\nu, \mathcal{S}\mu) \leq \lambda [\partial(\nu, \mathcal{S}\nu)^\alpha \cdot \partial(\mu, \mathcal{S}\mu)^{1-\alpha}] = \frac{\lambda \cdot 99^\alpha}{125}. \quad (4)$$

Since \mathcal{S} satisfies (2) for all $\nu, \mu \in X \setminus F(\mathcal{S})$, from (3) and (4), there exists a pair of constants $\lambda, \alpha \in [0, 1)$ with $\alpha \neq 0$, such that

$$\frac{49}{2} \leq \lambda \cdot \min\{99^{1-\alpha}, 99^\alpha\}. \quad (5)$$

Now, if $\lambda = 0$, a contradiction of (5) is obtained. Therefore, $\lambda \in (0, 1)$, and in such a case, there is

$$\frac{49}{\lambda} \leq 2 \cdot \min\{99^{1-\alpha}, 99^\alpha\}.$$

However, this again leads to a contradiction, as expressed by the following inequality

$$\inf_{\lambda \in (0,1)} \frac{49}{\lambda} > 2 \cdot \sup_{\alpha \in (0,1)} [\min\{99^{1-\alpha}, 99^\alpha\}].$$

Therefore, there does not exist any $\alpha \in (0, 1)$ and $\lambda \in (0, 1)$ for which equation (5) holds true for all $\nu, \mu \in X \setminus F(\mathcal{S})$. Thus, the initial assumption is incorrect, and \mathcal{S} does not satisfy condition (2).

Therefore, based on Example 1 and Example 2.3 of Karapinar et al. (2018a), it can be inferred that conditions (1) and (2) are independent. In the current study, these authors endeavor to establish connections between these conditions by extending them to a more generalized contraction condition in a relational metric space.

It is noteworthy that in relational metric spaces, one often considers weaker properties such as \mathcal{R} -continuous (not necessarily continuous), \mathcal{R} -complete (not necessarily complete), etc. In this setting, additional flexibility is beneficial in that the contraction condition need not be applied to every element but rather to related elements only. Importantly, these contraction conditions revert to their conventional counterparts when the universal relation is taken into account.

Preliminaries

Before presenting the main results of this paper, it is important to introduce formal notations that will be used throughout. Let X be a non-empty set, with a binary relation \mathcal{R} . In this context, the pair (X, \mathcal{R}) is acknowledged as a relational set. Similarly, within the framework of a metric space (X, ∂) , one designates the triplet $(X, \partial, \mathcal{R})$ which constitutes a relational metric space (RMS, for brevity). The collection of fixed points of the self-mapping S is indicated by $F(S)$, and let $X_{\mathcal{R}}$ denote the set defined by, $X_{\mathcal{R}} = \{(\nu, \mu) \in X^2 : (\nu, \mu) \in \mathcal{R} \text{ and } \nu, \mu \notin F(S)\}$. Furthermore, $X(S, \mathcal{R})$ is a subset of X , containing elements ν such that $(\nu, S\nu) \in \mathcal{R}$. These formalized notations ensure precision and consistency throughout the subsequent analyses and discussions.

DEFINITION 2. (Alam & Imdad, 2015) *Let S be self-map on X , and (X, \mathcal{R}) be a relational set,*

- (i) *any two elements $\nu, \mu \in X$ are considered \mathcal{R} -comparative if $(\nu, \mu) \in \mathcal{R}$ or $(\mu, \nu) \in \mathcal{R}$. This relationship is symbolically represented as $[\nu, \mu] \in \mathcal{R}$,*
- (ii) *a sequence $\{\nu_k\} \subset X$ satisfies the condition $(\nu_k, \nu_{k+1}) \in \mathcal{R}$ for all $k \in \mathbb{N}_0$, is referred to as an \mathcal{R} -preserving sequence.*
- (iii) *\mathcal{R} is designated as S -closed when it satisfies the condition that if (ν, μ) belongs to \mathcal{R} , then $(S\nu, S\mu)$ also belongs to \mathcal{R} , for any $\nu, \mu \in X$.*
- (iv) *\mathcal{R} is referred to as ∂ -self-closed under the condition that whenever there exists a \mathcal{R} -preserving sequence $\{\nu_k\}$ such that $\nu_k \xrightarrow{\partial} \nu$, there can always be found a subsequence $\{\nu_{k_n}\}$ of $\{\nu_k\}$ such that $[\nu_{k_n}, \nu]$ belongs to \mathcal{R} for all $n \in \mathbb{N}_0$.*

DEFINITION 3. (Alam & Imdad, 2017) *$(X, \partial, \mathcal{R})$ is considered \mathcal{R} -complete if every sequence in X , which is both \mathcal{R} -preserving and Cauchy, converges.*

DEFINITION 4. (Alam & Imdad, 2017) *A self-map S defined on X is termed \mathcal{R} -continuous at $\nu \in X$, if any \mathcal{R} -preserving sequence $\nu_k \xrightarrow{\partial} \nu$, implies $S\nu_k \xrightarrow{\partial} S\nu$. Furthermore, if S exhibits this behavior at every point in X , it is simply categorized as \mathcal{R} -continuous.*

DEFINITION 5. (Alam & Imdad, 2018) Consider a self-mapping S defined on X . If for every \mathcal{R} -preserving sequence $\{\nu_n\} \subset \mathcal{S}(X)$, with a range denoted as $E = \{\nu_n : n \in \mathbb{N}\}$, $\mathcal{R}|_E$ is transitive, then S is designated as locally S -transitive.

Samet et al. (2012) introduced the concept of α -admissible mappings, which has been applied by various authors in numerous fixed-point theorems.

DEFINITION 6. (Samet et al., 2012) Suppose S is a self-map on X , and $\alpha : X \times X \rightarrow \mathbb{R}^+$ is a function. Then, S is considered α -admissible if $\alpha(\nu, \mu) \geq 1 \Rightarrow \alpha(S\nu, S\mu) \geq 1$ for all $\nu, \mu \in X$.

In the following definition, this concept is generalized by incorporating certain relational metrical notions.

DEFINITION 7. Let (X, \mathcal{R}) be a relational set. A self-map S defined on X is termed \mathcal{R} -admissible if there exists a function $\vartheta : X \times X \rightarrow [0, +\infty)$, satisfying the following conditions:

- (r₁) $\vartheta(\nu, \mu) \geq 1$ for all $(\nu, \mu) \in \mathcal{R}$,
- (r₂) \mathcal{R} is S -closed.

REMARK 1. From the above two definitions, it can be observed that if S is α -admissible, it also holds that S is \mathcal{R} -admissible when considering $\mathcal{R} = \{(\nu, \mu) \in X^2 : \vartheta(\nu, \mu) \geq 1\}$. However, it should be noted that the converse is not necessarily true, as illustrated in the following example.

EXAMPLE 2. Let $X = \{0, 1, 2, 3\}$, $\vartheta : X \times X \rightarrow \mathbb{R}^+$ by

$$\vartheta(\nu, \mu) = \begin{cases} 2, & (\nu, \mu) \in \{(0, 1), (1, 2), (2, 3)\} \\ 1, & (\nu, \mu) \in \{(0, 2), (1, 1), (2, 1), (2, 2)\} \\ \frac{2}{\nu+5}, & \text{otherwise.} \end{cases}$$

and $S : X \rightarrow X$ is defined by $S0 = 0, S1 = 2, S2 = 1$, and $S3 = 3$. In this example, it is evident that $\vartheta(2, 3) \geq 1$, but $\vartheta(S2, S3) = \vartheta(1, 3) \not\geq 1$, indicating that S is not ϑ -admissible. Now, let us consider the binary relation \mathcal{R} defined as,

$$\mathcal{R} = \{(0, 1), (0, 2), (1, 2), (2, 1), (1, 1), (2, 2)\}.$$



It is straightforward to observe that \mathcal{R} is \mathcal{S} -closed, and for all $\nu, \mu \in X$ with $(\nu, \mu) \in \mathcal{R}$, $\vartheta(\nu, \mu) \geq 1$. Therefore, \mathcal{S} is \mathcal{R} -admissible.

Let $\psi, \phi : [0, +\infty) \rightarrow [0, +\infty)$ be two functions. Then the following conditions are considered:

- (C₁) ϕ is *u.s.c.* such that $\phi(0) = 0$,
- (C₂) ψ is *l.s.c.*,
- (C₃) ψ, ϕ are non-decreasing,
- (C₄) $\psi(t) > \phi(t)$, for all $t > 0$,
- (C₅) $\limsup_{t \rightarrow c+} \phi(t) < \psi(c+)$, for all $c > 0$,
- (C₆) $\limsup_{t \rightarrow 0} \phi(t) \leq \liminf_{t \rightarrow e+} \psi(t)$.

Main results

This section introduces a novel concept of a unified interpolative Kannan contraction condition and establishes some fixed-point results for such contractions. Through an example, it will be demonstrated how the unified interpolative Kannan contraction condition extends the classical notions of contraction mappings defined in (Kannan, 1968; Karapinar, 2018; Nazam et al., 2023a).

DEFINITION 8. Let $(X, \partial, \mathcal{R})$ be an RMS. A self-mapping \mathcal{S} defined on X is characterized as a unified interpolative Kannan contraction (UIKC, for brief) if there exist functions $\psi, \phi : [0, +\infty) \rightarrow [0, +\infty)$, and a function $\vartheta : X \times X \rightarrow [0, +\infty)$, along with a parameter $\alpha \in (0, 1)$, such that

$$\vartheta(\nu, \mu)\psi(\partial(\mathcal{S}\nu, \mathcal{S}\mu)) \leq \phi(\Omega(\partial(\nu, \mathcal{S}\nu), \partial(\mu, \mathcal{S}\mu))), \quad \text{for all } \nu, \mu \in X_{\mathcal{R}}, \quad (6)$$

where $\Omega : \mathbb{R}^2 \rightarrow \mathbb{R}$ be a function satisfying $\Omega(\nu, \mu) \leq \max\{\nu, \mu, \nu^\alpha \mu^{1-\alpha}\}$.

EXAMPLE 3. Let (X, d) be a metric space with $X = [0, +\infty)$ and ∂ is the usual metric, define the self-map \mathcal{S} on X by,

$$\mathcal{S}\nu = \begin{cases} \frac{\nu}{5}, & \text{if } \nu \leq 1, \\ \nu^2, & \text{if } \nu > 1. \end{cases}$$

Then, it is important to note that \mathcal{S} is not a Kannan contraction (Kannan, 1968). This is evident that when considering $\nu = \frac{1}{2}$ and $\mu = 2$, as there

does not exist any $\lambda \in [0, \frac{1}{2})$ that satisfies (1). Additionally, for the same values of $\nu = \frac{1}{2}$ and $\mu = 2$, there is no pair of $\lambda \in [0, 1)$ and $\alpha \in (0, 1)$ for which (2) holds. Consequently, \mathcal{S} is not an interpolative Kannan contraction (Karapinar, 2018). Now, let us define the binary relation \mathcal{R} on X as,

$$\mathcal{R} = \{(\nu, \mu) \in X^2 : \max\{\nu, \mu\} \leq 1\}.$$

Observing the definition of \mathcal{R} , it is evident that \mathcal{R} is not an orthogonal relation. It is important to recall that a binary relation \mathcal{R} is considered as an orthogonal relation if for any element $\nu_0 \in X$, either (for all $\mu, (\nu_0, \mu) \in \mathcal{R}$) or (for all $\mu, (\mu, \nu_0) \in \mathcal{R}$). As a consequence, the function \mathcal{S} is not a (ψ, ϕ) -orthogonal interpolative Kannan-type contraction (Nazam et al., 2023a). However, it will now be demonstrated that \mathcal{S} is indeed a unified interpolative Kannan contraction. Consider $\vartheta : X \times X \rightarrow [0, +\infty)$ defined by

$$\vartheta(\nu, \mu) = \begin{cases} \frac{3}{2}, & \text{if } \nu, \mu \in [0, 1], \\ \frac{1}{2}, & \text{otherwise.} \end{cases}$$

Observing that $\vartheta(\nu, \mu) > 1$ for all $\nu, \mu \in X$ with $(\nu, \mu) \in \mathcal{R}$, and that $(\nu, \mu) \in \mathcal{R}$ implies $(\mathcal{S}\nu, \mathcal{S}\mu) \in \mathcal{R}$, it follows that \mathcal{S} is \mathcal{R} -admissible. Suppose there exist functions $\psi, \phi : [0, +\infty) \rightarrow [0, +\infty)$ defined by $\phi(t) = \frac{t}{6}$,

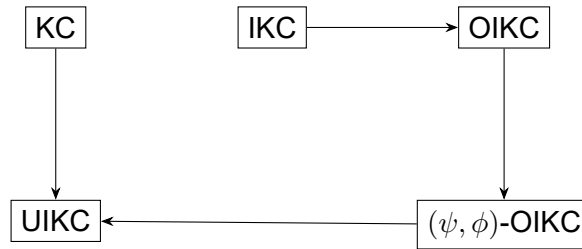
$$\text{and, } \psi(t) = \begin{cases} \frac{t}{5}, & \text{if } t \leq 1, \\ \frac{2t}{9}, & \text{if } t > 1. \end{cases}$$

The aim now is to show that \mathcal{S} satisfies (6). Consider the function $\Omega : X \times X \rightarrow [0, +\infty)$ defined as $\Omega(\nu, \mu) = \frac{\nu + \mu}{2}$. For every $\nu, \mu \in X_{\mathcal{R}}$, the following inequality holds,

$$\begin{aligned} \vartheta(\nu, \mu)\psi(\vartheta(\mathcal{S}\nu, \mathcal{S}\mu)) &= \frac{3}{2}\psi\left(\left|\frac{\nu}{5} - \frac{\mu}{5}\right|\right) \\ &= \frac{3}{50}|\nu - \mu| \\ &\leq \frac{1}{6}(\Omega(\vartheta(\nu, \mathcal{S}\nu), \vartheta(\mu, \mathcal{S}\mu))) \\ &= \phi(\Omega(\vartheta(\nu, \mathcal{S}\nu), \vartheta(\mu, \mathcal{S}\mu))). \end{aligned}$$

Consequently, it is deduced that \mathcal{S} is a unified interpolative Kannan contraction.

REMARK 2. From Example 1, Example 3, and Example 2.3 in Karapinar et al. (2018a), one arrives at the following conclusion



Now, let us proceed to establish this paper’s main results concerning the unified interpolative Kannan contraction maps.

THEOREM 2. Consider the RMS $(X, \partial, \mathcal{R})$ where \mathcal{R} is a locally \mathcal{S} -transitive binary relation. Suppose that \mathcal{S} is a unified interpolative Kannan contraction and there exist functions $\psi, \phi : [0, +\infty) \rightarrow [0, +\infty)$ satisfying conditions C_i , $(i = 1, 2, 3, 4)$. Under the following conditions:

- (D_1) \mathcal{S} is \mathcal{R} -admissible,
 - (D_2) there exists $Y \subseteq X$ with $\mathcal{S}(X) \subseteq Y$, such that $(Y, \partial, \mathcal{R})$ is \mathcal{R} -complete,
 - (D_3) $X(\mathcal{S}, \mathcal{R})$ is non-empty,
 - (D_4) either \mathcal{S} is $\mathcal{R}|_Y$ -continuous or \mathcal{R} is ∂ -self-closed,
- there exists at least one $\gamma \in X$ such that $\gamma \in F(\mathcal{S})$.

Proof. Under the assumption (D_3) , suppose that $\nu_0 \in X(\mathcal{S}, \mathcal{R})$. Define the sequence $\{\nu_n\}$ of Picard iterates with the initial point ν_0 , i.e. $\nu_n = \mathcal{S}^n \nu_0$ for all $n \in \mathbb{N}_0$. As $(\nu_0, \mathcal{S}\nu_0) \in \mathcal{R}$ and \mathcal{S} is \mathcal{R} -admissible, using (r_1) it follows that $(\mathcal{S}^n \nu_0, \mathcal{S}^{n+1} \nu_0) \in \mathcal{R}$. Consequently, $(\nu_n, \nu_{n+1}) \in \mathcal{R}$ for all $n \in \mathbb{N}_0$, and this yields that the sequence $\{\nu_n\}$ is \mathcal{R} -preserving and from (r_2) there holds $\vartheta(\nu_n, \nu_{n+1}) \geq 1$. Let $\partial_n = \partial(\nu_n, \nu_{n+1})$; applying contractive condition (1) yields that

$$\begin{aligned}
 \psi(\partial_n) &\leq \vartheta(\nu_{n-1}, \nu_n) \psi(\partial(\mathcal{S}\nu_{n-1}, \mathcal{S}\nu_n)) \\
 &\leq \phi(\Omega(\partial(\nu_{n-1}, \mathcal{S}\nu_{n-1}), \partial(\nu_n, \mathcal{S}\nu_n))) \\
 &= \phi(\Omega(\partial_{n-1}, \partial_n)) \\
 &\leq \phi(\max\{\partial_{n-1}, \partial_n, \partial_{n-1}^\alpha \cdot \partial_n^{1-\alpha}\}) \\
 &< \psi(\max\{\partial_{n-1}, \partial_n, \partial_{n-1}^\alpha \cdot \partial_n^{1-\alpha}\}).
 \end{aligned} \tag{7}$$

By the monotonicity of the function ψ one obtains

$$\partial_n < \max \{ \partial_{n-1}, \partial_n, \partial_{n-1}^\alpha \cdot \partial_n^{1-\alpha} \}. \tag{8}$$

Now suppose there exists $n \in \mathbb{N}$ for which $\partial_{n-1} \leq \partial_n$, then from (8) it yields that $\partial_n < \partial_n$, a contradiction. Therefore $\partial_n \leq \partial_{n-1}$, now it can be concluded that $\{\nu_n\}$ is a non-increasing sequence and thus a non-negative constant C exists such that, $\lim_{n \rightarrow +\infty} \partial_n = C+$. Suppose if possible $C > 0$, then from (7), it can be deduced that

$$\psi(C+) \leq \liminf \psi(\partial_n) \leq \limsup \phi(\partial_{n-1}) \leq \phi(C+),$$

but, from (C_4) there exists $\psi(\nu) > \phi(\nu)$ for all $\nu > 0$, therefore C must be 0, i.e. $\lim_{n \rightarrow +\infty} \partial_n = 0$. The next objective is to establish that the sequence $\{\nu_n\}$ is Cauchy. For the sake of contradiction, suppose it is not; then there exists a positive real number $\epsilon > 0$ along with sub-sequences $\{\nu_{n_k}\}$ and $\{\nu_{m_k}\}$ of $\{\nu_n\}$, with $n_k > m_k \geq k$, such that

$$\partial(\nu_{m_k}, \nu_{n_k}) \geq \epsilon, \quad \text{for all } k \in \mathbb{N}. \tag{9}$$

Selecting n_k as the smallest integer exceeding m_k such that (9) holds, it is deduced that

$$\partial(\nu_{m_k}, \nu_{n_k-1}) < \epsilon. \tag{10}$$

Using triangular inequality and (9), (10) one obtains that

$$\begin{aligned} \epsilon &\leq \partial(\nu_{m_k}, \nu_{n_k}) \leq \partial(\nu_{m_k}, \nu_{n_k-1}) + \partial(\nu_{n_k-1}, \nu_{n_k}) \\ &< \epsilon + \partial(\nu_{n_k-1}, \nu_{n_k}). \end{aligned}$$

on taking the limit $k \rightarrow +\infty$ and utilizing the fact that $\lim_{n \rightarrow +\infty} \partial_n = 0$, one gets

$$\lim_{k \rightarrow +\infty} \partial(\nu_{m_k}, \nu_{n_k}) = \epsilon + . \tag{11}$$

By using triangular inequality, one obtains that

$$|\partial(\nu_{m_k+1}, \nu_{n_k+1}) - \partial(\nu_{m_k}, \nu_{n_k})| \leq \partial\nu_{m_k} + \partial\nu_{n_k}.$$



Letting limit $k \rightarrow +\infty$ in the above inequality and employing (11) yields the following:

$$\lim_{k \rightarrow +\infty} \partial(\nu_{m_k+1}, \nu_{n_k+1}) = \lim_{k \rightarrow +\infty} \partial(\nu_{m_k}, \nu_{n_k}) = \epsilon + . \quad (12)$$

Since $\{\nu_n\} \subset \mathcal{S}(X)$ and $\{\nu_n\}$ is \mathcal{R} -preserving, the local \mathcal{S} -transitivity of \mathcal{R} leads to the implication that $(\nu_{m_k}, \nu_{n_k}) \in \mathcal{R}$. Thus, it can be deduced

$$\begin{aligned} \psi(\partial(\nu_{m_k+1}, \nu_{n_k+1})) &\leq \vartheta(\nu_{m_k}, \nu_{n_k})\psi(\partial(\mathcal{S}\nu_{m_k}, \mathcal{S}\nu_{n_k})) \\ &\leq \phi(\Omega(\partial(\nu_{m_k}, \mathcal{S}\nu_{m_k}), \partial(\nu_{n_k}, \mathcal{S}\nu_{n_k}))) \\ &= \phi(\Omega(\partial_{m_k}, \partial_{n_k})) \\ &\leq \phi(\max\{\partial_{m_k}, \partial_{n_k}, \partial_{m_k}^\alpha \cdot \partial_{n_k}^{1-\alpha}\}). \end{aligned}$$

Taking the limit as $k \rightarrow +\infty$ in the aforementioned inequality leads to the conclusion that $\epsilon < 0$, a contradiction. Hence, $\{\nu_n\}$ is the \mathcal{R} -preserving Cauchy sequence in Y . The \mathcal{R} -completeness of the metric space $(Y, \partial, \mathcal{R})$ now guarantees the existence of a point $\gamma \in Y$ such that, $\lim_{n \rightarrow +\infty} \nu_n = \gamma$.

First, one assumed that \mathcal{S} is \mathcal{R} -continuous; one can deduce that $\lim_{n \rightarrow +\infty} \nu_{n+1} = \lim_{n \rightarrow +\infty} \mathcal{S}\nu_n = \mathcal{S}\gamma$. Applying the uniqueness of the limit, one consequently establishes that $\mathcal{S}\gamma = \gamma$, indicating that $\gamma \in F(\mathcal{S})$.

Alternatively, let $\mathcal{R}|_Y$ is ∂ -self-closed. The fact that $\{\nu_n\}$ is \mathcal{R} -preserving and $\{\nu_n\} \rightarrow \gamma$ can be utilized again. This implies the existence of a subsequence $\{\nu_{n_k}\}$ of $\{\nu_n\}$ with $(\nu_{n_k}, \gamma) \in \mathcal{R}$, for all $k \in \mathbb{N}_0$. If $(\nu_{n_k}, \gamma) \in \mathcal{R}$, then since \mathcal{S} is a unified interpolative Kannan contraction, there exists

$$\begin{aligned} \psi(\partial(\mathcal{S}\nu_{n_k}, \mathcal{S}\gamma)) &\leq \vartheta(\nu_{n_k}, \gamma)\psi(\partial(\mathcal{S}\nu_{n_k}, \mathcal{S}\gamma)) \\ &\leq \phi(\Omega(\partial(\nu_{n_k}, \mathcal{S}\nu_{n_k}), \partial(\gamma, \mathcal{S}\gamma))) \\ &= \phi(\Omega(\partial_{n_k}, \partial(\gamma, \mathcal{S}\gamma))) \\ &\leq \phi(\max\{\partial_{n_k}, \partial(\gamma, \mathcal{S}\gamma), \partial_{n_k}^\alpha \cdot \partial(\gamma, \mathcal{S}\gamma)^{1-\alpha}\}), \quad (13) \end{aligned}$$

on taking the limit $k \rightarrow +\infty$, in (13), one obtains

$$\psi(\partial(\gamma, \mathcal{S}\gamma)) \leq \phi(\partial(\gamma, \mathcal{S}\gamma)). \quad (14)$$

It is important to note that in equation (14), if $\partial(\gamma, \mathcal{S}\gamma) \neq 0$, it is contradictory to (C_4) . Similarly, if $(\gamma, \nu_{n_k}) \in \mathcal{R}$, then by utilizing the symmetry of ∂ , we once again encounter a contradiction of (C_4) . Therefore, $\partial(\gamma, \mathcal{S}\gamma) = 0$, implying $\gamma \in F(\mathcal{S})$. \square

THEOREM 3. Consider the RMS $(X, \partial, \mathcal{R})$ where \mathcal{R} is a locally \mathcal{S} -transitive binary relation. Suppose that \mathcal{S} is a unified interpolative Kannan contraction and there exist functions $\psi, \phi : [0, +\infty) \rightarrow [0, +\infty)$ satisfying conditions C_i , ($i = 3, 4, 5, 6$) and D_j , ($j = 1, 2, 3, 4$) holds. Then, there exists at least one $\gamma \in X$ such that $\gamma \in F(\mathcal{S})$.

Proof. Following the steps of the previous theorem, one can obtain an \mathcal{R} -preserving and non-increasing sequence $\{\nu_n\}$ such that there exists some $C \geq 0$ and ν_n converges to $C+$ as $n \rightarrow +\infty$. Suppose $C > 0$, then (7) implies that

$$\begin{aligned} \psi(C+) &\leq \limsup_{n \rightarrow +\infty} \psi(\partial_n) \\ &\leq \limsup_{n \rightarrow +\infty} \phi \left(\max \{ \partial_{n-1}, \partial_n, \partial_{n-1}^\alpha \cdot \partial_n^{1-\alpha} \} \right) \\ &\leq \limsup_{k \rightarrow C+} \phi(k), \end{aligned}$$

a contradiction of (C_5) , thus $C = 0$ i.e. $\lim_{n \rightarrow +\infty} \partial_n = 0$. Now, to establish that the sequence $\{\nu_n\}$ is Cauchy, one makes a counter assumption. Suppose it is not Cauchy, then following the steps outlined in the previous theorem, there exists a positive real number $\epsilon > 0$, along with sub-sequences $\{\nu_{n_k}\}$ and $\{\nu_{m_k}\}$ of $\{\nu_n\}$, where $n_k > m_k \geq k$, satisfying condition (12). Since $\{\nu_n\} \subset \mathcal{S}(X)$ and $\{\nu_n\}$ is \mathcal{R} -preserving, the local \mathcal{S} -transitivity of \mathcal{R} leads to the implication that $(\nu_{m_k}, \nu_{n_k}) \in \mathcal{R}$. Thus, it can be deduced

$$\begin{aligned} \psi(\partial(\nu_{m_{k+1}}, \nu_{n_{k+1}})) &\leq \vartheta(\nu_{m_k}, \nu_{n_k}) \psi(\partial(\mathcal{S}\nu_{m_k}, \mathcal{S}\nu_{n_k})) \\ &\leq \phi \left(\max \{ \partial_{m_k}, \partial_{n_k}, \partial_{m_k}^\alpha \cdot \partial_{n_k}^{1-\alpha} \} \right), \end{aligned}$$

on taking the limit $k \rightarrow +\infty$ in the above equation, it implies that

$$\begin{aligned} \liminf_{a \rightarrow \epsilon+} \psi(a) &\leq \liminf_{k \rightarrow +\infty} \psi(\partial(\nu_{m_{k+1}}, \nu_{n_{k+1}})) \\ &\leq \limsup_{k \rightarrow +\infty} \phi \left(\max \{ \partial_{m_k}, \partial_{n_k}, \partial_{m_k}^\alpha \cdot \partial_{n_k}^{1-\alpha} \} \right) \\ &\leq \limsup_{a \rightarrow 0} \phi(a). \end{aligned}$$

This results in a contradiction of (C_6) , thus establishing that the $\{\nu_n\}$ is an \mathcal{R} -preserving Cauchy sequence is in Y . Given that $(Y, \partial, \mathcal{R})$ is an \mathcal{R} -complete metric space, there exists $\gamma \in Y$ such that $\lim_{n \rightarrow +\infty} \nu_n = \gamma$. If the

self-mapping S is \mathcal{R} -continuous, the desired conclusion can be derived, as demonstrated in the previous theorem.

Alternatively, let $\mathcal{R}|_Y$ be ∂ -self-closed then utilizing the fact that $\{\nu_n\}$ is \mathcal{R} -preserving and $\{\nu_n\} \rightarrow \gamma$. This implies the existence of a sub-sequence $\{\nu_{n_k}\}$ of $\{\nu_n\}$ with $[\nu_{n_k}, \gamma] \in \mathcal{R}$, for all $k \in \mathbb{N}_0$. One claims that $\partial(\gamma, S\gamma) = 0$. Let us assume that $\partial(\gamma, S\gamma) > 0$, if $(\nu_{n_k}, \gamma) \in \mathcal{R}$, then since S is a unified interpolative Kannan contraction, there exists

$$\begin{aligned} \psi(\partial(\nu_{n_k+1}, S\gamma)) &\leq \vartheta(\nu_{n_k}, \gamma)\psi(\partial(S\nu_{n_k}, S\gamma)) \\ &\leq \phi(\Omega(\partial(\nu_{n_k}, S\nu_{n_k}), \partial(\gamma, S\gamma))) \\ &= \phi(\Omega(\partial_{n_k}, \partial(\gamma, S\gamma))) \\ &\leq \phi(\max\{\partial_{n_k}, \partial(\gamma, S\gamma), \partial_{n_k}^\alpha \cdot \partial(\gamma, S\gamma)^{1-\alpha}\}) \\ &< \psi(\max\{\partial_{n_k}, \partial(\gamma, S\gamma), \partial_{n_k}^\alpha \cdot \partial(\gamma, S\gamma)^{1-\alpha}\}), \end{aligned}$$

by using (C_3) and taking the limit as $k \rightarrow +\infty$, one deduces $\partial(\gamma, S\gamma) < \partial(\gamma, S\gamma)$, which leads to a contradiction. Furthermore, if $(\gamma, \nu_{n_k}) \in \mathcal{R}$, then by utilizing the symmetry of ∂ , one encounters again a contradiction. Hence, $\partial(\gamma, S\gamma) = 0$, implying $\gamma \in F(S)$ \square

THEOREM 4. Consider the RMS $(X, \partial, \mathcal{R})$, where \mathcal{R} is a locally S -transitive and S -closed. Suppose the conditions D_j , ($j = 1, 2, 3, 4$) hold and there exist the functions $\psi, \phi : [0, +\infty) \rightarrow [0, +\infty)$ satisfying the conditions C_i , ($i = 1, 2, 3, 4$) or ($i = 3, 4, 5, 6$), such that

$$\psi(\partial(S\nu, S\mu)) \leq \phi(\Omega(\partial(\nu, S\nu), \partial(\mu, S\mu))), \quad \text{for all } \nu, \mu \in X_{\mathcal{R}} \quad (15)$$

Then there exists at least one $\gamma \in X$ such that $\gamma \in F(S)$.

By considering the specific values of the functions ψ, ϕ, Ω , and ν , in Theorem 4, one can derive the following relational theoretic versions of Kannan fixed-point results and Interpolative Kannan fixed-point results respectively.

COROLLARY 1. Let $(X, \partial, \mathcal{R})$ be an \mathcal{R} -complete RMS, where \mathcal{R} is a locally S -transitive and S -closed. Suppose that the conditions D_j , ($j = 1, 2, 3$) hold and there exists a parameter $0 \leq \lambda < \frac{1}{2}$, such that

$$\partial(S\nu, S\mu) \leq \lambda[\partial(\nu, S\nu) + \partial(\mu, S\mu)], \quad \text{for all } \nu, \mu \in X_{\mathcal{R}}.$$

Then there exists at least one $\gamma \in X$ such that $\gamma \in F(S)$.

COROLLARY 2. *Let $(X, \partial, \mathcal{R})$ be an \mathcal{R} -complete RMS, where \mathcal{R} is a locally S -transitive and S -closed. Suppose that the conditions D_j , ($j = 1, 2, 3$) hold and there exists a pair of constants $\alpha, \lambda \in [0, 1)$ with $\alpha \neq 0$, satisfying*

$$\partial(S\nu, S\mu) \leq \lambda [\partial(\nu, S\nu)^\alpha \cdot \partial(\mu, S\mu)^{1-\alpha}], \quad \text{for all } \nu, \mu \in X_{\mathcal{R}}.$$

Then there exists at least one $\gamma \in X$ such that $\gamma \in F(S)$.

An application

In this section, the authors have applied their research findings to derive a result concerning the existence of solutions for a nonlinear matrix equation. In this context, let the set denoted as $\mathcal{M}(n)$ encompasses all square matrices with dimensions of $n \times n$, while $\mathcal{H}(n)$, $\mathcal{P}(n)$, and $\mathcal{K}(n)$, respectively represent the sets of Hermitian matrices, positive definite positive, and semi-definite matrices. When there is a matrix \mathcal{C} from $\mathcal{H}(n)$, one uses the notation $\|\mathcal{C}\|_{tr}$ to refer to its trace norm, which is the sum of all its singular values. If there are matrices \mathcal{P} and \mathcal{Q} from $\mathcal{H}(n)$, the notation $\mathcal{P} \succeq \mathcal{Q}$ signifies that the matrix $\mathcal{P} - \mathcal{Q}$ is an element of the set $\mathcal{K}(n)$, while $\mathcal{P} \succ \mathcal{Q}$ indicates that $\mathcal{P} - \mathcal{Q}$ belongs to the set $\mathcal{P}(n)$. The upcoming discussion relies on the significance of the following lemmas.

LEMMA 1. (Ran & Reurings, 2002) *If $X \in \mathcal{H}(n)$ satisfies $X \prec \mathcal{I}_n$, then $\|X\| < 1$.*

LEMMA 2. (Ran & Reurings, 2002) *For $n \times n$ matrices $X \succeq O$ and $Y \succeq O$, the following inequalities hold:*

$$0 \leq tr(XY) \leq \|X\|tr(Y).$$

Examine now the following nonlinear matrix equation,

$$X = \mathcal{A} + \sum_{i=1}^u \sum_{k=1}^v \mathcal{C}_j^* \Upsilon_k(X) \mathcal{C}_j \tag{16}$$

In the above equation, \mathcal{A} is defined as a Hermitian and positive definite matrix. Additionally, the notation \mathcal{C}_j^* refers to the conjugate transpose of a square matrix \mathcal{C}_j of size $n \times n$. Furthermore, Υ_k represents continuous functions that preserve order, mapping from $\mathcal{H}(n)$ to $\mathcal{P}(n)$. It is noteworthy that $\Upsilon(O) = O$, where O represents a zero matrix.

THEOREM 5. Consider the nonlinear matrix equation expressed in (16) and assume the following:

- (H₁) there exists $\mathcal{A} \in \mathcal{P}(n)$ with $\sum_{j=1}^u \sum_{k=1}^v \mathcal{C}_j^* \Upsilon_k(\mathcal{A}) \mathcal{C}_j \succ 0$;
- (H₂) for every $X, Y \in \mathcal{P}(n)$, $X \preceq Y$ implies

$$\sum_{j=1}^u \sum_{k=1}^v \mathcal{C}_j^* \Upsilon_k(X) \mathcal{C}_j \preceq \sum_{j=1}^u \sum_{k=1}^v \mathcal{C}_j^* \Upsilon_k(Y) \mathcal{C}_j;$$

- (H₃) $\sum_{j=1}^u \mathcal{C}_j \mathcal{C}_j^* \prec N \mathcal{I}_n$, for some positive number N , and for all $X, Y \in \mathcal{P}(n)$ with $X \preceq Y$, the following inequality holds
- $$\max_k (\text{tr}(\Upsilon_k(Y) - \Upsilon_k(X))) \leq$$

$$\frac{1}{2Nv} \times \max \left\{ \begin{array}{l} \text{tr} \left(X - \mathcal{A} - \sum_{j=1}^u \sum_{k=1}^v \mathcal{C}_j^* \Upsilon_k(X) \mathcal{C}_j \right), \text{tr} \left(Y - \mathcal{A} - \sum_{j=1}^u \sum_{k=1}^v \mathcal{C}_j^* \Upsilon_k(Y) \mathcal{C}_j \right), \\ \left(\text{tr} \left(X - \mathcal{A} - \sum_{j=1}^u \sum_{k=1}^v \mathcal{C}_j^* \Upsilon_k(X) \mathcal{C}_j \right) \right)^{\frac{1}{2}} \cdot \left(\text{tr} \left(Y - \mathcal{A} - \sum_{j=1}^u \sum_{k=1}^v \mathcal{C}_j^* \Upsilon_k(Y) \mathcal{C}_j \right) \right)^{\frac{1}{2}} \end{array} \right\}.$$

Then, there exists at least one solution of the nonlinear matrix equation (16). Moreover, the iteration

$$X_r = \mathcal{A} + \sum_{j=1}^u \sum_{k=1}^v \mathcal{C}_j^* \Upsilon_k(X_{r-1}) \mathcal{C}_j, \tag{17}$$

where $X_0 \in \mathcal{P}(n)$ satisfies $X_0 \preceq \mathcal{A} + \sum_{j=1}^u \sum_{k=1}^v \mathcal{C}_j^* \Upsilon_k(X_0) \mathcal{C}_j$, Convergence towards the solution of the matrix equation, in the context of trace norm $\|\cdot\|_{tr}$.

Proof. Let $\mathfrak{T} : \mathcal{P}(n) \rightarrow \mathcal{P}(n)$ be a mapping defined by

$$\mathfrak{T}(X) = \mathcal{A} + \sum_{j=1}^u \sum_{k=1}^v \mathcal{C}_j^* \Upsilon_k(X) \mathcal{C}_j, \quad \text{for all } X \in \mathcal{P}(n).$$

Consider $\mathcal{R} = \{(X, Y) \in \mathcal{P}(n) \times \mathcal{P}(n) : X \preceq Y\}$. Consequently, the fixed point of \mathfrak{T} serves as a solution to the nonlinear matrix equation (16). It is pertinent to mention that \mathcal{R} is \mathfrak{T} -closed and \mathfrak{T} is well-defined as well as \mathcal{R} -continuous. From condition (H₁) there is $\sum_{j=1}^u \sum_{k=1}^v \mathcal{C}_j^* \Upsilon_k(X) \mathcal{C}_j \succ 0$ for some $X \in \mathcal{P}(n)$, thus $(X, \mathfrak{T}(X)) \in \mathcal{R}$ and consequently $\mathcal{P}(n)(\mathfrak{T}, \mathcal{R})$ is non-empty.

Define $\partial : \mathcal{P}(n) \times \mathcal{P}(n) \rightarrow \mathbb{R}^+$ by

$$\partial(X, Y) = \|X - Y\|_{tr}, \text{ for all } X, Y \in \mathcal{P}(n).$$

Then $(\mathcal{P}(n), \partial, \mathcal{R})$ is \mathcal{R} -complete RMS. Then

$$\begin{aligned} \|\mathfrak{T}(Y) - \mathfrak{T}(X)\|_{tr} &= tr(\mathfrak{T}(Y) - \mathfrak{T}(X)) \\ &= tr \left(\sum_{j=1}^u \sum_{k=1}^v C_j^* (\Upsilon_k(Y) - \Upsilon_k(X)) C_j \right) \\ &= \sum_{j=1}^u \sum_{k=1}^v tr(C_j C_j^* (\Upsilon_k(Y) - \Upsilon_k(X))) \\ &= tr \left(\left(\sum_{j=1}^u C_j C_j^* \right) \sum_{k=1}^v (\Upsilon_k(Y) - \Upsilon_k(X)) \right) \\ &\leq \left\| \sum_{j=1}^u C_j C_j^* \right\| \times v \times \max \|\Upsilon_k(Y) - \Upsilon_k(X)\|_{tr} \\ &\leq \frac{1}{2} \times \max \left\{ \|X - \mathfrak{T}X\|_{tr}, \|Y - \mathfrak{T}Y\|_{tr}, \right. \\ &\quad \left. \|X - \mathfrak{T}X\|_{tr}^{\frac{1}{2}} \cdot \|Y - \mathfrak{T}Y\|_{tr}^{\frac{1}{2}} \right\} \\ &= \frac{1}{2} (\Omega(\|X - \mathfrak{T}X\|_{tr}, \|Y - \mathfrak{T}Y\|_{tr})) \end{aligned} \tag{18}$$

Now, when considering $\psi(\nu) = \nu$, $\phi(\nu) = \frac{\nu}{2}$, then equation (18) becomes

$$\psi(\partial(\mathfrak{T}X, \mathfrak{T}Y)) \leq \phi(\Omega(\partial(X, \mathfrak{T}(X)), \partial(Y, \mathfrak{T}(Y)))).$$

Consequently, upon fulfilling all the hypotheses stated in Theorem 2, it can be deduced that there exists an element $X^* \in \mathcal{P}(n)$ for which $\mathfrak{T}(X^*) = X^*$ holds good. As a result, the matrix equation (16) is guaranteed to possess a solution within the set $\mathcal{P}(n)$. \square

EXAMPLE 4. Consider the nonlinear matrix equation (16) for $u = v = 2$, and $n = 3$, with $\Upsilon_1(X) = X^{\frac{1}{4}}$, $\Upsilon_2(X) = X^{\frac{1}{5}}$, i.e.,

$$X = \mathcal{A} + C_1^* X^{\frac{1}{4}} C_1 + C_1^* X^{\frac{1}{5}} C_1 + C_2^* X^{\frac{1}{4}} C_2 + C_2^* X^{\frac{1}{5}} C_2 \tag{19}$$

where

$$\mathcal{A} = \begin{bmatrix} 0.177855454222667 & 0.001123654123643 & 0.144563214565439 \\ 0.001123532012243 & 0.177856213654500 & 0.133214521452362 \\ 0.144562121365390 & 0.133214526352116 & 0.266521364125960 \end{bmatrix}$$

$$\mathcal{C}_1 = \begin{bmatrix} 0.222353216521933 & 0.104402312563210 & 0.077854213651530 \\ 0.277652136521619 & 0.122365475632174 & 0.066321541236599 \\ 0.144563125462493 & 0.111232145236838 & 0.244512365214147 \end{bmatrix}$$

$$\mathcal{C}_2 = \begin{bmatrix} 0.255541232145296 & 0.177563214532317 & 0.277854621452056 \\ 0.074456321236541 & 0.222351452365355 & 0.100321256321427 \\ 0.155462136521421 & 0.133652123652627 & 0.199663251400003 \end{bmatrix}$$

By taking $N = \frac{3}{5}$, the conditions specified in Theorem 5 can be validated numerically by evaluating various specific values for the matrices involved. For example, they can be tested (and verified to be true) for

$$X = \begin{bmatrix} 0.285221251452362 & 0.123815632145236 & 0.016912136521452 \\ 0.192072365214523 & 0.219152365214523 & 0.026932365214569 \\ 0.232862136541254 & 0.172062136521452 & 0.096802123652145 \end{bmatrix}$$

$$Y = \begin{bmatrix} 0.385224563214521 & 0.123811236521452 & 0.016912365214896 \\ 0.192076541236541 & 0.319150000000000 & 0.026931236541526 \\ 0.232861236541256 & 0.172061236521452 & 0.196823652145230 \end{bmatrix}$$

To ascertain the convergence of $\{X_n\}$ defined in (17), one commences with three distinct initial values.

$$U_0 = \begin{bmatrix} \frac{1}{20} & 0 & 0 \\ 0 & \frac{1}{15} & 0 \\ 0 & 0 & \frac{1}{15} \end{bmatrix}$$

$$V_0 = \begin{bmatrix} 0.500354112000372 & 0.454632123005061 & 0.398954120000949 \\ 0.022141236541532 & 0.151234561235184 & 0.104256348563137 \\ 0.054621236525374 & 0.045213625456758 & 0.103456212563418 \end{bmatrix}$$

$$W_0 = \begin{bmatrix} 0.100963214521244 & 0.066321213621732 & 0.005445632123530 \\ 0.255632122000784 & 0.210032145632300 & 0.288632512325983 \\ 0.111232152412246 & 0.080032356212332 & 0.177521363201611 \end{bmatrix}$$

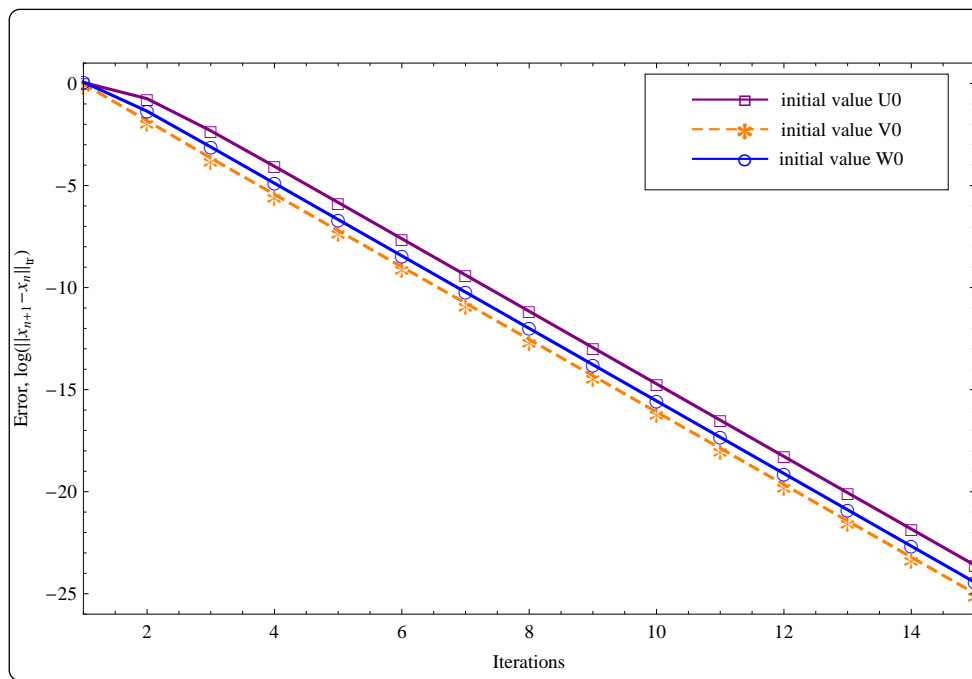


Figure - 1 Convergence behavior

After conducting 15 iterations, the subsequent approximation of the positive definite solution for the system presented in (16) is as follows:

$$\hat{U} \approx U_{15} = \begin{bmatrix} 0.683105295072446 & 0.342270947152747 & 0.548634067670387 \\ 0.342270819335426 & 0.468237110722328 & 0.450115496162419 \\ 0.548632937935167 & 0.450115485036356 & 0.678165537273724 \end{bmatrix}$$

with error 1.92601×10^{-11} ,

$$\hat{V} \approx V_{15} = \begin{bmatrix} 0.683105295076171 & 0.342270947155381 & 0.548634067673204 \\ 0.342270819338060 & 0.468237110724480 & 0.450115496164750 \\ 0.548632937937984 & 0.450115485038687 & 0.678165537276339 \end{bmatrix}$$

with error 1.1608×10^{-11} ,

$$\hat{W} \approx W_{15} = \begin{bmatrix} 0.683105295075270 & 0.342270947154744 & 0.548634067672523 \\ 0.342270819337423 & 0.468237110723960 & 0.450115496164186 \\ 0.548632937937303 & 0.450115485038123 & 0.678165537275706 \end{bmatrix}$$

with error 5.3354×10^{-12} .

Figure 1 is a graphical illustration of the convergence phenomenon.

References

- Alam, A. & Imdad, M. 2015. Relation-theoretic contraction principle. *Journal of Fixed Point Theory and Applications*, 17, pp.693-702. Available at: <https://doi.org/10.1007/s11784-015-0247-y>.
- Alam, A. & Imdad, M. 2017. Relation-theoretic metrical coincidence theorems. *Filomat*, 31(14), pp.4421-4439. Available at: <https://doi.org/10.2298/FIL1714421A>.
- Alam, A. & Imdad, M. 2018. Nonlinear contractions in metric spaces under locally T -transitive binary relations. *Fixed Point Theory*, 19(1), pp.13-24. Available at: <https://doi.org/10.24193/fpt-ro.2018.1.02>.
- Banach, S. 1922. Sur les opérations dans les ensembles abstraits et leur applications aux équations intégrales. *Fundamenta Mathematicae*, 3, pp.133-181 (in French). Available at: <https://doi.org/10.4064/fm-3-1-133-181>.
- Debnath, P., Konwar, N. & Radenović, S. 2021. *Metric Fixed Point Theory: Applications in Science, Engineering and Behavioural Sciences*. Springer Verlag, Singapore. Available at: <https://doi.org/10.1007/978-981-16-4896-0>.
- Debnath, P., Mitrović, Z.D. & Radenović, S. 2020. Interpolative Hardy-Rogers and Reich-Rus-Ćirić type contractions in b -metric spaces and rectangular b -metric spaces. *Matematički vesnik*, 72(4), pp.368-374 [online]. Available at: <https://www.vesnik.math.rs/landing.php?p=mv204.cap&name=mv20409> [Accessed: 28 May 2024].
- Hammad, H.A., Aydi, H. & Kattan, D.A. 2023. Hybrid interpolative mappings for solving fractional Navier–Stokes and functional differential equations. *Boundary Value Problems*, 2023, art.number:116. Available at: <https://doi.org/10.1186/s13661-023-01807-1>.
- Jain, S. & Radenović, S. 2023. Interpolative fuzzy Z -contraction with its application to Fredholm non-linear integral equation. *Gulf Journal of Mathematics*, 14(1), pp.84-98. Available at: <https://doi.org/10.56947/gjom.v14i1.1009>.
- Jain, S., Stojiljković, V.N. & Radenović, S.N. 2022. Interpolative generalised Meir-Keeler contraction. *Vojnotehnički glasnik/Military Technical Courier*, 70(4), pp.818-835. Available at: <https://doi.org/10.5937/vojtehg70-39820>.

Kannan, R. 1968. Some results on fixed points. *Bulletin of the Calcutta Mathematical Society*, 60, pp.71-76.

Karapinar, E. 2018. Revisiting the Kannan type Contractions via Interpolation. *Advances in the Theory of Nonlinear Analysis and its Application*, 2(2), pp.85-87. Available at: <https://doi.org/10.31197/atnaa.431135>.

Karapinar, E. 2021. Interpolative Kannan-Meir-Keeler type contraction. *Advances in the Theory of Nonlinear Analysis and its Application*, 5(4), pp.611-614. Available at: <https://doi.org/10.31197/atnaa.989389>.

Karapinar, E., Agarwal, R. & Aydi, H. 2018a. Interpolative Reich–Rus–Ćirić Type Contractions on Partial Metric Spaces. *Mathematics*, 6(11), art.number:256. Available at: <https://doi.org/10.3390/math6110256>.

Karapinar, E., Alqahtani, O. & Aydi, H. 2018b. On Interpolative Hardy-Rogers Type Contractions. *Symmetry*, 11(1), art.number:8. Available at: <https://doi.org/10.3390/sym11010008>.

Karapinar, E., Fulga, A. & Yesilkaya, S.S. 2021. New Results on Perov-Interpolative Contractions of Suzuki Type Mappings. *Journal of Function Spaces*, 2021(1), art.number:9587604. Available at: <https://doi.org/10.1155/2021/9587604>.

Nazam, M., Aydi, H. & Hussain, A. 2023a. Existence theorems for (Ψ, Φ) -orthogonal interpolative contractions and an application to fractional differential equations. *Optimization*, 72(7), pp.1899-1929. Available at: <https://doi.org/10.1080/02331934.2022.2043858>.

Nazam, M., Javed, K. & Arshad, M. 2023b. The (Ψ, Φ) -orthogonal interpolative contractions and an application to fractional differential equations. *Filomat*, 37(4), pp.1167-1185. Available at: <https://doi.org/10.2298/FIL2304167N>.

Ran, A.C.M. & Reurings, M.C.B. 2002. On the nonlinear matrix equation $X + A^*F(X)A = Q$: solutions and perturbation theory. *Linear Algebra and its Applications*, 346(1-3), pp.15-26. Available at: [https://doi.org/10.1016/S0024-3795\(01\)00508-0](https://doi.org/10.1016/S0024-3795(01)00508-0).

Samet, B., Vetro, C. & Vetro, P. 2012. Fixed point theorems for α - ψ -contractive type mappings. *Nonlinear Analysis: Theory, Methods & Applications*, 75(4), pp.2154-2165. Available at: <https://doi.org/10.1016/j.na.2011.10.014>.

Teoremas de existencia para una contracción unificada Kannan interpolativa con una aplicación en ecuaciones matriciales no lineales

Koti N. V. V. Vara Prasad^a, Vinay Mishra^a, **autor de correspondencia**, Stojan Radenović^b

^a Guru Ghasidas Vishwavidyalaya, Departamento de Matemáticas, Bilaspur, República de la India

^b Universidad de Belgrado, Facultad de Ingeniería Mecánica, Belgrado, República de Serbia



CAMPO: matemáticas

TIPO DE ARTÍCULO: artículo científico original

Resumen:

Introducción/objetivo: Este artículo estableció un nuevo marco matemático al descubrir las relaciones entre las contracciones Kannan y las contracciones Kannan interpolativas. El concepto de contracciones Kannan interpolativas unificadas se introdujo en el marco de un espacio métrico relacional. Además, el estudio tuvo como objetivo ampliar el concepto de admisibilidad alfa incorporando ideas métricas relacionales específicas.

Métodos: Se realizó una exploración detallada de las propiedades y características de las contracciones Kannan y las contracciones Kannan interpolativas. La investigación introdujo el concepto de contracciones Kannan interpolativas unificadas y formuló nuevos resultados de punto fijo para estas asignaciones.

Resultados: El estudio estableció con éxito resultados de punto fijo para las contracciones unificadas Kannan interpolativas dentro del marco de los espacios métricos relacionales. Además, se proporcionó una aplicación de estos resultados para resolver un problema relacionado con ecuaciones matriciales no lineales, enfatizando aún más su importancia.

Conclusión: Los hallazgos de este estudio han permitido avanzar significativamente en la comprensión de las contracciones Kannan y las contracciones Kannan interpolativas, ofreciendo un marco unificado para su análisis. La introducción de contracciones unificadas Kannan interpolativas y la expansión de la admisibilidad alfa tienen amplias implicaciones para el campo de las matemáticas.

Palabras claves: contracción interpolativa unificada de Kannan, \mathcal{R} -admisibilidad, espacio métrico relacional.

Теоремы существования унифицированного интерполяционного сокращения Каннана с применением нелинейных матричных уравнений

Коти Н. В. В. Вара Прасад^а, Винай Мишра^а, **корреспондент**, Стоян Раденович^б

^а Биласпурский университет Гуру Гасидас Вишвавидьялая, математический факультет, г. Биласпур, Республика Индия

^б Белградский университет, машиностроительный факультет, г. Белград, Республика Сербия

РУБРИКА ГРНТИ: 27.25.17 Метрическая теория функций
ВИД СТАТЬИ: оригинальная научная статья

Резюме:

Введение/цель: В данной статье были обозначены новые математические рамки, освещающие взаимосвязи между сокращениями Каннана и интерполяционными сокращениями Каннана. Концепция унифицированных интерполяционных сокращений Каннана была введена в рамках реляционного метрического пространства. Помимо того, целью исследования было развитие концепции альфа-допустимости за счет включения конкретных идей в отношении относительных показателей.

Методы: Было проведено подробное исследование свойств и характеристик сокращений Каннана и интерполяции сокращений Каннана. В ходе исследования была представлена концепция унифицированной интерполяции сокращений Каннана и сформулированы новые результаты с фиксированными точками.

Результаты: Исследование дало успешные результаты с фиксированной точкой для унифицированных интерполяционных сокращений Каннана в рамках реляционных метрических пространств. Помимо того, было представлено применение этих результатов для решения задачи, касающейся нелинейных матричных уравнений, тем самым подчеркивая их значимость.

Выводы: Результаты данного исследования значительно улучшили понимание сокращений Каннана и интерполяционных сокращений Каннана, представив единую основу для их анализа. Введение унифицированных интерполяционных сокращений Каннана и расширение допустимости альфа-допустимости широко применяются в области математики.

Ключевые слова: унифицированное интерполяционное сжатие Каннана, \mathcal{R} -допустимое, реляционное метрическое пространство.



Теореме постојања за јединствену интерполативну Кананову контракцију са применама код нелинеарних матричних једначина

Коти Н. В. В. Вара Прасад^а, Винај Мишра^а, аутор за преписку, Стојан Раденовић^б

^а Гуру Гасидас Вишвавидјалаја, Одељење математике, Биласпур, Република Индија

^б Универзитет у Београду, Машински факултет, Београд, Република Србија

ОБЛАСТ: математика

КАТЕГОРИЈА (ТИП) ЧЛАНКА: оригинални научни рад

Сажетак:

Увод/циљ: Овим радом успостављен је нови математички оквир откривањем односа између Кананове контракције и његове интерполативне контракције. Концепт обједињене интерполативне Кананове контракције уведен је у оквиру релационог метричког простора. Поред тога, студија је имала за циљ да прошири концепт алфа-прихватљивости уграђивањем специфичних релационих метричких идеја.

Метод: Детаљно истраживање својстава и карактеристика Кананове контракције и његове интерполативне контракције били су и раније разматрани. Овим истраживањем уведен је концепт унифициране интерполације Кананове контракције чиме су формулисани нови резултати фиксне тачке за њих.

Резултати: Студија је успешно потврдила резултате фиксне тачке за унифициране интерполативне Кананове контракције у оквиру релационих метричких простора. Поред тога, примена ових резултата за решавање проблема који се тиче нелинеарних матричних једначина додатно наглашава њихов значај.

Закључак: Налази ове студије значајно су унапредили недовољно разумевање Кананових контракција и његових интерполативних контракција, нудећи јединствен оквир за њихову анализу. Увод у унифициране интерполативне Кананове контракције и проширење алфа-прихватљивости има широку примену у области математике.

Кључне речи: унифицирана интерполативна Кананова контракција, \mathcal{R} -допустив, релациони метрички простор.

Paper received on: 30.04.2024.

Manuscript corrections submitted on: 20.09.2024.

Paper accepted for publishing on: 21.09.2024.

© 2024 The Authors. Published by Vojnotehnički glasnik / Military Technical Courier (<http://vtg.mod.gov.rs>, <http://vtr.mo.yrp.spb>). This article is an open access article distributed under the terms and conditions of the Creative Commons Attribution license (<http://creativecommons.org/licenses/by/3.0/rs/>).






On some fixed point results for expansive mappings in S -metric spaces

Nora Fetouci^a, Stojan Radenović^b

^aJijel University, LMPA Laboratory, Department of Mathematics,
Jijel, People's Democratic Republic of Algeria,
e-mail: n.fetouci@univ-jijel.dz, **corresponding author**,
ORCID iD:  <https://orcid.org/0000-0002-1474-6554>

^bUniversity of Belgrade, Faculty of Mechanical Engineering,
Belgrade, Republic of Serbia,
e-mail: sradenovic@mas.bg.ac.rs,
ORCID iD:  <https://orcid.org/0000-0001-8254-6688>

 <https://doi.org/10.5937/vojtehg72-50064>

FIELD: mathematics

ARTICLE TYPE: original scientific paper

Abstract:

Introduction/purpose: The aim of this paper is to establish some existence results of a fixed point for a class of expansive mappings defined on a complete S -metric space.

Methods: An iteration scheme was used.

Results: Some existing results of mappings satisfying contractive conditions are expanded to expansive ones, providing a new condition expressed in one variable under which the existence of a fixed point holds.

Conclusions: This work provides new tools to fixed point theory together with their applications.

Key words: fixed point, S -metric space, expansive mapping.

Introduction and preliminaries

One of the most important instruments to treat nonlinear problems with the aid of functional analytic methods is the fixed point approach. Metric fixed point theory provides essential tools for solving problems emerging from various areas of mathematical analysis, such as variational and linear inequalities, equilibrium problems, complementarity problems, optimization and approximation theory, as well as problems of proving the existence of a solution of integral and differential equations. The first important result of fixed points in metric spaces was the well known contraction mapping theorem, established by S. Banach in his dissertation and published for the

first time in 1922. Later, some generalized metric spaces have been studied to obtain new fixed point theorems.

In 2006, Z. Mustafa and B. Sims (Mustafa & Sims, 2006) introduced the notion of G -metric spaces as a generalization of ordinary metric spaces, and analysed the topological structure of G -metric spaces. In this first paper, the authors developed some fixed point results for various classes of mappings in the setting of a G -metric space. For this and more details, the reader can see (Abbas et al., 2016; An et al., 2015; Dosenovic et al., 2018; Vujaković et al., 2023). In 2012, S. Sedghi, N. Shobe and A. Aliouche (Sedghi et al., 2012) introduced S -metric spaces as a generalization of G -metric spaces and metric spaces, and proved several fixed point results in the setting of S -metric spaces. For other results, see (Mojaradiafra, 2016; Mojaradiafra & Sabbaghan, 2021; Sedghi & Dung, 2014). In 1984, (Wang et al., 1984), introduced the concept of expanding mappings and proved some fixed point theorems in metric spaces. For more details on expanding mappings and related results, we refer the reader to (Mohanta, 2012; Mojaradiafra et al., 2020; Mustafa et al., 2010). This paper establishes some existence results of a fixed point for a class of expansive mappings in S -metric spaces. Some existing results from G -metric and S -metric spaces are extended. The contribution of this paper is in providing new tools to fixed point theory together with their applications. Let us recall some basic definitions and properties of S -metric spaces.

DEFINITION 1. (Sedghi et al., 2012) *Let X be a non-empty set. An S -metric on X is a function*

$S : X \times X \times X \rightarrow [0, +\infty[$ that satisfies the following conditions for all $x, y, z, a \in X$:

$$(S1) \quad S(x, y, z) = 0 \text{ if and only if } x = y = z,$$

$$(S2) \quad S(x, y, z) \leq S(x, x, a) + S(y, y, a) + S(z, z, a).$$

The pair (X, S) is called an S -metric space.

EXAMPLE 1. 1. Let $X = \mathbb{R}^n$ and $\|\cdot\|$ a norm on X , then

$$S(x, y, z) = \|y + z - 2x\| + \|y - z\| \text{ is an } S\text{-metric on } X.$$

2. Let $X = \mathbb{R}^n$ and $\|\cdot\|$ a norm on X , then $S(x, y, z) = \|x - z\| + \|y - z\|$ is an S -metric on X .

3. Let X be a nonempty set, d is ordinary metric on X , then

$$S(x, y, z) = d(x, z) + d(y, z) \text{ is an } S\text{-metric on } X.$$



DEFINITION 2. (Bakhtin, 1989) Let X be a nonempty set. A b -metric on X is a function $d : X \times X \rightarrow [0, +\infty[$ if there exists a real number $b \geq 1$ such that the following conditions hold for all $x, y, z \in X$.

B1 $d(x, y) = 0$ if and only if $x = y$,

B2 $d(x, y) = d(y, x)$,

B3 $d(x, z) \leq b[d(x, y) + d(y, z)]$.

The pair (X, d) is called a b -metric space.

We will prove that every S -metric space (X, S) will define a b -metric space (X, d) .

PROPOSITION 1. (Sedghi & Dung, 2014) Let (X, S) an S -metric space and let

$$d(x, y) = S(x, x, y)$$

for all $x, y \in X$. Then

1. d is a b -metric on X ,
2. $x_n \rightarrow x$ in (X, S) if and only if $x_n \rightarrow x$ in (X, d) ,
3. (x_n) is a Cauchy sequence in (X, S) if and only if (x_n) is a Cauchy sequence in (X, d) .

DEFINITION 3. (Sedghi et al., 2012) Let (X, S) be an S -metric space. For $r > 0$ and $x \in X$, we define the open ball $B_S(x, r)$ and the closed ball $B_S[x, r]$ with the center x and the radius r as follows

$$B_S(x, r) = \{y \in X : S(y, y, x) < r\} \quad (1)$$

$$B_S[x, r] = \{y \in X : S(y, y, x) \leq r\}. \quad (2)$$

The topology induced by the S -metric is the topology generated by the base of all open balls in X .

DEFINITION 4. (Sedghi et al., 2012) Let (X, S) be an S -metric space.

1. A sequence (x_n) converges to $x \in X$ if $S(x_n, x_n, x) \rightarrow 0$ as $n \rightarrow +\infty$. That is, for each $\varepsilon > 0$, there exists $n_0 \in \mathbb{N}$ such that for all $n \geq n_0$ one gets $S(x_n, x_n, x) < \varepsilon$. We write $x_n \rightarrow x$ for brevity.
2. A sequence (x_n) is a Cauchy sequence if $S(x_n, x_n, x_m) \rightarrow 0$ as $n, m \rightarrow +\infty$. That is, for each $\varepsilon > 0$, there exists $n_0 \in \mathbb{N}$ such that for all $n, m \geq n_0$ one gets $S(x_n, x_n, x_m) < \varepsilon$.

3. The S -metric space (X, S) is complete if every Cauchy sequence is a convergent sequence.

LEMMA 1. (Sedghi et al., 2012) Let (X, S) be an S -metric space. If the sequence (x_n) in x converges to x , then x is unique.

The next three lemmas are well known, see for example (Sedghi et al., 2012).

LEMMA 2. In an S -metric space, there exists

$$S(x, x, y) = S(y, y, x),$$

for all $x, y \in X$.

LEMMA 3. Let (X, S) be an S -metric space. If $x_n \rightarrow x$ and $y_n \rightarrow y$ then $S(x_n, x_n, y_n) \rightarrow S(x, x, y)$.

LEMMA 4. (Mojaradiafra et al., 2020) Any S -metric space is Hausdorff.

DEFINITION 5. Let (X, S_1) and (Y, S_2) be S -metric spaces. A map $f : X \rightarrow Y$ is called continuous at $x \in X$ if for every $\varepsilon > 0$ there exists $\delta > 0$ such that

$S_1(x, x, y) < \delta$ implies that $S_2(f(x), f(x), f(y)) < \varepsilon$, or

$$f(B_{S_1}(x, \delta)) \subset B_{S_2}(f(x), \varepsilon).$$

The next result is also known, see (Sedghi et al., 2012).

LEMMA 5. Let (X, S) be an S -metric space. The map $f : X \rightarrow X$ is continuous at $x \in X$ if and only if $f(x_n) \rightarrow f(x)$ whenever $x_n \rightarrow x$.

DEFINITION 6. Let (X, S) be an S -metric space. A map $T : X \rightarrow X$ is said to be a contraction if there exists a constant $0 \leq k < 1$ such that

$$S(Tx, Tx, Ty) \leq kS(x, x, y), \text{ for all } x, y \in X.$$

THEOREM 1. Let (X, S) be a complete S -metric space and $T : X \rightarrow X$ be a contraction. Then T has a unique fixed point.



DEFINITION 7. Let (X, S) be an S -metric space and T be a self-map on X . Then T is called an expansive map if there exists a constant $a > 1$ such that for all $x, y \in X$, one gets

$$S(Tx, Tx, Ty) \geq aS(x, x, y).$$

The constant a is called the expansion coefficient.

REMARK 1. Expansive map on an S -metric space does not need to be continuous.

THEOREM 2. (Mojaradiafra et al., 2020) Let (X, S) be a complete S -metric space, and let $T : X \rightarrow X$ be an onto continuous mapping satisfying

$$S(Tx, Tx, T^2x) \geq aS(x, x, Tx) \tag{3}$$

for all $x \in X$, where $a > 1$. Then T has a fixed point in X .

EXAMPLE 2. (Mojaradiafra et al., 2020) Let

$T : (\mathbb{R}, S) \rightarrow (\mathbb{R}, S)$ be defined by

$$T(x) = \begin{cases} 4x & \text{for } x \leq 2, \\ 4x + 3 & \text{for } x > 2, \end{cases}$$

where $S(x, y, z) = \max\{|x - z|, |y - z|\}$. Then (\mathbb{R}, S) is a complete S -metric space and T is an expansive map with the coefficient $a = 2$.

Main results

Our first main result is as follows:

THEOREM 3. Let (X, S) be a complete S -metric space. Let $T : X \rightarrow X$ be an onto mapping such that,

$$S(Tx, Ty, Tz) \geq aN(x, y, z) \tag{4}$$

for all x, y, z , where $a > 1$ and

$$N(x, y, z) = \min \left\{ \begin{array}{l} S(x, y, Tx), S(Tx, Ty, y), S(Tx, Ty, x), S(Tx, Tx, y), \\ S(z, z, x), S(Tz, Tz, T^2x), S(T^2y, T^2x, Tz), S(Tx, Ty, z), \\ S(x, y, z), S(Tx, Tx, x), S(Ty, Ty, y), S(T^2x, T^2y, Tz), \\ S(Tx, Tx, z), S(Ty, Ty, x), S(Tz, Tz, T^2y) \end{array} \right\}. \tag{5}$$

Then T admits a fixed point.

Proof. Let $x_0 \in X$, since T is onto then there exists an element x_1 satisfying $x_1 \in T^{-1}(x_0)$. Continuing in this way, one gets a sequence (x_n) , where $x_n \in T^{-1}(x_{n-1})$. If $x_n = x_{n-1}$ for some n , then x_n is a fixed point of T . Assume $x_n \neq x_{n-1}$ for every $n \in \mathbb{N}$, then from (5) one obtains

$$S(x_{n-1}, x_{n-1}, x_{n-2}) = S(Tx_n, Tx_n, Tx_{n-1}) \geq aN(x_n, x_n, x_{n-1}),$$

where

$$N(x_n, x_n, x_{n-1}) = \tag{6}$$

$$= \min \left\{ \begin{array}{l} S(x_n, x_n, Tx_n), S(Tx_n, Tx_n, x_n), S(Tx_n, Tx_n, x_n), \\ S(Tx_n, Tx_n, x_n), S(x_{n-1}, x_{n-1}, x_n), S(Tx_{n-1}, Tx_{n-1}, T^2x_n), \\ S(T^2x_n, T^2x_n, Tx_{n-1}), S(Tx_n, Tx_n, x_{n-1}), S(x_n, x_n, x_{n-1}), \\ S(Tx_n, Tx_n, x_n), S(Tx_n, Tx_n, x_n), S(T^2x_n, T^2x_n, Tx_{n-1}), \\ S(Tx_n, Tx_n, x_{n-1}), S(Tx_n, Tx_n, x_n), S(Tx_{n-1}, Tx_{n-1}, T^2x_n) \end{array} \right\},$$

so

$$N(x_n, x_n, x_{n-1}) = \tag{7}$$

$$= \min \left\{ \begin{array}{l} S(x_n, x_n, x_{n-1}), S(x_{n-1}, x_{n-1}, x_n), S(x_{n-1}, x_{n-1}, x_n), \\ S(x_{n-1}, x_{n-1}, x_n), S(x_{n-1}, x_{n-1}, x_n), S(x_{n-2}, x_{n-2}, x_{n-2}), \\ S(x_{n-2}, x_{n-2}, x_{n-2}), S(x_{n-1}, x_{n-1}, x_{n-1}), S(x_n, x_n, x_{n-1}), \\ S(x_{n-1}, x_{n-1}, x_n), S(x_{n-1}, x_{n-1}, x_n), S(x_{n-2}, x_{n-2}, x_{n-2}), \\ S(x_{n-1}, x_{n-1}, x_{n-1}), S(x_{n-1}, x_{n-1}, x_n), S(x_{n-2}, x_{n-2}, x_{n-2}) \end{array} \right\},$$

then

$$S(x_{n-1}, x_{n-1}, x_{n-2}) \geq aS(x_n, x_n, x_{n-1}),$$

this implies that

$$S(x_n, x_n, x_{n-1}) \leq \frac{1}{a} S(x_{n-1}, x_{n-1}, x_{n-2}). \tag{8}$$

Set $k = \frac{1}{a}$, then $k < 1$. By induction one obtains

$$\begin{aligned} S(x_n, x_n, x_{n-1}) &\leq kS(x_{n-1}, x_{n-1}, x_{n-2}) \\ &\leq k^2 S(x_{n-2}, x_{n-2}, x_{n-3}) \end{aligned} \tag{9}$$

$$\begin{aligned} &\leq \dots \\ &\leq k^{n-1}S(x_1, x_1, x_0). \end{aligned}$$

Then, by (S2) and Lemma 2, we get for all $n, m \in \mathbb{N}; n < m$,

$$\begin{aligned} S(x_m, x_m, x_n) &\leq 2S(x_m, x_m, x_{m-1}) + S(x_n, x_n, x_{m-1}) & (10) \\ &= 2S(x_m, x_m, x_{m-1}) + S(x_{m-1}, x_{m-1}, x_n) \\ &\leq 2S(x_m, x_m, x_{m-1}) + 2S(x_{m-1}, x_{m-1}, x_{m-2}) \\ &\quad + S(x_n, x_n, x_{m-2}) \\ &= 2S(x_m, x_m, x_{m-1}) + 2S(x_{m-1}, x_{m-1}, x_{m-2}) \\ &\quad + S(x_{m-2}, x_{m-2}, x_n) \\ &\dots \\ &\leq 2 \sum_{i=n+2}^m S(x_i, x_i, x_{i-1}) + S(x_{n+1}, x_{n+1}, x_n), \end{aligned}$$

by (10), we obtain

$$\begin{aligned} S(x_m, x_m, x_n) &\leq 2 \sum_{i=n+2}^m S(x_i, x_i, x_{i-1}) + S(x_{n+1}, x_{n+1}, x_n) & (11) \\ &\leq 2 \sum_{i=n+2}^m k^{i-1}S(x_1, x_1, x_0) + k^n S(x_1, x_1, x_0) \\ &\leq 2k^{n+1} \frac{1 - k^{m-n-1}}{1 - k} S(x_1, x_1, x_0) + k^n S(x_1, x_1, x_0) \\ &\leq 2 \frac{k^{n+1}}{1 - k} S(x_1, x_1, x_0) + k^n S(x_1, x_1, x_0), \end{aligned}$$

so, $S(x_m, x_m, x_n) \rightarrow 0$ as $n, m \rightarrow +\infty$ and (x_n) is a Cauchy sequence. Since (X, S) is complete, then there exists $u \in X$ such that (x_n) is convergent to u .

We need to show that $Tu = u$, let $y \in T^{-1}(u)$, for n such that $x_n \neq u$, we get

$S(x_n, x_n, u) = S(Tx_{n+1}, Tx_{n+1}, Ty) \geq aN(x_{n+1}, x_{n+1}, y)$, where

$$N(x_{n+1}, x_{n+1}, y) = \tag{12}$$

$$= \min \left\{ \begin{array}{l} S(x_{n+1}, x_{n+1}, x_n), S(x_n, x_n, x_{n+1}), S(x_n, x_n, x_{n+1}), \\ S(x_n, x_n, x_{n+1}), S(y, y, x_{n+1}), S(Ty, Ty, x_{n-1}), \\ S(x_{n-1}, x_{n-1}, Ty), S(x_n, x_n, y), S(x_{n+1}, x_{n+1}, y), \\ S(x_n, x_n, x_{n+1}), S(x_n, x_n, x_{n+1}), S(x_{n-1}, x_{n-1}, Ty), \\ S(x_n, x_n, y), S(x_n, x_n, x_{n+1}), S(Ty, Ty, x_{n-1}) \end{array} \right\},$$

taking the limit as $n \rightarrow +\infty$ we obtain $S(u, u, y) \leq 0$, which implies that $Ty = u = y$; hence u is a fixed point of T . □

Our second result is given by

THEOREM 4. *Let (X, S) be a complete S -metric space and let $T : X \rightarrow X$ be an onto S -continuous mapping. Assume that there exist nonnegative reals a, b, c, d, e, f, g with $b < 1$, and $a + b + c + d + e + f + g > 1$ such that*

$$\begin{aligned} S^4(Tx, Ty, Tz) &\geq & (13) \\ &\geq aS^4(x, y, z) + bS^4(T^2x, T^2y, z) + cS^4(Tx, Ty, x) + \\ &+ dS^2(Tz, T^2y, Tx)S^2(y, x, Tx) + eS^2(z, Tx, y)S^2(z, Tx, y) + \\ &+ fS^2(z, Tx, T^2y)S^2(Tx, Ty, y) + gS^2(T^2x, T^2x, y)S^2(y, x, Tx), \end{aligned}$$

for all $x \in X$, then T has a fixed point in X .

Proof. Let $x_0 \in X$, since T is onto there exists $x_1 \in T^{-1}(x_0)$. Continuing in this way, we get a sequence (x_n) , where $x_n \in T^{-1}(x_{n-1})$.

If, $x_n = x_{n-1}$ for some n , then we obtain x_n as a fixed point of T . Hence, without loss of generality, we may assume that $x_n \neq x_{n-1}$ for every $n \in \mathbb{N}$.

By (13), we get

$$\begin{aligned} S^4(x_{n-1}, x_{n-1}, x_{n-2}) &= S^4(Tx_n, Tx_n, Tx_{n-1}) \\ &\geq aS^4(x_n, x_n, x_{n-1}) + bS^4(x_{n-2}, x_{n-2}, x_{n-1}) \\ &+ cS^4(x_{n-1}, x_{n-1}, x_n) \\ &+ dS^2(x_{n-2}, x_{n-2}, x_{n-1})S^2(x_n, x_n, x_{n-1}) \\ &+ eS^2(x_{n-1}, x_{n-1}, x_n)S^2(x_{n-1}, x_{n-1}, x_n) \\ &+ fS^2(x_{n-1}, x_{n-1}, x_{n-2})S^2(x_{n-1}, x_{n-1}, x_n) \\ &+ gS^2(x_{n-2}, x_{n-2}, x_n)S^2(x_n, x_n, x_{n-1}), \end{aligned}$$

hence, by Lemma 2 we obtain

$$(a + c)S^4(x_n, x_n, x_{n-1}) + \tag{14}$$

$$\begin{aligned}
 &+ (d + e + f + g)S^2(x_n, x_n, x_{n-1})S^2(x_{n-1}, x_{n-1}, x_{n-2}) - \\
 &- (1 - b)S^4(x_{n-1}, x_{n-1}, x_{n-2}) \leq 0,
 \end{aligned}$$

which is equivalent to

$$(a + c)r^4 + (d + e + f + g)r^2 - (1 - b) \leq 0, \tag{15}$$

where

$$r = \frac{S(x_n, x_n, x_{n-1})}{S(x_{n-1}, x_{n-1}, x_{n-2})}.$$

Let $f : [0, +\infty[\rightarrow \mathbb{R}$ be the function given by

$$f(r) = (a + c)r^4 + (d + e + f + g)r^2 - (1 - b) = 0,$$

then, using assumptions, we get $f(0) = b - 1 < 0$ and $f(1) = a + b + c + d + e + f + g - 1 > 0$.

One can deduce that, there exists $k \in]0, 1[$ for which inequality (15) holds whenever $r \leq k$, and hence

$$\begin{aligned}
 S(x_n, x_n, x_{n-1}) &\leq kS(x_{n-1}, x_{n-1}, x_{n-2}) \\
 &\leq k^2S(x_{n-2}, x_{n-2}, x_{n-3}) \\
 &\leq \dots \\
 &\leq k^{n-1}S(x_1, x_1, x_0),
 \end{aligned}$$

then, by (S2) and Lemma 2, we get for all $n, m \in \mathbb{N}; n < m$,

$$\begin{aligned}
 S(x_m, x_m, x_n) &\leq 2S(x_m, x_m, x_{m-1}) + S(x_n, x_n, x_{m-1}) & (16) \\
 &= 2S(x_m, x_m, x_{m-1}) + S(x_{m-1}, x_{m-1}, x_n) \\
 &\leq 2S(x_m, x_m, x_{m-1}) + 2S(x_{m-1}, x_{m-1}, x_{m-2}) \\
 &+ S(x_n, x_n, x_{m-2}) \\
 &= 2S(x_m, x_m, x_{m-1}) + 2S(x_{m-1}, x_{m-1}, x_{m-2}) \\
 &+ S(x_{m-2}, x_{m-2}, x_n) \\
 &\dots \\
 &\leq 2 \sum_{i=n+2}^m S(x_i, x_i, x_{i-1}) + S(x_{n+1}, x_{n+1}, x_n),
 \end{aligned}$$

by (16), we obtain

$$S(x_m, x_m, x_n) \leq 2 \sum_{i=n+2}^m S(x_i, x_i, x_{i-1}) + S(x_{n+1}, x_{n+1}, x_n) \tag{17}$$

$$\begin{aligned} &\leq 2 \sum_{i=n+2}^m k^{i-1} S(x_1, x_1, x_0) + k^n S(x_1, x_1, x_0) \\ &\leq 2k^{n+1} \frac{1 - k^{m-n-1}}{1 - k} S(x_1, x_1, x_0) + k^n S(x_1, x_1, x_0) \\ &\leq 2 \frac{k^{n+1}}{1 - k} S(x_1, x_1, x_0) + k^n S(x_1, x_1, x_0), \end{aligned}$$

so, $S(x_m, x_m, x_n) \rightarrow 0$ as $n, m \rightarrow +\infty$ and (x_n) is a Cauchy sequence, and by the completeness of (X, S) , there exists $u \in X$ such that (x_n) converges to u . By continuity of T , we get

$$T(x_n) = x_{n-1} \rightarrow Tu,$$

thus $u = Tu$. We conclude that u is a fixed point of T . □

We state our third result in the sequel.

THEOREM 5. *Let (X, S) be a complete S -metric space and let $T : X \rightarrow X$ be an onto continuous mapping satisfying*

$$\begin{aligned} S(Tx, Ty, Tz) &\geq c_1 S(Tx, Ty, x) + c_2 S(Tz, T^2y, Tx) + c_3 S(y, y, Ty) + \quad (18) \\ &+ c_4 S(Tx, Tx, Tz) + c_5 \left[\frac{S(Ty, z, T^2x) + S(z, Tx, y) + S(T^2x, T^2y, z)}{3} \right] + \\ &+ c_6 \left[\frac{S(z, Tx, T^2y) + S(T^2y, Tz, Tx) + S(x, y, z)}{3} \right] + \\ &+ c_7 \left[\frac{S(Tx, Ty, y) + S(Tz, T^2x, Ty) + S(y, y, z)}{3} \right], \end{aligned}$$

where $c_1, c_2, c_3, c_4, c_5, c_6, c_7$ are non negative reals that verify

$$c_1 + c_2 + c_3 + c_4 + c_5 + c_6 + c_7 > 1, \text{ and } 3 - 3c_2 - 3c_4 - 2c_5 - 2c_6 - c_7 > 0,$$

then, T has a fixed point in X .

Proof. Replacing y by x and z by Tx in (18), we obtain

$$\begin{aligned} S(Tx, Tx, T^2x) &\geq c_1 S(Tx, Tx, x) + c_2 S(T^2x, T^2x, Tx) \quad (19) \\ &+ c_3 S(x, x, Tx) + c_4 S(Tx, Tx, T^2x) \\ &+ c_5 \left[\frac{S(Tx, Tx, T^2x) + S(Tx, Tx, x) + S(T^2x, T^2x, Tx)}{3} \right] \end{aligned}$$

$$\begin{aligned}
 &+ c_6 \left[\frac{S(Tx, Tx, T^2x) + S(T^2x, T^2x, Tx) + S(x, x, Tx)}{3} \right] \\
 &+ c_7 \left[\frac{S(Tx, Tx, x) + S(T^2x, T^2x, Tx) + S(x, x, Tx)}{3} \right],
 \end{aligned}$$

without loss of generality, we may assume that $T(x) \neq T^2(x)$, then (19) entails

$$\begin{aligned}
 S(Tx, Tx, T^2x) &\geq (c_1 + \frac{c_5 + c_7}{3})S(Tx, Tx, x) \\
 &+ (c_2 + \frac{c_5 + c_6 + c_7}{3})S(T^2x, T^2x, Tx) \\
 &+ (c_3 + \frac{c_6 + c_7}{3})S(x, x, Tx) \\
 &+ (c_4 + \frac{c_5 + c_6}{3})S(Tx, Tx, T^2x). \tag{20}
 \end{aligned}$$

Using Lemma 2, we obtain

$$\begin{aligned}
 (1 - (c_2 + c_4 + \frac{c_5 + c_6}{3} + \frac{c_5 + c_6 + c_7}{3}))S(Tx, Tx, T^2x) &\geq \\
 (c_1 + c_3 + \frac{c_5 + c_7}{3} + \frac{c_6 + c_7}{3})S(x, x, Tx), \tag{21}
 \end{aligned}$$

which implies that

$$\begin{aligned}
 (3 - 3c_2 - 3c_4 - 2c_5 - 2c_6 - c_7)S(Tx, Tx, T^2x) &\geq (3c_1 + 3c_3 + \\
 &+ c_5 + c_6 + 2c_7)S(x, x, Tx), \tag{22}
 \end{aligned}$$

hence

$$S(Tx, Tx, T^2x) \geq \frac{3c_1 + 3c_3 + c_5 + c_6 + 2c_7}{3 - 3c_2 - 3c_4 - 2c_5 - 2c_6 - c_7} S(x, x, Tx). \tag{23}$$

Setting, $a = c_1 + c_2 + c_3 + c_4 + c_5 + c_6 + c_7$, then by assumption we obtain $a > 1$. So, (23) becomes condition (3); therefore, the result follows from Theorem 2. \square

Now, we give an example illustrating our result in Theorem 5.

EXAMPLE 3. Let $X = \mathbb{R}$ be the set of real numbers. Define

$$S(x, y, z) = \begin{cases} 0 & \text{if } x = y = z, \\ \max\{|x|, |y|, |z|\} & \text{otherwise.} \end{cases}$$

Then (X, S) is an S -metric space.

Assume

$$Tx = \begin{cases} \sqrt{2}x & \text{if } x < 0, \\ \frac{5}{2}x & \text{if } x \geq 0. \end{cases}$$

We get

$$T^2x = \begin{cases} 2x & \text{if } x < 0, \\ \frac{25}{4}x & \text{if } x \geq 0. \end{cases}$$

$$S(x, x, Tx) = |Tx| = \begin{cases} -\sqrt{2}x & \text{if } x < 0, \\ \frac{5}{2}x & \text{if } x \geq 0. \end{cases}$$

$$S(Tx, Tx, T^2x) = |T^2x| = \begin{cases} -2x & \text{if } x < 0, \\ \frac{25}{4}x & \text{if } x \geq 0. \end{cases}$$

Set: $c_1 = \frac{1}{20}$, $c_2 = \frac{1}{8}$, $c_3 = \frac{1}{5}$, $c_4 = \frac{1}{4}$, $c_5 = \frac{7}{40}$, $c_6 = \frac{3}{20}$ and $c_7 = \frac{3}{40}$, so conditions of Theorem 5 are verified; hence T admits a fixed point in \mathbb{R} . One can see that the fixed point here is zero.

References

- Abbas, M., Hussain, A., Popović, B. & Radenović, S. 2016. Istratescu-Suzuki-Ćirić-type fixed points results in the framework of G -metric spaces. *Journal of Non-linear Sciences and Applications*, 9(12), pp.6077-6095. Available at: <https://doi.org/10.22436/jnsa.009.12.15>.
- An, T.V., Dung, N.V., Kadelburg, Z. & Radenović, S. 2015. Various generalizations of metric spaces and fixed point theorems. *Revista de la Real Academia de Ciencias Exactas, Físicas y Naturales. Serie A. Matemáticas*, 109, pp.175-198. Available at: <https://doi.org/10.1007/s13398-014-0173-7>.
- Bakhtin, I.A. 1989. The contraction mapping principle in quasimetric spaces. *Func. An., Gos. Ped. Inst. Unianowsk*, 30, pp.26-37.
- Dosenovic, T., Radenovic, S. & Sedghi, S. 2018. Generalized metric spaces: Survey. *Turkic World Mathematical Society (TWMS) Journal of Pure and Applied Mathematics*, 9(1), pp.3-17 [online]. Available at: <https://www.twmsj.az/Abstract.aspx?Id=238> [Accessed: 26 April 2024].
- Mohanta, S.K. 2012. Some Fixed Point Theorems on G -Expansive Mappings. *Kyungpook Mathematical Journal*, 52(2), pp.155-165. Available at: <https://doi.org/10.5666/KMJ.2012.52.2.155>.
- Mojaradiafra, J. 2016. Fixed Point type Theorems in S -metric spaces. *Theory of Approximation and Applications*, 10(2), pp.33-41 [online]. Available at: <https://sanad.iau.ir/en/Article/909865> [Accessed: 26 April 2024].



Mojaradiafra, J. & Sabbaghan, M. 2021. Some new applications of S -metric spaces by weakly compatible pairs with a limit property. *The Pure and Applied Mathematics*, 28(1), pp.1-13. Available at: <https://doi.org/10.7468/jksmeb.2021.28.1.1>.

Mojaradiafra, J., Sabbaghan, M. & Taleghan, F. 2020. Some New Fixed Point Theorems For Expansive map on S -metric spaces. *Theory of Approximation and Applications*, 14(2), pp.57-64 [online]. Available at: <https://sanad.iau.ir/journal/msj/Article/690090?jid=690090> [Accessed: 26.4.2024].

Mustafa, Z., Awawdeh, F. & Shatanawi, W. 2010. Fixed Point Theorem for Expansive Mappings G -Metric Spaces. *International Journal of Contemporary Mathematical Sciences*, 5(50), pp.2463-2472 [online]. Available at: <https://www.m-hikari.com/ijcms-2010/49-52-2010/mustafalJCMS49-52-2010.pdf> [Accessed: 26 April 2024].

Mustafa, Z. & Sims, B. A. 2006. New approach to generalized metric spaces. *Journal of Nonlinear and Convex Analysis*, 7(2), pp.289-297 [online]. Available at: <http://www.yokohamapublishers.jp/online2/jncav7.html> [Accessed: 26 April 2024].

Sedghi, S. & Dung, N.V. 2014. Fixed point theorems on S -metric spaces. *Matematički vesnik*, 66(1), pp.113-124 [online]. Available at: <http://www.vesnik.math.rs/landing.php?p=mv141.cap&name=mv14112> [Accessed: 25 April 2024].

Sedghi, S., Shobe, N. & Aliouche, A. 2012. A generalization of fixed point theorems in S -metric spaces. *Matematički vesnik*, 64(3), pp.258-266 [online]. Available at: <http://www.vesnik.math.rs/landing.php?p=mv123.cap&name=mv12309> [Accessed: 25 April 2024].

Vujaković, J., Mitrović, S., Mitrović, Z. & Radenović, S. 2023. On Wardowski type results within G -metric spaces. *Research Gate* [online]. Available at: https://www.researchgate.net/publication/366440643_On_Wardowski_type_results_within_G-metric_spaces [Accessed: 26 April 2024].

Wang, S.Z., Li, B.Y., Gao, Z.M. & Iseki, K. 1984. Some fixed point theorems on expansion mappings. *Mathematica Japonica*, 29, pp.631-636.

Sobre algunos resultados de punto fijo para mapeos expansivos en espacios S -métricos

Nora Fetouci^a, Stojan Radenović^b

^a Universidad de Jijel, Laboratorio LMPA, Departamento de Matemáticas, Jijel, República Argelina Democrática y Popular, **autor de correspondencia**

^b Universidad de Belgrado, Facultad de Ingeniería Mecánica, Belgrado, República de Serbia

CAMPO: matemáticas

TIPO DE ARTÍCULO: artículo científico original

Resumen:

Introducción/objetivo: El objetivo de este artículo es establecer algunos resultados de existencia de un punto fijo para una clase de mapeos expansivos definidos en un espacio S -métrico completo.

Métodos: Se utilizó un esquema de iteración.

Resultados: Algunos resultados existentes de mapeos que satisfacen condiciones contractivas se expanden a resultados expansivos, proporcionando una nueva condición expresada en una variable bajo la cual se cumple la existencia de un punto fijo.

Conclusión: Este trabajo proporciona nuevas herramientas a la teoría del punto fijo junto con sus aplicaciones.

Palabras claves: punto fijo, espacio S -métrico, mapeo expansivo.

О некоторых результатах с неподвижной точкой в расширенных отображениях

Нора Фетучи^а, Стоян Раденович^б

^а Университет Джиджелы, лаборатория LMPA, математический факультет, г. Джиджел, Алжирская Народная Демократическая Республика, **корреспондент**

^б Белградский университет, машиностроительный факультет, г. Белград, Республика Сербия

РУБРИКА ГРНТИ: 27.25.17 Метрическая теория функций,
27.39.15 Линейные пространства,
снабженные топологией,
порядком и другими структурами

ВИД СТАТЬИ: оригинальная научная статья

Резюме:

Введение/цель: Цель данной статьи – выявить результаты о наличии неподвижной точки в классе расширяющихся отображений, определенных в полном S -метрическом пространстве.

Методы: В исследовании использована итерационная схема.

Результаты: В данной статье развернуты некоторые из существующих результатов расширяющихся отображений, которые были дополнены новыми сжимающими усло-



виями, выраженными одной переменной, при наличии неподвижной точки.

Выводы: В данной статье представлены способы применения новых инструментов в теории неподвижных точек.

Ключевые слова: неподвижная точка, S -метрическое пространство, расширенное отображение.

О неким резултатима фиксне тачке за експанзивна пресликавања у S -метричким просторима

Нора Фетучи^а, Стојан Раденовић^б

^а Универзитет у Цицелу, Лабораторија LMPA, Департман математике, Цицел, Народна Демократска Република Алжир, **аутор за преписку**

^б Универзитет у Београду, Машински факултет, Београд, Р. Србија

ОБЛАСТ: математика

КАТЕГОРИЈА (ТИП) ЧЛАНКА: оригинални научни рад

Сажетак:

Увод/циљ: Циљ овог рада јесте да установи неке резултате постојања фиксне тачке за класу експанзивних пресликавања дефинисаних на комплетном S -метричком простору.

Метод: У истраживању је примењена шема итерације.

Резултати: Проширени су неки постојећи резултати за експанзивна пресликавања са новим контрактивним условима израженим са једном променљивом под којом постоји фиксна тачка.

Закључак: Ауторски допринос пружа нове алате за теорију фиксне тачке и њихову примену.

Кључне речи: фиксна тачка, S -метрички простор, експанзивно пресликавање.

Paper received on: 28.03.2024.

Manuscript corrections submitted on: 23.09.2024.

Paper accepted for publishing on: 24.09.2024.

© 2024 The Authors. Published by Vojnotehnički glasnik / Military Technical Courier (<http://vtg.mod.gov.rs>, <http://vtr.mo.ynp.srb>). This article is an open access article distributed under the terms and conditions of the Creative Commons Attribution license (<http://creativecommons.org/licenses/by/3.0/rs/>).



Some considerations on the total stopping time for the Collatz problem

Nicola Fabiano^a, Nikola Mirkov^b, Stojan Radenović^c

^a University of Belgrade, “Vinča” Institute of Nuclear Sciences - National Institute of the Republic of Serbia, Belgrade, Republic of Serbia, e-mail: nicola.fabiano@gmail.com, **corresponding author**, ORCID iD: <https://orcid.org/0000-0003-1645-2071>

^b University of Belgrade, “Vinča” Institute of Nuclear Sciences - National Institute of the Republic of Serbia, Belgrade, Republic of Serbia, e-mail: nmirkov@vin.bg.ac.rs, ORCID iD: <https://orcid.org/0000-0002-3057-9784>

^c University of Belgrade, Faculty of Mechanical Engineering, Belgrade, Republic of Serbia, e-mail: radens@beotel.rs, ORCID iD: <https://orcid.org/0000-0001-8254-6688>

 <https://doi.org/10.5937/vojtehg72-50306>

FIELD: mathematics

ARTICLE TYPE: original scientific paper

Abstract:

Introduction/purpose: The Collatz conjecture has been considered and the stopping time needed for the recursive transformation to end has been investigated.

Methods: A statistical analysis on the stopping time has been used.

Results: The statistical approach shows that the probability of finding an infinite stopping time, that is a violation of the Collatz conjecture, is extremely low.

Conclusion: Picking precisely one particular atom in the Universe is still more favorable, by more than 61 orders of magnitude, than encountering an infinite total stopping time.

Key words: Collatz conjecture, recurrences, statistical analysis, curve fitting.

Introduction and definitions

The Collatz conjecture starts from a very simple function. For $N \in \mathbb{N}$ define $C(N)$ as

$$C(N) = \begin{cases} \frac{N}{2} & \text{if } N \text{ even,} \\ 3N + 1 & \text{if } N \text{ odd.} \end{cases} \quad (1)$$

This function applied recursively creates a sequence. Translating $C(N)$ to a sequence $\{a_i\}_{i \in \mathbb{N}}$, applying recursively the operation starting from a positive integer N , one could write a_i as follows:

$$a_i = \begin{cases} N & \text{for } i = 0 \\ C(a_{i-1}) & \text{for } i > 0, \end{cases} \quad (2)$$

so that a_i is obtained by iterating the application of C for i times, $C(C(C(\dots C(a_0))))$, written as $a_i = C(N)^i$.

Starting the sequence from $N = 12$, for instance, one has:

$$12, 6, 3, 10, 5, 16, 8, 4, 2, 1,$$

while the same procedure for $N = 3333$ leads to

$$3333, 10000, 5000, 2500, 1250, 625, 1876, 938, 469, 1408, 704, 352, 176, 88, 44, \\ 22, 11, 34, 17, 52, 26, 13, 40, 20, 10, 5, 16, 8, 4, 2, 1.$$

In both cases, the sequence ends in the same manner with the number 1. The number of steps necessary to end the sequence started with N , that is, to reach number 1, is called stopping time. The conjecture of Collatz, stated almost a hundred years ago in 1937 ([MacTutor, 2024](#)), is that for every $N \in \mathbb{N}$ the stopping time is finite. Up to now, there is no proof of the conjecture, or a counterexample disproving it. There is a huge amount of literature on the subject; for a short list, see, for example ([Applegate & Lagarias, 1995a,b](#); [Fabiano et al., 2021, 2023](#); [Guy, 2004](#); [Kurtz & Simon, 2007](#); [Lagarias, 1985](#); [Weisstein, 2024](#)) and the references therein. Empirical evidence, that is, numerical simulation, confirms the conjecture that the stopping time is finite for every N , and that there does not exist another ending sequence except from the one described above with the final number 1.

In this work, some results obtained for the stopping time and its consequences will be discussed.

Total stopping time

Collatz transformations (1) and (2) show that even numbers generate smaller numbers. In particular, powers of 2, 2^k , have the shortest total stopping times equal to k . Odd numbers clearly add more steps to the

sequence, thus increasing total stopping times. Therefore, even numbers generated from N tend to shorten the sequence, while odd numbers generate larger numbers that increase the stopping time. Let us define $E(N)$ as the number of even numbers generated by the sequence starting from the value N , and $O(N)$ as the number of odd numbers generated in the same sequence. Define the total stopping time $T(N)$ as

$$T(N) = \max_{N' \leq N} T(N') \quad (3)$$

for $N, N' \in \mathbb{N}$, being the largest stopping time for all numbers smaller or equal to N , which clearly has the property that $T(N) = E(N) + O(N)$. To provide some examples, the Collatz sequences for the first few numbers of \mathbb{N} are, respectively,

$N = 3$:

$$3, 10, 5, 16, 8, 4, 2, 1,$$

that is, $E(3) = 5$, $O(3) = 3$, so $T(3) = 8$.

$N = 4$:

$$4, 2, 1,$$

$E(4) = 2$, $O(4) = 1$, and $T(4) = 8$ because the loop of $N = 3$ is longer than the one of $N = 4$.

$N = 5$:

$$5, 16, 8, 4, 2, 1,$$

$E(5) = 4$, $O(5) = 2$, and $T(5) = 8$ once again for the same reason of the case $N = 4$.

From Collatz transformations (1) and (2), one could write the relation

$$2^{E(N)} = 3^{O(N)} \cdot N \cdot \text{Res}(N), \quad (4)$$

where $\text{Res}(N)$ is called the residue, and is defined as

$$\text{Res}(N) = \prod'_{0 \leq i < T(N)} \left(1 + \frac{1}{3C(N)^i} \right), \quad (5)$$

where \prod' means that the product is taken on all odd values of $C(N)^i$.

The coefficient R is defined as

$$R = \frac{E(N)}{O(N)}, \quad (6)$$

sometimes the inverse of R is called “completeness”. The following theorem could be stated:

THEOREM 1. For every $N \in \mathbb{N}$, $N > 1$:

$$R > \frac{\ln(3)}{\ln(2)} \approx 1.58. \quad (7)$$

Proof. Looking at eqs. (4) and (6) and taking the logarithm, it is possible to write

$$\frac{E(N)}{O(N)} = \frac{\ln(3)}{\ln(2)} + \frac{(\ln(N) + \ln \text{Res}(N))}{O(N) \ln(2)} > \frac{\ln(3)}{\ln(2)}. \quad (8)$$

□

The investigation shall now proceed further on the behaviour for large N of the residue (4). From eq. (1), $C(N) \geq N/2$, therefore

$$\text{Res}(N) \leq \prod'_{0 \leq i < T(N)} \left(1 + \frac{2^i}{3N^i}\right).$$

Rewriting the upper bound on the residue in the following manner

$$\text{Res}(N) \leq \exp \sum'_{0 \leq i < T(N)} \ln \left(1 + \frac{2^i}{3N^i}\right) \quad (9)$$

and taking the limit, one ends up with the result

$$\lim_{N \rightarrow +\infty} \ln(\text{Res}(N)) = 0. \quad (10)$$

The value of R (6) therefore could assume a range of values between $\ln(3)/\ln(2)$ and k , for $N = 2^k$, $N > 2$. The minimal value is reached in the case of an infinite total stopping time, while the value of k is reached when N equals powers of 2, 2^k . Conversely, the completeness has values in the range $[1/k, \ln(2)/\ln(3)]$.

Our analysis starts from the results shown in Figure 4a of (Fabiano et al., 2021, 2023) and further extends the analysis adding more points from

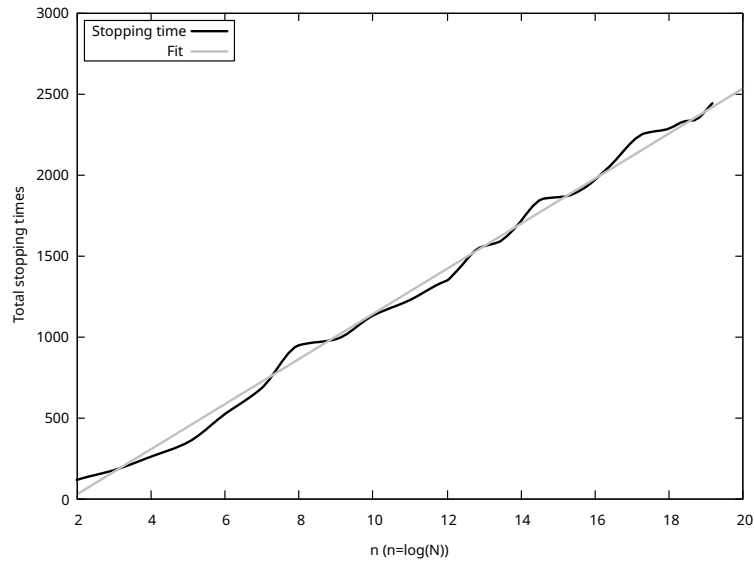


Figure 1 – Total stopping time as a function of $n = \log(N)$, compared to a linear fit

numerical analysis and also using the available data for the largest total stopping times discovered up to now (Roosendaal, 2024) for N of the order of 10^{20} .

Figure (1) shows the plot of the total stopping time as a function of n , $n = \log(N)$, together with a linear fit of the curve. There is clearly a behaviour with increasing n that reproduces remarkably well a linear function, from the fit $139.2n - 249.8$ with the correlation coefficient $r = 0.9972$ quite close to 1. Thus, the total stopping time does not departure significantly from its minimal value encountered for the discussed case of powers of 2, a purely linear function of $\log(N)$.

As a result, it is possible to infer that the behaviour of the total stopping time for large N is proportional to its log, that is,

$$T(N) \sim \log(N) . \tag{11}$$

Figure (2) presents the ratio of even to odd numbers for large N , formula (6), of the total stopping time when applying the Collatz procedure. It is apparent that this ratio decreases with growing N while seemingly approaching an asymptotic value larger than zero.

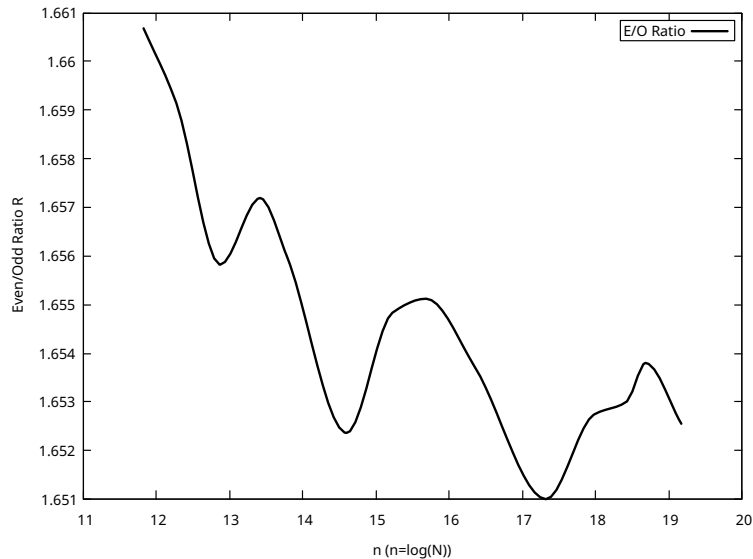


Figure 2 – Even to odd ratio for the total stopping time as a function of $n = \log(N)$

The statistics from the data of Figure (2) gives for the average of R and its standard deviation:

$$\bar{R} \pm \sigma_R = 1.65485 \pm 0.00272805 \quad (12)$$

We assumed that the results of eq. (12) represent a normal distribution. The hypothesis on the values of R being normally distributed has been supported by many tests effectuated on the data set, like Kolmogorov–Smirnov, Pearson χ^2 , Shapiro–Wilk, Anderson–Darling and Kuiper, which did not contradict it.

The distance of \bar{R} from the value of $\ln(3)/\ln(2)$ is given by 25.6181 times the standard deviation σ_R , that is, $\bar{R} - 25.6181\sigma_R = \ln(3)/\ln(2)$. The probability for this event to happen is smaller than 10^{-143} .

As a comparison term, the number of atoms in the Universe is of the order of 10^{82} , meaning that picking precisely one particular atom in the Universe is still more favorable, by more than 61 orders of magnitude, than encountering an infinite total stopping time. The current agreement for a discovery in particle physics should have at least a five sigma, 5σ , discrepancy with the already known physics of the Standard Model. Such an event has a probability to occur of less than 10^{-6} .

This result coming from statistical analysis infers that the probability of finding an infinite total stopping time is extremely tiny, being “zero” when compared to other already very small quantities encountered in Science.

It must be stressed however that this result for the finiteness of the total stopping time cannot rule out the possibility of existence of some values of N that under the Collatz procedure enter a different kind of loop not ending with 1.

References

Applegate, D. & Lagarias, J.C. 1995. Density bounds for the $3x + 1$ problem. I. Tree-search method. *Mathematics of Computation*, 64(209), pp.411-426. Available at: <https://doi.org/10.1090/S0025-5718-1995-1270612-0>.

Applegate, D. & Lagarias, J.C. 1995. Density Bounds for the $3x + 1$ Problem. II. Krasikov Inequalities. *Mathematics of Computation* 64(209), pp.427-438. Available at: <https://doi.org/10.1090/S0025-5718-1995-1270613-2>.

Fabiano, N., Mirkov, N. & Radenović, S. 2021. Collatz hypothesis and Planck’s black body radiation. *Journal of Siberian Federal University. Mathematics & Physics*, 17(3), pp.408-414 [online]. Available at: <https://www.mathnet.ru/eng/jsfu/v17/i3/p408> [Accessed: 4 April 2024].

Fabiano, N., Mirkov N., Mitrović, Z.D. & Radenović S. 2023. Chapter 3: Collatz Hypothesis and Kurepa’s Conjecture. In: *Advances in Number Theory and Applied Analysis*, pp.31-50. Available at: https://doi.org/10.1142/9789811272608_0003.

Guy, R.K. 2004. *Unsolved Problems in Number Theory, Third Edition*. Springer Science & Business Media. ISBN: 978-0387-20860-2.

Kurtz, S.A. & Simon, J. 2007. The Undecidability of the Generalized Collatz Problem. In: Cai, JY., Cooper, S.B. & Zhu, H. (Eds.) *Theory and Applications of Models of Computation. TAMC 2007. Lecture Notes in Computer Science*, 4484. Berlin, Heidelberg: Springer. Available at: https://doi.org/10.1007/978-3-540-72504-6_49.

Lagarias, J.C. 1985. The $3x + 1$ Problem and its Generalizations. *The American Mathematical Monthly*, 92(1), pp.3-23. Available at: <https://doi.org/10.1080/00029890.1985.11971528>.

MacTutor. 2024. Collatz conjecture. *MacTutor* [online]. Available at: <https://mathshistory.st-andrews.ac.uk/Biographies/Collatz> [Accessed: 4 April 2024].

Roosendaal, E. 2024. *On the $3x + 1$ problem* [online]. Available at: <http://www.ericr.nl/wondrous/delrecs.html> [Accessed: 4 April 2024].

Weisstein, E.W. 2024. Collatz Problem. *MathWorld—A Wolfram Web Resource* [online]. Available at: <https://mathworld.wolfram.com/CollatzProblem.html> [Accessed: 4 April 2024].

Algunas consideraciones sobre la detención del tiempo total para el problema de Collatz

Nicola Fabiano^a, **autor de correspondencia**, Nikola Mirkov^a, Stojan Radenović^b

^a Universidad de Belgrado, Instituto de Ciencias Nucleares "Vinča" - Instituto Nacional de la República de Serbia, Belgrado, República de Serbia

^b Universidad de Belgrado, Facultad de Ingeniería Mecánica, Belgrado, República de Serbia

CAMPO: matemáticas

TIPO DE ARTÍCULO: artículo científico original

Resumen:

Introducción/objetivo: Se ha considerado la conjetura de Collatz y el tiempo de parada necesario y se ha investigado la detención del tiempo necesaria para que finalice la transformación recursiva.

Métodos: Se ha utilizado un análisis estadístico de la detención del tiempo.

Resultados: El enfoque estadístico muestra que la probabilidad de encontrar una detención del tiempo infinito, es decir, una violación de la conjetura de Collatz, es extremadamente baja.

Conclusión: Escoger precisamente un átomo particular en el El universo es aún más favorable, en más de 61 órdenes de magnitud, que encontrar una detención del tiempo total infinita.

Palabras claves: Conjetura de Collatz, recurrencias, análisis estadístico, ajuste de curvas.

Некоторые соображения относительно общего времени остановки для задачи Коллатца

Никола Фабиано^a, **корреспондент**, Никола Мирков^a, Стоян Раденович^b

^a Белградский университет, Институт ядерных исследований «Винча» – Институт государственного значения для Республики Сербия, г. Белград, Республика Сербия

^b Белградский университет, факультет машиностроения, г. Белград, Республика Сербия

РУБРИКА ГРНТИ: 27.15.17 Элементарная теория чисел,
27.43.17 Математическая статистика

ВИД СТАТЬИ: оригинальная научная статья

Резюме:

Введение/цель: В данной статье рассмотрена гипотеза Коллатца и исследовано время остановки, необходимое для завершения рекурсивного преобразования.

Методы: Был использован статистический анализ времени остановки.

Результаты: Статистический подход показывает, что вероятность нахождения бесконечного времени остановки, то есть нарушения гипотезы Коллатца, чрезвычайно мала.

Вывод: Выбор именно одного конкретного атома во Вселенной большего на 61 порядок вероятнее, чем вероятность столкнуться с бесконечным общим временем остановки.

Ключевые слова: гипотеза Коллатца, рекуррентность, статистический анализ, подгонка кривой.

Нека разматрања о укупном времену заустављања за
Колацов проблем

Никола Фабиано^а, **аутор за преписку**, Никола Мирков^а,
Стојан Раденовић^б

^а Универзитет у Београду, Институт за нуклеарне науке “Винча” –
Национални институт Републике Србије,
Београд, Република Србија

^б Универзитет у Београду, Машински факултет,
Београд, Република Србија

ОБЛАСТ: математика

КАТЕГОРИЈА (ТИП) ЧЛАНКА: оригинални научни рад

Сажетак:

Увод/циљ: Размотрена је Колацова претпоставка и потребно време за заустављање рекурзивне трансформације.

Метод: Коришћена је статистичка анализа времена заустављања.

Резултати: Статистички приступ показује да је вероватноћа проналажења бесконачног времена заустављања, што нарушава Колацову хипотезу, изузетно ниска.

Закључак: Вероватноћа одабира тачно једног атома у целокупном универзуму је за више од 61 реда величине вероватнија од наилажења бројног низа са бесконачним временом заустављања у Колацовом проблему.

Кључне речи: Колацова хипотеза, понављања, статистичка анализа, апроксимација криве.

Paper received on: 08.04.2024.

Manuscript corrections submitted on: 23.09.2024.

Paper accepted for publishing on: 24.09.2024.

© 2024 The Authors. Published by Vojnotehnički glasnik / Military Technical Courier (<http://vtg.mod.gov.rs>, <http://vtr.mo.ynp.spb>). This article is an open access article distributed under the terms and conditions of the Creative Commons Attribution license (<http://creativecommons.org/licenses/by/3.0/rs/>).



New approach of Lebesgue integral in revised fuzzy cone metric spaces via unique coupled fixed point theorems

Ravichandhiran Thangathamizh^a, Angamuthu Muraliraj^b, Periyasamy Shanmugavel^c

^a Jeppiaar Institute of Technology (Autonomous), Department of Mathematics, Kanchipuram, Tamil Nadu, Republic of India, e-mail: thamizh1418@gmail.com, **corresponding author**, ORCID iD: <https://orcid.org/0000-0002-2449-5103>

^b Barathidasan University, Urumu Dhanalakshmi College, PG & Research Department of Mathematics, Trichy, Tamilnadu, Republic of India, e-mail: karguzali@gmail.com, ORCID iD: <https://orcid.org/0009-0007-6696-6683>

^c Periyar University, Selvamm Arts and Science College (Autonomous), Department of Mathematics, Namakkal, Tamil Nadu, Republic of India, e-mail: p.sham1988@gmail.com, ORCID iD: <https://orcid.org/0009-0004-8783-7088>

[doi https://doi.org/10.5937/vojtehg72-48816](https://doi.org/10.5937/vojtehg72-48816)

FIELD: mathematics

ARTICLE TYPE: original scientific paper

Abstract:

Introduction/purpose: This article introduces the concept of revised fuzzy cone contraction by using the concept of a triangular conorm and Revised Fuzzy Cone contractive conditions.

Methods: This article established new Revised Fuzzy Cone Contraction (RFC-C) type unique coupled Fixed Point theorems (FP theorems) in revised fuzzy cone metric spaces (RFCMS) by using the triangular property of RFCMS.

Results: The obtained results on fixed points in revised fuzzy cone metric spaces generalize some known results in the literature and present illustrative examples to support the main work.

Conclusion: The RFC contractive conditions generalize some important contraction types and examine the existence of a fixed point in revised fuzzy cone metric spaces. In addition, the Lebesgue integral type mapping is applied to get the existence result of a unique coupled fixed point in RFCMS to validate the main work.

Key words: revised fuzzy metric, revised fuzzy cone, fixed point.

Introduction

In the year 1965, Zadeh (Zadeh, 1965) introduced the concept of fuzzy sets which permit the gradual assessment of the membership of elements in a set. To use this concept in topology, Kramosil & Michálek (1975) introduced the class of fuzzy metric spaces [FMS]. After that, George & Veeramani (1994) modified the concept of fuzzy metric spaces and defined a Hausdorff topology on this fuzzy space. After that In 2015, the notion of fuzzy cone metric space (FCM space) was introduced by Öner et al. (2015). Grabiec (1988), gave the well-known Banach contraction principle in the case of fuzzy metric spaces, in the sense of Kramosil and Michalek.

Indeed, Huang & Zhang (2007) rediscovered the idea of a Banach-valued metric space. Indeed, many mathematicians proposed it, but it became popular after Huang and Zhang's study. By adopting the theory that the underlying cone is normal, they demonstrated the convergence properties and some FP-theorems. In 2015, Öner et al. (2015) gave the idea of a fuzzy cone metric space (FCM-space), and they also presented some fundamental properties and "a single-valued Banach contraction theorem for FP with the assumption that all the sequences are Cauchy." After that, Li et al. (2021) settled some generalized fuzzy cone contractive type FP-results neglecting that "all the sequences are Cauchy" in a complete FCM-space. And later, Jabeen et al. (2020) presented some common FP theorems for three self-mappings, by taking into consideration the idea of weakly compatible in FCM-spaces with an integral type application.

Chen et al. (2020), gave the idea of coupled fuzzy cone contractive-type mappings. They proved "some coupled FP-theorems in FCM-spaces with non-linear integral type application." Latterly Rehman & Aydi (2021) presented the concept of rational type fuzzy cone contraction mappings in FCM-spaces. They used "the triangular property of fuzzy metric" as a fundamental tool and proved some common FP-theorems and give an application. Guo & Lakshmikantham (1987) proved "coupled FP results for the nonlinear operator with applications". Later, Bhaskar & Lakshmikantham (2006) present some coupled FP-theorems in the context of partially ordered metric spaces, and this work is also presented by Lakshmikantham & Ćirić (2009). The concept of a cone metric space is introduced by Huang & Zhang (2007) and they also proved FP results. Some more fixed point results in a cone metric space and Fuzzy Metric spaces can be found in (Janković et al, 2010; Javed et al, 2021;

Kadelburg et al, 2011; Karapinar, 2010; Rezapour & Hambarani, 2008; Shamas et al, 2021) and the references therein.

Alexander Šostak (2018) additionally represented the idea of George-Veeramani Fuzzy Metrics Revised [RFMS]. Presently, Olga Grigorenko et al. (2020) introduced “On t-conorm primarily based Fuzzy (Pseudo) metrics”. In 2023, Muraliraj et al. (2023) proved some common coupled FP-results for commuting mappings in FMS. Muraliraj & Thangathamizh (2021b) introduced the concept of a Revised fuzzy modular metric space [RFMMS]. Moreover, Muraliraj & Thangathamizh (2023a) tend to prove that a Revised fuzzy cone topological space is pre-compact if and providing each sequence in it is a Cauchy subsequence. Further, we tend to show that $X_1 \times X_2$ may be a complete Revised fuzzy cone topological space if and providing X_1 and X_2 are complete Revised fuzzy cone metric areas. Finally, it is tried that each divisible Revised fuzzy cone topological space is second calculable and a mathematical space of a separable Revised fuzzy cone topological space is separable. Some more t-conorm results in various metric spaces can be found in (Kider, 2020, 2021; Muraliraj & Thangathamizh, 2021a, 2022, 2023b; Öner & Šostak, 2020; Parakath Nisha Bagam et al, 2024; Muraliraj et al, 2024) and the references therein.

This paper presents some unique coupled FP findings in RFCMS by taking the idea of Guo & Lakshmikantham (1987) and Chen et al. (2020). Furthermore, we have also presented an application of the two Lebesgue Integral Equations (LIE) for a common solution to uphold our work. This paper is organized as follows: Section 2 consists of preliminaries. Section 3 establishes some unique coupled FP-results in RFCMS with illustrative examples. Section 4 presents an application of Lebesgue integral mapping to get the existence result of unique coupled FP in RFCMS to hold up the main work. In Section 5, we discuss the conclusion of our work presenting the objectives and hypotheses of the research or intervention.

Prilimeries

Some fundamental definitions and lemmas are given in this section.

Definition 1 (George & Veeramani, 1994).

An operation $\odot : [0, 1]^2 \rightarrow [0, 1]$ is called a continuous t-conorm if

- (i) \odot is associative, commutative, and continuous
- (ii) $0 \odot q_1 = q_1$ and $q_1 \odot q_2 \leq q_3 \odot q_4$, whenever $q_1 \leq q_3$ and $q_2 \leq q_4$, $\forall q_1, q_2, q_3, q_4 \in [0, 1]$
- (iii) The maximum; $q_1 \odot q_2 = \max \{q_1, q_2\}$
- (iv) The product; $q_1 \odot q_2 = q_1 + q_2 - q_1 q_2$

(vi) The Lukasiewicz; $q_1 \odot q_2 = \min \{q_1 + q_2, 1\}$.

Definition 2 (Huang & Zhang, 2007).

Let E be a real Banach space and ϑ be the zero element of E , and p is a subset of E . Then, p is called a cone if,

- (i) p is closed and nonempty, and $p \neq \{\vartheta\}$
- (ii) $\alpha_1, \alpha_2 \in R, \alpha_1, \alpha_2 \geq 0$ and $\forall a, b \in p$, then $\alpha_1 a + \alpha_2 b \in p$
- (iii) both $a \in p$ and $-a \in p$ and then $a = \vartheta$

A partial ordering on a given cone $p \subset E$ is defined by $a \leq b \Leftrightarrow b - a \in p$. $a < b$ stands for $a \leq b$ and $a \neq b$, while $a \ll b$ stands for $b - a \in \text{int}\{p\}$. In this paper, all cones have nonempty interior.

Definition 3 (Šostak, 2018).

Let U be a set and $\odot: [0,1]^2 \rightarrow [0,1]$ is a continuous t-conorm. A RFMS, on the set U is a pair (N_0, \odot) or simply N_0 , where the mapping $N_0: U^2 \rightarrow [0, 1]$ satisfying the following conditions,

- (RF 1) $N_0(b_1, b_2, t) < 1$ and $N_0(b_1, b_2, t) = 0 \Leftrightarrow b_1 = b_2$
- (RF 2) $N_0(b_1, b_2, t) = N_0(b_2, b_1, t)$
- (RF 3) $N_0(b_1, b_2, t) \odot N_0(b_2, b_3, s) \geq N_0(b_1, b_3, t + s)$
- (RF 4) $N_0(b_1, b_2, -): (0, \infty) \rightarrow [0, 1]$ is right continuous $\forall b_1, b_2, b_3 \in U$ and $t, s > 0$. Then, (N_0, \odot) is said to be a RFM on \mathfrak{M} .

Definition 4 (Muraliraj & Thangathamizh, 2023).

A 3-tuple (U, N_0, \odot) is said to be RFCMS if p is a cone of E , U is an arbitrary set, \odot is a continuous t-conorm and (N_0, \odot) be a RFM on $U^2 \times \text{int}(p)$ satisfying the following conditions; $\forall b_1, b_2, b_3 \in U$ and $t, s \in \text{int}(p)$.

- i. $N_0(b_1, b_2, t) < 1$ and $N_0(b_1, b_2, t) = 0 \Leftrightarrow b_1 = b_2$
- ii. $N_0(b_1, b_2, t) = N_0(b_2, b_1, t)$
- iii. $N_0(b_1, b_2, t) \odot N_0(b_2, b_3, s) \geq N_0(b_1, b_3, t + s)$
- iv. $N_0(b_1, b_2, -): \text{int}(p) \rightarrow [0,1]$ is continuous.

Definition 5 (Muraliraj & Thangathamizh, 2023)

Let (U, N_0, \odot) is a RFCMS, $\exists b_1 \in U$ and $\{b_j\}$ be any sequence in U .

(i) $\{b_j\}$ converges to b_1 if for any $c \in (0, 1), t \gg \theta$, and $\exists j_1 \in N$ such that $N_0(b_j, b_1, t) < c$, for $j \geq j_1$. This can be written as $\lim_{j \rightarrow \infty} b_j = 0$, or $b_j \rightarrow b_1$ as $j \rightarrow \infty$.

(ii) (b_j) is Cauchy if for any $c \in (0, 1), t \gg \theta$ and $\exists j_1 \in N$ such that $N_0(b_j, b_k, t) < c$ for $j, k \geq j_1$.

(iii) (U, N_0, \odot) is complete if every Cauchy sequence is convergent in U

(iv) $\{b_j\}$ is RFC contractive if $\exists \alpha(0,1)$ so that

$$N_0(b_j, b_{j+1}, t) \leq \alpha \left(N_0(b_{j-1}, b_j, t) \right) \text{ for } t \gg \theta, j \geq 1. \quad (1)$$

Lemma 6

Let (U, N_0, \odot) is a RFCMS and a sequence

$$b_j \rightarrow b_1 \in U \Leftrightarrow N_0(b_j, b_1, t) \rightarrow 0 \text{ as } j \rightarrow \infty \text{ for each } t \gg \theta.$$

Definition 7

Let (U, N_0, \odot) is a RFCMS. The RFCM N_0 is triangular if

$$N_0(b_1, b_3, t) \leq N_0(b_1, b_2, t) + N_0(b_2, b_3, t), \forall b_1, b_2, b_3 \in U, t \gg \theta, \tag{2}$$

Definition 8

Let (U, N_0, \odot) is a RFCMS and $A: U \rightarrow U$. Then, A is called RFC contractive if there is $\alpha \in (0,1)$ so that

$$N_0(Ab_1, Ab_2, t) \leq \alpha(N_0(b_1, b_2, t)), \forall b_1, b_2 \in U \text{ and } t \gg \theta, \tag{3}$$

Definition 9

Let $(\lambda_j, \lambda_2) \in U^2$. Then, it is said to be coupled FP of a mapping $A : U^2 \rightarrow U$ if

$$\begin{aligned} A(b_2, b_3) &= b_2, \\ A(b_3, b_2) &= b_3. \end{aligned} \tag{4}$$

As a follow-up to our original work, we now prove a few special pair FP theorems in RFCMS with examples. Additionally, we offer a Lebesgue integral contractive type application.

Main results

Now, the first main result is presented.

Theorem 10.

Let $A : U^2 \rightarrow U$ is a mapping on complete RFCMS (U, N_0, \odot) in which N_0 is triangular and satisfies the following inequality

$$N_0(A(a, b), A(\xi, \zeta), t) \leq l(N_0(a, \xi, t)) + m(M(A(a, b), A(\xi, \zeta), t)) \tag{5}$$

where

$$M(A(a, b), A(\xi, \zeta), t) = \begin{cases} N_0(a, A(a, b), t) + N_0(\xi, A(\xi, \zeta), t) \\ + N_0(a, A(\xi, \zeta), t) + N_0(\xi, A(a, b), t) \end{cases} \tag{6}$$

$\forall a, b, \xi, \zeta \in U, t \geq \theta, l \in (0,1)$, and $m \geq 0$ with $(l + 4m) < 1$.

Then, A has a unique coupled FP in U .

Proof:

Any $a_0, b_0 \in U$; we define sequences $\{a_j\}$ and $\{b_j\}$ in U such that

$$A(a_j, b_j) = a_{j+1}, A(b_j, a_j) = b_{j+1}, \text{ for } j \geq 0. \tag{7}$$

From (5) for $t \geq \theta$, one gets

$$N_0(a_j, a_{j+1}, t) = N_0(A(a_{j-1}, b_{j-1}), A(a_j, b_j), t)$$

$$\leq l \left(N_0(a_{j-1}, a_j, t) \right) + m \left(M(A(a_{j-1}, b_{j-1}), A(a_j, b_j), t) \right), \quad (8)$$

where

$$\begin{aligned} M(A(a_{j-1}, b_{j-1}), A(a_j, b_j), t) &= \left(\begin{array}{c} N_0(a_{j-1}, A(a_{j-1}, b_{j-1}), t) + N_0(a_j, A(a_j, b_j), t) \\ + N_0(a_{j-1}, A(a_j, b_j), t) \end{array} \right) \quad (9) \\ &= \left(N_0(a_{j-1}, a_j, t), N_0(a_j, a_{j+1}, t), N_0(a_{j-1}, a_{j+1}, t) \right) \\ &\leq 2 \left(N_0(a_{j-1}, a_j, t) + N_0(a_j, a_{j+1}, t) \right) \end{aligned}$$

From (8) and (9), for $t \gg \vartheta$,

$$N_0(a_j, a_{j+1}, t) \leq l \left(N_0(a_{j-1}, a_j, t) \right) + 2m \left(N_0(a_{j-1}, a_j, t) + N_0(a_j, a_{j+1}, t) \right) \quad (10)$$

After simplification, one obtains

$$N_0(a_j, a_{j+1}, t) \leq \lambda \left(N_0(a_{j-1}, a_j, t) \right) \text{ for } t \gg \vartheta, \quad (11)$$

where $\lambda = \left(\frac{l+2m}{1-2m} \right) < 1$.

Similarly,

$$N_0(a_{j-1}, a_j, t) \leq \lambda \left(N_0(a_{j-2}, a_{j-1}, t) \right) \text{ for } t \gg \vartheta. \quad (12)$$

From (11) and (12), by induction, for $t \gg \vartheta$,

$$\begin{aligned} N_0(a_j, a_{j+1}, t) &\leq \lambda \left(N_0(a_{j-1}, a_j, t) \right) \leq \lambda^2 \left(N_0(a_{j-1}, a_j, t) \right) \\ &\leq \dots \leq \lambda^2 \left(N_0(a_0, a_1, t) \right) \rightarrow 0, \text{ as } j \rightarrow \infty. \end{aligned} \quad (13)$$

The above shows that $\{a_j\}$ be a RFC-C; therefore,

$$\lim_{j \rightarrow \infty} N_0(a_j, a_{j+1}, t) = 0, \text{ for } t \gg \vartheta. \quad (14)$$

Now for $i > j$ and for $t \gg \vartheta$, then

$$\begin{aligned} N_0(a_j + a_{j+1}, t) &\leq \left(N_0(a_j + a_{j+1}, t) + N_0(a_{j+1} + a_{j+2}, t) + \dots + \lambda^2 \left(N_0(a_{i-1} + a_i, t) \right) \right) \\ &\leq \lambda^j \left(N_0(a_0 + a_1, t) \right) + \lambda^{j+1} \left(N_0(a_0 + a_1, t) \right) + \dots + \lambda^{i-1} \left(N_0(a_0 + a_1, t) \right) \\ &= \left(\lambda^j + \lambda^{j+1} + \dots + \lambda^{i-1} \right) \left(N_0(a_0 + a_1, t) \right) \text{ as } j \rightarrow \infty. \\ &= \frac{\lambda^j}{1-\lambda} \left(N_0(a_0 + a_1, t) \right) \text{ as } j \rightarrow \infty. \end{aligned} \quad (15)$$

Hence, the sequence $\{a_j\}$ is Cauchy. Now for the sequence $\{b_j\}$ and from (5), for $t \gg \vartheta$, there is

$$\begin{aligned} N_0(b_j, b_{j+1}, t) &= N_0(A(b_{j-1}, b_{j-1}), A(b_j, a_j), t) \\ &\leq l \left(N_0(b_{j-1}, b_j, t) \right) + m \left(M(A(b_{j-1}, a_{j-1}), (b_j, a_j), t) \right), \end{aligned} \quad (16)$$

where

$$\begin{aligned} M(A(b_{j-1}, a_{j-1}), (b_j, a_j), t) &= \left(\begin{array}{c} N_0(b_{j-1}, A(b_{j-1}, a_{j-1}), t) + N_0(b_j, A(b_j, a_j), t) \\ + N_0(b_{j-1}, A(b_j, a_j), t) \end{array} \right) \\ &= \left(N_0(b_{j-1}, b_j, t) + N_0(b_j, b_{j+1}, t) + N_0(b_{j-1}, b_{j+1}, t) \right) \end{aligned}$$

$$= 2 \left(N_0(b_{j-1}, b_j, t) + N_0(b_j, b_{j+1}, t) \right) \tag{17}$$

Now, from (16) and (17), for $t \gg \vartheta$,

$$N_0(b_j, b_{j+1}, t) \leq l \left(N_0(b_{j-1}, b_j, t) \right) + 2m \left(N_0(b_{j-1}, b_j, t) + N_0(b_j, b_{j+1}, t) \right) \tag{18}$$

one gets, after simplification,

$$N_0(b_j, b_{j+1}, t) \leq \lambda \left(N_0(b_{j-1}, b_j, t) \right), \text{ for } t \gg \vartheta, \tag{19}$$

where $\lambda = \frac{(l+2m)}{(1-2m)} < 1$.

Similarly,

$$N_0(b_{j-1}, b_j, t) \leq \lambda \left(N_0(b_{j-2}, b_{j-1}, t) \right), \text{ for } t \gg \vartheta. \tag{20}$$

Now, from (19) and (20) and by induction, for $t \gg \vartheta$,

$$\begin{aligned} N_0(b_j, b_{j+1}, t) &\leq \lambda \left(N_0(b_{j-1}, b_j, t) \right) \leq \lambda^2 \left(N_0(b_{j-2}, b_{j-1}, t) \right) \\ &\leq \dots \leq \lambda^j \left(N_0(b_0, b_1, t) \right) \end{aligned} \tag{21}$$

It shows that the sequence $\{b_j\}$ is a RFC-C; therefore,

$$\lim_{j \rightarrow \infty} N_0(b_j, b_{j+1}, t) = 0, \text{ for } t \gg \vartheta. \tag{22}$$

Now, for $i > j$ and for $t \gg \vartheta$, there is

$$\begin{aligned} N_0(b_j, b_{j+1}, t) &\leq \left(N_0(b_j, b_{j+1}, t) \right) + \left(N_0(b_{j+1}, b_{j+2}, t) \right) + \dots + \lambda^2 \left(N_0(b_{i-1}, b_i, t) \right) \\ &\leq \lambda^j \left(N_0(b_0, b_1, t) \right) + \lambda^{j+1} \left(N_0(b_0, b_1, t) \right) + \dots + \lambda^{i-1} \left(N_0(b_0, b_1, t) \right) \\ &= \left(\lambda^j + \lambda^{j+1} + \dots + \lambda^{i-1} \right) \left(N_0(b_0, b_1, t) \right) \text{ as } j \rightarrow \infty. \\ &= \frac{\lambda^j}{1-\lambda} \left(N_0(b_0, b_1, t) \right) \text{ as } j \rightarrow \infty. \end{aligned} \tag{23}$$

Hence, the sequence $\{b_j\}$ is Cauchy. Since A is complete and $\{a_j\}, \{b_j\}$ are Cauchy sequences in A , so $\exists a, b \in A$ such that $a_j \rightarrow a$ and $b_j \rightarrow b$ as $j \rightarrow \infty$ or this can be written as $\lim_{j \rightarrow \infty} a_j = a$ and $\lim_{j \rightarrow \infty} b_j = b$.

Therefore,

$$\lim_{j \rightarrow \infty} N_0(a_j, a, t) = 0, \lim_{j \rightarrow \infty} N_0(b_j, b, t) = 0, \text{ for } t \gg \vartheta. \tag{24}$$

Hence,

$$\lim_{j \rightarrow \infty} a_{j+1} = \lim_{j \rightarrow \infty} A(a_j, b_j) = A(\lim_{j \rightarrow \infty} a_j, \lim_{j \rightarrow \infty} b_j) \Rightarrow A(a, b) = a. \tag{25}$$

Similarly,

$$\lim_{j \rightarrow \infty} b_{j+1} = \lim_{j \rightarrow \infty} A(b_j, a_j) = A(\lim_{j \rightarrow \infty} b_j, \lim_{j \rightarrow \infty} a_j) \Rightarrow A(b, a) = b. \tag{26}$$

Regarding its uniqueness, suppose (a_1, b_1) and (b_1, a_1) are another coupled FP pairs in U^2 such that $A(a_1, b_1) = a_1$ and $A(b_1, a_1) = b_1$. Now, from (5), for $t \gg \vartheta$, there exists

$$\begin{aligned} N_0(a, a_1, t) &= N_0(A(a, b), A(a_1, b_1), t) \\ &\leq l \left(N_0(a, a_1, t) \right) + m \left(M(A(a, b), (a_1, b_1), t) \right), \end{aligned} \tag{27}$$

where

$$\begin{aligned}
 M(A(a, b), (a_1, b_1), t) &= \left(N_0(a, A(a, b), t) + N_0(a_1, A(a_1, b_1), t) \right) \\
 &= \left(N_0(a, A(a_1, b_1), t) + N_0(a_1, A(a, b), t) \right) \\
 &= (N_0(a, a, t) + N_0(a_1, a_1, t) + N_0(a, a_1, t) + N_0(a_1, a, t)) \\
 &= 2(N_0(a, a_1, t)) .
 \end{aligned} \tag{28}$$

Now, from (27) and for $t \gg \vartheta$,

$$\begin{aligned}
 N_0(a, a_1, t) &\leq l(N_0(a, a_1, t)) + 2m(N_0(a, a_1, t)) = (l + 2m)(N_0(a, a_1, t)) \\
 &= (l + 2m) \leq (l + 2m)^2(N_0(a, a_1, t)) \\
 &\leq \dots \leq (l + 2m)^j(N_0(a, a_1, t)) \rightarrow 0, \text{ as } j \rightarrow \infty,
 \end{aligned} \tag{29}$$

where $(l + 2m) < 1$.

Hence, there exists $N_0(a, a_1, t) = 0$ for $a = a_1$ and $t \gg \vartheta$.

Similarly, again from (4), $t \gg \vartheta$, there is

$$\begin{aligned}
 N_0(b, b_1, t) &= N_0(A(b, a), A(b_1, a_1), t) \\
 &\leq l(N_0(b, b_1, t)) + m(M(A(b, a), (b_1, a_1), t)),
 \end{aligned} \tag{30}$$

where

$$\begin{aligned}
 M(A(b, a), (b_1, a_1), t) &= \left(N_0(b, A(b, a), t) + N_0(b_1, A(b_1, a_1), t) \right) \\
 &= \left(N_0(b, A(b_1, a_1), t) + N_0(b_1, A(b, a), t) \right) \\
 &= (N_0(b, b, t) + N_0(b_1, b_1, t) + N_0(b, b_1, t) + N_0(b_1, b, t)) \\
 &= 2(N_0(b, b_1, t))
 \end{aligned} \tag{31}$$

Now, from (30) and for $t \gg \vartheta$,

$$\begin{aligned}
 N_0(b, b_1, t) &\leq l(N_0(b, b_1, t)) + 2m(N_0(b, b_1, t)) = (l + 2m)(N_0(b, b_1, t)) \\
 &= (l + 2m) \leq (l + 2m)^2(N_0(b, b_1, t)) \\
 &\leq \dots \leq (l + 2m)^j(N_0(b, b_1, t)) \rightarrow 0, \text{ as } j \rightarrow \infty.
 \end{aligned} \tag{32}$$

Hence, there exists $N_0(b, b_1, t) = 0$ for $b = b_1$ and $t \gg \vartheta$.

Corollary 11

Let $A : U^2 \rightarrow U$ be a mapping on complete RFCMS (U, N_0, \odot) in which N_0 is triangular and satisfies

$$N_0(A(a, b), A(\xi, \zeta), t) \leq \left\{ \begin{array}{l} l(N_0(a, \xi, t)) \\ +m[N_0(a, A(a, b), t) + N_0(\xi, A(\xi, \zeta), t)] \end{array} \right\} \tag{33}$$

$\forall a, b, \xi, \zeta \in U, t \geq \vartheta, l \in (0, 1)$, and $m \geq 0$ with $(l + 2m) < 1$. Then, A has a unique coupled FP in U .

Corollary 12

Let $A : U^2 \rightarrow U$ be a mapping on complete RFCMS (U, N_0, \odot) in which N_0 is triangular and satisfies

$$N_0(A(a, b), A(\xi, \zeta), t) \leq \left\{ \begin{array}{l} l(N_0(a, \xi, t)) \\ +m[N_0(a, A(\xi, \zeta), t) + N_0(\xi, A(a, b), t)] \end{array} \right\} \tag{34}$$

$\forall a, b, \xi, \zeta \in U, t \geq \theta, l \in (0,1)$, and $m \geq 0$ with $(l + 2m) < 1$. Then, A has a unique coupled FP in U .

Example 13

$A = (0, \infty)$, \odot is a t-conorm, and $A : U^2 \times (0, \infty) \rightarrow [0,1]$ is defined as $N_0(a, b, t) = \frac{d(a,b)}{t+d(a,b)}, d(a, b) = |a - b|,$ (35)

$\forall a, b \in U$ and $t \geq \theta$. Then, it is easy to verify that N_0 is triangular and (U, N_0, \odot) is a complete RFCM-space. We define

$$A(g, h) = \begin{cases} \frac{a-b}{12}, & \text{if } a, b \in [0,1] \\ \frac{2a+2b-2}{3}, & \text{if } a, b \in [1, \infty). \end{cases} \quad (36)$$

Now from (5), for $t \geq \theta$, one obtains

$$N_0(A(a, b), A(\xi, \zeta), t) = \left(\begin{array}{c} \frac{1}{12}(N_0(a, \xi, t)) \\ + \frac{1}{12}(M(A(a, b), A(\xi, \zeta), t)) \end{array} \right), \text{ for } t \geq \theta. \quad (37)$$

It is easy to verify that conditions of Theorem 10 are satisfied with $l = m = \frac{1}{12}$. Then, A has unique coupled FP for $a = 2$ and $b = 2$.

$$A(a, b) = A(2,2) = \frac{2(2)+2(2)-2}{3} = 2 \Rightarrow A(2,2) = 2. \quad (38)$$

Theorem 14

Let $A : U^2 \rightarrow U$ be a mapping on complete RFCMS (U, N_0, \odot) in which N_0 is triangular and satisfies the inequality

$$N_0(A(a, b), A(\xi, \zeta), t) \leq \left\{ \begin{array}{c} l(N_0(a, \xi, t)) \\ + m(N_0(a, A(a, b), t) + N_0(\xi, A(\xi, \zeta), t)) \\ + n(N_0(\xi, A(a, b), t) \odot N_0(\xi, A(\xi, \zeta), t)) \end{array} \right\} \quad (39)$$

$\forall a, b, \xi, \zeta \in U, t \geq \theta, l \in (0,1)$, and $m, n \geq 0$ with $(l + 2m, n) < 1$. Then, A has a unique coupled FP in U .

Corollary 15

Let $A : U^2 \rightarrow U$ be a mapping on complete RFCMS (U, N_0, \odot) in which N_0 is triangular and satisfies the inequality

$$N_0(A(a, b), A(\xi, \zeta), t) \leq \left\{ \begin{array}{c} l(N_0(a, \xi, t)) \\ + n(N_0(\xi, A(a, b), t) \odot N_0(\xi, A(\xi, \zeta), t)) \end{array} \right\} \quad (40)$$

$\forall a, b, \xi, \zeta \in U, t \geq \theta, l \in (0,1)$, and $m, n \geq 0$ with $(l + 2m, n) < 1$. Then, A has a unique coupled FP in U .

Example 16

$A = (0, \infty)$, \odot is a t-conorm, and $A : U^2 \times (0, \infty) \rightarrow [0,1]$ is defined as

$$N_0(a, b, t) = \frac{d(a,b)}{t+d(a,b)}, d(a, b) = |a - b|, \quad (41)$$

$\forall a, b \in U$ and $t \geq \theta$. Then, it is easy to verify that N_0 is triangular and (U, N_0, \odot) is a complete RFCM-space. We define

$$A(g, h) = \begin{cases} \frac{a-b}{8}, & \text{if } a, b \in [0,1] \\ \frac{2a+2b-3}{3}, & \text{if } a, b \in [1, \infty). \end{cases} \quad (42)$$

Now from (39), for $t \geq \theta$, one obtains, for $t \geq \theta$,

$$N_0(A(a, b), A(\xi, \zeta), t) = \left(\begin{array}{c} \frac{1}{12}(N_0(a, \xi, t)) \\ + \frac{1}{8}(N_0(a, A(a, b), t) + N_0(\xi, A(\xi, \zeta), t)) \end{array} \right). \quad (43)$$

It is easy to verify that conditions of Theorem 13 are satisfied with $l = m = \frac{1}{8}$ and $n = 0$.

Then, A has unique coupled FP for $a = 2$ and $b = 2$.

$$A(a, b) = A(3,3) = \frac{2(3)+2(3)-2}{3} = 2 \Rightarrow A(3,3) = 3. \quad (44)$$

Application

In this section, we present an application of Lebesgue integral (LI) mapping to support our main work. In 2002, Branciari (Branciari, 2002) proved the following result on a complete metric space for a unique FP.

Theorem 17

Let (U, d) be a complete metric space, $\alpha \in (0,1)$, and $A: U \rightarrow U$ a mapping such that $\forall a, b \in U$,

$$\int_0^{d(Aa, Ab)} \varphi(s) ds \leq \alpha \int_0^{d(a,b)} \varphi(s) ds, \quad (45)$$

where $\varphi: (0, \infty) \rightarrow (0, \infty)$ is a Lebesgue integrable mapping which is summable (i.e., with finite integral on each compact subset of $(0, \infty)$) and for each $\tau > 0$,

$$\int_0^{d(a,b)} \varphi(s) ds. \quad (46)$$

Then, A has a unique FP $u \in U$ such that for any $a \in U$, $\lim_{j \rightarrow \infty} A_a^j = u$. Now, we are in the position to use the above concept and to prove a unique coupled FP-theorem in FCM-spaces.

Theorem 18

Let $A : U^2 \rightarrow U$ be a mapping on complete RFCMS (U, N_0, \odot) in which N_0 is triangular and satisfies the inequality

$$\int_0^{\tau} \varphi(s) ds \leq l \int_0^{\tau} \varphi(s) ds + m \int_0^{\tau} \varphi(s) ds$$

$$M(A(a, b), A(\xi, \zeta), t) = \left\{ \begin{array}{l} N_0(a, A(a, b), t) + N_0(\xi, A(\xi, \zeta), t) \\ + N_0(a, A(\xi, \zeta), t) + N_0(\xi, A(a, b), t) \end{array} \right\} \quad (47)$$

$\forall a, b, \xi, \zeta \in U, t \geq \theta, l \in (0,1)$, and $m \geq 0$ with $(l + 4m) < 1$ and where $\varphi: (0, \infty) \rightarrow (0, \infty)$ is a Lebesgue integrable mapping which is summable (i.e., with finite integral on each compact subset of $(0, \infty)$) and for each $\tau > 0$,

$$\int_0^{d(a,b)} \varphi(s) ds \quad (48)$$

Then, A has a unique coupled FP in U .

Conclusion

This article introduced the idea of coupled FP-results in RFCMS and used "the triangular property of RFCMS" to demonstrate certain special coupled FPT under the revised contractive type requirements. Some examples are provided that supported our conclusions as well. Furthermore, a Lebesgue integral mapping application is provided to enhance our primary findings. With the aid of this novel idea, it is possible to demonstrate more modified and universal contractive type coupled FP results with various integral contractive type of conditions and applications throughout the whole RFCMS.

References

Bhaskar, T.G. & Lakshmikantham, V. 2006. Fixed point theorems in partially ordered metric spaces and applications. *Nonlinear Analysis: Theory, Methods & Applications*, 65(7), pp.1379-1393. Available at: <https://doi.org/10.1016/j.na.2005.10.017>.

Branciari, A. 2002. A fixed point theorem for mappings satisfying a general contractive condition of integral type. *International Journal of Mathematics and Mathematical Sciences*, 29(9), pp.531-536 [online]. Available at: <https://eudml.org/doc/49397> [Accessed: 19 January 2024].

Chen, G.-X., Jabeen, S., Rehman, S.U., Khalil, A.M., Abbas, F., Kanwal, A. & Ullah, H. 2020. Coupled fixed point analysis in fuzzy cone metric spaces with

an application to nonlinear integral equations. *Advances in Differential Equations*, 2020, art.number: 671. Available at: <https://doi.org/10.1186/s13662-020-03132-8>.

George, A. & Veeramani, P. 1994. On some results in fuzzy metric spaces. *Fuzzy Sets and Systems*, 64(3), pp.395-399. Available at: [https://doi.org/10.1016/0165-0114\(94\)90162-7](https://doi.org/10.1016/0165-0114(94)90162-7).

Grabiec, M. 1988. Fixed points in fuzzy metric spaces. *Fuzzy Sets and Systems*, 27(3), pp.385-389. Available at: [https://doi.org/10.1016/0165-0114\(88\)90064-4](https://doi.org/10.1016/0165-0114(88)90064-4).

Grigorenko, O., Minana, J.J., Šostak, A. & Valero, O. 2020. On t -Conorm Based Fuzzy (Pseudo)metrics. *Axioms*, 9(3), art.number:78. Available at: <https://doi.org/10.3390/axioms9030078>.

Guo, D. & Lakshmikantham, V. 1987. Coupled fixed points of nonlinear operators with applications. *Nonlinear Analysis: Theory, Methods & Applications*, 11(5), pp.623-632. Available at: [https://doi.org/10.1016/0362-546X\(87\)90077-0](https://doi.org/10.1016/0362-546X(87)90077-0).

Huang, L.-G. & Zhang, X. 2007. Cone metric spaces and fixed point theorems of contractive mappings. *Journal of Mathematical Analysis and Applications*, 332(2), pp.1468-1476. Available at: <https://doi.org/10.1016/j.jmaa.2005.03.087>.

Jabeen, S., Rehman, S.U, Zheng, Z. & Wei, W. 2020. Weakly compatible and quasi-contraction results in fuzzy cone metric spaces with application to the Urysohn type integral equations. *Advances in Differential Equations*, 2020, art.number:280. Available at: <https://doi.org/10.1186/s13662-020-02743-5>.

Janković, S., Kadelburg, Z. & Radenović, S. 2011. On cone metric spaces: A survey. *Nonlinear Analysis: Theory, Methods & Applications*, 74(7), pp.2591-2601. Available at: <https://doi.org/10.1016/j.na.2010.12.014>.

Javed, K., Aydi, H., Uddin, F. & Arshad, M. 2021. On Orthogonal Partial b -Metric Spaces with an Application. *Journal of Mathematics*, 2021, art.ID:6692063. Available at: <https://doi.org/10.1155/2021/6692063>.

Kadelburg, Z., Radenović, S. & Rakočević, V. 2011. A note on the equivalence of some metric and cone metric fixed point results. *Applied Mathematics Letters*, 24(3), pp.370-374. Available at: <https://doi.org/10.1016/j.aml.2010.10.030>.

Karapinar, E. 2010. Some Nonunique Fixed Point Theorems of Ćirić Type on Cone Metric Spaces. *Abstract and Applied Analysis*, 2010, art.ID:123094. Available at: <https://doi.org/10.1155/2010/123094>.

Kider, J.R. 2020. Some Properties of Algebra Fuzzy Metric Space. *Journal of Al-Qadisiyah for Computer Science and Mathematics*, 12(2), pp.43-56. Available at: <https://doi.org/10.29304/jqcm.2020.12.2.695>.

Kider, J.R. 2021. Application of Fixed Point in Algebra Fuzzy Normed Spaces. *Journal of Physics: Conference Series*, 1879, art.number:022099. Available at: <https://doi.org/10.1088/1742-6596/1879/2/022099>.

Kramosil, I. & Michálek, J. 1975. Fuzzy metrics and statistical metric spaces. *Kybernetika*, 11(5), pp.336-344 [online]. Available at: <https://www.kybernetika.cz/content/1975/5/336> [Accessed: 19 January 2024].

Lakshmikantham, V. & Ćirić, L. 2009. Coupled fixed point theorems for nonlinear contractions in partially ordered metric spaces. *Nonlinear Analysis: Theory, Methods & Applications*, 70(12), pp.4341-4349. Available at: <https://doi.org/10.1016/j.na.2008.09.020>.

Li, X., Rehman, S.U., Khan, S.U., Aydi, H., Ahmad, J. & Hussain, N. 2021. Strong Coupled Fixed Point Results and Applications to Urysohn Integral Equations. *Dynamic Systems and Applications*, 30(2), pp.197-218. Available at: <https://doi.org/10.46719/dsa20213023>.

Muraliraj, A., Shanmugavel, P. & Thangathamizh, R. 2024. Fixed Point Theorems on Modular Revised Fuzzy Metric Spaces. *Communications on Applied Nonlinear Analysis*, 31(3s), pp.212-226. Available at: <https://doi.org/10.52783/cana.v31.760>.

Muraliraj, A. & Thangathamizh, R. 2021a. Fixed point theorems in revised fuzzy metric space. *Advances in Fuzzy Sets and Systems*, 26(2), pp.103-115. Available at: <https://doi.org/10.17654/FS026020103>.

Muraliraj, A. & Thangathamizh, R. 2021b. Introduction on Revised fuzzy modular spaces. *Global Journal of Pure and Applied Mathematics*, 17(2), pp.303-317. Available at: <https://doi.org/10.37622/GJPAM/17.2.2021.303-317>.

Muraliraj, A. & Thangathamizh, R. 2022. Relation-Theoretic Revised Fuzzy Banach Contraction Principle and Revised Fuzzy Edelstein Contraction Theorem. *JMSCM Journal of Mathematical Sciences & Computational Mathematics*, 3(2), pp.197-207. Available at: <https://doi.org/10.15864/jmscm.3205>.

Muraliraj, A. & Thangathamizh, R. 2023a. Some topological properties of revised fuzzy cone metric spaces. *Ratio Mathematica*, 47, pp.42-51. Available at: <https://doi.org/10.23755/rm.v47i0.734>.

Muraliraj, A. & Thangathamizh, R. 2023b. New Relation-Theoretic Fixed Point Theorems in Revised Fuzzy Metric Spaces with an Application to Fractional Differential Equations. *Communications in Mathematics and Applications*, 14(2), pp.865-880. Available at: <https://doi.org/10.26713/cma.v14i2.1772>.

Muraliraj, A., Thangathamizh, R., Popovic, N., Savic, A. & Radenovic, S. 2023. The First Rational Type Revised Fuzzy-Contractions in Revised Fuzzy Metric Spaces with an Applications. *Mathematics*, 11(10), art.number:2244. Available at: <https://doi.org/10.3390/math11102244>.

Öner, T., Kandemire, M.B. & Tanay, B. 2015. Fuzzy cone metric spaces. *Journal of Nonlinear Sciences and Applications*, 8(5), pp.610-616. Available at: <https://doi.org/10.22436/jnsa.008.05.13>.

Öner, T. & Šostak, A. 2020. On Metric-Type Spaces Based on Extended T -Conorms. *Mathematics*, 8(7), art.number:1097. Available at: <https://doi.org/10.3390/math8071097>.

Parakath Nisha Bagam, P., Sandhya, P., Thangathamizh, R., Shanmugavel, P., Sarathbabu, K. & Anusuya, R. 2024. Fixed Point Theorems in Revised Fuzzy Metric Space via R_F -Contraction. *Communications on Applied Nonlinear Analysis*, 31(3s), pp. Available at: <https://doi.org/10.52783/cana.v31.761>.

Rehman, S.U. & Aydi, H. 2021. Rational Fuzzy Cone Contractions on Fuzzy Cone Metric Spaces with an Application to Fredholm Integral Equations. *Journal*

of *Function Spaces*, 2021(1), art.number:5527864. Available at: <https://doi.org/10.1155/2021/5527864>.

Rezapour, S. & Hambarani, R. 2008. Some notes on the paper "Cone metric spaces and fixed point theorems of contractive mappings". *Journal of Mathematical Analysis and Applications*, 345(2), pp.719-724. Available at: <https://doi.org/10.1016/j.jmaa.2008.04.049>.

Shamas, I., Rehman, S.U., Aydi, H., Mahmood T. & Ameer, E. 2021. Unique Fixed-Point Results in Fuzzy Metric Spaces with an Application to Fredholm Integral Equations. *Journal of Function Spaces*, 2021, art.ID:429173. Available at: <https://doi.org/10.1155/2021/4429173>.

Šostak, A. 2018. George-Veeramani Fuzzy Metrics Revised. *Axioms*, 7(3), art.number:60. Available at: <https://doi.org/10.3390/axioms7030060>.

Zadeh, L.A. 1965. Fuzzy Sets. *Information and Control*, 8(3), pp.338-353. Available at: [https://doi.org/10.1016/S0019-9958\(65\)90241-X](https://doi.org/10.1016/S0019-9958(65)90241-X).

Nuevo enfoque de la integral de Lebesgue en espacios métricos de conos difusos revisados mediante teoremas de punto fijo acoplados únicos

Ravichandhira Thangathamizh^a, Angamuthu Muraliraj^b, Periyasamy Shanmugavel^c

^a Instituto de Tecnología Jeppiaar (Autónomo), Departamento de Matemáticas, Kanchipuram, Tamil Nadu, República de la India, **autor de correspondencia**

^b Universidad Barathidasan, Universidad Urumu Dhanalakshmi, PG y Departamento de Investigación de Matemáticas, Trichy, Tamilnadu, República de la India,

^c Universidad de Periyar, Facultad de Artes y Ciencias de Selvamm (autónoma), Departamento de Matemáticas, Namakkal, Tamil Nadu, República de la India,

CAMPO: matemáticas

TIPO DE ARTÍCULO: artículo científico original

Resumen:

Introducción/objetivo: Este artículo presenta el concepto de contracción revisada del cono difuso utilizando el concepto de conorma triangular y las condiciones contractivas revisadas del cono difuso.

Métodos: Este artículo estableció nuevos teoremas de punto fijo acoplados únicos (teoremas FP) del tipo de contracción difusa revisada (RFC-C) en espacios métricos de cono difuso revisados (RFCMS) mediante el uso de la propiedad triangular de RFCMS.

Resultados: Los resultados obtenidos en puntos fijos en espacios métricos de cono difuso revisados generalizan algunos resultados conocidos en la literatura y presentan ejemplos ilustrativos para respaldar el trabajo principal.

Conclusión: Las condiciones contractivas de RFC generalizan algunos tipos de contracción importantes y examinan la existencia de un punto fijo en espacios métricos de cono difuso revisados. Además, se aplica el mapeo de tipo integral de Lebesgue para obtener el resultado de existencia de un punto fijo acoplado único en RFCMS para validar el trabajo principal.

Palabras claves: métrica difusa revisada, cono difuso revisado, punto fijo.

Новый подход к интегралу Лебега в пересмотренных нечетких конусообразных метрических пространствах с помощью единой связанной неподвижной точки

Равичандиран Тангатамиж^а, Ангамуту Муралираджд^б,
Периясами Шанмуговилл^в

^а Технологический институт Джемпиара (автономный),
математический факультет, Канчипурам, Тамилнад, Республика Индия,
корреспондент

^б Университет Баратидасан, колледж Дханалакшми в Уруму,
Математический факультет и научно-исследовательский центр,
Тричи, Тамилнад, Республика Индия

^в Университет Перияр, Салемский колледж искусств и естественных наук
(автономный), математический факультет,
Намаккал, Тамилнад, Республика Индия

РУБРИКА ГРНТИ: 27.25.17 Метрическая теория функций,
27.39.15 Линейные пространства, снабженные
топологией, порядком и другими структурами

ВИД СТАТЬИ: оригинальная научная статья

Резюме:

Введение/цель: В данной статье представлена концепция пересмотренного сокращения нечеткого конуса с использованием концепции треугольника и пересмотренных условий сокращения нечеткого конуса.

Методы: В статье представлены новые пересмотренные теоремы об единой связанной неподвижной точке с типом сжатия нечеткого конуса (RFC-C) (теоремы FP) в пересмотренных метрических пространствах нечеткого конуса (RFCMS), используя свойство треугольности RFCMS.

Результаты: Полученные результаты по неподвижным точкам в пересмотренных нечетких конусообразных метрических пространствах обобщают некоторые известные результаты в литературе и представляют иллюстративные примеры в поддержку основной работы.

Выводы: Условия сжатия RFC обобщают некоторые важные типы сжатия и исследуют существование неподвижной точки в пересмотренных нечетких конусообразных метрических пространствах. Помимо того, отображение интегрального типа Лебега применяется для получения результата существования единой связанной фиксированной точки в RFCMS для подтверждения основной работы.

Ключевые слова: пересмотренная нечеткая метрика, пересмотренный нечеткий конус, неподвижная точка.

Нови приступ Лебеговом интегралу у прерађеним фази конусним метричким просторима помоћу теорема јединствене спрегнуте непокретне тачке

*Равичандиран Тангатамиж^а, Ангамуту Муралирац^б,
Перијасами Шанмугавил^в*

^а Институт за технологију Џепаир, Одељење за математику,
Канчипурам, Тамил Наду, Република Индија,
аутор за преписку

^б Универзитет Баратидасан, Уруну Даналакшми колеџ,
Одељење математике за последипломске и истраживачке студије,
Тиручирепали, Тамилнаду, Република Индија

^в Универзитет Периар, Колеџ уметности и науке Селвам (аутономни),
катедра математике, Намакал, Тамил Наду, Република Индија

ОБЛАСТ: математика

КАТЕГОРИЈА (ТИП) ЧЛАНКА: оригинални научни рад

Сажетак:

Увод/циљ: Овај рад уводи појам прерађене фазне конусне контракције помоћу концепта троугаоне конорме и прерађеног фазног конусног контрактивног услова.

Методе: Представљене су нове теореме јединствене спрегнуте непокретне тачке типа RFC-C (revised fuzzy cone contraction – преређене фази конусне контракције) у прерађеним фази конусним метричким просторима (RFCMS – revised fuzzy cone metric spaces) коришћењем својства троугла које поседују RFCMS.

Резултати: Добијени резултати на непокретним тачкама у прерађеним фази конусним метричким просторима генерализују неке познате резултате из литературе и представљају илустративне примере који подржавају основу овог рада.

Закључак: Контрактивни услови RFC генерализују неке важне типове контракција и испитују постојање непокретне тачке у прерађеним фази конусним метричким просторима. Примењено је и пресликавање типа Лебеговог интеграла за добијање резултата

јединствене спрегнуте непокретне тачке у RFCMS за валидацију овог рада.

Кључне речи: прерађена фази метрика, прерађен фази конус, непокретна тачка.

Paper received on: 20.01.2024.

Manuscript corrections submitted on: 22.09.2024.

Paper accepted for publishing on: 23.09.2024.

© 2024 The Authors. Published by Vojnotehnički glasnik / Military Technical Courier (www.vtg.mod.gov.rs, втг.мо.унп.срб). This article is an open access article distributed under the terms and conditions of the Creative Commons Attribution license (<http://creativecommons.org/licenses/by/3.0/rs/>).





Distinct features and validation of δ^* -algebras: an analytical exploration

Prakasam Muralikrishna^a, Perumal Hemavathi^b,
Raja Vinodkumar^c, Perumal Chanthini^d,
Kaliyaperumal Palanivel^e, Seyyed Ahmad Edalatpanah^f

^aMuthurangam Government Arts College (Autonomous), PG and Research
Department of Mathematics, Vellore, Republic of India,
e-mail: pmkrishna@rocketmail.com,
ORCID iD: <https://orcid.org/0000-0003-0652-2224>

^bSaveetha Institute of Medical and Technical Sciences (SIMATS),
Saveetha School of Engineering, Department of Mathematics,
Thandalam, Republic of India,
e-mail: hemavathip.sse@saveetha.com, **corresponding author**,
ORCID iD: <https://orcid.org/0000-0003-0607-2817>

^cPrathyusha Engineering College (Autonomous),
Department of Mathematics, Thiruvallur, Republic of India,
e-mail: vinodmaths85@gmail.com,
ORCID iD: <https://orcid.org/0000-0001-7847-4933>

^dCollege of Science & Humanities - SRMIST, Department of Computer
Applications, Potheri Campus, Republic of India,
e-mail: chanthini.srm@gmail.com,
ORCID iD: <https://orcid.org/0000-0003-0245-3065>

^eVellore Institute of Technology (VIT), School of Advanced Sciences,
Department of Mathematics, Vellore, Republic of India,
e-mail: drkpalanivel@gmail.com,
ORCID iD: <https://orcid.org/0000-0001-6389-7992>

^fAyandegan Institute of Higher Education, Department of
Applied Mathematics, Tonekabon, Islamic Republic of Iran,
e-mail: s.a.edalatpanah@aihe.ac.ir,
ORCID iD: <https://orcid.org/0000-0001-9349-5695>

 <https://doi.org/10.5937/vojtehg72-50294>

FIELD: mathematics

ARTICLE TYPE: original scientific paper

Abstract:

Introduction/purpose: This research introduces the concept of a δ^* -algebra, a unique structure in the field of abstract algebra. The study aims to explore the defining features and distinct properties of δ^* -algebras, distinguishing them from other algebraic systems and examining their interrelations with other types of algebras.

Methods: The methodology includes the formal definition and characterization of δ^* -algebras, a comparative analysis with the existing algebraic

structures, and an exploration of their interconnections. An algorithm is developed to verify whether a given structure meets the conditions of a δ^* -algebra.

Results: The results reveal that δ^* -algebras possess unique properties not found in other algebraic systems. The comparative study clarifies their distinctive place within the algebraic landscape and highlights significant interrelations with other structures. The verification algorithm proves effective in identifying δ^* -algebras, providing a systematic approach for further study.

Conclusions: In conclusion, δ^* -algebras represent a significant addition to abstract algebra, offering new theoretical insights and potential for future research. The study's findings enhance the understanding of algebraic systems and their interconnections, opening new avenues for exploration in the field.

Key words: δ^* -algebra, Fuzzy algebra, Fuzzy logic, Fuzzy sets.

Introduction

BCI and BCK algebras are foundational algebraic structures in universal algebra, first introduced by Iseki and Tanaka (Iséki & Tanaka, 1978). In 1999, the author pioneered the concept of QS-algebra, which is closely linked to BCI/BCK-algebras, and further explored the G-part of QS-algebra in the same context (Ahn & Kim, 1999). The author also delved into the concept of BP-algebra, examining its relationship with other associated algebras (Ahn & Han, 2013). Within the same study, the exploration of quadratic BP-algebra and its corresponding algebras was undertaken.

Akram and Kim (Akram & Kim, 2007) conducted research on BCI-algebra and K-algebra, presenting various studies and insights. A novel algebraic concept named Z-algebra was introduced in 2017 (Chandramouleeswaran et al., 2017), where the properties of this new notion were thoroughly reviewed and discussed. Kaviyarasu et al. (Kaviyarasu et al., 2017) introduced INK-algebras, which represents a significant development in algebraic theory. The notion of a J-algebra was initially introduced by Iseki et al. (Iséki et al., 2006). It was subsequently shown that a variety of d-algebras can be constructed from minimal sharp J-algebras. The study also delved into the disjointness digraph within J-algebras and explored Smarandache disjointness. Kim and Kim (Kim & Kim, 2008) extended the concept of B-algebras to BG-algebras by utilizing a non-group-derived, non-empty set as a foundation for constructing a BG-algebra. Furthermore,

several BG-algebra isomorphism theorems and associated properties were unveiled through the application of the concept of normal subalgebras.

As an extension of the BCK-algebra concept, a BE-algebra was introduced by Kim and Kim (Kim & Kim, 2006). Within BE-algebras, the concept of upper sets was leveraged to establish an equivalent condition for filters.

Kim and So (Kim & So, 2012) delved into the properties of β -algebras and their interconnections with β -algebras. They notably illustrated that $(\beta-, +)$ forms a semigroup with identity 0 when $(\beta-, -, +, 0)$ is a β -algebra. Specific constructions related to linear algebra within the field were also discussed.

Kim and Kim (Kim & Kim, 2006) introduced the notion of limited BM-algebras and delved into their properties. The concept of BO-algebra was initially introduced by Kim and Kim (Kim & Kim, 2012), highlighting that every BO-algebra is 0-commutative.

Expanding on dual BCK/BCI/BCH algebras and BE-algebras, Meng (Meng, 2010) proposed CI-algebras. This work explored the connections between BE-algebras and the core properties of CI-algebras, establishing that in transitive BE-algebras, the concept of ideals aligns with that of filters. Megalai and Tamilarasi (Megalai & Tamilarasi, 2010) introduced TM-algebra, offering comprehensive insights into its relationship with various algebraic structures. A group of algebras related to BCH, BCI, and BCK algebras, along with other notable groups, were introduced by Neggers and Kim (Neggers & Kim, 2002a). This class showcased an intriguing link between groups and B-algebras (Neggers & Kim, 2002b).

Neggers and Kim (Neggers & Kim, 1999) discussed a series of algebras that naturally bridge groups and sets. While this class encompasses various objects, it remains amenable to analysis using traditional methods.

Furthermore, after exploring the relationships between d-algebras and BCK-algebras, the concept of d-algebras emerged as another generalization of BCK-algebras. Jun et al. (Jun et al., 1998) introduced a BH-algebra which signifies a broader concept that encompasses BCH, BCI, and BCK-algebras. This generalization likely extends the understanding and application of these algebraic structures, offering a unified framework to study their properties and relationships. In 2007, BF-algebras were introduced as an extension of B-algebras, incorporating the concepts of an ideal and a normal ideal (Walendziak, 2007). This analytical exploration

aims to delve deeper into the unique attributes and defining characteristics of δ^* -algebras.

Preliminaries

This section presents some essential definitions with relevant examples that are needed to this article. Hereafter Σ is the Universal Set, $*$ is the binary operation on Σ , and 0 is the constant element in Σ unless otherwise specified.

DEFINITION 1. *The structure $(\Sigma, *, 0)$ is called a B-algebra, if*

- $\tilde{\Psi} * \tilde{\Psi} = 0$
- $\tilde{\Psi} * 0 = \tilde{\Psi}$
- $(\tilde{\Psi} * \tilde{\Lambda}) * \tilde{\Phi} = \tilde{\Psi} * (\tilde{\Phi} * (0 * \tilde{\Lambda}))$, $\forall \tilde{\Psi}, \tilde{\Lambda}, \tilde{\Phi} \in \Sigma$.

EXAMPLE 1. From the following table let $\Sigma = \{0, \alpha_{\varkappa_1}, \alpha_{\varkappa_2}\}$ be a B-algebra.

Table 1-B-algebra

$*$	0	α_{\varkappa_1}	α_{\varkappa_2}
0	0	α_{\varkappa_2}	α_{\varkappa_1}
α_{\varkappa_1}	α_{\varkappa_1}	0	α_{\varkappa_2}
α_{\varkappa_2}	α_{\varkappa_2}	α_{\varkappa_1}	0

DEFINITION 2. *The structure $(\Sigma, *, 0)$ is referred to as a BF-algebra, if*

- $\tilde{\Psi} * \tilde{\Psi} = 0$
- $\tilde{\Psi} * 0 = \tilde{\Psi}$
- $0 * (\tilde{\Psi} * \tilde{\Lambda}) = \tilde{\Lambda} * \tilde{\Psi} \quad \forall \tilde{\Psi}, \tilde{\Lambda} \in \Sigma$.

DEFINITION 3. *The structure $(\Sigma, *, 0)$ is called an AMR-algebra, if*

- $\tilde{\Psi} * 0 = \tilde{\Psi}$
- $(\tilde{\Psi} * \tilde{\Lambda}) * \tilde{\Phi} = \tilde{\Lambda} * (\tilde{\Phi} * \tilde{\Psi}) \quad \forall \tilde{\Psi}, \tilde{\Lambda}, \tilde{\Phi} \in \Sigma$.

*Let us define a binary relation $\tilde{\Psi} \leq \tilde{\Lambda}$ iff $\tilde{\Psi} * \tilde{\Lambda} = 0$*

EXAMPLE 2. Let $\Sigma = \{0, \alpha_{\varkappa_1}, \alpha_{\varkappa_2}, \alpha_{\varkappa_3}\}$ be a set with a binary operation $*$ defined by:

Table 2-AMR-algebra

$*$	0	α_{x_1}	α_{x_2}	α_{x_3}
0	0	α_{x_1}	α_{x_2}	α_{x_3}
α_{x_1}	α_{x_1}	α_{x_2}	α_{x_3}	0
α_{x_2}	α_{x_2}	α_{x_3}	0	α_{x_1}
α_{x_3}	α_{x_3}	0	α_{x_1}	α_{x_2}

Then $(\Sigma, *, 0)$ is an *AMR*-algebra.

DEFINITION 4. *The structure $(\Sigma, *, 0)$ is called a *Z*-algebra, if*

- $\tilde{\Psi} * \tilde{\Psi} = 0$
- $0 * \tilde{\Psi} = \tilde{\Psi}$
- $\tilde{\Psi} * \tilde{\Psi} = \tilde{\Psi}$
- $\tilde{\Psi} * \tilde{\Lambda} = \tilde{\Lambda} * \tilde{\Psi}$, when $\tilde{\Psi} \neq 0$ and $\tilde{\Lambda} \neq 0, \forall \tilde{\Psi}, \tilde{\Lambda} \in \Sigma$.

DEFINITION 5. *The structure $(\Sigma, *, 0)$ is called a *BCK*-algebra, if*

- $((\tilde{\Psi} * \tilde{\Lambda}) * (\tilde{\Psi} * \tilde{\Phi})) * (\tilde{\Phi} * \tilde{\Lambda}) = 0$
- $0 * \tilde{\Psi} = 0$
- $\tilde{\Psi} * \tilde{\Psi} = 0$
- $(\tilde{\Psi} * (\tilde{\Psi} * \tilde{\Lambda})) * \tilde{\Lambda} = 0$
- $\tilde{\Psi} * \tilde{\Lambda} = 0$ & $\tilde{\Lambda} * \tilde{\Psi} = 0$, imply $\tilde{\Psi} = \tilde{\Lambda}, \forall \tilde{\Psi}, \tilde{\Lambda} \in \Sigma$.

DEFINITION 6. *The structure $(\Sigma, *, 0)$ is called a *Q*-algebra, if*

- $\tilde{\Psi} * 0 = \tilde{\Psi}$
- $\tilde{\Psi} * \tilde{\Psi} = 0$
- $(\tilde{\Psi} * \tilde{\Lambda}) * \tilde{\Phi} = (\tilde{\Psi} * \tilde{\Phi}) * \tilde{\Lambda}, \forall \tilde{\Psi}, \tilde{\Lambda} \in \Sigma$.

DEFINITION 7. *The structure $(\Sigma, *, 0)$ is called a *TM*-algebra, if*

- $\tilde{\Psi} * 0 = \tilde{\Psi}$
- $(\tilde{\Psi} * \tilde{\Lambda}) * (\tilde{\Psi} * \tilde{\Phi}) = (\tilde{\Phi} * \tilde{\Lambda}), \forall \tilde{\Psi}, \tilde{\Lambda} \in \Sigma$.

DEFINITION 8. *The structure $(\Sigma, *, 0)$ is called a *BH*-algebra, if*

- $\tilde{\Psi} * 0 = \tilde{\Psi}$
- $\tilde{\Psi} * \tilde{\Psi} = 0$
- $\tilde{\Psi} * \tilde{\Lambda} = 0$ & $\tilde{\Lambda} * \tilde{\Psi} = 0$, implies $\tilde{\Psi} = \tilde{\Lambda}, \forall \tilde{\Psi}, \tilde{\Lambda} \in \Sigma$.

The structure of a δ^* -algebra

This section examines the features of a δ^* -algebra, a novel algebraic structure.

DEFINITION 9. *The structure $(\Sigma, *, 0)$ is called a δ^* -algebra, if*

(I) $0 * \tilde{\Psi} = \tilde{\Psi}$

(II) $\tilde{\Psi} * \tilde{\Psi} = 0$

(III) $(\tilde{\Psi} * (\tilde{\Lambda} * \tilde{\Phi})) * \tilde{\Psi} = (\tilde{\Psi} * \tilde{\Lambda}) * (\tilde{\Phi} * \tilde{\Psi}), \quad \forall \tilde{\Psi}, \tilde{\Lambda}, \tilde{\Phi} \in \Sigma.$

EXAMPLE 3. It is clear that $\Sigma = (\{0, \alpha_{\varkappa_1}, \alpha_{\varkappa_2}, \alpha_{\varkappa_3}\}, *, 0)$ is a δ^* -algebra from the following table.

Table 3- δ^ -algebra*

*	0	α_{\varkappa_1}	α_{\varkappa_2}	α_{\varkappa_3}
0	0	α_{\varkappa_1}	α_{\varkappa_2}	α_{\varkappa_3}
α_{\varkappa_1}	α_{\varkappa_1}	0	α_{\varkappa_1}	α_{\varkappa_2}
α_{\varkappa_2}	α_{\varkappa_2}	α_{\varkappa_1}	0	α_{\varkappa_3}
α_{\varkappa_3}	α_{\varkappa_3}	α_{\varkappa_2}	α_{\varkappa_3}	0

EXAMPLE 4. Consider the set $\Sigma = \{0, \alpha_{\varkappa_1}, \alpha_{\varkappa_2}, \alpha_{\varkappa_3}\}$ with a binary operation $*$ defined by

Table 4- δ^ -algebra*

*	0	α_{\varkappa_1}	α_{\varkappa_2}	α_{\varkappa_3}
0	0	α_{\varkappa_1}	α_{\varkappa_2}	α_{\varkappa_3}
α_{\varkappa_1}	α_{\varkappa_1}	0	α_{\varkappa_3}	α_{\varkappa_1}
α_{\varkappa_2}	α_{\varkappa_2}	α_{\varkappa_3}	0	α_{\varkappa_2}
α_{\varkappa_3}	α_{\varkappa_3}	α_{\varkappa_1}	α_{\varkappa_2}	0

Then $(\Sigma, *, 0)$ is a δ^* -algebra.

DEFINITION 10. *Let Σ be a non empty subset of a δ^* -algebra of Σ . Then Σ is referred to as a δ^* -subalgebra of Σ , if $\epsilon_1 * \epsilon_2 \in \Sigma, \forall \epsilon_1, \epsilon_2 \in \Sigma$.*

EXAMPLE 5. For the δ^* -algebra in Example 3.1, the subsets $A = \{\alpha_{\varkappa_1}, \alpha_{\varkappa_2}\} \subset \Sigma$ & $B = \{\alpha_{\varkappa_2}, \alpha_{\varkappa_3}\} \subset \Sigma$ are the δ^* -subalgebras of Σ , but the subset $C = \{\alpha_{\varkappa_1}, \alpha_{\varkappa_2}, \alpha_{\varkappa_3}\} \subset \Sigma$ is not a δ^* -subalgebra of Σ .

PROPOSITION 1. Let $(\Sigma, *, 0)$ be a δ^* -algebra. Then it is not a BCK-algebra (Iséki & Tanaka, 1978), INK-algebra (Kaviyarasu et al., 2017), BE-algebra (Kim & Kim, 2006), BF-algebra (Walendziak, 2007), QS-algebra (Ahn & Kim, 1999), BP-algebra (Ahn & Han, 2013), Z-algebra (Chandramouleeswaran et al., 2017), BM-algebra (Kim & Kim, 2006), BG-algebra (Kim & Kim, 2008), B-algebra (Neggers & Kim, 2002a) or BH-algebra (Jun et al., 1998).

Proof. In every aforementioned algebra mentioned here with the exception of a δ^* -algebra, observe that $(\tilde{\Psi} * (\tilde{\Lambda} * \tilde{\Phi})) * \tilde{\Psi} = (\tilde{\Psi} * \tilde{\Lambda}) * (\tilde{\Phi} * \tilde{\Psi}), \forall \tilde{\Psi}, \tilde{\Lambda}, \tilde{\Phi} \in \Sigma$. This Condition has been successfully introduced and implemented in example 3 and this type of condition was not used in any of the above cited algebras. \square

REMARK 1. The δ^* -algebra $(\Sigma, *, 0)$ provided in example 4 is not a B-algebra, since $(\alpha_{x_2} * \alpha_{x_1}) * \alpha_{x_3} = \alpha_{x_3} * \alpha_{x_3} = 0$ and $\alpha_{x_2} * (\alpha_{x_3} * (0 * \alpha_{x_1})) = \alpha_{x_2} * (\alpha_{x_3} * \alpha_{x_1}) = \alpha_{x_2} * \alpha_{x_1} = \alpha_{x_3}$ imply $(\alpha_{x_2} * \alpha_{x_1}) * \alpha_{x_3} \neq \alpha_{x_2} * (\alpha_{x_3} * (0 * \alpha_{x_1}))$.

LEMMA 1. If $(\Sigma, *, 0)$ is a δ^* -algebra, then $(\tilde{\Lambda} * \tilde{\Phi}) * \tilde{\Psi} = \tilde{\Lambda} * (\tilde{\Phi} * \tilde{\Psi})$ for any $\tilde{\Psi}, \tilde{\Lambda}, \tilde{\Phi} \in \Sigma$.

Proof. This follows from the axioms (I) and (II)

$$\begin{aligned} ie) (\tilde{\Lambda} * \tilde{\Phi}) * \tilde{\Psi} &= 0 * ((\tilde{\Lambda} * \tilde{\Phi}) * \tilde{\Psi}) && by(I) \\ &= (0 * \tilde{\Lambda}) * (\tilde{\Phi} * \tilde{\Psi}) && by(II) \\ &= \tilde{\Lambda} * (\tilde{\Phi} * \tilde{\Psi}) && by(I) \end{aligned}$$

\square

LEMMA 2. If $(\Sigma, *, 0)$ is a δ^* -algebra, then $(\tilde{\Psi} * (\tilde{\Lambda} * (0 * \tilde{\Lambda}))) * \tilde{\Psi} = \tilde{\Psi}$ for any $\tilde{\Psi}, \tilde{\Lambda} \in \Sigma$.

Proof. From axioms (III) $\tilde{\Phi} = 0 * \tilde{\Lambda}$, it is found that

$$\begin{aligned} (\tilde{\Psi} * (\tilde{\Lambda} * (0 * \tilde{\Lambda}))) * \tilde{\Psi} &= ((\tilde{\Psi} * \tilde{\Psi}) * (\tilde{\Lambda} * \tilde{\Psi})) \\ &= (0 * (\tilde{\Lambda} * \tilde{\Psi})) * \tilde{\Lambda} \end{aligned}$$

$$\begin{aligned}
 &= (\tilde{\Lambda} * \tilde{\Psi}) * \tilde{\Lambda} && \text{by(II)} \\
 &= \tilde{\Psi} * (\tilde{\Lambda} * \tilde{\Lambda}) && \text{by(I)} \\
 &= \tilde{\Psi} * 0 \\
 &= \tilde{\Psi} \quad \text{as claimed.}
 \end{aligned}$$

□

LEMMA 3. *If $(\Sigma, *, 0)$ is a δ^* -algebra, then $\tilde{\Phi} * \tilde{\Psi} = \tilde{\Phi} * \tilde{\Lambda}$ implies $\tilde{\Psi} = \tilde{\Lambda}$ for any $\tilde{\Psi}, \tilde{\Lambda}, \tilde{\Phi} \in \Sigma$.*

Proof. If $\tilde{\Phi} * \tilde{\Psi} = \tilde{\Phi} * \tilde{\Lambda}$, then $(\tilde{\Psi} * (\tilde{\Lambda} * (0 * \tilde{\Lambda}))) * \tilde{\Psi} = (\tilde{\Psi} * (\tilde{\Lambda} * (0 * \tilde{\Lambda}))) * \tilde{\Lambda}$ and thus by lemma 1 it follows that $\tilde{\Psi} = \tilde{\Lambda}$. □

LEMMA 4. *If $(\Sigma, *, 0)$ is a δ^* -algebra, then for any $\tilde{\Psi}, \tilde{\Lambda} \in \Sigma$ it follows that*

- (i) $\tilde{\Phi} * \tilde{\Psi} = 0$ implies $\tilde{\Psi} = \tilde{\Phi}$
- (ii) $0 * \tilde{\Psi} = 0 * \tilde{\Phi}$ implies $\tilde{\Psi} = \tilde{\Phi}$
- (iii) $\tilde{\Psi} * (0 * \tilde{\Psi}) = \tilde{\Psi}$.

Proof. (i) Since $\tilde{\Phi} * \tilde{\Psi} = 0$ implies $\tilde{\Phi} * \tilde{\Psi} = \tilde{\Phi} * \tilde{\Phi}$, it follows that $\tilde{\Psi} = \tilde{\Phi}$.

(ii) If $0 * \tilde{\Psi} = 0 * \tilde{\Phi}$, then $0 = \tilde{\Psi} * \tilde{\Psi} = (0 * (0 * \tilde{\Phi})) * \tilde{\Psi} = (0 * 0) * (\tilde{\Phi} * \tilde{\Psi}) = 0 * (\tilde{\Phi} * \tilde{\Psi}) = (\tilde{\Phi} * \tilde{\Psi})$ and thus by (i), $\tilde{\Psi} = \tilde{\Phi}$.

(iii) For any $\tilde{\Psi} \in \Sigma$, it is obtained that

$\tilde{\Psi} * (0 * \tilde{\Psi}) = (\tilde{\Psi} * (0 * \tilde{\Psi})) * \tilde{\Psi} = (\tilde{\Psi} * 0) * (\tilde{\Psi} * \tilde{\Psi})$ by axioms (I) and (II) it follows that $\tilde{\Psi} = \tilde{\Psi} * (0 * \tilde{\Psi})$ as claimed. □

Note that: Let $(\Sigma, *, 0)$ be a δ^* -algebra and let $\iota_* \in \Sigma$. Define $\iota_*^n = \iota_*^{(n-1)} * (0 * \iota_*) (n \geq 1)$ and $\iota_*^0 = \iota_*$. Note that $\iota_*^1 = \iota_*^0 * (0 * s) = s * (0 * \iota_*) = \iota_*$ by lemma 2.

LEMMA 5. *If $(\Sigma, *, 0)$ is a δ^* -algebra and let $s \in \Sigma$. Then $s^n * s^m = s^{n-m}$, where $n \geq m$.*

Proof. Let Σ is a δ^* -algebra. It is noted that by lemma 3 it follows that

$$s^2 * s = s^1 * (0 * s) * s = (s * 0) * (s * s) = s * 0 = s.$$

Assume that $s^{(n+1)} * s = s^n (n \geq 1)$. Then

$$\begin{aligned}
 s^{n+2} * s &= (s^{n+1} * (0 * s)) * s \\
 &= (s^{n+1} * 0) * (s * s) \\
 &= s^{n+1} * 0
 \end{aligned}$$

$$= s^{n+1}.$$

Assume $s^n * s^m = s^{n-m}$, where $n - m \geq 1$. Then

$$\begin{aligned} s^n * s^{m+1} &= s^n * ((0 * s^m) * s) \\ &= ((0 * s^m) * s) * s^n \\ &= (0 * s^m) * (s * s^n) \\ &= s^m * s^{n-1} \\ &= s^{n-1} * s^m \\ &= s^{n-(m+1)} \quad (n - m - 1 \geq 0). \end{aligned}$$

□

LEMMA 6. *If $(\Sigma, *, 0)$ is a δ^* -algebra and let $s \in \Sigma$. Then $s^n * s^m = s^{n-m}$, where $n \geq m$.*

Proof. Let Σ is a δ^* -algebra then note that by lemma 3 it follows that $s^2 * s = s^1 * (0 * s) * s = (s * 0) * (s * s) = s * 0 = s$.

Assume that $s^{(n+1)} * s = s^n$ ($n \geq 1$). Then

$$\begin{aligned} s^{n+2} * s &= (s^{n+1} * (0 * s)) * g \\ &= (s^{n+1} * 0) * (s * s) \\ &= s^{n+1} * 0 \\ &= s^{n+1}. \end{aligned}$$

Assume $s^n * s^m = s^{n-m}$, where $n - m \geq 1$. Then

$$\begin{aligned} s^n * s^{m+1} &= g^n * ((0 * s^m) * s) \\ &= ((0 * s^m) * s) * s^n \\ &= (0 * s^m) * (s * s^n) \\ &= s^m * s^{n-1} \\ &= s^{n-1} * s^m \\ &= s^{n-(m+1)} \quad (n - m - 1 \geq 0). \end{aligned}$$

□

LEMMA 7. *If $(\Sigma, *, 0)$ is a δ^* -algebra and let $s \in \Sigma$. Then $s^m * s^n = s^{n-1} * 0$, where $n \geq m$.*

Proof. Let Σ is a δ^* -algebra, By applying (I), (III) and lemma 3, it is follows that $s * s^2 = s * (s^1 * (0 * s)) = (s * 0) * (s^1 * s) = s * 0 = 0 * s$. Assume that $g * s^n = s^{(n-1)}$ where $(n \geq 1)$. Then

$$\begin{aligned} s * s^{n-1} &= g * (g^n * (0 * s)) \\ &= (s^n * (0 * s)) * s \\ &= (s^n * 0) * (s * s) \\ &= s^n * 0. \end{aligned}$$

Assume that $s^m * s^n = s^{n-m}$ where $n - m \geq 1$. Then

$$\begin{aligned} s^n * s^{m+1} &= s^n * ((s^m * (0 * s))) \\ &= (s^m * (0 * s)) * s^n \\ &= (s^m * 0) * (s * s^n) \\ &= s^m * s^{n-1} \\ &= s^{n-1} * s^m \\ &= 0 * s^{(n-m-1)} \quad (n - m - 1 \geq 0). \end{aligned}$$

□

It is summarized that the above lemmas:

THEOREM 1. *Let $(\Sigma, *, 0)$ is a δ^* -algebra and let $s \in \Sigma$. Then*

$$s^n * s^m = \begin{cases} s^{(n-m)} : & \text{if } n \geq m \\ 0 * s^{(n-m)} : & \text{otherwise.} \end{cases}$$

PROPOSITION 2. *Let $(\Sigma, *, 0)$ be a δ^* -algebra. Consequently, the subsequent outcomes are valid, for all $\varepsilon_x, \varepsilon_y \in \Sigma$.*

- (i) $(\varepsilon_x * (\varepsilon_x * (\varepsilon_y * \varepsilon_x))) = \varepsilon_x$, if $\varepsilon_y = 0$.
- (ii) $(\varepsilon_y * \varepsilon_x) = (\varepsilon_y * 0) * (x * 0)$.
- (iii) $(\varepsilon_x * \varepsilon_y) * [(\varepsilon_y * \varepsilon_x) * (\varepsilon_x * \varepsilon_y)] = \varepsilon_x * \varepsilon_y$.
- (iv) $0 * (\varepsilon_x * \varepsilon_y) = (0 * \varepsilon_x) * (0 * \varepsilon_y)$.
- (v) $(\Sigma, *, 0)$, $y * (0 * \varepsilon_x) = \varepsilon_y * \varepsilon_x$, $\varepsilon_x \neq \varepsilon_y$.



Proof. Let $(\Sigma, *, 0)$ be a δ^* -algebra, $\varepsilon_x, \varepsilon_y \in \Sigma$.
Suppose $y = 0$. Then,

$$\begin{aligned}
 (i) \quad (\varepsilon_x * (\varepsilon_x * (\varepsilon_y * \varepsilon_x))) &= (\varepsilon_x * (\varepsilon_x * (0 * \varepsilon_x))) \\
 &= (\varepsilon_x * (\varepsilon_x * \varepsilon_x)) \text{ by axiom(I)} \\
 &= (\varepsilon_x * 0) \text{ by axiom(II)} \\
 &= \varepsilon_x \text{ by axiom(I)}.
 \end{aligned}$$

$$\begin{aligned}
 (ii) \quad (\varepsilon_y * 0) * (\varepsilon_x * 0) &= (\varepsilon_y * (0 * \varepsilon_x)) * 0 \text{ by axiom(III)} \\
 &= (\varepsilon_y * \varepsilon_x) * 0 \text{ by axiom(I)} \\
 &= (\varepsilon_y * \varepsilon_x) \text{ by axiom(I)}.
 \end{aligned}$$

$$\begin{aligned}
 (iii) \quad (\varepsilon_x * \varepsilon_y) * [(\varepsilon_y * \varepsilon_x) * (\varepsilon_x * y)] \\
 &= (\varepsilon_x * \varepsilon_y) * [(\varepsilon_y * (\varepsilon_x * \varepsilon_x)) * \varepsilon_y] \text{ by axiom(III)}. \\
 &= (\varepsilon_x * \varepsilon_y) * ((\varepsilon_y * 0) * \varepsilon_y) \text{ by axiom(II)} \\
 &= (\varepsilon_x * \varepsilon_y) * (\varepsilon_y * \varepsilon_y) \text{ by axiom(I)} \\
 &= (\varepsilon_x * \varepsilon_y) * 0 \text{ by axiom(I)} \\
 &= \varepsilon_x * \varepsilon_y \text{ by axiom(I)}.
 \end{aligned}$$

$$\begin{aligned}
 (iv) \quad (0 * (\varepsilon_x * \varepsilon_y)) &= \varepsilon_x * \varepsilon_y \text{ by axiom(I)} \\
 &= (0 * \varepsilon_x) * (0 * \varepsilon_y) \text{ by axiom(II)}.
 \end{aligned}$$

$$\begin{aligned}
 (v) \quad (\varepsilon_y * (0 * \varepsilon_x)) &= (0 * \varepsilon_y) * (0 * \varepsilon_x) \text{ by axiom(I)} \\
 &= (\varepsilon_y * \varepsilon_x) \text{ by axiom(I)}.
 \end{aligned}$$

□

PROPOSITION 3. Let $(\Sigma, *, 0)$ and $(\Sigma', *', 0')$ be two δ^* -algebras. A mapping $z : \Sigma \rightarrow \Sigma'$ of a δ^* -algebras is referred to as a homomorphism, if $z(\varepsilon_x * \varepsilon_y) = z(\varepsilon_x) *' z(\varepsilon_y), \forall \varepsilon_x, \varepsilon_y \in \Sigma$.

DEFINITION 11. Let $(\Sigma, *, 0)$ and $(\Sigma', *', 0')$ be two δ^* -algebras. A mapping $z : \Sigma \rightarrow \Sigma'$ of δ^* -algebras is called a homomorphism. Then the kernel of z is the subset of Σ , defined by $\ker(z) = \{\varepsilon_x \in \Sigma : z(\varepsilon_x) = 0'\}$

LEMMA 8. Let $z : \Sigma \rightarrow \Sigma'$ be a homomorphism of a δ^* -algebra. Then $z(0) = 0', 0 \in \Sigma$.

Proof. Let $z : \Sigma \rightarrow \Sigma'$ be an homomorphism of δ^* -algebras. Then $z(0) = z(0 * 0) = z(0) *' z(0) = 0'$. \square

THEOREM 2. Let $(\Sigma, *, 0)$ and $(\Sigma', *', 0')$ be two δ^* -algebras. let $z : \Sigma \rightarrow \Sigma'$ be a surjective δ^* - homomorphism. If A is a δ^* -subalgebra of Σ , then $z(A)$ is a δ^* -subalgebra of Σ' .

Proof. Let $(\Sigma, *, 0)$ and $(\Sigma', *', 0')$ be two δ^* -algebras. Let $z : \Sigma \rightarrow \Sigma'$ be a homomorphism and A be a δ^* -subalgebra of Σ .

Now, $\varepsilon_a, \varepsilon_b \in A \Rightarrow \varepsilon_a * \varepsilon_b \in A \therefore z(\varepsilon_a), z(\varepsilon_b) \in z(A)$

$\Rightarrow z(\varepsilon_a) *' z(\varepsilon_b) = z(\varepsilon_a * \varepsilon_b) \in z(A)$

Hence $z(A)$ is a δ^* -algebra of Σ' . \square

THEOREM 3. Let $(\Sigma, *, 0)$ and $(\Sigma', *', 0')$ be two δ^* -algebras. Let $z : \Sigma \rightarrow \Sigma'$ be a surjective δ^* - homomorphism. If B is a δ^* -subalgebra of Σ' , then $z^{-1}(B)$ is a δ^* -subalgebra of Σ .

Proof. It is known that $z^{-1}(B) = \{x \in \Sigma : z(x) = y \text{ for some } y \in B\}$

Assume that x and $y \in z^{-1}(B)$. Then $z(\varepsilon_x), z(\varepsilon_y) \in (B)$.

Since B is a δ^* -subalgebra of Y ,

$\Rightarrow z(\varepsilon_x) *' z(\varepsilon_y) \in B$. Also, since z is a homomorphism, $z(\varepsilon_x * \varepsilon_y) = z(\varepsilon_x) *' z(\varepsilon_y) \in B, \therefore \varepsilon_x * \varepsilon_y \in z^{-1}(B)$.

Hence $z^{-1}(B)$ is a δ^* -algebra of Σ . \square

Algorithm for a δ^* -algebra

In this section, it is demonstrated that an algorithm to check the conditions of δ^* -algebras uses the values in between 0 and 1.

```
def generate_table(rows, cols):
```

```
# Create a list of labels for the rows and columns
```

```

labels = ['0'] + [chr(ord('a') + i) for i in range(cols - 1)]

# Print the header row
header = " ".join(labels[:cols])
print(header)

# Loop through the rows
for i in range(rows):
# Initialize the row with the label
row = [labels[i]]

# Loop through the columns
for j in range(1, cols):
# Fill in the cells based on the table pattern
if i == 0:
row.append(labels[j])
else:
row.append(labels[j] if j == i else labels[i])

# Print the row
print(" ".join(row))

# Call the function with 4 rows and 4 columns
generate_table(4, 4)

```

```

* 0 a b c
0 0 a b c
a a 0 a b
b b a 0 c
c c b c 0

```

Where $a = \alpha_{x_1}$, $b = \alpha_{x_2}$, $c = \alpha_{x_3}$ from the above pattern, the pattern according to the equation is the original table.

To prove the algebraic expression, it is necessary to show that the left-hand side (LHS) is equal to the right-hand side (RHS) for all possible combinations of the values 'a', 'b', and 'c'.

Let us break down the LHS and RHS step by step:

$$\text{LHS: } (a * (b * c)) * a$$

Start with ' a' '.

Find the value at the intersection of the row ' a' ' and the column corresponding to the value of $(b * c)$. In this case, $(b * c)$ can be found in the cell at the intersection of the row ' b' ' and the column ' c' '.

Finally, find the value at the intersection of the row corresponding to the result of $(a * (b * c))$ and the column ' a' '. In this case, the result of $(a * (b * c))$ can be found in the cell at the intersection of the row ' a' ' and the column corresponding to the value of $(b * c)$.

$$\text{RHS: } (a * b) * (c * a)$$

Start with ' a' '. Find the value at the intersection of the row ' a' ' and the column ' b' '. Find the value at the intersection of the row ' c' ' and the column ' a' '. Finally, find the value at the intersection of the row corresponding to the result of $(a * b)$ and the column corresponding to the result of $(c * a)$.

Now, let us go through the computations for each case:

LHS:

$$(a * (b * c)) * a = (a * (b * c)) * a = (a * (b * c))$$

RHS:

$$(a * b) * (c * a) = (a * b) * (c * a) = (a * (b * c))$$

It is evident that the LHS and RHS are both equal to $(a * (b * c))$, which means that the algebraic expression $(a * (b * c)) * a = (a * b) * (c * a)$ is true for all possible combinations of ' a' ', ' b' ', and ' c' '.

Therefore, the algebraic expression is proven to be true using the given table.

Conclusion

This study introduced a novel algebraic class, a δ^* -algebra which is deeply rooted in the foundational set theory principles. Through careful



analysis, it became evident that a δ^* -algebra stands apart from the existing algebraic structures, showcasing distinct characteristics and properties. Employing a unique methodology, the study meticulously formalized the concept of a δ^* -algebra, providing clarity and insight into its inner workings. As a result, a host of new results emerged from this exploration, each bolstered by relevant examples to illustrate its significance. This conceptual framework not only enriches our understanding of algebraic structures but also opens doors for further exploration and expansion into other algebraic substructures in future research endeavors.

References

- Ahn, S.S. & Kim, H.S. 1999. On QS-algebras. *Journal of the Chungcheong Mathematical Society*, 12(1), pp.33-41 [online]. Available at: <https://koreascience.kr/article/JAKO199917069750921.page> [Accessed: 15 May 2024].
- Ahn, S.S. & Han, J.S. 2013 On BP-Algebras. *Hacettepe Journal of Mathematics and Statistics*, 42(5), pp.551-557 [online]. Available at: <https://dergipark.org.tr/en/pub/hujms/issue/7746/101253> [Accessed: 15 May 2024].
- Akram, M. & Kim, H.S. 2007. On K-algebras and BCI-algebras. *International Mathematical Forum*, 2(9-12), pp.583-587. Available at: <https://doi.org/10.12988/imf.2007.07054>.
- Chandramouleeswaran, M., Muralikrishna, P., Sujatha, K. & Sabarinathan, S. 2017. A note on Z-algebra. *Italian Journal of Pure and Applied Mathematics*, 38, pp.707-714 [online]. Available at: https://ijpam.uniud.it/online_issue/201738/61-Chandramouleeswaran-Muralikrishna-Sujatha-Sabarinathan.pdf [Accessed: 15 May 2024].
- Iséki, K., Kim, H.S. & Neggers, J. 2006. On J-algebras. *Scientiae Mathematicae Japonicae*, 63(3), pp.413-420 [online]. Available at: <https://www.jams.or.jp/scm/contents/e-2006-3/2006-30.pdf> [Accessed: 15 May 2024].
- Iséki, K. & Tanaka, S. 1978. An introduction to the theory of BCK-algebras. *Mathematica Japonica*, 23(1), pp.1-26.
- Jun, Y.B., Roh, E.H. & Kim, H.S. 1998. On BH-Algebras. *Scientiae Mathematicae*, 1(3), pp.347-354 [online]. Available at: <https://www.jams.jp/scm/contents/Vol-1-3/1-3-12.pdf>. [Accessed: 15 May 2024].
- Kaviyarasu, M., Indhira, K. & Chandrasekaran, V.M. 2017. Introduction on INK-Algebras. *International Journal of Pure and Applied Mathematics*, 115(9), pp.1-9 [online]. Available at: <https://acadpubl.eu/jsi/2017-115-9/articles/9/1.pdf> [Accessed: 15 May 2024].

Kim, C.B. & Kim, H.S. 2006. On BM-algebras. *Scientiae Mathematicae Japonicae*, 63(3), pp.215-221 [online]. Available at: <https://www.jams.or.jp/scm/contents/e-2006-3/2006-22.pdf> [Accessed: 15 May 2024].

Kim, C.B. & Kim, H.S. 2008. On BG-algebras. *Demonstratio Mathematica*, 41(3), pp.497-506. Available at: <https://doi.org/10.1515/dema-2008-0303>.

Kim, C.B. & Kim, H.S. 2012. On BO-algebras. *Mathematica Slovaca*, 62(5), pp.855-864. Available at: <https://doi.org/10.2478/s12175-012-0050-9>.

Kim, H.S. & Kim, Y.H. 2006. On BE-algebras. *Scientiae Mathematicae Japonicae*, 66(1), pp.1299-1302 [online]. Available at: <https://www.jams.jp/scm/contents/e-2006-12/2006-120.pdf>. [Accessed: 15 May 2024].

Kim, Y.H. & So, K.S. 2012. β -algebras and related topics. *Communications of the Korean Mathematical Society*, 27(2), pp.217-222. Available at: <https://doi.org/10.4134/CKMS.2012.27.2.217>.

Megalai, K. & Tamilarasi, A. 2010. TM-algebra - An Introduction. *IJCA Special Issue on "Computer Aided Soft Computing Techniques for Imaging and Biomedical Applications" CASCT*, pp.17-23. Available at: <https://doi.org/10.5120/996-29>.

Meng, B.L. 2010. CI-algebras. *Scientiae Mathematicae Japonicae*, 71(1), pp.11-17. Available at: https://doi.org/10.32219/isms.71.1_11.

Neggers, J. & Kim, H.S. 1999. On d -algebras. *Mathematica Slovaca*, 49(1), pp.19-26 [online]. Available at: <http://dml.cz/dmlcz/129981> [Accessed: 15 May 2024].

Neggers, J. & Kim, H.S. 2002a. On B-algebras. *Matematički vesnik*, 54(1-2), pp.21-29 [online]. Available at: <https://scindeks.ceon.rs/article.aspx?artid=0025-51650202021N> [Accessed: 15 May 2024].

Neggers, J. & Kim, H.S. 2002b. On β -algebras. *Mathematica slovacica*, 52(5), pp.517-530 [online]. Available at: <http://dml.cz/dmlcz/131570> [Accessed: 15 May 2024].

Walendziak, A. 2007. On BF-algebras. *Mathematica Slovaca*, 57(2), pp.119-128. Available at: <https://doi.org/10.2478/s12175-007-0003-x>.

Características distintivas y validación de δ^* -álgebras: una exploración analítica

Prakasam Muralikrishna^a, Perumal Hemavathi^b,
Raja Vinodkumar^c, Perumal Chanthini^d,
Kaliyaperumal Palanivel^e, Seyyed Ahmad Edalatpanah^f

^a Muthurangam Escuela de Artes del Gobierno (Autónoma),
PG y Departamento de Investigación de Matemáticas,
Vellore, República de la India



- ^b Instituto Saveetha de Ciencias Médicas y Técnicas (SIMATS), Escuela de Ingeniería Saveetha, Departamento de Matemáticas, Thandalam, República de la India, **autor de correspondencia**
- ^c Prathyusha Facultad de Ingeniería (Autónoma), Departamento de Matemáticas, Thiruvallur, República de la India
- ^d Facultad de Ciencias y Humanidades - SRMIST, Departamento de Aplicaciones Informáticas, Campus Potheri, República de la India
- ^e Instituto de Tecnología Vellore (VIT), Facultad de Ciencias Avanzadas, Departamento de Matemáticas, Vellore, República de India
- ^f Instituto Ayandegan de Educación Superior, Departamento de Matemáticas Aplicadas, Tonekabon, República Islámica de Irán

CAMPO: matemáticas

TIPO DE ARTÍCULO: artículo científico original

Resumen:

Introducción/objetivo: Esta investigación introduce el concepto de δ^ -álgebra, una estructura única en el campo del álgebra abstracta. El estudio tiene como objetivo explorar las características determinantes y las propiedades distintivas de δ^* -álgebras, distinguiéndolos de otros sistemas algebraicos y examinando sus interrelaciones con otros tipos de álgebras.*

Métodos: La metodología incluye la definición formal y caracterización de δ^ -álgebras, un análisis comparativo con las estructuras algebraicas existentes y una exploración de sus interconexiones. Se desarrolla un algoritmo para verificar si una estructura determinada cumple las condiciones de un δ^* -álgebra.*

Resultados: Los resultados revelan que las δ^ -álgebras poseen propiedades únicas que no se encuentran en otros sistemas algebraicos. El estudio comparativo aclara su lugar distintivo dentro del panorama algebraico y destaca interrelaciones significativas con otras estructuras. El algoritmo de verificación resulta eficaz para identificar δ^* -álgebras, proporcionando un enfoque sistemático para estudios posteriores.*

Conclusión: En conclusión, las δ^ -álgebras representan una adición significativa al álgebra abstracta, ofreciendo nuevos conocimientos teóricos y potencial para investigaciones futuras. Los hallazgos del estudio mejoran la comprensión de los sistemas algebraicos y sus interconexiones, abriendo nuevas vías para la exploración en este campo.*

Palabras claves: δ^ -álgebra, Álgebra difusa, Lógica difusa, Conjuntos difusos.*

Отличительные особенности и валидация δ^* -алгебры:
аналитическое исследование

Пракасам Мураликришна^а, Перумал Хемавати^б,
Раджа Винодкумар^в, Перумалр Чантини^г,
Калияперумал Паланивел^д, Сейед Ахмад Эдалатпанах^е

^а Государственный колледж искусств Мутурангам (автономный),
Научно-исследовательский институт математического
факультета, Веллор, Республика Индия

^б Институт медицинских и технических наук Савиты (SIMATS),
инженерная школа Савиты, математический факультет,
Тандалам, Республика Индия, **корреспондент**

^в Инженерный колледж Пратьюша (автономный), математический
факультет, Тируваллур, Республика Индия

^г Колледж естественных и гуманитарных наук - SRMIST, кафедра
компьютерных приложений, кампус Потери, Республика Индия

^д Технологический институт Веллора (VIT), Школа передовых наук,
математический факультет, Веллор, Республика Индия

^е Аяндеганский институт высшего образования, факультет
прикладной математики, Тонекабон, Исламская Республика
Иран

РУБРИКА ГРНТИ: 27.17.00 Алгебра

ВИД СТАТЬИ: оригинальная научная статья

Резюме:

Введение/цель: В данном исследовании вводится понятие δ^* -алгебры с уникальной структурой в области абстрактной алгебры. Целью исследования является изучение определяющих особенностей и отличительных свойств δ^* -алгебр, отличающих ее от других алгебраических систем и изучение их взаимосвязи с другими типами алгебр.

Методы: Методология включает формальное определение и характеристику δ^* -алгебры, сравнительный анализ с существующими алгебраическими структурами и изучение их взаимосвязей. Разработан алгоритм для проверки, насколько данная структура удовлетворяет условия δ^* -алгебры.

Результаты: Результаты показали, что δ^* -алгебра обладает уникальными свойствами, которых нет в других алгебраических системах. Сравнительное исследование проясняет ее особое место в алгебраическом царстве и подчеркивает важные взаимосвязи с другими структурами.



ми. В статье также подтверждено, что алгоритм верификации эффективен в идентификации δ^* -алгебр и, таким образом, предоставляет систематический подход в дальнейших исследованиях.

Выводы: В заключении подчеркивается важная роль δ^* -алгебры в качестве значительного дополнения к абстрактной алгебре, представляя новые теоретические идеи и потенциал для будущих исследований. Результаты исследования расширяют понимание алгебраических систем и их взаимосвязей, открывая новые возможности для исследований в этой области.

Ключевые слова: δ^* -алгебра, нечеткая алгебра, нечеткая логика, нечеткие множества.

Изразите одлике и валидација δ^* -алгебри: аналитичко истраживање

Пракасам Мураликришна^а, Перумал Хемавати^б,
Раџа Винодкumar^в, Перумал Чантини^г,
Калиџалерумал Паланивел^д, Сејед Ахмад Едалатпанах^ђ

^а Државни уметнички колеџ Мутурангам (аутономни), Одељење математике за последипломске и истраживачке студије, Велор, Република Индија

^б Институт медицинских и техничких наука Савита (SIMATS), Електротехнички факултет Савита, Департман за математику, Тхандалам, Република Индија, **аутор за преписку**

^в Инжењерски колеџ Притушја (аутономни), Одсек за математику, Тирувалур, Република Индија

^г Факултет за науку и хуманистичке науке - SRMIST, Одељење за рачунарске апликације, Кампус Потхери, Република Индија

^д Технолошки институт Велор (VIT), Факултет напредних наука, Одсек за математику, Велор, Република Индија

^ђ Институт за високо образовање Ајандеган, Одсек за примењену математику, Тонекабон, Исламска Република Иран

ОБЛАСТ: математика

КАТЕГОРИЈА (ТИП) ЧЛАНКА: оригинални научни рад

Сажетак:

Увод/циљ: Ово истраживање уводи концепт δ^* -алгебре, јединствене структуре у области апстрактне алгебре. Циљ студије је да истражи карактеристичне црте и из-

разите одлике δ^* -алгебри да би се показало по чему се разликују од осталих алгебри и да би се испитали међусобни односи са другим врстама алгебри.

Методe: Методологија обухвата формалну дефиницију и карактеризацију δ^* -алгебри, компаративну анализу са постојећим алгебарским структурама као и истраживање њихових међусобних веза. Развијен је алгоритам да потврди да дата структура испуњава услове δ^* -алгебре.

Резултати: Резултати показују да δ^* -алгебре карактеришу јединствене одлике којих нема у другим алгебарским системима. Упоредна студија појашњава њихово посебно место у алгебарском царству и истиче важне међусобне везе са другим структурама. Показано је да је верификациони алгоритам ефикасан у идентификацији δ^* -алгебри, чиме се обезбеђује систематски приступ даљем истраживању.

Закључак: Може се закључити да су δ^* -алгебре значајан додатак апстрактној алгебри и да нуде нове теоријске увиде и потенцијале за даља истраживања. Налази ове студије проширују наше разумевање алгебарских система и њихових међусобних веза, отварајући истовремено нове путеве истраживања у овој области.

Кључне речи: δ^* -алгебра, фази алгебра, фази логика, фази скупови.

Paper received on: 07.04.2024.

Manuscript corrections submitted on: 24.09.2024.

Paper accepted for publishing on: 25.09.2024.

© 2024 The Authors. Published by Vojnotehnički glasnik / Military Technical Courier (<http://vtg.mod.gov.rs>, <http://vtr.mo.ynp.cb>). This article is an open access article distributed under the terms and conditions of the Creative Commons Attribution license (<http://creativecommons.org/licenses/by/3.0/rs/>).



Studying the dynamic characteristics of gas-operated guns using Solidworks Motion software

Phu M. Nguyen^a, Bien V. Vo^b,
Doan V. Dao^c, Dung V. Nguyen^d

Le Quy Don Technical University, Faculty of Special Equipments,
Hanoi City, Socialist Republic of Vietnam

^a e-mail: nguyenminhphu9793@gmail.com,
ORCID iD: <https://orcid.org/0009-0000-8599-1445>

^b e-mail: vovanbien@lqdtu.edu.vn, **corresponding author**,
ORCID iD: <https://orcid.org/0000-0002-1364-2884>

^c e-mail: daovandoan@lqdtu.edu.vn,
ORCID iD: <https://orcid.org/0000-0003-1360-3049>

^d e-mail: hdmta29@gmail.com,
ORCID iD: <https://orcid.org/0000-0002-2810-1204>

[doi https://doi.org/10.5937/vojtehg72-50987](https://doi.org/10.5937/vojtehg72-50987)

FIELD: mathematics, mechanical engineering

ARTICLE TYPE: original scientific paper

Abstract:

Introduction/purpose: This article presents a new approach to determining the dynamic characteristics of the automatic firing system of gas-operated automatic guns.

Methods: Based on the real structure of the automatic firing system of gas-operated automatic weapons, a 3D model of the gun is simulated using Solidworks software, and the dynamic characteristics of the automatic firing system are calculated on Solidworks Motion software.

Results: The obtained simulation results include displacement and velocity of the breech platform over time; the force exerted by the hammer on the bolt carrier over time; and impact force of the bolt carrier and gun body over time. These results are compared with data obtained from experiments to verify the mathematical model. The cycle of a shot according to test results is 0.0846 s and the firing rate error between theoretical and experimental results is 2.82%.

Conclusion: Research content allows users to visually evaluate the working process of all parts of the automatic firing system. The results of this research can be applied to calculations for automatic firing systems of different automatic guns. This is an important scientific basis for improving and upgrading existing automatic weapons and serving the process of designing and manufacturing new types of automatic weapons in the future.

Keywords: dynamics, automatic firing system, automatic weapons, gas-operated weapons, Solidworks Motion.

Introduction

For small automatic weapons, stability during firing is one of the factors that affect shooting accuracy, so studying the stability of weapons when firing is of significant importance for improving weapons to increase shooting accuracy. The stability of a gun is affected by many factors such as shooter's movements, surrounding environmental conditions, relative displacement, and collision of gun parts when shooting. In particular, the movement of parts in the gun's automatic firing system is a factor that can be determined. The characteristics of these movements are determined by solving the problem of the dynamics of the gun's automatic firing system when fired, see (Bien et al, 2021; Macko et al, 2021; Doan et al, 2023; Balla et al, 2010a).

Currently, there are two main methods commonly used to determine the dynamic characteristics of the automatic firing system of gas-operated automatic weapons. These are numerical methods and experimental methods. The numerical method is a method in which the establishment of a system of differential equations determining the relationship between components in the automatic firing system of a gun is carried out based on classical equations such as Newton's second law equation, Lagrange equation of the 2nd type, etc. The advantage of this method is that the calculation scope can be easily expanded and calculation options can be changed flexibly. In particular, the results of theoretical problems can be used to localize and predict experimental results during the research and design process. However, the structural shape of the parts of the automatic firing system is always complex, and the accuracy of the input parameters determined by sub-problems is not high (transmission ratio problem, efficiency problem, collision problem, etc.). Therefore, this method needs to use many assumptions, so the results obtained in all conditions are approximate and only capable of approaching reality, see (Balla & Mach, 2007; Balla et al, 2010b; Vitek, 2019). The experimental method is a method of determining the dynamic characteristics of an automatic firing system by measuring these parameters through specialized measuring equipment. The commonly used measuring equipment is mainly a high-speed camera system. The most outstanding advantage of using a high-speed camera system is its simplicity of use and quick preparation. With this method, any part of the gun can be identified.

However, the disadvantage of this method is that details with complex motion rules are difficult to determine, and high-precision measuring

devices are difficult to access. In addition, the implementation cost is relatively high (Vitek, 2019; Balla et al, 2015).

Today, with the high development of science and technology in the field of computers, associated with the evaluation/improvement/advancement of 3D simulation software (such as Inventor, SolidWorks, Adam, etc.), the application of simulation software to determine the dynamic components of structures has become easier and more accurate. There have been many studies on the application of 3D simulations in determining kinematic laws of simple structures and parts of the world, see (Fiser & Popelinsky, 2007; Fiser, 2007).

However, the application of 3D simulation software to determine the dynamic characteristics of the automatic firing system of automatic weapons is still limited. In this study, the authors applied 3D simulation software to determine the dynamic characteristics of an AK submachine gun in the Solidworks Motion working environment. The experimental process using a high-speed camera is used to determine the dynamic characteristics of the automatic machine. The dynamic simulation results are compared with the data obtained from experiments to evaluate the reliability of the implemented method.

Problem formulation

Set up a dynamic simulation model

The AK submachine gun is an automatic weapon that operates on the principle of gas extraction. The diagram of the working principle of a gas-operated automatic weapon is presented in Figure 1, see (Dung et al, 2023).

The working principle of gas-operated automatic weapons is that part of the gas in the barrel is extracted through the gas hole to provide energy for the automatic mechanism to perform the next shot. Gas-operated automatic weapons have many advantages such as simple structure, reliable operation, high accuracy, large effective range, and high rate of fire, see (Popelinsky & Balla, 2004; Allsop, 1997). With such outstanding advantages, it is widely used.

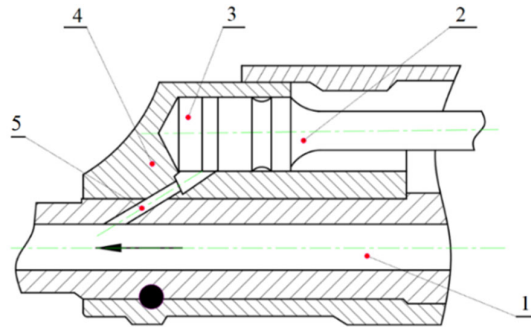


Figure 1 – Schematic arrangement of the gas piston
 1 - barrel; 2 - piston rod with the piston; 3 - cylinder; 4 - gas block; 5 - gas port

The main components of the AK submachine gun are listed in Figure 2.



Figure 2 – Main components of the AK submachine gun

With such a complex structure, using numerical methods to determine the dynamic characteristics of AK submachine guns is very difficult. Therefore, this method often uses many coefficients in the calculation process such as the collision recovery coefficient, the collapsed mass coefficient (Macko et al, 2021), etc. Experimental methods make it difficult to determine the movement characteristics of the hammer, the safety lever, and the characteristics of front and rear impacts between the bolt carrier and the gun body (Vitek, 2019). In addition, the cost of this method

is relatively high. Therefore, the method of using 3D computational simulation software is very suitable. The advantage of this method is that it provides intuitiveness in calculation. Determining the input parameters for this method is also relatively simple. This method gives relatively accurate and complete calculation results.

Creation of the parts geometry and the assembly mechanism

The automatic firing system of the AK submachine gun is a system with a complex structure. The connection between the details in the automatic firing system is in the form of pins, elastic springs, profile cams, or impact types. The assembly structure of the automatic firing system is divided into 8 main components as follows: gun body; bolt carrier and piston; carrier spring; hammer; safety lever; and magazine. The parts of the automatic firing system of the AK submachine gun are simulated according to the actual size of the part on Solidworks software as shown in Figure 3. In the Solidworks Assembly environment, it is necessary to click mate to assemble the gun parts.

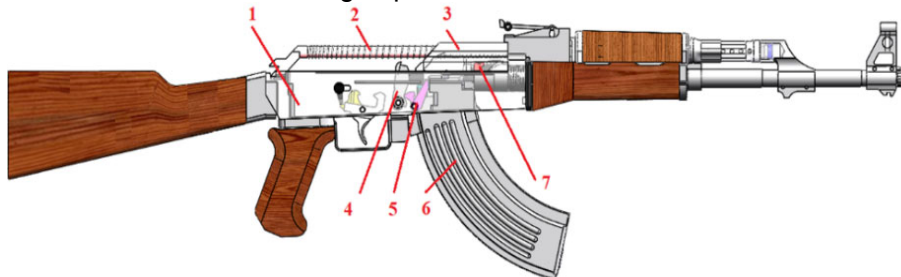


Figure 3 – 3D model of the AK submachine gun:
1 - gun body; 2 - return spring; 3 - bolt carrier and piston; 4 - hammer;
5 - safety lever; 6 - magazine, 7 - bolt

The stages of the SolidWorks Motion research

A motion study can be created from the Tools → Add-Ins menu and accessed from a Motion Study tab at the lower portion of the graphics area.

- Click Properties to set value in the Frames per second field. Activate Animate during the simulation and Show all Motion Analysis message options;

- Under Motion Analysis, click Advanced Options to Select GSTIFF solver, see (Nedelcu et al, 2020, 2011).

External forces acting on the automatic firing system

External forces acting on the automatic firing system when firing are shown in Figures 4 and 5. These forces have a cyclic nature when firing in series.

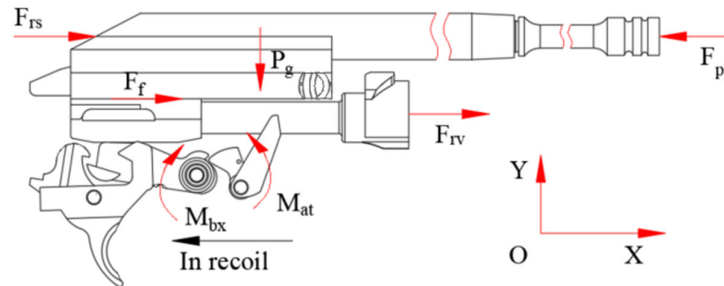


Figure 4 – External force acts on the automatic firing system when the bolt carrier recoils

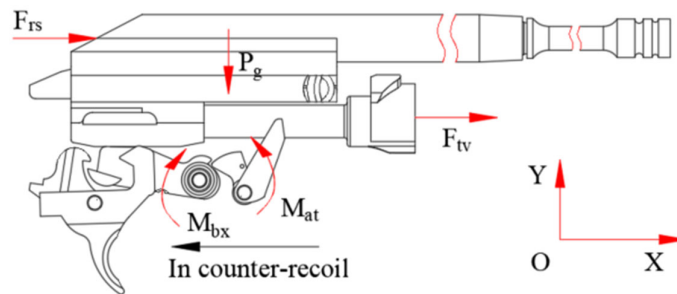


Figure 5 – External force acts on the automatic firing system when the bolt carrier is pushed up

The symbols of the force components in Figure 4 and Figure 5: F_{pi} – combustion gas pressure force acts on the piston; F_{rs} – force of the bolt carrier spring; F_f – friction force between the bolt carrier and the gun box; M_{bx} – torque of the torsion spring acts on the hammer; M_{at} – torque of the torsion spring acts on the safety lever; F_{rv} – bullet shell withdrawal force; F_{tv} – force that pushes the bullet into the chamber; and P_g – gravity of the bolt carrier.

- The force due to the combustion gas pressure in the gas chamber acts on the piston

For automatic firing systems of gas-operated automatic weapons, the force exerted on the piston by the combustion gas pressure in the gas

chamber is the energy for the automatic machine to work. Therefore, this is the input parameter to solve the dynamic problem of a gas-operated automatic machine. The force due to combustion gas pressure in the air chamber depends on the pressure in the air chamber and the piston cross-sectional area.

There are many methods to determine the pressure law in the air chamber. The Blagonrarov method does not reveal the law of variation of combustion gas pressure in the gas chamber over time, so it is not used currently, see (Allsop, 1997). The Mamontop method has solved the above deficiency, however, the calculation process is very complicated (Allsop, 1997). Calculation using the Bravin method is simpler and the results are also relatively accurate. Currently, with the development of computer science, the combustion gas pressure in the gas chamber is determined by simultaneously solving the interior ballistics equation, the gas chamber thermodynamic equation, and the motion equation of the automatic machine, see (Dung et al, 2023). However, the calculation volume of this method is too large, and continuously adjusting the calculation process is inappropriate. Therefore, the Bravin method chosen to determine the pressure in the air chamber is appropriate when the main concern is the pressure in the air chamber.

The equation for determining the combustion gas pressure in the gas chamber using the Bravin method is as follows:

$$p_b = p_\varphi e^{\frac{-t}{b}} (1 - e^{-\alpha \frac{t}{b}}) \quad (1)$$

The combustion gas pressure force in the gas chamber is determined according to the formula:

$$F_{pi} = p_b S_p \quad (2)$$

where: p_φ - gas pressure in the barrel at the moment the bullet passes through the gas hole. This pressure value is determined by solving the interior ballistics problem or by experimental methods; e - natural logarithm base; t - time during which the burning gas acts on the piston; α - coefficient takes into account the influence of the structural parameters of the air chamber (the method for determining this coefficient is presented in detail in the document (Fiser & Popelinsky, 2007)); and b is the Bravin coefficient. The results of calculating the pressure force in the gas chamber F_b are shown in Figure 6.

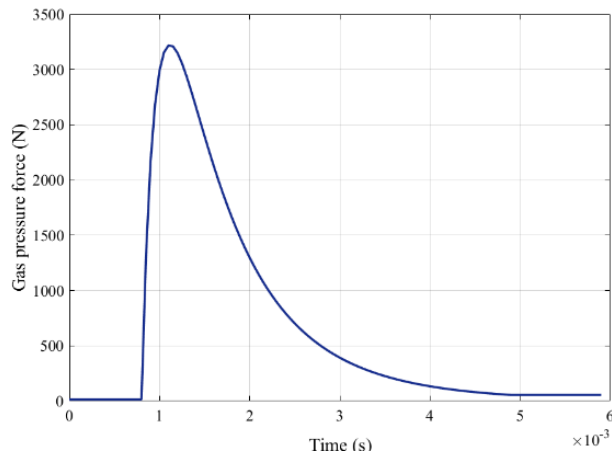


Figure 6 – Graph of combustion gas pressure force in the gas chamber

- The force of the return spring

This force acts on the weapon casing and the bolt carrier throughout the whole functional cycle. The return spring force significantly influences the function cycle of the weapon. It is usually considered linear and is determined by the following formula:

$$F_{rs} = F_{rs0} + k_{rs} \cdot X \quad (3)$$

where F_{rs0} is the return spring pre-tension force; k_{rs} is the stiffness of the return spring; and X is the deformation of the return spring.

The hardness of the return spring is determined by experimental methods. The return spring of the AK submachine gun and the fixture for the experiment are shown in Figure 7.



Figure 7 – Return springs

The jig model for the experiment is presented in Figure 8. The hardness of the return spring is determined experimentally using the ST-1000 SALT multi-purpose tensile and compression machine. When compressing the spring, the display screen of the compression machine will display the force according to the compression of the spring, see Figure 9. Based on the results obtained experimentally, the stiffness of the push-back spring is determined according to Huc's law.



Figure 8 – Deploy an experiment to measure spring hardness

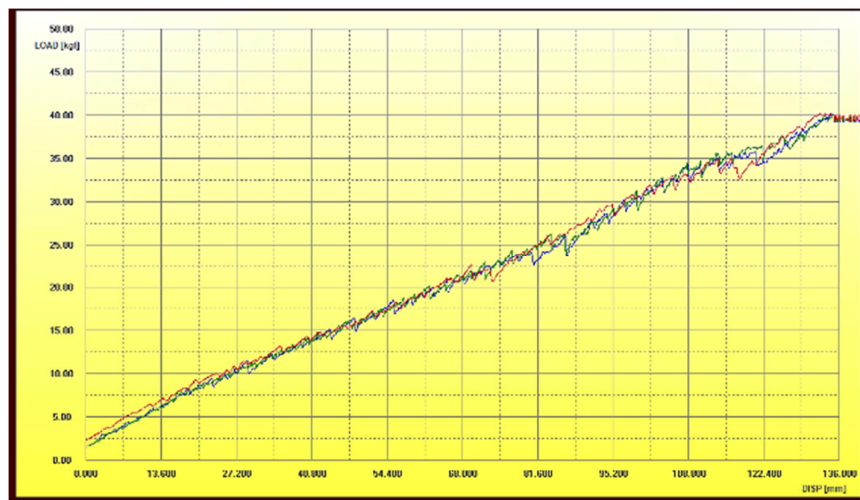


Figure 9 – Graph of compression force versus spring compression

- *The friction force between the bolt carrier and the gun box*

Friction force calculation is a very complex and important problem in calculating the dynamics of the automatic firing system. The friction force is the variable force during the movement of the breech block carrier, and it depends on a lot of factors. The friction force acting on the automatic firing system occurs in many positions, such as the friction force between the breech block carrier and the receiver assembly, the friction force between the breech block carrier and the bolt, the friction force between the breech block carrier and the working mechanisms, the friction force is caused by the collision, etc. In practice, however, the friction force between the breech block carrier and the receiver assembly is much larger than other friction forces. Therefore, to simplify the analysis, the authors only consider the friction force between the breech block carrier and the receiver assembly while the other friction forces are neglected. The effect of this simplification on the accuracy of the final solution is negligible.

The friction force between the breech block carrier and the receiver assembly is proportional to the normal contact force, as given in equation (4):

$$F_f = \mu \cdot N \tag{4}$$

The coefficient μ is called the coefficient of friction. Often two values of μ are quoted: the coefficient of static friction μ_s , which applies to the onset of sliding, and the coefficient of kinetic friction μ_k , which applies during a sliding motion. The coefficient of friction between the breech block carrier and the receiver assembly is determined by the experiment, see (Fiser & Popelinsky, 2007); N is the reaction force of the gun box acting on the bolt carrier.

The normal contact force is determined by the following formula:

$$N = m_{\Sigma} \cdot g \tag{5}$$

where m_{Σ} is the total breech block carrier mass and g is the acceleration of gravity.

- *Force to withdraw the bullet case*

The force required to remove the empty cartridge case from the chamber acts until the chamber is completely clear of the cartridge case. This force is determined by the friction force, F_{ms} , between the cartridge case and the chamber wall, which is determined by the propellant gas pressure acting on the inner surface of the cartridge case. The diagram used to calculate the cartridge case extraction force is illustrated in Figure 10, see (Tien et al, 2021).

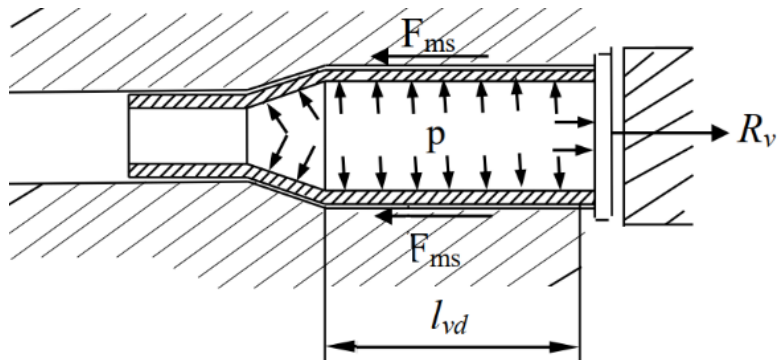


Figure 10 – Diagram to calculate force when extracting the cartridge case:
 R_v - the force of casing withdrawal; p is the pressure in the combustion chamber;
 F_{ms} - the friction force between the casing and the bullet chamber wall;
 l_{vd} - the length of the cylindrical part of the casing

Normally, small automatic weapons usually use cartridges which are cylindrical cartridge cases and short. Therefore, the cartridge case extraction force, R_v is determined according to the following approximate formula, see (Tien et al, 2022; Dung et al, 2023):

$$R_v = 2\pi f \cdot l_{vd} \cdot E_n \cdot \delta \cdot \Delta \quad (6)$$

where: f – coefficient of friction between the cartridge chamber and the cartridge case; l_{vd} – length of the cartridge case in the cartridge chamber; E_n – modulus of elasticity of the cartridge case material; δ – wall thickness of the cartridge case; Δ – relative interference (the magnitude of this value depends mostly on the maximum pressure and the cartridge case material).

- Gravity of gun parts

The object's gravity is located at the center of the object. This force is perpendicular to the horizontal plane and has a vertical downward direction. The magnitude of these forces is determined according to the following formula:

$$P_g = m \cdot g \quad (7)$$

where m is the mass of the object and g is the acceleration of gravity.

Install forces in Solidwork software

After determining the rules of the forces acting on the bolt carrier during the process of recoil and return, the results are exported to a spreadsheet on Excel software. They are then added to the Solidworks environment. The setting parameters are shown in Figures 11-16.

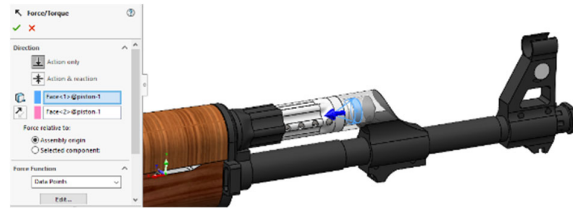


Figure 11 – Set the position and the set point of the gas chamber pressure force

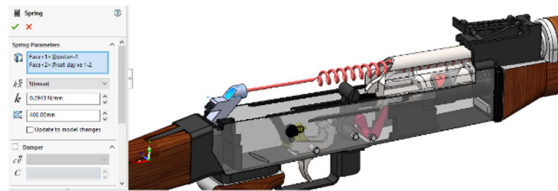


Figure 12 – Set the direction, the magnitude, and the set point of the return spring

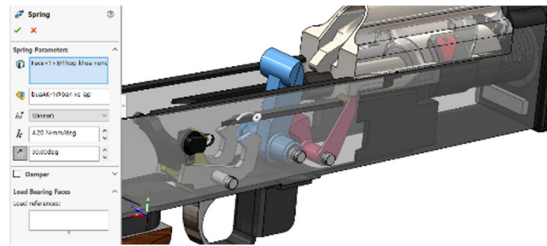


Figure 13 – Set the direction and the magnitude of the hammer's torsion spring

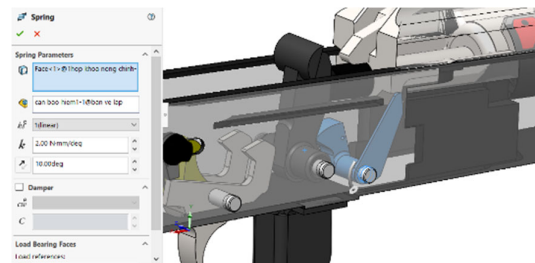


Figure 14 – Set the direction and the magnitude of the torsion spring of the safety lever

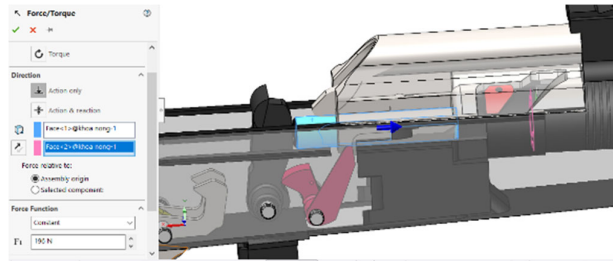


Figure 15 – Set the direction and the magnitude of the bullet casing force

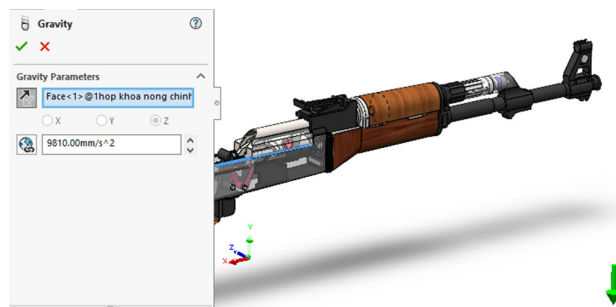


Figure 16 – Set the direction and the magnitude of gravity

After establishing the direction and the magnitude of the forces in the Solidworks environment, the contacts when moving the parts of the automatic firing system on the AK submachine gun need to be established. The contacts are set up with the parameters entered as shown in Figure 17.

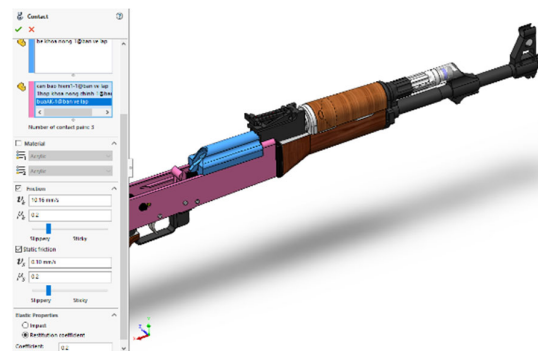



Figure 17 – Set up the contacts between the parts in the automatic firing system

Results and the discussion

Problem solution

After setting the initial parameters and connections between the parts of the AK submachine gun, a calculation model is established as shown in Figure 18. The calculation process is performed in the following order:

Click Calculate  to run the computational model. During the computing period, the Motion Analysis Messages window will display specific information.

The initial position and the study's time are determined as follows:

The initial position of the mechanism is determined as shown in Figure 18.

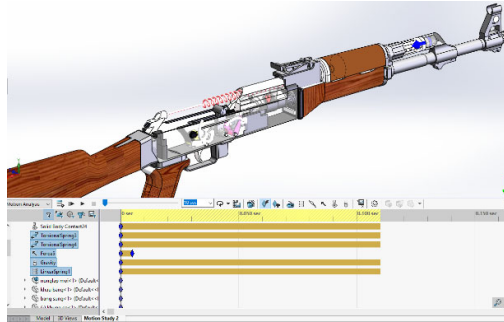


Figure 18 – Dynamic computational model of the automatic firing system

After the calculation is finished, the following options will be available:

- Click Results and Plots to see the parameters as a function of time;
- In this section, select the parameters that need to display the results such as displacement, velocity, acceleration, applied force, and moment of the part of interest, see Figure 19. These parameters can also be exported to an Excel table.



Figure 19 – Select the parameters to display

The results presented in Figures 20 to 25 are the dynamic parameters of the automatic firing system of the AK submachine gun when firing. These parameters include the velocity of the bolt carrier, the movement law of the bolt carrier, the law of rotation angle of the hammer, the force of the hammer acting on the bolt carrier, and the collision force between the bolt carrier and the gun body.

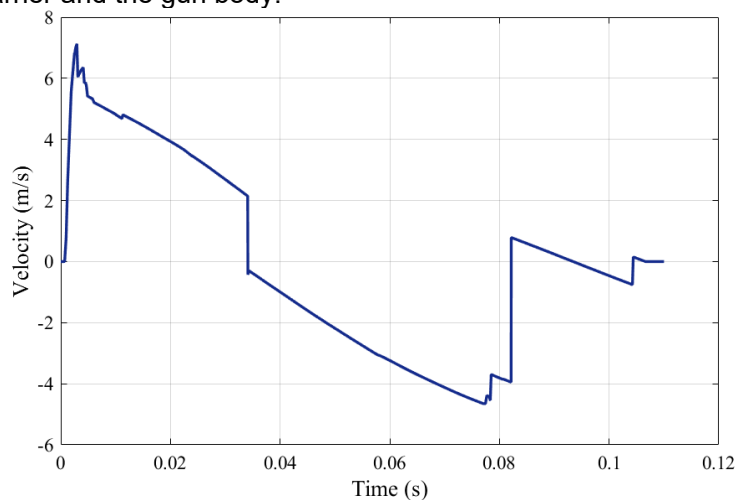


Figure 20 – Graph of the velocity of the bolt carrier over time

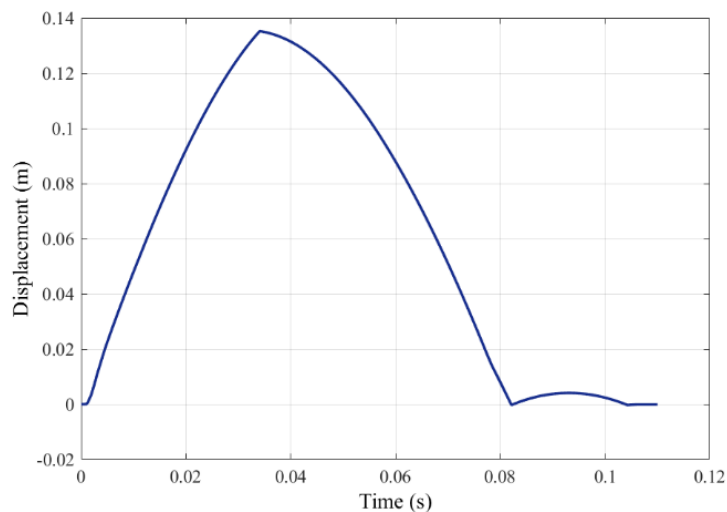


Figure 21 – Graph of the displacement of the bolt carrier over time

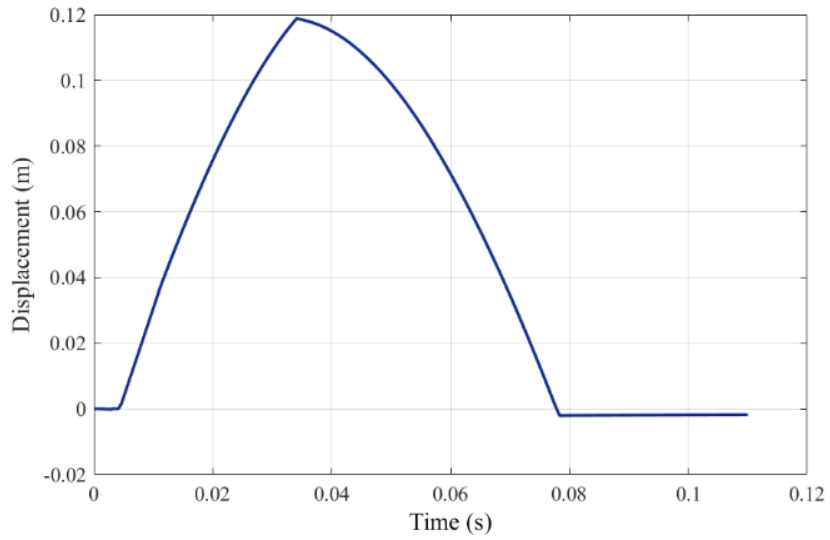


Figure 22 – Graph of the displacement of the bolt over time

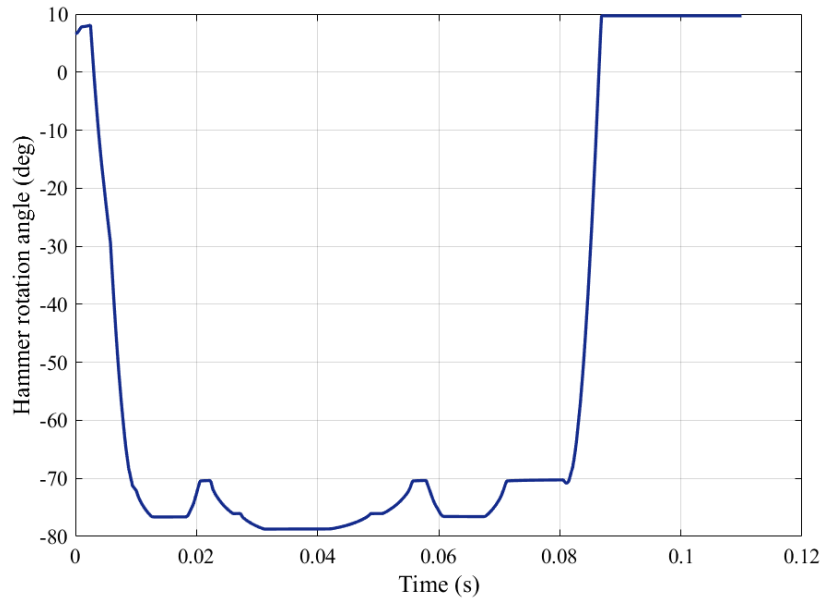


Figure 23 – Graph of the hammer rotation angle over time

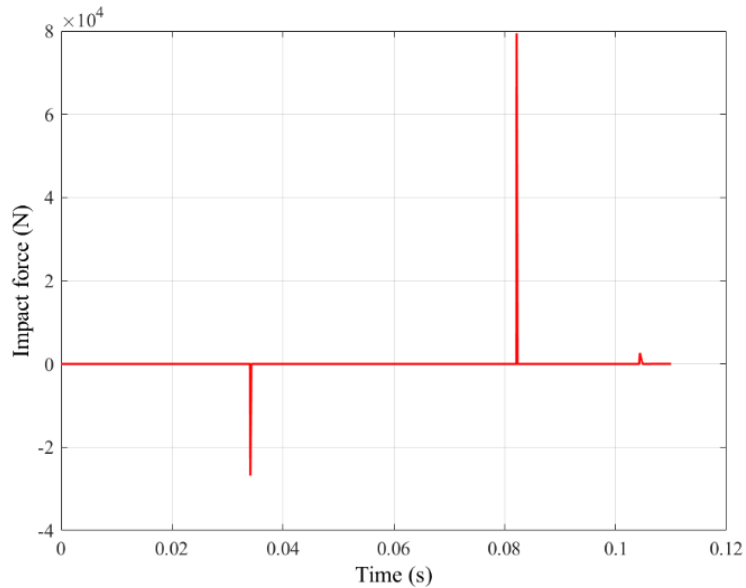


Figure 24 – Graph of the impact force between the breech and the gun body over time

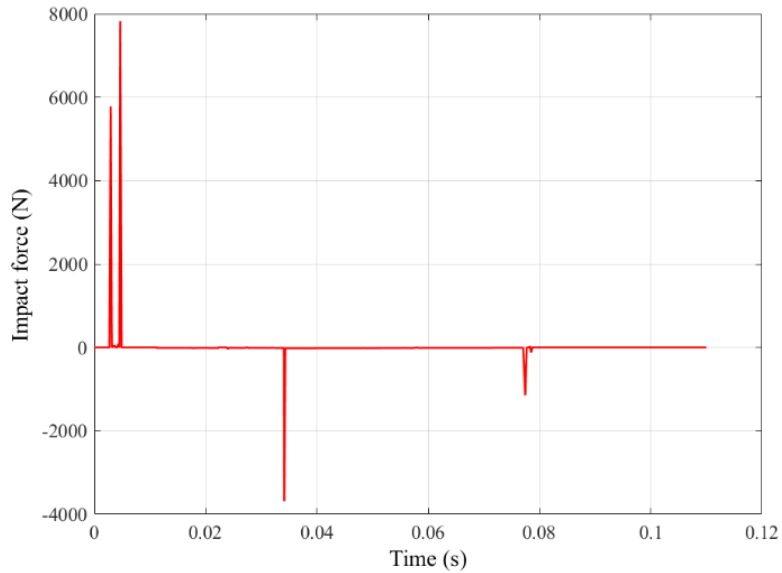


Figure 25 – Graph of the impact force between the bolt and the bolt carrier over time

Some comments are pointed out as follows:

The special points of the graph in Figures 20 and 21 show the moment of collision of the bolt carrier with the other parts of the automatic machine. The time it takes for the bolt carrier to move back is less than the time it takes for the bolt carrier to be pushed up. After an impact at the top position, the bolt carrier bounces back a distance before the hammer hits the firing pin to fire.

The change in the direction of movement of the bolt is shown in Figure 22. At this time, there is a collision between the breech bolt and the bolt carrier when the bolt moves within the cam-shaped section of the bolt carrier.

When the bolt carrier moves backward, the hammer is pressed down and it rotates around the axis (see Figure 23). This impact reduces the speed of movement of the bolt carrier, which is the cause of the decrease in the rate of fire.

The impact with the largest amplitude is when the bolt carrier is in the rearmost position and the top position (see Figure 24). In these two positions, the amplitude of collision force between the bolt carrier and the gun box is the largest, which causes strong fluctuations in the gun barrel, reducing the gun's accuracy when firing in series.

Evaluate the reliability of the calculation method

To evaluate the reliability of the new calculation method, an experimental method was used to verify the calculation model. The dynamic parameters of the bolt carrier are the basis for evaluating the ability of the automatic firing system to operate reliably. Therefore, the purpose of this experiment is to determine the displacement and the movement speed of the bolt carrier. The results obtained are the basis for verifying the established calculation method. In the experimental part of this study, we used a non-contact measurement technique. The high-speed camera system FASTCAM SA1.1 model 675K - C1 was used to measure the movement of the bolt carrier, see Figure 26 (Doan et al, 2023). This system includes a Fastcam SA1.1 high-speed camera with the basic parameters in Table 1, a computer used to install PFV software and store information, a lighting system, and a connection cable. PFV software is used to control high-speed cameras from a computer. TEMA software is used to process the records as well as collect the necessary data, (Tien et al, 2022, Vo et al, 2021). The system deployment diagram in the laboratory is shown in Figure 27.



Figure 26 – SA1.1 High-speed camera system

Table 1 – Some basic parameters of the camera

Parameters	Value
Maximum write speed	675000 fps @ 64x16 pixels
Data memory	8GB is equivalent to 5457 64x16 pixels photos or 5400 1024x1024 pixels photos
Sensor	12bit DAC

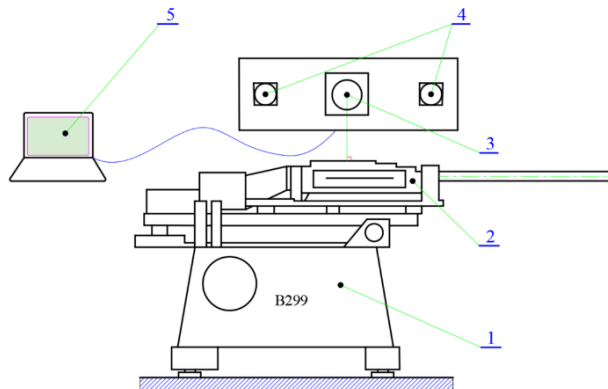


Figure 27 – Diagram of the arrangement for measuring the displacement of the bolt carrier using the SA1.1 high-speed camera system:

- 1 - B299 firing platform; 2 - AK submachine gun; 3 - SA1.1 high-speed camera;
- 4 - lighting system; 5 - computer with processing software

The testing was conducted at the Weapons Technical Center/Military Technical Academy under the environmental conditions: a temperature of 24°C and a humidity of 75%. AK submachine guns and 7.62mm ammunition are of the same batch and are insulated under the same environmental conditions. The layout diagram of the equipment used in the test is described in Figure 28. The camera installation mode is described in Figure 29.

Based on the records, the displacement and the velocity of the bolt carrier can be determined. TeMA software is used to process records as well as collect necessary data.



Figure 28 – Arrangement of the equipment in testing

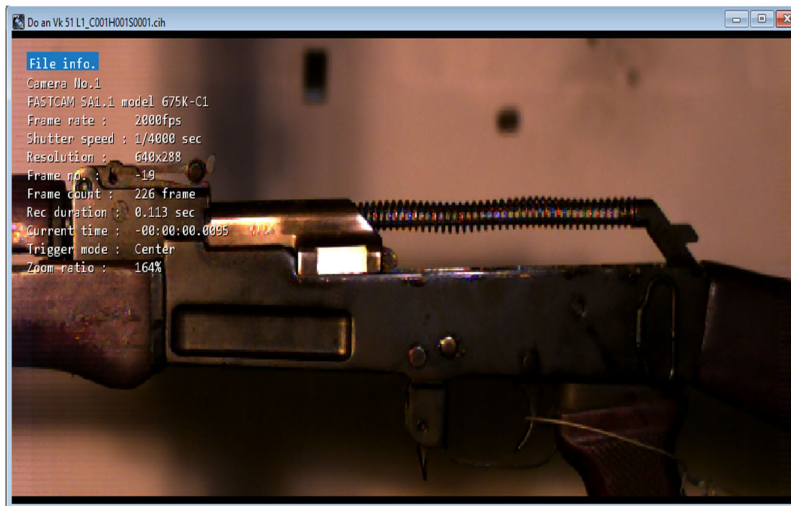


Figure 29 – Set parameters of the high-speed camera

Discussion

The experimental data are used to compare with the data from the computational model. The results of comparing the displacement and the velocity of the bolt carrier are shown in Figure 30 and Figure 31.

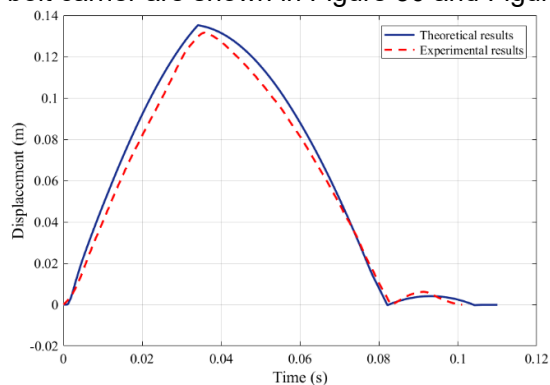


Figure 30 – Comparison of the displacement of the bolt carrier

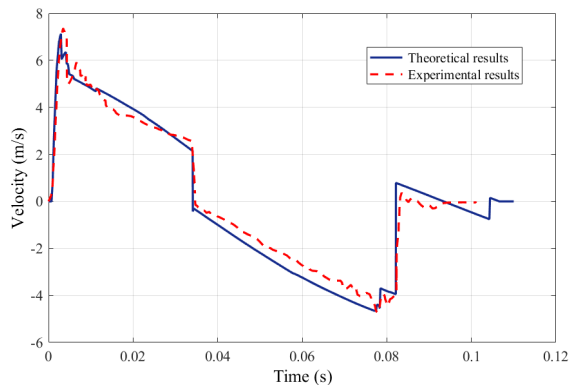


Figure 31 – Comparison of the velocity of the bolt carrier

The obtained results can be commented on as follows:

- The comparison results between the theoretical data and the experimental data show that the calculation model is highly accurate and suitable, see Figure 30 and Figure 31. The maximum deviation does not exceed 6%.

- The simulation results show that the working cycle of a shot is 0.0823s and this value is equivalent to the theoretical rate of fire of 729 (shots/minute).

The cycle of a shot according to the test results is 0.0846 s and this value is equivalent to the theoretical rate of fire of 709 (shots/minute), with an error of 2.82%.

- The comparison results demonstrate that the theoretical simulation model ensures reliability and can be used in further research and surveys on AK submachine guns.

Conclusion

With a new approach to calculating the automatic machine dynamics of the AK submachine gun using Solidworks Motion software, the dynamic parameters of all parts of the automatic machine of the gun are determined relatively accurately. From the calculated results and the comparison with the experimental results, some conclusions are drawn as follows:

- Solidworks Motion software allows users to set up 3D calculation models so it is more intuitive. The input parameters are relatively simple and easy to set, reducing the need to calculate additional problems.

- By creating links between many parts in the automatic machine, many problems are solved simultaneously, so the calculation results are more accurate. In contrast to the theoretical method, secondary problems such as the problem of determining the hammer force and the collision problem need to be solved first. These are the input parameters for the main problem.

- The results calculated using Solidworks Motion software are relatively accurate compared to the results obtained from experiments; the error is no more than 5% for the movement speed of the bolt carrier and 3% for the firing cycle.

By using Solidworks Motion software in dynamic calculations, designers will have more advantages in designing, manufacturing, and improving other types of automatic weapons.

In the future, the models determining other dynamic characteristics of weapons will be established on Solidworks Motion software by the author. In particular, the author continues to research calculations for weapons operating according to the principle of receding barrel or free breech principle.

References

Allsop, D.F. 1997. *Brassey's Essential Guide to Military Small Arms: Design Principles and Operating Methods*. London: Brassey's. ISBN: 978-1-85753-107-8.

Balla, J., Havlicek, M., Jedlicka, L., Krist, Z. & Racek, F. 2010a. Dynamics of automatic weapon mounted on the tripod. In: *Proceedings of the Advances in mathematical and computational methods: 12th WSEAS international conference on Mathematical and computational methods in science and engineering*, pp.122-127. Stevens Point, Wisconsin, USA: World Scientific and Engineering Academy and Society (WSEAS). ISBN: 9789604742431.

Balla, J., Krist, Z. & Le, C.I. 2015. Experimental study of turret-mounted automatic weapon vibrations. *International journal of mechanics*, 9(1), pp.16-25 [online]. Available at: <https://www.naun.org/main/NAUN/mechanics/2015/a062003-137.pdf> [Accessed: 10 May 2024].

Balla, J. & Mach, R. 2007. Kinematics and dynamics of Gatling weapons. *Advances in Military Technology*, 2(2), pp.121-133 [online]. Available at: <https://www.aimt.cz/index.php/aimt/article/view/1691> [Accessed: 10 May 2024].

Balla, J., Popelinsky, L. & Krist, Z. 2010b. Theory of high rate of fire automatic weapon with together bound barrels and breeches. *WSEAS Transactions on Applied and Theoretical Mechanics*, 5(1), pp.71-80 [online]. Available at: <http://www.wseas.us/e-library/transactions/mechanics/2010/89-283.pdf> [Accessed: 10 May 2024].

Bien, V.V., Phuc, T.V. & Macko, M. 2021. Effect of Some Structural Parameters on Firing Stability of Shooter-Weapon System. *Advances in Military Technology*, 16(2), pp.235-251. Available at: <https://doi.org/10.3849/aimt.01487>.

Doan, D.V., Bien, V.V., Quang, M.A. & Phu, N.M. 2023. A Study on Multi-Body Modeling and Vibration Analysis for Twin-Barrel Gun While Firing on Elastic Ground. *Applied Engineering Letters*, 8(1), pp.36-43. Available at: <https://doi.org/10.18485/aeletters.2023.8.1.5>.

Dung, T., Nguyen, M.P., Vo, V.B., Nguyen, D.P., Macko, M. & Vitek, M. 2023. Analysis of gas flow losses in a gas-operated gun. In: *2023 International Conference on Military Technologies (ICMT)*, Brno, Czech Republic, pp.1-7, May 23-26. Available at: <https://doi.org/10.1109/ICMT58149.2023.10171337>.

Fiser, M., 2007. *Automatic weapons – design and testing*. Trenčin, Slovak Republic: Alexander Dubček University of Trenčín. ISBN: 80-8575-089-0.

Fiser, M. & Popelinsky, L. 2007. *Small Arms*. Brno, Czech Republic: University of Defence. ISBN: 978-80-7231-475-1.

Macko, M., Vo, B.V. & Mai, Q.A. 2021. Dynamics of Short Recoil-operated Weapon. *Problems of Mechatronics. Armament, Aviation, Safety Engineering*, 12(3), pp.9-26. Available at: <https://doi.org/10.5604/01.3001.0015.2432>.

Nedelcu, D., Gillich, G., Bloju, A. & Padurean, I. 2020. The kinematic and kinetostatic study of the shaker mechanism with SolidWorks Motion. *Journal of Physics: Conference Series*, 1426, art.number:012025. Available at: <https://doi.org/10.1088/1742-6596/1426/1/012025>.

Nedelcu, D., Nedeloni, M.-D. & Daia, D. 2011. The kinematic and dynamic analysis of the crank mechanism with solidworks motion. In: *GAVTASC'11: Proceedings of the 11th WSEAS international conference on Signal processing, computational geometry and artificial vision, and Proceedings of the 11th WSEAS*

international conference on Systems theory and scientific computation, pp.245-250. Stevens Point, Wisconsin, USA: World Scientific and Engineering Academy and Society (WSEAS). Available at: ISBN: 978-1-61804-027-5.

Popelinsky, L. & Balla, J. 2004. *High rate of fire automatic weapons – design and projecting*. Brno, Czech Republic: University of Defence. ISBN: 80-85960-80-X.

Tien, V.D., Macko, M., Procházka, S. & Bien, V.V. 2022. Mathematical Model of a Gas-Operated Machine Gun. *Advances in Military Technology*, 17(1), pp.63-77. Available at: <https://doi.org/10.3849/aimt.01449>.

Tien, V.D., Procházka, S., Krist, Z. & Vo, B.V. 2021. Influence of Gas Port on Forces and Their Impulses Acting in an Automatic Weapon. In: *2021 International Conference on Military Technologies (ICMT)*, Brno, Czech Republic, pp.1-8, June 08-11. Available at: <https://doi.org/10.1109/ICMT52455.2021.9502832>

Vitek, R. 2019. Analyses of the Measurement Accuracy of the Optical Light Gates. In: *2019 International Conference on Military Technologies (ICMT)*, Brno, Czech Republic, pp.1-11, May 30-31. Available at: <https://doi.org/10.1109/MILTECHS.2019.8870114>.

Vo, V.B., Macko, M. & Dao, H.M. 2021. Experimental Study of Automatic Weapon Vibrations when Burst Firing. *Problems of Mechatronics. Armament, Aviation, Safety Engineering*, 12(4), pp.9-28. Available at: <https://doi.org/10.5604/01.3001.0015.5984>.

Estudio de las características dinámicas de pistolas accionadas por gas utilizando el software Solidworks Motion

Phu M. Nguyen, Bien V. Vo, **autor de correspondencia**,
Doan V. Dao, Dung V. Nguyen

Universidad Técnica Le Quy Don, Facultad de Equipos Especiales,
Hanói, República Socialista de Vietnam

CAMPO: matemáticas, ingeniería mecánica
TIPO DE ARTÍCULO: artículo científico original

Resumen:

Introducción/objetivo: Este artículo presenta un nuevo enfoque para determinar las características dinámicas del sistema de disparo automático de pistolas automáticas operadas por gas.

Métodos: Basado en la estructura real del sistema de disparo automático de armas automáticas operadas por gas, se simula un modelo 3D del arma utilizando el software Solidworks y las características dinámicas del sistema de disparo automático se calculan en el software Solidworks Motion.

Resultados: Los resultados de la simulación obtenidos incluyen el desplazamiento y la velocidad de la plataforma de recámara a lo largo del tiempo; la fuerza ejercida por el martillo sobre el portacerrojo a lo largo del tiempo; y la fuerza de impacto del portacerrojo y el cuerpo de la pistola a lo

largo del tiempo. Estos resultados se comparan con datos obtenidos de experimentos para verificar el modelo matemático. El ciclo de un disparo según los resultados de la prueba es de 0,0846 s y el error en la tasa de disparo entre los resultados teóricos y experimentales es del 2,82%.

Conclusión: El contenido de la investigación permite a los usuarios evaluar visualmente el proceso de trabajo de todas las partes del sistema de disparo automático. Los resultados de esta investigación se pueden aplicar a los cálculos de sistemas de disparo automático de diferentes armas automáticas. Esta es una base científica importante para mejorar y modernizar las armas automáticas existentes y servir al proceso de diseño y fabricación de nuevos tipos de armas automáticas en el futuro.

Palabras claves: dinámica, sistema de disparo automático, armas automáticas, armas accionadas por gas, Solidworks Motion.

Изучение динамических характеристик газового огнестрельного оружия с использованием программного обеспечения Solidworks Motion

Фу М. Нуиен, Биен В. Во, **корреспондент**, Зоан В. Цао, Зунг В. Нуиен

Технический университет Ле Квай Дон,
факультет специального оборудования,
Ханой, Социалистическая Республика Вьетнам

РУБРИКА ГРНТИ: 55.68.00 Производство оружия

ВИД СТАТЬИ: оригинальная научная статья

Резюме:

Введение/цель: В данной статье представлен новый подход к определению динамических характеристик автоматической системы выстрелов из газового автоматического огнестрельного оружия.

Методы: На основании реальной структуры автоматической системы выстрелов из газового автоматического огнестрельного оружия моделируется 3D-модель винтовки с использованием программного обеспечения Solidworks, а динамические характеристики системы автоматической стрельбы рассчитываются с помощью программного обеспечения Solidworks Motion.

Результаты: Полученные результаты моделирования включают в себя перемещение и скорость затворной рамы за период времени; усилие, оказываемое ударником на затворную раму за период времени; и силу удара затворной рамы и винтовки за период времени. Эти результаты для проверки математической модели сравниваются с данными, полученными в результате экспериментов. Продолжительность цикла

выстрелов, согласно результатам испытаний, составляет 0,0846 секунд, а погрешность между теоретическими и экспериментальными результатами составляет 2,82%.

Выводы: Содержание данного исследования позволяет пользователям визуально оценить рабочий процесс всех частей автоматической системы стрельбы. Результаты этого исследования могут быть применены для расчета систем автоматической стрельбы из различных видов автоматического оружия. Результаты исследования являются важной научной основой для совершенствования и модернизации существующего автоматического огнестрельного оружия и послужат в процессе проектирования и изготовления новых видов автоматического оружия в будущем.

Ключевые слова: динамика, автоматическая система стрельбы, автоматическое оружие, газовое оружие, Solidworks Motion.

Проучавање динамичких карактеристика пушака које функционишу по принципу позајмице барутних гасова помоћу софтвера Solidworks Motion

Фу М. Нуиен, Биен В. Во, **аутор за преписку**, Зоан В. Цао, Зунг В. Нуиен
Технички универзитет Ле Квај Дон, Факултет за специјалну опрему,
Ханој, Социјалистичка Република Вијетнам

ОБЛАСТ: математика, машинство
КАТЕГОРИЈА (ТИП) ЧЛАНКА: оригинални научни рад

Сажетак:

Увод/циљ: Овај рад представља нов приступ одређивању динамичких карактеристика аутоматског система опалјивања код аутоматских пушака које функционишу по принципу позајмице барутних гасова.

Метод: На основу реалне структуре аутоматског система опалјивања аутоматских оружја која функционишу по принципу позајмице барутних гасова, симулиран је 3Д модел пушке помоћу софтвера Solidworks, а динамичке карактеристике аутоматског система опалјивања израчунате су помоћу софтвера Solidworks Motion.

Резултати: Добијени резултати симулације обухватају померање и брзину затварачког блока у функцији времена, силу којом ударач делује на носач затварача у функцији времена, као и силу удара носача затварача и тела оружја у функцији времена. Резултати су упоређени с експериментално добијеним подацима ради верификације математичког модела. Циклус опалјења, према

результатима испитивања, износи 0,0846 s, а грешка брзине паљбе између теоријских и експерименталних резултата је 2,82%.

Закључак: Ово истраживање омогућава корисницима визуелан приказ процеса рада свих делова аутоматског система опаљивања. Његови резултати могу да се примене за израчунавања аутоматских система опаљивања различитих аутоматских пушака. То представља важну научну основу за побољшање и усавршавање постојећег аутоматског оружја, као и за пројектовање и производњу нових типова тог оружја у будућности.

Кључне речи: динамика, аутоматски систем опаљивања, аутоматско оружје, оружје које функционише по принципу позајмице барутних гасова, Solidworks Motion.

Paper received on: 12.05.2024.

Manuscript corrections submitted on: 24.09.2024


Paper accepted for publishing on: 25.09.2024


© 2024 The Authors. Published by Vojnotehnički glasnik / Military Technical Courier (www.vtg.mod.gov.rs, втг.мо.унр.срб). This article is an open access article distributed under the terms and conditions of the Creative Commons Attribution license (<http://creativecommons.org/licenses/by/3.0/rs/>).




Improvement of the operations planning process using a hybridized fuzzy-multi-criteria decision-making approach

Ivan B. Petrović^a, Milan Ž. Milenković^b

^a University of Defence in Belgrade, Military Academy, Belgrade, Republic of Serbia, e-mail: ivanpetrovic1977@gmail.com, **corresponding author**, ORCID iD:  <https://orcid.org/0000-0001-7372-637X>

^b University of Defence in Belgrade, School of National Defence "Field Marshal Radomir Putnik", Belgrade, Republic of Serbia, e-mail: micko0307@gmail.com, ORCID iD:  <https://orcid.org/0009-0008-9315-3802>

 <https://doi.org/10.5937/vojtehg72-51473>

FIELD: applied mathematics, military sciences

ARTICLE TYPE: original scientific paper

Abstract:

Introduction/purpose: The possibility of optimizing decision making in the operations planning process in air defence units by applying a multi-criteria decision-making approach in a fuzzy environment is shown in the paper. By analyzing the content of the available literature, the selection criteria were determined based on which it is possible to evaluate and compare the courses of action of air defence units. The criteria are based on the evaluation parameters of the courses of action from the decision matrix in the phase of the operations planning process called the courses of action validation and comparison.

Methods: The proposed approach combines the Laboratory for Testing and Evaluation of Decision Making (DEMATEL) and the Compressed Proportional Assessment (COPRAS) which have been successfully modified by fuzzy triangular sets. The fuzzy-DEMATEL method was applied to determine the criteria's weights, and the fuzzy-COPRAS method was applied to evaluate the alternatives - courses of action.

Results: Multiple fuzzy-multi-criteria decision-making methods were integrated into a unique model that can be applied in the operations planning process with the aim of optimizing the decision-making process.

Conclusion: The paper contributes to military science in making decisions related to the operations planning process at the tactical level in air defence units.

Keywords: Multi-Criteria Decision-Making (MCDM), DEMATEL, COPRAS, Triangular Fuzzy Sets, Operations Planning Process.

ACKNOWLEDGMENT: This paper was written as a part of the scientific research project funded by the Ministry of Defence, Republic of Serbia: VA-DH/1/22-24 "Model upravljanja razvojem sposobnosti sistema odbrane" ("Defence system capability development management model").

Introduction

Making the decision for the use of the air defence missile battalion in the operations planning process is a train of thought established by the coordinating officer based on the decision of the commander in order to logically analyze significant information during the work of the command. It is implemented through a procedure that allows the commander to control the operational planning process. This process globally has variable dynamics, depending on the scenario, that is, the decision-making environment.

The sequence of planning activities is a series of logical, sequential, and analytical processes to: examine a mission; develop, analyze, and compare the courses of action, selecting the best course of action; and produce a plan or order during a military operation (in this case an air defence operation).

The operations planning process in the air defence missile battalion is realized through six phases: initiation, mission analysis, courses of action development, courses of action validation and comparison, commander's courses of action decision, and plan development. The operations planning process in the air defence missile battalion is regulated by a special instruction that is harmonized with the Guide for Operational Planning of the Armed Forces Commands (Canadian Army Command and Staff College, 2018).

In the air defence missile battalion, the operations planning process takes place through the decision-making process implemented by the operations planning group.

The operations planning group is formed by members of the battalion command. If necessary, subordinate commanders as well as members of superior command (air defence missile brigade) are involved in the operations planning process.

The composition of the operations planning group is defined by the Standard Procedure for Operations Planning Process, which is developed by each air defence missile battalion command at its own level, in accordance with the Guide for Operational Planning of the Armed Forces Commands (UK Ministry of Defence, 2019). The operations planning group of the air defence missile battalion has seven members of command, while in the expanded composition this group can have up to twelve members.

The fourth phase of the decision-making process, the courses of action validation and comparison, begins with an ongoing analysis that evaluates the advantages and disadvantages of all courses of action. Each

member of the operations planning group presents their conclusions for further consideration. Using previously developed commander's selection criteria, the operations planning group analyzes each course of action. By comparing the courses of action, their advantages and disadvantages are identified in relation to each other, in order to finally identify the one with the highest probability of success, in relation to the most likely and most dangerous enemy's courses of action.

One of the problems in the work of the operations planning group is that, in the process of selecting group members, no expertise process was carried out, but the composition of the operations planning group was determined based on the duties of the members of the air defence missile battalion command. Bearing this in mind, the subjectivity of the operations planning group members can significantly influence the decision-making process.

The paper considers the optimization and improvement of the operations planning process by applying appropriate objective tools in the decision-making approach, in this case the methods of multi-criteria decision-making.

Namely, on the basis of adequate input values, multi-criteria decision-making methods provide a quick optimal output - response, based on modern computer technologies and soft computing and which can be applied in the decision-making process in the operations planning process in the air defence missile battalion. The application of these methods enables the optimization of the process in an objective way; based on the subjective judgment of the respondents (those methods are subjectively oriented programming methods in soft computing). The possibility of improving the operations planning process was considered in accordance with the principle of limitations, that is, it was examined only in the phase of the courses of action validation and comparison. The object of the application of multi-criteria decision-making methods is the decision-making matrix, which is used in the phase of the courses of action validation and comparison to select the best alternative - course of action from the offered courses of action. In the paper, MCDM methods were first applied for the prioritization of the criteria, and then for the evaluation of the courses of action. There are two types of MCDM methods used in scientific research. The first type is represented by multiple attribute decision making (MADM) methods, while the second type is represented by multiple objective decision making (MODM) methods. MADM involves the selection of the "best" alternative from pre-specified alternatives described in terms of multiple attributes (Zavadskas et al, 2014; Sabaei et al, 2015). These methods enable the prioritization of a discrete - finite

number of criteria, sub-criteria and attributes in hierarchically structured qualitative - quantitative ambiguous (imperfect) problems. The second category, MODM, involves the design of alternatives which optimize the multiple objectives of the decision maker (Zavadskas et al, 2014; Sabaei et al, 2015). Bearing in mind that the main goal of the paper is to objectively solve the problem of selecting the optimal course of action based on the final number of offered courses of action, as well as that the evaluation of the courses of action is also performed on the basis of a finite number of criteria, the MCDM methods that belong to the category of MADM methods, are applied in the paper. Furthermore, the application of MADM methods is based on the fact that the decision made is the product of the thought process of the members of the operations planning group, which ensures the validity of the application of these operational research methods. Therefore, the application of the MADM method provides a solution to the structural problem of selecting the optimal alternative (course of action) from the finite number of alternatives by ranking them based on the subjective opinion of decision makers (the operations planning group). The decision makers subjectively ranked the alternatives for each of the final number of criteria (with which they previously determined the weights) using linguistic variables, which required the application of fuzzy sets, instead of "crisp" values. Bearing in mind that fuzzy sets provide a suitable mathematical apparatus for solving problems based on uncertainty, ambiguity, subjectivity and indeterminacy, their application was necessary in solving this research problem in the paper. Namely, the criteria, which were used in the decision matrix, are of an undetermined type (they cannot be determined exactly mathematically) that depend on many factors (space, weather conditions, enemies, etc.) and the decision makers made a subjective assessment of their values, which conditioned the application of fuzzy sets. The evaluation of the courses of action is also based on subjectivity and uncertainty, which caused the application of fuzzy sets. Bearing in mind that, in type-1 fuzzy sets, each element has a degree of membership which is described with a membership function valued in the interval between 0 and 1, as well as linguistic variables (intended for decision makers to assess the mutual influence of criteria and evaluate the criteria for each alternative) are unambiguous, type-1 fuzzy sets in the form of triangular fuzzy sets were applied in the paper.

In addition to the introduction and conclusion, the paper consists of three more sections. In the first section, the review of literature was done. In the second section, the methodological basis used in the paper is

explained, while in the third section, the results of the research are presented an explained.

Analysis of literature

Multi-criteria decision-making methods are included in operational research methods. The application of these methods for military purposes has been known since their inception. Namely, with the objective of optimizing the radar network, during the Second World War, the British armed forces optimized radar positions by applying operational research methods. After the Second World War, these methods were further enhanced, and they found a very significant application in the Yugoslav Army (the Laboratory for Operational Research at the Faculty of Organizational Sciences in Belgrade is named after Jovan Petrić, colonel of the Yugoslav Army) because their basic purpose was related to the optimization of decision-making processes in organizational systems (the army and its units essentially represent organizational systems). Multi-criteria decision-making methods were developed later, and experienced complete affirmation with the development of computer technologies. There are numerous papers dealing with the application of multi-criteria decision-making methods for military purposes. For example, Indić et al. (2018) dealt with the selection of unmanned aerial vehicles for the needs of chemical accident area reconnaissance, for the purposes of chemical recognition. Božanić et al. (2016) investigated the possibility of applying multi-criteria optimization methods in the operations planning process in the defense operation. The possibility of optimizing military decision-making by applying the FUCOM–EWAA–COPRAS-G MCDM model was researched by Tešić & Božanić (2023). Most of the mentioned papers are in the process of finding practical application in the realization of combat tasks.

Bearing in mind the aforementioned, it can be concluded that there is no single theoretical fund that refers to the application of multi-criteria decision-making methods in the operations planning process in order to select the optimal course of action of a military unit.

Methodological background

For the purposes of this research, the hybridized DEMATEL-COPRAS approach of multi-criteria decision-making on triangular fuzzy sets was applied.

A small number of respondents within the operations planning process in the air defence missile battalion results in the application of

fuzzy sets. Namely, as mentioned earlier in the paper, in contrast to "crisp" values, which give representative results on a large sample, in the case of a small sample, as is the case in this paper, the representativeness and reliability of the results is obtained by applying triangular fuzzy sets (the application of this type of numbers is related to decision making in the conditions of uncertainty and subjectivity of experts' opinion).

The triangular fuzzy set \tilde{A} for each number a is $\mu(a)$, where $\mu(a)$ is a membership function a of the triangular fuzzy set \tilde{A} in the interval $[0,1]$ for two triangular fuzzy sets:

$$\tilde{A}_1 = (l_1, m_1, u_1) \text{ and}$$

$$\tilde{A}_2 = (l_2, m_2, u_2).$$

The elementary operations necessary for the application of multi-criteria decision-making methods on the aforementioned triangular fuzzy sets are as follows (Chang, 1996; Kahraman et al, 2014; Petrović & Petrović, 2021):

$$\tilde{A}_1 + \tilde{A}_2 = (l_1 + l_2, m_1 + m_2, u_1 + u_2) \quad (1)$$

$$\tilde{A}_1 - \tilde{A}_2 = (l_1 - u_2, m_1 - m_2, u_1 - l_2) \quad (2)$$

$$\tilde{A}_1 \times \tilde{A}_2 = (l_1 \times l_2, m_1 \times m_2, u_1 \times u_2) \quad (3)$$

$$\tilde{A}_1 \div \tilde{A}_2 = (l_1 \div u_2, m_1 \div m_2, u_1 \div l_2) \quad (4)$$

$$k \times \tilde{A}_i = (k \times l_i, k \times m_i, k \times u_i) \quad (5)$$

$$\frac{\tilde{A}_i}{k} = \left(\frac{l_i}{k}, \frac{m_i}{k}, \frac{u_i}{k} \right) \quad (6)$$

where k is a scalar ("crisp value") – a real number

$$\frac{1}{\tilde{A}_i} = \left(\frac{1}{u_i}, \frac{1}{m_i}, \frac{1}{l_i} \right) \quad (7)$$

$$\sqrt[m]{\tilde{A}_i} = \left(\sqrt[m]{l_i}, \sqrt[m]{m_i}, \sqrt[m]{u_i} \right) \quad (8)$$

Defuzzification of the triangular fuzzy sets is done by using the following formula (Kahraman et al, 2014; Petrović & Petrović, 2021):

$$a_i = \frac{l_i + 4 \times m_i + u_i}{6} . \quad (9)$$

There are a number of MCDM methods that can be used to prioritize criteria in a structured model: FUCOM (Full Consistency Method), LBWA (Level Based Weight Assessment), OPA (Ordinal Priority Approach), etc. The FUCOM algorithm is based on the pairwise comparisons of criteria, where only the $n - 1$ comparison in the model is necessary. One of the characteristics of the developed new method is the lowering of decision-maker's subjectivity, which leads to consistency or symmetry in the weight values of the criteria (Khan et al, 2022; Tešić & Božanić, 2023). The LBWA method enables the involvement of experts from different fields with the purpose of defining the relations between criteria and providing rational decision making. The LBWA model has several key advantages: (1) the LBWA model allows the calculation of weight coefficients with a small number of criteria comparisons, only $n-1$ comparison; (2) the algorithm of the LBWA model does not become more complex with the increase of the number of criteria, which makes it suitable for use in complex MCDM models with a large number of criteria; (3) by applying the LBWA model, optimal values of weight coefficients are obtained with a simple mathematical apparatus that eliminates inconsistencies in expert preferences, which are tolerated in certain subjective models (Žižović & Pamučar, 2019). An advantage of the OPA method is that it does not make use of the pairwise comparison matrix, the decision-making matrix (no need for a numerical input), normalization methods, averaging methods for aggregating the opinions of experts (in GDM), and linguistic variables. Another advantage of the OPA method is the possibility for experts to only comment on the attributes and alternatives for which they have sufficient knowledge and experience (Ataei et al, 2020).

The validation of the selection criteria was carried out by using the fuzzy-DEMATEL (Decision – Making Trialand Evaluation Laboratory) method. This method is based on the determination of direct and indirect influences between each criterion on each criterion (Kahraman et al, 2014; Petrović & Petrović, 2021). It was developed with the aim of studying groups with complex and connected relationships. This method was chosen for the prioritization of criteria because it analyzes structures with complex causal relationships between their elements in partially determined or non-deterministic organizational systems and processes. Namely, as already mentioned, the criteria used in the paper are partially

deterministic or non-deterministic. They are partially determined through the components of the operational environment such as one's own military forces, a physical combat component (qualitative-quantitative properties of land and relief), and a weather component (complex meteorological conditions). However, these criteria also depend on the enemy's forces and their ability to reduce the values of the courses of action for all criteria, which makes the criteria both non-deterministic and partially disordered. Also, the advantage of the DEMATEL method is that it enables the identification and elimination of less important criteria during the detailed analytical process of determining a large number of criteria for evaluating the courses of action.

The degree of direct and indirect influences (no influence, low, medium, high or very high influence) between each criterion on all other criteria was gathered by all members of the operations planning group, individually, by using the DEMATEL questionnaire. Based on this data, the initial matrix of influence was formed for each member of the operations planning group. The element values per row represent the degree of influence that each criterion has on other criteria (direct influence), and the element values per column represent the influence that other criteria have on each criterion (indirect influence). These matrices provided the application of the fuzzy-DEMATEL method.

The procedure of the fuzzy-DEMATEL method is done as follows (Kahraman et al, 2014; Petrović & Petrović, 2021):

The first step: The initial average fuzzy set matrix of the influence between the criteria is obtained by aggregating the individual (initial) fuzzy set of influence (after the transformation of the linguistic variables in the triangular fuzzy sets values) for each ij - element of $\tilde{A} = [\tilde{a}_{ij}]_{n \times n}$:

$$\tilde{A} = [\tilde{a}_{ij}]_{n \times n} = \left[\frac{\tilde{a}_{ij}^{(1)} \oplus \tilde{a}_{ij}^{(2)} \oplus \dots \oplus \tilde{a}_{ij}^{(k)}}{k} \right]_{n \times n} \quad (10)$$

where $\tilde{a}_{ij} = (l_{ij}, m_{ij}, u_{ij})$ is the triangular fuzzy set element of the non-negative matrix ($1 \leq i \leq n$ - number of columns, $1 \leq j \leq n$ - number of rows in the initial average fuzzy matrix of the influence).

k - the number of members of the operations planning group (decision makers).

The second step: The normalized direct-relation matrix is:

$$\tilde{X} = [\tilde{x}_{ij}] = s \times \tilde{A} \tag{11}$$

where $s = 1 / \max_{1 \leq i \leq n} \sum_{j=1}^n u_{ij}$.

The third step: The total relation matrix is:

$$\begin{aligned} \tilde{T} &= [\tilde{t}_{ij}]_{n \times n}, \tilde{t}_{ij} = (l_{ij}^t, m_{ij}^t, u_{ij}^t), \\ l_{ij}^t &= l_{ij}^x \times (l_{ij}^i - l_{ij}^x)^{-1}, \\ m_{ij}^t &= m_{ij}^x \times (m_{ij}^i - m_{ij}^x)^{-1}, \\ u_{ij}^t &= u_{ij}^x \times (u_{ij}^i - u_{ij}^x)^{-1}, i, j = 1, 2, \dots, n \end{aligned} \tag{12}$$

$\tilde{I} = [\tilde{i}_{ij}]_{n \times n}$, $\tilde{i}_{ij} = (l_{ij}^i, m_{ij}^i, u_{ij}^i)$, $i, j = 1, 2, \dots, n$ is the triangular fuzzy set identity square matrix with the values on the main diagonal:

$$\tilde{i}_{ij} = (1, 1, 1), 1 \leq i \leq n, 1 \leq j \leq n, i = j,$$

Other values of the triangular fuzzy set identity square are:

$$\tilde{i}_{ij} = (0, 0, 0), 1 \leq i \leq n, 1 \leq j \leq n, i \neq j$$

The fourth step: After defuzzification of the triangular fuzzy total relation matrix elements $T_{ij}^{def} = [t_{ij}^{def}]_{n \times n}$ (using formula 9), the sum of the rows $D_i, i = 1, 2, \dots, n$ and the sum of the columns $R_j, j = 1, 2, \dots, n$ of the defuzzificated total relation matrix T_{ij}^{def} is calculated using the following formulas (Baykasoğlu & Gölcük, 2017; Kahraman et al, 2014; Petrović & Petrović, 2021):

$$D_i = \sum_{j=1}^n t_{ij}^{def} \tag{13}$$

$$R_j = \sum_{i=1}^n t_{ij}^{def} \tag{14}$$

The fifth step: The weights of the criteria are (Baykasoğlu & Gölcük, 2017):

$$w_i = \sqrt{(D_i + R_i)^2 + (D_i - R_i)^2} \quad (15)$$

The sixth step: The normalized criteria's weights are:

$$W_i = \frac{w_i}{\sum_{i=1}^n w_i}, \quad i = 1, \dots, n \text{ - the number of the criteria} \quad (16)$$

As in the case of the prioritization criteria, there are numerous methods that can be used to evaluate alternatives (MABAC, VIKOR, MARCOS, COPRAS, etc.). The Multi-Attributive Border Approximation area Comparison (MABAC) method was introduced by Pamučar & Čirović (2015). The basic assumption in this method is to define the distance of the alternatives from the border approximation area. The basic advantage of the MABAC method is that this method is a simple but stable mathematical tool that can be integrated with other methods, and the potential values of gains and losses are taken into consideration so that the final result can be comprehensive (Yu et al, 2017). The Visekriterijumska Optimizacija i Kompromisno Resenje (VIKOR) method was developed by Opricovic (Opricovic & Tzeng, 2004) as an MCDM method to solve a discrete multi criteria problem with noncommensurable and conflicting criteria (Gul et al, 2016; Opricovic & Tzeng, 2004). It is aimed to determine a compromise solution for ranking and selecting considering conflicting criteria. The compromise solution is a feasible solution which is the closest to the ideal solution (Gul et al, 2016; Opricovic & Tzeng, 2004). The advantage of this method is that it calculates the ratio of positive and negative ideal solutions. The Measurement of Alternatives and Ranking according to Compromise Solution (MARCOS) method was introduced by Stević et al. (2020). The advantages of this method are: the consideration of an anti-ideal and ideal solution at the very beginning of the formation of an initial matrix, closer determination of the utility degree in relation to both solutions, the proposal of a new way to determine utility functions and their aggregation, the possibility to consider a large set of criteria and alternatives while maintaining the stability of the method (Stević et al, 2020).

In addition to the listed methods, after the prioritization of the criteria in the decision matrix was completed, the selection of the optimal alternative (course of action) was done by using the COPRAS (COPRAS - Compressed Proportional Assessment) method on triangular fuzzy sets. This method is used to assess the maximizing and minimizing index values and the effect of maximizing and minimizing indexes of attributes on the

results assessment is considered separately (Alinezhad et al, 2019). The COPRAS method determines a solution with the ratio to the ideal solution and the ratio with the ideal-worst solution (Zavadskas et al, 2008). The feature of the COPRAS method, that it is applied when solving problems in risk management, made it suitable for application in this paper. Other features of this method, which ensure its application in this paper, are: the COPRAS is a compensatory method, criteria and alternatives are independent and the qualitative attributes are converted into the quantitative attributes (Alinezhad et al, 2019). Compensatory of this method and the independence of criteria and alternatives ensures an independent assessment of each member of the operations planning group from the influence of the commander or deputy commander of the unit whose formal influence in the military organization is most often decisive in the decision-making process. Also, all the values of the criteria for evaluating the courses of action are of a qualitative type, which makes this method suitable for application in this paper.

The procedure of the fuzzy-COPRAS method is done as follows (Ghorabae et al, 2014; Tešić & Božanić, 2023):

The first step: The average fuzzy decision matrix is obtained by aggregating the individual fuzzy decision matrix (after the transformation of the linguistic variables in triangular fuzzy sets values) from the alternative values per criteria for each ij - element of \tilde{F} (Ghorabae et al, 2014):

$$\tilde{F} = [\tilde{f}_{ij}]_{n \times m} = \left[\frac{\tilde{f}_{ij}^{(1)} \oplus \tilde{f}_{ij}^{(2)} \oplus \dots \oplus \tilde{f}_{ij}^{(k)}}{k} \right]_{n \times m}, 1 \leq i \leq n, 1 \leq j \leq m \quad (17)$$

where $\tilde{f}_{ij} = (l_{ij}^f, m_{ij}^f, u_{ij}^f)$ is

the fuzzy element of the decision matrix,

n - the number of the criteria,

m - the number of the alternative (courses of action), and

k - the number of members of the operations planning group (decision makers).

The second step: The calculation of the normalized fuzzy decision matrix:

$$\tilde{R} = [\tilde{r}_{ij}]_{n \times m} = \left[\tilde{f}_{ij} / \sum_{j=1}^m \tilde{f}_{ij} \right], 1 \leq i \leq n, 1 \leq j \leq m \quad (18)$$

where $\tilde{r}_{ij} = (l_{ij}^r, m_{ij}^r, u_{ij}^r)$ is

the fuzzy element of the normalized decision matrix.

The third step: The calculation of the weighted normalized fuzzy decision matrix (Ghorabae et al, 2014; Tešić & Božanić, 2023):

$$\tilde{Z} = [\tilde{z}_{ij}]_{n \times m} = [W_i \otimes \tilde{r}_{ij}]_{n \times m} \quad (19)$$

where $\tilde{z}_{ij} = (l_{ij}^z, m_{ij}^z, u_{ij}^z)$ is

the fuzzy element of the weighted normalized decision matrix.

The fourth step: Summarizing the values of the weighted normalized decision matrix by the benefit criteria \tilde{P}_j (criteria that are maximized) and by the cost criteria \tilde{S}_j (criteria that are minimized) (Ghorabae et al, 2014):

$$\tilde{P}_j = \sum_{i=1}^p \tilde{z}_{ij}^+, i^+ \in G^+, G^+ = \{\tilde{z}_{1j}^+, \tilde{z}_{2j}^+, \dots, \tilde{z}_{pj}^+\}, G^+ - \text{the set of} \quad (20)$$

benefit criteria $\tilde{z}_{ij}^+, i = 1, \dots, p$

$$\tilde{S}_j = \sum_{i=1}^s \tilde{z}_{ij}^-, i^- \in G^-, G^- = \{\tilde{z}_{1j}^-, \tilde{z}_{2j}^-, \dots, \tilde{z}_{sj}^-\}, G^- - \text{the set of cost} \quad (21)$$

criteria $\tilde{z}_{ij}^-, i = 1, \dots, s$

$p + s = n$, the set of benefit and cost criteria.

The fifth step: After the defuzzification of the sums \tilde{P}_j and \tilde{S}_j (using formula 9), the values of the relative importance of each alternative for the benefit criteria P_j and for the cost criteria S_j are obtained. In the next step, the importance of each alternative from the total number of alternatives is determined:

$$Q_j = P_j + \frac{\sum_{j=1}^m S_j}{S_j \times \sum_{j=1}^m \frac{1}{S_j}} \quad (22)$$

Finally, the alternatives are ranked. The optimal alternative is the one that has the largest value of Q_j (Ghorabae et al, 2014).

Results and the discussion

In the first step of applying the fuzzy multi-criteria decision-making approach, the criteria of the decision-making matrix that can be used in the phase of the operations planning process courses of action validation and comparison were determined. Based on the literature analysis, the following criteria were determined: ability to command (C1), fire ability (C2), maneuver ability (C3), spatial ability (C4), logistical support (C5), and force protection (C6).

In the next step, five members of the operations planning group evaluated the mutual influence of the criteria using a questionnaire with linguistic variables and adequate triangular sets shown in Table 1 and in Figure 1.

Table 1 - DEMATEL Causal influence linguistic variables and the triangular fuzzy set values

Causal influence linguistic variables	Triangular fuzzy set values
No influence (N)	(0,0,0)
Low influence (L)	(0,0.25,0.5)
Medium influence (M)	(0.25,0.5,0.75)
High influence (H)	(0.5,0.75,1)
Very high influence (VH)	(0.75,1,1)

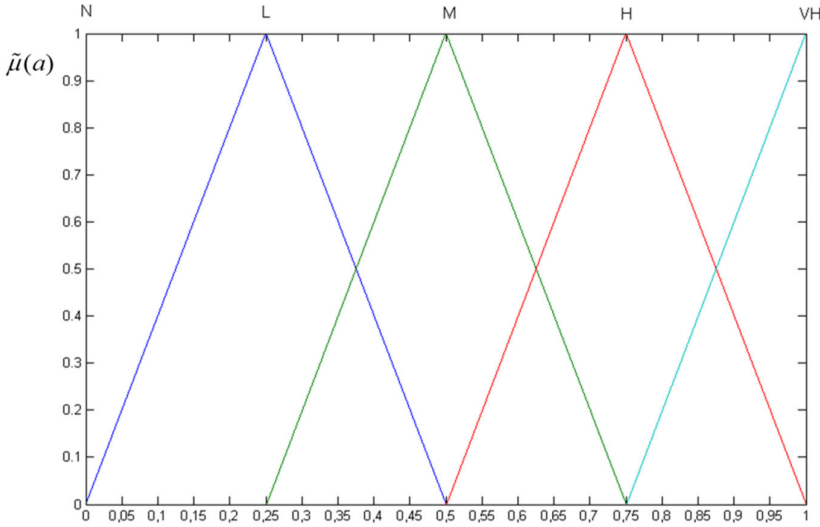


Figure 1 – Triangular fuzzy set for the linguistic variables of influence

The obtained results in the form of the linguistic variables are shown in Table 2.

Table 2 – Answers of the members of the operations planning group in the linguistic variables - matrix of mutual influence

C	C1	C2	C3	C4	C5	C6
C1	N	M+4S	S+4M	4M+H	4S+M	S+M+3H
C2	3S+2H	N	S+4M	5M	5S	3M+2H
C3	VH+3H+M	3S+2M	N	2M+3H	5M	M+3H+VH
C4	M+2VH+2H	5H	M+4H	N	4S+M	M+4H
C5	3M+2H	2S+2M+H	3S+2M	5S	N	4M+H
C6	3H+2VH	2M+2H+VH	5H	5VH	2M+3H	N

After the transformation of the linguistic variables into the triangular fuzzy sets (in accordance with Table 1) was completed, the average fuzzy set matrix of the influence was calculated using formula 10. The obtained results are shown in Table 3.

Table 3 – The average fuzzy set matrix of the influence

C	C1	C2	C3
C1	0,0,0	0.05,0.3,0.55	0.2,0.45,0.7
C2	0.2,0.45,0.7	0,0,0	0.2,0.45,0.7
C3	0.5,0.75,0.95	0.1,0.35,0.6	0,0,0
C4	0.55,0.8,0.95	0.5,0.75,1	0.45,0.7,0.95
C5	0.35,0.6,0.85	0.2,0.45,0.7	0.1,0.35,0.6
C6	0.6,0.85,1	0.4,0.65,0.85	0.5,0.75,1
C	C4	C5	C6
C1	0.3,0.55,0.8	0.05,0.3,0.55	0.35,0.6,0.85
C2	0.25,0.5,0.75	0,0.25,0.5	0.35,0.6,0.85
C3	0.4,0.65,0.9	0.25,0.5,0.75	0.5,0.75,0.95
C4	0,0,0	0.05,0.3,0.55	0.45,0.7,0.95
C5	0,0.25,0.5	0,0,0	0.3,0.55,0.8
C6	0.75,1,1.05	0.4,0.65,0.9	0,0,0

In the next step, formula 11 was used to calculate the normalized direct-relation matrix, and formula 12 was used to calculate the total relation matrix, respectively. The obtained results are shown in Tables 4 and 5.

Table 4 – The average normalized direct-relation matrix

C	C1	C2	C3
C1	0.00,0.00,0.00	0.01,0.06,0.11	0.04,0.09,0.15
C2	0.04,0.09,0.15	0.00,0.00,0.00	0.04,0.09,0.15
C3	0.10,0.16,0.20	0.02,0.07,0.13	0.00,0.00,0.00
C4	0.11,0.17,0.20	0.10,0.16,0.21	0.09,0.15,0.20
C5	0.07,0.13,0.18	0.04,0.09,0.15	0.02,0.07,0.13
C6	0.13,0.18,0.21	0.08,0.14,0.18	0.10,0.16,0.21
C	C4	C5	C6
C1	0.06,0.11,0.17	0.01,0.06,0.11	0.07,0.13,0.18
C2	0.05,0.10,0.16	0.00,0.05,0.10	0.07,0.13,0.18
C3	0.08,0.14,0.19	0.05,0.10,0.16	0.10,0.16,0.20
C4	0.00,0.00,0.00	0.01,0.06,0.11	0.09,0.15,0.20
C5	0.00,0.05,0.10	0.00,0.00,0.00	0.06,0.11,0.17
C6	0.16,0.21,0.22	0.08,0.14,0.19	0.00,0.00,0.00

Table 5 – The total relation matrix

C	C1	C2	C3
C1	0.00,0.00,0.00	0.00,0.06,0.08	0.00,0.09,0.11
C2	0.00,0.09,0.12	0.00,0.00,0.00	0.00,0.09,0.11
C3	0.02,0.16,0.19	0.00,0.07,0.10	0.00,0.00,0.00
C4	0.02,0.17,0.20	0.01,0.16,0.18	0.01,0.15,0.18
C5	0.01,0.13,0.15	0.00,0.09,0.10	0.00,0.07,0.09
C6	0.02,0.18,0.22	0.01,0.14,0.16	0.01,0.16,0.21
C	C4	C5	C6
C1	0.01,0.11,0.13	0.00,0.06,0.07	0.01,0.13,0.15
C2	0.00,0.10,0.12	0.00,0.05,0.06	0.01,0.13,0.15
C3	0.01,0.14,0.17	0.00,0.10,0.12	0.01,0.16,0.19
C4	0.00,0.00,0.00	0.00,0.06,0.08	0.01,0.15,0.20
C5	0.00,0.05,0.07	0.00,0.00,0.00	0.00,0.11,0.13
C6	0.03,0.21,0.22	0.01,0.14,0.16	0.00,0.00,0.00

In the next step, the defuzzificated total relation matrix was obtained using formula 9, and formulas 13 and 14 were used to calculate the sum values of rows and columns. In the last step, the criteria's weights were calculated and their normalization was done using formulas 15 and 16. The obtained results are shown in Table 6 and Figure 2.

Table 6 – Defuzzificated total relation matrix and criteria's weights

C	C1	C2	C3	C4	C5	C6	D_i	R_j	w_i	W_i
C1	0.000	0.020	0.032	0.041	0.018	0.046	0.157	0.313	0.496	0.176
C2	0.035	0.000	0.032	0.037	0.016	0.047	0.166	0.195	0.363	0.129
C3	0.069	0.027	0.000	0.056	0.035	0.067	0.254	0.220	0.475	0.169
C4	0.075	0.063	0.061	0.000	0.022	0.066	0.287	0.248	0.537	0.191
C5	0.046	0.029	0.024	0.019	0.000	0.041	0.159	0.142	0.302	0.108
C6	0.088	0.056	0.071	0.096	0.052	0.000	0.362	0.267	0.636	0.227

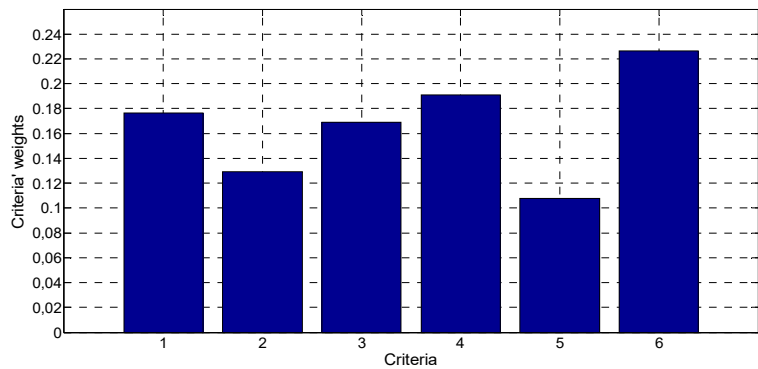


Figure 2 – Criteria's weights of the decision-making matrix

After the prioritization of the selection criteria was completed, using the fuzzy-COPRAS method, the evaluation of alternatives (courses of action of the air defence missile battalion) was carried out. In this case, three courses of action of the air defence missile battalion are proposed. The members of the operations planning group evaluated the alternatives according to the selection criteria. The evaluation was carried out using the answers with the linguistic variables (based on the Likert scale values) shown in Table 7 and in Figure 3.

Table 7 – COPRAS-Likert scale (linguistic variables and triangular fuzzy sets values)

The selection criteria's quality	Likert scale value	Fuzzy sets
Very bad (VB)	1	(0,0,0)
Bad (B)	2	(0,0.25,0.5)
Good (G)	3	(0.25,0.5,0.75)
Very good (VG)	4	(0.5,0.75,1)
Excellent(E)	5	(0.75,1,1)

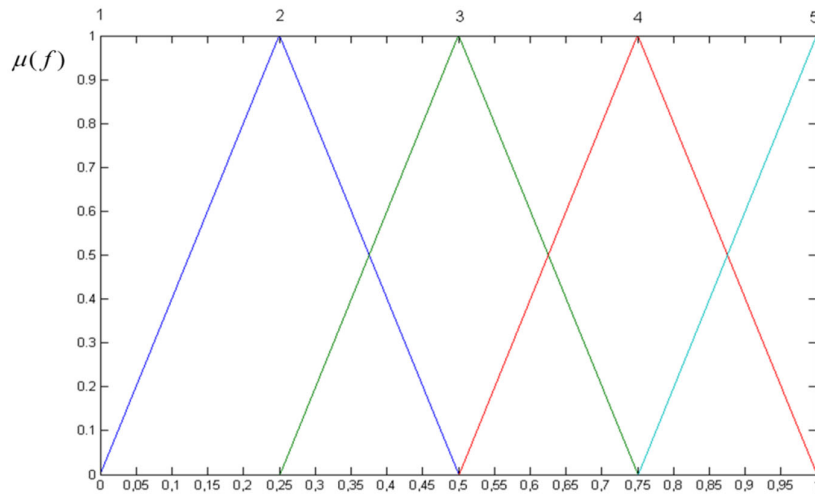


Figure 3 – Triangular fuzzy set for the numerical values of the Likert scale

After the transformation of the values of the linguistic variables into the fuzzy triangular sets, the formation of the average fuzzy decision matrix was done using formula 17. The obtained results are shown in Table 8.

Table 8 – COPRAS linguistic and fuzzy decision matrix

\tilde{F}	COA1		COA2		COA3	
C1	3VG+2G	0.4,0.65,0.9	2G+2VG+E	0.45,0.7,0.9	VG+4E	0.7,0.95,1
C2	4G+VG	0.3,0.55,0.8	G+4E	0.65,0.9,0.95	4VG+E	0.55,0.8,1
C3	G+VG+3E	0.6,0.85,0.95	2G+3VG	0.4,0.65,0.9	3VG+2E	0.6,0.85,1
C4	G+2VG+2E	0.55,0.8,0.95	2G+2VG+E	0.45,0.7,0.9	2VG+3E	0.65,0.9,1
C5	G+VG+3E	0.6,0.85,0.95	4VG+E	0.55,0.8,1	2G+3VG	0.4,0.65,0.9
C6	2L+G+2VG	0.25,0.5,0.75	G+3VG+E	0.5,0.75,0.95	2VG+3E	0.65,0.9,1

Using formula 18, the normalized decision matrix was calculated. The obtained results are shown in Table 9.

Table 9 – COPRAS normalized fuzzy decision matrix

\tilde{R}	W_i	COA1	COA2	COA3	$\sum_{j=1}^m \tilde{f}_{ij}$
C1	0.176	0.143,0.283,0.581	0.161,0.304,0.581	0.161,0.413,0.645	1.55,2.3,2.8
C2	0.129	0.109,0.244,0.533	0.236,0.400,0.633	0.236,0.356,0.667	1.5,2.25,2.75
C3	0.169	0.211,0.362,0.594	0.140,0.277,0.563	0.140,0.362,0.625	1.6,2.35,2.85
C4	0.191	0.193,0.333,0.576	0.158,0.292,0.545	0.158,0.375,0.606	1.65,2.4,2.85
C5	0.108	0.211,0.370,0.613	0.193,0.348,0.645	0.193,0.283,0.581	1.55,2.3,2.85
C6	0.227	0.093,0.233,0.536	0.185,0.349,0.679	0.185,0.419,0.714	1.4,2.15,2.7

Using formula 19, the values of the weighted normalized decision matrix were obtained, and using formula 20, the sums of the values of the weighted normalized decision matrix were calculated for the benefit criteria. Bearing in mind that all criteria are of a benefit type (the values of all criteria must be maximized), the sums of the values of the weighted normalized decision matrix by the cost criteria were not calculated. After the defuzzification of the sum of the values of the weighted normalized decision matrix according to the benefit criteria (formula 9), the courses of action were ranked. The obtained results are shown in Table 10.

Table 10 – COPRAS weighted normalized decision matrix

\tilde{R}	COA1	COA2	COA3
C1	0.025,0.050,0.102	0.028,0.054,0.102	0.044,0.073,0.114
C2	0.014,0.032,0.069	0.031,0.052,0.082	0.026,0.046,0.086
C3	0.036,0.061,0.100	0.024,0.047,0.095	0.036,0.061,0.106
C4	0.037,0.064,0.110	0.030,0.056,0.104	0.044,0.072,0.116
C5	0.023,0.040,0.066	0.021,0.037,0.069	0.015,0.030,0.062
C6	0.021,0.053,0.121	0.042,0.079,0.154	0.055,0.095,0.162
\tilde{P}_j	0.155,0.299,0.569	0.176,0.324,0.607	0.219,0.377,0.646
P_j	0.319931286	0.346612618	0.395352904
$p = n, s = 0$ $\Rightarrow Q_j = P_j$	0.319931286	0.346612618	0.395352904
Rang	3	2	1

Based on the obtained results, it is concluded that the third course of action of the air defence missile battalion is optimal. In this example, the fuzzy-DEMATEL method ensured the prioritization of the criteria on the basis of which the course of action was chosen in the operations planning process. After presenting the subjective opinion on the mutual influence of the criteria in the questionnaire with the DEMATEL linguistic variables by the member of the operations planning group and by applying the fuzzy-DEMATEL procedure, the evaluation of the criteria was carried out in an objective way and the subjective influence of the respondents was minimized.

In the next step, the courses of action were ranked using the fuzzy-COPRAS method. Again, the members of the operations planning group gave their subjective opinions on the values of the criteria for each course of action, and the further procedure of ranking the alternatives – courses of action was carried out by using the fuzzy-COPRAS method procedure.

Bearing in mind that the rank value, in this example, is the highest for the course of action 3, it turns out that this course is also optimal; the second in rank is course of action 2, while course 1 is the weakest.

A sensitivity analysis was done through changes in the criteria's weights. The sensitivity analysis was carried out through 24 scenarios (Table 11). In each scenario, the weight of one criterion is increased (reduced) by 20%, and 40%, respectively. The weights of the other criteria are increased (decreased) so that the sum of the criteria's values is 1.

Table 11 – The sensitivity analysis of the results

$W_1 = W_{old} \times 1.2$	$W_1 = W_{old} \times 1.4$	$W_1 = W_{old} \times 0.8$	$W_1 = W_{old} \times 0.6$
$COB > COZ > COA$	$COB > COZ > COA$	$COB > COZ > COA$	<u>$COB > COI > COZ$</u>
$W_2 = W_{old} \times 1.2$	$W_2 = W_{old} \times 1.4$	$W_2 = W_{old} \times 0.8$	$W_2 = W_{old} \times 0.6$
$COB > COZ > COA$	$COB > COZ > COA$	$COB > COZ > COA$	$COB > COZ > COA$
$W_3 = W_{old} \times 1.2$	$W_3 = W_{old} \times 1.4$	$W_3 = W_{old} \times 0.8$	$W_3 = W_{old} \times 0.6$
$COB > COZ > COA$	$COB > COZ > COA$	$COB > COZ > COA$	$COB > COZ > COA$
$W_4 = W_{old} \times 1.2$	$W_4 = W_{old} \times 1.4$	$W_4 = W_{old} \times 0.8$	$W_4 = W_{old} \times 0.6$
$COB > COZ > COA$	<u>$COZ > COB > COA$</u>	$COB > COZ > COA$	$COB > COZ > COA$
$W_5 = W_{old} \times 1.2$	$W_5 = W_{old} \times 1.4$	$W_5 = W_{old} \times 0.8$	$W_5 = W_{old} \times 0.6$
$COB > COZ > COA$	$COB > COZ > COA$	$COB > COZ > COA$	$COB > COZ > COA$
$W_6 = W_{old} \times 1.2$	$W_6 = W_{old} \times 1.4$	$W_6 = W_{old} \times 0.8$	$W_6 = W_{old} \times 0.6$
$COB > COZ > COA$	<u>$COZ > COB > COA$</u>	$COB > COZ > COA$	<u>$COZ > COB > COA$</u>

The results in the table show that the ranking of the courses of action changed through four scenarios. In other scenarios, the ranking of the courses of action did not change. The correlation of the results was tested using Kendall's coefficient of concordance W. This coefficient represents a measure of the agreement between several judges (in this case 24 scenarios) who have rank ordered a set of entities (in this case three courses of action) (Field, 2005). The value of Kendall's coefficient of concordance for all 24 scenarios and 3 variables (the courses of action) is 0.845. The value of the coefficient of 0.845 is extremely significant for a significance of 0.05 (the limit value of Kendall's coefficient of concordance for 24 judges - scenarios and 3 entities - the courses of action is 0.12). Thus, it can be concluded that there is a very high correlation (closeness) of ranks through the scenarios and that the results obtained using the hybridized fuzzy-DEMATEL-COPRAS approach are credible.

To see the advantages of the proposed model, decision making in the fourth phase of the process is briefly explained by applying the Standard Procedure for Operations Planning Process (Table 12).

Table 12 – An example of a decision matrix used in the Standard Procedure for Operations Planning Process

Criteria	Coefficient	Ranking	COA1	Ranking	COA2	Ranking	COA3
C1	2	1	2	2	4	1	2
C2	1	1	1	1	1	2	2
C3	2	2	4	2	4	1	2
C4	2	2	4	1	2	2	4
C5	1	2	2	2	2	2	2
C6	3	2	6	1	3	1	3
Rang of COA			19 (3)		16 (2)		15 (1)

The coefficients in the Standard Procedure for Operations Planning Process are determined by an individual, commander or deputy commander without discussion with other members of the operational planning group. The deputy battalion commander, after consultation, proposes criteria ranks for each course of action. In the last step, the values obtained by multiplying the value of the coefficient with the rank value for each course of action are added and the course of action with the lowest value is chosen as the best. As can be noted, the process does not use scientific methods, values are assigned randomly without in-depth analysis and decision making is influenced by individuals. Bearing in mind the above, there is no doubt that the main contribution of the paper is based on the following facts: the process of the courses of action valuation is based on the application of MCDM scientific methods; group decision making reduces the influence of individuals in the group; the application of the MCDM method enables an objective approach to decision making based on the subjective opinion of the respondents. Also, the application of fuzzy sets ensures the elimination of ambiguity and indeterminacy. Namely, decision makers evaluate the criteria using linguistic variables that are transformed into triangular fuzzy sets. These fuzzy sets, in discrete form, have three values. In the middle value, the fuzzy number membership function has the maximum value, while the first and third values represent the limits of the left distribution and the right distribution of the confidence interval of fuzzy sets (in this way, the approximate value "about" was introduced into the operational planning process – for example "about 1", "about 2", etc.). This MCDM model also has its limits, which are reflected in the following: MCDM methods are mainly applied by

examining experts (expertise is not carried out in the operational planning process, but group members are pre-determined from the battalion command); sometimes it is difficult for the members of the operations planning group to assess the mutual influence of the criteria due to a number of factors whose mutual influences are often intertwined; mathematical formulations are generally rejected by the members of the operations planning group due to the lack of a unique interface that would significantly facilitate the application of the MCDM model, etc. The aforementioned shortcomings can be eliminated by forming a scientific and professional team that would analyze the possibility of forming a unique MCDM model. The mentioned model would be based on professional experiences from corps units. The final design of the model would have a unique interface that would facilitate the use of the MCDM model and would resemble the information system models already used in the Army (interfaces for planning defense functions, human resources, logistical support, etc.).

Conclusion

The paper shows the possibility of applying a multi-criteria decision-making approach in the fuzzy environment with the aim of optimizing the operations planning process in air defence units. A multi-criteria optimization approach can support the decision-making process, which will minimize subjectivity. Namely, despite the fact that the subjective assessments of individuals are taken as a starting point, the scientific-methodological approach in further steps enables the objectification of the decision-making process. Multi-criteria optimization is performed using the mathematical software MATLAB, which cannot fully ensure the ease of application of these methods to the end user. Future research should be focused on creating a unique procedure for optimizing the operations planning process based on multi-criteria decision-making methods (AHP, BEST-WORST, DEMATEL, COPRAS, MABAC, TOPSIS, etc.), with the creation of a unique programming code that would be transformed into a suitable programming language. This approach would lead to the creation of a unique interface that would significantly facilitate the operations planning process for the end user. Also, in that case, the subjective influence of each individual in the operational planning process would be significantly reduced.

References

Alinezhad, A., Khalili, J., Alinezhad, A. & Khalili, J. 2019. *New Methods and Applications in Multiple Attribute Decision Making (MADM)*. Cham: Springer. Available at: <https://doi.org/10.1007/978-3-030-15009-9>.

Ataei, Y., Mahmoudi, A., Feylizadeh, M.R. & Li, D.-F. 2020. Ordinal Priority Approach (OPA) in Multiple Attribute Decision-Making. *Applied Soft Computing*, 86, art.number:105893. Available at: <https://doi.org/10.1016/j.asoc.2019.105893>.

Baykasoğlu, A. & Gölcük, İ. 2017. Development of an interval type-2 fuzzy sets based hierarchical MADM model by combining DEMATEL and TOPSIS. *Expert Systems with Applications*, 70, pp.37-51. Available at: <https://doi.org/10.1016/j.eswa.2016.11.001>.

Božanić, D.I., Pamučar, D.S. & Karović, S.M. 2016. Application the MABAC method in support of decision-making on the use of force in a defensive operation. *Tehnika*, 71(1), pp.129-136 (in Serbian). Available at: <https://doi.org/10.5937/tehnika1601129B>.

-Canadian Army Command and Staff College. 2018. *The Operational Planning Process: OPP Handbook CACSC-PUB-500*. Kingston, Ontario, Canada: Canadian Army Command and Staff College [online]. Available at: <https://www.canada.ca/content/dam/dnd-mdn/army/lineofsight/files/articlefiles/en/CACSC-PUB-500-2018.pdf> [Accessed: 10 May 2024].

Chang, D.Y. 1996. Applications of the extent analysis method on fuzzy AHP. *European journal of operational research*, 95(3), pp.649-655. Available at: [https://doi.org/10.1016/0377-2217\(95\)00300-2](https://doi.org/10.1016/0377-2217(95)00300-2).

Field A.P. 2005. Kendall's Coefficient of Concordance. In: Everitt, B.S. & Howell, D.C. (Eds.) *Encyclopedia of Statistics in Behavioral Science*, 2, pp.1010-1011. New York: Wiley [online]. Available at: https://discoveringstatistics.com/repository/kendall's_coefficient_of_concordance_ebs.pdf [Accessed: 05 July 2024]. ISBN: 978-0-470-86080-9

Ghorabae, M.K., Amiri, M., Sadaghiani, J.S. & Goodarzi, G.H. 2014. Multiple criteria group decision-making for supplier selection based on COPRAS method with interval type-2 fuzzy sets. *The International Journal of Advanced Manufacturing Technology*, 75, pp.1115-1130. Available at: <https://doi.org/10.1007/s00170-014-6142-7>.

Gul, M., Celik, E., Aydin, N., Gumus, A.T. & Guneri, A.F. 2016. A state of the art literature review of VIKOR and its fuzzy extensions on applications. *Applied Soft Computing*, 46, pp.60-89. Available at: <https://doi.org/10.1016/j.asoc.2016.04.040>.

Indić, D., Petrović, I., Ivanković, N. & Đukić, Đ. 2018. Chemical accident area reconnaissance by unmanned aircraft. *Vojno delo*, 70(8), pp.109-127. Available at: <https://doi.org/10.5937/vojdela1808109I>.

Kahraman, C., Öztayşi, B., Sarı, İ.U. & Turanoğlu, E. 2014. Fuzzy analytic hierarchy process with interval type-2 fuzzy sets. *Knowledge-Based Systems*, 59, pp.48-57. Available at: <https://doi.org/10.1016/j.knosys.2014.02.001>.

Khan, F., Ali, Y. & Pamucar, D. 2022. A new fuzzy FUCOM-QFD approach for evaluating strategies to enhance the resilience of the healthcare sector to combat the COVID-19 pandemic. *Kybernetes*, 51(4), pp.1429-1451. Available at: <https://doi.org/10.1108/K-02-2021-0130>.

Opricovic, S. & Tzeng, G.-H. 2004. Compromise solution by MCDM methods: A comparative analysis of VIKOR and TOPSIS. *European Journal of operational research*, 156(2), pp.445-455. Available at: [https://doi.org/10.1016/S0377-2217\(03\)00020-1](https://doi.org/10.1016/S0377-2217(03)00020-1).

Pamučar, D. & Ćirović, G. 2015. The selection of transport and handling resources in logistics centers using Multi-Attributive Border Approximation area Comparison (MABAC). *Expert Systems with Applications*, 42(6), pp.3016-3028. Available at: <https://doi.org/10.1016/j.eswa.2014.11.057>.

Petrović, J. & Petrović, I. 2021. What makes a successful helicopter pilot? A fuzzy multi-criteria decision-making approach. *International Journal for Traffic and Transport Engineering*, 11(4), pp.507-527. Available at: [https://doi.org/10.7708/ijtte2021.11\(4\).02](https://doi.org/10.7708/ijtte2021.11(4).02).

Sabaei, D., Erkoyuncu, J. & Roy, R. 2015. A Review of Multi-criteria Decision Making Methods for Enhanced Maintenance Delivery. *Procedia CIRP*, 37, pp.30-35. Available at: <https://doi.org/10.1016/j.procir.2015.08.086>.

Stević, Ž., Pamučar, D., Puška, A. & Chatterjee, P. 2020. Sustainable supplier selection in healthcare industries using a new MCDM method: Measurement of alternatives and ranking according to COmpromise solution (MARCOS). *Computers & Industrial Engineering*, 140, art.number:106231. Available at: <https://doi.org/10.1016/j.cie.2019.106231>.

Tešić, T. & Božanić, D. 2023. Optimizing Military Decision-Making: Application of the FUCOM– EWAA–COPRAS-G MCDM Model. *Acadlore Transactions on Applied Mathematics and Statistics*, 1(3), pp.148-160. Available at: <https://doi.org/10.56578/atams010303>.

-UK Ministry of Defence. 2019. *Allied Joint Publication-5 Allied Joint Doctrine for the Planning of Operations*. Ministry of Defence UK [e-book]. Bristol: UK Ministry of Defence [online]. Available at: https://assets.publishing.service.gov.uk/media/6054d017e90e0724be025a8f/20210310-AJP_5_with_UK_elem_final_web.pdf [Accessed: 12 May 2024].

Yu, S.M., Wang, J. & Wang, J.Q. 2017. An Interval Type-2 Fuzzy Likelihood-Based MABAC Approach and Its Application in Selecting Hotels on a Tourism Website. *International Journal of Fuzzy Systems*, 19, pp.47-61. Available at: <https://doi.org/10.1007/s40815-016-0217-6>.

Zavadskas, E.K., Kaklauskas, A., Turskis, Z. & Tamošaitiene, J. 2008. Selection of the effective dwelling house walls by applying attributes values determined at intervals. *Journal of Civil Engineering and Management*, 14(2), pp.85-93. Available at: <https://doi.org/10.3846/1392-3730.2008.14.3>.

Zavadskas, E.K., Turskis, Z. & Kildienė, S. 2014. State of art surveys of overviews on MCDM/MADM methods. *Technological and Economic Development of Economy*, 20(1), pp.165-179. Available at: <https://doi.org/10.3846/20294913.2014.892037>.

Žižović, M. & Pamučar, D. 2019. New model for determining criteria weights: Level Based Weight Assessment (LBWA) model. *Decision Making: Applications in Management and Engineering*, 2(2), pp.126-137. Available at: <https://doi.org/10.31181/dmame1902102z>.

Mejora del proceso de planificación de operaciones mediante un enfoque híbrido de toma de decisiones difusa y multicriterio

Ivan B. Petrović^a, Milan Ž. Milenković^b

^a Universidad de Defensa de Belgrado, Academia Militar, Belgrado, República de Serbia, **autor de correspondencia**

^b Universidad de Defensa de Belgrado, Escuela de Defensa Nacional "Mariscal de campo Radomir Putnik", Belgrado, República de Serbia

CAMPO: matemáticas aplicadas, ciencias militares

TIPO DE ARTÍCULO: artículo científico original

Resumen:

Introducción/objetivo: En el artículo se muestra la posibilidad de optimizar la toma de decisiones en el proceso de planificación de operaciones en unidades de defensa aérea mediante la aplicación de un enfoque de toma de decisiones multicriterio en un entorno difuso. Analizando el contenido de la bibliografía disponible, se determinaron los criterios de selección a partir de los cuales es posible evaluar y comparar los planes de acción de las unidades de defensa aérea. Los criterios se basan en los parámetros de evaluación de los planes de acción de la matriz de decisión en la fase del proceso de planificación de operaciones denominada los planes de acción validación y comparación.

Métodos: El enfoque propuesto combina el Laboratorio de Pruebas y Evaluación de la Toma de Decisiones (DEMATEL) y la Evaluación Proporcional Comprimida (COPRAS) que han sido modificados con éxito mediante conjuntos triangulares difusos. Se aplicó el método difuso-DEMATEL para determinar los pesos de los criterios y el método difuso-COPRAS para evaluar las alternativas - planes de acción.

Resultados: Se integraron múltiples métodos de toma de decisiones difusos y multicriterio en un modelo único que se puede aplicar en el proceso de planificación de operaciones con el objetivo de optimizar el proceso de toma de decisiones.

Conclusión: El artículo contribuye a la ciencia militar en la toma de decisiones relacionadas con el proceso de planificación de operaciones a nivel táctico en unidades de defensa aérea.

Palabras claves: Toma de Decisiones Multicriterio (MCDM), DEMATEL, COPRAS, Conjuntos Difusos Triangulares, Proceso de Planificación de Operaciones.

Совершенствование процесса планирования операций с использованием гибридного нечетко-многокритериального подхода к принятию решений

Иван Б. Петрович^а, Милан Ж. Миленкович^б

^а Университет обороны в г. Белград, Военная академия,
г. Белград, Республика Сербия, **корреспондент**

^б Университет обороны в г. Белград, Школа национальной обороны,
«Фельдмаршал Радомир Путник», г. Белград, Республика Сербия

РУБРИКА ГРНТИ: 27.47.19 Исследование операций,
28.17.31 Моделирование процессов управления
ВИД СТАТЬИ: оригинальная научная статья

Резюме:

Введение/цель: В статье представлена возможность оптимизации процесса принятия решений по планированию операций в подразделениях противовоздушной обороны путем применения многокритериального подхода к принятию решений в нечеткой среде. С помощью анализа содержания доступной литературы были определены критерии отбора, на основании которых можно оценивать и сравнивать действия подразделений противовоздушной обороны. Критерии основаны на параметрах оценки вариантов действий из матрицы принятия решений на этапе процесса сравнения вариантов применения.

Методы: Предлагаемый подход объединяет лабораторные испытания и оценку процесса принятия решений (DEMATEL) с методом комплексной пропорциональной оценки (COPRAS), которые были успешно модифицированы с помощью нечеткого треугольного числа. Для определения весовых коэффициентов критериев был применен метод fuzzy-DEMATEL, а для оценки альтернатив – вариантов действий был применен метод fuzzy-COPRAS.

Результаты: Несколько нечетких многокритериальных методов принятия решений были интегрированы в единую модель, которая может быть применена в процессе планирования операций с целью оптимизации процесса принятия решений.

Выводы: Данная статья вносит вклад в военную науку, в частности, в области принятия решений, связанных с процессом планирования операций на тактическом уровне в подразделениях противовоздушной обороны.

Ключевые слова: многокритериальное принятие решений (MCDM), DEMATEL, COPRAS, треугольные нечеткие числа, процесс планирования операций.

Унапређење процеса оперативног планирања применом хибридног фази-вишекритеријумског приступа одлучивању

Иван Б. Петровић^а, Милан Ж. Миленковић^б

^а Универзитет одбране у Београду, Војна академија,
Београд, Република Србија, **аутор за преписку**

^б Универзитет одбране у Београду, Школа националне одбране
„Војвода Радомир Путник“, Београд, Република Србија

ОБЛАСТ: примењена математика, војне науке

КАТЕГОРИЈА (ТИП) ЧЛАНКА: оригинални научни рад

Сажетак:

Увод/циљ: У раду је приказана могућност оптимизације доношења одлука у процесу оперативног планирања у артиљеријско-ракетним јединицама за противваздухопловна дејства применом метода вишекритеријумског одлучивања у фази окружењу. Анализом садржаја доступне литературе, одређени су критеријуми на основу којих је могуће вредновати и поредити варијанте употребе артиљеријско-ракетних јединица за противваздухопловна дејства које развијају чланови групе за оперативно планирање у току процеса оперативног планирања. Критеријуми се заснивају на параметрима оцењивања варијанти употребе из матрице одлучивања у фази поређења варијанти употребе.

Метод: Предложени приступ који комбинује методе ДЕМАТЕЛ и КОПРАС успешно је модификован троугластим фази скуповима. Метода фази-ДЕМАТЕЛ примењена је за одређивање тежине критеријума, а фази-КОПРАС метода за вредновање алтернатива – варијанти употребе.

Резултати: Интегрисано је више фази-вишекритеријумских метода одлучивања у јединствен модел који се може применити у процесу планирања операција ради оптимизације процеса доношења одлука.

Закључак: Рад доприноси војној науци приликом доношења одлука у процесу оперативног планирања на тактичком нивоу у артиљеријско-ракетним јединицама за противваздухопловна дејства.

Кључне речи: вишекритеријумско одлучивање (ВКО), ДЕМАТЕЛ, КОПРАС, троугласти фази скупови, оперативно планирање.


Paper received on: 06.02.2024.
Manuscript corrections submitted on: 24.09.2024.
Paper accepted for publishing on: 25.09.2024.


© 2024 The Authors. Published by Vojnotehnički glasnik / Military Technical Courier (www.vtg.mod.gov.rs, втг.мо.унп.срб). This article is an open access article distributed under the terms and conditions of the Creative Commons Attribution license (<http://creativecommons.org/licenses/by/3.0/rs/>).





Application of multi-criteria decision making for the selection of a location for crossing a water obstacle by fording in a defense operation

Duško Z. Tešić^a, Darko I. Božanić^b, Adis Puška^c

^a University of Defence in Belgrade, Military Academy, Dean Office, Belgrade, Republic of Serbia, e-mail: tesic.dusko@yahoo.com, **corresponding author**, ORCID iD:  <https://orcid.org/0000-0002-5277-3270>

^b University of Defence in Belgrade, Military Academy, Department of Tactics with Weapon Systems, Belgrade, Republic of Serbia, e-mail: dbozanic@yahoo.com, ORCID iD:  <https://orcid.org/0000-0002-9657-0889>

^c Government of the Brčko District of Bosnia and Herzegovina, Department of Public Safety, Brčko, Bosnia and Herzegovina, e-mail: adispuska@yahoo.com, ORCID iD:  <https://orcid.org/0000-0003-3274-0188>

 <https://doi.org/10.5937/vojtehg72-51249>

FIELD: applied mathematics, military sciences

ARTICLE TYPE: original scientific paper

Abstract:

Introduction/purpose: The paper presents the multi-criteria Fuzzy DIBR-Fuzzy DIBR II-EWAA-BM-DEXi-Fuzzy LMAW model for choosing a location for crossing water obstacles by fording in a defense operation. After the identification of the criteria by experts in this field, the mentioned model was applied and the optimal point was determined. In order to test the consistency of the results and the validity of the model, experts were consulted again, and the sensitivity analysis and the comparative analysis were performed.

Methods: The Fuzzy DIBR and Fuzzy DIBR II methods were used to determine the weighting coefficients of the identified criteria, while the aggregation of the expert opinions and the obtained values was performed using the EWAA and BM operators. To select the optimal location, the Fuzzy LMAW method was applied, while the linguistic descriptors were determined using the DEXi decision support system.

Results: The proposed methodology made it possible to identify all the criteria that determine the choice of a location and the choice of the optimal point for crossing a water obstacle in a defense operation. The testing of the model by experts, the analysis of the sensitivity of the output results to

changes in the weights of the criteria and the comparison of the obtained results with the results of other methods indicated the fact that the model is valid and that it gives consistent results.

Conclusion: It was concluded that the multi-criteria model provides the necessary help to decision makers in conditions of imprecise and unspecified information and that it is applicable in real situations. Also, the proposed model takes into consideration all the aspects that must be considered when making such a complex decision and helps less experienced officers in the decision-making process, reducing the possibility of errors, which can result in human casualties. Finally, directions for further research in the field of overcoming water obstacles and multi-criteria decision making are suggested.

Key words: wading, location, selection, military, MCDM, DIBR, DIBR II, Fuzzy, LMAW, EWAA, BM, DEXi.

Introduction

Overcoming water obstacles is a challenge that is present in all armies around the world and is considered one of the most difficult, most dangerous and complex combat actions and is a type of counter-engineering action aimed at ensuring the movement (maneuver) of units in combat operations (Pifat, 1980, p.13; Falkowski & Model, 2019). Considering a great number of waterways in our country, overcoming water obstacles in defensive actions against the enemy will be of great importance. Depending on deployment needs, different crossing points can be established: raft crossing point, bridge crossing point, ice crossing point, swimming crossing point, ford crossing point, deep fording crossing point, and underwater fording crossing point (Pifat, 1980, pp.225-233). The specifics of each of the operations determine the different conditions in which the water obstacle is overcome. Successfully overcoming such obstacles requires knowledge of various techniques and tactics, as well as detailed preparation. The preparation process includes collecting information on locations for crossing points, deciding on the most suitable location, and as a final step, establishing the crossing point itself. This is where the role of engineering officers comes into play - they must have a good understanding of the tactical and technical aspects of using various means to overcome water obstacles. Due to the complexity of these tasks, long-term experience of officers working in pontoon units and training is required to ensure the efficiency and safety of operations.

The location where the crossing over the water obstacle is established must meet the necessary conditions (criteria) in the assigned area, in accordance with the given task. The very choice of a location, for each of

the crossing points, is basically defined by the normative - legal regulations that regulate this area in the Serbian Armed Forces. The existing documents only outline the criteria and rely on the experience of officers. The criteria that have been established do not consider in detail all the factors that influence the decision on the location, i.e., they are not complete. Also, the mentioned factors are not elaborated in detail, nor are they described to such an extent that they can serve as a standard operating procedure when choosing a location, especially for officers who do not have enough experience in this area. Part of the criteria is of a qualitative nature, so its assessment is influenced by the subjectivity of the decision maker.

In order to eliminate errors when deciding on the choice of locations for overcoming water obstacles in a defense operation, primarily due to the lack of experience of decision makers and the inaccuracy and incompleteness of available information, it is necessary to establish a decision-support model that would allow decision makers to choose the optimal location, based on previously defined criteria, in which subjectivity would be reduced to the smallest possible error. It is necessary to note that mistakes made during the selection of a location for the establishment of a crossing point over a water obstacle can result in human casualties and cause damage to weapons and military equipment.

In order to make faster and better decisions about the choice of the site of crossing by fording, i.e., the point on the water obstacle that is "overcome by treading on the bottom of its bed" (Pifat, 1980, p.226), and better optimization of time and assistance to less experienced officers for making such a decision in a defense operation, in this research a decision support model was established, which includes all the factors necessary for making an optimal decision on the choice of a location. The mentioned model includes the application of multi-criteria decision-making (MCDM) methods for the subject choice. The application of different MCDM methods, for solving different decision-making problems in different areas, is shown in numerous papers (Keshavarz-Ghorabae et al, 2022; Mishra et al, 2023; Sahoo & Goswami, 2024; De & Nandi, 2024; Aldaghi & Muzik, 2024; Radovanović et al, 2024; Kumar et al, 2024; etc.). The selection of different locations using different methods was also the subject of different research studies (Ulutaş & Karakuş, 2021; Ao Xuan et al, 2022; Aykac et al, 2023; Maghfiroh & Kavirathna, 2023; Nghiem & Chu, 2024; Alwedyan, 2024; Raad & Rajendran, 2024; Yücenur & Maden, 2024; etc.). The field of MCDM was also applied to solving various problems in the military field, including location selection, as evidenced by a large number of papers (Sánchez-Lozano & Rodríguez, 2020; de Araújo Costa et al, 2022;

Swethaa & Felix, 2023; Kurnaz et al, 2023; Tešić & Božanić, 2023; Dağıstanlı & Kurtay, 2024; Bilgin et al, 2024; etc.). The specific choice of locations (points) for crossing a water obstacle using multi-criteria decision-making methods is presented in a small number of papers, which are mainly research studies conducted by the authors of this article, e.g (Tešić & Božanić, 2018; Božanić et al, 2018; Setiadji et al, 2020; Žnidaršič et al, 2024; etc.), but no research deals with the choice of a fording crossing site in a defensive operation. Given that the choice of indicators is conditioned by data that confirm or refute the hypothesis and reflect the properties of the subject and research objectives, the indicators are based on previous scientific knowledge about the subject of research (Bazić & Danilović, 2015), and, given that there are no detailed criteria that influence the subject selection, that there are no previous research studies in this specific area, and that the area is defined by normative-legal documents, there was a need for this research as well as for this way of defining indicators.

The most frequently used criteria for evaluating alternatives, in the previous research in this area, were: Concealment of preparations, Degree of exposure to enemy fire, Characteristics of shores/banks, Camouflage, Bank characteristics, Characteristics of the terrain for the redirection of units and vehicles, Depth of water obstacles, Protection of own forces, Width of water obstacles, Speed of water current, Quality and number of access routes, Scope of work on the approaches to banks, Bottom composition, Existence of material deposits, Existence of obstacles, etc. From the aforementioned research, it is concluded that the problems of choosing locations for overcoming water obstacles can be successfully solved by applying MCDM methods.

Given that the aspects from which the subject of research is viewed represent incomplete and imprecise data, i.e., that most of them are known through linguistic descriptions, and that in previous research Fuzzy theory was used (which gave good output results with this type of data (Rashid et al, 2023; Božanić et al, 2018; Setiadji et al, 2020; Wang et al, 2024)), the authors in this paper also decided to use methods that were improved using Fuzzy theory. The model formed and used in this paper includes relevant MCDM methods for defining the weighting coefficients of the criteria Fuzzy DIBR (Defining Interrelationships Between Ranked) and the Fuzzy DIBR II, based on expert opinions, with the DEXi decision support system (used to form linguistic descriptors for qualitative criteria), as well as the Fuzzy LMAW (Logarithm Methodology of Additive Weights) method for determining the optimal location from a set of possible solutions in conditions of imprecise and incomplete input parameters. The EWAA

(Einstein Weighted Arithmetic Average) operator was used for the aggregation of expert opinions, while the BM (Bonferoni Mean) operator was used for the aggregation of weighting coefficients obtained by different methods (Fuzzy DIBR and Fuzzy DIBR II). The validity of the proposed methodology was tested by experts in this field. In order to check the stability and validity of the proposed model, a sensitivity analysis of the output results of the proposed methodological procedure was performed, as well as a comparison of the obtained results with the results obtained using six other fuzzy MCDM methods. The reasons for the formation of such a multi-criteria model are reflected in the following: considering that experts are not always completely sure of their claims, the degree of confidence of the experts was used to form a triangular fuzzy number, which, by reducing the expert's confidence in the statement, blurs the fuzzy number and reduces its crisp value; in order to obtain more precise values of the weights of the criteria, two methods were used to determine the weights, which use different scales to define the relationship between the criteria; and when defining the weights, the competences of the experts were also taken into account using the EWAA operator. The reasons for applying Fuzzy theory have been previously explained. In Figure 1, the algorithm of the proposed methodology is presented.

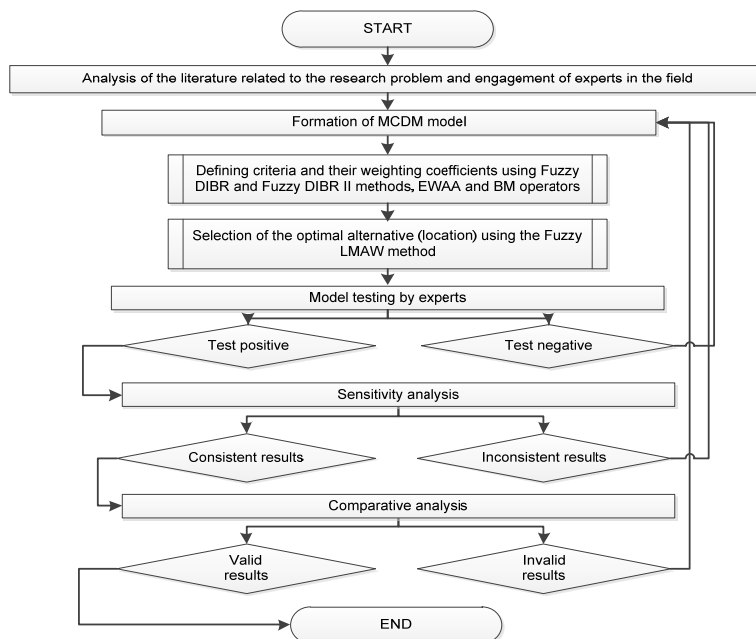


Figure 1 – Algorithm of the proposed MCDM methodology

Description of the methods

So far, various MCDM methods have been developed, both for determining the weighting coefficients of the criteria and for the calculation of the optimal alternative; they have been used in numerous areas to solve various decision-making problems. For the purpose of this research, DIBR, DIBR II, and LMAW methods were used, improved by triangular fuzzy numbers formed using degrees of confidence.

More about Fuzzy theory and numbers can be seen in (Zadeh, 1965; Zadeh, 1973; Pathinathan et al, 2015). Figure 2 shows an example of a triangular fuzzy number based on the degree of confidence of the decision maker in the given statement (Tešić et al, 2024).

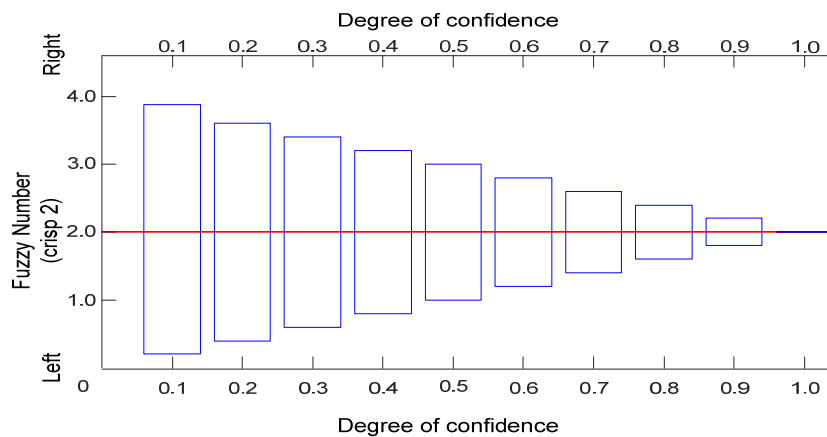


Figure 2 – Example of a triangular fuzzy number based on the degree of confidence of the decision maker

Fuzzy DIBR

The DIBR method (Pamucar et al, 2021a), with its simple mathematical apparatus, is intended for the calculation of weighting coefficients of criteria. In order to apply this method to imprecise and incomplete data, it was improved using triangular fuzzy numbers (Pamucar et al, 2022).

Figure 3 shows the steps of applying the method.

```

# Step 1: Ranking criteria by importance
IF there exists a set of criteria and criterion is chosen as most importance THEN
    Rank the other criteria in set C by importance so that criterion is at the first place.
ENDIF

# Step 2: Comparing criteria by importance and defining mutual relationships
FOR each criterion in set C DO
    FOR each other criterion in set C DO
        IF is not equal to THEN
            Enter the value of relationship
            # Ratio values are triangular fuzzy numbers.
        ENDIF
    ENDFOR
ENDFOR

# Step 3: Defining relations for calculating weight coefficients
FOR each criterion in set C DO
    Define relations for calculating weight coefficients of criteria based on defined relationships and
ENDFOR

# Step 4: Calculating the weight coefficient of the most influential criterion
Calculate the weight coefficient for criterion based on defined relationships
    # The values of the weight coefficients of the criteria are triangular fuzzy numbers

Calculate the weight coefficients for other criteria ( to ) based on defined relationships

Calculate the crisp value of weight coefficients and and

# Step 5: Defining the degree of satisfaction of subjective relationships between criteria
FOR and DO
    Calculate
        IF Difference between and is less than 10% THEN
            Print "Relationship between criteria is satisfied."
        ELSE
            Print "Relationship between criteria is not satisfied."
            # It is necessary to define new relationships between the criteria in order to satisfy the stated condition.
        ENDIF
    ENDFOR
ENDFOR
    
```

Figure 3 – Pseudocode of the Fuzzy DIBR method

Fuzzy DIBR II

The DIBR II method (Božanić & Pamučar, 2023) represents an improved DIBR method, based on a small number of pairwise comparisons, and has so far found application in various research areas. The method is additionally improved by Fuzzy theory (Tešić et al, 2024), and the steps of the method are presented in Figure 4.


```

# Step 1: Identification of the criteria
Identify_criteria_C(m) # Where m is the total number of criteria
Print "C(m)"

# Step 2: Determining the importance of each identified criterion
IF there exists a set of criteria C(m) and criterion is chosen as most importance THEN
  Rank the other criteria in set C(m) by importance so that criterion is at the first place.

# Step 3: Defining the relationship between criteria
FOR each criterion DO
  FOR each criterion DO
    IF is not equal to THEN
      Determine_degree_of_confidence( )
      IF Degree_of_confidence satisfies condition THEN
        Define_relationship_between_criteria() based on
      ENDIF
    ENDIF
  ENDFOR
ENDFOR

# Step 4: Defining the relationship between the most significant and other criteria
Define_relationship_between_most_significant_and_other_criteria():

# Step 5: Determination of the value of the weight coefficient of the most significant criterion
Determine_weight_coefficient_of_most_significant_criterion():
# The values of the weight coefficients of the criterion is triangular fuzzy number

# Step 6: Determination of the value of the weight coefficient of the other criteria
# The values of the weight coefficients of the criteria are triangular fuzzy numbers
Determine_weight_coefficient_of_other_criteria( to )

# Step 7: Defuzzification of the value of the weight coefficient of the criteria
Defuzzify_weight_coefficient_of_criteria():

# Step 8: Determining the quality of the relationship between the criteria
Determine_quality_of_relationship_between_criteria():
Calculate_deviation_values() # Using Equation
Calculate_control_value() # Using Equation
IF Deviation_values satisfy condition THEN
  Print "Relationship quality between criteria is satisfactory."
ELSE
  Print "Relationship quality between criteria is not satisfactory."
  # It is necessary to define new relationships between the criteria in order to satisfy the stated condition.
ENDIF

```

Figure 4 – Pseudocode of the Fuzzy DIBR II method

Aggregation operators

For aggregating expert opinions, the EWAA operator, presented in (Tešić & Božanić, 2023), was used. The mathematical expression of the operator is presented by expression (1).

$$EWAA\{\chi_1, \chi_2, \dots, \chi_j\} = \sum_{j=1}^e \chi_j^e \frac{\prod_{j=1}^e (1 + f(\chi_j^e))^{\lambda} - \prod_{j=1}^e (1 - f(\chi_j^e))^{\lambda}}{\prod_{j=1}^e (1 + f(\chi_j^e))^{\lambda} + \prod_{j=1}^e (1 - f(\chi_j^e))^{\lambda}} \quad (1)$$

where e is the total number of experts, $\lambda = 1/e$ when all experts have the same competence coefficient, and $\lambda = \omega^e$ when the competences of the experts are different (ω^e).

The BM operator was used to aggregate the obtained values of the weighting coefficients of the criteria using the Fuzzy DIBR and Fuzzy DIBR II methods and to obtain the final criteria weights (Bonferroni, 1950; Tešić & Božanić, 2023), and its mathematical formulation is presented by expression (2).

$$BM^{r,s}(x_1, x_1, \dots, x_n) = \left(\frac{1}{n(n-1)} \sum_{i,j=1}^n x_i^r x_j^s \right)^{\frac{1}{r+s}} \quad (2)$$

Fuzzy LMAW

Pamučar et al. (2021b) presented the LMAW method in 2021. It has a dual purpose: 1) determining the weighting coefficients of the criteria, and 2) calculating the optimal alternative. Like the previous methods, this method has been improved using triangular fuzzy numbers and applied in various research areas (Tešić et al, 2023). The mathematical apparatus of the Fuzzy LMAW method for determining the weights of the criteria is presented in the following text.

Step 1: Formation of the initial decision matrix ($\tilde{X} = [\tilde{x}_{ij}]_{m \times n}$)

Step 2. Normalization of the elements of the initial decision matrix ($\tilde{N} = [\tilde{n}_{ij}]_{m \times n}$)

$$\tilde{n}_{ij} = \begin{cases} \left\{ 1 + \frac{\tilde{x}_{ij}}{\tilde{x}_j^{(+)}}, 1 + \frac{x_j^{(l)}}{\tilde{x}_j^{(+)}}, 1 + \frac{x_j^{(s)}}{\tilde{x}_j^{(+)}}, 1 + \frac{x_j^{(d)}}{\tilde{x}_j^{(+)}} \right\} & \text{if } j \in \text{Benefit,} \\ \left\{ 1 + \frac{\tilde{x}_j^{(-)}}{\tilde{x}_{ij}}, 1 + \frac{x_j^{(-)}}{x_j^{(d)}}, 1 + \frac{x_j^{(-)}}{x_j^{(s)}}, 1 + \frac{x_j^{(-)}}{x_j^{(l)}} \right\} & \text{if } j \in \text{Cost} \end{cases} \quad (3)$$

where \tilde{n}_{ij} represents the normalized values of the initial decision matrix, $x_j^{(+)} = \max(x_j^{(d)})$, and $x_j^{(-)} = \min(x_j^{(l)})$, l represents the left, d - on the right is the distribution of the fuzzy number, and s is the value where the membership function of the fuzzy number is equal to 1.

Step 3. Calculation of the weighted matrix ($\tilde{Z} = [\tilde{z}_{ij}]_{m \times n}$).

$$\tilde{z}_{ij} = \frac{2\tilde{\tau}_{ij}^{w_j}}{(2 - \tilde{\tau}_{ij})^{w_j} + \tilde{\tau}_{ij}^{w_j}} = \left(\frac{2\tau_j^{(l)w_j}}{(2 - \tau_j^{(d)})^{w_j} + \tau_j^{(d)w_j}}, \frac{2\tau_j^{(s)w_j}}{(2 - \tau_j^{(s)})^{w_j} + \tau_j^{(s)w_j}}, \frac{2\tau_j^{(d)w_j}}{(2 - \tau_j^{(l)})^{w_j} + \tau_j^{(l)w_j}} \right) \quad (4)$$

$$\text{where } \tilde{\tau}_{ij} = \frac{\ln(\tilde{n}_{ij})}{\ln\left(\prod_{i=1}^m \tilde{n}_{ij}\right)} = \left(\frac{\ln(n_{ij}^{(l)})}{\ln\left(\prod_{i=1}^m n_{ij}^{(d)}\right)}, \frac{\ln(n_{ij}^{(s)})}{\ln\left(\prod_{i=1}^m n_{ij}^{(s)}\right)}, \frac{\ln(n_{ij}^{(d)})}{\ln\left(\prod_{i=1}^m n_{ij}^{(l)}\right)} \right) \quad (5)$$

Step 4. Calculation of the final index for ranking the alternatives (\tilde{Q}_i)

$$\tilde{Q}_i = \sum_{j=1}^n \tilde{\tau}_{ij} = \left(\sum_{j=1}^n \tau_{ij}^{(l)}, \sum_{j=1}^n \tau_{ij}^{(s)}, \sum_{j=1}^n \tau_{ij}^{(d)} \right) \quad (6)$$

The ranking of the alternatives is formed on the basis of defuzzificated index values (\tilde{Q}_i), i.e., a higher value of the index of the alternative implies a higher rank and vice versa.

Application of the MCDM model

For the purpose of this research, 26 experts in this particular field were engaged. The experts were sent a questionnaire to identify the criteria that influence the choice of a location for crossing a water obstacle by fording in a defense operation. After applying the Delphi method and processing the obtained data, the opinions of four experts were rejected due to a large deviation from the opinion of the expert group, so that in the end 22 experts were engaged in the entire research process, i.e. $E \in \{E_1, E_2, \dots, E_{22}\}$, and, by applying the methodology presented in Tešić & Božanić (2024), their competencies were defined $E_{\omega} \in \left\{ \begin{matrix} 0.0484, 0.0535, 0.0365, 0.0439, 0.038, 0.0375, 0.0424, 0.043, 0.0388, 0.0372, 0.0364, \\ 0.0375, 0.0498, 0.0579, 0.0554, 0.0536, 0.0496, 0.0492, 0.0417, 0.0444, 0.0529, 0.0526 \end{matrix} \right\}$. Based on expert opinions, a total of 13 criteria affecting the location choice $C \in \{C_1, C_2, \dots, C_{13}\}$ were identified (Table 1).

After defining the criteria, each of the experts defined the ranking of the criteria in accordance with their significance and the relationships between the criteria, as well as their degree of confidence.

Table 1 – Criteria that affect the choice of a fording location

Criterion	Criterion type	
	Benefit/Cost	Numerical/ Linguistic
C ₁ - Quality of access routes on both banks	Benefit	Linguistic
C ₂ - Scope of works on the entry and exit banks	Cost	Linguistic
C ₃ - Water obstacle width (m)	Cost	Numerical
C ₄ - Water obstacle depth (m)	Cost	Numerical
C ₅ - Water current speed (m/sec)	Cost	Numerical
C ₆ - Composition of the water obstacle bed	Benefit	Linguistic
C ₇ - Camouflage conditions	Benefit	Linguistic
C ₈ - Vulnerability of the crossing point to the enemy attacks	Cost	Linguistic
C ₉ - Natural and man-made obstructions in and along the water obstacle	Benefit	Linguistic
C ₁₀ - Conditions for bank preparations	Benefit	Linguistic
C ₁₁ - Existence of local material sites, resources and workshops (industrial plants)	Benefit	Linguistic
C ₁₂ - Water level change tendency	Benefit	Linguistic
C ₁₃ - Possibility of deploying tanks for action and maneuvering on the exit bank	Benefit	Linguistic

By applying the steps of the Fuzzy DIBR method (Figure 3) and the Fuzzy DIBR II method (Figure 4), for each of the experts, aggregation was performed using the EWAA operator, expression (1), and the coefficients of the expert competences, which resulted in the criteria weight values for each method (Table 2).

Table 2 – Aggregated values of the criteria weights for each of the methods

	C ₁	C ₂	C ₃	C ₄	C ₅	C ₆	C ₇
Fuzzy DIBR	0.0438	0.0410	0.1219	0.1741	0.1462	0.1417	0.0440
Fuzzy DIBR II	0.0429	0.0396	0.1199	0.1846	0.1511	0.1431	0.0407
	C ₈	C ₉	C ₁₀	C ₁₁	C ₁₂	C ₁₃	
Fuzzy DIBR	0.0906	0.0345	0.0271	0.0179	0.0552	0.0620	
Fuzzy DIBR II	0.0905	0.0337	0.0263	0.0162	0.0564	0.0550	

In order to arrive at the final values of the weighting coefficients of the criteria using the BM operator, expression (2), the data from Table 2, i.e., the weights of each of the criteria for both methods are aggregated. The final values of the criteria weights are presented in Table 3 and represent the input data for the initial decision matrix.

Table 3 – Final values of the criteria weights

	C₁	C₂	C₃	C₄	C₅	C₆	C₇
w	0.0434	0.0403	0.1209	0.1793	0.1487	0.1424	0.0423
	C₈	C₉	C₁₀	C₁₁	C₁₂	C₁₃	C₈
w	0.0906	0.0341	0.0267	0.0170	0.0558	0.0584	0.0906

In order to choose the optimal location for crossing a water obstacle by fording in a defense operation, it is necessary to evaluate the defined alternatives in accordance with each identified criterion. The evaluation for the linguistic type criteria is performed using Fuzzy linguistic descriptors, presented in Table 4.

Table 4 – Fuzzy linguistic criteria descriptors

Linguistic descriptors for criterion C ₁₀		Linguistic descriptors for criterion C ₁₃	
Description of the linguistic descriptor	Scale value	Description of the linguistic descriptor	Scale value
Excellent (OD)	(8, 9, 10)	Favorable conditions (PU)	(8, 9, 10)
Very Good (VD)	(5, 6, 7)	Partially favorable conditions (SP)	(5, 6, 7)
Good (DO)	(3, 4, 5)	Partially adverse conditions (DN)	(2, 3, 4)
Sufficient (DV)	(1, 2, 3)	Unfavorable conditions (NU)	(1, 1, 1)
Insufficient (NDV)	(1, 1, 1)		
Linguistic descriptors for criterion C ₉		Linguistic descriptors for criterion C ₁₂	
Description of the linguistic descriptor	Scale value	Description of the linguistic descriptor	Scale value
Positive impact (P)	(8, 9, 10)	Favorable Trend (PT)	(8, 9, 10)
Partial positive impact (PD)	(5, 6, 7)	Partially Favorable Trend (DPT)	(5, 6, 7)
Partially negative impact (ND)	(2, 3, 4)	Partially Unfavorable Trend (DNT)	(2, 3, 4)
Negative impact (N)	(1, 1, 1)	Unfavorable Trend (NT)	(1, 1, 1)

Linguistic descriptors for criterion C ₇		Linguistic descriptors for criterion C ₁	
Description of the linguistic descriptor	Scale value	Description of the linguistic descriptor	Scale value
Excellent (O)	(8, 9, 10)	Excellent (OD)	(8, 9, 10)
Very good (V)	(5, 6, 7)	Very Good (VD)	(5, 6, 7)
Good (D)	(3, 4, 5)	Good (DO)	(3, 4, 5)
Satisfactory (Z)	(1, 2, 3)	Sufficient (DV)	(1, 2, 3)
Unsatisfactory (NZ)	(1, 1, 1)	Insufficient (ND)	(1, 1, 1)
Linguistic descriptors for criterion C ₆		Linguistic descriptors for criterion C ₈	
Description of the linguistic descriptor	Scale value	Description of the linguistic descriptor	Scale value
The bottom of the water obstacle has sufficient bearing capacity and is flat (DDR)	(8, 9, 10)	Very Large (VV)	(8, 9, 10)
The bottom of the water obstacle has sufficient bearing capacity, but it is not flat (DDN)	(5, 6, 7)	Large (VE)	(5, 6, 7)
The bottom of the water obstacle does not have sufficient load-bearing capacity (the load-bearing capacity can be increased), but it is flat (DNR)	(3, 4, 5)	Middle (SR)	(3, 4, 5)
The bottom of the water obstacle does not have sufficient load-bearing capacity (the load-bearing capacity can be increased) and is not flat (DMN)	(1, 2, 3)	Small (MA)	(1, 2, 3)
The bottom of the water obstacle does not have sufficient load capacity (the load capacity cannot be increased) and is not flat (DNN)	(1, 1, 1)	Does not exist (NP)	(1, 1, 1)
Linguistic descriptors for criterion C ₁₁		Linguistic descriptors for criterion C ₂	
Description of the linguistic descriptor	Scale value	Description of the linguistic descriptor	Scale value
Exist (P)	(6, 8, 10)	Big (VEL)	(6, 8, 10)
Partially Exist (DP)	(2, 4, 6)	Medium (SRE)	(2, 4, 6)
Non Existant (NPo)	(1, 1, 1)	Small (MAL)	(1, 1, 2)

To determine the linguistic descriptor, for the purposes of this research, the DEXi decision support system (Bohanec, 2023), based on the DEX methodology (Bohanec et al, 2013), was used. The DEXi uses a

system of logical rules to make decisions. Each linguistic descriptor is broken down into several criteria and sub-criteria and depending on the logical rules, its value is determined.

Based on all the above, an initial decision-making matrix was formed. It consists of five alternatives $A \in \{A_1, A_2, \dots, A_5\}$ and 13 criteria (Table 1), previously identified by experts (Table 5).

Table 5 – Initial decision matrix

	C₁	C₂	C₃	C₄	C₅	C₆	C₇
A₁	DO	SRE	60	1.1	0.8	DDR	D
A₂	DV	SRE	55	1.1	0.9	DNR	O
A₃	DV	MAL	58	1.2	0.8	DDN	NZ
A₄	ND	SRE	51	1	2	DDR	Z
A₅	ND	MAL	60	0.9	2.1	DDN	D
	C₈	C₉	C₁₀	C₁₁	C₁₂	C₁₃	
A₁	VV	ND	DO	DP	DPT	PU	
A₂	VE	ND	NDV	DP	PT	PU	
A₃	VE	N	VD	NP _o	DNT	DP	
A₄	VV	N	DV	DP	DPT	DN	
A₅	SR	ND	NDV	P	PT	PD	

The initial decision matrix (Table 5), using fuzzy linguistic descriptors (Table 4), is translated into the Fuzzy initial decision matrix (Table 6).

Table 6 – Fuzzy initial decision matrix

	C₁	C₂	C₃	C₄	C₅	C₆	C₇
A₁	(3, 4, 5)	(2, 4, 6)	(60, 60, 60)	(1.1, 1.1, 1.1)	(0.8, 0.8, 0.8)	(8, 9, 10)	(3, 4, 5)
A₂	(1, 2, 3)	(2, 4, 6)	(55, 55, 55)	(1.1, 1.1, 1.1)	(0.9, 0.9, 0.9)	(3, 4, 5)	(8, 9, 10)
A₃	(1, 2, 3)	(1, 1, 2)	(58, 58, 58)	(1.2, 1.2, 1.2)	(0.8, 0.8, 0.8)	(5, 6, 7)	(1, 1, 1)
A₄	(1, 1, 1)	(2, 4, 6)	(51, 51, 51)	(1, 1, 1)	(2, 2, 2)	(8, 9, 10)	(1, 1, 1)
A₅	(1, 1, 1)	(1, 1, 2)	(60, 60, 60)	(0.9, 0.9, 0.9)	(2.1, 2.1, 2.1)	(5, 6, 7)	(3, 4, 5)
	C₈	C₉	C₁₀	C₁₁	C₁₂	C₁₃	
A₁	(8, 9, 10)	(2, 3, 4)	(3, 4, 5)	(2, 4, 6)	(5, 6, 7)	(8, 9, 10)	

A₂	(5, 6, 7)	(2, 3, 4)	(1, 1, 1)	(2, 4, 6)	(8, 9, 10)	(8, 9, 10)
A₃	(5, 6, 7)	(1, 1, 1)	(5, 6, 7)	(1, 1, 1)	(2, 3, 4)	(5, 6, 7)
A₄	(8, 9, 10)	(1, 1, 1)	(1, 2, 3)	(2, 4, 6)	(5, 6, 7)	(2, 3, 4)
A₅	(3, 4, 5)	(2, 3, 4)	(1, 1, 1)	(6, 8, 10)	(8, 9, 10)	(5, 6, 7)

The formation of the initial decision matrix represents the first step in the application of the Fuzzy LMAW method. After the other steps of the method, expressions from (3) to (6), have been applied, the final ranking indices are defined for each of the alternatives, and, by dephasing the specified values, the final rankings of the alternatives are obtained (Table 7).

Table 7 – Values of the final index (Q) and the ranking of the alternatives

Alternative	\tilde{Q}_i	Q_i	Rank
A₁	(11.71, 11.95, 12.21)	11.950	1
A₂	(11.64, 11.9, 12.18)	11.907	2
A₃	(11.63, 11.87, 12.11)	11.866	4
A₄	(11.56, 11.79, 12.04)	11.797	5
A₅	(11.67, 11.9, 12.13)	11.898	3

In order to validate the obtained results, the experts were asked to rank the alternatives (Table 8) based on the initial decision matrix (Table 5).

Table 8 – Ranking alternatives based on the expert opinions

	A₁	A₂	A₃	A₄	A₅		A₁	A₂	A₃	A₄	A₅
E1	2	1	4	5	3	E12	1	4	2	3	5
E2	1	2	5	4	3	E13	2	1	4	5	3
E3	1	3	2	5	4	E14	2	1	3	5	4
E4	2	1	5	4	3	E15	1	2	4	5	3
E5	3	2	1	4	5	E16	1	2	4	5	3
E6	1	5	3	2	4	E17	1	2	5	4	3
E7	1	2	4	5	3	E18	1	2	4	5	3
E8	1	2	4	5	3	E19	1	2	4	5	3
E9	2	1	4	5	3	E20	1	2	4	5	3
E10	1	2	5	4	3	E21	1	2	4	5	3
E11	1	3	2	5	4	E22	1	3	2	5	4

Given that there is a consensus of expert opinions (Tešić & Božanić, 2024), the ranks were aggregated using the EWAA operator and the final ranking of the alternatives was obtained by the experts (Table 9).

Table 9 – Final ranking of the alternatives based on the expert opinions

Alternative	EWAA	Rank
A ₁	1.286692	1
A ₂	2.058976	2
A ₃	3.778465	4
A ₄	4.528116	5
A ₅	3.350265	3

Based on the ranks obtained by expert evaluation, it can be concluded that the proposed methodology is valid, i.e., that it gives correct results.

Sensitivity analysis

In order to check the stability of the model to changes in the weighting coefficients of the criteria, 40 different change scenarios were formed (Figure 5).

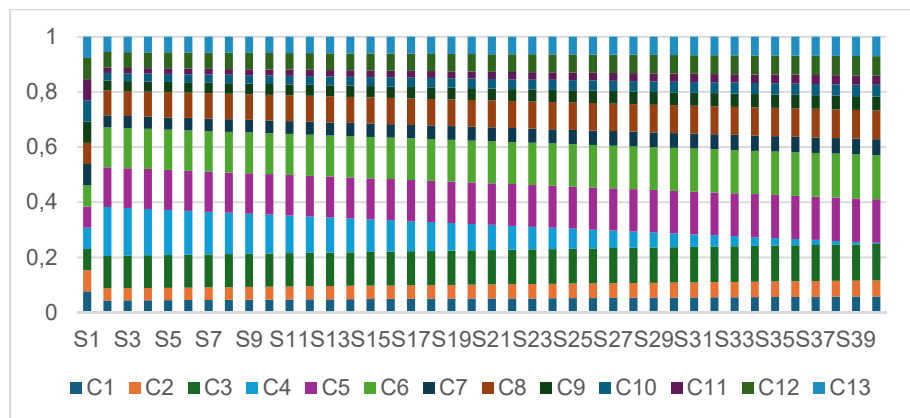


Figure 5 – Scenarios of changes in criteria weights

Applying the mentioned scenarios in the Fuzzy LMAW method leads to the following results (Figure 6):

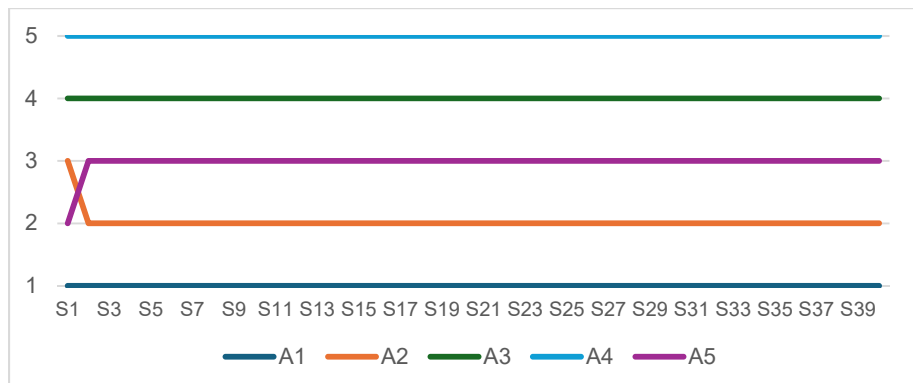


Figure 6 – Rankings of the alternatives obtained by applying scenarios

As it can be seen from the previous figure, the methodology used in this research produces very consistent results. The first-ranked alternative A_1 was chosen as optimal in all cases, while the last-ranked alternative was in the last place in all cases. Also, it can be stated that the ranking of alternatives A_5 and A_2 changes slightly in the scenario S_1 , i.e., in the case when all criteria have equal weights.

Comparative analysis

In order to validate the model, the obtained results were compared with the results obtained by the Fuzzy WASPAS (Weighted Aggregated Sum Product Assessment) (Turskis et al, 2015), Fuzzy VIKOR (Višekriterijumsko KOmpromisno Rangiranje) (Chang, 2014), Fuzzy SAW (Simple Additive Weighting) (Roszkowska & Kacprzak, 2016), Fuzzy MABAC (Multi-Attributive Border Approximation Area Comparison) (Bozanić et al, 2018), Fuzzy COPRAS (Complex Proportional Assessment) (Zarbahshnia et al, 2018) and Fuzzy CoCoSo (Combined Compromise Solution) (Fernández-Portillo et al, 2023) methods. As it can be concluded from the obtained results shown in Figure 7, the alternative A_1 is ranked first in all methods. Also, in Figure 8, it can be seen that the Pearson correlation coefficient of the ranks (Rodgers & Nicewander, 1988) obtained by the mentioned methods, in relation to the Fuzzy LMAW method, tends to an ideal positive correlation.

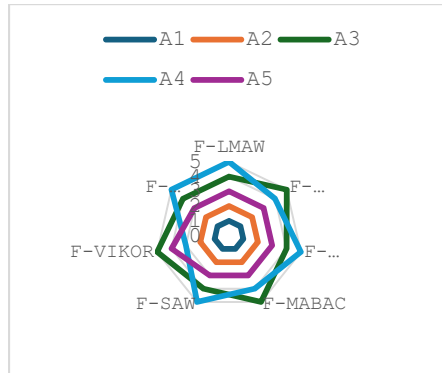


Figure 7 – Rankings of the alternatives obtained by different methods

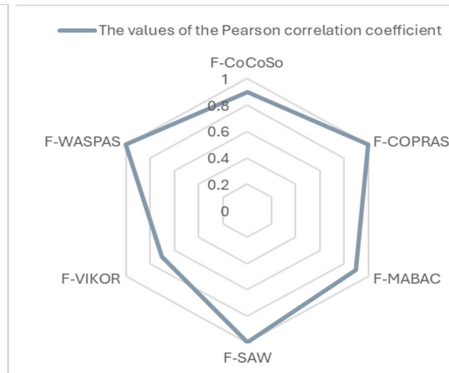


Figure 8 – The values of the Pearson correlation coefficient of the obtained ranks

Conclusion

In this research, a model was developed for the selection of a location for fording a water obstacle in a defense operation using MCDM methods, i.e., the Fuzzy DIBR-Fuzzy DIBR II-EWAA-BM-Fuzzy LMAW model. The proposed model represents significant progress in the field of overcoming water obstacles and decision making, enabling more accurate and efficient decisions in choosing a site to cross a water obstacle in conditions of uncertainty and inaccuracy, in a defense operation. The application of the Fuzzy DIBR and Fuzzy DIBR II methods, which are based on expert opinions and use the DEXi decision system, allows the inclusion of imprecision in the decision process, which is of extreme importance in the context of defense operations where information is usually incomplete or unclear. At the same time, the application of the Fuzzy LMAW method contributes to the determination of the optimal location in conditions of uncertainty in the input parameters. The use of the EWAA and BM operators for the aggregation of expert opinions and weighting coefficients implies the importance of taking into account different aspects in decision making. This approach provides a complex evaluation of various criteria and aspects that influence the choice of location.

The validity of the proposed methodology was confirmed by expert testing, which guarantees the relevance and applicability of the model in real situations. Additionally, the performed sensitivity analysis and a comparison with other MCDM methods confirm the stability and validity of the proposed model.

The developed model represents a significant contribution to the field of military decision making and provides necessary assistance to less experienced officers. Its application can significantly improve the selection of the location for fording water obstacles, which is crucial for the successful execution of defense operations. The main innovation in this research is the introduction of MCDM methods and DEXi software in this area, specifically in solving this problem, as well as comprehensively defining the criteria that condition the subject choice. Practical application is reflected in clearly defined criteria and the MCDM model that can easily be converted into an application, the use of which will be adjusted to the user.

This research opens up new opportunities for further research and applications of other theories that deal well with inaccuracies and uncertainties, as well as the development of application software for wider use. Also, the proposed methodology can be used for any research problem, with the definition of new criteria and new decision models in DEXi software. The main limitations of this research are related to the subject of the research itself; namely, the criteria that have been defined refer exclusively to deciding on a location in a defense operation while for other types of operations it would be necessary to redefine the criteria.

References

Aldaghi, T. & Muzik, J. 2024. Multicriteria Decision-Making in Diabetes Management and Decision Support: Systematic Review. *JMIR medical informatics*, 12, e47701. Available at: <https://doi.org/10.2196/47701>.

Alwedyan, S. 2024. Optimal location selection of a casual-dining restaurant using a multi-criteria decision-making (MCDM) approach. *International review for spatial planning and sustainable development*, 12(1), pp.156-172. Available at: https://doi.org/10.14246/irspsd.12.1_156.

Ao Xuan, H., Vu Trinh, V., Techato, K. & Phoungthong, K. 2022. Use of hybrid MCDM methods for site location of solar-powered hydrogen production plants in Uzbekistan. *Sustainable Energy Technologies and Assessments*, 52(A), art.number:101979. Available at: <https://doi.org/10.1016/j.seta.2022.101979>.

Aykac, Y.E., Yucesan, M. & Gul, M. 2023. Development of a Best-Worst Method based MCDM approach for solar power plant location selection: An Application to Tunceli, Turkey. *International Journal of Multicriteria Decision Making (IJMCDM)*, 9(4), pp.322-350. Available at: <https://doi.org/10.1504/ijmcdm.2023.10056276>.

Bazić, M. & Danilović, N. 2015. Draft scientific concept of the research project. *Megatrend revija/Megatrend Review*, 12(3), pp.5-28 (in Serbian). Available at: <https://doi.org/10.5937/MegRev1503005B>.

Bilgin, N.G., Bozma, G. & Riaz, M. 2024. Location selection criteria for a military base in border region using N-AHP method. *AIMS Mathematics*, 9(3), pp.7529-7551. Available at: <https://doi.org/10.3934/math.2024365>.

Bohanec, M. 2023. DEXi: A Program for Multi-Attribute Decision Making Version 5.0. In: *Jožef Stefan Institute (Ljubljana, Slovenia)*, June 6 [online]. Available at: <https://kt.ijs.si/MarkoBohanec/dexi.html> [Accessed: 18 April 2024].

Bohanec, M., Žnidaršič, M., Rajkovič, V., Bratko, I., & Zupan, B. 2013. DEX Methodology: Three Decades of Qualitative Multi-Attribute Modeling. *Informatica*, 37(1), pp.49-54 [online]. Available at: <https://www.informatica.si/index.php/informatica/article/view/433/437> [Accessed: 20 April 2024].

Bonferroni, C. 1950. Sulle medie multiple di potenze. *Bollettino Della Unione Matematica Italiana*, 5(3-4), pp.267-270 [online]. Available at: https://www.bdim.eu/item?id=BUMI_1950_3_5_3-4_267_0&fmt=pdf (in Italian) [Accessed: 18 April 2024].

Božanić, D., Tešić, D. & Milićević, J. 2018. A hybrid Fuzzy AHP-MABAC model: Application in the Serbian Army – The selection of the location for deep wading as a technique of crossing the river by tanks. *Decision Making: Applications in Management and Engineering*, 1(1), pp.143-164. Available at: <https://doi.org/10.31181/dmame1801143b>.

Božanić, D. & Pamucar, D. 2023. Overview of the Method Defining Interrelationships Between Ranked Criteria II and Its Application in Multi-criteria Decision-Making. In: Chatterjee, P., Pamucar, D., Yazdani, M. & Panchal, D. (Eds.) *Computational Intelligence for Engineering and Management Applications. Lecture Notes in Electrical Engineering*, 984, pp.863-873. Singapore: Springer. Available at: https://doi.org/10.1007/978-981-19-8493-8_64.

Chang, T.-H. 2014. Fuzzy VIKOR method: A case study of the hospital service evaluation in Taiwan. *Information Sciences*, 271, pp.196-212. Available at: <https://doi.org/10.1016/j.ins.2014.02.118>.

Dağıstanlı, H.A. & Kurtay, K.G. 2024. Facility Location Selection for Ammunition Depots based on GIS and Pythagorean Fuzzy WASPAS. *Journal of Operations Intelligence*, 2(1), pp.36-49. Available at: <https://doi.org/10.31181/jopi2120247>.

de Araújo Costa, I.P.de Araújo Costa, A.P., Sanseverino, A.M., Gomes, C.F.S. & dos Santos, M. 2022. Bibliometric studies on multi-criteria decision analysis (MCDA) methods applied in military problems. *Pesquisa Operacional*, 42, e249414, pp.1-26 Available at: <https://doi.org/10.1590/0101-7438.2022.042.00249414>.

De, S.K. & Nandi, S. 2024. The exact defuzzification method under polynomial approximation of various fuzzy sets. *Yugoslav Journal of Operations Research*, 34(1), pp.51-72. Available at: <https://doi.org/10.2298/yjor2306017d>.

Falkowski, M. & Model, A. 2019. Procedures of crossing water obstacles in the light of binding normative documents. *Scientific Journal of the Military University of Land Forces*, 193(3), pp.443-458. Available at: <https://doi.org/10.5604/01.3001.0013.5001>.

Fernández-Portillo, L.A., Yazdani, M., Estepa-Mohedano, L. & Sisto, R. 2023. Prioritisation of strategies for the adoption of organic agriculture using BWM and fuzzy CoCoSo. *Soft Computing*, 2023, pp.1-32. Available at: <https://doi.org/10.1007/s00500-023-09431-y>.

Keshavarz-Ghorabae, M., Amiri, M., Zavadskas, E.K., Turskis, Z. & Antuchevičienė, J. 2022. MCDM approaches for evaluating urban and public transportation systems: A short review of recent studies. *Transport*, 37(6), pp.411-425. Available at: <https://doi.org/10.3846/transport.2022.18376>.

Kumar, V., Vrat, P. & Shankar, R. 2024. MCDM model to rank the performance outcomes in the implementation of Industry 4.0. *Benchmarking: An International Journal*, 31(5), pp.1453-1491. Available at: <https://doi.org/10.1108/BIJ-04-2022-0273>.

Kurnaz, S., Özdağoğlu, A. & Keleş, M.K. 2023. Method of evaluation of military helicopter pilot selection criteria: A novel Grey SWARA approach. *Aviation*, 27(1), pp.27-35. Available at: <https://doi.org/10.3846/aviation.2023.18596>.

Maghfiroh, M. & Kavirathna, C. 2023. Location Selection of Battery Swap Station using Fuzzy MCDM Method: A Case Study in Indonesia. *Jurnal teknik industri*, 24(2), pp.81-94. Available at: <https://doi.org/10.22219/jtiimm.vol24.no2.81-94>.

Mishra, A.R., Rani, P., Cavallaro, F. & Alrasheedi, A.F. 2023. Assessment of sustainable wastewater treatment technologies using interval-valued intuitionistic fuzzy distance measure-based MAIRCA method. *Facta Universitatis, Series: Mechanical Engineering*, 21(3), pp.359-386. Available at: <https://doi.org/10.22190/FUME230901034M>.

Nghiem, T.B.H. & Chu, T.-C. 2024. A total distance ranking approach to fuzzy AHP-based MCDM method for selecting sustainable manufacturing facility location. *Journal of Intelligent & Fuzzy Systems*, 46(2), pp.3085-3115. Available at: <https://doi.org/10.3233/jifs-223962>.

Pamucar, D., Deveci, M., Gokasar, I., Işık, M. & Zizovic, M. 2021a. Circular economy concepts in urban mobility alternatives using integrated DIBR method and fuzzy Dombi CoCoSo model. *Journal of Cleaner Production*, 323, art.number:129096. Available at: <https://doi.org/10.1016/j.jclepro.2021.129096>.

Pamucar, D., Simic, V., Lazarević, D., Dobrodolac, M. & Deveci, M. 2022. Prioritization of sustainable mobility sharing systems using integrated fuzzy DIBR and fuzzy-rough EDAS model. *Sustainable Cities and Society*, 82, art.number:103910. Available at: <https://doi.org/10.1016/j.scs.2022.103910>.

Pamučar, D., Žižović, M., Biswas, S. & Božanić, D. 2021b. A new logarithm methodology of additive weights (LMAW) for multi-criteria decision-making: application in logistics. *Facta Universitatis, Series: Mechanical Engineering*, 19(3), p.361. Available at: <https://doi.org/10.22190/fume210214031p>.

Pathinathan, T., Ponnivalavan, K. & Dison, M.E. 2015. Different Types of Fuzzy Numbers and Certain Properties. *Journal of Computer and Mathematical Sciences*, 6(11), pp.631-651 [online]. Available at: <https://www.researchgate.net/publication/344877599> [Accessed: 18 April 2024].

Pifat, V. 1980. *Prelaz preko reka*. Belgrade, Serbia: Vojnoizdavački zavod (in Serbian).

Raad, N.G. & Rajendran, S. 2024. A hybrid robust SBM-DEA, multiple regression, and MCDM-GIS model for airport site selection: Case study of Sistan and Baluchestan Province, Iran. *Transportation Engineering*, 16, art.number:100235. Available at: <https://doi.org/10.1016/j.treng.2024.100235>.

Radovanović, M., Petrovski, A., Cirkin, E., Behlić, A., Jokić, Ž., Chemezov, D., Hashimov, E.G., Bouraima, M.B. & Jana, C. 2024. Application of the new hybrid model LMAW-G-EDAS multi-criteria decision-making when choosing an assault rifle for the needs of the army. *Journal of Decision Analytics and Intelligent Computing*, 4(1), pp.16-31. Available at: <https://doi.org/10.31181/jdaic10021012024r>.

Rashid, M.R., Ghosh, S.K., Alam, Md.F.B. & Rahman, M.F. 2023. A fuzzy multi-criteria model with Pareto analysis for prioritizing sustainable supply chain barriers in the textile industry: Evidence from an emerging economy. *Sustainable Operations and Computers*, 5, pp.29-40. Available at: <https://doi.org/10.1016/j.susoc.2023.11.002>.

Rodgers, J.L. & Nicewander, W.A. 1988. Thirteen Ways to Look at the Correlation Coefficient. *The American Statistician*, 42(1), pp.59-66. Available at: <https://doi.org/10.2307/2685263>.

Roszkowska, E. & Kacprzak, D. 2016. The fuzzy saw and fuzzy TOPSIS procedures based on ordered fuzzy numbers. *Information Sciences*, 369, pp.564-584. Available at: <https://doi.org/10.1016/j.ins.2016.07.044>.

Sahoo, S.K. & Goswami, S.S. 2024. Green Supplier Selection using MCDM: A Comprehensive Review of Recent Studies. *Spectrum of Engineering and Management Sciences*, 2(1), pp.1-16. Available at: <https://doi.org/10.31181/sems1120241a>.

Sánchez-Lozano, J.M. & Rodríguez, O.N. 2020. Application of Fuzzy Reference Ideal Method (FRIM) to the military advanced training aircraft selection. *Applied Soft Computing*, 88, art.number:106061. Available at: <https://doi.org/10.1016/j.asoc.2020.106061>.

Setiadji, A., Sukandari, B., Widjayanto, J. & Najib, R. 2020. Decision selection model of landing beach in amphibious operations exercise with Fuzzy MCDM. *ASRO Journal - STTAL*, 11(2), p.22-34. Available at: <https://doi.org/10.37875/asro.v11i2.266>.

Swethaa, S. & Felix, A. 2023. An intuitionistic dense fuzzy AHP- TOPSIS method for military robot selection. *Journal of Intelligent & Fuzzy Systems*, 44(4), pp.6749-6774. Available at: <https://doi.org/10.3233/jifs-223622>.

Tešić, D. & Božanić, D. 2023. Optimizing Military Decision-Making: Application of the FUCOM– EWAA–COPRAS-G MCDM Model. *Acadlore transactions on applied mathematics and statistics*, 1(3), pp.148-160. Available at: <https://doi.org/10.56578/atams010303>.

Tešić, D., Božanić, D. & Khalilzadeh, M. 2024. Enhancing Multi-Criteria Decision-Making with Fuzzy Logic: An Advanced Defining Interrelationships Between Ranked II Method Incorporating Triangular Fuzzy Numbers. *Journal of*

intelligent management decision, 3(1), pp.56-67. Available at: <https://doi.org/10.56578/jimd030105>.

Tešić, D., Božanić, D., Puška, A., Milić, A. & Marinković, D. 2023. Development of the MCDM fuzzy LMAW-grey MARCOS model for selection of a dump truck. *Reports in Mechanical Engineering*, 4(1), pp.1-17 [online]. Available at: <http://rme-journal.org/index.php/asd/article/view/95> [Accessed: 18 April 2024].

Tešić, D.Z. & Božanić, D.I. 2018. Application of the MAIRCA method in the selection of the location for crossing tanks under water. *Tehnika*, 73(6), pp.860-867 (in Serbian). Available at: <https://doi.org/10.5937/tehnika1806860t>.

Tešić, D.Z. & Božanić, D.I. 2024. Model for determining competences of experts in the field of Military Science. *Vojno delo*, 76(1), pp.1-22. Available at: <https://doi.org/10.5937/vojdelo2401001T>.

Turskis, Z., Zavadskas, E.K., Antuchevičienė, J. & Kosareva, N. 2015. A Hybrid Model Based on Fuzzy AHP and Fuzzy WASPAS for Construction Site Selection. *International Journal of Computers Communications & Control*, 10(6), pp.113-128 [online]. Available at: <https://www.univagora.ro/jour/index.php/ijccc/article/view/2078> [Accessed: 18 April 2024].

Ulutaş, A. & Karakuş, C.B. 2021. Location selection for a textile manufacturing facility with GIS based on hybrid MCDM approach. *Industria Textila*, 72(2), pp.126-132. Available at: <https://doi.org/10.35530/it.072.02.1736>.

Wang, S., Yu, L., Cao, P., Hu, H., Pang, B., Luo, W. & Ge, X. 2024. A Scheme for Charging Load Prediction of EV Based on Fuzzy Theory [e-book]. In: *IOS Press Ebooks. Series: Frontiers in Artificial Intelligence and Applications*, 381: Electronics, Communications and Networks, pp.425-432. Available at: <https://doi.org/10.3233/faia231222>.

Yücenur, G.N. & Maden, A. 2024. Sequential MCDM methods for site selection of hydroponic geothermal greenhouse: ENTROPY and ARAS. *Renewable Energy*, 226, art.number:120361. Available at: <https://doi.org/10.1016/j.renene.2024.120361>.

Zadeh, L.A. 1965. Fuzzy sets. *Information and Control*, 8(3), pp.338-353. Available at: [https://doi.org/10.1016/s0019-9958\(65\)90241-x](https://doi.org/10.1016/s0019-9958(65)90241-x).

Zadeh, L.A. 1973. Outline of a New Approach to the Analysis of Complex Systems and Decision Processes. *IEEE Transactions on Systems, Man, and Cybernetics*, SMC-3(1), pp.28-44. Available at: <https://doi.org/10.1109/tsmc.1973.5408575>.

Zarbakhshnia, N., Soleimani, H., & Ghaderi, H. 2018. Sustainable third-party reverse logistics provider evaluation and selection using fuzzy SWARA and developed fuzzy COPRAS in the presence of risk criteria. *Applied Soft Computing*, 65, pp.307-319. Available at: <https://doi.org/10.1016/j.asoc.2018.01.023>.

Žnidaršič, V., Dojić, K.V. & Milić, L.N. 2024. Selection of Landing Site for Infantry River Crossing Using Aluminum Boat M70: Application of DIBR and Topsis Method. In: *The 30th International Scientific Conference: The KNOWLEDGE-BASED ORGANIZATION*, Sibiu, Romania, 30(1), pp.1-8, June 13-15. Available at: <https://doi.org/10.2478/kbo-2024-0027>.

Aplicación de la toma de decisiones multicriterio para la selección de un lugar para cruzar un obstáculo de agua mediante vadeo en una operación de defensa

Duško Z. Tešić^a, Darko I. Božanić^b, Adis Puška^c

^a Universidad de Defensa de Belgrado, Academia Militar, Oficina del Decano, Belgrado, República de Serbia, **autor de correspondencia**

^b Universidad de Defensa de Belgrado, Academia Militar, Departamento de Tácticas con Sistemas de Armas, Belgrado, República de Serbia

^c Gobierno del Distrito de Brčko de Bosnia y Herzegovina, Departamento de Seguridad Pública, Brčko, Bosnia y Herzegovina

CAMPO: matemáticas aplicadas, ciencias militares

TIPO DE ARTÍCULO: artículo científico original

Resumen:

Introducción/objetivo: El artículo presenta el modelo multicriterio Fuzzy DIBR-Fuzzy DIBR II-EWAA-BM-DEXi-Fuzzy LMAW para elegir una ubicación para cruzar obstáculos de agua al vadear en una operación de defensa. Luego de la identificación de los criterios por parte de expertos en este campo, se aplicó el modelo mencionado y se determinó el punto óptimo. Para comprobar la consistencia de los resultados y la validez del modelo, se consultó nuevamente a expertos y se realizaron análisis de sensibilidad y análisis comparativo.

Métodos: Se utilizaron los métodos Fuzzy DIBR y Fuzzy DIBR II para determinar los coeficientes de ponderación de los criterios identificados, mientras que la agrupación de las opiniones de los expertos y los valores obtenidos se realizó utilizando los operadores EWAA y BM. Para seleccionar la ubicación óptima se aplicó el método Fuzzy LMAW, mientras que los descriptores lingüísticos se determinaron mediante el sistema de soporte a la decisión DEXi.

Resultados: La metodología propuesta permitió identificar todos los criterios que determinan la elección de una ubicación y la elección del punto óptimo para cruzar un obstáculo de agua en una operación de defensa. La prueba del modelo por parte de expertos, el análisis de la sensibilidad de los resultados de salida a los cambios en los pesos de los criterios y la comparación de los resultados obtenidos con los resultados de otros métodos indicaron el hecho de que el modelo es válido y que proporciona resultados consistentes.

Conclusión: Se concluyó que el modelo multicriterio brinda la ayuda necesaria a los tomadores de decisiones en condiciones de información imprecisa y no especificada y que es aplicable en situaciones reales. Además, el modelo propuesto toma en consideración todos los aspectos que deben considerarse al tomar una decisión tan compleja y ayuda a los

oficiales menos experimentados en el proceso de toma de decisiones, reduciendo la posibilidad de errores que pueden resultar en víctimas humanas. Finalmente, se sugieren direcciones para futuras investigaciones en el campo de la superación de los obstáculos del agua y la toma de decisiones multicriterio.

Palabras claves: vadeo, ubicación, selección, militar, MCDM, DIBR, DIBR II, Fuzzy, LMAW, EWAA, BM, DEXi

Применение многокритериального принятия решений для выбора места преодоления водного препятствия вброд в ходе оборонительной операции

Душко З. Тешич^а, Дарко И. Божанич^б, Адис Пушка^в

^а Университет обороны в г. Белград, Военная академия, деканат, г. Белград, Республика Сербия, **корреспондент**

^б Университет обороны в г. Белград, Военная академия, департамент тактики и системы вооружения, г. Белград, Республика Сербия

^в Правительство округа Брчко Боснии и Герцеговины, департамент общественной безопасности, г. Брчко, Босния и Герцеговина

РУБРИКА ГРНТИ: 27.47.19 Исследование операций,
78.21.53 Исследования и разработки в области
эффективности, надежности и боевого
использования вооружения и военной техники

ВИД СТАТЬИ: оригинальная научная статья

Резюме:

Введение/цель: В данной статье представлена многокритериальная модель Fuzzy DIBR-Fuzzy DIBR II-EWAA-BM-DEXi-Fuzzy LMAW для выбора места преодоления водных преград вброд в ходе оборонительной операции. После определения критериев экспертами в данной области была применена упомянутая модель и определено оптимальное место. Для проверки согласованности результатов и достоверности модели были проведены повторные консультации с экспертами, а также анализ чувствительности и сравнительный анализ.

Методы: Для определения весовых коэффициентов выявленных критериев использовались методы Fuzzy DIBR и Fuzzy DIBR II, а агрегирование мнений экспертов и полученных значений осуществлялось с помощью операторов EWAA и BM. Для выбора оптимального местоположения применялся метод Fuzzy LMAW, а лингвистические дескрипторы определялись с помощью системы поддержки принятия решений DEXi.

Результаты: Предложенная методология позволила выявить все критерии, обуславливающие выбор местоположения и сам выбор оптимального места для преодоления водной преграды

вброд в ходе оборонительной операции. Тестирование модели экспертами, анализ чувствительности выходных результатов к изменению весов критериев и сравнение полученных результатов с результатами других методов показали, что модель надежна и результативна.

Выводы: На основании результатов исследования сделан вывод, что многокритериальная модель оказывает необходимую помощь лицам, принимающим решения в условиях неточной и неопределенной информации, и что она применима в реальных ситуациях. Также предложенная модель учитывает все аспекты, которые необходимо иметь в виду при принятии столь сложного решения. Помимо того, она помогает менее опытным командирам в процессе принятия решения, снижая вероятность ошибок, которые могут привести к человеческим жертвам. В заключение предложены направления дальнейших исследований в области преодоления водных препятствий и многокритериального принятия решений.

Ключевые слова: брод, локация, выбор, армия, многокритериальное принятие решений, DIBR, DIBR II, Fuzzy, LMAW, EWAA, BM, DEXi.

Примена вишекритеријумског одлучивања за избор локације за савлађивање водене препреке газом у одбрамбеној операцији

Душко З. Тешић^а, Дарко И. Божанић^б, Адис Пушка^в

^а Универзитет одбране у Београду, Војна академија, Деканат, Београд, Република Србија, **аутор за преписку**

^б Универзитет одбране у Београду, Војна академија, Катедра тактике са системима наоружања, Београд, Република Србија

^в Влада Брчко дистрикта Босне и Херцеговине, Одјељење за јавну безбједност, Брчко, Босна и Херцеговина

ОБЛАСТ: математика, операциона истраживања, војне науке
КАТЕГОРИЈА (ТИП) ЧЛАНКА: оригинални научни рад

Сажетак:

Увод/циљ: У раду је приказан вишекритеријумски модел Fuzzy DIBR-Fuzzy DIBR II-EWAA-BM-DEXi-Fuzzy LMAW помоћу којег се врши избор локације за савлађивање водених препрека газом у одбрамбеној операцији. Након идентификације критеријума од стране експерата, примењен је наведени модел и одређена је оптимална локација. Ради тестирања конзистентности

резултата и валидности модела, поново су ангажовани експерти, извршена је анализа осетљивости и компаративна анализа.

Методе: Методе Fuzzy DIBR и Fuzzy DIBR II коришћене су за одређивање тежинских коефицијената идентификованих критеријума, док је агрегација експертских мишљења и добијених вредности вршена помоћу EWAA и VM оператора. За избор оптималне локације примењена је метода Fuzzy LMAW, док су лингвистички дескриптори одређивани помоћу DEXi система за подршку одлучивању.

Резултати: Предложена методологија омогућила је идентификацију свих критеријума који условљавају избор локације и сам избор оптималне локације за прелазак газом преко водене препреке у одбрамбеној операцији. Тестирањем модела, анализом осетљивости излазних резултата на промене тежина критеријума и поређењем добијених резултата са резултатима других метода, указано је на чињеницу да је модел валидан и да даје конзистентне резултате.

Закључак: Закључено је да вишекритеријумски модел пружа неопходну помоћ доносиоцима одлука у условима непрецизних и неодређених информација и да је примењив у реалним ситуацијама. Такође, предложени модел разматра све аспекте које је неопходно сагледати приликом доношења једне комплетне одлуке и помаже мање искусним старешинама у процесу одлучивања, смањујући могућност настанка грешака, које за последицу могу имати и људске жртве. На крају, предложени су правци даљих истраживања из области савлађивања водених препрека и вишекритеријумског одлучивања.

Кључне речи: газ, локација, избор, војска, вишекритеријумско одлучивање, DIBR, DIBR II, Fuzzy, LMAW, EWAA, VM, DEXi.

Paper received on: 27.01.2024.

Manuscript corrections submitted on: 24.09.2024.

Paper accepted for publishing on: 25.09.2024.

© 2024 The Authors. Published by Vojnotehnički glasnik / Military Technical Courier (www.vtg.mod.gov.rs, втг.мо.унр.срб). This article is an open access article distributed under the terms and conditions of the Creative Commons Attribution license (<http://creativecommons.org/licenses/by/3.0/rs/>).



Application of the AHP and VIKOR methods of individual decision making and the Borda method of group decision making when choosing the most efficient way of performing preparatory shooting at serial number one from a 12.7 mm long range rifle M-93


Aleksandar R. Aleksić^a, Boris V. Delibašić^b,
Željko M. Jokić^c, Marko R. Radovanović^d

^a University of Defense in Belgrade, Military Academy,
Department of Tactics with Weapon Systems,
Belgrade, Republic of Serbia,
e-mail: aleksic.aleksandar1004@gmail.com, **corresponding author**,
ORCID iD: <https://orcid.org/0000-0003-1103-8410>

^b University of Belgrade, Faculty of Organizational Sciences,
Department of Business Systems Organization,
Belgrade, Republic of Serbia,
e-mail: boris.delibasic@fon.bg.ac.rs,
ORCID iD: <https://orcid.org/0000-0002-6153-5119>

^c University of Defense in Belgrade, Military Academy,
Department of Tactics with Weapon Systems,
Belgrade, Republic of Serbia,
e-mail: antras1209@gmail.com,
ORCID iD: <https://orcid.org/0000-0002-3646-1787>

^d University of Defense in Belgrade, Military Academy,
Department of Tactics with Weapon Systems,
Belgrade, Republic of Serbia,
e-mail: markoradovanovicgdb@yahoo.com,
ORCID iD: <https://orcid.org/0000-0002-9866-9639>

 <https://doi.org/10.5937/vojtehg72-52204>

FIELD: applied mathematics, mechanical engineering, military sciences
(tactics with weapons systems)

ARTICLE TYPE: original scientific paper

Abstract:

Introduction/purpose: The paper presents the method of applying multi-criteria decision-making methods in order to improve shooting and select the most favorable conditions for shooting. Alternatives were ranked by individual multi-criteria decision-making methods AHP and VIKOR by experts, and then the most favorable alternative was selected using the Borda method of group decision making. The aim of the work is to select

Aleksić, A. et al, Application of the AHP and VIKOR methods of individual decision making and the Borda method of group decision making when choosing the most efficient way of performing preparatory shooting at serial number one from a 12.7 mm long range rifle M-93, pp.1147-1170

the most efficient way of shooting with minimal human fatigue, consumption of movable things and in the shortest possible time through a combination of multi-criteria decision-making methods, which will ensure the accuracy and precision of the rifle for subsequent shooting and other operations.

Methods: The paper presents one of the ways of using multidisciplinary methods of multi-criteria decision making for a specific problem in the field of tactics with weapon systems. Experts from the field of armaments, using the AHP and VIKOR methods of individual multi-criteria decision making, selected the most favorable alternative in accordance with four given criteria. Then, by applying the Borda method of group decision making, the the most favorable alternative was selected - the most favorable conditions for the execution of preparatory shooting at serial number one with a 12.7 mm long range rifle. The alternatives are four shootings, namely, two ways of performing preparatory shooting with a 12.7 mm long range rifle at serial number one, one from the current Instructions and Program of Shooting with Infantry Weapons and the other newly proposed method, as well as two ways of realizing shooting for testing the accuracy and precision of a long range rifle.

Results: The selection of the most effective conditions for the execution of the first initial preparatory shooting at serial number one with a long range rifle, which will ensure maximum accuracy of the weapon and the minimum consumption of resources - time, ammunition, targets, and personnel fatigue.

Conclusion: The solution takes into account the simultaneous optimization of several criteria in order to select the most efficient way of performing preparatory shooting at serial number one in order to ensure rested and trained personnel as well as accurate and precise long range rifles for subsequent shootings, which leads to the maximum saving of resources, the satisfaction of personnel, and precise weapons.

Key words: long range rifle, rectification, shooting, AHP, VIKOR, Borda method.

Introduction

The application of individual and group methods of multi-criteria decision making is an unavoidable segment in the decision-making process in complex organizational systems such as the Serbian Armed Forces. The work represents one of the models for choosing the most economical conditions for the execution of preparatory shooting at serial number one with a 12.7 mm long range rifle M-93 with the application of the individual AHP and VIKOR methods and the Borda method of group multi-criteria decision making (Suknović et al, 2021).

The symbiosis of multi-criteria decision-making methods in solving problems in the field of tactics and weapons is already known, as well as in other fields. Jokic et al. (2024) write about the best caliber for rifles, while Petrović et al. (2018) used the DEMATEL-AHP method to select the best jet for the protection of Serbia's airspace. The same authors apply the Fuzzy - AHP approach in evaluating the criteria for choosing a missile system for anti-aircraft operations (Petrović et al, 2018). Radovanović & Stevanović (2020) apply the fuzzy AHP-VIKOR method to select the best method for testing the accuracy and precision of sniper rifles. Akmaludin et al. (2023) use the AHP-VIKOR methods for smartphone selection. Demir et al. (2023) use the AHP-VIKOR method extended by the Pythagorean set of fuzzy numbers to evaluate the railway transport system in Turkey. Akmaludin et al. (2021) use a combination of the AHP-VIKOR methods for the selection of the best swimming athletes. Radovanović et al. (2021) analyze the accuracy and precision of shooting with automatic rifles using the AHP method. Oufella (2024) uses a hybrid model of the Borda number and the PROMETHEE method to select a maintenance strategy. Sonatha et al. (2021) use the AHP, Topsis and Borda methods to support a group decision-making system.

The 12.7 mm long range rifle M-93 (named BLACK ARROW) is a tool of high accuracy and precision, which achieves its firepower by shooting immediate targets at distances of up to 1800 m (Zastava Arms, 2024) or 2000 m, depending on the optical sight it has. The stated conditions for the execution of the first shooting with a long range rifle in the Serbian Army do not give satisfactory results and require a lot of time. The subject of the research is the arrival of more efficient conditions for the execution of initial shooting with a long range rifle.

The paper proposes the conditions for the execution of preparatory shooting at serial number one, which at the same time represent a test of the accuracy and precision of a long range rifle and a check of a sniper in uniform aiming and firing. The described rectification procedure with the help of binoculars is unique and requires the introduction of binoculars into the tool kit. The aim of the work is to choose the most efficient and effective shooting procedure in relation to the presented alternatives by applying multi-criteria decision-making methods whose contribution will be a reduction in shooting time and a smaller amount of ammunition as well as, at the same time, an improvement in accuracy and weaponry for all subsequent shooting and combat tasks.

Problem description

During the realization of the preparatory shooting at number one in accordance with the regulations, certain problems appear. The existing way of performing preparatory shooting at serial number one with a long range rifle is realized at a distance of 400 m, and before that it is necessary to test the accuracy and precision of the rifle at a distance of 100 m or 400 m, depending on the optical sight it has. The optical sight M-93 has an aiming distance on the distance mechanism of 0, and it is possible to carry out a test at both 100 and 400 m, while the optical sight M-94 has an aiming distance of 4, and no rule or instruction describes the use of the existing targets for testing accuracy and precision. This work is the first place where a unique procedure for the rectification of both optical sights and the procedure for testing the accuracy and precision of the sights at the same target for testing accuracy and precision at a distance of 100 m is described, which can also represent preparatory shooting at serial number one. The rectification procedure is necessarily performed after every removal and re-installation of the optical sight on the rifle.

The optical sight rectification procedure is carried out in such a way that the test target is placed at a distance of 100 m and with the help of a universal stand and binoculars for the rectification of a long range rifle, the barrel is aimed at the control point 400, and that the optical sight, on which the distance mechanism is set to 4 and the direction mechanism to 0, brings it to the aiming point which is at the bottom of the target, i.e., 30 cm vertically below the control point 400. Then, with 4 bullets, the accuracy and precision of the rifle is tested on the same target with sight 4, aiming at the aiming point at the bottom of the target. Hits should be grouped around control point 400 in a 12 cm diameter circle described around the control point. The procedure for testing accuracy and precision can also be a preparatory shooting at serial number one, which, compared to the existing conditions, saves 3 test bullets and shortens the distance from 400 m to 100 m.

The procedure can also be implemented at control point 800, which is 72 cm above the aiming point, sight 8; then, at the same distance of 100 m, the hits will be grouped around control point 800 in a circle with a diameter of 12 cm. This method of rectification and testing of accuracy and precision combines shooting for testing accuracy and precision with preparatory shooting at serial number one and ensures the accuracy of the rifle at all aiming distances depending on the model of the optical sight.

Description of the methods used

The work will use the AHP and VIKOR individual multi-criteria decision-making methods (Hanif et al, 2022; Göbeloğlu & Urgan, 2023; Abdilllah et al, 2023; Komazec & Petrović, 2019); and the Borda group multi-criteria decision-making method.

Description of the AHP method

The Analytical Hierarchy Process method was developed by Thomas Satti (1988). The method has undergone a large number of modifications (Petrović et al, 2018; Božanić et al, 2016; Ayvaz et al, 2024), but in some cases it is still used in its original form (Radovanović & Stevanović, 2020) both in individual and group decision making (Tešić et al, 2024), and is used in a large number of different decision-making cases.

For pairwise comparisons, which are the basis of this method, the Saati scale is used, Table 1. The pairwise comparison leads to the initial decision matrix. Satie's scale is used to determine the value of criteria and can also be used to rank alternatives.

Table 1 – Saati's scale of comparison

Standard values	Dominance of strength	Derived/invasive values
1	same meaning	1
3	weak dominance	1/3
5	strong dominance	1/5
7	very strong dominance	1/7
9	absolute dominance	1/9
2, 4, 6, 8	limit	1/2, 1/4, 1/6, 1/8

The first step of using the method is to compare the alternatives in accordance with the criteria. In individual as well as in group decision making and the application of the AHP method, it is first necessary to perform a comparison of alternatives in pairs in accordance with each criterion separately, respecting the following: on the diagonals of the matrix, the value is

$$a_{ij} = 1/a_{ji} \quad (1)$$

Then a new matrix is formed for the same criteria and all alternatives, and it is filled based on the previous one in such a way that the sum total value of the column is divided by the value from the cell of that column of the previous matrix and the value is entered in the same cell of the new matrix. The next step is to determine the mean value of each type of the

second matrix. In this way, a certain value of the criterion column is obtained for all alternatives in accordance with the given criterion in the decision matrix. The sum of the resulting column is 1 and represents the degree of confidence in the alternatives for the given criterion.

The next step is the comparison of n pairs of criteria, i.e., determining the eigenvector W for the criteria - determining the degree of confidence in the criteria or the weight of the criteria or weights. A matrix of criteria by type and column is formed and filled in as described above. Then the types are summed up and a new matrix is formed as mentioned above. The mean value of the species of the second tick is represented by the vector W and the sum of that column is 1.

The next step is to calculate the consistency ratio of the CR matrix, which must be less than 0.1.

$$CR=CI/RI \quad (2)$$

where

- CI is the consistency index

$$CI = (\lambda_{max}-n) / (n-1) \quad (3)$$

- RI is a random index according to Sati and depends on the number of criteria and is taken from the table (in this case it is 4 criteria, i.e., 0.9)

- λ_{max} is its own value which is calculated in accordance with the formula for each criterion

$$\lambda_{max} = (Aw*w)/w*w \quad (4)$$

A - is the criteria comparison matrix.

Table 2 – Random index by Saati

n	3	4	5	6	7	8	9	10
RI	0.58	0.9	1.12	1.24	1.32	1.41	1.45	1.49

The matrix is multiplied by the vector by multiplying W by each row-cell and summing the products. If the consistency ratio (CR) is greater than 0.1, the criteria matrix is inconsistent and it is necessary to check the comparisons or change the method. The closer CR is to 0, the more consistent the matrix is, and one goes to the initial - main matrix.

Then the weighted sum is calculated for all alternatives, by multiplying the matrix by W. This is done by writing W below the alternatives and adding the product of the cells of the matrix and the vector W. In this way, the cells of the alternatives are joined. Again, the number of columns is 1. By comparing the numbers, the most favorable alternative is reached. The higher the value, the more acceptable the alternative.

Description of the VIKOR method

Multi-criteria Compromise Ranking is a method proposed by the Serbian scientist Serafim Opricović in 1998 (Opricović, 1998). The VIKOR method was applied in a large number of works in its original form (Nisel, 2014; Opricović & Tzeng, 2004; Delibašić et al, 2023; Yue & Lv, 2024; Khan et al, 2024; Sennaroglu & Celebi, 2018) as well as in vague environment (Chatterjee & Chakraborty, 2016). It is favorable in cases where decision makers do not have equality in decision making, when individuals have the right of veto, when they are committed to certain criteria, and when the criteria are easily measurable. It represents a compromise when choosing alternatives, observing the minimum or the maximum in the desired criteria.

First, the initial matrix is filled based on the qualitative properties of the criteria for each alternative, where the criteria are in the first row, and the alternatives are in the first column of the matrix. Then, another type is formed above the criteria, where it is defined whether it is necessary for the criterion to be minimal if it is a negative property, for example, costs, or the maximum if good performance is in question.

It is necessary to define the weighting coefficients of the criteria obtained on the basis of some other method, in this case on the basis of the AHP method. A weight-normalized matrix is formed by multiplying each cell of the previous matrix by the weight coefficient of the criterion.

Then, at the end of each column, two more types of the minimum and the maximum are formed. The minimum and the maximum for each criterion are extracted from each column.

Then, the strategy S is calculated as the sum value of each type, that is, the sum of all criteria for a given alternative, as well as the strategy R which is obtained as the minimum of each type, that is, criteria for each alternative. If more than one strategy R is minimal, i.e., 0, it is necessary to determine the corrected value of the strategy R* by subtracting Rmin from S.

The matrix is formed based on the formulas:

$$\text{for MAX: } t = X - X(\min) / X(\max) - X(\min) \quad (5)$$

$$\text{for MIN: } t = X(\max) - X / X(\max) - X(\min) \quad (6)$$

The next step is to determine the normalized strategy Sn, in accordance with the formula:

$$S_n = (S - S_{\min}) / (S_{\max} - S_{\min}) \quad (7)$$

Next, it is necessary to determine the normalized strategy Rn, which is obtained by the formula:

$$R_n = (R^* - R^{\min}) / (R^{\max} - R^{\min}) \quad (8)$$

Finally, a compromise strategy Q is obtained for the value of the parameter $v=0.5$. The highest value of Q represents the most favorable alternative, but if the conditions are met:

that it is sufficiently better than the second-ranked alternative

$$DQ(a'') - DQ(a''') \geq DQ \quad (9)$$

$$DQ = \min(0,25, 1 / 1 - J) \quad (10)$$

where J-number is an alternative.

That is, $J = 4$ in this case. So, DQ is 0.25 because it is less than 0.333; and

that it has a strong enough position, that one of the three conditions is met: (it maintains the first position for $v=0.25$ and for $v=0.75$; or it maintains the first position for $v=1$ or it maintains the first position for $v=0$).

Description of the Borda method of group reading

The Borda method is one of the oldest methods of group decision making, developed by the Frenchman Borda in 1781. It was widely used in the process of voting for the election of deputies in many countries of the world (Barberà et al, 2023; Sonatha et al, 2021; Saari, 2023; Suknović et al, 2021). It can be used in its original form (Murti et al, 2021; Everaere et al, 2023; Ilmiyah et al, 2023), and there are a number of modifications (Costa, 2017; Lin & Lin, 2023; Jones & Wilson, 2024). The basis of the method is to choose the alternative that in most cases was the first or tended to be the first one.

First, a matrix is formed in accordance with the rank of all decision makers, where the first column is the rank of alternatives and the first type is decision makers. Then, the second matrix is formed where the decision makers are in the left-wing column of the alternatives and in the first row, and the cells - fields of the matrix are filled by assigning the value 0 to the last ranked alternative for each decision maker, the second ranked alternative from the back the value 1 and the best placed alternative An the value $n - 1$. Finally, the vector W is obtained in the new right column where the values by species are summarized. The best placed alternative - the most acceptable alternative is the one that has the highest value of the vector W.

If it happens that two alternatives have the same rank, then the following is examined: the independence of the irrelevant alternative (the rank of the third alternative is changed and it is monitored whether it affects the two that have a higher rank); the group agreement (which is the order

of ranks of two equally ranked alternatives among all decision makers); and non-dictatorship (check whether the result was obtained as the opinion of one individual).

Description of the alternatives and the criteria

Multi-criteria decision making was implemented for four alternatives in accordance with four criteria:

Alternative 1 - Preparatory shooting at serial number one with a 12.7 mm long range rifle M-93 from the 2020 provisional Instructions and Programs of Shooting with Infantry Weapons temporarily at a distance of 400 m, with $3 + 4 = 7$ bullets at target number 1 with the aiming point - black circle with a diameter of 10 cm. It is necessary to go to the target twice for one executor, which is 800 m and requires 40 minutes to execute the shooting. If the rifle is not accurate and precise, it may happen that the entire 1x1 m target is missed, and the accuracy and precision of the rifle must be tested additionally, which increases the time required for shooting, as well as the amount of ammunition.

Alternative 2 - Testing the accuracy and precision of the rifle at a distance of 400 m with $4 + 4 = 8$ bullets. It requires a time of 40 minutes and consumes one bullet more and is carried out at the same target number 1 with the aiming point - black circle with a diameter of 10 cm. It is favorable that both optical sights, M-93 and M-94, can be tested, and unfavorable that it may happen that there are no hits on the target.

Alternative 3 - Testing the accuracy and precision of the rifle at a distance of 100 m with $4 + 4 = 8$ bullets. It requires a time of 10 minutes and consumes one bullet more compared to A1 and is carried out at the same target number 1 with the aiming point - a black circle with a diameter of 10 cm or some other aiming point on the target. It is favorable that the distance is 100 m, but it is unfavorable that the optical sight M-94 has a minimum aiming distance of 400 m, and it is necessary to define a control point in relation to the elevation of the bullet path at 100 m, because the aiming point and the control point do not coincide, which requires another target.

Alternative 4 - Proposal for preparatory shooting on regular color 1 at a target for testing accuracy and precision with the aiming point and control point 400 at 30 cm above the aiming point and control point 800 at 72 cm above the aiming point, at a distance of 100 m (with prior optical sight rectification) with 4 bullets at one of the control points. A distance of 200 m is covered, which is four times less compared to A1, 4 bullets are used and fired at the same target on which rectification is performed.

The criteria are as follows:

Criterion 1 - The time for which the shooting procedure ends, which is directly related to the shooting distance and the number of bullets. It is preferred to be the minimum value;

Criterion 2 - Ammunition consumption ranging from 4 to 8 rounds. A minimum value is also desirable;

Criterion 3 – The target is determined by type and it can be: target number three with a black circle aiming point with a diameter of 10 cm; a target with a crosshair as an aiming point; a target for testing accuracy and precision into which both rectification and shooting are performed. In the target for accuracy testing, we perform two actions, but it must be sketched, while target number 1 exists, and the second in order should be sketched or the aiming point marked on a clean target support. The criterion is of a linguistic type and depends on the choice of an alternative. The maximum value is preferred; and

Criterion 4 - Fatigue of personnel, which carries weights from 1 to 4 and is directly related to the shooting distance, shooting time, and the number of bullets. It is preferred to be the minimum value.

The alternatives and the criteria are evaluated by decision makers, experts in the field of weapons with shooting training who work at the Military Academy with many years of teaching experience and experience in the troops, and experts in the field of weapons with experience of working in the Serbian Army units.

Ranking results

The first and the second decision maker used the AHP method of individual multi-criteria decision making, for the third decision maker (DO3) the alternative ranking method is unknown and the rank is (the best is A1; the second place is A2; the third place is A3, and the last place is the A4 alternative), while the fourth decision maker used the VIKOR method of multi-criteria decision making.

The first decision maker ranked the alternatives as follows:

Table 3 – Ranking of alternatives in accordance with the time criterion

Time	A1	A2	A3	A4
A1	1	0.5	0.5	0.3333
A2	2	1	0.25	0.25
A3	2	4	1	0.2
A4	3	4	5	1

Decision maker 1 works as follows: The first matrix is filled in with respect to (1), while the second is filled in based on the first, and so on for all four criteria. It can be concluded that for alternative A4, the criterion "time" has the greatest importance, then for alternative A3, and for A2, and for A-1 it has the least importance.

Table 4 – Ranking of alternatives in accordance with the ammunition criterion

Ammunition	A1	A2	A3	A4
A1	1	2	2	2
A2	0.5	1	0.8	0.8
A3	0.5	1.25	1	1
A4	0.5	1.25	1	1

From the above tables, it can be seen that the ammunition is the most important for A1, the target for A4, while the fatigue of the executor is equal for A3 and A4 because the shortest distance is covered.

Table 5 – Ranking of alternatives in accordance with the target criterion

Target	A1	A2	A3	A4
A1	1	1	2	0.5
A2	1	1	0.5	0.5
A3	0.5	2	1	0.5
A4	2	2	2	1

Table 6 – Ranking of alternatives in accordance with the fatigue criterion

Fatigue	A1	A2	A3	A4
A1	1	1	0.25	0.25
A2	1	1	0.25	0.25
A3	4	4	1	1
A4	4	4	1	1

The following tables check the importance of the criteria "ammunition", "target" and "fatigue", according to Satie's scale of comparison of Tables 4 - 6. The procedure is identical to the previous case and requires attention when filling out the initial matrix.

Now it is necessary to check the consistency of the matrix and the consistency ratio CR (2), by ranking the criteria in Table 7. The procedure is identical to the previous two cases and requires attention when filling out the initial matrix.

Table 7 – Ranking of the criteria and determining the weighted sum of the criteria

	K-1	K-2	K-3	K-4
K-1	1	0.33	0.33	1
K-2	3	1	0.25	4
K-3	3	4	1	5
K-4	1	0.25	0.2	1

The mean values of other matrices represent the initial values for the initial decision matrix, Table 8.

Table 8 – Formation of the initial matrix and the priority vector - weighting W

	Time	Ammunition	Target	Fatigue
A-1	0.1097	0.3992	0.2381	0.1
A-2	0.1331	0.1788	0.1699	0.1
A-3	0.2328	0.2110	0.2066	0.4
A-4	0.5244	0.2110	0.3854	0.4
W	0.1156	0.2645	0.5267	0.0932

Table 9 – Matrix consistency check

A*w	λ_{max}	CI	RI	CR
0.47	4.09	0.078	0.9	0.087
1.12	4.22			
2.4	4.55			
0.38	4.08			
	4.23			

From Table 9, it can be concluded that the CR=0.087, which is less than 0.1, the matrix is consistent, and the alternatives are then ranked using the same procedure.

Table 10 shows that, for decision maker 1 (DO1), A4 was ranked best, followed by A1, then A3 and the lowest ranked one was A2.

Table 10 – Final ranking of the alternatives with weighted sums for DO1

A-1	0.2530	2.
A-2	0.1615	4.
A-3	0.2288	3.
A-4	0.3567	1.

In the same way, the second decision maker, DO2, with the help of the AHP methods, arrived at the final decision-making matrix and ranked the alternatives as in Table 11.

Table 11 – Formation of the initial matrix and the priority vector - weighting *W*

	Time	Ammunition	Target	Fatigue
A-1	0.1339	0.4	0.2	0.1
A-2	0.1339	0.2	0.2	0.1
A-3	0.2054	0.2	0.2	0.4
A-4	0.5268	0.2	0.4	0.4
W	0.1981	0.2748	0.3873	0.1397

For decision maker 2 (DO2), the CR is 0.045, better than for DO1. Since this is less than 0.1, it means that the matrix is consistent, Table 12.

Table 12 – Final ranking of the alternatives with weighted sums for DO2

A-1	0.2279	3.
A-2	0.1729	4.
A-3	0.229	2.
A-4	0.3702	1.

Decision maker 4 (DO4) used the VIKOR method and formed the initial decision matrix as in Table 13.

Table 13 – Initial decision matrix

L max-min	min	min	max	min
	K1	K2	K3	K4
A1	40	7	1	4
A2	40	8	1	4
A3	10	8	2	1
A4	10	4	2	1
MAX	40	8	2	4
MIN	10	4	1	1

Then in Table 14, the field of the previous matrix is multiplied with the weight vector from the AHP.

Table 14 – Normalized decision matrix

W	0.1953	0.35007	0.21867	0.2758
L max-min	min	min	max	min
	K1	K2	K3	K4
A1	7.812	2.450	0.219	1.103
A2	7.812	2.801	0.219	1.103
A3	1.953	2.801	0.437	0.276
A4	1.953	1.400	0.437	0.276
MAX	7.812	2.801	0.437	1.103
MIN	1.953	1.400	0.219	0.276

Table 15 – Second normalized decision matrix

	K1	K2	K3	K4	S	R	R*	Sn	Rn	Q
A1	0	0,5	0	0	0.25	0	0.0025	0.0625	0.0625	0.0625
A2	0	0	0	0	0	0	0	0	0	0
A3	1	0	1	1	3	0	0.03	0.75	0.75	0.75
A4	1	1	1	1	4	1	0.04	1	1	1
				min	0	0	0			
				max	4	1	0.04			

Then, in accordance with (5) and (6), he formed a normalized decision matrix, Table 15. From there, he determined the strategies S and R, then R*, then with formulas (7) and (8).

The strategies Sn, Rn and finally the compromise strategy Q, for the probability $v = 0.5$, a simple comparison of which leads to the ranking of the alternatives, if certain conditions of sufficient advantage and a sufficiently firm position of the first-ranked alternative compared to the second-ranked alternative are met.

The complete procedure for calculating the strategies is described in the text above.

Table 16 – Checking the sufficient advantage of the first-ranked alternative

	Q	Rang
A1	0.0625	3.
A2	0	4.
A3	0.75	2.
A4	1	1.

In accordance with (9), $DQ = 1 - 0.75 = 0.25$. In accordance with (10), the sufficient advantage of the first-placed alternative A4 in relation to the

second-placed alternative A3 is $0.33333 \geq 0.25$. Further, from Table 17, it is checked whether one of the three conditions is fulfilled, so that the first ranked alternative satisfies the condition of a sufficiently firm position.

Table 17 – Checking a sufficiently firm position

	v=1	v=0	v=0.75	v=0.25
A1	0.0625	0.0625	0.0469	0.0156
A2	0	0	0	0
A3	0.75	0.75	0.5625	0.1875
A4	1	1	0.75	0.25

Although only one of the three conditions needs to be met, in this case all three conditions are met. It is concluded that the first-ranked alternative maintains a strong enough position in relation to the second-ranked alternative both when $v=0$ and when $v=1$ and when $v=0.75$ and 0.25 . It can be concluded that the individual methods of multi-criteria decision making, the VIKOR and the AHP, gave similar results. In certain cases, the use of one of the methods does not give the expected results, and it is necessary to change the method.

From Table 18, it can be concluded that for the first, second and fourth decision maker, the best alternative is A4, while the opinion of the third decision maker deviates and for him the best alternative is A1 and the lowest ranked alternative is A4. Regardless of everything, his opinion is taken into consideration even if he does not agree with the others.

Table 18 – Results of the individual multi-criteria decision-making methods

METOD	AHP	AHP		VIKOR
RANG	DO 1	DO 2	DO 3	DO 4
1.	A4	A4	A1	A4
2.	A1	A3	A2	A3
3.	A3	A1	A3	A1
4.	A2	A2	A4	A2

When the alternative rankings of all four decision makers are entered in Table 18, the following results are obtained. From the aforementioned table, a new Table 19 is formed, which represents the summarization and ranking of the results of all decision makers while respecting the rule that the worst-placed alternative is assigned 3, the second-placed 2, the third-

placed 1, and the last or fourth-placed 0. In Table 19, a simple sum of the ranks leads to the best ranked alternatives to A4.

Table 19 – Use of the Borda method in the ranking of the alternatives

	DO 1	DO 2	DO 3	DO 4	W	RANG
A1	2	1	3	1	7	2.
A2	0	0	2	0	2	4.
A3	1	2	1	2	6	3.
A4	3	3	0	3	9	1.

The Borda method gives the final ranking of alternatives A4, A1, A3, and A2. The best alternative is A4, while the least favorable is A2.

Conclusion

Individual multi-criteria decision-making methods AHP and VIKOR can give different results or be less favorable for a certain problem. In this case, the decision makers obtained favorable results by applying two different methods. Using the VIKOR method, the first-ranked alternative A4 satisfied the criterion of sufficient advantage and sufficiently solid position for all three conditions, out of which only one is sufficient to be fulfilled in relation to the second-ranked alternative A3. The third decision maker only presented the results without explaining the method used. All four decision makers had an equal right to vote in the decision. By applying the Borda group decision-making method, their results were summarized and the most favorable alternative was selected, which is the fourth alternative, A4.

The paper presents a model of the application of multi-criteria decision-making methods for solving a specific problem in the field of weapon use for the purpose of training and realization of the first initial preparatory shooting at serial number one with a 12.7 mm long range rifle, through the selection of the most favorable conditions for shooting. The mentioned procedure combines three actions into one, rectification of the sight - without the use of ammunition, testing the accuracy and precision of the rifle and at the same time the implementation of preparatory shooting, i.e., checking the sniper's training in uniform aiming and firing. The rectification procedure is the product of the author's experiment and for the first time in any official literature in Serbia it is shown here; it was tested in practice where it gave positive results. The idea for the procedure was taken from the shooting with the 30 mm Automatic Grenade Launcher M-93, where the preparatory shooting at serial number one is also the

shooting for testing accuracy and precision and checking the operator's training in proper aiming and firing.

The results show that there is a need for a justified change in the conditions for the execution of preparatory shooting with a long range rifle, and the mentioned procedure can be used to select any other four alternatives with four criteria in any field with the ranking of alternatives and criteria by experts in that field.

Multi-criteria decision-making methods have shown results and are used in all areas, both in natural and social spheres of life, in order to obtain maximum product performance. The proposal for future research is that before purchasing and putting weapons into use, multi-criteria optimization methods should be used, the existing and new systems should be compared with the proposed procedure, and the results and the opinions of experts should be followed when purchasing or modernizing assets. Through the aforementioned procedure, the performance of the M-19 modular rifle or the M-20 modular machine gun can be compared with the existing rifles and machine guns or the Kornet EM anti-armor system with the existing anti-armor weapons.

References

- Abdillah, A.I.J., Danang Rimbawa, H.A. & Asnar, Y. 2023. Evaluation of the determination of it infrastructure personnel in the al navy using a combination of ahp and vikor methods. *Antivirus*, 17(1), pp.144-154. Available at: <https://doi.org/10.35457/antivirus.v17i2.3094>.
- Akmaludin, A., Sidik, S., Iriadi, N., Arfian, A. & Suriyanto, A.D. 2021. Selection of the Best Swimming Athletes using MCDM-AHP and VIKOR Methods. *Sinkron: Jurnal Dan Penelitian Teknik Informatika*, 5(2B), pp.44-52. Available at: <https://doi.org/10.33395/sinkron.v6i1.10998>.
- Akmaludin, A., Suriyanto, A.D., Iriadi, N., Santoso, B. & Sukendar, T. 2023. Decision Support System for SmartPhone Selection with AHP-VIKOR Method Recommendations. *Sinkron: Jurnal Dan Penelitian Teknik Informatika*, 7(2), pp.657-665. Available at: <https://doi.org/10.33395/sinkron.v8i2.11845>.
- Ayvaz, B., Tatar, V., Sağır, Z. & Pamucar, D. 2024. An integrated Fine-Kinney risk assessment model utilizing Fermatean fuzzy AHP-WASPAS for occupational hazards in the aquaculture sector. *Process Safety and Environmental Protection*, 186, pp.232-251. Available at: <https://doi.org/10.1016/j.psep.2024.04.025>.
- Barberà, S., Bossert, W. & Moreno-Tertero, J.D. 2023. Wine rankings and the Borda method. *Journal of Wine Economics*, 18(2), pp.122-138. Available at: <https://doi.org/10.1017/jwe.2023.7>.
- Božanić, D.I., Pamučar, D.S. & Karović, S.M. 2016. Use of the fuzzy AHP-MABAC hybrid model in ranking potential locations for preparing laying-up

positions. *Vojnotehnički glasnik/Military Technical Courier*, 64(3), pp.705-729. Available at: <https://doi.org/10.5937/vojtehg64-9261>.

Chatterjee, P. & Chakraborty, S. 2016. A comparative analysis of VIKOR method and its variants. *Decision Science Letters*, 5, pp.469-486. Available at: <https://doi.org/10.5267/j.dsl.2016.5.004>.

Costa, H.G. 2017. AHP-De Borda: a hybrid multicriteria ranking method. *Brazilian Journal of Operations & Production Management*, 14(3), pp.281-287. Available at: <https://doi.org/10.14488/BJOPM.2017.v14.n3.a1>.

Delibašić, B., Glavić, D., Radovanović, S., Petrović, A., Milenković, M. & Suknović, M. 2023. Multi-actor VIKOR Method for Highway Selection in Montenegro. In: Liu, S., Zaraté, P., Kamissoko, D., Linden, I. & Papathanasiou, J. (Eds.) *Decision Support Systems XIII. Decision Support Systems in An Uncertain World: The Contribution of Digital Twins. ICDSST 2023. Lecture Notes in Business Information Processing*, 474. Cham: Springer. Available at: https://doi.org/10.1007/978-3-031-32534-2_1.

Demir, E., Ak, M. F. & Sari, K. 2023. Pythagorean Fuzzy Based AHP-VIKOR Integration to Assess Rail Transportation Systems in Turkey. *International Journal of Fuzzy Systems*, 25(2), pp.620-632. Available at: <https://doi.org/10.1007/s40815-022-01404-x>.

Everaere, P., Fella, C., Konieczny, S. & Pino Pérez, R. 2023. On the links between belief merging, the Borda voting method, and the cancellation property. *AI Communications*, 37(3), pp.1-19. Available at: <https://doi.org/10.3233/AIC-220306>.

Göbeloğlu, E.D. & Urgan, M.C. 2023. Solar power plant location selection with AHP-VIKOR hybrid method. *Sakarya Üniversitesi İşletme Enstitüsü Dergisi*, 5(2), pp.95-109. Available at: <https://doi.org/10.47542/sauied.1388986>.

Hanif, K.H., Yudhana, A. & Fadlil, A. 2022. Penentuan Guru Berprestasi Menggunakan Metode Analytical Hierarchy Process (AHP) dan ViseKriterijumska Optimizacija I Kompromisno Resenje (VIKOR). *Jurnal Teknologi Informasi Dan Ilmu Komputer*, 9(6), pp.1119-1128. Available at: <https://doi.org/10.25126/jtiik.2022934628>.

Ilmiyah, N.F., Al Hasani, S.Z.N. & Renaningtyas, D. 2023. Combination of saw-topsis and borda count methods in sequencing potential convalescent plasma donors. *Barekeng: Jurnal Ilmu Matematika dan Terapan*, 17(3), pp.1521-1532. Available at: <https://doi.org/10.30598/barekengvol17iss3pp1521-1532>.

Jokic, Z., Delibasic, B. & Randjelovic, A. 2024. Selection of Rifle Caliber in Rearming Process of the Serbian Army. *Management: Journal of Sustainable Business and Management Solutions in Emerging Economies*, 29(1), pp.41-52. Available at: <https://doi.org/10.7595/management.fon.2021.0011>.

Jones, M.A. & Wilson, J. 2024. The Colley Method is an Extension of the Borda Count. *Mathematics Magazine*, 97(2), pp.140-150. Available at: <https://doi.org/10.1080/0025570X.2024.2312781>.

Khan, H.U., Ali, F., Sohail, M., Nazir, S. & Arif, M. 2024. Decision making for selection of smart vehicle transportation system using VIKOR approach.

International Journal of Data Science and Analytics, pp.1-15. Available at: <https://doi.org/10.1007/s41060-024-00537-6>.

Komazec, N. & Petrović, A. 2019. Application of the AHP-VIKOR hybrid model in media selection for informing about the endangered in situations of emergency. *Operational Research in Engineering Sciences: Theory and Applications*, 2(2), pp.12-23 [online]. Available at: <https://oresta.org/article-view/?id=21> [Accessed: 15 July 2024].

Lin, H. & Lin, D. 2023. Evaluation of Online Learners' Learning Performance Based on Fuzzy Borda Method. *International Journal of Emerging Technologies in Learning*, 18(14), pp.244-255. Available at: <https://doi.org/10.3991/ijet.v18i14.40397>.

Murti, P.H.K., Wirjodirdjo, B., Bastari, A. & Ahmadi, A. 2021. Using of profile matching and Borda method in predicting threats country in ASEAN. *Journal ASRO*, 12(01), pp.173-184. Available at: <https://doi.org/10.37875/asro.v12i01.395>.

Nisel, S. 2014. An Extended VIKOR Method for Ranking Online Graduate Business Programs. *International Journal of Information and Education Technology*, 4(1), pp.103-107. Available at: <https://doi.org/10.7763/IJIE.T.2014.V4.378>.

Opricović, S. 1998. *Višekriterijumska optimizacija sistema u građevinarstvu*. Belgrade: University of Belgrade, Faculty of Civil Engineering (in Serbian). ISBN: 86-80049-82-4.

Opricović, S. & Tzeng, G.-H. 2004. Compromise solution by MCDM methods: A comparative analysis of VIKOR and TOPSIS. *European Journal of Operational Research*, 156(2), pp.445-455. Available at: [https://doi.org/10.1016/S0377-2217\(03\)00020-1](https://doi.org/10.1016/S0377-2217(03)00020-1).

Oufella, S. 2024. Hybrid use of Borda count and PROMETHEE method for maintenance strategy selection problem. *Foundations of Computing and Decision Sciences*, 49(2), pp.139-160. Available at: <https://doi.org/10.2478/fcds-2024-0009>.

Petrović, I., Gordić, M. & Kankaraš, M. 2018. Fuzzy – AHP pristup u vrednovanju kriterijuma za izbor raketnog sistema za protivvazduhoplovna dejstva. *Vojno delo*, 70(2), pp.298-308 (in Serbian). Available at: <https://doi.org/10.5937/vojdela1802298P>.

Radovanović, M., Milić, A. & Petrovski, A. 2021. Analysis of accuracy and precision of shooting with home: Made automatic rifles using the AHP method. *Scientific Technical Review*, 71(1), pp.30-37. <https://doi.org/10.5937/str2101030R>.

Radovanovic, M., Randelović, A. & Jokić, Ž. 2020. Application of hybrid model fuzzy AHP-VIKOR in selection of the most efficient procedure for rectification of the optical sight of the long-range rifle. *Decision Making: Applications in Management and Engineering*, 3(2), pp.131-148. Available at: <https://doi.org/10.31181/dmame2003131r>.

Radovanović, M. & Stevanović, M. 2020. Analysis of the construction characteristics of automatic domestic production rifles for the purpose of

equipping units of the Serbian Army. *Serbian Journal of Engineering Management*, 5(1), pp.40-49. Available at: <https://doi.org/10.5937/SJEM2001040R>.

Saari, D.G. 2023. Selecting a voting method: the case for the Borda count. *Constitutional Political Economy*, 34(3), pp.357-366. Available at: <https://doi.org/10.1007/s10602-022-09380-y>.

Sennaroglu, B. & Celebi, G.V. 2018. A military airport location selection by AHP integrated PROMETHEE and VIKOR methods. *Transportation Research Part D: Transport and Environment*, 59, pp.160-173. Available at: <https://doi.org/10.1016/j.trd.2017.12.022>.

Sonatha, Y., Azmi, M. & Rahmayuni, I. 2021. Group Decision Support System Using AHP, Topsis and Borda Methods for Loan Determination in Cooperatives. *International Journal on Informatics Visualization*, 5(4), pp.372-379. Available at: <https://doi.org/10.30630/Joiv.5.4.640>.

Suknović, M., Delibašić, B., Jovanović, M., Vukićević, M. & Radovanović, S. 2021. *Odlučivanje, sedmo prerađeno i dopunjeno izdanje*. Belgrade: University of Belgrade, Faculty of Organizational Sciences [online]. Available at: https://id.fon.bg.ac.rs/uploads/documents/empire_plugin/A0032%20Odlucivanje.pdf (in Serbian). ISBN: 978-86-7680-370-5 [Accessed: 15 July 2024].

Tešić, D., Božanić, D. & Khalilzadeh, M. 2024. Enhancing Multi-Criteria Decision-Making with Fuzzy Logic: An Advanced Defining Interrelationships Between Ranked II Method Incorporating Triangular Fuzzy Numbers. *Journal of Intelligent Management Decision*, 3(1), pp.56-67. Available at: <https://doi.org/10.56578/jimd030105>.

Yue, L. & Lv, Y. 2024. VIKOR Optimization Decision Model Based on Poset. *Journal of Intelligent & Fuzzy Systems*. Pre-press. Available at: <https://doi.org/10.3233/JIFS-230680>.

-Zastava Arms. 2024. *Long Range Rifle M93 Black Arrow* [online]. Available at: <https://www.zastava-arms.rs/en/long-range-rifle-m93-black-arrow/> [Accessed: 15 July 2024].

Aplicación de los métodos AHP y VIKOR de toma de decisiones individuales y del método Borda de toma de decisiones grupales al elegir la forma más eficiente de realizar el tiro preparatorio al número de serie uno con un rifle de largo alcance M-93 de 12,7 mm

Aleksandar R. Aleksić^a, autor de correspondencia, Boris V. Delibašić^b, Željko M. Jokić^a, Marko R. Radovanović^a

^a Universidad de Defensa de Belgrado, Academia Militar, Departamento de Tácticas con Sistemas de Armas, Belgrado, República de Serbia

^b Universidad de Belgrado, Facultad de Ciencias Organizacionales, Departamento de Organización de Sistemas Empresariales, Belgrado, República de Serbia

CAMPO: matemáticas aplicadas, ingeniería mecánica, ciencias militares
(tácticas con sistemas de armas)

TIPO DE ARTÍCULO: artículo científico original

Resumen:

Introducción/objetivo: El artículo presenta el método de aplicar métodos de toma de decisiones multicriterio para mejorar disparos y seleccionar las condiciones más favorables para disparos. Los expertos clasificaron las alternativas mediante los métodos individuales de toma de decisiones multicriterio AHP y VIKOR, y luego se seleccionó la alternativa más favorable utilizando el método Borda de toma de decisiones grupales. El objetivo del trabajo es seleccionar la forma más eficiente de disparar con el mínimo cansancio humano, consumo de objetos móviles y en el menor tiempo posible mediante una combinación de métodos de toma de decisiones multicriterio, que garanticen la exactitud y precisión del disparo del rifle para disparos posteriores y otras operaciones.

Métodos: El artículo presenta una de las formas de utilizar métodos multidisciplinarios de toma de decisiones multicriterio para un problema específico en el campo de la táctica con sistemas de armas. Los expertos en el campo de armamentos, utilizando los métodos AHP y VIKOR de toma de decisiones individuales según múltiples criterios, seleccionaron la alternativa más favorable de acuerdo con cuatro criterios dados. Luego, aplicando el método Borda de toma de decisiones en grupo, se eligió la alternativa más favorable: las condiciones más favorables para realizar el tiro preparatorio en el número de serie uno con un rifle de largo alcance de 12,7 mm. Las alternativas son cuatro tiros, a saber, dos modos de realizar el tiro preparatorio con un fusil de largo alcance calibre 12,7 mm número de serie uno, uno del actual Instructivo y Programa de Tiro con Armas de Infantería y el otro método recientemente propuesto, así como dos modos de realizar tiros para probar la exactitud y precisión de un rifle de largo alcance.

Resultados: La selección de las condiciones más efectivas para la ejecución del primer tiro preparatorio inicial en el número de serie uno con un rifle de largo alcance, que garantizará la máxima precisión del arma y el mínimo consumo de recursos: tiempo, municiones, objetivos y fatiga del personal.

Conclusión: La solución tiene en cuenta la optimización simultánea de varios criterios para seleccionar la forma más eficiente de realizar tiros preparatorios en el número de serie uno para garantizar personal descansado y capacitado, así como rifles de largo alcance precisos y exactos para tiros posteriores. lo que conduce al máximo ahorro de recursos, la satisfacción del personal y armas precisas.

Palabras claves: rifle de largo alcance, rectificación, tiro, AHP, VIKOR, método Borda.

Aleksić, A. et al., Application of the AHP and VIKOR methods of individual decision making and the Borda method of group decision making when choosing the most efficient way of performing preparatory shooting at serial number one from a 12.7 mm long range rifle M-93, pp. 1147-1170

Применение методов индивидуального принятия решений АНР и VIKOR и метода группового принятия решений Borda при выборе наиболее эффективного способа выполнения подготовительных упражнений №1 по стрельбе из дальнобойной винтовки М-93 калибра 12,7-мм

Александр Р. Алексич^а, **корреспондент**, Борис В. Делибашич^б,
Желько М. Йокич^а, Марко Р. Радованович^а

^а Университет обороны в г. Белград, Военная академия,
кафедра тактики и систем вооружения, г. Белград, Республика Сербия

^б Белградский университет, факультет организационных наук,
кафедра организации бизнес-систем, г. Белград, Республика Сербия

РУБРИКА ГРНТИ: 27.47.19 Исследование операций,
78.25.00 Вооружение и военная техника

ВИД СТАТЬИ: оригинальная научная статья

Резюме:

Введение/цель: В данной статье представлен способ применения метода многокритериального принятия решений с целью совершенствования стрельбы и выбора наиболее благоприятных условий для стрельбы. Альтернативы ранжировались экспертами на основании использования индивидуальных многокритериальных методов принятия решений „АНР“ и „VIKOR“, после чего лучшая альтернатива выбиралась методом группового принятия решений „Borda“. Цель данной статьи – выбрать наиболее эффективный способ стрельбы с минимальным утомлением человека, расходом вещей и в кратчайшие сроки, используя сочетание многокритериальных методов принятия решений, обеспечивающих точность стрельбы и оружия в последующих учениях и других действиях.

Методы: В данной статье представлен один из способов использования мультидисциплинарных методов многокритериального принятия решений по конкретной задаче в области тактики систем вооружения. Эксперты по баллистике выбрали наиболее выгодную альтернативу с помощью методов индивидуального многокритериального принятия решений „АНР“ и „VIKOR“ по четырем заданным критериям. Затем с применением метода группового принятия решений „Borda“ был произведен окончательный выбор наиболее благоприятного альтернативного варианта-условия выполнения подготовительных упражнений по стрельбе №1 из дальнобойной винтовки калибра 12,7 мм. Альтернативными являются четыре способа стрельбы, а именно два способа выполнения подготовительных упражнений по стрельбе № 1 из

дальнобойной винтовки калибра 12,7 мм, один способ согласно Инструкции и программе стрельбы из стрелкового оружия и второй – новый способ, а также два способа выполнения упражнений по стрельбе для проверки точности дальнобойной винтовки.

Результаты: Выбор наиболее благоприятных условий для проведения первого подготовительного упражнения по стрельбе №1 из дальнобойной винтовки обеспечивает максимальную точность оружия и минимальный расход ресурсов – времени, боеприпасов, мишеней, усталости состава.

Выводы: Решение учитывает одновременную оптимизацию нескольких критериев с целью выбора наиболее эффективного способа выполнения подготовительных упражнений по стрельбе № 1 с целью обеспечения отдохнувшего и подготовленного личного состава и точности дальнобойной винтовки для последующих учений, что приводит к максимальной экономии ресурсов, удовлетворению состава и точности оружия.

Ключевые слова: дальнобойная винтовка, исправление, стрельба, АНР, VIKOR, метод Borda.

Примена АНР и VIKOR метода индивидуалног одлучивања и Borda метода групног одлучивања при избору најефикаснијег начина извршења припремног гађања на редном броју 1 далекометном пушком М-93 калибра 12,7 mm

Александар Р. Алексић^а, аутор за преписку, Борис В. Делибашић^б, Жељко М. Јокић^а, Марко Р. Радовановић^а

^а Универзитет одбране у Београду, Војна академија, Катедра тактике са системима наоружања, Београд, Република Србија

^б Универзитет у Београду, Факултет организационих наука, Катедра за организацију пословних система, Београд, Република Србија

ОБЛАСТ: примењена математика, машинство, војне науке (тактика са системима наоружања)

КАТЕГОРИЈА (ТИП) ЧЛАНКА: оригинални научни рад

Сажетак:

Увод/циљ: У раду је представљен начин примене метода вишекритеријумског одлучивања чији је циљ унапређење гађања и одабира што повољнијих услова за извршење гађања. Алтернативе су рангиране индивидуалним методама вишекритеријумског одлучивања АНР и VIKOR од стране експерата, након чега је најповољнија алтернатива одабрана применом Borda метода групног одлучивања. Циљ рада јесте да се

комбинацијом метода вишекритеријумског одлучивања одабере најефикаснији начин извршења гађања уз минималан замор људства, утршак покретних ствари и за што краће време, који ће обезбедити тачност и прецизност оруђа за наредна гађања и друга дејства.

Метод: Приказан је један од начина употребе мултидисциплинарних метода вишекритеријумског одлучивања на конкретном проблему из области тактике са системима наоружања. Експерти из области наоружања су применом АНР и VIKOR методе индивидуалног вишекритеријумског одлучивања, према четири задата критеријума, извршили избор најповољније алтернативе. Затим је применом Borda метода групног одлучивања извршен коначан одабир најповољније алтернативе – услова за извршење припремног гађања на редном броју 1 далекометном пушком М-93, калибра 12,7 mm. Алтернативе су четири гађања – два начина извршења припремног гађања на редном броју 1, један из „Упутства и програма гађања пешадијским наоружањем” и други новопредложени начин, као и два начина реализације гађања за испитивање тачности и прецизности далекометне пушке.

Резултат: Изабрани су најповољнији услови за извршење првог почетног припремног гађања на редном броју 1 далекометном пушком, који ће обезбедити максималну тачност оруђа и минималан утршак ресурса – времена, муниције, мета и замора људства.

Закључак: Решење узима у обзир истовремену оптимизацију више критеријума ради одабира најефикаснијег начина извршења припремног гађања на редном броју 1. На тај начин обезбеђује се одморно и обучено људство, као и прецизност далекометне пушке за наредна гађања, што доводи до максималне уштеде ресурса.

Кључне речи: далекометна пушка, ректификација, гађање, АНР, VIKOR, метод Borda.

Paper received on: 15.02.2024.

Manuscript corrections submitted on: 24.09.2024.

Paper accepted for publishing on: 25.09.2024.

© 2024 The Authors. Published by Vojnotehnički glasnik / Military Technical Courier (www.vtg.mod.gov.rs, втр.мо.унп.срб). This article is an open access article distributed under the terms and conditions of the Creative Commons Attribution license (<http://creativecommons.org/licenses/by/3.0/rs/>).



Effect of a crack on the nonlinear behavior of a stiffened composite panel

Houda Beghdad^a, Nacer Rahal^b, Abdelaziz Souici^c, Sara Zatir^d, Khaled Benmahdi^e, Halima Aouad^f

^a Mustapha Stambouli University, Department of Civil Engineering, Mascara, People's Democratic Republic of Algeria, e-mail: houda.beghdad@univ-mascara.dz, **corresponding author**, ORCID iD: <https://orcid.org/0009-0001-3548-5138>


^b Mustapha Stambouli University, Department of Civil Engineering, Mascara, People's Democratic Republic of Algeria; University of Sciences and Technology, Laboratory of Mechanical Structure and Construction Stability, Oran, People's Democratic Republic of Algeria, e-mail: n.rahal@univ-mascara.dz, ORCID iD: <https://orcid.org/0009-0002-0400-8360>

^c Mustapha Stambouli University, Department of Civil Engineering, Mascara, People's Democratic Republic of Algeria; University of Sciences and Technology, Laboratory of Mechanical Structure and Construction Stability, Oran, People's Democratic Republic of Algeria, e-mail: a.souici@univ-mascara.dz, ORCID iD: <https://orcid.org/0009-0004-3845-7409>

^d University Tahri Mohamed of Bechar, Architecture and Urban Department, Bechar, People's Democratic Republic of Algeria, e-mail: zatir.sara@univ-bechar.dz, ORCID iD: <https://orcid.org/0000-0002-6187-3441>

^e Mustapha Stambouli University, Department of Civil Engineering, Mascara, People's Democratic Republic of Algeria, e-mail: k.benmahdi@univ-mascara.dz, ORCID iD: <https://orcid.org/0000-0002-8244-5817>

^f Mustapha Stambouli University, Department of Civil Engineering, Mascara, People's Democratic Republic of Algeria, e-mail: aouadhal@gmail.com, ORCID iD: <https://orcid.org/0009-0004-1999-1489>

 <https://doi.org/10.5937/vojtehg72-47123>

FIELD: mechanics, materials

ARTICLE TYPE: original scientific paper

Abstract:

Introduction/purpose: During their lifetime, ships and aircraft are subjected to severe service and aerodynamic loads that can cause structural damage and cracking. These cracks grow and propagate over time. Extending the life of a damaged structure is a very important area of research. In this

context, the repair of composite panels is recommended to restore the performance of cracked structures.

Methods: In order to minimize the concentration of stresses at the bottom of a crack, to stop and even to delay the propagation of this crack, this study seeks to propose a two-dimensional analysis by the software ANSYS to predict the effect of the propagation of a possible crack on the nonlinear behavior of cracked stiffened composite panels.

Results: The results from this analysis will be a very good reference for improving performance and repairing cracked composite panels using stiffeners.

Conclusion: It is recommended to provide patches for repairing cracked panels based on the modeling given in this study.

Key words: composite panels, damaged structure, crack propagation, ANSYS, concentration of stresses.

Introduction

Over the past two decades, composite materials have played an important role in the development of high-performance structures. Researchers have studied different topics in this field such as the control of cracks, vibrations, shape, buckling, and stresses in structures (Fesharaki et al, 2016).

Unfortunately, an important aspect of the behaviour of composites is their impact resistance as ships and aircraft are subjected to severe service and aerodynamic loads that can cause structural damage and cracking. During their service, cracks develop in the structures of ships and aircraft. In addition, other unexpected damaging loads or use beyond their service life exaggerate the growth of these cracks (Mall & Conley, 2009). The occurrence of cracks in the stiffened plates will reduce their ultimate compressive strength (Bayatfar et al, 2014; Shi et al, 2019; Xu et al, 2014; Xu et al, 2021), as the damage will induce earlier collapse (Shi et al, 2021). This situation constitutes a subject of great importance and a temptation to resolve it has become necessary. Therefore, repair techniques for cracked aerospace structures are needed (Mall & Conley, 2009).

To regain the initial structural capacity for which the device was designed, repairing or reinforcing the cracked or weakened part of the structure is an essential operation, thus requiring in-depth mastery. In recent years, a bonded composite patch is widely used as a very good alternative to repair cracked aerospace structures (Duong & Wang, 2007; Baker et al, 2003). In this context, to better understand the effect of crack propagation on the behavior of structures repaired by bonded patches,

many studies have been carried out (Baker, 1993; Sun et al, 1996; Young et al, 1993; Jones et al, 1982; Jones et al, 1988; Rose, 1982; Tarn & Shek, 1991; Naboulsi & Mall, 1998, 1999; Denney & Mall, 1997; Heller et al, 1989; Chue et al, 1994; Xu & Guedes Soares, 2012; Xu & Guedes Soares, 2013; Shi et al, 2017). The bonded patch repair reduces the stresses near the crack, it retards or completely stops the growth of this crack. Bonded composite patch repairs offer advantages such as the absence of additional stress concentration, a higher stiffness-to-weight ratio, the ability of the patch to be formed into complex shapes, and the ability to repair irregular components (Makwana et al, 2021).

Modeling

This present research consists of modeling, using the ANSYS software, the nonlinear behaviour of a composite panel with a crack. The considered panel is simply supported on its periphery and is subjected to a bidirectional tensile loading (Figure 1).

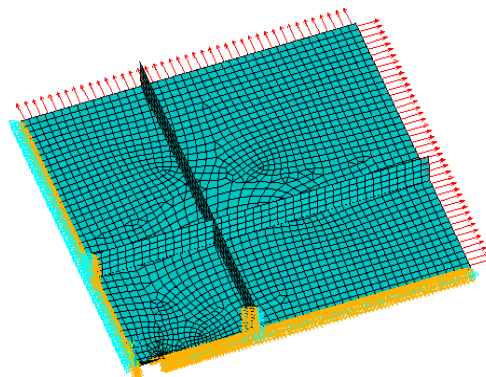


Figure 1 – Simply supported panel under a bi-axial tensile loading

The panel is made entirely of a graphite/epoxy composite with the mechanical characteristics given in Tables 1 and 2.

Table 1 – Mechanical characteristics of an epoxy graphite composite

E ₁ (GPa)	E ₂ (GPa)	E ₃ (GPa)	G ₁₂ (GPa)	G ₁₃ (GPa)	G ₂₃ (GPa)	ν ₁₂	ν ₁₃	ν ₂₃
130	10	10	4.85	4.85	3.62	0.31	0.31	0.52

Table 2 – Strengths of a graphite epoxy composite

X _T (MPa)	X _C (MPa)	Y _T (MPa)	Y _C (MPa)	S (MPa)
1933	1051	51	141	61

Ratio and the resistance index

In the ANSYS software, the resistance ratio R, also called the safety factor, is expressed by:

$$R = 1.0 / \left(-\frac{B}{2A} + \sqrt{\left(\frac{B}{2A}\right)^2 + 1.0/A} \right) \quad (1)$$

$$A = \frac{(\sigma_x)^2}{\sigma_{xt}^f \sigma_{xc}^f} + \frac{(\sigma_y)^2}{\sigma_{yt}^f \sigma_{yc}^f} + \frac{(\sigma_z)^2}{\sigma_{zt}^f \sigma_{zc}^f} + \frac{(\sigma_{xy})^2}{(\sigma_{xy}^f)^2} + \frac{(\sigma_{yz})^2}{(\sigma_{yz}^f)^2} + \frac{(\sigma_{xz})^2}{(\sigma_{xz}^f)^2} + \frac{C_{xy} \sigma_x \sigma_y}{\sqrt{\sigma_{xt}^f \sigma_{xc}^f \sigma_{yt}^f \sigma_{yc}^f}} + \frac{C_{yz} \sigma_y \sigma_z}{\sqrt{\sigma_{yt}^f \sigma_{yc}^f \sigma_{zt}^f \sigma_{zc}^f}} + \frac{C_{xz} \sigma_x \sigma_z}{\sqrt{\sigma_{xt}^f \sigma_{xc}^f \sigma_{zt}^f \sigma_{zc}^f}} \quad (2)$$

$$B = \left(\frac{1}{\sigma_{xt}^f} + \frac{1}{\sigma_{xc}^f} \right) \sigma_x + \left(\frac{1}{\sigma_{yt}^f} + \frac{1}{\sigma_{yc}^f} \right) \sigma_y + \left(\frac{1}{\sigma_{zt}^f} + \frac{1}{\sigma_{zc}^f} \right) \sigma_z \quad (3)$$

C_{xy}, C_{yz}, C_{xz} = x-y, y-z, x-z are respectively the coupling coefficients for the Tsai-Wu theory.

The rupture will take place if this resistance report satisfies the condition 0 < R < 1.

The resistance index ξ can also be expressed as:

$$\xi = A + B \quad (4)$$

If ξ < 1, the structure is completely safe. Otherwise, breakage is likely to occur.

Finding the critical zone

In order to find the critical values of the resistance index ξ, three points likely to have the critical stresses have been chosen. The first point is at the tip of the crack, the second one is in the position of the transverse stiffener and the third point is at the end of the panel (Figure 2). Figure 2 represents the distribution of the resistance index under a loading P=50MPa.

In order to find the most critical zone, the authors analysed the evolution of this index as a function of time for the three points chosen on the screen. The modeling results (Figure 3) show that the most important

values are offered at point 1 (point of the crack). Therefore, point 1 represents more risk for the panel because of the presence of the crack which tends to propagate for resistance indices greater than the value 1. To this end, the analysis focuses on the point 1 strong constraint.

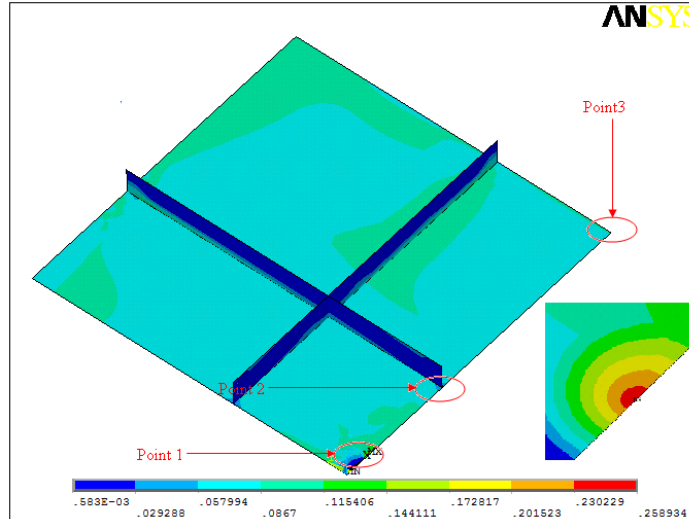


Figure 2 – Resistance index ξ of a stiffened panel for a load of 50 N/m

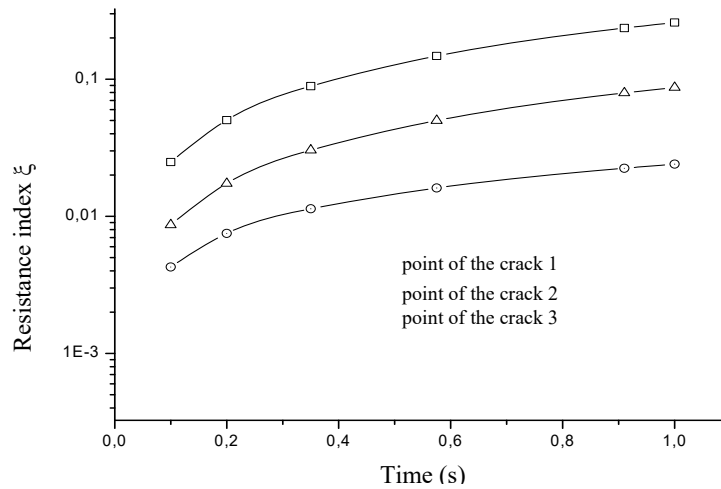


Figure 3 – Evolution of the resistance index ξ as a function of time for three points

Results and the discussion

Effect of loading

In order to see the effect of the load variation on the evolution of the resistance ratio R and the resistance index ξ , the cracked panel was subjected to several loadings.

The results obtained (Figure 4) clearly show that initially, at time $t = 0.1$ second, this ratio is very high and decreases as the simulation time increases. In parallel, this ratio R increases with increasing load. For example, at time $t = 1$ s, this ratio goes from 40.225 for $P=5$ MPa to 0.47504 for $P=400$ MPa. This means that the load has a considerable effect on the evolution of the resistance ratio R .

Since the resistance index ξ is the inverse of the resistance ratio R , the curves of Figure 5 are therefore inverse of those of Figure 4. By way of example, at time $t = 1$ s, the resistance index ξ reached = 0.02486 for a load of 5 MPa. Under the application of a load of 400 MPa, the latter is = 2.1051.

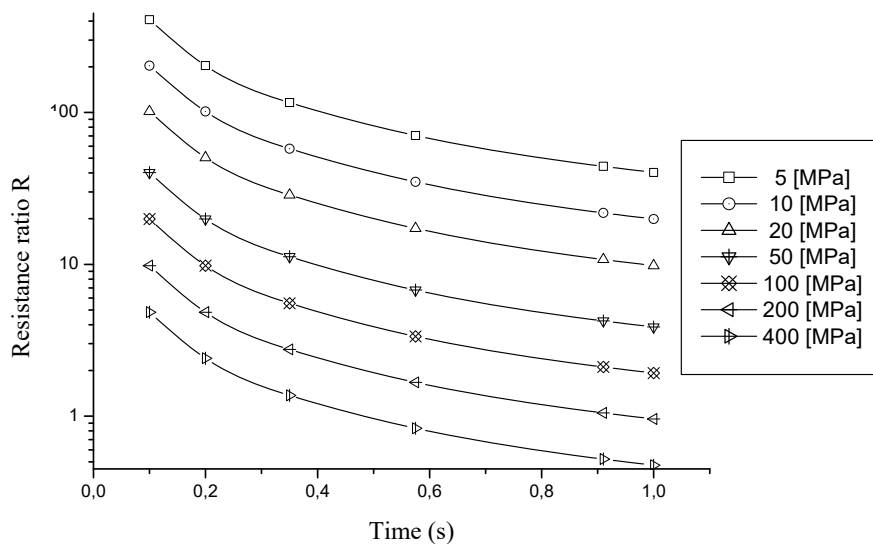


Figure 4 – Evolution of the resistance ratio R at point 1 as a function of time and the applied loading

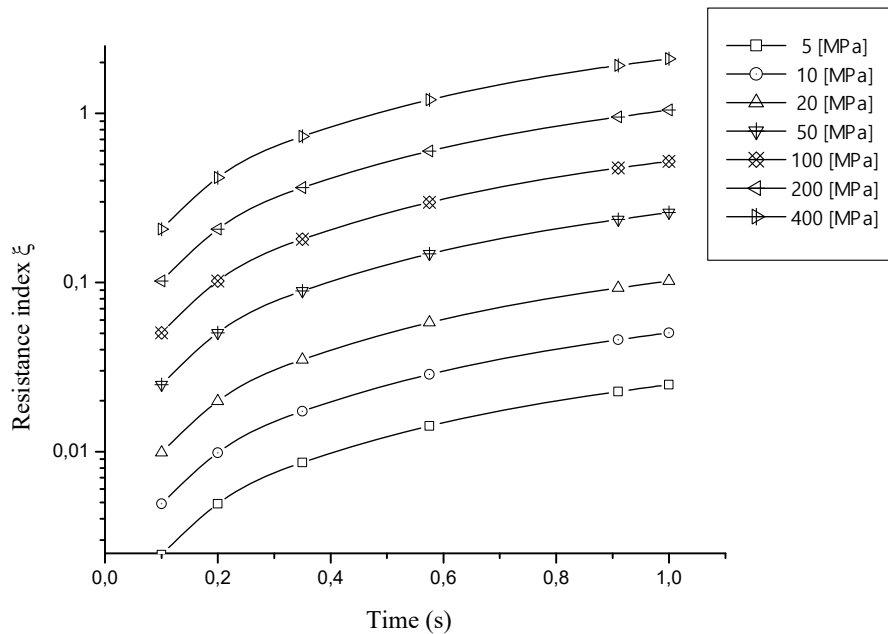


Figure 5 – Evolution of the resistance index ξ at point 1 as a function of time and the applied loading

Effect of the position of the transverse stiffeners

In order to analyse the influence of the spacing of the stiffeners on the evolution of the index and the resistance ratio, the position of the stiffeners was varied.

The stiffeners were located 40mm (Figure 6), 80mm (Figure 7) and 120mm (Figure 8) from the end of the panel.

Under a loading $P= 50$ MPa, it is obvious that the safety index is very high at the crack tip (Figures 6, 7, and 8). Moving away from the tip of the crack, the safety index values show that the panel is completely safe.

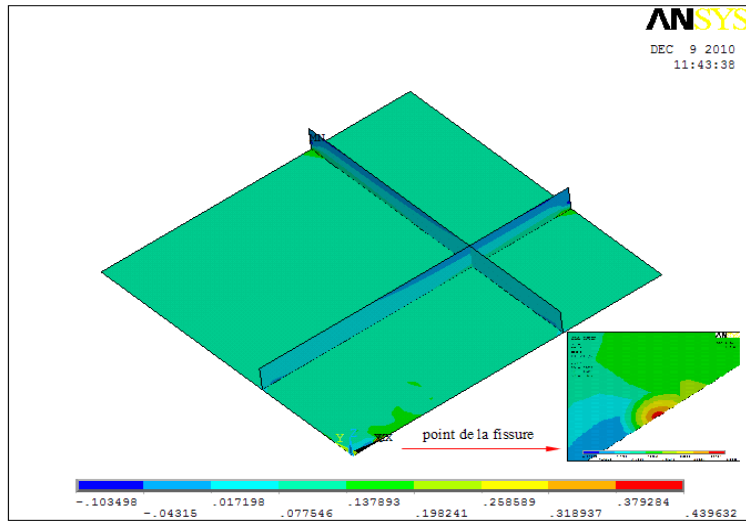


Figure 6 – Strength index for the non-linear behavior of a stiffened panel with 40mm end spacing

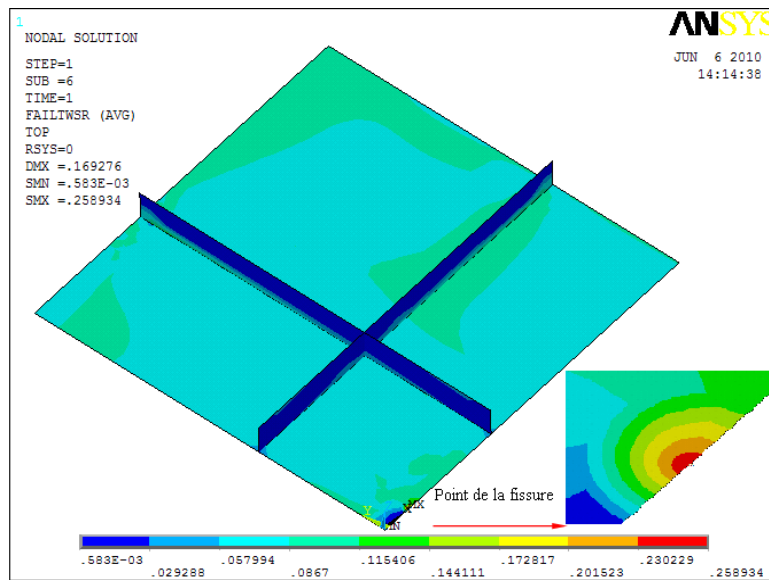


Figure 7 – Strength index for the non-linear behavior of a stiffened panel with 80mm end spacing

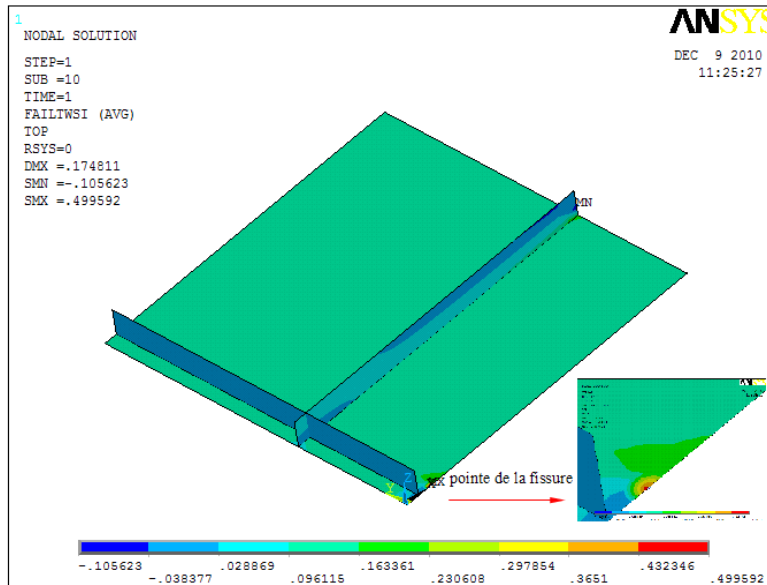


Figure 8 – Strength index for the non-linear behavior of a stiffened panel with 120mm end spacing

The results (Figure 9) provided by this modeling indicate that the position of the stiffeners considerably affects the evolution of the resistance index ξ . The latter becomes smaller with the approximation of the stiffeners to the crack tip (for $t=1s$, $=0.00446$).

So there is more security. In addition, the evolution of the resistance ratio as a function of time, for the three positions of the stiffeners, is presented in Figure 10. In this figure, the resistance ratio tends towards zero when the position of the stiffeners moves away from the crack tip.

It can therefore be concluded that bringing the stiffeners closer to the tip of the crack prevents the propagation of the cracks and ensures fairly high resistance ratios.

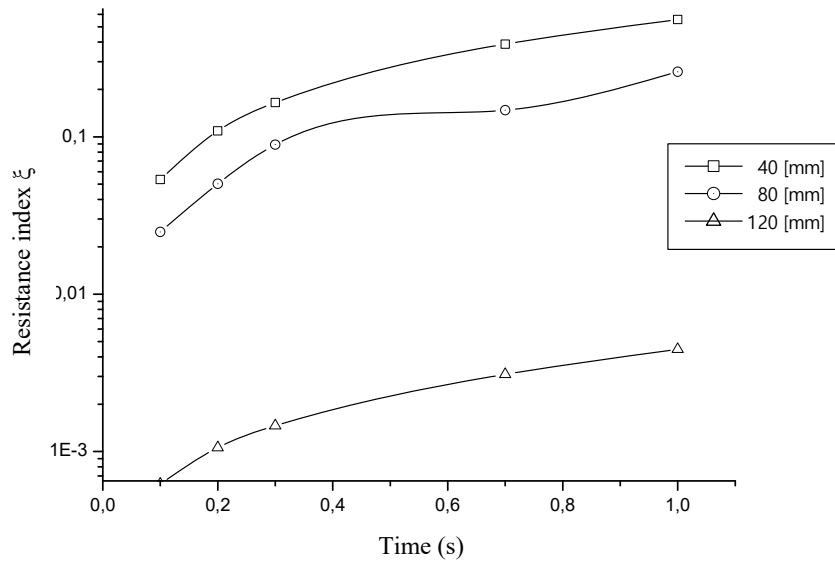


Figure 9 – Evolution of the resistance index ξ as a function of time of the cracked panel for different spacings of the transverse stiffeners

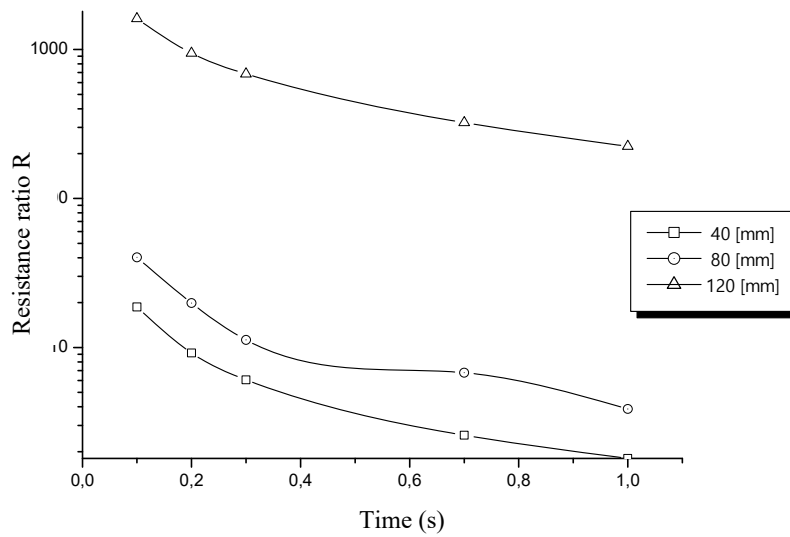


Figure 10 – Evolution of the resistance ratio R as a function of time for different spacings of the transverse stiffeners

Effect of the variation of the thickness of the stiffeners

To analyse this parameter, the stiffener thickness was changed while keeping the initial thickness of the panel constant.

From the results obtained (Figures 11 and 12), it is evident that the progressive increase in the thickness of the stiffener leads to a significant reduction in the resistance index ξ and an increase in the resistance ratio R.

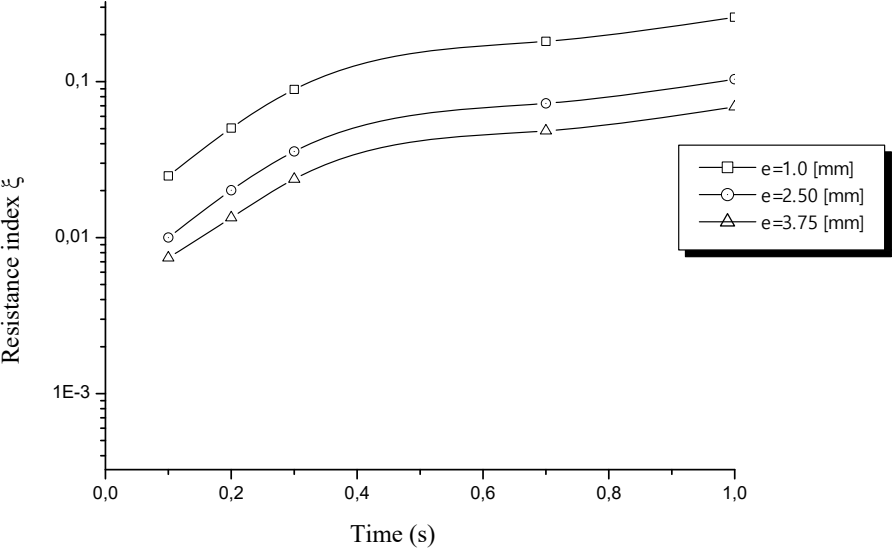


Figure 11 – Evolution of the resistance index ξ depending on the thickness of the stiffener

In Figure 11, the resistance index at t=1s goes from 0.26 for a thickness of 1 mm to 0.06 for a thickness of 3.75 mm.

On the other hand, in Figure 12, the resistance ratio at t=1s is 3.86 for a thickness of 1 mm. On the other hand, for a thickness of 3.75 mm, it increases to 14.48.

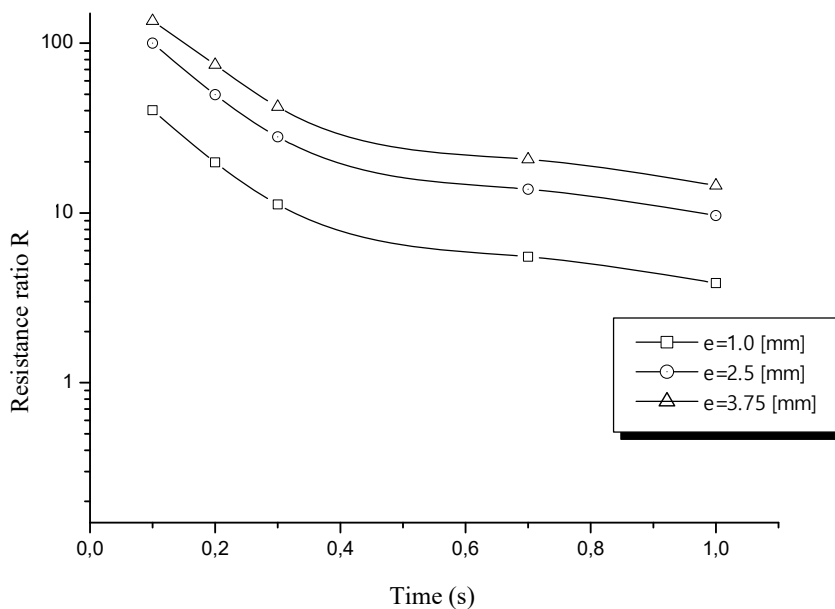


Figure 12 – Evolution of the resistance ratio R depending on the thickness of the stiffener

Conclusion

In order to follow the behaviour of a composite panel with a crack in its center in the case of large displacements, it seemed logical to carry out an analysis in the nonlinear domain.

In order to find the critical values of the index and the resistance ratio, along the panel, three points likely to have the critical stresses were chosen. The first point is at the bottom of the crack, the second one is at the level of the transverse stiffener while the third point is at the end of the panel.

From all the results provided by this modelling, it was noticed that the safety ratio increases remarkably, as a function of time, for the three chosen points. But the first point represents the most critical case because it is at the tip of the crack.

Regarding the effect of the variation of the load on the evolution of the safety ratio at the bottom of the crack, it was found that the initial state presents more risk for the panel because the resistance ratio registers to these lower values. On the other hand, the resistance index is quite important.

Following the results of this analysis, it is recommended to provide patches for the repair of cracked panels based on the presented modelling. In order to ensure structural stability, the authors intend to address panel buckling and associated stiffener-sheet separation in future research.

References

Baker, A.A. 1993. Repair efficiency in fatigue-cracked aluminum components reinforced with boron/epoxy patches. *FFEMS – Fatigue & Fracture of Engineering Materials & Structures*, 16(7), pp.753-765. Available at: <https://doi.org/10.1111/j.1460-2695.1993.tb00117.x>.

Baker, A.A., Rose, L.R.F. & Jones, R. 2003. *Advances in the Bonded Composite Repair of Metallic Aircraft Structure, 1st Edition*. Elsevier Science. ISBN: 9780080522951.

Bayatfar, A., Khedmati, M.R. & Rigo, P. 2014. Residual ultimate strength of cracked steel unstiffened and stiffened plates under longitudinal compression. *Thin-Walled Structures*, 84, pp.378-392. Available at: <https://doi.org/10.1016/j.tws.2014.07.002>.

Chue, C.-H., Chang, L.-C. & Tsai, J.-S. 1994. Bonded repair of a plate with inclined central crack under biaxial loading. *Composite Structures*, 28(1), pp.39-45. Available at: [https://doi.org/10.1016/0263-8223\(94\)90004-3](https://doi.org/10.1016/0263-8223(94)90004-3).

Denney, J.J. & Mall, S. 1997. Characterization of disbond effects on fatigue crack growth behavior in aluminum plate with bonded composite patch. *Engineering Fracture Mechanics*, 57(5), pp.507-525. Available at: [https://doi.org/10.1016/S0013-7944\(97\)00050-7](https://doi.org/10.1016/S0013-7944(97)00050-7).

Duong, C.N. & Wang, C.H. 2007. *Composite Repair: Theory and Design*. Elsevier. Available at: <https://doi.org/10.1016/B978-0-08-045146-6.X5000-0>.

Fesharaki, J.J., Madani, S.G. & Golabi, S. 2016. Effect of stiffness and thickness ratio of host plate and piezoelectric patches on reduction of the stress concentration factor. *International Journal of Advanced Structural Engineering*, 8, pp.229-242. Available at: <https://doi.org/10.1007/s40091-016-0125-x>.

Heller, M, Hill, T.G., Williams, J.F. & Jones, R. 1989. Increasing the fatigue life of cracked fastener holes using bonded repairs. *Theoretical and Applied Fracture Mechanics*, 11(1), pp.1-8. Available at: [https://doi.org/10.1016/0167-8442\(89\)90020-7](https://doi.org/10.1016/0167-8442(89)90020-7).

Jones, R., Davis, M., Callinan, R.J. & Mallinson, G.D. 1982. Crack Patching: Analysis and Design. *Journal of Structural Mechanics*, 10(2), pp.177-190. Available at: <https://doi.org/10.1080/03601218208907409>.

Jones, R., Molent, L, Baker, A.A. & Davis, M.J. 1988. Bonded repair of metallic components: Thick sections. *Theoretical and Applied Fracture Mechanics*, 9(1), pp.61-70. Available at: [https://doi.org/10.1016/0167-8442\(88\)90049-3](https://doi.org/10.1016/0167-8442(88)90049-3).

Makwana, A.H., Vyas, N. & Barot. R.S. 2021. Numerical investigation of composite patch repair of inclined cracked panel using XFEM. *Materials Today: Proceedings*, 45(6), pp.5128-5133. Available at: <https://doi.org/10.1016/j.matpr.2021.01.643>.

Mall, S. & Conley, D.S. 2009. Modeling and validation of composite patch repair to cracked thick and thin metallic panels. *Composites Part A: Applied Science and Manufacturing*, 40(9), pp.1331-1339. Available at: <https://doi.org/10.1016/j.compositesa.2008.08.007>.

Naboulsi, S. & Mall, S. 1998. Nonlinear analysis of bonded composite patch repair of cracked aluminum panels. *Composite Structures*, 41(3-4), pp.303-313. Available at: [https://doi.org/10.1016/S0263-8223\(98\)00052-X](https://doi.org/10.1016/S0263-8223(98)00052-X).

Naboulsi, S. & Mall, S. 1999. Methodology to analyze aerospace structures repaired with a bonded composite patch. *Journal of Strain Analysis*, 34(6), pp.395-412. Available at: <https://doi.org/10.1243/0309324991513849>.

Rose, L.R.F. 1982. A cracked plate repaired by bonded reinforcements. *International Journal of Fracture*, 18, pp.135-144. Available at: <https://doi.org/10.1007/BF00019638>.

Shi, X.H., Zhang, J. & Guedes Soares, C. 2017. Experimental study on collapse of cracked stiffened plate with initial imperfections under compression. *Thin-Walled Structures*, 114, pp.39-51. Available at: <https://doi.org/10.1016/j.tws.2016.12.028>.

Shi, X.H., Zhang, J. & Guedes Soares, C. 2019. Numerical assessment of experiments on the residual ultimate strength of stiffened plates with a crack. *Ocean Engineering*, 171, pp.443-457. Available at: <https://doi.org/10.1016/j.oceaneng.2018.10.043>.

Shi, X., Hu, Z., Zhang, J. & Guedes Soares, C.G. 2021. Ultimate strength of a cracked stiffened panel repaired by CFRP and stop holes. *Ocean Engineering*, 226, art.number:108850. Available at: <https://doi.org/10.1016/j.oceaneng.2021.108850>.

Sun, C.T., Klug, G.J. & Arendt, C. 1996. Analysis of cracked aluminum plates repaired with bonded composite patches. *AIAA Journal*, 34(2), pp.369-374. Available at: <https://doi.org/10.2514/3.13073>.

Tarn, J.-Q. & Shek, K.-L. 1991. Analysis of cracked plates with a bonded patch. *Engineering Fracture Mechanics*, 40(6), pp.1055-1065. Available at: [https://doi.org/10.1016/0013-7944\(91\)90170-6](https://doi.org/10.1016/0013-7944(91)90170-6).

Xu, M. & Guedes Soares, C.G. 2012. Assessment of the ultimate strength of narrow stiffened panel test specimens. *Thin-Walled Structures*, 55, pp.11-21. Available at: <https://doi.org/10.1016/j.tws.2012.02.006>.

Xu, M. & Guedes Soares, C.G. 2013. Experimental study on the collapse strength of wide stiffened panels. *Marine Structures*, 30, pp.33-62. Available at: <https://doi.org/10.1016/j.marstruc.2012.10.003>.

Xu, M., Garbatov, Y. & Guedes Soares, C. 2014. Residual ultimate strength assessment of stiffened panels with locked cracks. *Thin-Walled Structures*, 85, pp.398-410. Available at: <https://doi.org/10.1016/j.tws.2014.09.011>.

Xu, M. & Guedes Soares, C.G. 2021. Numerical study on the influence of experimental conditions on the collapse behaviour of stiffened panels. *Ocean Engineering*, 220, art.number:108410. Available at: <https://doi.org/10.1016/j.oceaneng.2020.108410>.

Efecto de una grieta en el comportamiento no lineal de un panel compuesto rigidizado

Houda Beghdad^a, **autor de correspondencia**, Nacer Rahal^{ab}, Abdelaziz Souici^{ab}, Sara Zatir^c, Khaled Benmahdi^a, Halima Aouad^a

^a Universidad Mustapha Stambouli, Departamento de Ingeniería Civil, Mascara, República Argelina Democrática y Popular

^b Universidad de Ciencias y Tecnología, Laboratorio de Estructura Mecánica y Estabilidad de la Construcción, Orán, República Argelina Democrática y Popular

^c Universidad Tahri Mohamed de Bechar, Departamento de Arquitectura y Urbanismo, Bechar, República Argelina Democrática y Popular

CAMPO: mecánica, materiales

TIPO DE ARTÍCULO: artículo científico original

Resumen:

Introducción/objetivo: Durante su vida útil, los barcos y aeronaves están sometidos a cargas aerodinámicas y de servicio severas que pueden causar daños estructurales y grietas. Estas grietas crecen y se propagan con el tiempo. Extender la vida útil de una estructura dañada es un área de investigación muy importante. En este contexto, se recomienda la reparación de paneles compuestos para restaurar el rendimiento de las estructuras agrietadas.

Métodos: Con el fin de minimizar la concentración de tensiones en el fondo de una grieta, detener e incluso retrasar la propagación de esta grieta, este estudio busca proponer un análisis bidimensional mediante el software ANSYS para predecir el efecto de la propagación de una posible grieta en el comportamiento no lineal de paneles compuestos rígidos agrietados.

Resultados: Los resultados de este análisis serán una muy buena referencia para mejorar el rendimiento y reparar paneles compuestos agrietados utilizando rigidizadores.

Conclusión: Se recomienda proporcionar parches para reparar paneles agrietados en función del modelado proporcionado en este estudio.

Palabras claves: paneles compuestos, estructura dañada, propagación de grietas, ANSYS, concentración de tensiones.

Влияние трещин на нелинейное поведение упрочненной композитной панели

Хауда Бегдад^а, **корреспондент**, Насер Рахал^{аб}, Абдулазиз Соици^{аб}, Сара Затар^в, Халед Бенмахди^а, Халима Авед^а

^а Университет Туши Мустафы Стамбули, строительный факультет, г. Маскара, Алжирская Народная Демократическая Республика

^б Университет естественных наук и технологий, Лаборатория машиностроения и прочности конструкций, г. Оран, Алжирская Народная Демократическая Республика

^в Университет Тахри Мохаммед Бешар, департамент архитектуры и урбанизма, г. Бешар, Алжирская Народная Демократическая Республика

РУБРИКА ГРНТИ: 67.09.33 Бетоны. Железобетон. Строительные растворы, смеси, составы

ВИД СТАТЬИ: оригинальная научная статья

Резюме:

Введение/цель: В течение срока службы суда и самолеты подвергаются серьезным эксплуатационным и аэродинамическим нагрузкам, которые могут привести к повреждению конструкции и образованию трещин. Эти трещины со временем увеличиваются и распространяются. Продление срока службы поврежденной конструкции является весьма важной областью исследований. В связи с этим рекомендуется ремонт композитных панелей для восстановления эксплуатационных характеристик конструкций с трещинами.

Методы: Для того, чтобы свести к минимуму концентрацию нагрузки на дно трещины и для того, чтобы остановить или задержать распространение этой трещины в данном исследовании предлагается двухмерный анализ с помощью программного обеспечения ANSYS в прогнозировании влияния распространения трещины на нелинейное поведение поврежденных упрочненных композитных панелей.

Результаты: Результаты данного исследования будут хорошим руководством для улучшения эксплуатационных характеристик и ремонта треснувших композитных панелей с использованием ребер жесткости.

Выводы: Рекомендуется использование заплат в ремонте треснувших панелей на основе моделирования, приведенного в этом исследовании.

Ключевые слова: композитные панели, поврежденная конструкция, распространение трещин, ANSYS, концентрация нагрузки.

Утицај прслине на нелинеарно понашање ојачаног композитног панела

Хауда Бегдад^а, **аутор за преписку**, Насер Рахал^{а^б}, Абделаиз Соици^{а^б}, Сара Затар^б, Калед Бенмахди^а, Халима Авед^а

^а Универзитет „Мустафа Стамболи“, Одсек за грађевинарство, Маскара, Народна Демократска Република Алжир

^б Универзитет природних наука и технологије, Лабораторија за машинске структуре и стабилност конструкције, Оран, Народна Демократска Република Алжир

^в Универзитет „Тахри Мохамед“, Одељење за архитектуру и урбанизам, Бешар, Народна Демократска Република Алжир

ОБЛАСТ: механика, материјали

КАТЕГОРИЈА (ТИП) ЧЛАНКА: оригинални научни рад

Сажетак:

Увод/циљ: Током свог животног века, бродови и авиони су изложени изузетним експлоатационим и аеродинамичким оптерећењима која могу да изазову структурална оштећења и прслине које временом расту и шире се. Продужавање живота оштећеној структури представља веома важну област истраживања. С тим у вези, поправка композитних панела препоручује се ради враћања перформанси структурама са прслинама.

Метод: Да би се концентрација напона на дну неке прслине свела на најмању могућу меру, као и да би се зауставио, па чак и одложио раст прслине, овом студијом се предлаже дводимензионална анализа помоћу ANSYS софтвера како би се предвидео утицај раста неке прслине на нелинеарно понашање напрслих ојачаних композитних панела.

Резултати: Резултати ове студије биће добра референца за побољшавање перформанси и поправку напрслих композитних панела помоћу учвршћивача.

Закључак: Препоручује се коришћење закрпа за поправку напрслих панела на основу моделовања приказаног у овој студији.

Кључне речи: композитни панели, оштећена структура, раст прслине, ANSYS, концентрација напона.

Paper received on: 14.10.2023.

Manuscript corrections submitted on: 24.09.2024.


Paper accepted for publishing on: 25.09.2024.


© 2024 The Authors. Published by Vojnotehnički glasnik / Military Technical Courier (www.vtg.mod.gov.rs, втг.мо.унр.срб). This article is an open access article distributed under the terms and conditions of the Creative Commons Attribution license (<http://creativecommons.org/licenses/by/3.0/rs/>).





Tensile examination of progressive damage and failure in porous ceramic composite materials using the XFEM


Aicha Metehri^a, Kouider Madani^b, Belaïd Mechab^c,
Mohammed Mokhtari^d, Ilias M.A. Ghermaoui^e


^a University of Sidi Bel Abbes, Faculty of Technology,
Mechanical Engineering Department,
Laboratory of Physical Mechanics of Materials,
Sidi Bel Abbès, People's Democratic Republic of Algeria,
e-mail: ametehri@yahoo.com, **corresponding author**,
ORCID iD:  <https://orcid.org/0009-0002-2221-6833>

^b University of Sidi Bel Abbes, Faculty of Technology,
Mechanical Engineering Department,
Laboratory of Physical Mechanics of Materials,
Sidi Bel Abbès, People's Democratic Republic of Algeria,
e-mail: koumad10@yahoo.fr,
ORCID iD:  <https://orcid.org/0000-0003-3277-1187>

^c University of Sidi Bel Abbes, Faculty of Technology,
Mechanical Engineering Department,
Laboratory of Physical Mechanics of Materials,
Sidi Bel Abbès, People's Democratic Republic of Algeria,
e-mail: bmechab@yahoo.fr,
ORCID iD:  <https://orcid.org/0009-0000-7483-5527>

^d ENPO-MA - National Polytechnic School of Oran-Maurice Audin,
Mechanical Engineering Department,
Mechanical Manufacturing Technology Research Laboratory,
Oran, People's Democratic Republic of Algeria,
e-mail: mokhtarimohamed44@yahoo.fr,
ORCID iD:  <https://orcid.org/0000-0001-7255-2312>

^e University of Sidi Bel Abbes, Faculty of Technology,
Mechanical Engineering Department,
Laboratory of Physical Mechanics of Materials,
Sidi Bel Abbès, People's Democratic Republic of Algeria,
e-mail: ghermaoui_ilias@hotmail.fr,
ORCID iD:  <https://orcid.org/0000-0001-7935-5362>

 <https://doi.org/10.5937/vojtehg72-50091>

FIELD: mechanics
ARTICLE TYPE: original scientific paper

Abstract:

Introduction/purpose: Porosity is a significant factor that causes voids to become trapped in materials during composite material fabrication. This study is dedicated to modelling fracture modes within highly stressed areas of an advanced SiC/C_f component at a macroscopic scale.

Methods: The finite element method is used to analyze defects within composites, considering factors such as porosity size, shape, and tensile stress. The Monte Carlo method predicts the distribution function (F).

Results: Three pores are distributed across the width of the material, which reduces the active cross-sectional area of the material and, consequently, leads to a significant reduction in strength. Overall, resistance tends to decrease, with a more noticeable drop.

Conclusion: It is concluded how the form and the size affect the failure load, employing the Extended Finite Element Method (XFEM) to predict mode-I fracture behaviour. The porosity parameter significantly affects the durability of the structure. It is noted that the size of pores (ϕ) is a crucial component that affects the distribution function (F). The variability in this parameter substantially elevates the likelihood of plate failure and diminishes the longevity of a structure.

Keywords: composite, XFEM, tensile load, failure load, fibre reinforced, size.

Introduction

A composite material is a mixture of two or more materials that exhibit improved properties when combined. Each material retains its unique chemical, physical, and mechanical properties, as demonstrated by various studies, in contrast to metallic alloys. (Kumari et al, 2018; Venkatesan et al, 2020; Michael et al, 2021; Muthalagu et al, 2021; Kishore et al, 2021; Hatti et al, 2021; Mizerska et al, 2022)

Ceramic matrix composites (CMC) demonstrate exceptional characteristics such as superior strength, stiffness, stiffness-to-density ratios, and thermal stability at elevated temperatures (Gavalda Diaz et al, 2019; Gowayed et al, 2013; Xia et al, 2019). Ceramic composite materials are increasingly used in major industrial sectors such as aeronautics, automotive, and nuclear industries. Defects can sometimes arise within composite materials, including ceramic matrix composites, during manufacturing, regardless of the specific method employed. These imperfections may occur during the forming process because of the uneven composition of composite materials. A porosity defect is characterized by the presence of small cavities that contain gaseous matter known as pores. These pores are classified based on their size, including micro, meso, and macro-pores. There are various methods to characterize porosity; the thermal and mechanical properties of porous ceramic bodies are influenced by factors such as the size, shape, distribution, orientation, volume fraction, and interconnection of pores (Meille et al, 2012; Bartuli et al, 2009). Various models have been

suggested to explain the strength of brittle materials, but the Weibull analysis is widely utilized, as demonstrated by Cui et al. (2017) and Keleş et al. (2018). An approach to calculate the pore volume and the area distribution directly from the isotherm desorption of porous substances was introduced by Barrett et al. (1951).

The approach has effectively been used for adsorbents with various maximum pore volumes. An innovative numerical simulation technique utilizing the Finite Element Analysis (FEA) is regarded as a powerful tool for enhancing the utilization of ceramics in components and members. This method can accurately assess the likelihood of fractures produced by fault distribution characteristics. Evans et al. (1979) presented data regarding microstructure distribution, including relative density, pore size, aspect ratio, and grain size. These data were used as input values and incorporated into a continuum damage model through a fracture mechanical model. The fracture mechanical model was based on a circumferential circular crack originating from an oval spherical pore. The findings indicate that the suggested Finite Element Analysis (FEA) approach is applicable for assessing the likelihood of fractures in ceramics. Zimmermann & Rödel (2004) have illustrated and given results based on a model that describes the instability of the cracks that occur with the configuration of a micro-crack positioned in the effect of concentration of the stresses of a large pore. The study conducted by Rezaee et al. (2020) established that pores exhibit a nearly spherical shape, consistent size and distribution, and strong connection. This work aimed to enhance the strength of porous alumina-zirconia ceramic composites by combining the toughening and strengthening properties of tetragonal zirconia with the positive densification impact of niobium oxide. In this study, Ying et al. (2018) examined how the amount of Al_2O_3 fibre in ceramic materials affects pore size distribution, porosity, compressive strength, and load-displacement behaviour. The materials were created using the gel-casting process. Pia et al. (2016) have introduced an intertwined fractal model that can establish a connection between the thermal characteristics of ceramic materials and their pore microstructure.

The investigation into fracture phenomena such as crack propagation and delamination in composite materials continues to evolve, aiming for a more precise modelling approach. (Luan et al, 2018; Carrère et al, 2000). The ongoing refinement of assumptions and methodologies aims to accurately predict damage, optimize computational resources, and facilitate progressive damage modelling. The finite element technique (XFEM) has been widely employed in the prediction of fracture propagation in composite materials, as demonstrated by the research

conducted by Swati et al. (2019) and Benzaama et al. (2018). XFEM methodology has recently emerged as a distinctive way of tackling the simultaneous propagation of mode-I cracks and delamination in composites. This has been proved in research conducted by Hu et al. (2016), and Daggumati et al. (2020). Previous applications of this method have mainly concentrated on either simulating large-scale specimens in carbon fibre-reinforced polymer (CFRP) composites, as demonstrated in the research conducted by Stuparu et al. (2016), or simulating individual fibres in SiC/SiC composites at a microscopic level, as investigated by Daggumati et al. (2020) and Lang et al. (2018). Hence, the primary objective of the present investigation is to replicate different types of fractures occurring in the concentrated area of high stress within a non standard SiC/SiC component but on a larger scale. To accomplish this, XFEM methodology was utilized to forecast fracture behaviour in both mode-I and mode-II, using the strategy described by Sun et al. (2013).

This study aimed to reproduce the fracture behaviour in the highly strained region of an advanced SiC/C_f component on a macroscopic scale. This inquiry utilized the Extended Finite Element Method (XFEM) to analyze a defect in a composite material. An analysis was conducted on factors like the dimensions, the configuration, and the alignment of the pores, the interplay between multiple holes and the rigidity of the matrix when subjected to tensile stress. An evaluation was conducted on the influence of the interaction among the pores on the load at which failure occurs. In addition, the extended finite element approach was used to predict the behaviour of mode-I fracture.

XFEM input parameter and materials

The cell of a unidirectional composite domain is created as a solid part of the solid section. The XFEM enrichment domain function is input as follows:

*Enrichment, name=Crack-1, type=Propagation Crack, activate= On
The solid composite section is used for the XFEM domain.

The evaluated damage is maximal at the crack opening and is calculated using the following equation (Dassault Systems, The 3D EXPERIENCE platform, 2014):

$$\left(\frac{G_I}{G_{IC}}\right) + \left(\frac{G_{II}}{G_{IIC}}\right) + \left(\frac{G_{III}}{G_{IIIC}}\right) = 1 \quad (1)$$

The maximum principal stress measured for the composite material SiC/C_f is (178±25.7) MPa and the shear stress measured is 93 MPa (Udayakumar et al, 2014). The damage evaluation criteria also take into account the maximum traction energy (the maximum crack opening of the composite specimen has been experimentally determined to be 2.8KJ/m² (Udayakumar et al, 2014). The ABAQUS code included various mechanical properties and their failure parameters as damage parameters (See Table 1), in order to simulate an increase in the failure/damage level after reaching the ultimate stress.

Table 1 – Mechanical properties of the constituents of the composite material used (Vijayakumar et al, 2016; Metehri et al, 2009)

Materials	SiC-matrix	Epoxy R368-1-matrix	Al 6061-matrix	Carbon-fiber
E (GPa)	410	3.05	72	230
v	0.14	0.35	0.33	0.3
Max principal stress (GPa)	3	0.08	0.12	3.2
Displacement failure damage	0.007	0.4	0.2	0.013

The XFEM technique and the Irwin hypothesis (Irwin, 1960) are used to calculate the energy release rate components, G_I, G_{II}, and G_{III}, by multiplying the nodal forces. This analysis is performed to study crack propagation in the SiC/C_f porous composite material, specifically at the crack tips of the matrix and fibres.

According to Griffith's fracture theory (Griffith, 1921), a crack will propagate when the variation in elastic energy is more significant than surface energy.

$$\sigma = \sigma_r = \sqrt{\frac{EG_{Ic}}{\pi a}} \quad (2)$$

where: E: Young modulus and
σ_r: failure stress.

This corresponds to a decrease in the system's free energy, meaning that the total energy release rate (G_T), measured at a particular location along the crack front, will reach a critical value denoted by G_C.

$$G_T = G_I + G_{II} + G_{III} \quad (3)$$

where G_I , G_{II} , and G_{III} represent the energy release rates for Mode I, II, and III, respectively.

To achieve crack propagation, it is necessary: $G_T \geq G_C$.

Table 2 – Mechanical interface properties of composites materials (Monerie, 2000)

	G_{Ic} (J/m ²)	G_{IIc} (J/m ²)	G_{IIIc} (J/m ²)
SiC/SiC	9	1	0

Finite element modeling of the problem

Residual strains are generated during the elaboration process as the temperature lowers from the elaboration temperature to the ambient temperature. The stresses frequently occur due to the difference in stiffness and thermal expansion coefficient between the reinforcing material (fibre) and the matrix.

As a result, this encourages the development and spread of fatigue micro-cracks and geometric or metallurgical flaws. Therefore, examining the escalated failure or damage in these areas and the fibres is crucial. A three-dimensional model has been created for this study.

The model consists of a ceramic matrix shaped like a parallelepiped, with two capillaries running down its central axis. Inside these capillaries, two cylindrical carbon fibres have been placed (Figure 1). The latter refers to a basic unit of a composite material that is unidirectional and has porosity.

The model dimensions are 60µm in length, 30µm in width, and 15µm in thickness. The carbon fibres are separated by 16µm and their diameter is 7µm. The porosity is situated at the core of the ceramic matrix and is represented as a pore with a diameter of 6µm. This pore serves as a reference point for comparing the dimensions of the cells in a unidirectional composite.

Figure 1 provides a diagrammatic representation of the composite material with porosity. A study was conducted to analyse the material properties and geometric characteristics. The porosity is located within the ceramic matrix at a distance of 25µm from the bottom of the structure.

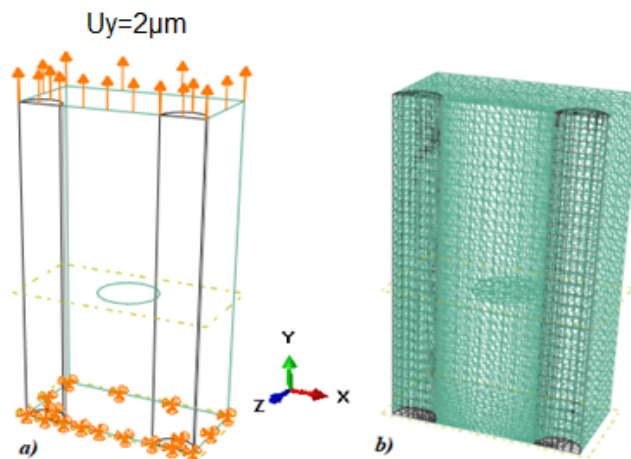


Figure 1 – The finite element model: a) Boundary conditions, b) Total meshes structure

This structure is subjected to tensile behaviour, with the fixing and loading conditions involving fixing the structure at one edge direction ($U_x = U_y = U_z = 0$) and applying a traction displacement on the opposite edge ($U_y = 2\mu\text{m}$). (Refer to Figure 1a).

This behaviour, fixed at one edge and subjected to traction displacement on the opposite edge.

The accuracy of the numerical computation is highly dependent on the mesh quality surrounding the porosity and the interface between the fibre and matrix. It is essential to have an adequate number of mesh elements in the areas between the pores and the matrix, as well as in the fibres and matrix, on which the damage properties rely. For this analysis, we used 1980 linear hexahedral elements of type C3D8R (8 Nodes Linear Brick, reduced integration) for the fibres and 35377 quadratic tetrahedral elements of type C3D10 (10 nodes Linear tetrahedron) for the matrix (refer to Table 3). Figure 1b displays the finite element model, which features a dense grid in the porosity considering the concentration of stresses and the appearance of cracks.

Table 3 – Number of nodes and the element types of the mesh

Element type	Number of elements	Total number of nodes
Fibre: C3D8R	1980	54796
Matrix: C3D10	34711	

Results and analysis

Numerical models have been developed to evaluate the effect of the presence of porosity of different shapes and sizes in the matrix on the mechanical resistance of the composite material. In all of this work, it is considered that the stress analysis is given at a displacement equal to $1.7\mu\text{m}$, i.e., just before the damage of ceramic composite material. The two sections A-A of this structure are taken to demonstrate the stress distribution at the porosity level, as shown in Figure 2.

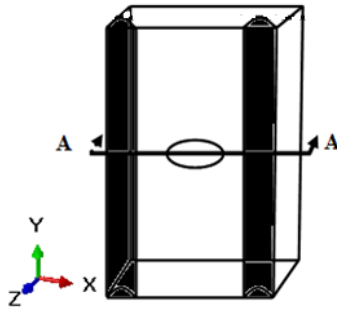


Figure 2 – Unidirectional composite cell with the sections

Tensile simulation and experimental

This study considers the SiC/C_f couple with a porosity of $4\mu\text{m}$ diameter.

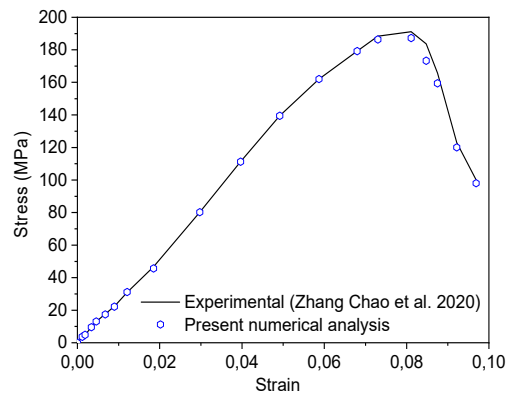


Figure 3 – Comparative analysis of the experimental and computational results for the SiC/C_f

This section demonstrates that the software can accurately simulate the beginning and the propagation of the fibre/matrix interfacial fracture by validating the numerical approach results against experimental data. The results agreed with the experimental values (Zhang et al, 2020; Udayakumar et al, 2020). A good agreement is observed for a couple of composite materials, SiC/C_f, from Figure 3. These results are helpful for further studying the fracture toughness of SiC. The current results are in good agreement with the analytical solution, with a difference of around 3%.

Effect of porosity size

The influence of the porosity size (diameter) on the variation of the breaking force was considered. The force-displacement curves representing the numerical analysis results consider the average displacement and response force.

Figure 4 presents the distribution of the equivalent stresses in SiC/C_f for a displacement in tension U_y of 2 μm . This result shows a concentration of equivalent stresses around the porosity and the fibre/matrix interface. Further from the porosity, the deformation and the normal stresses became weaker and weaker.

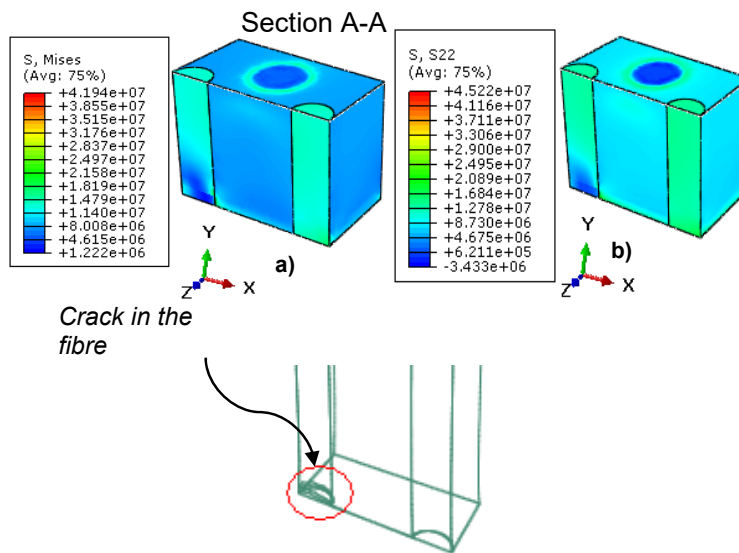


Figure 4 – vonMises and normal longitudinal stress distribution ($U_y=2\mu\text{m}$, $\phi_P=10\mu\text{m}$)

Compared to the section A-A, one can note an interaction between the fibre-porosity and porosity-free edge; this porosity generates a low material resistance compared to the applied stress.

The level of the standard stress σ_{22} follows the direction Y, and according to the section A-A, it shows areas of high concentrations. Compressive stresses are generated at the porosity level. A high concentration of stress generates a crack in the fibre.

The variation of the failure load as a function of the displacement for different sizes of the porosity is shown in Figure 5. It is noted that the breaking force is in an order of value of ~ 13KN, decreased proportionally with the increase of the pores to reach a minimum value for a large porosity size, which shows that the strength of the material becomes low. On the other hand, if the porosity size is minimal, it can be observed that the SiC/C_f couple is more rigid, which means that the damage will appear sooner.

The existence of porosity in the composite material enables the identification of the crack's starting point, which is challenging to determine due to its dependence on factors such as the elastic displacement of the constituent materials and the characteristics of the fibre/matrix interface and porosity/matrix.

In other words, referring to the material response to the applied displacement, the increase in the porosity volume generates the most considerable drop in the material resistance; the maximum breaking force appears sooner than in the case of a material without porosity.

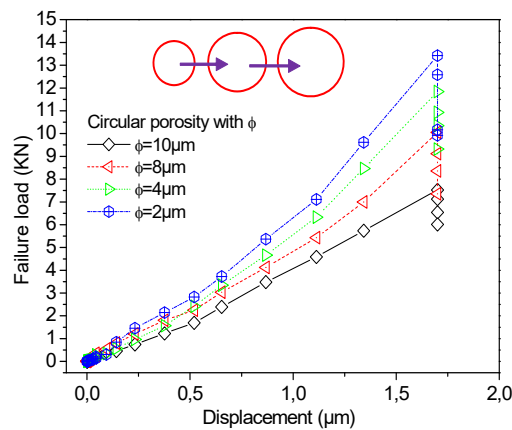


Figure 5 – XFEM stress-displacement curve for different porosity sizes

Cubic shape

In this part of the work, the effect of the geometric shape (characterized by different porosity lengths in a composite material) on the damage force was analyzed.

In the presence of a cubic-shaped porosity, the value of the von Mises stresses increases more considerably than in the case of the presence of circular and elliptical-shaped porosity. This is mainly due to four wedges, areas of high-stress concentration.

The high concentration of stresses at the porosity level lightens the stresses compared to the rest of the structure. It is noted that compressive stresses are present at the porosity level. Therefore, the crack is initiated in the two fibres. The results of this analysis are shown in Figure 6.

Section A-A

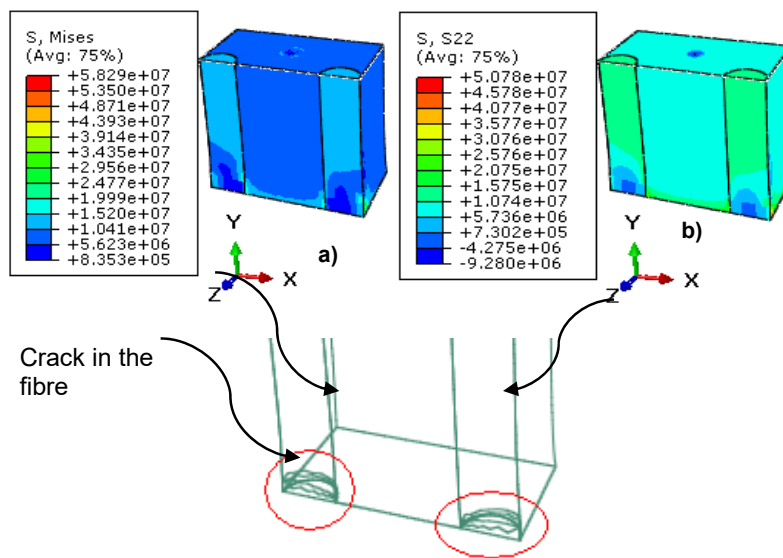


Figure 6 – vonMises stresses distribution for the cubic porosity ($U_y= 2\mu\text{m}$, $l_p=4\mu\text{m}$)

Comparing these curves (Figure7), the changes in the ultimate failure load are almost the same, but with an increase in the level in all cases; a higher level is observed in the case of cubic shapes with lengths equal to $2\mu\text{m}$. When subjected to tensile stress, the crack propagation rate is significantly reduced as it nears the interface between the fibre and the matrix. However, it then quickly expands within the fibre. This behaviour

becomes more pronounced as the stresses increase for all the examples tested (lengths ranging from 2 to 6 μm). In these circumstances, the failure load is relatively modest compared to spherical porosity.

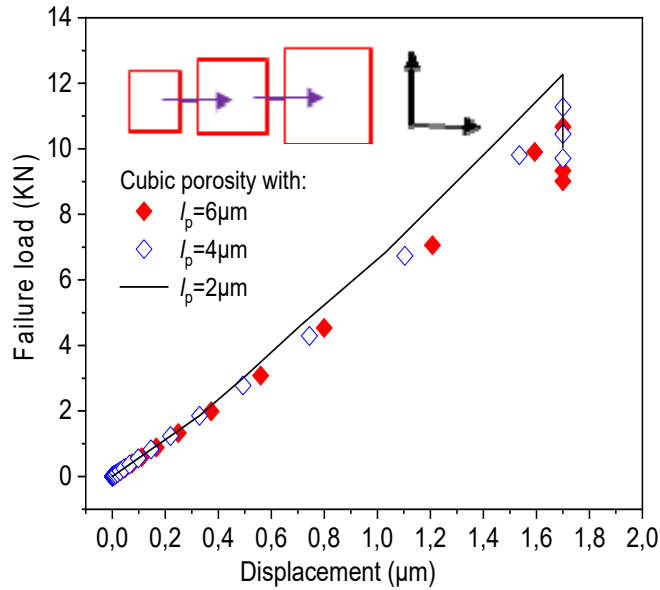


Figure 7 – XFEM load-displacement curve related to the cubic porosity

Comparative analysis

These models were developed to evaluate the influence of the organization of the porous structure on the effective mechanical resistance. They have closed porosities. In the first case, closed-pore composites are connected in the same direction (direction x), and in the second case, they have a composite with closed pores that is only distributed.

This paper proposes an ideological model that considers the probability of multiple porosities and the influence of the interaction with the surrounding existing porosity, suggesting that mono-porosity is insufficient.

Figure 8 represents the equivalent stresses of von Mises along the y direction of the three cylindrical connected unidirectional pores with $\Phi_p = 6\mu\text{m}$ (See Figure 8a), the three cubic pores with the length $l_p = 6\mu\text{m}$

connected unidirectionally (Figure 8b). The last one is one of the three randomly dispersed pores with $\Phi_p = 6\mu\text{m}$ (Figure 8c).

Section A-A

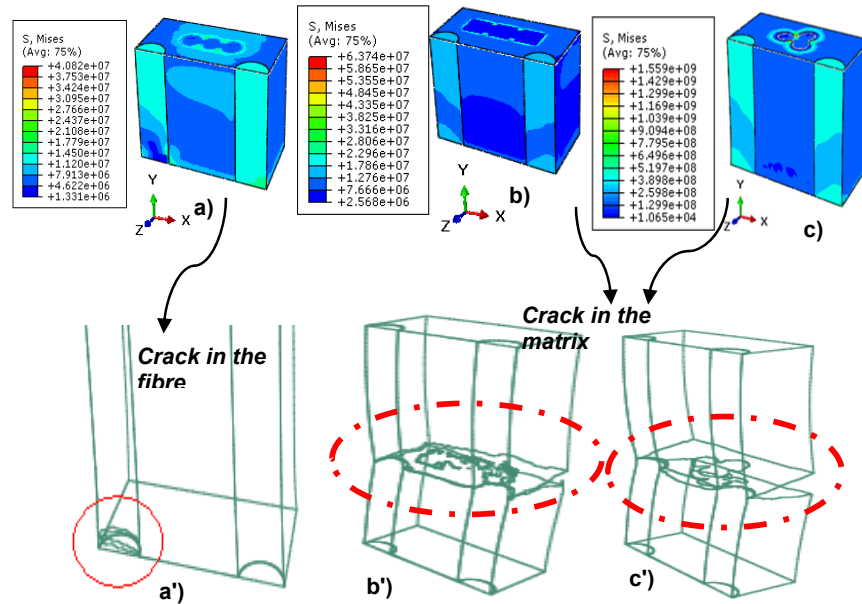


Figure 8 – vonMises stresses distribution with closed pores connected to the cylindrical cubic organization and the triangle organization ($\phi_p=6\mu\text{m}$)

Some three-dimensional models of composite materials with closed pores, possibly connected, were studied to evaluate the ultimate failure damage on the mechanical resistance at a displacement $U_y=2\mu\text{m}$ —the pores of cylindrical, cubic, and triangle shapes.

In the presence of three porosities of a circular shape arranged linearly along the width, the value of the von Mises stress is very high only if the arrangement is according to the case of Figure 8a.

However, the cubic and triangular shapes of the porosity are always the most dangerous for the material (Figures 8b, 8c), especially if there will be more porosity arranged along the width. The stress concentration is at the acute point of the porosity with a high concentration between porosities. At the same time, in the case of the triangular and cubic shapes, we notice a high stress concentration between the porosities and another

stress concentration between the porosity and the free edge of the material.

Figures 8b and 8c show the fracture microstructure of the composite material after the tensile test where the cracks propagated and deflected along the edge of the fibres in the matrix under the applied displacement, and the existence of the fibres effectively blocked the further expansion of the cracks, as well as broken fibres at the same time.

The tensile response of the material following the presence of three porosities according to different arrangements clearly shows a considerable drop in the curve of the force-displacement variation, especially in the case of the cubic shape of the porosity.

Figure 9 shows the variation of the damage force for three defect shapes, i.e., cylindrical, cubic, and triangular, with the organization of the porous structure (ordered and randomly). Comparing these porosity shapes, the change in the curve of the ultimate failure load is observed, though a higher level is observed in the case of a triangular shape.

The structure of the composite material has the propagation crack in the fibres in the case of the circular shape, but in the case of triangular and cubic pores, we observed very clearly that the crack has been initiated in the matrix and propagated to the other side; the composite material is not very strong. More porosity can trigger the rupture of the composite material too early and for low applied stress.

Suppose there is the presence of three porosities arranged along the width of the material. In that case, this minimizes the active section of the material and, therefore, a considerable drop in its resistance. Higher, linked pore densities tend to result in a more notable decrease in overall resistance.

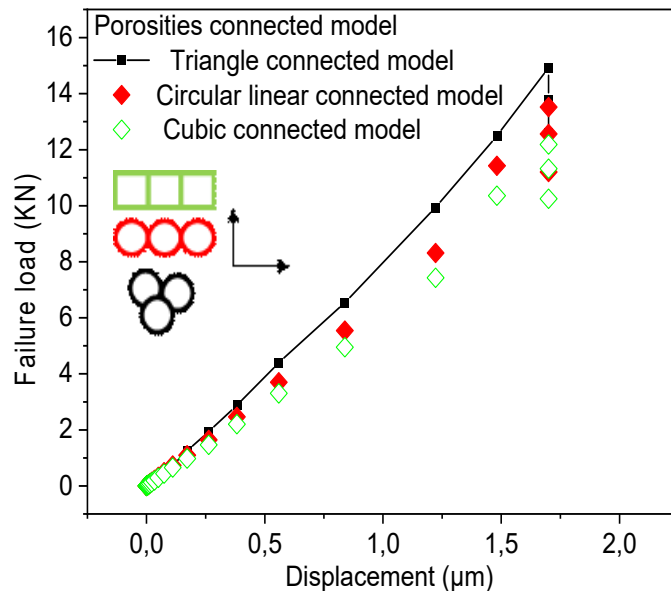


Figure 9 – XFEM load-displacement curve related to the porosity organization (circular, cubic, and triangle)

Effect of the matrix type

In this section, the impact of the matrix on the natural behaviour is examined, taking into account the severity of the tensile loading and the size of circular porosity ($\phi=10\mu\text{m}$). The matrix chosen for this study is Epoxy R368-1 and Al alloy with a carbon fiber; tensile loading is applied for comparative analysis.

For Figure 10, the most intense longitudinal stresses are observed in the pores of the SiC/C_f and Epoxy/C_f couples, which reduce the rigidity of the composite material structure and its resistance to the damage to chemical bonds. As it loses its strength. Epoxy/C_f has a long breaking path and a corresponding curve segment. The shape of this segment depends on the matrix type and the nature of the interface. The most damage-resistant couple is Al/C_f. Conversely, the Al/C_f combination with relatively slow damage responds to loading for this behaviour.

As a result, porosity significantly impacts how composites fracture when external displacement is applied. It modifies the location and

evolution of damage and results in a notable reduction in the tensile strength of the composites. In summary, porosity-induced longitudinal stresses need to be considered in both the design and the analysis of composites since they can significantly impact the damage behaviour of materials.

- 1- Appearance of a crack which first drops in stress at point (1).
- 2- Propagation of this break (from point (1) to point (2)).
- 3- Stabilization of the damage (no propagation), which causes an increase in stress with a resistance lower than the initial resistance. This step is between points (2) and (3).
- 4- Appearance of new cracks that cause the total ruin of the composite material and the relaxation of longitudinal stresses in the case of Epoxy/ C_f .

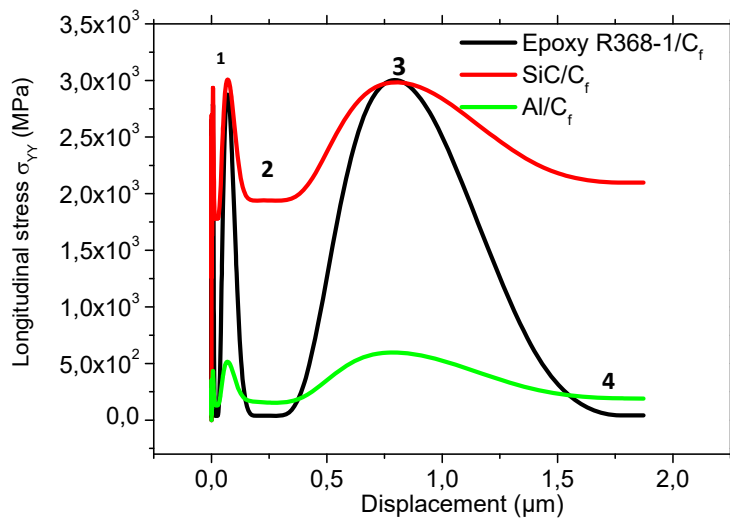


Figure 10 – XFEM Stress-displacement curve as a function of the matrix nature and the tensile load intensity

Figure 11 displays the PHILSM profile of the ceramic unidirectional composites containing a single circular pore with a diameter of $8 \mu\text{m}$.

It also shows the location of the signed distance function, which is utilized to represent the surface of the fracture.

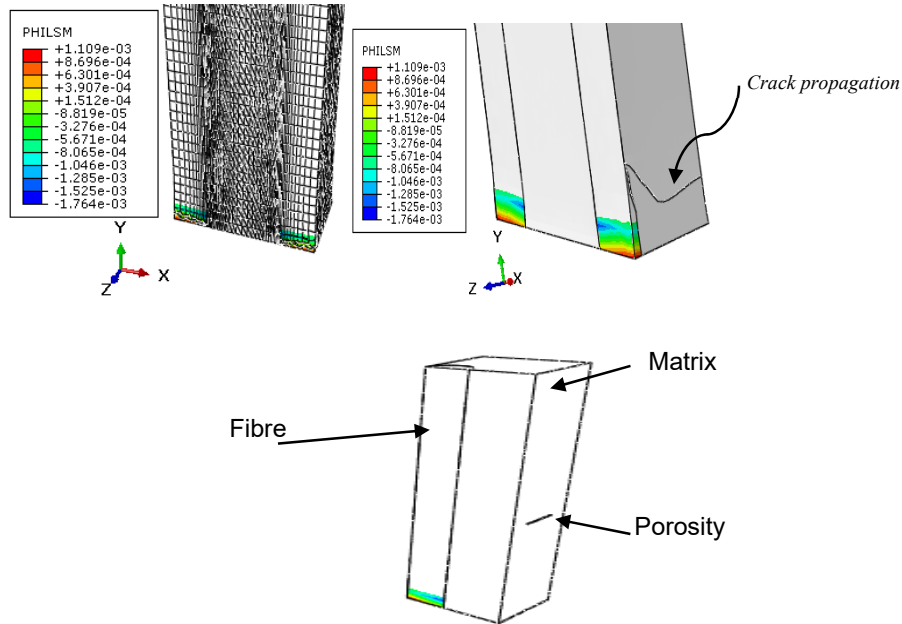


Figure 11 – Contours of PHILSM of the XFEM technique (1 circular pore $\phi=8\mu\text{m}$)

Probabilistic Fracture Mechanic Analysis

Monte Carlo methods find extensive application in diverse scientific and mathematical domains, including physics, chemistry, biology, and engineering (Mechab et al, 2016). Monte Carlo methods are frequently employed through computer simulations to yield approximate answers for situations that are otherwise difficult or too intricate to evaluate mathematically.

A probabilistic technique has been created to estimate different response statistics and the reliability of a structure. The uncertainties are associated with the estimation of load and the attributes of the geometry and materials. These parameters are depicted as stochastic variables, distinguished by their distribution type and parameters. To ensure safety, it is necessary to manage the uncertainties in the system design. For this instance, the five random variables represent the uncertainties related to the plate geometry (thickness and height), Young modulus, and crack length.

Probabilistic results

The histogram of the (F) obtained from the Monte Carlo run is shown in Figure 12. The probability density function (pdf) uses theory models to fit the histogram. Three distribution laws are being examined: Gaussian and polynomial (8th order). Based on the information presented in Figure 12, it is evident that all three distributions provide a reasonably accurate approximation of the variable (F). The polynomial function provides a higher mean value compared to the Gaussian function. Based on the data presented in Figure 12 and Table 4, it can be inferred that the Gaussian distribution offers a reasonably precise approximation of the probability density function (F) and a dependable calculation of the mean.

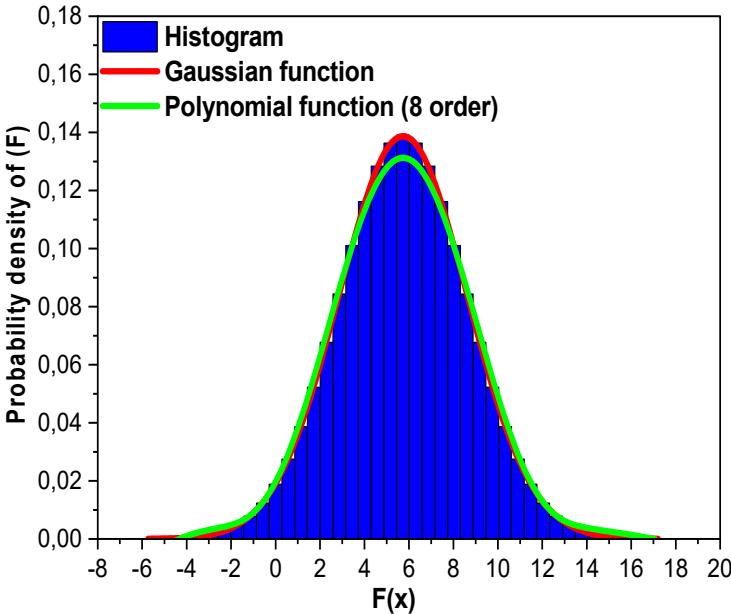


Figure 12 – Histogram and the density function of (F)

Table 4 – Mean (F) and the fitting error for probabilistic distributions

Probability density functions	Average (F)	Fitting error
Gaussian	0.1388	0
Polynomial	0.13236	0.00221

Figure 13 displays the probability density of (F) for various crack (a) lengths. It is observed that when the diameter (ϕ) of porosities is large, the probability density of (F) also increases significantly. The margin experiences a significant increase when faced with uncertainties surrounding the diameter (ϕ), resulting in a higher probability of failure. Ultimately, the failure probabilities are contingent upon the value of the diameter of porosities (ϕ).

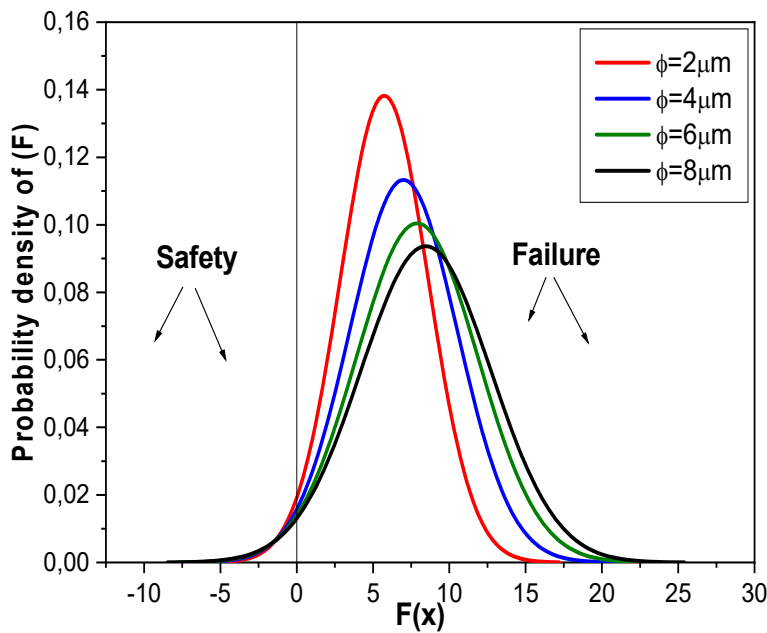


Figure 13 – Probability density of (F) for different diameter (ϕ) values

Conclusion

A finite element model using a single cell of a unidirectional composite (MCC) based on the progressive failure analysis was effectively utilized to examine the impact of geometrical characteristics (such as size and shape of the porosity) and the density of porosities (specifically the connected porosities) under a uniform uniaxial tensile load. This analysis aimed to estimate the mechanical resistance accurately. Furthermore, examining

the interaction effects between porosity and the ultimate damage force was of interest. The primary findings can be inferred as the culmination of this investigation:

The XFEM has proven to be highly effective in accurately predicting fracture behaviour during crack propagation, leading to the failure of unidirectional ceramic composite materials—nevertheless, the existence of pores in ceramics results in decreased mechanical strength.

- The more significant equivalent stresses are concentrated near the interface between the matrix and the pore while they are positioned at the interface between the fibre and the matrix.
- The size of the pores influences the extent of damage. It has been noted that the intensity of this phenomenon increases in direct proportion to the diameter of the porosity.
- The contact between the matrix and the pore and the interface between the fibre and the matrix strongly influences the propagation of cracks. These interfaces are areas where normal and tangential stresses are concentrated.
- Triangle and cubic porosities in composite materials exhibited fracture propagation primarily and deflected along the edge of the fibres in the matrix, and the existence of the fibres effectively blocked the further expansion of the cracks.
- The material Al/C_f porous enhances the structural stiffness and damage resistance of composite materials.
- The Monte Carlo method forecasts the probability distribution function of (F). It is vital to recognize that the size of the pores (ϕ) has a significant role in determining the distribution function of (F). The variability in this parameter substantially impacts the likelihood of plate failure and the structure's longevity.

References

Barrett, E.P., Joyner, L.G. & Halenda, P.P. 1951. The Determination of Pore Volume and Area Distributions in Porous Substances. I. Computations from Nitrogen Isotherms. *Journal of the American Chemical Society*, 73(1), pp.373-380. Available at: <https://doi.org/10.1021/ja01145a126>.

Bartuli, C., Bemporad, E., Tulliani, J.M., Tirillò, J., Pulci, G. & Sebastiani, M. 2009. Mechanical properties of cellular ceramics obtained by gel casting: Characterization and modeling. *Journal of the European Ceramic Society*, 29(14), pp.2979-2989. Available at: <https://doi.org/10.1016/J.Jeurceramsoc.2009.04.035>.

Benzaama, A., Mokhtari, M., Benzaama, H., Gouasmi, S. & Tamine, T. 2018. Using XFEM technique to predict the damage of unidirectional CFRP composite notched under tensile load. *Advances in aircraft and spacecraft science*, 5(1), pp.129-139. Available at: <https://doi.org/10.12989/aas.2018.5.1.129>.

Carrère, N., Martin, E. & Lamon, J. 2000. The influence of the interphase and associated interfaces on the deflection of matrix cracks in ceramic matrix composites. *Composites Part A: Applied Science and Manufacturing*, 31(11), pp.1179–1190. Available at: [https://doi.org/10.1016/s1359-835x\(00\)00095-6](https://doi.org/10.1016/s1359-835x(00)00095-6).

Cui, Z., Huang, Y. & Liu, H. 2017. Predicting the mechanical properties of brittle porous materials with various porosity and pore sizes. *Journal of the Mechanical Behavior of Biomedical Materials*, 71, pp.10-22. Available at: <https://doi.org/10.1016/j.jmbbm.2017.02.014>.

-Dassault Systems, The 3D EXPERIENCE platform. 2014. *Simulia: Abaqus Finite Element Analysis for Mechanical Engineering and Civil Engineering* [online]. Available at: <https://www.3ds.com/products/simulia/abaqus> [Accessed: 25 March 2024].

Evans, A.G, Biswas, D.R. & Fulrath, R.M. 1979. Some Effects of Cavities on the Fracture of Ceramics: II, Spherical Cavities. *Journal of the American Ceramic Society (JACerS)*, 62(1-2), pp.101-106. Available at: <https://doi.org/10.1111/j.1151-2916.1979.tb18815.x>.

Gavalda Diaz, O., Axinte, D.A., Butler-Smith, P. & Novovic, D. 2019. On understanding the microstructure of SiC/SiC Ceramic Matrix Composites (CMCs) after a material removal process. *Materials Science and Engineering: A*, 743, pp.1-11. Available at: <https://doi.org/10.1016/j.msea.2018.11.037>.

Gowayed, Y., Ojard, G., Prevost, E., Santhosh, U. & Jefferson, G. 2013. Defects in ceramic matrix composites and their impact on elastic properties. *Composites Part B: Engineering*, 55, pp.167-175. Available at: <https://doi.org/10.1016/j.compositesb.2013.06.026>.

Griffith, A.A. 1921. VI. The phenomena of rupture and flow in solids. *Philosophical Transactions of the Royal Society of London. Series A, Containing Papers of a Mathematical or Physical Character*, 221, pp.163-198. Available at: <https://doi.org/10.1098/rsta.1921.0006>.

Hatti, P.S., Sampath Kumar, L., Somanakatti, A.B. & Rakshith, M.N. 2021. Investigation on tensile behavior of glass-fiber reinforced polymer matrix composite with varying orientations of fibers. *Materials Today: Proceedings*, 54(2), pp.137-140. Available at: <https://doi.org/10.1016/j.matpr.2021.08.196>.

Irwin, G.R. 1960. Fracture Mode Transition for a Crack Traversing a Plate. *Journal of Basic Engineering*, 82(2), pp.417-423. Available at: <https://doi.org/10.1115/1.3662608>.

Keleş, Ö., Anderson, E.H., Huynh, J., Gelb, J., Freund, J. & Karakoç, A. 2018. Stochastic fracture of additively manufactured porous composites. *Scientific Reports*, 8, art.number:15437. Available at: <https://doi.org/10.1038/S41598-018-33863-4>.

Kishore, C., Jaiswal, R., Bhatt, V., Jugran, S., Rawat, D. & Verma, D. 2021. Analysis of glass fiber reinforced with epoxy resin using FEM. *Materials Today:*

Proceedings, 46(20), pp.11120-11128. Available at: <https://doi.org/10.1016/j.matpr.2021.02.273>.

Kumari, N.B.V.L., Mehar, A., Abdulrahman, M., Tatineni, S., Venkateshwara Shashank, E. & Ted Muthyala, J. 2018. Performance Analysis of Ply Orientation in Composite Laminates. *Materials Today: Proceedings*, 5(2), pp.5984-5992. Available at: <https://doi.org/10.1016/j.matpr.2017.12.200>.

Lang, Y., Zhao, L., Dai, X. & Wang, C.-A., 2018. Effect of alumina fiber content on pore structure and properties of porous ceramics. *International Journal of Applied Ceramic Technology*, 16(2), pp.814-819. Available at: <https://doi.org/10.1111/ijac.13123>.

Luan, K., Liu, J., Sun, B., Zhang, W., Hu, J., Fang, X., Ming, C., Song, E. 2018. High strain rate compressive response of the C_f/SiC composite. *Ceramics International*, 45(6), pp.6812-6818. Available at: <https://doi.org/10.1016/j.ceramint.2018.12.174>.

Mechab, B., Chama, M., Kaddouri, K. & Slimani, D. 2016. Probabilistic elastic-plastic analysis of repaired cracks with bonded composite patch. *Steel and Composite Structures*, 20(6), pp.1173-1182. Available at: <https://doi.org/10.12989/scs.2016.20.6.1173>.

Meille, S., Lombardi, M., Chevalier, J. & Montanaro, L. 2012. Mechanical properties of porous ceramics in compression: On the transition between elastic, brittle, and cellular behavior. *Journal of the European Ceramic Society*, 32(15), pp. 3959-3967. Available at: <https://doi.org/10.1016/J.Jeurceramsoc.2012.05.006>.

Metehri, A., Serier, B., Bachir bouiadjra, B., Belhouari, M. & Mecirdi, M.A. 2009. Numerical analysis of the residual stresses in polymer matrix composites. *Materials & Design*, 30(7), pp.2332-2338. Available at: <https://doi.org/10.1016/j.matdes.2008.11.009>.

Michael, Z., Mahisham, I., Mahadi, M.F., Mohd Amin, A.N., Syed Ahmad, S. I.H. & Mahmud, J. 2021. Deformation and failure behavior of hybrid composite laminates made of Glass Epoxy and woven Kevlar Epoxy. *Materials Today: Proceedings*, 46(4), pp.1618-1625. Available at: <https://doi.org/10.1016/j.matpr.2020.07.253>.

Mizerska, U., Fortuniak, W., Chojnowski, J., Rubinsztajn, S., Zakrzewska, J., Bak-Sypien, I. & Nyczyk-Malinowska, A. 2022. Porous SiC and SiC/Cf Ceramic Microspheres Derived from Polyhydromethyl siloxane by Carbothermal Reduction. *Materials*, 15(1), art.number: 81. Available at: <https://doi.org/10.3390/ma15010081>.

Monerie, Y. 2000. *Fissuration des matériaux composites : rôle de l'interface fibre-matrice*. PhD thesis. Marseille: Université de la méditerranée aix-Marseille II [online]. Available at: <https://theses.fr/2000AIX22054> [Accessed: 25March 2024].

Muthalagu, R., Murugesan, J., Sathees Kumar, S. & Sridhar Babu, B. 2021. Tensile attributes and material Analysis of kevlar and date palm fibers reinforced epoxy composites for automotive bumper applications. *Materials Today: Proceedings*, 46(1), pp.433-438. Available at: <https://doi.org/10.1016/j.matpr.2020.09.777>.

Pia, G., Casnedi, L. & Sanna, U. 2016. Porosity and pore size distribution influence on thermal conductivity of yttria-stabilized zirconia: Experimental findings and model predictions. *Ceramics International*, 42(5), pp.5802-5809. Available at: <https://doi.org/10.1016/J.Ceramint.2015.12.122>.

Rezaee, S., Ranjbar, K. & Kiasat, A.R. 2020. Characterization and strengthening of porous alumina-20 wt% zirconia ceramic composites. *Ceramics International*, 46(1), pp.893-902. Available at: <https://doi.org/10.1016/j.ceramint.2019.09.047>.

Udayakumar, A., Basha, M.R., Singh, S., Kumari, S. & Prasad, V.V.B. 2020. Carbon Fiber Reinforced Silicon Carbide Ceramic Matrix Composites. In: Mahajan, Y. & Roy, J. (Eds.) *Handbook of Advanced Ceramics and Composites*. Cham: Springer. Available at: https://doi.org/10.1007/978-3-319-73255-8_26-1.

Udayakumar, A., Basha, M., Stalin, M. & Prasad, V. 2014. Mechanical Properties of 3D Noninterlaced Cf/SiC Composites Prepared through Hybrid Process (CVI+PIP). *World Academy of Science, Engineering and Technology, Open Science Index 93, International Journal of Materials and Metallurgical Engineering*, 8(9), pp.1021-1028 [online]. Available at: <https://publications.waset.org/9999514/mechanical-properties-of-3d-non-interlaced-cf/sic-composites-prepared-through-hybrid-process-cvipip> [Accessed: 25 March 2024].

Venkatesan, K., Ramanathan, K., Vijayanandh, R., Selvaraj, S., Raj Kumar, G. & Senthil Kumar, M. 2020. Comparative structural Analysis of advanced multi-layer composite materials. *Materials Today: Proceedings*, 27(3), pp.2673-2687. Available at: <https://doi.org/10.1016/j.matpr.2019.11.247>.

Vijayakumar, S., Soundarrajan, M., Palanisamy, P. & Pasupathi, K. 2016. Studies on Mechanical Properties of Al-SiC Metal Matrix Composite. *SSRG International Journal of Material Science and Engineering*, 2(3), pp.1-5 Available at: <https://doi.org/10.14445/23948884/IJMSE-V2I6P101>.

Xia, Y., Lu, Z., Cao, J., Miao, K., Li, J. & Li, D. 2019. Microstructure and mechanical property of C/SiC core/shell composite fabricated by direct ink writing. *Scripta Materialia*, 165, pp.84-88. Available at: <https://doi.org/10.1016/j.scriptamat.2019.02.016>.

Zhang, C., Ren, T., Zhang, X., Hu, W., Wang, Z., Wang, B. & Suo, T. 2020. Study of dynamic compressive behaviors of 2D C/SiC composites at elevated temperatures based on in-situ observation. *Journal of the European Ceramic Society*, 40(15), pp.5103-5119. Available at: <https://doi.org/10.1016/j.jeurceramsoc.2020.06.036>.

Zimmermann, A. & Rödel, J. 2004. Fracture Statistics Based on Pore/Grain-Size Interaction. *Journal of the American Ceramic Society*, 82(8), pp.2279-2281. Available at: <https://doi.org/10.1111/j.1151-2916.1999.tb02080.x>.

Examen de tracción de daño progresivo y falla en material cerámico poroso compuesto utilizando el XFEM

Aicha Metehri^a, **autor de correspondencia**, Kouider Madani^a,
Belaïd Mechab^a, Mohammed Mokhtari^b, Ilias M. A. Ghermaoui^a

^a Universidad de Sidi Bel Abbès, Facultad de Tecnología, Departamento de Ingeniería Mecánica, Laboratorio de Mecánica Física de Materiales, Sidi Bel Abbès, República Argelina Democrática y Popular

^b ENPO-MA - Escuela Politécnica Nacional de Orán-Maurice Audin, Departamento de Ingeniería Mecánica, Laboratorio de Investigación en Tecnología de Fabricación Mecánica, Orán, República Argelina Democrática y Popular

CAMPO: mecánica

TIPO DE ARTÍCULO: artículo científico original

Resumen:

Introducción/objetivo: La porosidad es un factor significativo que hace que los huecos queden atrapados en los materiales durante la fabricación de materiales compuestos. Este estudio está dedicado a modelar los modos de fractura dentro de áreas altamente estresadas de un componente avanzado de SiC/Cf a escala macroscópica.

Métodos: El método de elementos finitos es utilizado para analizar los defectos dentro de los materiales compuestos, considerando factores como el tamaño de la porosidad, la forma y la tensión de tracción. El método de Monte Carlo predice la función de distribución (F).

Resultados: Tres poros se distribuyen a lo ancho del material, lo que reduce el área transversal activa del material y, en consecuencia, conduce a una reducción significativa de la resistencia. En general, la resistencia tiende a disminuir, con una caída más notoria.

Conclusión: Se concluye cómo la forma y el tamaño afectan la carga de falla, empleando el Método de Elementos Finitos Extendido (XFEM) para predecir el comportamiento de fractura en modo- I. El parámetro de porosidad afecta significativamente la durabilidad de la estructura. Se observa que el tamaño de los poros (ϕ) es un componente crucial que afecta la función de distribución (F). La variabilidad de este parámetro eleva sustancialmente la probabilidad de falla de la placa y disminuye la longevidad de una estructura.

Palabras claves: composite, XFEM, carga de tracción, carga de falla, reforzado con fibra, tamaño.

Исследование растяжений при прогрессирующих деформациях и разрушении пористых керамических композиционных материалов с применением метода конечных элементов (МКЭ)

Айша Метери^а **корреспондент**, Куидер Мадани^а,
Белаид Мехаба^а, Мухаммед Муктери^б, Илиас М. А. Гермауи^а

^а Университет Сиди-Бель-Аббес, технологический факультет,
кафедра машиностроения,
Сиди-Бель-Аббес, Алжирская Народная Демократическая Республика

^б Национальная политехническая школа в Оране „Морис Аудин“,
кафедра машиностроения,
Оран, Алжирская Народная Демократическая Республика

РУБРИКА ГРНТИ: 30.19.00 Механика деформируемого твердого тела
ВИД СТАТЬИ: оригинальная научная статья

Резюме:

Введение/цель: Пористость является важным фактором, который приводит к образованию пустот в материалах при изготовлении композиционных материалов. Данное исследование посвящено моделированию видов разрушения в высоконапряженных областях усовершенствованного компонента из SiC/Cf в макроскопическом масштабе.

Методы: Метод конечных элементов используется для анализа дефектов в композитных материалах с учетом таких факторов, как размер пористости, форма и растягивающее напряжение. Метод Монте-Карло прогнозирует функцию распределения (F).

Результаты: По ширине материала были распределены три поры, благодаря чему уменьшается активная площадь поперечного сечения материала, что приводит к значительному снижению прочности. В целом сопротивление имеет тенденцию к значительному снижению.

Выводы: С целью прогнозирования поведения разрушения в первом режиме с помощью расширенного метода конечных элементов (МКЭ) был сделан вывод о том, как форма и размер влияют на разрушающую нагрузку. Параметры пористости существенно влияют на долгосрочность структуры. Следует отметить, что размер пор (θ) является важнейшим компонентом, влияющим на функцию распределения (F). Изменчивость этого параметра существенно повышает вероятность разрушения пластины и снижает долгосрочность структуры.

Ключевые слова: композит, МКЭ, растягивающая нагрузка, разрушающая нагрузка, армирующее волокно, размер.

Испитивање затезања прогресивног оштећења и лома у порозним керамичким композитним материјалима помоћу проширеног метода коначних елемената (XFEM)

Ајша Метери^а, аутор за преписку, Куидер Мадани^а,
Белаид Мехаба^а, Мухамад Муктери^б, Илиас М. А. Гермауи^а

^а Универзитет Сиди Бел Абес, Технолошки факултет, Одсек машинства,
Сиди Бел Абес, Народна Демократска Република Алжир

^б Национална политехничка школа у Орану „Морис Аудин“,
Одсек машинства,
Лабораторија за истраживање технологије машинске производње,
Оран, Народна Демократска Република Алжир

ОБЛАСТ: механика
КАТЕГОРИЈА (ТИП) ЧЛАНКА: оригинални научни рад

Сажетак:

Увод/циљ: Порозност је значајан фактор који проузрокује задржавање шупљина у материјалима током производње композитних материјала. Ова студија се бави моделирањем типова лома унутар високонапрегнуте области напредне SiC/Cf компоненте на макроскопској скали.

Метод: Методом коначних елемената анализирају се дефекти унутар композита, уз разматрање фактора попут величине и облика порозности, као и затезног напона. Методом Монте Карло предвиђа се функција дистрибуције (F).

Резултати: Три поре су распоређене свом ширином материјала што смањује активну област попречног пресека материјала и, последично, води до знатног смањивања чврстоће. Укупна отпорност показује тенденцију ка смањивању, уз приметан пад.

Закључак: Изводи се закључак да облик и величина утичу на оптерећење лома уз коришћење проширене методе коначних елемената (XFEM) за предвиђање понашања лома у моду 1. Параметар порозности знатно утиче на трајност структуре. Уочава се да је величина пора (ϕ) кључна компонента која утиче на функцију дистрибуције (F). Варијабилност овог параметра знатно повећава вероватноћу лома плоче и смањује животни век структуре.

Кључне речи: композит, XFEM, затезно оптерећење, оптерећење лома, ојачање влакнима, величина.

Paper received on: 27.03.2024.

Manuscript corrections submitted on: 24.09.2024.

Paper accepted for publishing on: 25.09.2024.

© 2024 The Authors. Published by Vojnotehnički glasnik / Military Technical Courier (www.vtg.mod.gov.rs, vtg.mo.ynp.spb). This article is an open access article distributed under the terms and conditions of the Creative Commons Attribution license (<http://creativecommons.org/licenses/by/3.0/rs/>).



JPEG and BPG visually lossless image compression via KonJND-1k database

Boban P. Bondžulić^a, Nenad M. Stojanović^b,
Vladimir V. Lukin^c, Sergii S. Kryvenko^d

^a University of Defence in Belgrade, Military Academy, Department of Telecommunications and Informatics, Belgrade, Republic of Serbia, e-mail: bondzulici@yahoo.com, ORCID iD: <https://orcid.org/0000-0002-8850-9842>

^b University of Defence in Belgrade, Military Academy, Department of Telecommunications and Informatics, Belgrade, Republic of Serbia, e-mail: nivzvkc@hotmail.com, **corresponding author**, ORCID iD: <https://orcid.org/0000-0001-9328-5348>

^c National Aerospace University, Department of Information-Communication Technologies, Kharkiv, Ukraine, e-mail: lukin@ai.kharkov.com, ORCID iD: <https://orcid.org/0000-0002-1443-9685>

^d National Aerospace University, Department of Information-Communication Technologies, Kharkiv, Ukraine, e-mail: krivenkos@ieee.org, ORCID iD: <https://orcid.org/0000-0001-6027-5442>

[doi https://doi.org/10.5937/vojtehg72-50300](https://doi.org/10.5937/vojtehg72-50300)

FIELD: telecommunications

ARTICLE TYPE: original scientific paper

Abstract:

Introduction/purpose: This paper presents the results of the research on visually lossless image compression which is of particular interest because it achieves a high degree of compression, while the visual quality of the image is not impaired, i.e., end users are very satisfied with the image quality. The analysis was carried out using the publicly available large-scale picture-wise KonJND-1k database which contains the results of subjective tests on JPEG and BPG compressed images.

Methods: Thanks to the availability of images from the KonJND-1k database, the dependence of objective assessments of image quality on parameters that control the degree of compression of source signals (quality factor for JPEG and quantization parameter for BPG) is analyzed. The results of the visually lossless subjective tests are used for a deep analysis of the boundary and typical values of the parameters that control these two types of compression, as well as for the analysis of the corresponding values of the objective quality scores. Furthermore, reliable features for predicting the boundary between visually lossless and visually lossy compression have been identified. For that purpose, the degree of agreement between the predictions and the ground truth values of the peak

signal-to-noise ratio (PSNR) and image representation in bits per pixel (bpp) is used. The visually lossless compression ratio is used to compare JPEG and BPG techniques.

Results: It is shown that the boundary between visually lossless and visually lossy image compression is found in a wide range of PSNR values (about 20 dB for JPEG and 15 dB for BPG). The corresponding JPEG image compression quality factor values at this threshold also range widely from 31 to 79, with concentration between 40 and 45. For the BPG encoder, the values of the quantization parameter are grouped around 30, and the boundary values are 25 and 34. Furthermore, it is shown that this boundary can be reliably determined based on simple features derived from the original uncompressed image. Gradient-based features known as spatial frequency and spatial information proved to be the best predictors. The degree of agreement between the predictions obtained from these features with the ground truth values of PSNR and bpp in both types of compression is greater than 85%. A comparative analysis has showed that, using BPG compression, it is possible, on the average, to achieve a twice larger compression ratio of visually lossless compression than for JPEG (80 versus 40).

Conclusion: Although a high degree of agreement is achieved between the predictions and the ground truth values of PSNR and bpp of the boundary between visually lossless and visually lossy compression, there is a need for the development of new prediction approaches, especially with the BPG technique, which through the compression ratio proved to be superior to the JPEG technique. The existing databases used for the analysis of visually lossless compression contain color images from the visible part of the electromagnetic spectrum. Considering the increasing use of images from the infrared part of the spectrum, there is a need to conduct similar tests in this spectral range.

Key words: BPG compression, JPEG compression, just noticeable difference (JND), peak signal-to-noise ratio (PSNR), visually lossless image compression.

Introduction

With the increasing use of images and videos in everyday life, compression of visual signals is gaining more and more importance. The compression process adapts the image/video to the bandwidth of the transmission system while the requirements for memory resources are reduced. It is well known that compression techniques can be divided into lossless compression and lossy compression (Bull & Zhang, 2021). In real applications, the degree of compression of lossless techniques is often not sufficient, while lossy compression techniques can achieve a significantly

higher degree of compression, but at the expense of impairing the visual quality of the signal. As a compromise solution, visually lossless techniques have been increasingly used in recent years. Some researchers classify these techniques as the third type of compression, while some of them divide lossy compression techniques into visually lossless and visually lossy (Krivenko et al, 2018).

The just noticeable difference (JND) concept is very important within the visually lossless techniques, and it refers to the smallest degree of degradation that the observer is able to notice if the image is compressed with some compression process (Kovalenko & Lukin, 2023). The JND threshold can be defined for individual pixels (pixel-wise), at the region level (patch-wise), or at the level of the entire image (picture-wise) (Shen et al, 2021).

Thanks to the publicly available JND image databases with subjective test results, such as MCL-JCI (Jin et al, 2016), JND-Pano (Liu et al, 2018), JND-VVC (Shen et al, 2020), VLT (Mikhailiuk et al, 2021), KonJND-1k (Lin et al, 2022), researchers are enabled to analyze the JND concept in different types of compression. The JPEG compression type has been included in MCL-JCI and JND-Pano databases, JND-VVC database uses Versatile Video Coding (VVC) compression, VLT database contains JPEG and WebP compressed images, and the large-scale crowdsourced JND database KonJND-1k contains test results on JPEG and Better Portable Graphics (BPG) compressed images. The JPEG standard was developed more than 30 years ago and is still widely used, while the BPG coder is one of the promising lossy compression coders (Bellard, 2018; Kovalenko et al, 2022). The degree of JPEG compression is controlled using a quality factor (QF) that ranges from 1 to 100, where lower QF values provide a higher degree of compression. BPG compression uses a quantization parameter (QP) that ranges from 0 to 51, where lower values correspond to better visual quality (Lin et al, 2022). As BPG relies on the H.265/HEVC video compression standard, this dynamic range corresponds to the QP values used to adjust the quality of the H.265/HEVC compressed video signal. Recently introduced JND databases include subjective tests on a larger number of codecs (Testolina et al, 2023), and on a larger number of degradation types (Liu et al, 2023).

The boundary between visually lossless and visually lossy image compression (first JND point or JND #1) can be determined through QF/QP prediction, image representation prediction in bits per pixel (bpp) or through objective quality prediction using some of the measures such as PSNR (Saha & Vemuri, 2000), PSNR-HVS-M (Zemliachenko et al, 2016), SSIM (Cai et al, 2019), FSIM (Li et al, 2021), MDSI (Li et al, 2022),

VIF (Fiorucci et al, 2012) and similar measures. The simple approach presented in (Bondžulić et al, 2021) to predict the PSNR of the first JND point of JPEG compressed images uses only one feature of the original uncompressed image (the mean gradient magnitude). The effectiveness and acceptable prediction error of the PSNR value of the first JND point of this approach inspired the authors in (Pavlović et al, 2023) to analyze the prediction based on other features, where it was shown that good predictors are spatial information, spatial frequency, contrast and degree of compression. Deep learning approaches (Fan et al, 2019; Lin et al, 2020; Liu et al, 2020) for the prediction of the position of the first JND point of JPEG compressed images provide a smaller PSNR prediction error and can be used for direct QF/QP prediction.

The proposed approaches, where the prediction of the position of the first JND point is carried out through bpp or objective measures, require that the desired bpp or objective quality be reached through an iterative way by changing QF/QP (Zemliachenko et al, 2016). In the literature, one can find approaches such as the two-step approach (Li et al, 2024) or the approach with linear interpolation of the rate distortion curve (Poth et al, 2020; Bondžulić et al, 2024) by which the process of achieving the desired quality is carried out in a few iterations. However, the error introduced by such approaches is superimposed on the prediction error of the position of the first JND point.

In this paper, the results of subjective tests of the KonJND-1k database are analyzed, as it is the largest JND database, which covers JPEG and BPG compressed images, and instead of tests in a laboratory environment, the authors used a crowdsourcing framework. The positions of the JND points in both types of compression are analyzed through the values of PSNR (Wang & Bovik, 2009), PSNR-HVS-M (Ponomarenko et al, 2007) and bpp. Dependences of objective quality measures on parameters that control the degree of compression are shown. The possibility of predicting objective quality scores of visually lossless compressions based on simple features derived from original uncompressed images is analyzed. Finally, the gain (compression ratio) that can be achieved with both types of compression at the JND threshold is given.

KonJND-1k database content analysis

KonJND-1k is a publicly available picture-wise JND image database (Lin et al, 2022). The database consists of 1008 source images and their JPEG and BPG compressed versions with dimensions of 640x480 pixels,

together with the results of JND subjective tests. One half of the source images is compressed with JPEG, while the other half is compressed using the BPG encoder. The degree of compression of JPEG images is controlled by the quality factor (QF) which ranges from 1 to 100, so that for one original image there are 100 JPEG compressed images. The degree of compression of BPG images is controlled by the quantization parameter (QP) which is changed from 1 to 51, so that there are 51 BPG compressed images per one original image.

A total of 503 observers participated in the subjective tests, and an average of 42 opinions per original image were collected. Unlike the MCL-JCI (Jin et al, 2016) where the subjective results were collected using binary search comparison, in the KonJND-1k database the results were collected using slider adjustment and a flicker test to determine the position of the first JND point. In the flicker test, the original image and its compressed version alternate at a frequency of 8 Hz, whereby subjects drag the slider to the position corresponding to the smallest distortion level with a noticeable flicker effect. With the flicker approach, the duration of the subjective test can be reduced by 50% while doubling the perceptual sensitivity compared to the standard binary search approach, in which the compressed images are compared side by side with their original.

Figure 1 shows two original images from the KonJND-1k database, their JPEG and BPG compressed versions corresponding to the first JND points, and SSIM (Wang et al, 2004) maps of the structural similarity between the original and compressed version. From Figure 1, it is visually very difficult to find the differences between the original and its compressed versions. Furthermore, in Figure 1(e) and Figure 1(f), the regions with structural information degradation can be observed. For Figure 1(a), it is the lower part of the original image, while for Figure 1(b), it is the central part of the image. The differences in quality can be seen visually if parts of the images are enlarged, as shown in Figure 2, with 150x150 pixel patches. In Figure 2, a blocking effect is observed with the JPEG compressed image, while a blurring effect is observed with the BPG compressed image. In both cases, the SSIM image similarities are close to the maximum value, and the PSNR-HVS-M values are very high. The PSNR values are greater than 30 dB.



Figure 1 – (a) (b) original images, (c) JPEG JND #1 compressed image, (d) BPG JND #1 compressed image, (e) structural similarity map for JPEG image, and (f) structural similarity map for BPG image



Figure 2 – Patches of: (a) original image SRC0336.bmp, (b) JPEG compressed image, (c) original image SRC0845.bmp and (d) BPG compressed image

Subjective tests conducted by (Alakuijala et al, 2020) showed that H.265/HEVC Intra and JPEG 2000 codecs, with a noticeable blurring effect, generally result in better rate distortion curves when compared to JPEG, with a dominant blocking effect. This means that by blurred (H.265/HEVC Intra and JPEG 2000) images, more visually pleasing images can be obtained.

The content of the source images of the KonJND-1k database is wide, including the categories of people, animals, plants, things, buildings and transport means. Spatial information (SI) and colorfulness (CF) are used as indicators of the complexity of images that need to be compressed. While the definition of colorfulness is unified, different approaches are used to determine spatial information. After determining the local values of image gradient magnitudes, the spatial information can be determined as their maximum value, mean value, root mean square value or as standard

deviation of local scores. Although the ITU recommends using the maximum value, (Yu & Winkler, 2013) has showed that it is better to use the mean gradient magnitude (SI_{mean}) to estimate the complexity of the image in compression. Thus, Figure 3 shows scatterplots of SI_{mean} versus CF, along with the convex hulls for two subsets of original KonJND-1k database images. From Figure 3, it can be concluded that both subsets have approximately the same dynamic range of both indicators and that the contents are almost uniformly distributed within their convex hulls.

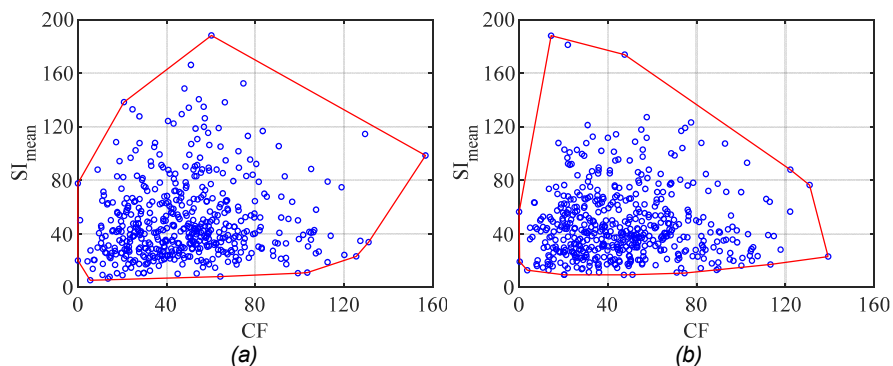


Figure 3 – Spatial information (SI_{mean}) versus colorfulness (CF) plots of the source images belonging to the: (a) JPEG and (b) BPG subsets

Visually lossless compression and objective quality assessment

Objective image quality assessment measures are often used with the aim of achieving the desired quality of the visually lossless compressed image. In some papers, visually lossless quality is defined using fixed thresholds of objective measures, and algorithms for predicting objective values on the boundary between visually lossless and visually lossy compression can also be used. Therefore, it is interesting to analyze the relationship between the objective quality scores and the parameters that control the compression, together with the positions of this boundary.

Figure 4 shows the dependences of PSNR, PSNR-HVS-M and bpp on the quality factor of JPEG compression (rate distortion curves, RDCs). A subset of the KonJND-1k images used for JPEG compression is utilized. Additionally, the positions of the first JND points obtained in the subjective tests (marked with x symbols) are shown.

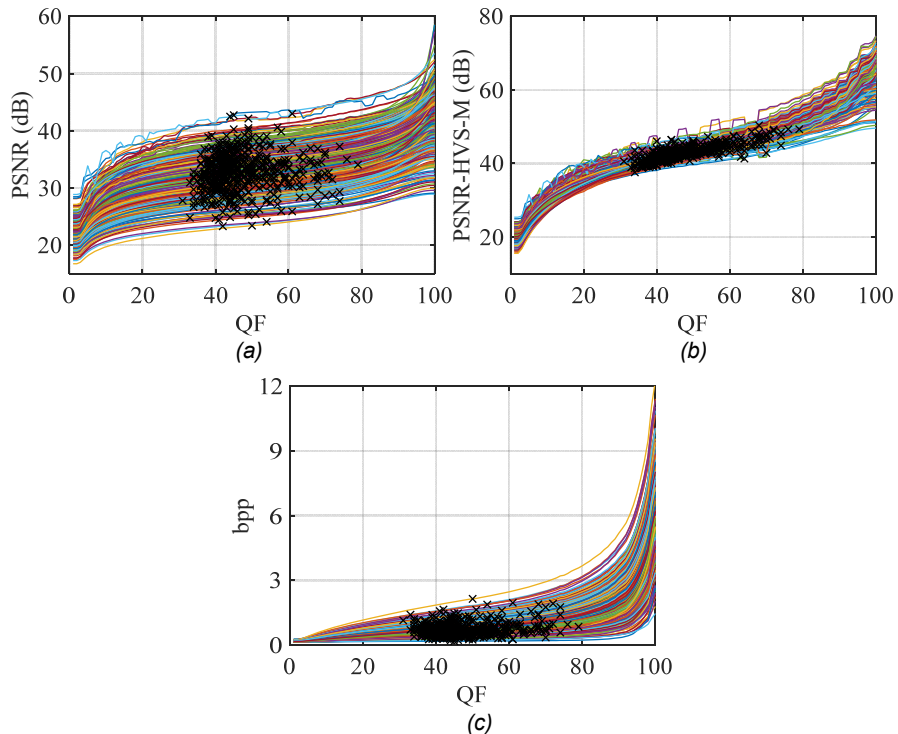


Figure 4 – RDCs PSNR, PSNR-HVS-M and bpp on QF, along with JND #1 points, for a subset of scene images taken from the KonJND-1k database and compressed by JPEG

From Figure 4, no relationship can be observed between the objective quality scores (PSNR, PSNR-HVS-M and bpp) and the QF values of the first JND points (visually lossless compression). It can be observed that the dynamic range of PSNR is significantly higher than the dynamic range of PSNR-HVS-M quality scores. Furthermore, some PSNR and PSNR-HVS-M rate distortion curves show a non-monotonous dependence on the quality factor, known as the strange effect (Bondžulić et al, 2022). This effect does not exist in bpp curves. Similarly, Figure 5 shows the RDCs, along with the positions of the first JND points on the subset of the KonJND-1k images that were used for BPG compression. In this case, the RDCs are monotonous so that the strange effect does not exist for BPG compressed images.

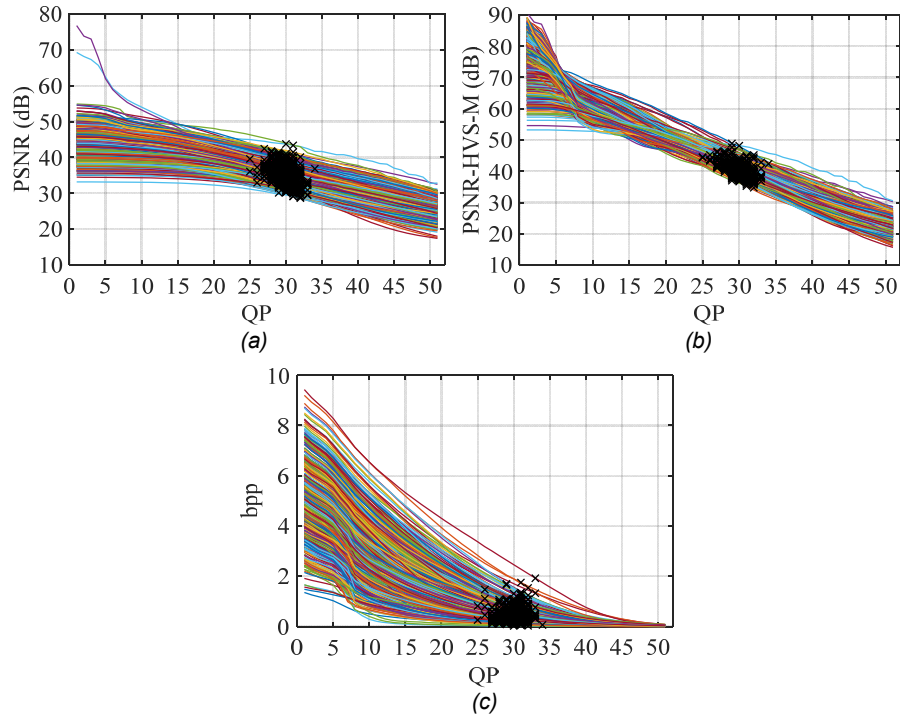


Figure 5 – RDCs PSNR, PSNR-HVS-M and bpp on QP, along with JND #1 points, for a subset of scene images taken from the KonJND-1k database and compressed by BPG

Table 1 provides the boundary values of QF/QP, bpp and objective quality scores for the first JND points of JPEG and BPG subsets. The positions of the first JND points are found in a wide range of PSNR quality values, of almost 20 dB for the JPEG subset, and about 15 dB for the BPG subset. According to PSNR-HVS-M, the range corresponding to the positions of the first JND points on both subsets is about 14 dB. If bpp is used as an indicator, it can be concluded that the positions of the first JND points can be reached by applying lower bpp values in BPG compressed images, which means that a higher degree of compression is achieved than in JPEG compressed images. Additionally, a wide range of QF factors is observed in JPEG compressed images (from 31 to 79). For BPG compressed images, the boundary values of the QP quantization parameter are 25 and 34.

Table 1 – Boundary values of PSNR, PSNR-HVS-M, QF/QP and bpp of the first JND points of the JPEG and BPG subsets

Subset		JPEG	BPG
PSNR	minimum	23.3149	28.6247
	maximum	42.9831	43.7344
PSNR-HVS-M	minimum	37.5680	34.7033
	maximum	50.3154	48.9101
QF/QP	minimum	31	25
	maximum	79	34
bpp	minimum	0.1841	0.0237
	maximum	2.1429	1.9232

With the histograms of QF/QP values, Figure 6, it can be concluded that the positions of the first JND points of JPEG compressed images are grouped between the QF values of 40 and 45, while in BPG compressed images, the QP values are grouped around 30.

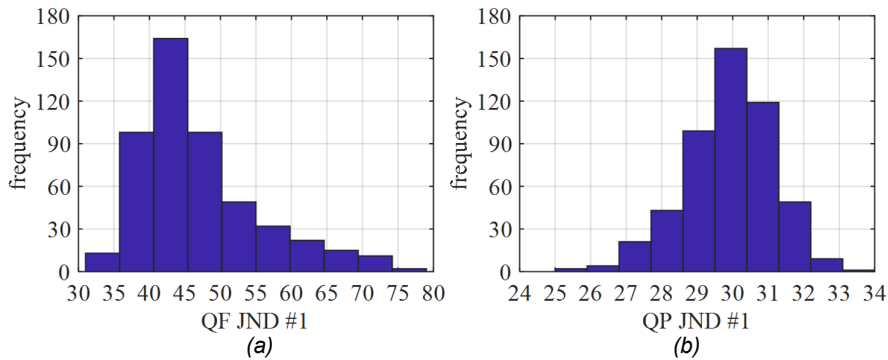


Figure 6 – Histograms of: (a) JND #1 JPEG quality factors, and (b) JND #1 BPG quantization parameters for the subsets of the KonJND-1k database

Identification of the features for visually lossless compression

In recent research (Pavlović et al, 2023), the relationship between simple features derived from the original uncompressed image and the position of the first JND point has been analyzed, with the aim of predicting the values of PSNR JND #1 or bpp JND #1. Here, the analysis is performed on both subsets of the KonJND-1k database, and for the first time on BPG compressed images. The linear correlation coefficient (LCC),

the root mean square error (RMSE) and the sum of the squared error (SSE) are used in the analysis as quantitative indicators. These values are calculated between the bpp/PSNR JND #1 predictions obtained from the original image features and the ground truth bpp/PSNR values obtained in subjective tests. The second-order mapping law is used to map feature values into JND predictions.

To predict the boundary between visually lossless and visually lossy compression, simple features that have already been used in the literature as complexity measures or can be related to the complexity of the image are chosen. Only one of the adopted features uses color information, while the other features are calculated on grayscale versions of the original images. The following features have been adopted:

- Entropy, E_1 ; it quantifies the information content of the image and can be used to characterize the randomness of the original image intensity distribution.
- Standard Deviation, STD; it is a statistical measure of the pixel intensity values variability.
- Spatial Information, SI, and Spatial Frequency, SF; these are gradient-based features of the image, calculated on the basis of local gradient magnitudes obtained by applying Sobel spatial masks (SI), i.e., differences of pixel intensity values along rows and columns (SF) (Pavlović et al, 2023). The final values are calculated as their mean value (mean), the root mean square value (rms) and the standard deviation (std).
- Image Power Spectra Slope, IPSS; it is calculated as the slope of the fitted line in the log-log plot of radially averaged spectral power (Pavlović et al, 2023).
- Two-dimensional Entropy, E_2 , Contrast, Correlation, Energy and Homogeneity; this feature set is calculated based on the gray level co-occurrence matrix (GLCM), known in image texture analysis and classification (Corchs et al, 2016). The frequencies of occurrence of pairs of gray levels at the positions (m,n) and $(m+1,n+1)$ are used to determine the GLCM.
- Compression Ratio, CR_i ; as a feature, here, it is calculated as the ratio of the size of the uncompressed image to the size of its JPEG compressed version with a quality factor of $QF=100$ (Corchs et al, 2016).
- Edge Density, ED; represents the percentage of edge pixels in relation to the dimensions of the image. The well-known Canny detector is used to determine edge pixels.

- Shape, α , and scaling, σ , parameters of the Generalized Gaussian Distribution (GGD), which models the distribution of Mean Subtracted Contrast Normalized (MSCN) coefficients. The MSCN coefficients distribution parameters are used in the literature to determine the type of degradation and image quality assessment (Mittal et al, 2012).
- Mean Percentage Intensity Uniformity, mPIU; it is determined based on the uniformity within 8x8 non-overlapping blocks of the original image (Goerner et al, 2013).
- Colorfulness, CF; can be used as an estimator of the variety and intensity of colors in an image. It is calculated based on the mean values and standard deviations within the planes obtained after the conversion of the RGB color image into the opponent color space (Hasler & Suesstrunk, 2003).

Tables 2 and 3 show the degree of agreement between the predictions and the ground truth PSNR and bpp values for both subsets of the KonJND-1k database.

Table 2 – Agreement between the predicted and ground truth PSNR (PSNR JND #1) for the KonJND-1k image subsets

Subset	PSNR JND #1					
	JPEG			BPG		
	LCC	RMSE	SSE	LCC	RMSE	SSE
Entropy, E_1	0.3943	3.049	4658	0.4663	2.389	2859
Standard Deviation, STD	0.3043	3.167	5024	0.2165	2.636	3482
Spatial Information, SI_{mean}	0.9056	1.407	992.3	0.8585	1.385	960.7
Spatial Information, SI_{rms}	0.8628	1.681	1415	0.7268	1.855	1723
Spatial Information, SI_{std}	0.7807	2.077	2162	0.6065	2.147	2309
Spatial Frequency, SF_{mean}	0.9178	1.32	873	0.8662	1.349	912.3
Spatial Frequency, SF_{rms}	0.9042	1.42	1010	0.7634	1.744	1524
Spatial Frequency, SF_{std}	0.8545	1.727	1495	0.6727	1.998	2000
Image Power Spectra Slope, PSS	0.7209	2.304	2660	0.5568	2.243	2521
Entropy, E_2	0.7353	2.253	2543	0.7475	1.794	1612
Contrast	0.8438	1.784	1595	0.7059	1.913	1833
Correlation	0.6867	2.412	2914	0.5763	2.207	2440
Energy	0.1043	3.306	5477	0.2319	2.627	3457

Subset	PSNR JND #1					
	JPEG			BPG		
	LCC	RMSE	SSE	LCC	RMSE	SSE
Homogeneity	0.7446	2.219	2468	0.7878	1.663	1385
Compression Ratio, CR _r	0.8246	1.881	1772	0.8508	1.419	1009
Edge Density, ED	0.7921	2.029	2063	0.8294	1.509	1140
GGD, shape α	0.4574	2.956	4378	0.4883	2.357	2782
GGD, scale σ	0.7706	2.119	2249	0.7597	1.756	1545
mPIU	0.7253	2.289	2624	0.5818	2.196	2416
Colorfulness, CF	0.3036	3.167	5026	0.2605	2.607	3405

Table 3 – Agreement between the predicted and ground truth bpp (bpp JND #1) for the KonJND-1k image subsets

Subset	bpp JND #1					
	JPEG			BPG		
	LCC	RMSE	SSE	LCC	RMSE	SSE
Entropy, E ₁	0.4620	0.2758	38.12	0.4422	0.2686	36.14
Standard Deviation, STD	0.2798	0.2986	44.67	0.2178	0.2923	42.79
Spatial Information, SI _{mean}	0.9052	0.1322	8.759	0.9052	0.1273	8.116
Spatial Information, SI _{rms}	0.8255	0.1755	15.43	0.7934	0.1823	16.65
Spatial Information, SI _{std}	0.6974	0.2229	24.89	0.6439	0.2291	26.3
Spatial Frequency, SF _{mean}	0.9006	0.1352	9.153	0.9302	0.1099	6.054
Spatial Frequency, SF _{rms}	0.8500	0.1638	13.44	0.8534	0.1561	12.21
Spatial Frequency, SF _{std}	0.7627	0.2012	20.27	0.7459	0.1994	19.93
Image Power Spectra Slope, PSS	0.6291	0.2418	29.28	0.6131	0.2366	28.04
Entropy, E ₂	0.7926	0.1897	18.02	0.7824	0.1865	17.43
Contrast	0.8275	0.1746	15.28	0.8218	0.1706	14.58
Correlation	0.6753	0.2294	26.36	0.6859	0.2179	23.79
Energy	0.1703	0.3065	47.06	0.2034	0.2932	43.07
Homogeneity	0.7861	0.1922	18.51	0.7854	0.1854	17.22
Compression Ratio, CR _r	0.8131	0.181	16.42	0.8445	0.1604	12.89
Edge Density, ED	0.8061	0.1841	16.97	0.7975	0.1807	16.35
GGD, shape α	0.5479	0.2602	33.91	0.4924	0.2606	34.03
GGD, scale σ	0.7253	0.2141	22.97	0.7562	0.1959	19.23
mPIU	0.7670	0.1996	19.95	0.7415	0.2009	20.23
Colorfulness, CF	0.3430	0.2921	42.76	0.1247	0.2971	44.23

It can be concluded that gradient-based spatial information (SI) and spatial frequency (SF) are the two best features for prediction, with SF performing better. Additionally, the earlier observation that the mean gradient magnitude is a better predictor than the root mean square value or the standard deviation is confirmed (see $SI_{\text{mean}}/SF_{\text{mean}}$ vs. $SI_{\text{rms}}/SF_{\text{rms}}$ and $SI_{\text{std}}/SF_{\text{std}}$). If LCC is considered as a quantitative indicator, it can be concluded that the performance of these two most reliable prediction features is worse in predicting PSNR JND #1 within the BPG subset, and in contrast, the success in predicting bpp JND #1 is observed within the BPG subset.

Also, in earlier research related to JPEG compressed images, it has been concluded that it is better to predict PSNR than bpp, which is also confirmed here. However, it can be concluded here that, for BPG compressed images, it is better to use bpp predictions than PSNR. By predicting bpp based on SF_{mean} , the degree of agreement with the ground truth values is better than 90% for both subsets. Apart from the mentioned two features, contrast, edge density and a compression ratio stand out as good predictors.

As spatial frequency proved to be the best predictor, Figure 7 presents the relationship between SF_{mean} and the ground truth positions of JND #1 points. On both subsets, a linear relationship can be observed between the feature values and the ground truth bpp JND #1 positions, while the trends slightly deviate from the linear law at PSNR JND #1 points. In this way, it is confirmed that the second-order mapping law is a good choice in predicting the positions of JND #1 points.

Additionally, it can be observed that the positions of the first JND points can be reached with lower bpp values, i.e., with a higher degree of compression using BPG. In addition to a higher degree of compression, the PSNR objective quality of BPG compressed images is also better. Finally, it can be concluded that BPG compression at the JND threshold provides both a higher degree of compression and a better PSNR objective quality than JPEG compression.

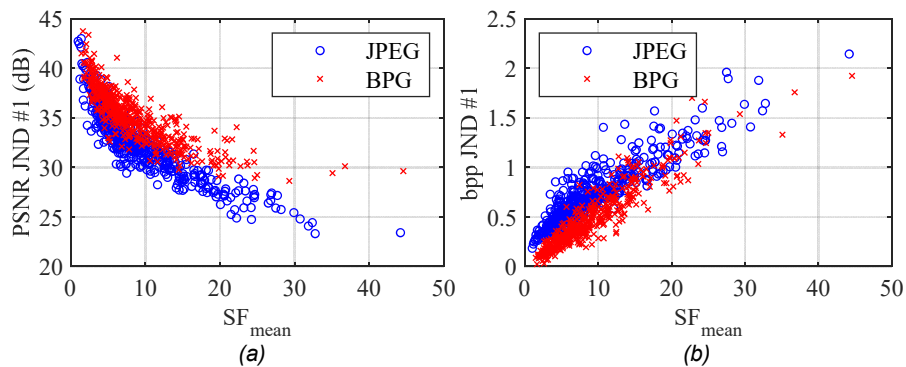


Figure 7 – Spatial frequency and: (a) PSNR and (b) bpp of the first JND points on the KonJND-1k image subsets

The optimal functions for mapping the SF_{mean} feature into PSNR JND #1 and bpp JND #1 predictions determined on the KonJND-1k image database results are given in Table 4. In this case, the second-order laws used to map SF_{mean} to PSNR JND #1 must be decreasing functions (see Fig. 7(a)) which remain constant after reaching the minimum values (25.4 dB with JPEG and 29.5 dB with BPG compression). Without this restriction, they would be U-shaped symmetric curves (parabolas). From the law of mapping SF_{mean} to bpp JND #1 of JPEG compressed images, it can be concluded that when SF_{mean} tends to zero, bpp JND #1 tends to 0.2504. For BPG compressed images, it is necessary to introduce a prediction limit ($SF_{\text{mean}}=0.75$) because without it bpp JND #1 values would be negative as SF_{mean} approaches zero (see Fig. 7(b)).

However, if the relationship between SF_{mean} and PSNR-HVS-M of the first JND points is analyzed, Figure 8, it can be concluded that the quality of JPEG compressed images is better. This quality inversion can be explained by the fact that PSNR is a simple measure that uses the difference of the amplitudes between individual pixels in the quality assessment, while PSNR-HVS-M additionally takes into account the characteristics of the human visual system. Thus, there is a decorrelation between SF_{mean} and PSNR-HVS-M values, so that instead of an orderly trend of scores there is a cloud of points in the 2D space SF_{mean} versus PSNR-HVS-M.

Table 4 – Optimal functions for mapping the SF_{mean} feature into PSNR JND #1 and bpp JND #1 predictions determined on the KonJND-1k subsets

JPEG	
PSNR	$PSNR(SF_{mean}) = \begin{cases} 0.01376SF_{mean}^2 - 0.8645SF_{mean} + 38.97, & SF_{mean} \leq 31 \\ 25.4, & SF_{mean} > 31 \end{cases}$
bpp	$bpp(SF_{mean}) = -0.0003719SF_{mean}^2 + 0.05558SF_{mean} + 0.2504$
BPG	
PSNR	$PSNR(SF_{mean}) = \begin{cases} 0.01336SF_{mean}^2 - 0.7618SF_{mean} + 40.36, & SF_{mean} \leq 28 \\ 29.5, & SF_{mean} > 28 \end{cases}$
bpp	$bpp(SF_{mean}) = \begin{cases} -0.0003425SF_{mean}^2 + 0.05989SF_{mean} - 0.02376, & SF_{mean} \geq 0.75 \\ 0.0201, & SF_{mean} < 0.75 \end{cases}$

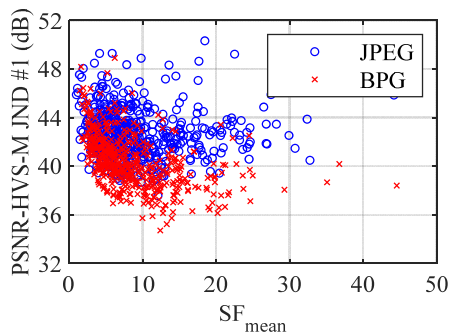


Figure 8 – Spatial frequency and PSNR-HVS-M of the first JND points on the KonJND-1k image subsets

JPEG and BPG visually lossless compression comparison

In several previous illustrations, it has been observed that, at the JND threshold, a higher degree of compression can be obtained if BPG compression is used instead of JPEG. This observation is further illustrated in Figure 9, where the relationship between the achieved gain (compression ratio, G_r) calculated as the ratio of the size of the

uncompressed image and its visually lossless version and the SI/SF feature is shown. These scatter plots confirm the previous observation, whereby it can be additionally concluded that the degree of BPG compression is significantly higher than JPEG for lower values of SI/SF, i.e., with low complexity images (with large homogeneous and without textured regions). The degree of compression in both cases is approximately the same for images with higher SI/SF values (images rich in details). On the average, Table 5, the degree of compression at the JND threshold is two times higher if BPG is used instead of JPEG (80.5 vs. 39.4). From Table 5, in which the boundary values of compression are given, it can be concluded that the BPG compression ratio G_f goes over 1000 times (in Figure 9 it is not visible because the dynamic range is shown up to a value of 300) in images with uniform regions. The maximum compression ratio using JPEG is approximately 130. From Figure 9, it can be additionally concluded that SI and SF can be used for reliable prediction of the achieved gain. In this case, due to the large dynamic gain and the slope of the dependence of G_f on the mentioned characteristics, it is desirable to use the mapping law of a higher order.

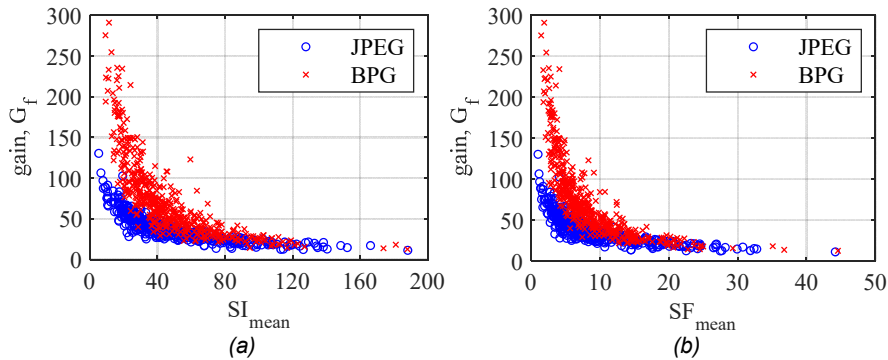


Figure 9 – The gain achieved by applying visually lossless compression versus: (a) spatial information and (b) spatial frequency

Table 5 – Gain boundary values of visually lossless compression for the KonJND-1k subsets

Subset		JPEG	BPG
gain, G_f	minimum	11.1996	12.4795
	maximum	130.3536	1012.7
	mean	39.3763	80.5105

Conclusion

The conducted analysis on visually lossless image compression using the KonJND-1k database confirmed some earlier observations about the prediction of the first JND point position of JPEG compressed images, but also brought new conclusions about the prediction of the first JND position of BPG compressed images.

It has been confirmed that the prediction of the first JND point position, as the boundary between visually lossless and visually lossy compression, in JPEG compression can be achieved using simple features derived from the original uncompressed image. The gradient-based features spatial information and spatial frequency are singled out as reliable features for prediction, where the degree of agreement with the results of subjective tests is greater than 90% for both indicators, PSNR and bits per pixel.

The analysis conducted on the prediction of the first JND point position of BPG compressed images has showed that spatial information and spatial frequency can also be used for reliable prediction. The degree of agreement between the predictions derived from these features and the results of subjective tests is greater than 90% if the representation is predicted in bits per pixel. If the PSNR of the first JND point is predicted, the degree of agreement is worse and is around 86%. In addition to these two features, good predictors are contrast, edge density and compression ratio.

A special contribution of the paper is the comparative analysis of the compression ratio on the boundary between visually lossless and visually lossy JPEG and BPG compression. The analysis has showed that the advantage in the degree of compression is on the side of BPG coding, where on average the degree of compression is twice as high compared to JPEG (80 versus 40). The degree of compression of BPG is significantly higher than JPEG for low complexity images (with homogeneous regions), slightly higher for medium complexity images, while for high complexity images with pronounced texture, the degree of compression is approximately the same for both codecs.

Due to the increasing use of images from the infrared part of the spectrum, visually lossless compression in this spectral band will be analyzed in further work. The goal is to conduct subjective tests and additional analyzes using objective image quality assessment measures.

References

- Alakuijala, J., Boukourt, S., Ebrahimi, T., Kliuchnikov, E., Sneyers, J., Upenik, E., Vandevenne, L., Versari, L. & Wassenberg, J. 2020. Benchmarking JPEG XL image compression. In: Schelkens, P. & Kozacki, T. (Eds.) *Proceedings SPIE Photonics Europe: Optics, Photonics and Digital Technologies for Imaging Applications VI*, Online Only, France, 11353, pp.113530X-1-113530X-20, April 06-10. Available at: <https://doi.org/10.1117/12.2556264>.
- Bellard, F. 2018. BPG Image format. *Bellard.org*, 21 April [online]. Available at: <https://bellard.org/bpg/> [Accessed: 05. April 2024].
- Bull, D. & Zhang, F. 2021. *Intelligent Image and Video Compression: Communicating Pictures, 2nd Edition*. Academic Press. ISBN: 9780128203545.
- Bondžulić, B., Stojanović, N., Petrović, V., Pavlović, B. & Miličević, Z. 2021. Efficient Prediction of the First Just Noticeable Difference Point for JPEG Compressed Images. *Acta Polytechnica Hungarica*, 18(8), pp.201-220. Available at: <https://doi.org/10.12700/APH.18.8.2021.8.11>.
- Bondžulić, B., Bujaković, D., Li, F. & Lukin, V. 2022. On strange images with application to lossy image compression. *Radioelectronic and Computer Systems*, 104(4), pp.143-152. Available at: <https://doi.org/10.32620/reks.2022.4.11>.
- Bondžulić, B., Pavlović, B., Stojanović, N., Petrović, V. & Bujaković, D. 2024. A simple and reliable approach to providing a visually lossless image compression. *The Visual Computer, International Journal of Computer Graphics*, 40, pp.3747-3763. Available at: <https://doi.org/10.1007/s00371-023-03062-y>.
- Cai, Y.-Q., Zou, H.-X. & Yuan, F. 2019. Adaptive compression method for underwater images based on perceived quality estimation. *Frontiers of Information Technology & Electronic Engineering*, 20(5), pp.716-730. Available at: <https://doi.org/10.1631/FITEE.1700737>.
- Corchs, S.E., Ciocca, G., Bricolo, E. & Gasparini, F. 2016. Predicting complexity perception of real world images. *PLoS ONE*, 11(6), e0157986. Available at: <https://doi.org/10.1371/journal.pone.0157986>.
- Fan, C., Lin, H., Hosu, V., Zhang, Y., Jiang, Q., Hamzaoui, R. & Saupe, D. 2019. SUR-Net: Predicting the satisfied user ratio curve for image compression with deep learning. In: *2019 Eleventh International Conference on Quality of Multimedia Experience (QoMEX)*, Berlin, Germany, pp.1-6, June 5-7. Available at: <https://doi.org/10.1109/QoMEX.2019.8743204>.
- Fiorucci, F., Baruffa, G. & Frescura, F. 2012. Objective and subjective quality assessment between JPEG XR with overlap and JPEG 2000. *Journal of Visual Communication and Image Representation*, 23(6), pp.835-844. Available at: <https://doi.org/10.1016/j.jvcir.2012.04.011>.
- Goerner, F.L., Duong, T., Stafford, R.J. & Clarke, G.D. 2013. A comparison of five standard methods for evaluating image intensity uniformity in partially parallel imaging MRI. *Medical Physics*, 40(8), art.number:082302. Available at: <https://doi.org/10.1118/1.4816306>.

Hasler, D. & Suesstrunk, S.E. 2003. Measuring colourfulness in natural images. In: Rogowitz, B.E. & Pappas, T.N. (Eds.) *Proceedings Electronic Imaging: Human Vision and Electronic Imaging VIII*, Santa Clara, CA, USA, 5007, pp.87-95, January 20-24. Available at: <https://doi.org/10.1117/12.477378>.

Jin, L., Lin, J.Y., Hu, S., Wang, H., Wang, P., Katsavounidis, I., Aaron, A. & Kuo, C.-C. J. 2016. Statistical study on perceived JPEG image quality via MCL-JCI dataset construction and analysis. In: *IS&T International Symposium on Electronic Imaging – Image Quality and System Performance XIII*, San Francisco, CA, USA, art.ID:art00026, February 14-18. Available at: <https://doi.org/10.2352/ISSN.2470-1173.2016.13.IQSP-222>.

Kovalenko, B., Lukin, V., Kryvenko, S., Naumenko, V. & Vozel, B. 2022. Prediction of parameters in optimal operation point for BPG-based lossy compression of noisy images. *Ukrainian Journal of Remote Sensing*, 9(2), pp.4-12. Available at: <https://doi.org/10.36023/ujrs.2022.9.2.212>.

Kovalenko, B. & Lukin, V. 2023. Analysis of distortions due to BPG-based lossy compression of noise-free and noisy images. *Herald of Khmelnytskyi National University. Technical Sciences*, 325(1), pp.128-135.

Krivenko, S.S., Krylova, O., Bataeva, E. & Lukin, V.V. 2018. Smart lossy compression of images based on distortion prediction. *Telecommunications and Radio Engineering*, 77(17), pp.1535-1554. Available at: <https://doi.org/10.1615/TelecomRadEng.v77.i17.40>.

Li, F., Lukin, V., Okarma, K. & Fu, Y. 2021. Providing a Desired Quality of BPG Compressed Images for FSIM Metric. In: *2021 IEEE 3rd International Conference on Advanced Trends in Information Theory (ATIT)*, Kyiv, Ukraine, pp.10-14, December 15-17. Available at: <https://doi.org/10.1109/ATIT54053.2021.9678522>.

Li, F., Lukin, V., Ieremeiev, O. & Okarma, K. 2022. Quality control for the BPG lossy compression of three-channel remote sensing images. *Remote Sensing*, 14(8), art.number:1824. Available at: <https://doi.org/10.3390/rs14081824>.

Li, F., Abramov, S., Dohtiev, I. & Lukin, V. 2024. Advantages and drawbacks of two-step approach to providing desired parameters in lossy image compression. *Advanced Information Systems*, 8(1), pp.57-63. Available at: <https://doi.org/10.20998/2522-9052.2024.1.07>.

Lin, H., Hosu, V., Fan, C., Zhang, Y., Mu, Y., Hamzaoui, R. & Saupe, D. 2020. SUR-FeatNet: Predicting the satisfied user ratio curve for image compression with deep feature learning. *Quality and User Experience*, 5, art.number:5. Available at: <https://doi.org/10.1007/s41233-020-00034-1>.

Lin, H., Chen, G., Jenadeleh, M., Hosu, V., Reips, U.-D., Hamzaoui, R. & Saupe, D. 2022. Large-Scale Crowdsourced Subjective Assessment of Picturewise Just Noticeable Difference. *IEEE Transactions on Circuits and Systems for Video Technology*, 32(9), pp.5859-5873. Available at: <https://doi.org/10.1109/TCSVT.2022.3163860>.

Liu, X., Chen, Z., Wang, X., Jiang, J. & Kwong, S. 2018. JND-Pano: Database for just noticeable difference of JPEG compressed panoramic images. In: Hong, R., Cheng, W.H., Yamasaki, T., Wang, M. & Ngo, C.W. (Eds.) *Advances in Multimedia Information Processing. PCM 2018. Lecture Notes in Computer Science*, 11164, pp.458-468. Cham: Springer. Available at: https://doi.org/10.1007/978-3-030-00776-8_42.

Liu, H., Zhang, Y., Zhang, H., Fan, C., Kwong, S., Kuo C.-C. J. & Fan, X. 2020. Deep Learning-Based Picture-Wise Just Noticeable Distortion Prediction Model for Image Compression. *IEEE Transactions on Image Processing*, 29, pp.641-656. Available at: <https://doi.org/10.1109/TIP.2019.2933743>.

Liu, Y., Jin, J., Xue, Y. & Lin, W. 2023. The First Comprehensive Dataset with Multiple Distortion Types for Visual Just-Noticeable Differences. In: *2023 IEEE International Conference on Image Processing (ICIP)*, Kuala Lumpur, Malaysia, pp.2820-2824, October 08-11. Available at: <https://doi.org/10.1109/ICIP49359.2023.10221977>.

Mikhailiuk, A., Ye, N. & Mantiuk, R.K. 2021. The effect of display brightness and viewing distance: A dataset for visually lossless image compression. In: *IS&T International Symposium on Electronic Imaging: Human Vision and Electronic Imaging*, Virtual Event, 33, art.ID:art00005, January 21st. Available at: <https://doi.org/10.2352/ISSN.2470-1173.2021.11.HVEI-152>.

Mittal, A., Moorthy, A.K. & Bovik, A.C. 2012. No-Reference Image Quality Assessment in the Spatial Domain. *IEEE Transactions on Image Processing*, 21(12), pp.4695-4708. Available at: <https://doi.org/10.1109/TIP.2012.2214050>.

Pavlović, B., Bondžulić, B., Stojanović, N., Petrović, V. & Bujaković, D. 2023. Prediction of the first just noticeable difference point based on simple image features. In: *2023 Zooming Innovation in Consumer Technologies Conference (ZINC)*, Novi Sad, Serbia, pp.125-130, May 29-31. Available at: <https://doi.org/10.1109/ZINC58345.2023.10173865>.

Ponomarenko, N., Silvestri, F., Egiazarian, K., Carli, M., Astola, J. & Lukin, V. 2007. On between-coefficient contrast masking of DCT basis functions. In: *3rd International Workshop on Video Processing and Quality Metrics for Consumer Electronics (VPQM)*, Scottsdale, Arizona, USA, pp.1-4, January 25-26 [online]. Available at: http://ponomarenko.info/vpqm07_p.pdf [Accessed: 05. April 2024].

Poth, M., Trpovski, Ž. & Lončar-Turukalo, T. 2020. Analysis and improvement of JPEG compression performance using custom quantization and block boundary classifications. *Acta Polytechnica Hungarica*, 17(6), pp.171-191. Available at: <https://doi.org/10.12700/APH.17.6.2020.6.10>.

Saha, S. & Vemuri, R. 2000. An analysis on the effect of image features on lossy coding performance. *IEEE Signal Processing Letters*, 7(5), pp.104-107. Available at: <https://doi.org/10.1109/97.841153>.

Shen, X., Ni, Z., Yang, W., Zhang, X., Wang, S. & Kwong, S. 2020. A JND Dataset Based on VVC Compressed Images. In: *2020 IEEE International Conference on Multimedia & Expo Workshops (ICMEW)*, London, United Kingdom, pp.1-6, July 6-10. Available at: <https://doi.org/10.1109/ICMEW46912.2020.9105955>.

Shen, X., Ni, Z., Yang, W., Zhang, X., Wang, S. & Kwong, S. 2021. Just Noticeable Distortion Profile Inference: A Patch-Level Structural Visibility Learning Approach. *IEEE Transactions on Image Processing*, 30, pp.26-38. Available at: <https://doi.org/10.1109/TIP.2020.3029428>.

Testolina, M., Hosu, V., Jenadeleh, M., Lazzarotto, D., Saupe, D. & Ebrahimi T. 2023. JPEG AIC-3 Dataset: Towards Defining the High Quality to Nearly Visually Lossless Quality Range. In: *2023 15th International Conference on Quality of Multimedia Experience (QoMEX)*, Ghent, Belgium, pp.55-60, June 20-22. Available at: <https://doi.org/10.1109/QoMEX58391.2023.10178554>.

Wang, Z. & Bovik, A.C. 2009. Mean squared error: Love it or leave it? A new look at Signal Fidelity Measures. *IEEE Signal Processing Magazine*, 26(1), pp.98-117. Available at: <https://doi.org/10.1109/MSP.2008.930649>.

Wang, Z., Bovik, A.C., Sheikh, H.R. & Simoncelli, E.P. 2004. Image quality assessment: From error visibility to structural similarity. *IEEE Transactions on Image Processing*, 13(4), pp.600-612. Available at: <https://doi.org/10.1109/TIP.2003.819861>.

Yu, H. & Winkler, S. 2013. Image complexity and spatial information. In: *2013 Fifth International Workshop on Quality of Multimedia Experience (QoMEX)*, Klagenfurt am Worthersee, Austria, pp.12-17, July 3-5. Available at: <https://doi.org/10.1109/QoMEX.2013.6603194>.

Zemliachenko, A., Ponomarenko, N., Lukin, V., Egiazarian, K. & Astola, J. 2016. Still image/video frame lossy compression providing a desired visual quality. *Multidimensional Systems and Signal Processing*, 27(3), pp.697-718. Available at: <https://doi.org/10.1007/s11045-015-0333-8>.

Compresión de imágenes JPEG y BPG sin pérdida visual a través de la base de datos KonJND-1k

Boban P. Bondžulić^a, Nenad M. Stojanović^a, **autor de correspondencia**, Vladimir V. Lukin^b, Sergij S. Kryvenko^b

^a Universidad de Defensa de Belgrado, Academia Militar, Departamento de Telecomunicaciones e Informática, Belgrado, República de Serbia

^b Universidad Aeroespacial Nacional, Departamento de Tecnologías de la Información y la Comunicación, Kharkiv, Ucrania

CAMPO: telecomunicación

TIPO DE ARTÍCULO: artículo científico original

Resumen:

Introducción/objetivo: Este artículo presenta los resultados de la investigación sobre la compresión de imágenes sin pérdida visual, que es de particular interés porque logra un alto grado de compresión, mientras que la calidad visual de la imagen no se ve afectada, es decir, los usuarios finales están muy satisfechos con la calidad de la imagen. El análisis se llevó a cabo utilizando la base de datos KonJND-1k de

imágenes a gran escala disponible públicamente, que contiene los resultados de pruebas subjetivas en imágenes comprimidas JPEG y BPG.

Métodos: Gracias a la disponibilidad de imágenes de la base de datos KonJND-1k, se analiza la dependencia de las evaluaciones objetivas de la calidad de la imagen en los parámetros que controlan el grado de compresión de las señales de origen (factor de calidad para JPEG y parámetro de cuantificación para BPG). Los resultados de las pruebas subjetivas sin pérdida visual se utilizan para un análisis profundo de los valores límite y típicos de los parámetros que controlan estos dos tipos de compresión, así como para el análisis de los valores correspondientes de las puntuaciones de calidad objetivas. Además, se han identificado características fiables para predecir el límite entre la compresión visual sin pérdida y la compresión visual con pérdida. Para ello, se utiliza el grado de acuerdo entre las predicciones y los valores de verdad fundamental de la relación señal-ruido (PSNR) de pico y la representación de la imagen en bits por píxel (bpp). La relación de compresión visual sin pérdida se utiliza para comparar las técnicas JPEG y BPG.

Resultados: Se muestra que el límite entre la compresión de imágenes visual sin pérdida y visual con pérdida se encuentra en un amplio rango de valores de PSNR (aproximadamente 20 dB para JPEG y 15 dB para BPG). Los valores del factor de calidad de compresión de imágenes JPEG correspondientes en este umbral también varían ampliamente de 31 a 79, con una concentración entre 40 y 45. Para el codificador BPG, los valores del parámetro de cuantificación se agrupan alrededor de 30, y los valores límite son 25 y 34. Además, se muestra que este límite se puede determinar de forma fiable basándose en características simples derivadas de la imagen original sin comprimir. Las características basadas en gradientes conocidas como frecuencia espacial e información espacial demostraron ser los mejores predictores. El grado de acuerdo entre las predicciones obtenidas a partir de estas características con los valores de verdad fundamental de PSNR y bpp en ambos tipos de compresión es superior al 85%. Un análisis comparativo ha demostrado que, utilizando la compresión BPG, es posible, en promedio, lograr una relación de compresión de compresión sin pérdida visual dos veces mayor que para JPEG (80 frente a 40).

Conclusión: Aunque se logra un alto grado de acuerdo entre las predicciones y los valores de verdad fundamental de PSNR y bpp del límite entre la compresión sin pérdida visual y la compresión con pérdida visual, existe la necesidad de desarrollar nuevos enfoques de predicción, especialmente con la técnica BPG, que a través de la relación de compresión demostró ser superior a la técnica JPEG. Las bases de datos existentes utilizadas para el análisis de la compresión sin pérdida visual contienen imágenes en color de la parte visible del espectro

electromagnético. Considerando el uso creciente de imágenes de la parte infrarroja del espectro, existe la necesidad de realizar pruebas similares en este rango espectral.

Palabras claves: compresión BPG, compresión JPEG, diferencia apenas perceptible (JND), relación señal-ruido máxima (PSNR), compresión de imágenes sin pérdida visual.

Сжатие изображений JPEG и BPG без визуальных потерь с помощью базы данных KopJND-1k

Бобан П. Бонджулич^а, Ненад М. Стоянович^а, корреспондент, Владимир В. Лукин^б, Сергей С. Кривенко^б

^а Университет обороны в г. Белград, Военная академия, кафедра телекоммуникаций и информатики, г. Белград, Республика Сербия

^б Национальный аэрокосмический университет им. М. Е. Жуковского «Харьковский авиационный институт», Кафедра информационно-коммуникационных технологий им. О.А. Зеленского, г. Харьков, Украина

РУБРИКА ГРНТИ: 28.23.00 Искусственный интеллект;
28.23.15 Распознавание образов. Обработка изображений

ВИД СТАТЬИ: оригинальная научная статья

Резюме:

Введение/цель: В данной статье представлены результаты исследований по сжатию изображений без визуальных потерь, которое представляет особый интерес, поскольку позволяет достичь высокой степени сжатия, при этом визуальное качество изображения не ухудшается, т.е. конечные пользователи очень довольны качеством изображения. Анализ проводился с использованием общедоступной крупномасштабной картинной базы данных KopJND-1k, содержащей результаты субъективных тестов изображений, сжатых в форматах JPEG и BPG.

Методы: Благодаря наличию изображений из базы данных KopJND-1k проанализирована зависимость объективных оценок качества изображения от параметров, управляющих степенью сжатия исходных сигналов (коэффициента качества для JPEG и параметра квантования для BPG). Результаты субъективных тестов без визуальных потерь используются для тщательного анализа граничных и типичных значений параметров, управляющих этими двумя типами сжатия, а также для анализа соответствующих значений объективных показателей качества. Кроме того, были идентифицированы надежные функции для прогнозирования границы между сжатием без визуальных потерь и сжатием с визуальными потерями. Для этой цели используется степень

согласия между прогнозируемыми и фактическими значениями пикового отношения сигнал/шум (PSNR) и представления изображения в битах на пиксель (bpp). Степень сжатия без визуальных потерь используется для сравнения методов JPEG и BPG.

Результаты: Показано, что граница между сжатием изображений без визуальных потерь и сжатием изображений с визуальными потерями находится в широком диапазоне значений PSNR (около 20 дБ для JPEG и 15 дБ для BPG). Соответствующие значения коэффициента качества сжатия изображения JPEG при этом пороге также широко варьируются от 31 до 79 с накоплением от 40 до 45. Значения параметра квантования группируются около 30, а граничные значения составляют 25 и 34. Показано, что эту границу можно надежно определить на основе простых признаков, полученных из исходного несжатого изображения. Градиентные характеристики, известные как пространственная частота и пространственная информация, оказались лучшими предикторами. Степень согласия между прогнозируемыми и фактическими значениями PSNR и bpp при обоих типах сжатия превышает 85%. Сравнительный анализ показал, что при использовании BPG сжатия в среднем можно добиться вдвое большей степени сжатия без визуальных потерь, чем при JPEG (80 против 40).

Выводы: Несмотря на достигнутую высокую степень согласия между прогнозируемыми и основными значениями PSNR и bpp на границе между сжатием без визуальных потерь и сжатием с визуальными потерями, существует необходимость в разработке новых подходов к прогнозированию, особенно с использованием метода BPG, который по коэффициенту сжатия превосходит метод JPEG. Современные базы данных, используемые для анализа сжатия без визуальных потерь, содержат цветные изображения видимой части электромагнитного спектра. Учитывая широкое использование изображений инфракрасной части спектра, возникает необходимость проведения аналогичных испытаний и в этом спектральном диапазоне.

Ключевые слова: сжатие BPG, сжатие JPEG, едва заметная разница (JND), пиковое соотношение сигнал/шум (PSNR), сжатие изображения без визуальных потерь.

Компресија JPEG и BPG без губитка визуелних информација на примеру базе KonJND-1k

Бобан П. Бонцулић^а, Ненад М. Стојановић^а, аутор за преписку,
Владимир В. Лукин^б, Сергеј С. Кривенко^б

^а Универзитет одбране у Београду, Војна академија, Катедра
телекомуникација и информатике, Београд, Република Србија

^б Национални ваздухопловни универзитет, Департман информационо-
комуникационих технологија, Харков, Украјина

ОБЛАСТ: телекомуникације

КАТЕГОРИЈА (ТИП) ЧЛАНКА: оригинални научни рад

Сажетак:

Увод/циљ: У овом раду представљени су резултати истраживања компресије без губитка визуелних информација. Она је од посебног значаја јер се њоме остварује висок степен компресије, при чему визуелни квалитет слике није нарушен, па су крајњи корисници веома задовољни. Анализа је спроведена коришћењем обимне, јавно доступне базе KonJND-1k, која садржи резултате субјективних тестова на компримованим сликама JPEG и BPG.

Метод: Захваљујући доступности слика базе KonJND-1k анализирана је зависност објективних мера процене квалитета слике од параметара којима се контролише степен компресије изворних сигнала (фактор квалитета код JPEG, односно параметар квантизације код BPG). Резултати субјективних тестова искоришћени су за детаљнију анализу граничних и типичних вредности параметара којима се контролишу ова два типа компресије, као и за анализу одговарајућих вредности објективних скорова квалитета. Такође, извршена је идентификација поузданих обележја за предикцију границе између компресије без и са губитком визуелних информација. У ту сврху коришћен је степен слагања између предикција и тачних вредности вршног односа сигнал/шум (PSNR) и репрезентације слике у битима по пикселу (bpp). Степен компресије остварен применом компресије без губитка визуелних информација искоришћен је за поређење техника JPEG и BPG.

Резултати: Показано је да се граница између компресије без и са губитком визуелних информација налази у широком опсегу вредности PSNR (око 20 dB код JPEG и 15 dB код BPG). Одговарајуће вредности фактора квалитета слика JPEG на овој граници се, такође, налазе у широком опсегу од 31 до 79, са груписањем између 40 и 45. Вредности параметра квантизације групишу се око 30, а граничне вредности су 25 и 34. Такође, потврђено је да се ова граница може поуздано одредити на основу једноставних обележја изведених из оригиналне некомпримоване слике. Показало се да су

најбољи предиктори градијентна обележја позната као просторна фреквенција и просторна информација. Степен слагања предикција добијених из ових обележја са тачним вредностима PSNR и brr код оба типа компресије већи је од 85%. Компаративном анализом доказано је да се применом компресије BPG, у просеку, може остварити дупло већи степен компресије без губитка визуелних информација него применом компресије JPEG (80 насупрот 40).

Закључак: Иако је остварен висок степен слагања између предикција и тачних вредности PSNR и brr на граници између компресије без и са губитком визуелних информација, постоји потреба за развојем нових приступа предикције, нарочито код технике BPG која се кроз степен компресије показала супериорном у односу на технику JPEG. Постојеће базе које се користе за анализу компресије без губитка визуелних информација су са сликама из видљивог дела електромагнетног спектра. Имајући у виду све већу употребу слика из инфрацрвеног дела спектра, постоји потреба за спровођењем сличних тестова у овом спектралном опсегу.

Кључне речи: компресија BPG, компресија JPEG, једва уочљиве разлике (JND), вршни однос сигнал/шум (PSNR), компресија без губитка визуелних информација.

EDITORIAL NOTE: The first author of this article, Boban P. Bondžulić, is a current member of the Editorial Board of the Military Technical Courier. Therefore, the Editorial Team has ensured that the double blind reviewing process was even more transparent and more rigorous. The Team made additional effort to maintain the integrity of the review and to minimize any bias by having another associate editor handle the review procedure independently of the editor – author in a completely transparent process. The Editorial Team has taken special care that the referee did not recognize the author's identity, thus avoiding the conflict of interest.

Paper received on: 07.04.2024.
Manuscript corrections submitted on: 24.09.2024.
Paper accepted for publishing on: 25.09.2024.

© 2024 The Authors. Published by Vojnotehnički glasnik / Military Technical Courier (www.vtg.mod.gov.rs, втр.мо.унр.срб). This article is an open access article distributed under the terms and conditions of the Creative Commons Attribution license (<http://creativecommons.org/licenses/by/3.0/rs/>).



Analytical investigation on the buckling and free vibration of porous laminated FG-CNTRC plates

Tahir Ghazoul^a, Mohamed Atif Benatta^b,
Abdelwahhab Khatir^c, Youcef Beldjelili^d,
Baghdad Krour^e, Mohamed Bachir Bouiadjra^f

^a University of Djillali Liabes, Structures and Advanced Materials in Civil Engineering and Public Works Laboratory, Sidi Bel Abbes, People's Democratic Republic of Algeria, e-mail: tahir.ghazoul@univ-sba.dz, **corresponding author**, ORCID iD: <https://orcid.org/0009-0006-9869-4339>


^b University of Djillali Liabes, Structures and Advanced Materials in Civil Engineering and Public Works Laboratory, Sidi Bel Abbes, People's Democratic Republic of Algeria, e-mail: bematif@gmail.com, ORCID iD: <https://orcid.org/0009-0007-5854-9054>

^c Polytechnic University of Marche, Structural Section DICEA, Ancona, Italian Republic, e-mail: a.khatir@pm.univpm.it, ORCID iD: <https://orcid.org/0000-0003-4920-5165>

^d University of Djillali Liabes, Structures and Advanced Materials in Civil Engineering and Public Works Laboratory, Sidi Bel Abbes, People's Democratic Republic of Algeria, e-mail: beldjelili.youcef@gmail.com, ORCID iD: <https://orcid.org/0000-0003-3877-9665>

^e University of Djillali Liabes, Structures and Advanced Materials in Civil Engineering and Public Works Laboratory, Sidi Bel Abbes, People's Democratic Republic of Algeria, e-mail: baghdad.krour@univ-sba.dz, ORCID iD: <https://orcid.org/0000-0002-8265-9807>

^f University of Djillali Liabes, Structures and Advanced Materials in Civil Engineering and Public Works Laboratory, Sidi Bel Abbes, People's Democratic Republic of Algeria; Thematic Agency for Research in Science and Technology, Algiers, People's Democratic Republic of Algeria, e-mail: mohamedbachirbouiadjra@gmail.com, ORCID iD: <https://orcid.org/0009-0008-4814-6187>

 <https://doi.org/10.5937/vojtehg72-50469>

FIELD: mechanics, materials

ARTICLE TYPE: original scientific paper

Abstract:

Introduction/purpose: The aim of this study is to examine the buckling and free vibration behavior of laminated composite plates reinforced with carbon

nanotubes when various sources of uncertainty are taken into account with the main focus being the existence of porosity.

Methods: A porous laminated plate model is developed using a high order shear deformation theory. Different configurations of functionally graded aligned single-walled carbon nanotubes throughout the thickness of each layer are being investigated. The effective properties of materials are evaluated through the extended rule of mixture while considering an upper bound for the effect of porosity. The governing equations are derived and solved using the virtual work principle and Navier's approach. The validity of the current formulation is confirmed by comparing the results with the existing data from literature sources. The impact of numerous parameters such as porosity, carbon nanotube volume fraction, reinforcement distribution types, lamination scheme, and the number of layers on the buckling and free vibration responses is investigated in detail.

Results: A key finding of this study is the significant reduction in buckling resistance of laminated FG-CNTRC plates due to porosity, contrasting with the minor impact on the free vibration response.

Conclusion: The results of this paper emphasize the critical role of porosity in structural integrity and provide novel insights into the behaviour of advanced composite materials.

Key words: buckling, free vibration, laminated composite plate, porosity, functionally graded material, carbon nanotubes.

Introduction

Carbon nanotubes (CNTs) are recognized as excellent reinforcements for advanced composites owing to their superior properties and low density. In contemporary industries such as aeronautical, mechanical and civil engineering, these advanced composite materials integrated in the form of shells, plates or beams as structural components have found significant applications. As required, the accurate evaluation of the mechanical reactions of structures fabricated from CNTs reinforced composite materials (CNTRC) becomes crucial for engineering design and manufacture.

Over recent years, significant attention has been devoted by researchers to functionally graded CNTRC materials (FG-CNTRC) featuring spatially varying characteristics based on a specific non-uniform distribution of the reinforcement phase. The discovery of this interesting feature led to different studies on the mechanics of CNTRC structures. Shen (2009) has introduced the first study on FG-CNTRC. His findings suggested that functionally graded reinforcement might increase the bending moment. According to Kwon et al. (2011), FG-CNTRC can be

achieved utilizing a powder metallurgy manufacturing method with a non-uniform dispersion of CNTs throughout the layer. The bending and free vibration of different kinds of FG-CNTRC plates were investigated by Zhu et al. (2012). They discover that reinforcements distributed near the bottom and top are more effective than those dispersed close to the mid-plane in enhancing the stiffness of CNTRC plates. Lei et al. (2013) used the element-free kp-Ritz method to study the buckling of FG-CNTRC plates. They found that for all different distributions of CNTs, those closer to the bottom and top exhibit larger buckling load values contrasted with other types of reinforcement arrangements. Liew et al. (2015) conducted a comprehensive review of the existing literature encompassing static, buckling, dynamic and non-linear analyses of FG-CNTRC.

On the other hand, researchers assert that multi-layered composite structures offer superior mechanical performance compared to single-layer structures. Laminated composite plates are highly attractive for structural applications due to their exceptional weight-to-stiffness ratio and the capacity to tailor the lamination scheme to meet specific design requirements. In conjunction with the expansion application of laminated composites in engineering structures, numerous deformation plate theories have been developed to precisely forecast their behavior. Kirchhoff (1850) developed the simplest theory, known as the classical plate theory (CLPT); however, it is not applicable to thick plates as it ignores completely the effects of shear deformation. Mindlin (1951) proposed the first-order shear deformation plate theory (FSDT) which considers shear deformation effects and is applicable to both thin and moderately thick plates. Nevertheless, the FSDT requires the use of a shear correction factor to meet zero shear conditions on the surfaces of the plate. Determining the correct value of this factor is challenging, which is considered a shortcoming of the FSDT. Later, higher-order shear deformation theories (HSDT) were developed (Reddy, 1984; Shimpi et al, 2003; Mantari et al, 2012) to overcome the limitations of the FSDT. These theories avoid the need for shear correction factors by assuming non-linear stress variation through the thickness. Subsequently, researchers arrived at a class of the refined plate theory (RPT) by disassembling transverse displacements into bending and shear components (Thai & Choi, 2011; Thai & Vo, 2013). The HSDT is often desirable for its superior accuracy over the CLPT and the FSDT. However, HSDTs with five or six variables are even more accurate for analyzing laminated composite plates than RPTs. Sayyad & Ghugal (2015) provided a synthesis of recent research conducted on multi-layered composite plates that utilized various shear deformation theories.

Stimulated by the concept of FG-CNTRC and the benefits of multi-layered composite structures, researchers have been inspired to study FG-CNTRC multi-layered structures. This approach has the advantage of arranging the CNTs where the reinforcement is most effective and the ability to orient them in such a way as to obtain the highest mechanical properties from the laminated composite structures. Malekzadeh & Shojaee (2013) examined the buckling of CNTRC quadrilateral laminated plates using the FSDT. Zhang & Selim (2017) incorporated Reddy's HSDT for free vibration analyses of FG-CNTRC thick laminated plates. Lei et al. (2018) used the CLPT combined with the element-free method to analyse the vibration behavior of matrix-cracked hybrid (FG-CNT/conventional fiber) laminated composite plates. Alimradzadeh et al. (2023) analysed the thermo-mechanical buckling of FG-Fiber laminated composite beams using the Euler-Bernoulli beam theory. Chiker et al. (2023) investigated how the uncertainty caused by the non-ideal aligned distribution of FG-CNTs nano-fillers affects the free vibration characteristics of laminated FG-CNTRC plates. Fu et al. (2019) introduced a model based on the nth-order shear deformation theory to conduct static analysis of FG-CNTRC laminated plates supported by elastic foundations under thermal conditions. Arani et al. (2021) used Reddy's shear deformation theory to analyze the forced and free vibrations of FG-CNTRC laminated cylindrical panels. Tran et al. (2020) devised a novel four-variable RPT to perform static analysis on smart FG-CNTRC laminated plates incorporating a piezoelectric actuator and subjected to electro-mechanical loads. Daikh et al. (2023) analyzed the static bending response of composite laminated beams reinforced with randomly oriented FG-CNTs and fiber reinforcements on an elastic foundation, employing the finite element method. An analytical model for examining the free vibration of thick laminated plates reinforced with FG-graphene composites was introduced by Ma & Jin (2023).

However, perfection remains elusive, and fiber composite materials are no exception. During their manufacturing, there are many imperfections that are created. These imperfections exert a considerable influence on the mechanical characteristics of composite materials, often causing them to deviate from expected values. Thoughtfully planned and tightly controlled manufacturing processes can decrease the occurrence of defects, thereby enhancing material properties, albeit typically resulting in increased costs (Ciriscioli et al, 1991). This would change if one could evaluate and quantify the effect of defects and, based on that, allow a certain level of defects in composite materials parts as a means to estimate the quality of a composite. In this way, the desired properties and safety

factors can be achieved at a lower cost and with reduced manufacturing energy.

As a result of its importance in fiber composite materials, porosity stands out as the most extensively studied manufacturing defect. In modern composite materials, removing pores has become increasingly challenging, due to a higher complexity of parts and the heightened viscosity of modified polymers (Lee et al, 2006). Mehdikhani et al. (2019) conducted a review on porosity in fiber composite materials, including its formation, characteristics, and effects.

The literature contains a considerable amount of research on the impact of porosity on the inter-laminar shear strength of Fiber/epoxy composites (Hernández et al, 2011; Stamopoulos et al, 2016; Hayashi & Takahashi, 2017). Others are keen on assessing how porosity affects the physical and mechanical characteristics of unidirectional fiber plant composites (Madsen & Lilholt, 2003; Madsen et al, 2009). However, studies focusing on the effect of porosity on CNTRCs are rare, particularly concerning the analysis of their mechanical responses. Guessas et al. (2018) analytically studied the impact of matrix porosity on the buckling response of a CNTRC porous plate via FSDT considering a semi-empirical approach established by Phani & Niyogi (1987) describing the relationship between porosity and Young's modulus in brittle solids. Medani et al. (2019) employed identical assumptions to study the static and dynamic behavior of an FG-CNTRC porous sandwich plate. In their studies, it was found that porosity has an undeniable effect on the mechanical responses of CNTRC structures.

From the aforementioned review, it is clear that a limited number of studies have been conducted to analyze the structural responses of CNTRCs with porosities. The literature currently available also indicates that multi-layered FG-CNTRC structures have captured the interest of numerous researchers, not only because of their intricate construction, but also because they pose challenges.

The current study focuses on developing an analytical model to analyze the buckling and free vibration performance of laminated FG-CNTRC plates while accounting for the presence of porosity. The extended rule of mixture is formulated to assess the effective material properties of the resulting nanocomposites in the presence of porosity, taking into account an upper limit for its influence. Four different distribution types of CNTs along the thickness of the layers are being examined, encompassing uniform distribution as well as three other functionally graded distributions. The adopted shear deformation theory ensures the appropriate distribution of transverse shear strains throughout the

thickness and imposes tangential stress-free boundary conditions on the surfaces. The governing equations are derived through the virtual work principle and solved using Navier's solutions. The results obtained by the present method are compared with the results from the existing literature. Detailed parametric analyses are performed to investigate the influences of porosity, CNTs distributions, CNTs volume fraction, the number of layers, CNTs fiber orientation, stacking sequence and aspect ratio on the buckling and free vibration characteristics of porous laminated FG-CNTRC plates.

Theoretical formulations

Effective material properties

Consider a rectangular plate with the total thickness h , the length a and the width b , composed of N perfectly bonded layers, with reference to the coordinate system depicted in Figure 1.

The component layers are presumed to consist of a blend of single-walled CNTs (SWCNTs) and an isotropic matrix. In consideration, there are four different types of CNT distribution throughout the layer thickness: uniform distribution (UD) and functionally graded distributions denoted by FG-O, FG-V and FG-X.

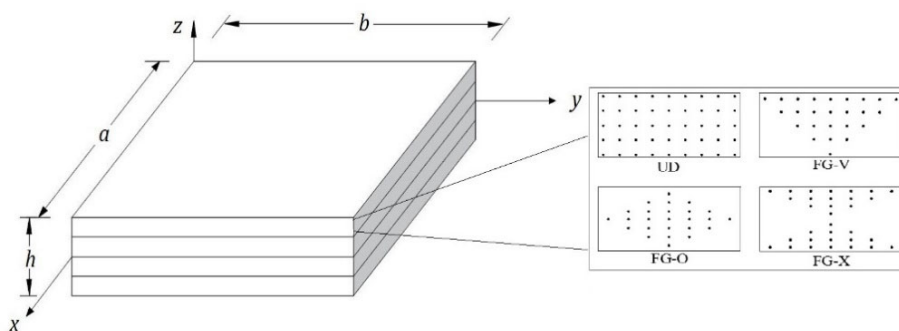


Figure 1 – Different configurations of CNTs through the layer thickness

As a result, the volume fraction of CNTs can be expressed based on their configuration throughout the thickness of each individual layer as:

$$V_{CNT} = \begin{cases} V_{CNT}^* & UD \\ \left(1 + \frac{2z}{h}\right) V_{CNT}^* & FG-V \\ 2\left(1 - \frac{2|z|}{h}\right) V_{CNT}^* & FG-O \\ 2\left(\frac{2|z|}{h}\right) V_{CNT}^* & FG-X \end{cases} \quad (1)$$

where

$$V_{CNT}^* = \frac{W_{CNT}}{W_{CNT} + (\rho^{CNT} / \rho^m) - (\rho^{CNT} / \rho^m) W_{CNT}} \quad (2)$$

W_{CNT} is the mass fraction of CNTs, ρ^{CNT} and ρ^m are the densities of the CNTs and the matrix, respectively. V_{CNT} and V_{CNT}^* are the volume fractions of CNTs for UD and FG-CNTRC, respectively.

It is assumed that the mass volume of CNTs in the UD-CNTRC layer and the FG-CNTRC layers is the same, meaning: $V_{CNT} = V_{CNT}^*$.

The extended rule of mixture, as a straightforward and convenient micromechanics model, is used to determine the effective material properties of the CNTRC layer (Shen, 2009):

$$E_1 = \eta_1 V_{CNT} E_1^{CNT} + V_m E^m \quad (3a)$$

$$\frac{\eta_2}{E_2} = \frac{V_{CNT}}{E_2^{CNT}} + \frac{V_m}{E^m} \quad (3b)$$

$$\frac{\eta_3}{G_{12}} = \frac{V_{CNT}}{G_{12}^{CNT}} + \frac{V_m}{G^m} \quad (3c)$$

where E_1^{CNT} and E_2^{CNT} are the Young's moduli of CNTs in longitudinal and transverse directions, respectively, and G_{12} is the shear modulus. G_{12}^{CNT} is the shear modulus of CNTs, E^m and G^m are the Young's modulus and shear modulus of the matrix. η_1 , η_2 and η_3 are the efficiency parameters which serve to account for load transfer between CNTs and the polymeric matrix. V_{CNT} and V_m are CNTs and matrix volume fractions which satisfy the relation:

$$V_{CNT} + V_m = 1 \quad (4)$$

In the previous study, Hagstrand et al. (2005) theoretically and experimentally investigated how void content affects the structural flexural performance of unidirectional glass fiber reinforced polypropylene composite. Consequently, they set an upper threshold for the impact of void content on the composite elastic modulus using the relationship:

$$E(v_{void}) = E_0(1 - v_{void}) \quad (5)$$

where $E(v_{void})$ and E_0 represent the elastic modulus in the presence and absence of voids, respectively. v_{void} represents the void volume fraction.

Similarly, the effective elastic moduli of the CNTRC in equation (3) as a function of porosity can be derived as follows:

$$E_i^P = E_i(1 - P), i = 1, 2, 12 \quad (6)$$

where P represents the volume fraction of porosity and E_i^P is the effective elastic modulus in the presence of porosity.

As Poisson's ratio exhibits weak dependence on the position, it is assumed that v_{12} remains constant across the thickness of CNTRC plates:

$$v_{12} = V_{CNT} v_{12}^{CNT} + V_m v^m \quad (7)$$

where v_{12}^{CNT} and v^m are the Poisson's ratios of CNTs and the matrix, respectively.

Density ρ as a function of porosity is given by:

$$\rho = V_{CNT} \rho^{CNT} + (V_m - P) \rho^m \quad (8)$$

where ρ^{CNT} and ρ^m are the density of CNTs and the matrix, respectively.

Kinematics equations

According to the theory of material point situated at (x, y, t) in the plate domain, the displacements field can be formulated as follows:

$$u(x, y, z, t) = u_0(x, y, t) - z.w_{,x} + f(z)\phi_x \quad (9a)$$

$$v(x, y, z, t) = v_0(x, y, t) - z.w_{,y} + f(z)\phi_y \quad (9b)$$

$$w(x, y, z, t) = w_0(x, y, t) \quad (9c)$$

Here u , v and w represent the displacements in the x , y and z directions, respectively. u_0 , v_0 and w_0 denote mid-plane displacements, while ϕ_x and ϕ_y denote shear rotations. All generalized displacements are the functions of x , y and time t . $f(z)$ denotes the shape function governing the

transverse shear strain and stress distribution across the thickness. In terms of HSDTs, it is defined as (Sayyad & Ghugal, 2015):

$$f(z) = z - \frac{4}{3} \left(\frac{z^3}{h^2} \right) \quad (10)$$

It is crucial to note that, depending on the selected shape function, the displacement field in (9) can be readily adjusted to fit other plate theories. For instance, the CLPT is achieved by using the zero shape function while the FSDT is obtained with $f(z) = z$. From the theory of small deformations, the non-zero strain components related to the displacement field in (9) are defined as follows:

$$\begin{Bmatrix} \varepsilon_x \\ \varepsilon_y \\ \gamma_{xy} \end{Bmatrix} = \begin{Bmatrix} u_{0,x} \\ v_{0,y} \\ u_{0,y} + v_{0,x} \end{Bmatrix} + z \begin{Bmatrix} -w_{0,xx} \\ -w_{0,yy} \\ -2w_{0,xy} \end{Bmatrix} + f(z) \begin{Bmatrix} \phi_{x,x} \\ \phi_{y,y} \\ \phi_{x,y} + \phi_{y,x} \end{Bmatrix}; \begin{Bmatrix} \gamma_{yz} \\ \gamma_{xz} \end{Bmatrix} = f'(z) \begin{Bmatrix} \phi_y \\ \phi_x \end{Bmatrix} \quad (11)$$

with

$$f'(z) = \frac{df(z)}{dz} \quad (12)$$

Constitutive relations

Given that the plate consists of multiple orthotropic layers, the stress state within each layer is expressed as:

$$\begin{Bmatrix} \sigma_x \\ \sigma_y \\ \sigma_{xy} \\ \sigma_{yz} \\ \sigma_{xz} \end{Bmatrix}^k = \begin{bmatrix} \bar{Q}_{11} & \bar{Q}_{12} & \bar{Q}_{16} & 0 & 0 \\ \bar{Q}_{12} & \bar{Q}_{22} & \bar{Q}_{26} & 0 & 0 \\ \bar{Q}_{16} & \bar{Q}_{26} & \bar{Q}_{66} & 0 & 0 \\ 0 & 0 & 0 & \bar{Q}_{44} & \bar{Q}_{45} \\ 0 & 0 & 0 & \bar{Q}_{45} & \bar{Q}_{55} \end{bmatrix}^k \begin{Bmatrix} \varepsilon_x \\ \varepsilon_y \\ \gamma_{xy} \\ \gamma_{yz} \\ \gamma_{xz} \end{Bmatrix} \quad (13)$$

where $\{\sigma\}^k$; $\{\varepsilon\}$ and $[\bar{Q}_{ij}]^k$ are the stress vector, the strain vector and the transformed stiffness matrix, respectively.

The components of the transformed stiffness matrix $[\bar{Q}_{ij}]^k$ are defined as follows:

$$\begin{aligned}
 \bar{Q}_{11}^k &= Q_{11}^k \cos^2 \theta + 2(Q_{12}^k + 2Q_{66}^k) \cos^2 \theta \sin^2 \theta + Q_{22}^k \sin^4 \theta; \\
 \bar{Q}_{12}^k &= (Q_{11}^k + Q_{22}^k - 4Q_{66}^k) \cos^2 \theta \sin^2 \theta + Q_{12}^k (\sin^4 \theta + \cos^4 \theta); \\
 \bar{Q}_{22}^k &= Q_{11}^k \sin^4 \theta + 2(Q_{12}^k + 2Q_{66}^k) \cos^2 \theta \sin^2 \theta + Q_{22}^k \cos^4 \theta; \\
 \bar{Q}_{16}^k &= (Q_{11}^k - Q_{12}^k - 2Q_{66}^k) \cos^3 \theta \sin \theta + (Q_{12}^k - Q_{22}^k + 2Q_{66}^k) \sin^3 \theta \cos \theta; \\
 \bar{Q}_{26}^k &= (Q_{11}^k - Q_{12}^k - 2Q_{66}^k) \cos \theta \sin^3 \theta + (Q_{12}^k - Q_{22}^k + 2Q_{66}^k) \sin \theta \cos^3 \theta; \\
 \bar{Q}_{66}^k &= (Q_{11}^k + Q_{22}^k - 2Q_{12}^k - 2Q_{66}^k) \cos^2 \theta \sin^2 \theta + Q_{66}^k (\sin^4 \theta + \cos^4 \theta); \\
 \bar{Q}_{44}^k &= Q_{44}^k \cos^2 \theta + Q_{55}^k \sin^2 \theta; \\
 \bar{Q}_{45}^k &= (Q_{55}^k - Q_{44}^k) \cos \theta \sin \theta; \\
 \bar{Q}_{55}^k &= Q_{55}^k \cos^2 \theta + Q_{44}^k \sin^2 \theta;
 \end{aligned} \tag{14}$$

where θ is the angle formed by the global plate coordinate and the individual layer's local material coordinate. Q_{ij}^k are the plane stress-reduced stiffnesses expressed in terms of the engineering constants along the material axes of the layer as follows:

$$Q_{11}^k = \frac{E_{11}}{1 - \nu_{12}\nu_{21}}; Q_{12}^k = \frac{\nu_{12}E_{22}}{1 - \nu_{12}\nu_{21}}; Q_{22}^k = \frac{E_{22}}{1 - \nu_{12}\nu_{21}}; Q_{66}^k = G_{12}; Q_{44}^k = G_{23}; Q_{55}^k = G_{13} \tag{15}$$

Equations of motion

The governing equations are derived here using the virtual work principle. The principle can be expressed analytically as:

$$\int_{t_1}^{t_2} \delta(U_p + V - T) dt = 0 \tag{16}$$

The strain energy of the plate is computed by:

$$\delta U_p = \int_V [\sigma_x \delta \varepsilon_x + \sigma_y \delta \varepsilon_y + \sigma_{xy} \delta \gamma_{xy} + \sigma_{yz} \delta \gamma_{yz} + \sigma_{xz} \delta \gamma_{xz}] dx dy dz \tag{17}$$

$$\delta U_p = \int_A \left[\begin{aligned} &N_x \delta u_{0,x} + N_y \delta v_{0,y} + N_{xy} (\delta u_{0,y} + \delta v_{0,x}) - \\ &M_x^w \delta w_{0,xx} - M_y^w \delta w_{0,yy} - 2M_{xy}^w \delta w_{0,xy} + \\ &M_x^f \delta \phi_{x,x} + M_y^f \delta \phi_{y,y} + M_{xy}^f (\delta \phi_{x,y} + \delta \phi_{y,x}) + \\ &Q_{yz} \delta \phi_y + Q_{xz} \delta \phi_x \end{aligned} \right] dx dy \tag{18}$$

where

$$(N_i, M_i^w, M_i^f) = \sum_{k=1}^N \int_{z_{k-1}}^{z_k} (1, z, f(z)) \sigma_i^k dz, i = x, y, xy \tag{19a}$$

$$Q_i = \sum_{k=1}^N \int_{z_{k-1}}^{z_k} f(z) \sigma_i^k dz, i = xz, yz \quad (19b)$$

By substituting equation (13) into equation (19) and integrating across the thickness of the plate, the stress resultants can be linked to the strain through the following relations:

$$\begin{Bmatrix} N_x \\ N_y \\ N_{xy} \\ M_x^w \\ M_y^w \\ M_{xy}^w \\ M_x^f \\ M_y^f \\ M_{xy}^f \end{Bmatrix} = \begin{bmatrix} A_{11} & A_{12} & A_{16} \\ A_{12} & A_{22} & A_{26} \\ A_{16} & A_{26} & A_{66} \\ [B_{ij}] & [C_{ij}] \\ [B_{ij}] & [D_{ij}] & [E_{ij}] \\ [C_{ij}] & [E_{ij}] & [F_{ij}] \end{bmatrix} \begin{Bmatrix} u_{0,x} \\ v_{0,y} \\ u_{0,y} + v_{0,x} \\ -w_{0,xx} \\ -w_{0,yy} \\ -2w_{0,xy} \\ \phi_{x,x} \\ \phi_{y,y} \\ \phi_{x,y} + \phi_{y,x} \end{Bmatrix}; i, j = 1, 2, 6 \quad (20a)$$

$$\begin{Bmatrix} Q_{yz} \\ Q_{xz} \end{Bmatrix} = \begin{bmatrix} H_{44} & H_{45} \\ H_{45} & H_{55} \end{bmatrix} \begin{Bmatrix} \gamma_{yz}^f \\ \gamma_{xz}^f \end{Bmatrix} \quad (20b)$$

where

$$(A_{ij}, B_{ij}, D_{ij}, C_{ij}, E_{ij}, F_{ij}) = \sum_{k=1}^N \int_{z_{k-1}}^{z_k} \bar{Q}_{ij}^k (1, z, z^2, f(z), zf(z), f^2(z)) dz; i, j = 1, 2, 6 \quad (21a)$$

$$H_{ij} = \sum_{k=1}^N \int_{z_{k-1}}^{z_k} \bar{Q}_{ij}^k (f'(z))^2 dz; i, j = 4, 5 \quad (21b)$$

The virtual potential energy of the external applied load is computed by:

$$\delta V = \int_V [N_x^0 w_{0,x} \delta w_{0,x} + N_y^0 w_{0,y} \delta w_{0,y}] dx dy dz \quad (22)$$

where $N_x^0 = \gamma_x N_{cr}$ and $N_y^0 = \gamma_y N_{cr}$ are the in-plan compressive forces.

The expression for the kinetic energy of the mass system is as follows:

$$\delta T = \int_V \rho [\dot{u} \delta \dot{u} + \dot{v} \delta \dot{v} + \dot{w} \delta \dot{w}] dx dy dz \quad (23)$$

$$\delta T = \int_A \left[\begin{array}{l} I_1 (\dot{u}_0 \delta \dot{u}_0 + \dot{v}_0 \delta \dot{v}_0 + \dot{w}_0 \delta \dot{w}_0) + \\ I_2 (\dot{w}_{0,x} \delta \dot{u}_0 + \dot{w}_{0,y} \delta \dot{v}_0 + \dot{u}_0 \delta \dot{w}_{0,x} + \dot{v}_0 \delta \dot{w}_{0,y}) + \\ I_3 (\dot{w}_{0,x} \delta \dot{w}_{0,x} + \dot{w}_{0,y} \delta \dot{w}_{0,y}) + \\ I_4 (\dot{\phi}_x \delta \dot{u}_0 + \dot{u}_0 \delta \dot{\phi}_x + \dot{\phi}_y \delta \dot{v}_0 + \dot{v}_0 \delta \dot{\phi}_y) - \\ I_5 (\dot{\phi}_x \delta \dot{w}_{0,x} + \dot{w}_{0,x} \delta \dot{\phi}_x + \dot{\phi}_y \delta \dot{w}_{0,y} + \dot{w}_{0,y} \delta \dot{\phi}_y) + \\ I_6 (\dot{\phi}_x \delta \dot{\phi}_x + \dot{\phi}_y \delta \dot{\phi}_y) \end{array} \right] dx dy \quad (24)$$

where

$$(I_1, I_2, I_3, I_4, I_5, I_6) = \sum_{k=1}^N \int_{z_{k-1}}^{z_k} \rho^k (1, z, z^2, f(z), zf(z), f^2(z)) dz \quad (25)$$

Substituting (18), (22) and (24) into (16) gives the equations of motion for the plate:

$$\begin{aligned} \delta u_0 : N_{x,x} + N_{xy,y} &= I_1 \ddot{u}_0 - I_2 \ddot{w}_{0,x} + I_4 \ddot{\phi}_x \\ \delta v_0 : N_{xy,x} + N_{y,y} &= I_1 \ddot{v}_0 - I_2 \ddot{w}_{0,y} + I_4 \ddot{\phi}_y \\ \delta w_0 : M_{x,xx}^w + 2M_{xy,xy}^w + M_{y,yy}^w + N_x^0 w_{0,xx} + N_y^0 w_{0,yy} \\ &= I_1 \ddot{w}_0 + I_2 (\ddot{u}_{0,x} + \ddot{v}_{0,y}) - I_3 (\ddot{w}_{0,xx} + \ddot{w}_{0,yy}) + I_5 (\ddot{\phi}_{x,x} + \ddot{\phi}_{y,y}) \\ \delta \phi_x : M_{x,x}^f + M_{xy,y}^f - Q_{xz} &= I_4 \ddot{u}_0 - I_5 \ddot{w}_{0,x} + I_6 \ddot{\phi}_x \\ \delta \phi_y : M_{y,y}^f + M_{xy,x}^f - Q_{yz} &= I_4 \ddot{v}_0 - I_5 \ddot{w}_{0,y} + I_6 \ddot{\phi}_y \end{aligned} \quad (26)$$

Analytical solutions

In the current study, the rectangular plates are taken to be simply supported at all edges. The exact solution of (26) can be derived analytically by applying the following boundary conditions:

$$\begin{aligned} v_0 = w_0 = \phi_y = N_x = M_x^w = M_x^f = 0 \text{ at } x=0, a \\ u_0 = w_0 = \phi_x = N_y = M_y^w = M_y^f = 0 \text{ at } y=0, b \end{aligned} \quad (27)$$

The following displacement expansions are provided to derive the closed-form solutions of (26) and fulfill the simply supported boundary conditions given in (27), following Navier's approach:

$$\begin{aligned}
 u_0(x, y, t) &= \sum_{m=1}^{\infty} \sum_{n=1}^{\infty} U_{mn} e^{i\omega t} \cos(\alpha x) \sin(\beta y) \\
 v_0(x, y, t) &= \sum_{m=1}^{\infty} \sum_{n=1}^{\infty} V_{mn} e^{i\omega t} \sin(\alpha x) \cos(\beta y) \\
 w_0(x, y, t) &= \sum_{m=1}^{\infty} \sum_{n=1}^{\infty} W_{mn} e^{i\omega t} \sin(\alpha x) \sin(\beta y) \\
 \phi_x(x, y, t) &= \sum_{m=1}^{\infty} \sum_{n=1}^{\infty} \Phi_{xmn} e^{i\omega t} \cos(\alpha x) \sin(\beta y) \\
 \phi_y(x, y, t) &= \sum_{m=1}^{\infty} \sum_{n=1}^{\infty} \Phi_{ymn} e^{i\omega t} \sin(\alpha x) \cos(\beta y)
 \end{aligned} \tag{28}$$

where U_{mn} , V_{mn} , W_{mn} , Φ_{xmn} and Φ_{ymn} are arbitrary parameters that need to be determined. ω represents the eigen frequency linked to the (m, n) eigen mode. $\alpha = m\pi / a$ and $\beta = n\pi / b$.

By substituting equations (20) and (28) into equation (26), we can then derive the analytical solutions from the following equations

$$\left(\begin{bmatrix} S_{11} & S_{12} & S_{13} & S_{14} & S_{15} \\ S_{12} & S_{22} & S_{23} & S_{24} & S_{25} \\ S_{13} & S_{23} & S_{33} & S_{34} & S_{35} \\ S_{14} & S_{24} & S_{34} & S_{44} & S_{45} \\ S_{15} & S_{25} & S_{35} & S_{45} & S_{55} \end{bmatrix} - \omega^2 \begin{bmatrix} m_{11} & m_{12} & m_{13} & m_{14} & m_{15} \\ m_{12} & m_{22} & m_{23} & m_{24} & m_{25} \\ m_{13} & m_{23} & m_{33} & m_{34} & m_{35} \\ m_{14} & m_{24} & m_{34} & m_{44} & m_{45} \\ m_{15} & m_{25} & m_{35} & m_{45} & m_{55} \end{bmatrix} \right) \begin{bmatrix} 0 \\ 0 \\ 0 \\ 0 \\ 0 \end{bmatrix} \tag{29}$$

where

$$\begin{aligned}
 s_{11} &= -A_{11}\alpha^2 - A_{66}\beta^2; s_{12} = -\alpha\beta(A_{12} + A_{66}); s_{13} = B_{11}\alpha^3 + B_{12}\alpha\beta^2 + 2B_{66}\alpha\beta^2; \\
 s_{14} &= -C_{11}\alpha^2 - C_{66}\beta^2; s_{15} = -\alpha\beta(C_{12} + C_{66}); s_{22} = -A_{22}\beta^2 - A_{66}\alpha^2; \\
 s_{23} &= B_{12}\alpha^2\beta + B_{22}\beta^3 + 2B_{66}\beta\alpha^2; s_{24} = s_{15}; s_{25} = -C_{22}\beta^2 - C_{66}\alpha^2; \\
 s_{33} &= -D_{11}\alpha^4 - 2(D_{12} + 2D_{66})\alpha^2\beta^2 - D_{22}\beta^2 + N_x^0\alpha^2 + N_y^0\beta^2; \\
 s_{34} &= E_{11}\alpha^3 + E_{12}\alpha\beta^2 + 2E_{66}\alpha\beta^2; s_{35} = E_{12}\alpha^2\beta + E_{22}\beta^3 + 2E_{66}\beta\alpha^2; \\
 s_{44} &= -F_{11}\alpha^2 - F_{66}\beta^2 - H_{55}; s_{45} = -\alpha\beta(F_{12} + F_{66}); s_{55} = -F_{22}\beta^2 - F_{66}\alpha^2 - H_{44}
 \end{aligned} \tag{30a}$$

$$\begin{aligned}
 m_{11} &= m_{22} = -I_1; m_{12} = m_{15} = m_{24} = m_{45} = 0; m_{13} = I_2\alpha; \\
 m_{14} &= m_{25} = -I_4; m_{23} = I_2\beta; m_{33} = -I_1 - I_3(\alpha^2 + \beta^2); \\
 m_{34} &= I_5\alpha; m_{35} = I_5\beta; m_{44} = m_{55} = -I_6
 \end{aligned} \tag{30b}$$

The numerical results in this study are presented using the subsequent dimensionless parameters:

$$\bar{N}_{cr} = \frac{N_{cr} a^2}{\pi^2 D_0}, D_0 = \frac{E^m h^3}{12[1-(\nu^m)^2]}, \bar{\omega} = \omega \frac{b^2}{h} \sqrt{\frac{\rho_m}{E_m}} \tag{31}$$

Results and the discussion

The material properties of the CNTRC layers utilized throughout this work are provided in Table 1. (10,10) armchair SWCNTs are selected as reinforcements, and Poly{(mphenylenevinylene)-co-[(2,5-dioctoxy-p-phenylene) vinylene]}, referred to as PmPV, as the matrix. G_{13}^{CNT} and G_{23}^{CNT} are assumed to be equal to G_{12}^{CNT} .

Table 1 – Characteristics of the CNTs and the matrix

		E_1 (GPa)	E_2 (GPa)	G_{12} (GPa)	ρ (kg/m ³)	ν_{12}
CNTs	(10,10) armchair SWCNT	5.6466x103	7.08x103	1.9445x103	1400	0.175
Matrix	PmPV	2.1	2.1	0.7358	1150	0.34

The efficiency parameters η_i for the CNTs are defined in Table 2. η_3 is assumed to be equal to η_2 (Zhu et al, 2012).

Table 2 – Efficiency parameters of the CNTs

V_{CNT}^*	η_1	η_2
0.11	0.149	0.934
0.14	0.150	0.941
0.17	0.149	1.381

Buckling analysis

It is worth mentioning that the FG-V distribution type is excluded from consideration in this section. This is due to the presence of stretching-bending coupling attribute in the FG-V layer, provoked by its asymmetry, causing deflections and bending moments when the plate experiences compressive loading.

As a first step, it is crucial to verify the accuracy and efficiency of the mathematical formulation presented in earlier sections for forecasting the buckling behavior of porous laminated FG-CNTRC plates. For this purpose, a comparison is conducted between the dimensionless critical buckling load \bar{N}_{cr} of an FG-CNTRC plate obtained by the present method and those reported by Zhu et al. (2012) (HSDT), Wattanasakulpong & Chaikittiratana (2015) (TSDPT, SSDPT) and Guessas et al. (2018) (FSDT) based on various theories, as shown in Table 3. The results confirm the excellent agreement between the current results and those of previous studies.

Table 3 – Comparison of the dimensionless critical buckling load of FG-CNTRC square plates

b/h	V_{CNT}^*	Source	Uniaxial compressive load ($\gamma_x = -1; \gamma_y = 0$)			Biaxial compressive load ($\gamma_x = -1; \gamma_y = -1$)		
			UD	FG-O	FG-X	UD	FG-O	FG-X
10	0.11	HSDT	20.6814	14.4990	24.2864	10.3407	7.2495	12.1432
		TSDPT	20.6814	14.4990	24.2864	10.3407	7.2495	12.1432
		SSDPT	20.7286	14.4515	24.3943	10.3643	7.2257	12.1972
		FSDT	20.5412	14.9792	23.9594	10.2706	7.4896	11.9797
		present	20.6814	14.4990	24.2864	10.3407	7.2495	12.1432
100	0.17	TSDPT	65.0043	35.1143	94.7137	32.5021	17.5572	47.3569
		SSDPT	65.0053	35.1126	94.7163	32.5026	17.5563	47.3581
		present	65.0043	35.1143	94.7137	32.5021	17.5572	47.3569

Table 4 presents the dimensionless critical buckling load of symmetric cross-ply laminated FG-CNTRC plate with and without porosity (P) under uniaxial and biaxial compressive loading. The results reveal that porosity exerts a significant influence on the critical buckling load, which decreases considerably with an increase in porosity. This decrease is attributed to the negative effect of porosity on the rigidity of the plate. Furthermore, It can be observed that the critical buckling load is high for the FG-X distribution type and low for the FG-O distribution type. In agreement with Lei et al. (2013), it is concluded that CNTs distributed near the top and bottom surfaces of each layer outperform those distributed closer to the mid-plane in enhancing the stiffness of the laminated FG-CNTRC plate. Additionally, regarding the effect of the number of layers on the critical buckling load, it is observed that increasing the number of layers leads to an increase in the critical buckling load.

Table 4 – Effect of porosity on the dimensionless critical buckling load of the porous cross-ply laminated FG-CNTRC square plate ($b/h=10$; $V_{CNT}^* = 0.11$)

Lamination scheme	P	Uniaxial compressive load ($\gamma_x = -1; \gamma_y = 0$)			Biaxial compressive load ($\gamma_x = -1; \gamma_y = -1$)		
		UD	FG-O	FG-X	UD	FG-O	FG-X
[0°/90°/0°]	0	21.7292	20.1795	23.3611	10.8646	10.0898	11.6806
	0.1	19.5563	18.1615	21.0250	9.7781	9.0808	10.5125
	0.2	17.3833	16.1436	18.6889	8.6917	8.0718	9.3445
[0°/90°/90°/0°]	0	23.6661	22.7649	24.6746	11.8331	11.3825	12.3373
	0.1	21.2995	20.4884	22.2072	10.6500	10.2442	11.1036
	0.2	18.9329	18.2119	19.7397	9.4665	9.1060	9.8699
[0°/90°/0°/90°/0°]	0	24.9562	24.4626	25.5669	12.4781	12.2313	12.7835
	0.1	22.4606	22.0164	23.0102	11.2303	11.0082	11.5051
	0.2	19.9649	19.5701	20.4535	9.9825	9.7850	10.2268
[0°/90°/0°/90°/0°/90°/0°]	0	25.8034	25.5837	26.1409	12.9017	12.7918	13.0705
	0.1	23.2231	23.0253	23.5268	11.6115	11.5127	11.7634
	0.2	20.6427	20.4669	20.9127	10.3214	10.2335	10.4564
[0°/90°/0°/90°/0°/90°/0°/90°/0°]	0	26.1425	26.0335	26.3688	13.0712	13.0168	13.1844
	0.1	23.5282	23.4302	23.7320	11.7641	11.7151	11.8660
	0.2	20.9140	20.8268	21.0951	10.4570	10.4134	10.5475

Table 5 – Dimensionless critical buckling load of the porous cross-ply laminated FG-CNTRC square plate for different CNTs volume fractions ($b/h=10$)

V_{CNT}^*	P	Uniaxial compressive load ($\gamma_x = -1; \gamma_y = 0$)			Biaxial compressive load ($\gamma_x = -1; \gamma_y = -1$)		
		UD	FG-O	FG-X	UD	FG-O	FG-X
0.11	0	24.9562	24.4626	25.5669	12.4781	12.2313	12.7835
	0.1	22.4606	22.0164	23.0102	11.2303	11.0082	11.5051
	0.2	19.9649	19.5701	20.4535	9.9825	9.7850	10.2268
0.14	0	28.9296	28.3851	29.7241	14.4648	14.1925	14.8620
	0.1	26.0366	25.5466	26.7517	13.0183	12.7733	13.3758
	0.2	23.1437	22.7081	23.7793	11.5718	11.3540	11.8896
0.17	0	38.8356	38.2169	39.9517	19.4178	19.1084	19.9758
	0.1	34.9521	34.3952	35.9565	17.4760	17.1976	17.9783
	0.2	31.0685	30.5735	31.9613	15.5343	15.2868	15.9807

The dimensionless critical buckling load of porous symmetric cross-ply $[0^\circ/90^\circ/0^\circ/90^\circ/0^\circ]$ laminated FG-CNTRC plates for various CNTs volume fractions and different porosity volume fraction are presented in Table 5. The findings indicate that that as the volume fraction of CNTs increases, the critical buckling load rises accordingly. This is attributed to the fact that the stiffness of the laminated FG-CNTRC plate further increases by adding an extra amount of CNTs volume fraction. However, this increase becomes less significant in the presence of porosity.

Figure 2 provides the variation of the dimensionless critical buckling load of porous symmetric angle-ply laminated FG-CNTRC plates $[\theta^\circ/-\theta^\circ/\theta^\circ/-\theta^\circ/\theta^\circ]$ in relation to the variation of the CNTs orientation angle θ for different porosity volume fractions. Upon inspection of Figure 2, it is evident that the critical buckling load increases as θ changes from 0° to 45° , then decreases as θ changes from 45° to 90° , with the critical buckling loads being symmetric to $\theta = 45^\circ$. The latter presents the largest values of critical buckling load for all reinforcement types and in both uniaxial and biaxial compressive loading. Consistent with previous findings, plates with porosity exhibit low resistance against buckling compared to plates without porosity.

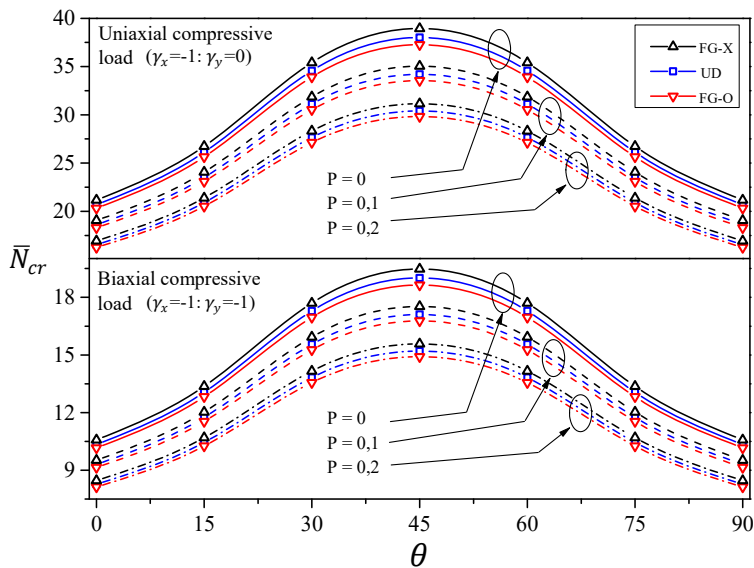


Figure 2 – Dimensionless critical buckling load of the porous angle-ply laminated FG-CNTRC square plate ($b/h=10$; $v_{CNT}^* = 0.11$)

Free vibration analysis

For free vibration analysis, numerical validation is also performed. The present method is compared with that of Huang et al. (2017) for the free vibration of anti-symmetrically laminated FG-CNTRC plates in the absence of porosity, and the results show good agreement, as illustrated in Table 6. Table 6 lists the dimensionless fundamental frequency $\bar{\omega}$ for varying patterns of the CNTs distribution, the number of layers, the CNTs volume fraction V_{CNT}^* and the width-to-thickness ratio b/h . The small variation in the lower b/h ratios is attributed to the model proposed by Huang et al. (2017), which is a four-variable FSDT.

Table 6 – Comparison of dimensionless fundamental frequencies of FG-CNTRC anti-symmetric cross-ply laminated square plates

	Source	$\frac{b}{h}$	[0°/90°/0°/90°]			[0°/90°/0°/90°/0°/90°/0°/90°]		
			V_{CNT}^*					
			0.11	0.14	0.17	0.11	0.14	0.17
UD	Present	10	14.405	15.546	17.840	15.161	16.344	18.779
		20	16.776	18.500	20.707	17.866	19.711	22.049
		50	17.696	19.701	21.810	18.943	21.122	23.340
	Huang et al. (2017)	10	14.640	15.832	18.124	15.338	16.555	18.993
		20	16.872	18.624	20.820	17.944	19.811	22.142
		50	17.714	19.726	21.831	18.958	21.142	23.358
FG-V	Present	10	14.299	15.444	17.737	15.150	16.348	18.799
		20	16.621	18.330	20.529	17.838	19.687	22.032
		50	17.518	19.498	21.597	18.906	21.081	23.303
	Huang et al. (2017)	10	14.518	15.717	17.993	15.302	16.534	18.975
		20	16.683	18.424	20.596	17.881	19.754	22.078
		50	17.495	19.484	21.565	18.883	21.065	23.271
FG-O	Present	10	14.166	15.293	17.574	15.116	16.308	18.757
		20	16.496	18.190	20.375	17.808	19.652	21.995
		50	17.396	19.362	21.448	18.878	21.050	23.269
	Huang et al. (2017)	10	14.450	15.649	17.909	15.288	16.519	18.957
		20	16.581	18.314	20.470	17.859	19.729	22.049
		50	17.378	19.354	21.421	18.856	21.036	23.238
FG-X	Present	10	14.668	15.852	18.202	15.238	16.445	18.910
		20	17.071	18.839	21.092	17.944	19.806	22.165
		50	18.003	20.054	22.204	19.019	21.211	23.445
	Huang et al. (2017)	10	14.794	16.007	18.344	15.363	16.596	19.052
		20	17.099	18.888	21.120	17.977	19.859	22.197
		50	17.975	20.032	22.165	18.995	21.193	23.411

Table 7 presents the three lowest dimensionless frequencies for symmetric cross-ply porous laminated FG-CNTRC plates with different porosity volume fractions. Upon comparing the results, it can be observed that the frequencies show weak dependence on porosity, with the frequency decreasing very slightly with the increase of porosity. The same observation can be made from Figures 4 and 5. This can be attributed to the fact that the effect of porosity on the density is as important as its effect on the rigidity of the plate. Additionally, the FG-X distribution type exhibits the largest frequencies compared to the UD, FG-V and FG-O for every mode. It is also evident that the effect of the number of layers is manifested in the increase of the frequency as the number of layers increases.

Table 7 – Effect of porosity on the dimensionless frequency of the porous cross-ply laminated FG-CNTRC square plate ($b/h = 10$; $V_{CNT}^* = 0.11$)

	P	[0°/90°/0°]				[0°/90°/0°/90°/0°]			
		UD	FG-V	FG-O	FG-X	UD	FG-V	FG-O	FG-X
1 st Mode	0	13.8958	13.6781	13.3887	14.4106	14.9041	14.9219	14.7553	15.0858
	0.1	13.8779	13.6604	13.3713	14.3919	14.8848	14.9026	14.7362	15.0662
	0.2	13.8555	13.6383	13.3498	14.3687	14.8608	14.8786	14.7124	15.0419
2 nd Mode	0	20.8993	20.0286	19.2837	22.2633	26.8626	26.9065	26.5834	27.2181
	0.1	20.8722	20.0027	19.2588	22.2344	26.8278	26.8716	26.5490	27.1828
	0.2	20.8386	19.9704	19.2277	22.1985	26.7845	26.8283	26.5062	27.1390
3 rd Mode	0	33.2531	32.8548	32.0150	34.4913	33.7417	33.8055	33.3006	34.2971
	0.1	33.2100	32.8123	31.9736	34.4466	33.6980	33.7617	33.2575	34.2527
	0.2	33.1564	32.7594	31.9220	34.3909	33.6436	33.7072	33.2038	34.1974
		[0°/90°/0°/90°/0°/90°/0°]				[0°/90°/0°/90°/0°/90°/0°/90°/0°]			
1 st Mode	0	15.1576	15.1748	15.0925	15.2564	15.2578	15.2748	15.2257	15.3237
	0.1	15.1379	15.1552	15.0729	15.2367	15.2381	15.2551	15.2060	15.3039
	0.2	15.1135	15.1307	15.0486	15.2121	15.2135	15.2304	15.1814	15.2792
2 nd Mode	0	28.5479	28.5952	28.4286	28.7590	29.4004	29.4495	29.3453	29.5527
	0.1	28.5109	28.5581	28.3918	28.7217	29.3624	29.4114	29.3073	29.5144
	0.2	28.4649	28.5121	28.3460	28.6754	29.3150	29.3639	29.2600	29.4668
3 rd Mode	0	33.6851	33.7463	33.4966	33.9928	33.4966	33.5563	33.4098	33.7017
	0.1	33.6415	33.7026	33.4532	33.9488	33.4533	33.5128	33.3665	33.6580
	0.2	33.5872	33.6482	33.3992	33.8940	33.3993	33.4588	33.3127	33.6037

Figure 3 depicts the effect of porosity on the amplitude of a four layered unidirectional [0°/0°/0°/0°] porous laminated FG-CNTRC plate in

different modes of vibration. It is clear that the results are almost identical in terms of values for all modes of vibration.

Thus, we can state that porosity has a negligible effect on the amplitude of the plate.

This result further confirms the weakening effect of porosity on the free vibration response of the laminated FG-CNTRC plate.

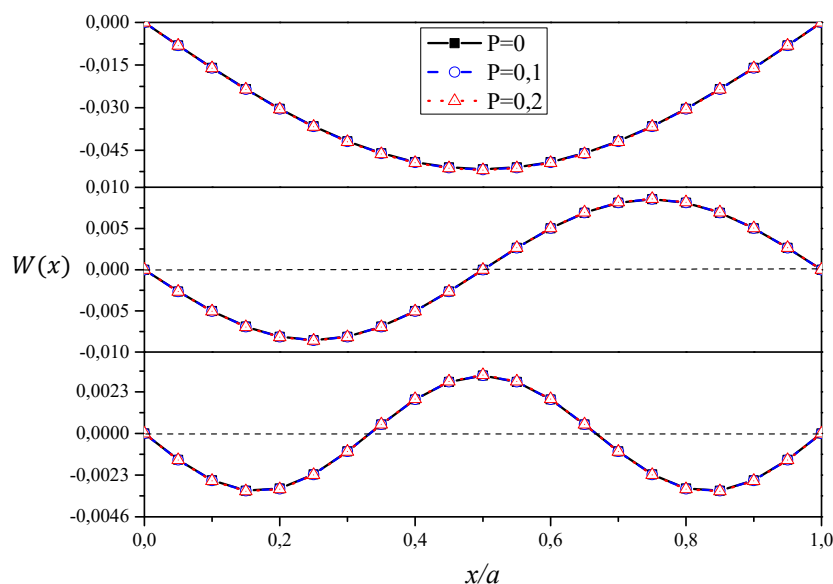


Figure 3 – Amplitude of the unidirectional porous laminated FG-CNTRC square plate ($b/h=10$; $V_{CNT}^*=0.11$)

The variation in the dimensionless fundamental frequency of porous anti-symmetric cross-ply laminated FG-CNTRC plates $[0^\circ/90^\circ/0^\circ/90^\circ]$ with respect to the variation of the CNTs volume fraction and the porosity volume fraction is depicted in Figure 4.

It is noticeable that the increase in the CNTs volume fraction leads to a significant increase in the fundamental frequency for all CNTs distribution types.

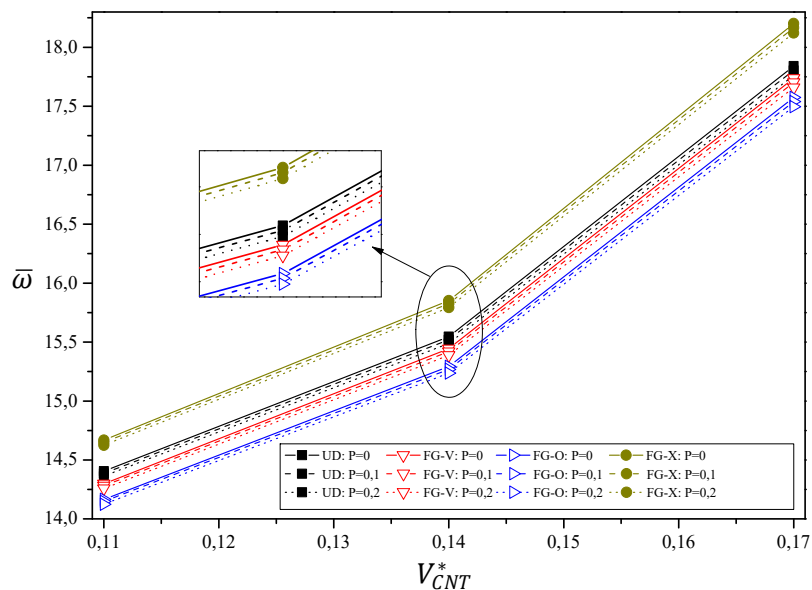


Figure 4 – Variation of the dimensionless frequency of the four layered porous anti-symmetric cross-ply laminated FG-CNTRC square plate in the function of the variation of the CNTs volume fraction ($b/h = 10$)

Figure 5 presents the variation of the dimensionless fundamental frequency of the anti-symmetric angle-ply laminated FG-CNTRC plate [$\theta^\circ / -\theta^\circ / \theta^\circ / -\theta^\circ$] in relation to the variation of the CNTs orientation angle (θ) for different porosity volume fractions.

The fundamental frequency increases as θ changes from 0° to 45° , then decreases as θ changes from 45° to 90° , in which the fundamental frequencies are symmetric to $\theta = 45^\circ$. This last mentioned value ($\theta = 45^\circ$) presents the largest values of fundamental frequency for all cases.

According to the above investigations, it can be noticed that porosity has a low impact on the frequency of laminated FG-CNTRC plates compared to the effects of the other parameters.

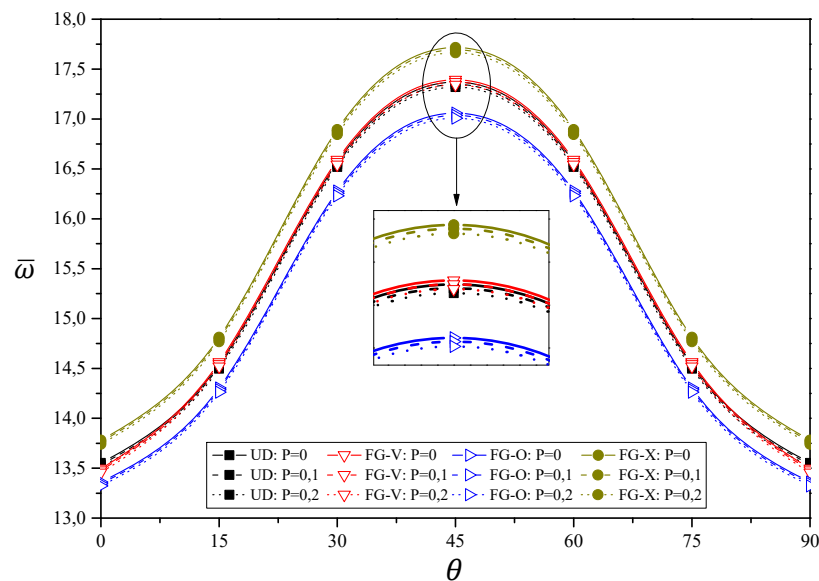


Figure 5 – Dimensionless frequency of the porous angle-ply laminated FG-CNTRC square plate ($b/h = 10$; $V_{CNT}^* = 0.11$)

The minimal influence of porosity on the plate's amplitude and frequency across various vibration modes suggests the resilient nature of the laminated FG-CNTRC plate structure to porosity effects. While porosity typically alters material stiffness, the specific arrangement of composite layers in this case seems to counteract such effects. Consistently uniform results imply effective mitigation of porosity-induced changes in amplitude and frequency by the plate's design and material composition. This highlights the robustness of the laminated FG-CNTRC plate against porosity-induced variations in vibrational characteristics, further confirming its weakened free vibration response due to porosity.

Conclusion

In this paper, the buckling and free vibration of laminated FG-CNTRC plates in the presence of porosity are analytically examined. A mathematical model based on a five-unknown HSDT is developed. The assumption is made that the laminates consist of layers that are perfectly bonded, with carbon nanotubes (CNTs) distributed throughout the thickness of each layer, accounting for different types of FG distributions.

The effective material properties are determined using the extended rule of mixture considering an upper limit of the impact of porosity. The accuracy of the present formulation has been validated, and detailed parametric studies have been conducted to examine the effects of several parameters on the critical buckling load and natural frequency of porous laminated FG-CNTRC plates. Some typical conclusions are noted:

- In terms of porosity, it is found that porosity has a considerable negative effect on the critical buckling load.
- Porosity has a weak effect on the free vibration characteristics.
- Increasing the CNTs volume fraction enhances plate rigidity. The enhancement becomes less significant in the presence of porosity.
- For the CNTs distribution type, it is derived that reinforcements distributed near the top and bottom surfaces of the layer outperform those distributed closer to the mid-plane in enhancing the stiffness of the plate.
- The number of layers significantly impacts the responses to free vibration and buckling. The critical buckling load and natural frequency rise in proportion to the increase in the number of layers.
- The lamination angle significantly influences both the critical buckling load and natural frequency. Because of the axial symmetry of the laminated square plate orientations at 45°, any changes in these properties are also symmetrical.

In future works, it would be beneficial to explore the influence of environmental conditions on laminated FG-CNTRC plates' mechanical properties and durability. Additionally, investigating dynamic responses under various loading conditions and conducting experimental validation could enhance reliability. Exploring advanced manufacturing techniques and novel materials could also improve performance and expand application possibilities.

References

Alimoradzadeh, M., Heidari, H., Tornabene, F. & Dimitri, R. 2023. Thermo-Mechanical Buckling and Non-Linear Free Oscillation of Functionally Graded Fiber-Reinforced Composite Laminated (FG-FRCL) Beams. *Applied Sciences*, 13(8), art.number:4904. Available at: <https://doi.org/10.3390/app13084904>.

Arani, A.G., Kiani, F. & Afshari, H. 2021. Free and forced vibration analysis of laminated functionally graded CNT-reinforced composite cylindrical panels. *Journal of Sandwich Structures & Materials*, 23(1), pp.255-278. Available at: <https://doi.org/10.1177/1099636219830787>.

Chiker, Y., Bachene, M., Attaf, B., Hafaifa, A. & Guemana, M. 2023. Uncertainty influence of nanofiller dispersibilities on the free vibration behavior of multi-layered functionally graded carbon nanotube-reinforced composite laminated plates. *Acta Mechanica*, 234(4), pp.1687-1711. Available at: <https://doi.org/10.1007/s00707-022-03438-6>.

Ciriscioli, P.R., Springer, G.S. & Lee, W.I. 1991. An Expert System for Autoclave Curing of Composites. *Journal of Composite Materials*, 25(12), pp.1542-1587. Available at: <https://doi.org/10.1177/002199839102501201>.

Daikh, A.A., Belarbi, M.-O., Salami, S.J., Ladmek, M., Belkacem, A., Houari, M.S.A., Ahmed, H.M. & Eltahir, M.A. 2023. A three-unknown refined shear beam model for the bending of randomly oriented FG-CNT/fiber-reinforced composite laminated beams rested on a new variable elastic foundation. *Acta Mechanica*, 234(10), pp.5171-5186. Available at: <https://doi.org/10.1007/s00707-023-03657-5>.

Fu, T., Chen, Z., Yu, H., Wang, Z. & Liu, X. 2019. Mechanical behavior of laminated functionally graded carbon nanotube reinforced composite plates resting on elastic foundations in thermal environments. *Journal of Composite Materials*, 53(9), pp.1159-1179. Available at: <https://doi.org/10.1177/0021998318796170>.

Guessas, H., Zidour, M., Meradjah, M. & Tounsi, A. 2018. The critical buckling load of reinforced nanocomposite porous plates. *Structural Engineering and Mechanics*, 67(2), pp.115-123. Available at: <https://doi.org/10.12989/sem.2018.67.2.115>.

Hagstrand, P.-O., Bonjour, F. & Månson, J.-A.E. 2005. The influence of void content on the structural flexural performance of unidirectional glass fibre reinforced polypropylene composites. *Composites Part A: Applied Science and Manufacturing*, 36(5), pp.705-714. Available at: <https://doi.org/10.1016/j.compositesa.2004.03.007>.

Hayashi, T. & Takahashi, J. 2017. Influence of void content on the flexural fracture behaviour of carbon fiber reinforced polypropylene. *Journal of Composite Materials*, 51(29), pp.4067-4078. Available at: <https://doi.org/10.1177/0021998317698215>.

Hernández, S., Sket, F., Molina-Aldaregui, J.M., González, C. & LLorca, J. 2011. Effect of curing cycle on void distribution and interlaminar shear strength in polymer-matrix composites. *Composites Science and Technology*, 71(10), pp.1331-1341. Available at: <https://doi.org/10.1177/0021998317698215>.

Huang, B., Guo, Y., Wang, J., Du, J., Qian, Z., Ma, T. & Yi, L. 2017. Bending and free vibration analyses of antisymmetrically laminated carbon nanotube-reinforced functionally graded plates. *Journal of Composite Materials*, 51(22), pp.3111-3125. Available at: <https://doi.org/10.1177/0021998316685165>.

Kirchhoff, G. 1850. Über das Gleichgewicht und die Bewegung einer elastischen Scheibe. *Journal für die reine und angewandte Mathematik (Crelles Journal)*, 1850(40), pp.51-88. Available at: <https://doi.org/10.1515/crll.1850.40.51>.

Kwon, H., Bradbury, C.R. & Leparoux, M. 2011. Fabrication of Functionally Graded Carbon Nanotube-Reinforced Aluminum Matrix Composite. *Advanced Engineering Materials*, 13(4), pp.325-329. Available at: <https://doi.org/10.1002/adem.201000251>.

Lee, J., Kim, J. & Hyeon, T. 2006. Recent Progress in the Synthesis of Porous Carbon Materials. *Advanced Materials*, 18(16), pp.2073-2094. Available at: <https://doi.org/10.1002/adma.200501576>.

Lei, Z.X., Liew, K.M. & Yu, J.L. 2013. Buckling analysis of functionally graded carbon nanotube-reinforced composite plates using the element-free kp-Ritz method. *Composite Structures*, 98, pp.160-168. Available at: <https://doi.org/10.1016/j.compstruct.2012.11.006>.

Lei, Z.X., Zhang, L.W. & Liew, K.M. 2018. Modeling large amplitude vibration of matrix cracked hybrid laminated plates containing CNTR-FG layers. *Applied Mathematical Modelling*, 55, pp.33-48. Available at: <https://doi.org/10.1016/j.apm.2017.10.032>.

Liew, K.M., Lei, Z.X. & Zhang, L.W. 2015. Mechanical analysis of functionally graded carbon nanotube reinforced composites: A review. *Composite Structures*, 120, pp.90-97. Available at: <https://doi.org/10.1016/j.compstruct.2014.09.041>.

Ma, R. & Jin, Q. 2023. Free Vibration Analysis of Functionally Graded Graphene-Reinforced Composite-Laminated Plates. *Journal of Aerospace Engineering*, 36(3), art.ID:04023016. Available at: <https://doi.org/10.1061/JAEEZ.ASENG-4657>.

Madsen, B. & Lilholt, H. 2003. Physical and mechanical properties of unidirectional plant fibre composites—an evaluation of the influence of porosity. *Eco-Composites*, 63(9), pp.1265-1272. Available at: [https://doi.org/10.1016/S0266-3538\(03\)00097-6](https://doi.org/10.1016/S0266-3538(03)00097-6).

Madsen, B., Thygesen, A. & Lilholt, H. 2009. Plant fibre composites – porosity and stiffness. *Composites Science and Technology*, 69(7), pp.1057-1069. Available at: <https://doi.org/10.1016/j.compscitech.2009.01.016>.

Malekzadeh, P. & Shojaei, M. 2013. Buckling analysis of quadrilateral laminated plates with carbon nanotubes reinforced composite layers. *Thin-Walled Structures*, 71, pp.108-118. Available at: <https://doi.org/10.1016/j.tws.2013.05.008>.

Mantari, J.L., Oktem, A.S. & Guedes Soares, C. 2012. A new trigonometric shear deformation theory for isotropic, laminated composite and sandwich plates. *International Journal of Solids and Structures*, 49(1), pp.43-53. Available at: <https://doi.org/10.1016/j.ijsolstr.2011.09.008>.

Medani, M., Benahmed, A., Zidour, M., Heireche, H. & Tounsi, A. 2019. Static and dynamic behavior of (FG-CNT) reinforced porous sandwich plate using energy principle. *Steel and Composite Structures*, 32(5), pp.595-610. Available at: <https://doi.org/10.12989/scs.2019.32.5.595>.

Mehdikhani, M., Gorbatikh, L., Verpoest, I. & Lomov, S.V. 2019. Voids in fiber-reinforced polymer composites: A review on their formation, characteristics, and effects on mechanical performance. *Journal of Composite Materials*, 53(12), pp.1579-1669. Available at: <https://doi.org/10.1177/0021998318772152>.

Mindlin, R.D. 1951. Influence of rotatory inertia and shear on flexural motions of isotropic, elastic plates. *Journal of Applied Mechanics*, 18(1), pp.31-38. Available at: <https://doi.org/10.1115/1.4010217>.

Phani, K.K. & Niyogi, S.K. 1987. Young's modulus of porous brittle solids. *Journal of Materials Science*, 22(1), pp.257-263. Available at: <https://doi.org/10.1007/BF01160581>.

Reddy, J.N. 1984. A Simple Higher-Order Theory for Laminated Composite Plates. *Journal of Applied Mechanics*, 51(4), pp.745-752. Available at: <https://doi.org/10.1115/1.3167719>.

Sayyad, A.S. & Ghugal, Y.M. 2015. On the free vibration analysis of laminated composite and sandwich plates: A review of recent literature with some numerical results. *Composite Structures*, 129, pp.177-201. Available at: <https://doi.org/10.1016/j.compstruct.2015.04.007>.

Shen, H.S. 2009. Nonlinear bending of functionally graded carbon nanotube-reinforced composite plates in thermal environments. *Composite Structures*, 91(1), pp.9-19. Available at: <https://doi.org/10.1016/j.compstruct.2009.04.026>.

Shimpi, R.P., Arya, H. & Naik, N.K. 2003. A Higher Order Displacement Model for the Plate Analysis. *Journal of Reinforced Plastics and Composites*, 22(18), pp.1667-1688. Available at: <https://doi.org/10.1177/073168403027618>.

Stamopoulos, A.G., Tserpes, K.I., Průcha, P. & Vavřík, D. 2016. Evaluation of porosity effects on the mechanical properties of carbon fiber-reinforced plastic unidirectional laminates by X-ray computed tomography and mechanical testing. *Journal of Composite Materials*, 50, pp.2087-2098. Available at: <https://doi.org/10.1077/0021998315602049>.

Thai, H.-T. & Choi, D.-H. 2011. A refined plate theory for functionally graded plates resting on elastic foundation. *Composites Science and Technology*, 71(16), pp.1850-1858. Available at: <https://doi.org/10.1016/j.compscitech.2011.08.016>.

Thai, H.-T. & Vo, T.P. 2013. A new sinusoidal shear deformation theory for bending, buckling, and vibration of functionally graded plates. *Applied Mathematical Modelling*, 37(5), pp.3269-3281. Available at: <https://doi.org/10.1016/j.apm.2012.08.008>.

Tran, H.Q., Vu, V.T., Tran, M.T. & Nguyen-Tri, P. 2020. A new four-variable refined plate theory for static analysis of smart laminated functionally graded carbon nanotube reinforced composite plates. *Mechanics of Materials*, 142, art.number:103294. Available at: <https://doi.org/10.1016/j.mechmat.2019.103294>.

Wattanasakulpong, N. & Chaikittiratana, A. 2015. Exact solutions for static and dynamic analyses of carbon nanotube-reinforced composite plates with Pasternak elastic foundation. *Applied Mathematical Modelling*, 39(18), pp.5459-5472. Available at: <https://doi.org/10.1016/j.apm.2014.12.058>.

Zhang, L.W. & Selim, B.A. 2017. Vibration analysis of CNT-reinforced thick laminated composite plates based on Reddy's higher-order shear deformation theory. *Composite Structures*, 160, pp.689-705. Available at: <https://doi.org/10.1016/j.compstruct.2016.10.102>.

Zhu, P., Lei, Z.X. & Liew, K.M. 2012. Static and free vibration analyses of carbon nanotube-reinforced composite plates using finite element method with first order shear deformation plate theory. *Composite Structures*, 94(4), pp.1450-1460. Available at: <https://doi.org/10.1016/j.compstruct.2011.11.010>.

Investigación analítica sobre el pandeo y la vibración libre de placas laminadas porosas FG-CNTRC

Tahir Ghazoul^a, **autor de correspondencia**, Mohamed Atif Benatta^a, Abdelwahhab Khatir^b, Youcef Beldjelili^a, Baghdad Krour^a, Mohamed Bachir Bouiadja^a

^a Universidad de Djillali Liabes, Laboratorio de Estructuras y Materiales Avanzados en Ingeniería Civil y Obras Públicas, Sidi Bel Abbes, República Argelina Democrática y Popular,

^b Universidad Politécnica de Marche, Sección Estructural DICEA, Ancona, República Italiana

CAMPO: mecánica, materiales

TIPO DE ARTÍCULO: artículo científico original

Resumen:

Introducción/objetivo: El objetivo de este estudio es examinar el comportamiento de pandeo y vibración libre de las placas compuestas laminadas, reforzadas con nanotubos de carbono cuando se tienen en cuenta varias fuentes de incertidumbre, siendo el enfoque principal la existencia de porosidad.

Métodos: Se desarrolla un modelo de placa laminada porosa utilizando la teoría de la deformación por corte de alto orden. Se investigan diferentes configuraciones de nanotubos de carbono de pared simple alineados y funcionalmente graduados en todo el espesor de cada capa. Las propiedades efectivas de los materiales se evalúan a través de la regla extendida de mezcla mientras se considera un límite superior para el efecto de la porosidad. Las ecuaciones que rigen se derivan y resuelven utilizando el principio de trabajo virtual y el enfoque de Navier. La validez de la formulación actual se confirma comparando nuestros resultados con los datos existentes de fuentes bibliográficas. Se investiga en detalle el impacto de numerosos parámetros como la porosidad, la fracción de volumen de nanotubos de carbono, los tipos de distribución de refuerzo, el esquema de laminación y el número de capas en las respuestas de pandeo y vibración libre.

Resultados: Un hallazgo clave de este estudio es la reducción significativa en la resistencia al pandeo de las placas laminadas FG-CNTRC debido a la porosidad, en contraste con el impacto menor en la respuesta de vibración libre.

Conclusión: Los resultados de este artículo enfatizan el papel crítico de la porosidad en la integridad estructural y brindan nuevos conocimientos sobre el comportamiento de los materiales compuestos avanzados.

Palabras claves: pandeo, vibración libre, placa compuesta laminada, porosidad, material funcionalmente graduado, nanotubos de carbono.

Аналитическое исследование изгиба и свободной вибрации пористых слоистых пластин FG-CNTRC

Тахир Газул^а, **корреспондент**, Мухаммед Атиф Бената^а,
Абделвахаб Катир^б, Йусуф Белджелили^а,
Багдад Кроур^а, Мухаммед Башир Бујажера^а

^а Университет Джиллали Лиабес, Лаборатория конструкций и современных материалов в гражданском строительстве и общественных работах,
г. Сиди-Бель-Аббес, Алжирская Народно-Демократическая Республика

^б Политехнический университет Марке, структурное подразделение DICEA, г. Анкона, Итальянская Республика

РУБРИКА ГРНТИ: 30.19.00 Механика деформируемого твердого тела,
81.09.00 Материаловедение

ВИД СТАТЬИ: оригинальная научная статья

Резюме:

Введение/цель: Целью данного исследования является изучение изгиба и свободной вибрации многослойных композитных пластин, армированных углеродными нанотрубками, при учете различных источников неопределенности с акцентом на наличие пористости.

Методы: Модель многослойной пористой пластины разработана с применением теории сдвиговой деформации высокого порядка. Исследовались различные конфигурации функционально упорядоченных выровненных одностенных углеродных нанотрубок по толщине каждого слоя. Эффективные свойства материалов оцениваются с помощью расширенного правила смешивания с учетом верхнего предела пористости. Управляющие уравнения получены и решены с помощью принципа виртуальной работы и подхода Навье. Обоснованность этой формулировки подтверждается сравнением результатов с данными из существующих научных источников. Подробно исследовано влияние многочисленных параметров, таких как пористость, объемная доля углеродных нанотрубок, виды распределения армирования, схема ламинирования и количество слоев на изгибе и реакция на свободную вибрацию.

Результаты: Ключевым выводом данного исследования является значительное снижение сопротивления

ламинированных пластин FG-CNTRC на изгиб из-за их пористости, в отличие от незначительного влияния на отклик на свободную вибрацию.

Выводы: Результаты данной статьи подчеркивают критическую роль пористости в целостности структуры и дают новое представление о поведении современных композитных материалов.

Ключевые слова: изгиб, свободная вибрация, многослойная композитная пластина, пористость, функционально распределенный материал, углеродные нанотрубки.

Аналитичко испитивање порозних ламинираних плоча од функционално градираних композита ојачаних угљеничним наноцевима (FG-CNTRC) на извијање и слободне вибрације

Тахир Газул^а, аутор за преписку, Мухамед Атиф Бената^а, Абделвахаб Катир^б, Јусуф Белцелили^а, Багдад Кроур^а, Мухамед Башир Бујаџера^а

^а Универзитет Ђилали Лиабес, Лабораторија за напредне конструкције и материјале у грађевинарству и јавним радовима, Сиди Бел Абес, Народна Демократска Република Алжир

^б Политехнички универзитет Марке, Структурни одсек DICEA, Анкона, Република Италија

ОБЛАСТ: механика, материјали
КАТЕГОРИЈА (ТИП) ЧЛАНКА: оригинални научни рад

Сажетак:

Увод/циљ: Циљ ове студије јесте да испита понашање ламинираних композитних плоча ојачаних угљеничним наноцевима при извијању и слободним вибрацијама када се узимају у обзир различити извори несигурности и када је фокус на постојању порозности.

Метод: Модел порозне ламиниране плоче развијен је помоћу смицајне деформационе теорије вишег реда. Испитане су различите конфигурације функционално градираних угљеничних наноцеви с једноструким зидом, поређаних целом дебелином сваког слоја. Ефективна својства материјала процењена су кроз проширено правило о смешама, узимајући у обзир горњу границу ефекта порозности. Водеће једначине изведене су и решене помоћу принципа виртуалног рада и Навијеровог приступа. Валидност наведене формулације потврђена је поређењем добијених резултата са подацима из постојеће литературе. Детаљно је испитан утицај бројних параметара попут порозности, запреминског удела угљеничних наноцеви, типова дистрибуције

ојачања, шеме ламинације, као и броја слојева на извијање и одговора на слободне вибрације.

Резултати: Кључни налаз ове студије јесте да је знатно смањена отпорност на извијање ламинираних FG-CNTRC плоча услед порозности, за разлику од минорног утицаја на одговор на слободне вибрације.

Закључак: Резултати овог рада истичу критичну улогу порозности у интегритету структуре и пружају нове увиде у понашање напредних композитних материјала.

Кључне речи: извијање, слободна вибрација, ламинирана композитна плоча, порозност, функционално градиран материјал, угљеничне наноцеви.

Paper received on: 15.04.2024.

Manuscript corrections submitted on: 24.09.2024.


Paper accepted for publishing on: 25.09.2024.


© 2024 The Authors. Published by Vojnotehnički glasnik / Military Technical Courier (www.vtg.mod.gov.rs, втг.мо.упр.срб). This article is an open access article distributed under the terms and conditions of the Creative Commons Attribution license (<http://creativecommons.org/licenses/by/3.0/rs/>).




Forced dynamic analysis of functionally graded beams under harmonic moving loads on elastic foundation with the finite element method

Amine Zemri^a, Ismail Mechab^b

^a University of Relizane,
Civil Engineering and Public Works Department,
Relizane, People's Democratic Republic of Algeria;
University of Sidi Bel Abbes,
Civil Engineering and Environmental Laboratory,
Sidi Bel Abbes, People's Democratic Republic of Algeria,
e-mail: amine.btp@hotmail.fr, **corresponding author**,
ORCID iD:  <https://orcid.org/0000-0001-7995-6248>

^b University of Sidi Bel Abbes,
Civil Engineering and Public Works Department,
Statistics and Stochastic Processes Laboratory,
Sidi Bel Abbes, People's Democratic Republic of Algeria,
e-mail: ismail.mechab@gmail.com,
ORCID iD:  <https://orcid.org/0009-0004-4922-6980>

 <https://doi.org/10.5937/vojtehg72-50200>

FIELD: mechanical engineering, materials
ARTICLE TYPE: original scientific paper

Abstract:

Introduction/purpose: This paper presents a numerical study of the forced dynamic behavior of a functionally graded beam subjected to a harmonically varying transversely concentrated moving force using a higher-order shear deformation theory.

Methods: The governing equations are derived using Hamilton's principle. These equations are then transformed into the weak form using the Galerkin method. The problem is solved using the finite element method by developing a three-node finite element with four degrees of freedom per node. The Newmark beta method is chosen for the time integration and the Gauss method for the spatial integration.

Results: The effects of several parameters were investigated, including the slenderness ratio, the material index, foundation stiffness, velocity and the frequency of the moving load. Good agreement was observed with the results obtained from the literature.

Conclusion: This study illustrates the importance of using a higher order theory in the case of short beams and clearly shows the change in the behavior of the FGM beam as a function of different parameters.

Key words: higher-order shear deformation theory, functionally graded material, finite element method, moving load, Newmark beta method.

Introduction

Due to their importance, functionally graded materials (FGMs) have attracted the attention of many researchers around the world (Reddy, 2007; Mena et al, 2012; Zemri et al, 2015; Berrabah & Boudarba, 2023). These new materials were initially created with the aim of using them as thermal barriers in high-temperature environments (Fuchiyama & Noda, 1995; Praveen & Reddy, 1998). Today, they are used in a wide range of engineering fields, including aerospace, nuclear energy, biology, electromagnetism, optics, energy and other fields through the ingenious combination of two or more materials such as metals, ceramics, and plastics (Saleh et al, 2020).

Literature related to this field is significant, including studies of bending, buckling, and free vibration (Dey et al, 2019). These studies have utilized various resolution methods, especially numerical and analytical techniques. Each of these two main methods has its advantages and disadvantages. The finite element method is one of the most widely used numerical methods for structural analysis because it offers both ease of programming and adaptability. One program can be used to solve a variety of problems with minimal changes, making it a highly efficient and flexible tool.

Extensive research has been conducted on the dynamic behavior of the FGM structures. Yang et al. (2008) conducted an analytical investigation on the vibrational behavior of Euler-Bernoulli beams with open edge cracks and exponential through-thickness variation in material properties. They considered the effects of axial compressive force and concentrated transverse load, and obtaining analytical solutions for natural frequencies and dynamic deflections of different boundary conditions beam types with exponential through-thickness variation in material properties. Şimşek & Kocatürk (2009) investigated the free vibration and dynamic behavior of a simply supported functionally graded beam under a concentrated moving harmonic load. Lagrange's equations, Euler-Bernoulli beam theory, and polynomial trial functions are employed to derive the equations of motion. Hasheminejad & Rafsanjani (2009) presented a precise three-dimensional analysis of the steady-state dynamic response of an arbitrarily thick, isotropic, and functionally graded plate strip under a transverse moving line load. Utilizing the Fourier transformation and a laminate model, Khalili et al. (2010) introduced a mixed method for analyzing the dynamic behavior of functionally graded

beams under moving loads. Utilizing Euler–Bernoulli beam theory and Lagrange equations, the Rayleigh–Ritz method discretizes spatial derivatives, while a step-by-step differential quadrature method (DQM) handles temporal derivatives. The proposed method demonstrated efficiency and reliability, providing improved accuracy compared to single-step methods like Newmark and Wilson. Şimşek (2010) investigated vibration of a functionally graded simply-supported beam, influenced by a moving mass using Euler–Bernoulli, Timoshenko, and third-order shear deformation beam theories. Yan et al. (2011) explored the dynamic response of functionally graded beams with an open-edge crack on an elastic foundation, subjected to a transverse load moving at a constant speed. Yan & Yang (2011) studied the forced flexural vibration of functionally graded beams with open-edge cracks under axial compressive force and moving transverse load, where the cracked section was modeled as a rotational spring and the vibration responses were determined using the modal series expansion technique. Le et al. (2014) developed a finite element procedure for analyzing the vibration of multi-span functionally graded material (FGM) beams under a moving harmonic load. The finite element formulation incorporated the exact solution of the FGM Timoshenko beam segment's governing differential equations, considering the shift in the neutral axis position. Malekzadeh & Monajjemzadeh (2016) explored the dynamic response of functionally graded (FG) beams in a thermal environment under the influence of a moving load, employing the first-order shear deformation theory (FSDT). Initial thermal stresses are determined through the solution of thermoelastic equilibrium equations. A finite element method solution procedure is developed for FG beams with various loading and boundary conditions. Lin & Lee (2016) predicted the instability and vibration of a concentrated mass moving along a curved beam. While the existing literature commonly approximates the moving mass model using the moving load model, this paper introduces a semi-analytical method for the moving mass problem and compares it with the traditional model. Wang et al. (2017) introduced a novel N-node weak form quadrature beam element, based on the physical neutral surface. Explicit formulas for stiffness and mass matrices computation are provided. This element is applied to analyze the dynamic behavior of functionally graded material beams subjected to a moving point load. Gan et al. (2017) explored the effects of an intermediate elastic support on the vibration behavior of functionally graded Euler-Bernoulli beams that are subjected to a moving point load. To analyze the dynamic responses, a finite element model is utilized, while a thorough examination of the stiffness and position of the elastic support sheds light on their impact on the dynamic

characteristics of the functionally graded material beams. Barati & Zenkour (2018) examined the behavior of forced vibration in functionally graded nanobeams, which is dependent on their size. This behavior occurs under in-plane hygro-thermal loading and lateral dynamic loads. By utilizing a higher-order refined beam theory that does not incorporate shear correction factors, the nanobeam interacts with a foundation that follows the three-parameter Kerr model. Beskou & Muho (2018) have studied analytically and numerically the dynamic response of a simply supported elastic beam on a Winkler-type elastic foundation with viscous damping to a harmonically varying, moving point load. Parametric assessments include the effects of foundation stiffness, damping, beam damping, and load acceleration, providing practical insights for various scenarios. Barati et al. (2019) explored the forced vibrations of nanobeams under the nonlocal strain gradient theory on a viscoelastic substrate subjected to moving loads. The nanobeam experiences varied hygro-thermal environments. Dynamic deflections were obtained using Galerkin and inverse Laplace transform methods. The influence of nonlocal parameter, strain gradient, moving load, temperature, moisture, and viscoelastic foundation on forced vibration behavior were discussed. Esen (2019) studied an improved Finite Element Method for analyzing transverse vibrations in Timoshenko beams made of functionally graded materials on a two-parameter foundation, under the influence of a variable-velocity moving mass. The investigation thoroughly explores the effects of inertia, foundation parameters, and material constituents, revealing significant changes in dynamic behavior shaped by frequency variations in the system. El Khouddar et al. (2024) analyzed gradient materials with piezoelectric actuators using the Euler–Bernoulli beam theory and the nonlinear Von-Karman deformation field. Analytical predictions for nonlinear free and forced vibrations of a beam on an elastic foundation were validated against the existing literature. Li et al. (2021) proposed an efficient method for accurate free vibration analysis of functionally graded beams with variable cross-sections on Pasternak elastic foundations. Utilizing the separate variable method and the Laplace transform, they provided general expressions for displacements and stresses, validated through various examples, offering a precise alternative for ultra-high precision requirements in mechanical systems. Esen et al. (2023) investigated the dynamic responses of Timoshenko beams with symmetric and sigmoid functionally graded gradations, resting on an elastic foundation and subjected to a moving mass. Using the Hamilton principle, system equations are derived and solved with a finite element method. Parametric studies explore influences of gradation type, index, elastic

foundation stiffness, inertia, and variable velocity of the moving mass. Javidi et al. (2023) presented an analytical study using the Optimal Homotopy Analysis Method and enriched multiple scales to investigate the dynamics of a beam with a moving mass and resting on a viscoelastic foundation. The authors considered a fifth-order nonlinear term to account for the bending vibration of the flexible beam and use the Galerkin method to form the corresponding ordinary differential equation. He et al. (2023) investigated the vibration of a cylindrical beam made of functionally graded materials under thermal conditions, validating the theoretical model against the finite element analysis. The displacement function was built using Carrera unified formulation, Taylor polynomials, and the improved Fourier series method. Guo et al. (2022) presented the dynamic analysis of exponentially functionally graded material micro plates with porosities. Utilizing the general third-order shear deformation theory and a modified couple stress theory, the research investigated the forced vibration response to accelerating moving loads. Safaei et al. (2024) investigated the out-of-plane free vibrational behaviors and responses to moving loads of sandwich-curved beams with graphene platelets reinforced composite face sheets and porous core (GPLRC-FS-PC). By employing the first-order shear deformation theory, the differential quadrature method, and Newmark's method, this study investigates the impacts of GPLs on the fundamental frequency and displacement amplitudes. It specifically accentuates the dependencies on distribution patterns as well as the ratio between the face sheet and the core thickness.

From this literature review, it is noted that a higher-order shear theory is rarely used to study the dynamic behavior of FGM beams under the effect of moving loads. In this context, the objective of this work is to present a three-node finite element model to study the dynamic behavior of an FGM beam under the effect of a harmonic moving load and on an elastic foundation, using a higher-order shear theory. Hamilton's principle is used to find the differential equations governing the behavior of the beam. Galerkin's method is used to transform the strong formulation into a weak one. Spacial integration is then performed using the Gauss method, and the Newmark beta method is used for time integration.

Mathematical modeling

Properties of functionally graded materials

This study examines a beam with dimensions of length (L), thickness (h), and width (b) within the conventional Cartesian coordinate system (x ,

y, z), as illustrated in Figure 1. Herein, the longitudinal direction is denoted by x , and the vertical transverse direction is represented by z .

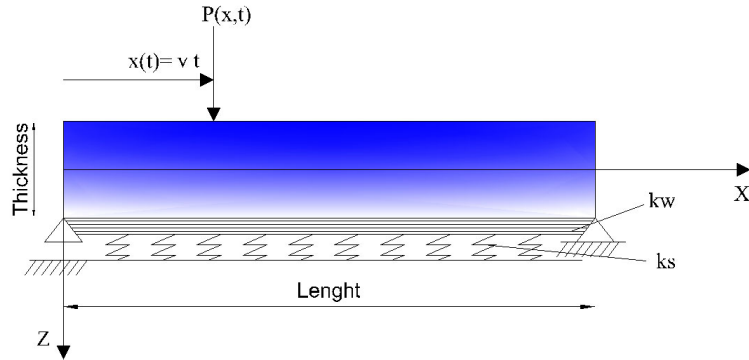


Figure 1 – FGM beam on a two-parameter linear elastic foundation subjected to a moving load

The material properties of the beam are assumed to be varied in the direction of thickness, in accordance with a polynomial function. These properties of each point in the beam can be written as a function of the volume fractions of each material constituting the beam under the following law:

$$P(z) = P_c V_c + P_m V_m \quad (1)$$

The mechanical property ' P ' can be Young's modulus or mass density. The volume fraction of each material is denoted by ' V ', with the subscripts ' c ' and ' m ' representing ceramic and metal components, respectively. The relationship between the fractions of metal and ceramic is expressed in the following manner (Ebrahimi & Jafari, 2018):

$$V_c + V_m = 1 \Rightarrow V_m = 1 - V_c \quad (2)$$

with $V_c = \left(\frac{z}{h} + \frac{1}{2}\right)^k$ and k is a material index.

The law governing the combination of Young's modulus and the mass density within a mixture can be expressed as follows:

$$\begin{aligned} E(z) &= (E_c - E_m) \cdot V_c + E_m \\ \rho(z) &= (\rho_c - \rho_m) \cdot V_c + \rho_m \end{aligned} \quad (3)$$

The beam is subjected to a moving load, denoted as $F(x,t)$. This moving load maintains a constant velocity v as it traverses the beam from the left to the right. This moving load has the following expression:

$$F(x,t) = F_0 \cdot \sin(\Omega \cdot t) \quad (4)$$

where Ω is the frequency of excitation.

The position of the load as a function of time can be determined through the following relation:

$$x(t) = v \cdot t + x_0 \quad (5)$$

x_0 is initial position when $t=0$. We take $x_0 = 0$

The higher-order shear deformation theory is employed to represent the displacement field. In this theory, shear is considered through a function that represents the distortion of the cross-sectional area. Additionally, this theory ensures the nullity of shear forces at both the upper and lower interfaces. This field takes the following form (Thai & Vo, 2012):

$$u_1(x, z, t) = u(x, t) - z \cdot \frac{\partial w(x, t)}{\partial x} - f(z) \cdot \phi(x, t) \quad (6)$$

$$u_2(x, z, t) = w(x, t)$$

where u , w and ϕ represent the axial displacement, the transverse displacement and the shear rotation of the cross-section. Due to the negligible transverse deformations, all points within the same cross section have identical displacements. Thus, the w component is independent of z . $f(z)$ is the n^{th} -order shape function of the transverse shear strains given by (Xiang & Kang, 2013; Nguyen & Phung, 2023):

$$f(z) = \frac{z}{n} \left(\frac{2z}{h} \right)^{n-1} \quad \text{with } n=3, 5, 7 \dots$$

The elastic strain at a given point in time is written in the following way:

$$\varepsilon_x = \frac{\partial u(x, t)}{\partial x} - z \cdot \frac{\partial^2 w(x, t)}{\partial x^2} - f(z) \cdot \frac{\partial \phi(x, t)}{\partial x} \quad (7)$$

$$\gamma_{xz} = f'(z) \cdot \frac{\partial w(x, t)}{\partial x}$$

Hamilton's principle asserts that the time integral of the variation in total energy is zero when the system is in equilibrium. This principle can be expressed as follows:

$$\int_{t_1}^{t_2} (\delta U + \delta U_f - \delta V - \delta K) dt = 0 \quad (8)$$

U , U_f , V and K denote the elastic deformation energy, the elastic foundation strain energy, the work of external forces, and the kinetic energy, respectively.

The elastic strain energy depends on the normal and tangential stresses and the corresponding strains. This association can be expressed as follows:

$$\delta U = \int (\sigma_x \delta \varepsilon_x + \tau_{xz} \delta \gamma_{xz}) dV = \int_0^L \left(N \frac{\partial \delta u}{\partial x} - M_b \frac{\partial^2 \delta w}{\partial x^2} + M_s \frac{\partial \delta \phi}{\partial x} + Q \delta \phi \right) dx \quad (9)$$

N , M_b , M_s and Q represent the internal forces which are defined by the following expressions:

$$\{N, M_b, M_s\} = \int \sigma_x \{1, z, f(z)\} dz \quad (10)$$

$$Q = \int G(z) f'(z) dz$$

The determination of the strain energy in an elastic foundation is carried out using the subsequent expression:

$$\delta U_f = \int_0^L \left(k_w \delta w - k_s \frac{\partial^2 \delta w}{\partial x^2} \right) dx \quad (11)$$

where k_w and k_s are the Winkler elastic foundation and the shear foundation modulus.

The work of the external forces can be written as follows:

$$\delta V = \int_0^L (q \delta w) dx + \int_0^L (F(x, t) \cdot \delta x(t) \cdot \delta w) dx \quad (12)$$

with q being the load distributed over the length of the beam.

The variation in the kinetic energy of the beam is as follows:

$$\delta K = \int_0^L \int_{-h/2}^{h/2} \rho(z) \left(\dot{u} \delta \dot{u} + \dot{w} \delta \dot{w} \right) dx \quad (13)$$

$$= \int_0^L \left(-I_0 \ddot{u} \delta u - I_1 \frac{\partial \ddot{u}}{\partial x} \delta w - K_1 \ddot{u} \delta \phi + I_1 \frac{\partial \ddot{w}}{\partial x} \delta u + I_2 \frac{\partial^2 \ddot{w}}{\partial x^2} \delta w \right. \\ \left. + K_2 \frac{\partial \ddot{w}}{\partial x} \delta \phi - K_1 \ddot{\phi} \delta u - K_2 \frac{\partial \ddot{\phi}}{\partial x} \delta w - J \ddot{\phi} \delta \phi - I_0 \ddot{w} \delta w \right) dx$$

where $\{I_0, I_1, I_2, K_1, K_2, J\} = \int \rho(z) \{1, z, z^2, f(z), zf(z), f(z)^2\} dz$

By substituting equations (9), (11), (12), and (13) in equation (8), one obtains the following system of differential equations:

$$\delta u : -\frac{\partial N}{\partial x} = -I_0 \ddot{u} + I_1 \frac{\partial \ddot{w}}{\partial x} - K_1 \ddot{\phi}$$

$$\delta w : -\frac{\partial^2 M_b}{\partial x^2} - kw + \frac{\partial^2 k_s}{\partial x^2} = -I_1 \frac{\partial \ddot{u}}{\partial x} + I_2 \frac{\partial^2 \ddot{w}}{\partial x^2} - K_2 \frac{\partial \ddot{\phi}}{\partial x} - I_0 \ddot{w}$$

$$+ q + F(x, t)$$

(14)

$$\delta \phi : -\frac{\partial M_s}{\partial x} + Q = -K_1 \ddot{u} + K_2 \frac{\partial \ddot{w}}{\partial x} - J \ddot{\phi}$$

The relationship between stresses and strains can be written using Hooke's law:

$$\sigma_x = E(z) \varepsilon_x$$

$$\tau_{xz} = G(z) \gamma_{xz}$$

(15)

By integrating the given expression (10) and the corresponding equations (15), one can formulate the internal forces in the following manner:

$$N = A \frac{\partial u}{\partial x} - B \frac{\partial^2 w}{\partial x^2} + C \frac{\partial \phi}{\partial x}$$

$$M_b = B \frac{\partial u}{\partial x} - B_s \frac{\partial^2 w}{\partial x^2} + D_s \frac{\partial \phi}{\partial x}$$

$$M_s = C \frac{\partial u}{\partial x} - D_s \frac{\partial^2 w}{\partial x^2} + H_s \frac{\partial \phi}{\partial x}$$

$$Q = H_{s2} \phi$$

(16)

with: $\{A, B, C, B_s, D_s, H_s\} = \int E(z) \{1, z, f(z), z^2, zf(z), f(z)^2\} dz$ and

$$H_{s2} = \int G(z) g(z)^2 dz$$

By replacing expressions (16) in the system of equations (14), the differential equations in terms of displacement under moving force of FGM beams with the presence of a foundation are obtained as follows:

$$-A \frac{\partial^2 u}{\partial x^2} + B \cdot \frac{\partial^3 w}{\partial x^3} - C \cdot \frac{\partial^2 \phi}{\partial x^2} = -I_0 \ddot{u} + I_1 \frac{\partial \ddot{w}}{\partial x} - K_1 \phi \tag{17a}$$

$$\begin{aligned} & -B \frac{\partial^3 u}{\partial x^3} + B_s \cdot \frac{\partial^4 w}{\partial x^4} - D_s \cdot \frac{\partial^3 \phi}{\partial x^3} - k_w + \frac{\partial^2 k_s}{\partial x^2} \\ & = -I_1 \frac{\partial \ddot{u}}{\partial x} + I_2 \frac{\partial^2 \ddot{w}}{\partial x^2} - K_2 \frac{\partial \ddot{\phi}}{\partial x} - I_0 \ddot{w} + q + F(x, t) \end{aligned} \tag{17b}$$

$$C \frac{\partial^2 u}{\partial x^2} - D_s \cdot \frac{\partial^3 w}{\partial x^3} - H_s \cdot \frac{\partial^2 \phi}{\partial x^2} + H_{s2} = -K_1 \ddot{u} + K_2 \frac{\partial \ddot{w}}{\partial x} - J \ddot{\phi} \tag{17c}$$

Galerkin finite element formulation

There are several techniques for discretizing the system of differential equations, among which the Galerkin finite element method is a widely used and effective technique (Phadikar & Pradhan, 2010). By using this method, the following weak form is obtained:

$$\begin{aligned} & \int_{x_1^e}^{x_2^e} \left(-A \frac{\partial \psi}{\partial x} \frac{\partial u}{\partial x} + B \cdot \frac{\partial \psi}{\partial x} \frac{\partial^2 w}{\partial x^2} - C \cdot \frac{\partial \psi}{\partial x} \frac{\partial \phi}{\partial x} \right) dx \\ & = \int_{x_1^e}^{x_2^e} \psi \left(-I_0 \ddot{u} + I_1 \frac{\partial \ddot{w}}{\partial x} - K_1 \phi \right) dx \end{aligned} \tag{18a}$$

$$\begin{aligned} & \int_{x_1^e}^{x_2^e} \left(-B \frac{\partial^2 \psi}{\partial x^2} \frac{\partial u}{\partial x} + B_s \cdot \frac{\partial^2 \psi}{\partial x^2} \frac{\partial^2 w}{\partial x^2} - D_s \cdot \frac{\partial^2 \psi}{\partial x^2} \frac{\partial \phi}{\partial x} - \psi(kw) \right) dx \\ & = - \int_{x_1^e}^{x_2^e} \left(I_1 \frac{\partial \psi}{\partial x} \ddot{u} + I_2 \frac{\partial \psi}{\partial x} \frac{\partial \ddot{w}}{\partial x} - K_2 \frac{\partial \psi}{\partial x} \ddot{\phi} - I_0 \psi \ddot{w} - \psi(q + F(x, t)) \right) dx \end{aligned} \tag{18b}$$

$$\int_{x_1^e}^{x_2^e} \left(C \frac{\partial \psi}{\partial x} \frac{\partial u}{\partial x} - D_s \cdot \frac{\partial \psi}{\partial x} \frac{\partial^2 w}{\partial x^2} - H_s \cdot \frac{\partial \psi}{\partial x} \frac{\partial \phi}{\partial x} + H_{s2} \psi \phi \right) dx$$

$$= \int_{x_1^e}^{x_2^e} \left(-K_1 \ddot{u} + K_2 \frac{\partial \ddot{w}}{\partial x} - J \ddot{\phi} \right) dx \tag{18c}$$

with ψ being the weight function.

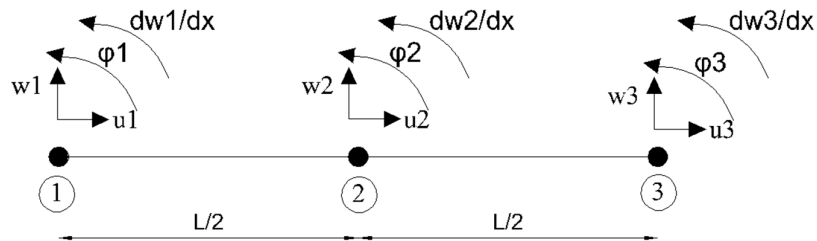


Figure 2 – Finite beam element with three nodes and three degrees of freedom per node

In order to construct the finite element beam employed in this study, we will consider a Hermitian element with three nodes (Figure 2). The displacements u , w , and ϕ are expressed in the subsequent manner:

$$u = [N_1 \quad N_2 \quad N_3] \begin{Bmatrix} u_1 \\ u_2 \\ u_3 \end{Bmatrix} \tag{19a}$$

$$\phi = [N_1 \quad N_2 \quad N_3] \begin{Bmatrix} \phi_1 \\ \phi_2 \\ \phi_3 \end{Bmatrix} \tag{19b}$$

$$w = [N_{w1} \quad N_{w2} \quad N_{w3} \quad N_{w4} \quad N_{w5} \quad N_{w6}] \begin{Bmatrix} w_1 \\ \theta_1 \\ w_2 \\ \theta_2 \\ w_3 \\ \theta_3 \end{Bmatrix} \tag{19c}$$

N_i and N_{w_i} are the polynomial shape functions related to nodes, given by the following expressions:

$$N_1 = 1 - \frac{3x}{L} + \frac{2x^2}{L^2} \tag{20a}$$

$$N_2 = \frac{4x}{L} - \frac{4x^2}{L^2} \tag{20b}$$

$$N_3 = -\frac{x}{L} + \frac{2x^2}{L^2} \tag{20c}$$

$$N_{w1} = 1 - \frac{23x^2}{L^2} + \frac{66x^3}{L^3} - \frac{68x^4}{L^4} + \frac{24x^5}{L^5} \tag{20d}$$

$$N_{w2} = x - \frac{6x^2}{L^2} + \frac{13x^3}{L^3} - \frac{12x^4}{L^4} + \frac{4x^5}{L^5} \tag{20e}$$

$$N_{w3} = \frac{16x^2}{L^2} - \frac{32x^3}{L^3} + \frac{16x^4}{L^4} \tag{20f}$$

$$N_{w4} = -\frac{8x^2}{L^2} + \frac{32x^3}{L^3} - \frac{40x^4}{L^4} + \frac{16x^5}{L^5} \tag{20g}$$

$$N_{w5} = \frac{7x^2}{L^2} - \frac{34x^3}{L^3} + \frac{52x^4}{L^4} - \frac{24x^5}{L^5} \tag{20h}$$

$$N_{w6} = -\frac{x^2}{L^2} + \frac{5x^3}{L^3} - \frac{8x^4}{L^4} + \frac{4x^5}{L^5} \tag{20i}$$

and $\theta = \frac{\partial w}{\partial x}$.

Using the shape functions in the weak form and integrating along the length of element, we obtain the following elementary equation:

$$\left([K^{elem}] + [K_f^{elem}] \right) \{U^{elem}\} + [M^{elem}] \left\{ \ddot{U}^{elem} \right\} = \{F^{elem}\} \tag{21}$$

K^{elem} , K_f^{elem} , U^{elem} , M^{elem} and F^{elem} are the elemental beam's stiffness matrix, the foundation stiffness matrix, the displacement vector, the mass matrix, and the vector of external forces. The elemental equations can be assembled to form global equations and one can solve the simultaneous

algebraic equations. Three separate analyses have been used for solving this problem. Table 1 shows these three systems of equations.

Table 1 – Three systems of equations to be analysed

$([K] + [K_f])\{U\} = \{F\}$	for solving the static problem by applying static concentrated force P_0 at the mid span, in the first case, and a uniform distributed load, in the second case
$([K] + [K_f])\{U\} + [M]\{\ddot{U}\} = 0$	for solving the free vibration problem and obtaining the natural frequencies
$([K] + [K_f])\{U\} + [M]\{\ddot{U}\} = \{F\}$	for solving the forced vibration problem by applying the moving load $P(x,t)$. The Newmark β method is used for integrating in time the system of equations.

For the case of forced vibration, the Newmark β method is used to integrate the system of equations. Newmark's β method is considered to be a special type of finite difference techniques commonly used by engineers and researchers to solve second-order differential equations with multiple degrees of freedom. The authors present here a summary of the methodology introduced by Newmark (Chopra, 2014; Yang et al, 2004).

The equations of motion of the structure at time $t+\Delta t$ are as follows:

$$([K] + [K_f])\{U\}_{t+\Delta t} + [C]\{\dot{U}\}_{t+\Delta t} + [M]\{\ddot{U}\}_{t+\Delta t} = \{F\}_{t+\Delta t} \quad (22)$$

where Δt is a small time increment, and $[C]$ is the damping matrix which is neglected in this work.

Newmark's method is characterized by its one-step approach, requiring only information from the structure at time t for resolution. The method uses two fundamental equations proposed by Newmark to determine the displacements and velocities of the structure at time $t+\Delta t$:

$$\begin{aligned} \{U\}_{t+\Delta t} &= \{U\}_t + \{\dot{U}\}_t \Delta t + \left[\left(\frac{1}{2} - \beta \right) \{\ddot{U}\}_t + \beta \{\ddot{U}\}_{t+\Delta t} \right] (\Delta t)^2 \\ \{\dot{U}\}_{t+\Delta t} &= \{\dot{U}\}_t + \left[(1 - \gamma) \{\ddot{U}\}_t + \gamma \{\ddot{U}\}_{t+\Delta t} \right] \Delta t \end{aligned} \quad (23)$$

The method has been shown to be unconditionally stable under the conditions where $\gamma \geq 1/2$ and $\beta \geq 1/4(1/2 + \gamma)^2$. Throughout this paper, the combination of $\gamma = 1/2$ and $\beta = 1/4$ will be chosen.

The accelerations and velocities of the structure at time $t+\Delta t$ can be determined from equation (23):

$$\begin{aligned} \left\{ \ddot{U} \right\}_{t+\Delta t} &= a_0 \left(\left\{ U \right\}_{t+\Delta t} - \left\{ U \right\}_t \right) - a_2 \left\{ \dot{U} \right\}_t - a_3 \left\{ \ddot{U} \right\}_t \\ \left\{ \dot{U} \right\}_{t+\Delta t} &= \left\{ \dot{U} \right\}_t + a_6 \left\{ \ddot{U} \right\}_t + a_7 \left\{ \ddot{U} \right\}_{t+\Delta t} \end{aligned} \quad (24)$$

The coefficients a_0 to a_7 are provided as follows:

$$\begin{aligned} a_0 &= \frac{1}{\beta \Delta t^2}, \quad a_1 = \frac{\gamma}{\beta \Delta t}, \quad a_2 = \frac{1}{\beta \Delta t}, \quad a_3 = \frac{1}{2\beta} - 1, \quad a_4 = \frac{\gamma}{\beta} - 1, \\ a_5 &= \frac{\Delta t}{2} \left(\frac{\gamma}{\beta} - 2 \right), \quad a_6 = \Delta t(1 - \gamma), \quad a_7 = \gamma \Delta t \end{aligned} \quad (25)$$

By substituting the preceding expression (24) into equation (22), the equivalent stiffness equations are obtained:

$$[K_{eff}] \left\{ U \right\}_{t+\Delta t} = \left\{ F_{eff} \right\}_{t+\Delta t} \quad (26)$$

where the effective stiffness matrix $[K_{eff}]$ and the effective load vector $\{P_{eff}\}_{t+\Delta t}$ are defined as follows:

$$\begin{aligned} [K_{eff}] &= a_0 [M] + a_1 [C] + ([K] + [K_f]) \\ \left\{ P_{eff} \right\}_{t+\Delta t} &= \left\{ P \right\}_{t+\Delta t} \\ &+ [M] \left(a_0 \left\{ \dot{U} \right\}_t + a_2 \left\{ \dot{U} \right\}_t + a_3 \left\{ \ddot{U} \right\}_t \right) + [C] \left(a_1 \left\{ \dot{U} \right\}_t + a_4 \left\{ \dot{U} \right\}_t + a_5 \left\{ \ddot{U} \right\}_t \right) \end{aligned} \quad (27)$$

Based on equation (26), the structural displacements $\{U\}$ at time $t+\Delta t$ can be calculated as follows:

$$\left\{ U \right\}_{t+\Delta t} = [K_{eff}]^{-1} \left\{ F_{eff} \right\}_{t+\Delta t} \quad (28)$$

The three sets of equations for static, free, and forced vibration problems were solved using a MATLAB algorithm specifically developed for this purpose.

Numerical results

The numerical results examine the static, free and forced vibrations of the simply supported (SS) FG beam subjected to moving harmonic loads.

Validation study

The results obtained from the formulation presented in this article are confirmed through validation against other studies. To this end, we compare the static responses and free vibration natural frequencies with the results reported in the references. The characteristics adopted are as follows (Şimşek & Al-shujairi, 2017):

- Steel: $E_m=70$ GPa, $\rho_m=2702$ kg/m³, $\nu_m=0.3$.
- Alumina: $E_c=380$ GPa, $\rho_c=3960$ kg/m³, $\nu_c=0.3$.

Table 2 shows the maximum transverse deflection of an FGM beam simply supported under a uniformly distributed load compared with the results found in the literature (Şimşek & Al-shujairi, 2017).

Table 2 – Non-dimensional deflection of the mid-span of FG beam under uniform load

L/h		k		
		0	1	10
5	CBT	2.8783	5.7746	9.6072
	TBT	3.1657	6.2599	10.7194
	Presente	3.0107	5.9983	10.0200
20	CBT	2.8783	5.7746	9.6072
	TBT	2.8962	5.8049	9.6767
	Presente	2.8866	5.7886	9.6330

The following dimensionless quantities are used:

$$\bar{\omega} = \frac{\omega L^2}{h} \sqrt{\frac{\rho_m}{E_m}}$$

$$\bar{w} = 100 \frac{E_m h^3}{q L^4} w(L/2) \text{ for a Simply-Simply beam (SS) and a Clamped-}$$

Clamped (CC)

$$\bar{w} = 100 \frac{E_m h^3}{q L^4} w(L) \text{ for a Clamped-Free beam (CF)}$$

$$K_w = \frac{k_w \cdot L^4}{E_m I}, \quad K_s = \frac{k_s \cdot L^2}{E_m I}.$$

Firstly, it is observed that the present work's values of dimensional static deflection agree well with those of the references. It is evident that the deflection of FG beam increases with increasing the material index k . This trend is explained by the fact that when the gradient index increases, the modulus of elasticity and the stiffness of the beam decrease and the beam becomes more flexible.

Table 3 – First three non-dimensional frequencies of the FG SS beam for the slenderness ratios 5 and 20 and the gradient index k (0, 1, and 10)

			k		
L/h	mode		0	1	10
5	1	CBT	5.3953	4.1484	3.4921
		TBT	5.1527	3.9904	3.2816
		Presente	5.1910	4.0151	3.3587
	2	CBT	20.6187	15.7982	13.2376
		TBT	17.8812	14.0100	11.0240
		Presente	15.0990	14.6846	11.9147
	3	CBT	43.3483	33.0278	27.4752
		TBT	34.2097	27.0979	20.5561
		Presente	33.0444	27.0358	21.7556
20	1	CBT	5.4777	4.2163	3.5547
		TBT	5.4603	4.2051	3.5390
		Presente	5.4640	4.2075	3.5457
	2	CBT	21.8438	16.8100	14.1676
		TBT	21.5732	16.6344	13.9263
		Presente	21.6279	16.6685	14.0248
	3	CBT	48.8999	37.6173	31.6883
		TBT	47.5930	36.7679	30.5369
		Presente	47.8323	36.8329	30.8015

In the second part of the validation study, the vibratory characteristics of the studied FGM beam are analyzed. Table 3 shows the first three natural frequencies of vibration of an FGM beam for different values of k

and for two values of the L/h ratio, compared with the results found in the references (Şimşek & Al-Shujairi, 2017). Table 4 shows the non-dimensional frequencies of the FG beam for low slenderness ratios (10 and 100) and several values of the index k (0, 1 and 10) compared with the results found in the references (Zemri et al, 2015).

Table 4 – Non-dimensional frequencies of the FG SS beam for the slenderness ratios 10 and 100 and the gradient index k (0, 1, and 10)

L/h		k		
		0	1	10
10	TBT	5.3383	2.4194	1.5799
	(Zemri et al, 2015)	5.3383	2.4194	1.579
	Presente	5.3287	2.418	1.5771
100	TBT	5.2096	2.3679	1.5453
	(Zemri et al, 2015)	5.2096	36794	1.5454
	Presente	5.2091	2.3674	1.5452

Table 5 – Non-dimensional frequencies of the FG beam for the slenderness ratios 5 and 20 and different cases of boundary conditions (SS, CC, and CF)

L/h		Boundary conditions	k		
			0	1	10
5	SS	TBT	5.1524	3.9708	3.2960
		Presente	5.1910	4.0151	3.3587
	CC	TBT	9.9975	7.8997	6.3147
		Presente	10.3200	8.2828	6.8150
	CF	TBT	1.8944	1.4627	1.2236
		Presente	1.9034	1.4721	1.2370
20	SS	TBT	5.4603	4.2036	3.5403
		Presente	5.4640	4.2075	3.5457
	CC	TBT	12.2201	9.4292	7.9101
		Presente	12.2621	9.4716	7.9701
	CF	TBT	1.9495	1.5010	1.2649
		Presente	1.9502	1.5017	1.2659

The results obtained in the present study were compared to those calculated using the Timoshenko beam theory, TBT. Notably, a good agreement was observed with the results in the references. The provided table clearly indicates that the fundamental non-dimensional frequency decreases as the power law index increases, emphasizing the influence of this index on the beam's behavior.

In Table 5, the non-dimensional frequencies of the FG beam are compared with the results found by Şimşek & Al-shujairi (2017) for different cases of boundary conditions (SS, CC, and CF). An excellent agreement is observed.

Convergence study

Firstly, the convergence of the results of the model developed in this study must be studied. For this purpose, an isotropic beam is taken with the following characteristics: $E=380$ MPa, $L=10$ m $b=1$ m, $F_0=100$ KN, $\Omega=0$. Two values of the L/h ratio are considered, namely $L/h=5$ and $L/h=20$ and with two speeds $v=20$ Km/h and $v=100$ Km/h.

The results of the convergence study of the static and dynamic deflection and the free vibration frequency of the isotropic beam under the effect of a moving concentrated load, as a function of the number of finite elements, are shown in Figures 3, 4, 5 and 6.

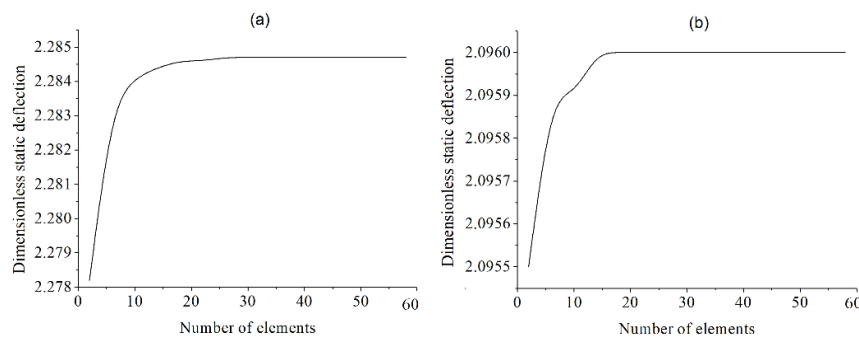


Figure 3 – Study of convergence of the dimensionless static deflection for: a) $L/h=5$ and b) $L/h=20$

From these figures, it can be seen that the deflection converges rapidly (by using 5, 10, or 15 elements) for the two cases of the L/h ratio and two cases of speed.

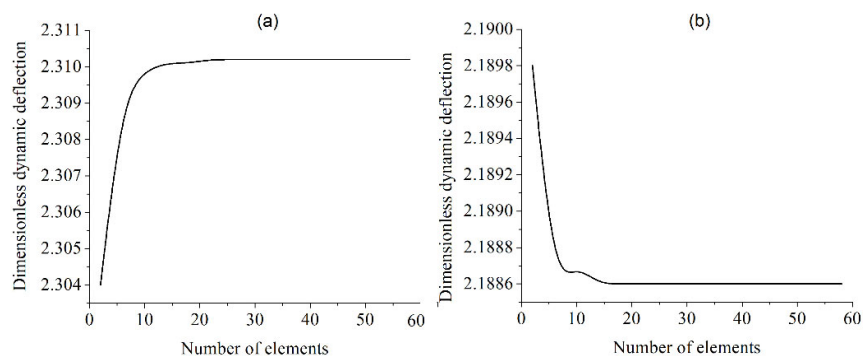


Figure 4 – Study of convergence of the dimensionless dynamic deflection with $v=20\text{m/s}$ for: a) $L/h=5$ and b) $L/h=20$

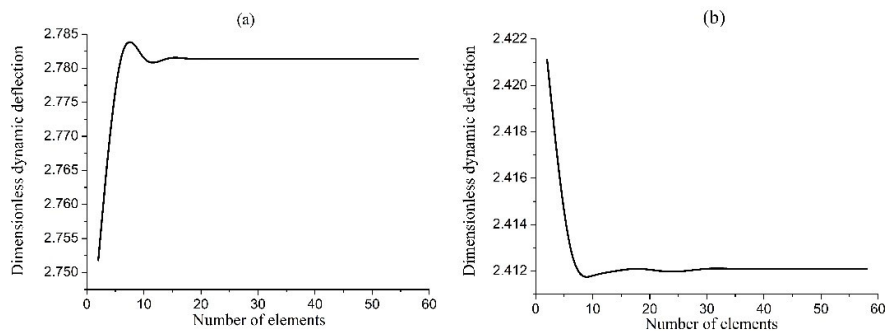


Figure 5 – Study of convergence of the dimensionless dynamic deflection with $v=100\text{m/s}$ for: a) $L/h=5$ and b) $L/h=20$

For the natural frequency (Figure 7), it can be seen that fewer than 10 elements are sufficient for the frequency value to converge. In our work, 30 elements are used to discretize the FGM beam for all the cases studied.

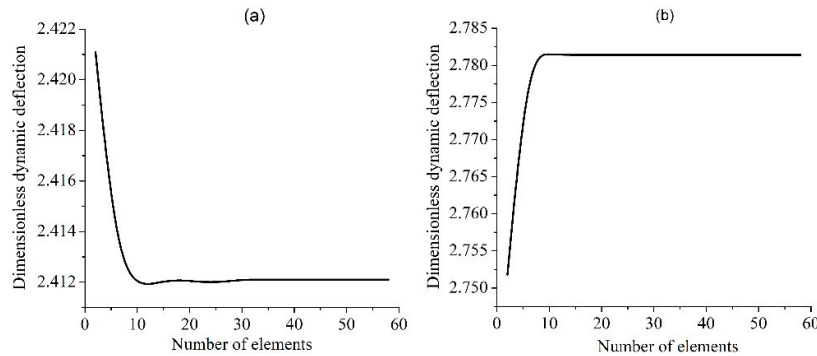


Figure 6 – Study of convergence of the dimensionless dynamic deflection for: a) $L/h=5$ and b) $L/h=20$

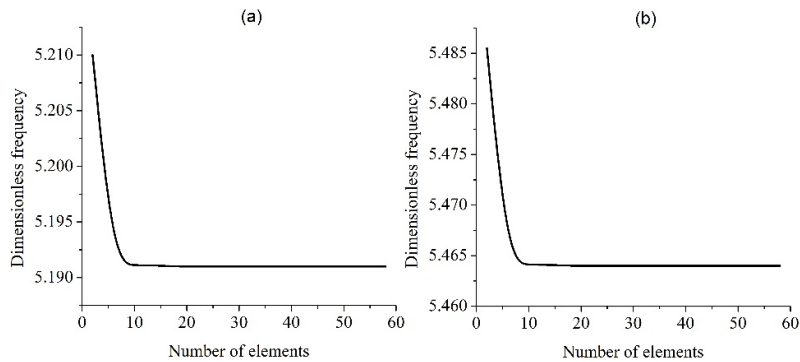


Figure 7 – Study of convergence of the dimensionless frequency for: a) $L/h=5$ and b) $L/h=20$

Forced vibration

This section studies the forced vibration of the FG beam under the effect of a moving load with a constant velocity. It considers a beam with the following characteristics: $L=20\text{m}$, $h=0.9\text{m}$, $b=0.4\text{m}$, $E_f=210\text{MPa}$, $\rho_f=8166\text{kg/m}^3$, $E_b=390\text{MPa}$, $\rho_b=3960\text{kg/m}^3$ and the material index $k=0$.

The dynamic amplification factor is defined as the ratio between the maximum dynamic deflection at the mid-span and the maximum static deflection at the same section.

For the purpose of validation of our formulation, the dynamic amplification factor (DAF) obtained by our study is compared with the results of Ismail Esen's article (Esen, 2019) for various values of k and shown in Table 5. Each value of the DAF is related with its corresponding velocity of the moving load expressed in m/s . A good agreement is found between the results of this work and those found in the reference.

Table 6 – DAF and corresponding velocities of the FG beam for different values of k

Source	Ceramic	$k=0.2$	$k=0.5$	$k=1$	$k=2$	Metal
Reference (Esen, 2019)	0.9326 (252 m/s)	1.0336 (222 m/s)	1.1435 (198 m/s)	1.269 (179 m/s)	1.3365 (164 m/s)	1.7316 (132 m/s)
Present	0.9371 (250 m/s)	1.0382 (218 m/s)	1.1488 (194 m/s)	1.2554 (174 m/s)	1.3433 (160)	1.7403 (127 m/s)

By increasing the value of k the dynamic amplification factor increases and the corresponding velocity decreases. This is due to the fact that the increase in k corresponds to an increase in Young's modulus, which means that the beam is more flexible and therefore a lower speed of the moving load is required to achieve the maximum displacement.

Table 6 shows the variation of the dimensionless fundamental frequency for different values of L/h and different values of K_w and K_s compared with the results found in Chen et al. (2004). There is also good agreement between the results obtained by the present model and those found in the literature.

For the subsequent figures, the following characteristics are considered: $E_t=320.23 \times 10^9$ MPa; $\rho_t=3750$ kg/m³; $E_b=207.78 \times 10^9$ MPa; $\rho_b=8166$ kg/m³.

Figure 8 shows the dynamic mid-span displacement of an isotropic beam as a function of time under the effect of a moving load of a constant value over time. The length $L=5$ m, the width $b=1$ m, and the slenderness ratio $L/h=5$. The values of this displacement are multiplied by 10^4 for greater visibility. Several values of the moving load speed are taken. It can be seen that the amplitude of the vibration increases proportionally with

the speed. The maximum difference between the amplitude obtained by the two speeds 5 m/s and 120 m/s is of the order of 14.77%.

Table 7 – Variation of the dimensionless fundamental frequency for different values of L/h and different values of Kw and Ks

Kw	Ks	L/h=120		L/h=15		L/h=5	
		Reference (Chen et al, 2004)	Present	Reference (Chen et al, 2004)	Present	Reference (Chen et al, 2004)	Present
0	0	3.1414	3.1414	3.1323	3.1318	3.0637	3.0567
	100	3.7359	3.7365	3.7278	3.7238	3.6665	3.6739
	250	4.2969	4.2974	4.2889	4.2810	4.2232	4.2329
100	0	3.7482	3.7942	3.7401	3.7861	3.6788	3.7339
	100	4.1436	4.1739	4.1356	3.8298	4.0720	4.1160
	250	4.5823	4.6000	4.5741	3.8923	4.5028	4.5428
10000	0	10.0240	10.2602	9.9958	10.2286	7.3408	7.2772
	100	10.0481	10.2825	10.0197	10.2558	7.3410	7.2772
	250	10.0839	10.3161	10.0552	10.2342	7.3412	7.2772

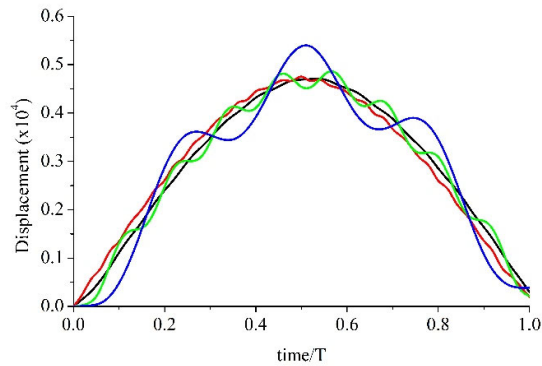


Figure 8 – Time history of the mid-span displacements of a simply supported isotropic beam: a) v=5 m/s, b) v=20 m/s, c) v= 50 m/s et d) v=120 m/s

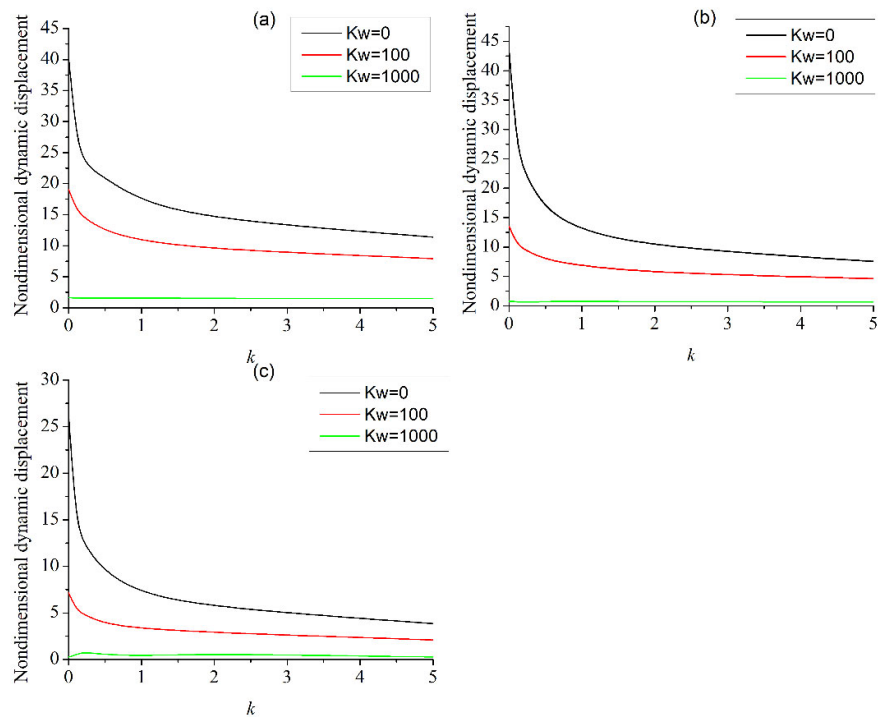


Figure 9 – Non-dimensional dynamic displacement of the mid-span section as a function of the index k for different values of K_w for: a) $L/h=20$ b) $L/h=10$ and c) $L/h=5$

Figure 9 shows the maximum dimensional displacement at the mid-span of an FGM beam as a function of the index k for different values of the foundation stiffness K_w and three slenderness ratios $L/h=5$, $L/h=10$ and $L/h=20$. The transverse displacement values decrease as k increases. Increasing the value of k leads to an increase in Young's modulus, i.e., greater stiffness.

The presence of the elastic foundation leads to a decrease in beam displacements. The non-dimensional displacements are almost the same in the two cases of $L/h=20$ and $L/h=10$. For the short beam ($L/h=5$), there is a decrease in this value due to the main effect of the shear force in short beams.

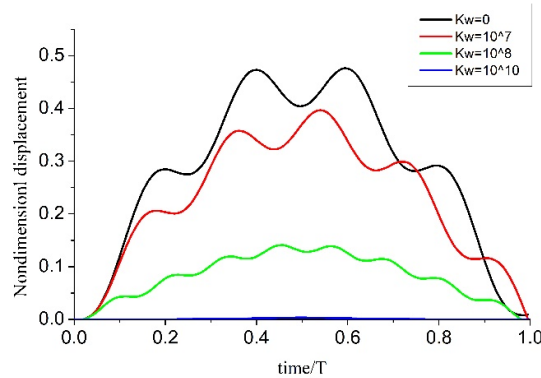


Figure 10 – Time history of the mid-span displacements of a simply supported FG beam for $k=1$ and $v=50\text{m/s}$

Figure 10 shows the effect of the elastic foundation on the forced vibration of an FGM beam ($k=1$) subjected to a moving load with a speed of 50 m/s . T is the time taken for the moving load to traverse the beam from left to right. There is: $T = \frac{L}{v}$. It is clear that the amplitude of vibration decreases with increasing the elastic foundation coefficient K_w .

Figures 11, 12, 13, and 14 show the dynamic amplification factor of a simply supported FGM beam. This factor represents the ratio between the maximum dynamic displacement at mid-span and the static displacement at the mid-span, which is equal to $\frac{P_0 L^3}{48 E_c I}$. The following characteristics are taken: $E_f=320.23 \times 10^9\text{ MPa}$, $\rho_f=3750\text{ kg/m}^3$, $E_b=207.78 \times 10^9\text{ MPa}$, $\rho_b=8166\text{ kg/m}^3$, $L=20\text{ m}$, and $b=0.5\text{ m}$.

Figure 11 shows the variation of the dynamic amplification factor of an FGM beam as a function of the velocity of the moving load and the index k , with $L/h=20$: (a) $K_w=0$ and $K_s=0$ and (b) $K_w=1000$ and $K_s=100$. The impact of velocity on the beam's response is evident in this figure. By increasing the speed, the DAF increases to reach its maximum and then decreases again. This factor reaches the same maximum value of 1.73 for all values of k but at different corresponding speeds: 260 m/s for $k=0$, 230 m/s for $k=0.2$, 180 m/s for $k=1$, 170 m/s for $k=2$ and 140 m/s for $k=1000$. Analyzing Figure 8(b), we can see that the presence of the elastic foundation results in a reduction of system flexibility, leading to a decrease in the normalized mid span deflection.

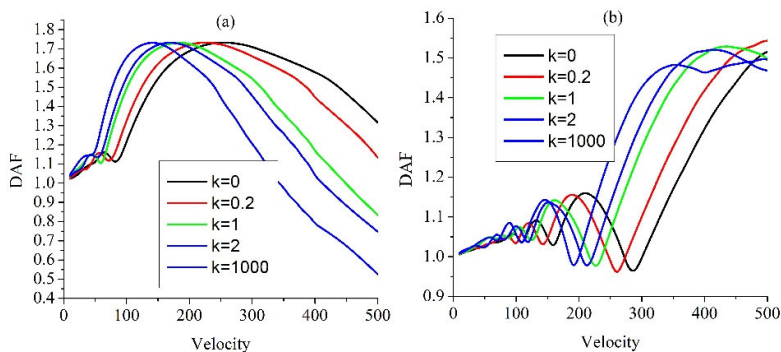


Figure 11 – Variation of the DAF as a function of velocity and the index k , for $L/h=20$ (a) $K_w=0$ et $K_s=0$ et (b) $K_w=1000$ et $K_s=100$

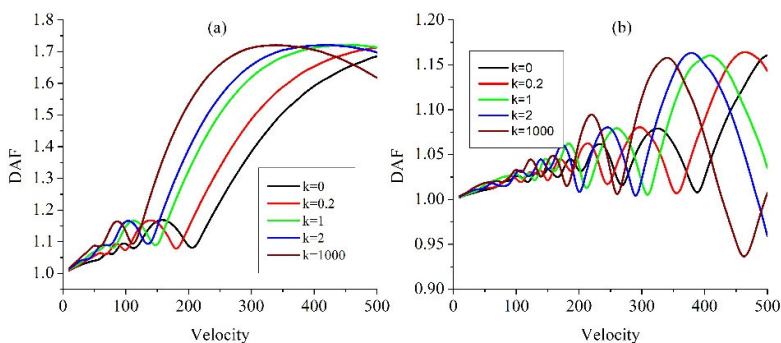


Figure 12 – Variation of the DAF as a function of velocity and the index k for $L/h=8$ (a) $K_w=0$ et $K_s=0$ et (b) $K_w=1000$ et $K_s=100$

Figure 12 shows the variation of the DAF as a function of speed and the index k for $L/h=8$. The same thing can be seen here as in the previous figure (Figure 12) but with higher values of corresponding velocities. These results reveal that the maximum dynamic magnification factors remain independent of the power-law exponent k .

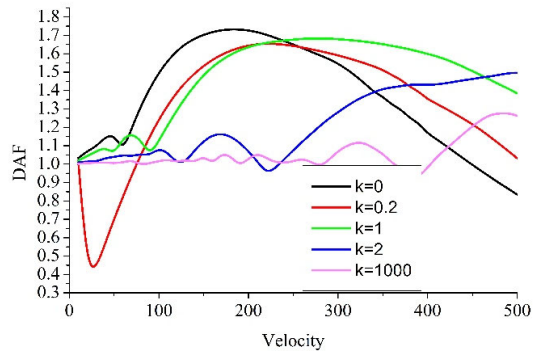


Figure 13 – Variation of the DAF as a function of K_w for $k=1$ and $L/h=20$

The variation of the DAF as a function of the speed of the moving load and for different values of K_w is shown in Figure 13. By increasing the value of the foundation stiffness, the DAF maximum value is reduced and reaches its maximum at higher values of speed. In the cases of $K_w = 0$, 10, and 100, the graphs show greater stability and reach higher maximum values compared to the case with $K_w = 1000$ and 10000. The increase in the stiffness of the elastic foundation leads to an increase in the rigidity of the beam-foundation system and consequently to smaller values of transverse displacement of the beam.

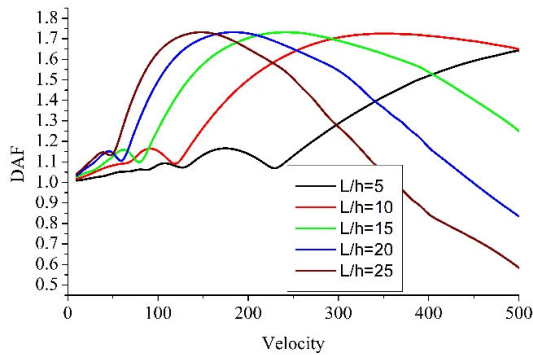


Figure 14 – Variation of the DAF as a function of L/h for $k=1$, $K_w=0$ and $K_s=0$

The variation of the DAF of the FGM beam ($k=1$) as a function of speed and slenderness L/h is shown in Figure 11. The factor is always maximal for longer beams. The maximum of this factor is almost the same (1.73) but at different speeds: 690 m/s for $L/h=5$, 360 m/s for $L/h=10$, 240 m/s for $L/h=15$, 190 m/s for $L/h=20$ and 150 m/s for $L/h=25$.

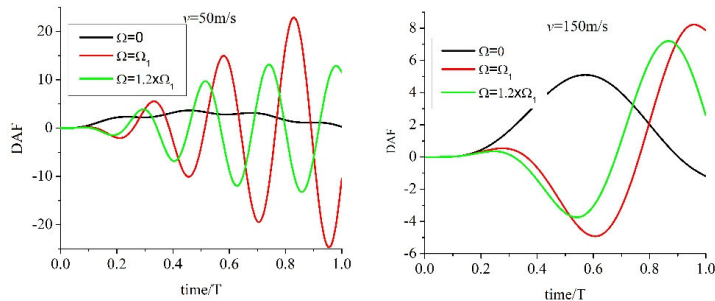


Figure 15 – Vibration of the mid-span section in relation to Ω for $v=50$ and $v=150$ and $K_w=0$ and $K_s=0$

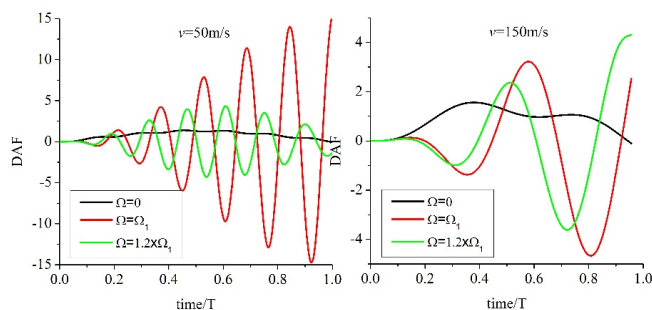


Figure 16 – Vibration of the mid-span section in relation to Ω for $v=50$ and $v=150$ and $K_w=100$ and $K_s=10$

Figures 15 and 16 illustrate the phenomenon of resonance of an FGM beam ($k=1$) for two speeds, $v=50$ m/s and $v=150$ m/s, with the foundation stiffnesses $K_w=100$ and $K_s=10$. The moving load is harmonic, with a frequency that takes three values: 0, Ω_1 and $1.2 \times \Omega_1$, with Ω_1 being the fundamental frequency. The length of the beam is 10m, $b=1$ m and $L/h=15$. The displacement values are multiplied by 1000. For a speed of 50 m/s, the amplitude of vibration reaches 3.66×10^3 m, whereas the presence of excitation frequency, which is equal to the natural frequency, raises the amplitude to more than 25×10^3 m and it continues to increase. The amplitudes in the case where $\Omega = \Omega_1$ are 630% greater than in the case where $\Omega=0$. A frequency close to the natural frequency (20% greater) gives amplitudes (13.38×10^3 m) even much greater than in the case of zero frequency of excitation of the moving load. Increasing the speed to $v=150$ m/s (Figure 14 (b)) induces amplitudes greater than in the case of zero frequency, but much less than in the first case where $v=50$ m/s. The amplitudes in the $\Omega = \Omega_1$ case are 58% greater than in the $\Omega=0$ case. The presence of the elastic foundation causes a reduction in amplitudes.

Conclusion

In the present work, a three-node finite element model using the higher-order shear deformation theory is developed to investigate the dynamic behavior of FGM beams under harmonic moving loads and elastic foundation support. By employing Hamilton's principle and the Galerkin method, we were able to derive the governing differential equations for the beam's behavior and effectively solve them. It has been shown in this article that the present finite element design is convergent, efficient and accurate, and that it is consistent with the results in the existing literature. The effects of various parameters on the free and forced vibration of FGM beams are also discussed. Our results underline the importance of taking the higher-order shear deformation theory into account in the dynamic analysis of FGM beams, thus providing a better understanding of their response to moving loads. This knowledge is essential for improving the design and performance of structures in various fields of engineering.

References

- Barati, M.R., Faleh, N.M. & Zenkour, A.M. 2019. Dynamic response of nanobeams subjected to moving nanoparticles and hygro-thermal environments based on nonlocal strain gradient theory. *Mechanics of Advanced Materials and Structures*, 26(19), pp.1661-1669. Available at: <https://doi.org/10.1080/15376494.2018.1444234>.
- Barati, M.R. & Zenkour, A. 2018. Forced vibration of sinusoidal FG nanobeams resting on hybrid Kerr foundation in hygro-thermal environments. *Mechanics of Advanced Materials and Structures*, 25(8), pp.669-680. Available at: <https://doi.org/10.1080/15376494.2017.1308603>.
- Berrabah, H.M. & Bouderra, B. 2023. Mechanical buckling analysis of functionally graded plates using an accurate shear deformation theory. *Mechanics of Advanced Materials and Structures*, 30(22), pp.4652-4662. Available at: <https://doi.org/10.1080/15376494.2022.2102701>.
- Beskou, N.D. & Muho, E.V. 2018. Dynamic response of a finite beam resting on a Winkler foundation to a load moving on its surface with variable speed. *Soil Dynamics and Earthquake Engineering*, 109, pp.222-226. Available at: <https://doi.org/10.1016/j.soildyn.2018.02.033>.
- Chen, W.Q., Lü, C.F. & Bian, Z.G. 2004. A mixed method for bending and free vibration of beams resting on a Pasternak elastic foundation. *Applied Mathematical Modelling*, 28(10), pp.877-890. Available at: <https://doi.org/10.1016/j.apm.2004.04.001>.
- Chopra, A.K. 2014. *Dynamics of Structures: Theory and Applications to Earthquake Engineering, fourth edition*. Pearson. ISBN: 978-0-273-77424-2.
- Ebrahimi, F. & Jafari, A. 2018. A four-variable refined shear-deformation beam theory for thermo-mechanical vibration analysis of temperature-dependent

FGM beams with porosities. *Mechanics of Advanced Materials and Structures*, 25(3), pp.212-224. Available at: <https://doi.org/10.1080/15376494.2016.1255820>.

El Khouddar, Y., Adri, A., Outassafte, O., Rifai, S. & Benamar, R. 2023. An analytical approach to geometrically nonlinear free and forced vibration of piezoelectric functional gradient beams resting on elastic foundations in thermal environments. *Mechanics of Advanced Materials and Structures*, 30(1), pp.131-143. Available at: <https://doi.org/10.1080/15376494.2021.2009601>.

Esen, I. 2019. Dynamic response of a functionally graded Timoshenko beam on two-parameter elastic foundations due to a variable velocity moving mass. *International Journal of Mechanical Sciences*, 153-154, pp.21-35. Available at: <https://doi.org/10.1016/j.ijmecsci.2019.01.033>.

Esen, I., Eltaher, M.A. & Abdelrahman, A.A. 2023. Vibration response of symmetric and sigmoid functionally graded beam rested on elastic foundation under moving point mass. *Mechanics Based Design of Structures and Machines*, 51(5), pp.2607-2631. Available at: <https://doi.org/10.1080/15397734.2021.1904255>.

Fuchiyama, T. & Noda, N. 1995. Analysis of thermal stress in a plate of functionally gradient material. *JSAE Review*, 16(3), pp.263-268. Available at: [https://doi.org/10.1016/0389-4304\(95\)00013-W](https://doi.org/10.1016/0389-4304(95)00013-W).

Gan, B.S., Kien, N.D. & Ha, L.T. 2017. Effect of Intermediate Elastic Support on Vibration of Functionally Graded Euler-Bernoulli Beams Excited by a Moving Point Load. *Journal of Asian Architecture and Building Engineering*, 16(2), pp.363-369. Available at: <https://doi.org/10.3130/jaabe.16.363>.

Guo, L., Xin, X., Shahsavari, D. & Karami, B. 2022. Dynamic response of porous E-FGM thick microplate resting on elastic foundation subjected to moving load with acceleration. *Thin-Walled Structures*, 173, art.number:108981. Available at: <https://doi.org/10.1016/j.tws.2022.108981>.

Hasheminejad, S.M. & Rafsanjani, A. 2009. Three-Dimensional Vibration Analysis of Thick FGM Plate Strips Under Moving Line Loads. *Mechanics of Advanced Materials and Structures*, 16(6), pp.417-428. Available at: <https://doi.org/10.1080/15376490902781209>.

He, C., Zhu, J., Hua, Y., Xin, D. & Hua, H. 2023. A study on the vibration characteristics of functionally graded cylindrical beam in a thermal environment using the Carrera unified formulation. *Mechanics of Advanced Materials and Structures*, pp.1-13. Available at: <https://doi.org/10.1080/15376494.2023.2242861>.

Javidi, R., Rezaei, B. & Moghimi Zand, M. 2023. Nonlinear Dynamics of a Beam Subjected to a Moving Mass and Resting on a Viscoelastic Foundation Using Optimal Homotopy Analysis Method. *International Journal of Structural Stability and Dynamics*, 23(08), art.number:2350084. Available at: <https://doi.org/10.1142/S0219455423500840>.

Khalili, S.M.R., Jafari, A.A. & Eftekhari, S.A. 2010. A mixed Ritz-DQ method for forced vibration of functionally graded beams carrying moving loads. *Composite Structures*, 92(10), pp.2497-2511. Available at: <https://doi.org/10.1016/j.compstruct.2010.02.012>.

Le, T.H., Gan, B.S., Trinh, T.H. & Nguyen, D.K. 2014. Finite element analysis of multi-span functionally graded beams under a moving harmonic load. *Mechanical Engineering Journal*, 1(3), art.number:CM0013. Available at: <https://doi.org/10.1299/mej.2014cm0013>.

Li, Z., Xu, Y. & Huang, D. 2021. Analytical solution for vibration of functionally graded beams with variable cross-sections resting on Pasternak elastic foundations. *International Journal of Mechanical Sciences*, 191, art.number:106084. Available at: <https://doi.org/10.1016/j.ijmecsci.2020.106084>.

Lin, S.-M. & Lee, K.-W. 2016. Instability and vibration of a vehicle moving on curved beams with different boundary conditions. *Mechanics of Advanced Materials and Structures*, 23(4), pp.375-384. Available at: <https://doi.org/10.1080/15376494.2014.981618>.

Malekzadeh, P. & Monajjemzadeh, S.M. 2016. Dynamic response of functionally graded beams in a thermal environment under a moving load. *Mechanics of Advanced Materials and Structures*, 23(3), pp.248-258. Available at: <https://doi.org/10.1080/15376494.2014.949930>.

Mena, R., Tounsi, A., Mouaici, F., Mechab, I., Zidi, M. & Bedia, E.A.A. 2012. Analytical Solutions for Static Shear Correction Factor of Functionally Graded Rectangular Beams. *Mechanics of Advanced Materials and Structures*, 19(8), pp.641-652. Available at: <https://doi.org/10.1080/15376494.2011.581409>.

Nguyen, V.D. & Phung, V.B. 2023. Static bending, free vibration, and buckling analyses of two-layer FGM plates with shear connectors resting on elastic foundations. *Alexandria Engineering Journal*, 62, pp.369-390. Available at: <https://doi.org/10.1016/j.aej.2022.07.038>.

Phadikar, J.K. & Pradhan, S.C. 2010. Variational formulation and finite element analysis for nonlocal elastic nanobeams and nanoplates. *Computational Materials Science*, 49(3), pp.492-499. Available at: <https://doi.org/10.1016/j.commatsci.2010.05.040>.

Praveen, G.N. & Reddy, J.N. 1998. Nonlinear transient thermoelastic analysis of functionally graded ceramic-metal plates. *International Journal of Solids and Structures*, 35(33), pp.4457-4476. Available at: [https://doi.org/10.1016/S0020-7683\(97\)00253-9](https://doi.org/10.1016/S0020-7683(97)00253-9).

Reddy, J.N. 2007. Nonlocal theories for bending, buckling and vibration of beams. *International Journal of Engineering Science*, 45(2-8), pp.288-307. Available at: <https://doi.org/10.1016/j.ijengsci.2007.04.004>.

Safaei, M., Malekzadeh, P. & Golbahar Haghighi, M.R. 2024. Out-of-plane moving load response and vibrational behavior of sandwich curved beams with GPLRC face sheets and porous core. *Composite Structures*, 327, art.number:117658. Available at: <https://doi.org/10.1016/j.compstruct.2023.117658>.

Saleh, B., Jiang, J., Fathi, R., Al-hababi, T., Xu, Q., Wang, L., Song, D. & Ma, A. 2020. 30 Years of functionally graded materials: An overview of manufacturing methods, Applications and Future Challenges. *Composites Part B: Engineering*, 201, art.number:108376. Available at: <https://doi.org/10.1016/j.compositesb.2020.108376>.

Şimşek, M. 2010. Vibration analysis of a functionally graded beam under a moving mass by using different beam theories. *Composite Structures*, 92(4), pp.904-917. Available at: <https://doi.org/10.1016/j.compstruct.2009.09.030>.

Şimşek, M. & Al-shujairi, M. 2017. Static, free and forced vibration of functionally graded (FG) sandwich beams excited by two successive moving harmonic loads. *Composites Part B: Engineering*, 108, pp.18-34. Available at: <https://doi.org/10.1016/j.compositesb.2016.09.098>.

Şimşek, M. & Kocatürk, T. 2009. Free and forced vibration of a functionally graded beam subjected to a concentrated moving harmonic load. *Composite Structures*, 90(4), pp.465-473. Available at: <https://doi.org/10.1016/j.compstruct.2009.04.024>.

Thai, H.-T. & Vo, T.P. 2012. Bending and free vibration of functionally graded beams using various higher-order shear deformation beam theories. *International Journal of Mechanical Sciences*, 62(1), pp.57-66. Available at: <https://doi.org/10.1016/j.ijmecsci.2012.05.014>.

Wang, X., Liang, X. & Jin, C. 2017. Accurate dynamic analysis of functionally graded beams under a moving point load. *Mechanics Based Design of Structures and Machines*, 45(1), pp.76-91. Available at: <https://doi.org/10.1080/15397734.2016.1145060>.

Xiang, S. & Kang, G.-W. 2013. A n th-order shear deformation theory for the bending analysis on the functionally graded plates. *European Journal of Mechanics - A/Solids*, 37(Jan-Feb), pp.336-343. Available at: <https://doi.org/10.1016/J.EUROMECHSOL.2012.08.005>.

Yan, T., Kitipornchai, S., Yang, J. & He, X.Q. 2011. Dynamic behaviour of edge-cracked shear deformable functionally graded beams on an elastic foundation under a moving load. *Composite Structures*, 93(11), pp.2992-3001. Available at: <https://doi.org/10.1016/j.compstruct.2011.05.003>.

Yan, T. & Yang, J. 2011. Forced Vibration of Edge-Cracked Functionally Graded Beams Due to a Transverse Moving Load. *Procedia Engineering*, 14, pp.3293-3300. Available at: <https://doi.org/10.1016/j.proeng.2011.07.416>.

Yang, J., Chen, Y., Xiang, Y. & Jia, X.L. 2008. Free and forced vibration of cracked inhomogeneous beams under an axial force and a moving load. *Journal of Sound and Vibration*, 312(1-2), pp.166-181. Available at: <https://doi.org/10.1016/j.jsv.2007.10.034>.

Yang, Y.B., Yau, J.D. & Wu, Y.S. 2004. *Vehicle–Bridge Interaction Dynamics: With Applications to High-Speed Railways*. World Scientific. Available at: <https://doi.org/10.1142/5541>.

Zemri, A., Houari, M.S.A., Bousahla, A.A. & Tounsi, A. 2015. A mechanical response of functionally graded nanoscale beam: an assessment of a refined nonlocal shear deformation theory beam theory. *Structural Engineering and Mechanics*, 54(4), pp.693-710. Available at: <https://doi.org/10.12989/sem.2015.54.4.693>.

Análisis dinámico forzado de vigas funcionalmente graduadas bajo cargas móviles armónicas sobre cimentación elástica con el método de elementos finitos

Amine Zemri^a, **autor de correspondencia**, *Ismail Mechab*^b

^a Universidad de Relizane, Departamento de Ingeniería Civil y Obras Públicas, Relizane, República Argelina Democrática y Popular; Universidad de Sidi Bel Abbes, Laboratorio de Ingeniería Civil y Medio Ambiente, Sidi Bel Abbes, República Argelina Democrática y Popular

^b Universidad de Sidi Bel Abbes, Departamento de Ingeniería Civil y Obras Públicas, Laboratorio de Estadística y Procesos Estocásticos, Sidi Bel Abbes, República Argelina Democrática y Popular

CAMPO: ingeniería mecánica, materiales

TIPO DE ARTÍCULO: artículo científico original

Resumen:

Introducción/objetivo: Este artículo presenta un estudio numérico del comportamiento dinámico forzado de una viga funcionalmente graduada sometida a una fuerza de movimiento transversal concentrada que varía armónicamente utilizando una teoría de deformación cortante de orden superior.

Métodos: Las ecuaciones que rigen el problema se derivan utilizando el principio de Hamilton. Luego, estas ecuaciones se transforman en la forma débil utilizando el método de Galerkin. El problema se resuelve utilizando el método de elementos finitos mediante el desarrollo de un elemento finito de tres nodos con cuatro grados de libertad por nodo. Se elige el método beta de Newmark para la integración temporal y el método de Gauss para la integración espacial.

Resultados: Se investigaron los efectos de varios parámetros, entre ellos la relación de esbeltez, el índice de material, la rigidez de la cimentación, la velocidad y la frecuencia de la carga en movimiento. Se observó una buena concordancia con los resultados obtenidos de la bibliografía.

Conclusión: Este estudio ilustra la importancia de utilizar una teoría de orden superior en el caso de vigas cortas y muestra claramente el cambio en el comportamiento de la viga FGM en función de diferentes parámetros.

Palabras claves: teoría de deformación cortante de orden superior, material funcionalmente graduado, método de elementos finitos, carga móvil, método beta de Newmark.

Анализ вынужденного динамического поведения функционально-градиентных балок при гармонической подвижной нагрузке на упругом основании методом конечных элементов

Амине Земри^a, **корреспондент**, *Исмаил Мечаб*^b

- ^a Университет Релизана,
Факультет гражданского строительства и общественных работ,
Релизан, Алжирская Народная Демократическая Республика;
Университет Сиди-Бель-Аббеса,
Лаборатория гражданского строительства и охраны окружающей среды,
Сиди-Бель-Аббес, Алжирская Народная Демократическая Республика
- ^b Университет Сиди-Бель-Аббес, Факультет гражданского строительства и
общественных работ, Лаборатория статистики и случайных процессов,
Сиди-Бель-Аббес, Алжирская Народная Демократическая Республика

РУБРИКА ГРНТИ: 30.19.00 Механика деформируемого твердого тела,
81.09.00 Материаловедение

ВИД СТАТЬИ: оригинальная научная статья

Резюме:

Введение/цель: В данной статье представлено численное исследование вынужденного динамического поведения функционально-градиентных балок под воздействием гармонически изменяющихся поперечных сил, с использованием теории сдвиговой деформации высокого порядка.

Методы: Управляющие уравнения получены с использованием принципа Гамильтона. Затем эти уравнения преобразованы в слабую форму с использованием метода Галеркина. Задача решается с использованием метода конечных элементов путем разработки трехузлового конечного элемента с четырьмя степенями свободы в узле. Для интегрирования по времени выбран бета-метод Ньюмарка, а для пространственного интегрирования – метод Гаусса.

Результаты: В статье было исследовано влияние нескольких параметров, включая коэффициент гибкости, индекс материала, жесткость основания, скорость и частоту перемещения нагрузки. Результаты исследования совпадают с результатами из научной литературы.

Выводы: Данное исследование иллюстрирует значимость теории высокого порядка в случае коротких балок и наглядно показывает изменение поведения функционально-градиентных балок в зависимости от различных параметров.

Ключевые слова: теория сдвиговой деформации высокого порядка, функционально-градиентный материал, метод конечных элементов, подвижная нагрузка, бета-метод Ньюмарка.

Анализа изазваног динамичког понашања функционално степенованих греда под хармоничним покретним оптерећењем на еластичној основи помоћу методе коначних елемената

Амин Земри^а, аутор за преписку, Исмаил Мехаб^б

^а Универзитет у Релизану, Одељење за грађевинарство и јавне радове, Релизане, Народна Демократска Република Алжир;
Универзитет Сиди Бел Абес,
Лабораторија за грађевинарство и заштиту животне средине,
Сиди Бел Абес, Народна Демократска Република Алжир

^б Универзитет Сиди Бел Абес, Одељење за грађевинарство и јавне радове, Лабораторија за статистику и случајне процесе,
Сиди Бел Абес, Народна Демократска Република Алжир

ОБЛАСТ: машинство, материјали
КАТЕГОРИЈА (ТИП) ЧЛАНКА: оригинални научни рад

Сажетак:

Увод/циљ: У раду је представљено нумеричко испитивање изазваног динамичког понашања функционално степеноване греде подврнуте хармонично променљивој и трансферзално концентрисаној покретној сили уз коришћење теорије деформације смицањем вишег реда.

Метод: Најважније једначине изведене су помоћу Хамилтоновог принципа, а затим трансформисане у слаби облик помоћу методе Галеркина. Проблем је решен коришћењем методе коначних елемената путем развијања коначног елемента са три чвора од којих сваки има четири степена слободе. За интеграцију у времену изабрана је Њумаркова бета-метода, а за интеграцију у простору Гаусова метода.

Резултати: Испитан је утицај неколико параметара, укључујући виткост, индекс материјала и крутост, као и брзину и фреквенцију покретног оптерећења. Уочено је добро слагање са резултатима из литературе.

Закључак: Ово испитивање илуструје значај коришћења теорије вишег реда у случају кратких греда и јасно указује на промену у понашању функционално степеноване греде зависно од различитих параметара.

Кључне речи: теорија деформације смицањем вишег реда, функционално степенован материјал, метода коначних елемената, покретно оптерећење, Њумаркова бета-метода.

Paper received on: 02.04.2024.

Manuscript corrections submitted on: 24.09.2024.

Paper accepted for publishing on: 25.09.2024.

© 2024 The Authors. Published by Vojnotehnički glasnik / Military Technical Courier (www.vtg.mod.gov.rs, втг.мо.унр.срб). This article is an open access article distributed under the terms and conditions of the Creative Commons Attribution license (<http://creativecommons.org/licenses/by/3.0/rs/>).



Evaluating the structural performance of masonry walls incorporating recycled plastic bricks under monotonic and cyclic loading

Youcef Moulai Arbi^a, Nouredine Mahmoudi^b,
Mohammed Bentahar^c

^a University of Mustapha Stambouli, Laboratory of Quantum Physics of Matter and Mathematical Modeling (LPQ3M), Mascara, People's Democratic Republic of Algeria, e-mail: youcef.moulaiarbi@univ-mascara.dz, **corresponding author**, ORCID ID: <https://orcid.org/0000-0002-6534-8820>

^b University of Saida Dr. Moulay Tahar, Faculty of Technology, Department of Civil Engineering and Hydraulics, Saida, People's Democratic Republic of Algeria, e-mail: mahmoudi.nouredine@yahoo.fr, ORCID ID: <https://orcid.org/0000-0002-9740-0857>

^c University of Saida Dr. Moulay Tahar, Faculty of Technology, Department of Civil Engineering and Hydraulics, Saida, People's Democratic Republic of Algeria, e-mail: bentahae@yahoo.fr, ORCID ID: <https://orcid.org/0000-0002-2166-678X>

[doi https://doi.org/10.5937/vojtehg72-50560](https://doi.org/10.5937/vojtehg72-50560)

FIELD: mechanical engineering, civil engineering

ARTICLE TYPE: original scientific paper

Abstract:

Introduction/purpose: This study evaluates the structural performance of masonry walls made from recycled plastic bricks under monotonic and cyclic loading. The purpose was to investigate the feasibility of using recycled plastic bricks as an alternative for masonry construction, focusing on their structural viability and potential environmental benefits.

Methods: A simplified micro-modeling approach in Abaqus was employed to simulate the behavior of these walls. The plastic bricks were represented with solid elements, while the mortar joints were modeled through cohesive interactions. The numerical model underwent validation through a mesh sensitivity analysis and was subjected to vertical compression followed by horizontal loading.

Results: The findings indicated a reduction in strength compared to traditional masonry materials. However, the study successfully captured the structural response and damage evolution of masonry walls under the specified loading conditions. Despite the reduced strength, the structural

viability of recycled plastic bricks was strongly affirmed, and the behavior observed under load conditions was particularly informative.

Conclusions: The investigation underscored the potential of plastic composite bricks in contributing to sustainable building practices. The outcomes validated the feasibility of incorporating plastic bricks into construction, highlighting their environmental benefits and sustainable implications. This study advanced the field of sustainable construction materials by demonstrating the practical application and benefits of using recycled plastic bricks.

Key words: finite element analysis, plastic bricks, masonry wall, in-plane loads, in-plan cyclic loads.

Introduction

Masonry is one of the oldest and most used building materials throughout the world because of its rich history spreading over hundreds of years. It has been used widely among various cultures and regions of the world in construction. Masonry is made up of filled units, like bricks, stones, or blocks, with mortar. These units, in their turn, can consist of different materials and possess some mechanical characteristics (Abdelmegeed, 2015; Lourenço, 1998). This great variety of constituents is what makes it that masonry becomes heterogeneous in nature; thus, the properties and contents of the masonry vary (Bucknall, 2020; Ellen MacArthur Foundation, 2017).

This study answers a clarion call across the globe on the management of plastic waste, coupled with the demand by the building and construction industry on materials sustainable to the ecosystem. The structural performance under cyclic loading is still quite poorly appreciated in the in-plane, though the potential for applications of recycled plastic is recognized (Rashid et al, 2019; Ramos Huarachi et al, 2020; Desai, 2018).

The use of plastic bricks made of recycled PET, HDPE, and others is potentially applicable in masonry structures according to several studies (Pacheco-Torgal et al, 2018). Certainly, such kind of materials serves the purpose of waste reduction, rather characterized by qualities like improvement in thermal insulation and reduction of overall construction cost. However, the mechanical behavior and the structural integrity when the masonry structures are built with the help of such sophisticated materials do remain underexplored areas requiring suitable research (Lamba et al, 2022).

Composite materials, blending polymeric matrices with ceramic particles, have seen broad application across industries, leveraging the strengths of both components (Abdelhak et al, 2018). Another avenue

explored involves bricks comprising plastics like PET, PP, or HDPE mixed with sand, clay, or brick powder, with studies varying proportions to optimize mechanical and thermal properties. For instance, Kurian et al. experimented with thermocol, plastic, and sand mixtures, observing no water absorption and achieving a peak compressive strength of 11 N/mm² with 25% plastic content (Kurian et al, 2016). Similarly, Kulkarni et al. investigated the compressive strength of HDPE and PP bricks, resulting in strengths of 11.19 N/mm² for HDPE and 10.02 N/mm² for PP, comparable to the 10.5 N/mm² strength of first-class conventional bricks (Kulkarni et al, 2022). Singhal & Netula combined melted PET, LDPE, HDPE, and PP with stone dust, achieving a water-resistant material boasting a compressive strength of 5.6 N/mm² (Mahmoudi, 2014, 2015; Singhal & Netula, 2018).

Youcef et al. examined the reinforcement of brick particles in a PET matrix. Four unique samples, designated C1, C2, C3, and C4, were examined as part of the study. PET constituted a different weight proportion in each sample, ranging from 70%, 65%, 60%, and 55%, respectively. To test the performance of these samples as reinforced composites, their mechanical properties were evaluated. The results showed that compared to the other compositions, the C1 sample produced better results. Therefore, the analysis and potential applications of the C1 sample will be discussed in more detail in the following sections of this study (Moulai Arbi et al, 2023).

Recent literature in numerical tests focuses more on understanding masonry wall behavior under various conditions, spanning experimental and numerical analysis. Celano et al. (2021) focus on the in-plane resistance and design formulations, Choudhury et al. (2020) explore unreinforced masonry components against seismic loads, Radnić et al, (2012) offer a comprehensive numerical model for static and dynamic analyses. Koocheki & Pietruszczak (2023) innovate with artificial neural networks for analyzing large structures. However, these studies primarily focus on traditional materials, and the incorporation of innovative materials like plastic bricks in numerical simulations remains largely unexplored, indicating a potential area for future research in enhancing sustainability and material innovation in masonry construction.

The present numerical study focuses to further explore this avenue and open a way for exploration to be carried out in the case of plastic bricks made up of sand and PET (Polyethylene Terephthalate), providing a different avenue for exploring sustainable materials in construction.

This study helps in deciding the possibility of integrating plastic bricks made from sand and PET (Moulai Arbi et al, 2023), into the masonry wall

using computer software (Abaqus/CAE) (Dassault Systems, The 3DEXPERIENCE platform, 2017) to create a 3D computer model of the masonry wall using plastic bricks instead of the conventional masonry unit. To confirm accuracy, this model is compared to a previous numerical model (Abdulla et al, 2017) and an experimental model (Mojsilović et al, 2009). Python is an open-source programming language used in Abaqus products for customization and scripting (Van Rossum, 1995).

Numerical modeling approaches

Several numerical modeling methods have been developed to simulate the behavior of masonry in both linear and nonlinear states. The most common are the discrete element method (DEM) (Rafiee & Vinches, 2013), the limit analysis (Roca et al, 2010), the applied element method (AEM) (Pandey & Meguro, 2004), and the finite element method (FEM) (Zhai et al, 2017). As it has been mentioned, the numerical model is based on the finite element method and implemented in the Abaqus software, used within the presented work.

The approaches used in masonry by the finite element method generally fall into two categories: micro-modeling and macro-modeling (Abdulla et al, 2017). It chooses the appropriate one depending on the level of accuracy and complexity that is sought. To the extent that the micro-modeling technique is done in detail, the simulation has individual units and mortar as continuous, interfacing with discontinuous elements between units and mortar.

While the detailed micro model in Figure 1a predicts accurate results, the computational requirements limit its use to relatively small masonry components (Petraçca et al, 2017). This seeks to decrease some of the pitfalls involved in much more complicated and comprehensive micro-methodologies by adopting a simple and manageable micro-modeling strategy, as presented in Figure 1(b).

In the macro-modelling technique, masonry is modelled as a homogeneous material; see Figure 1(c), without separating individual pieces and mortar. The material attributes are generated with the characteristics of the averaged masonry constituents by a series of continuous elements defining a masonry construction in its entirety (Lourenço, 2002). It is intended to solve somewhat larger and more complicated brick structures, focusing generally on behavior but may not be able to capture detailed failure modes.

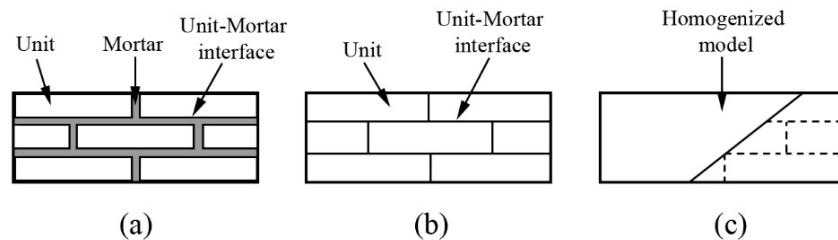


Figure 1 – Finite element modeling approaches (a) micro-detailed model (b) simplified micro-model (c) macro model (Koocheki & Pietruszczak, 2023)

Engineers can safely simulate potentially dangerous or destructive loads and failure scenarios using the finite element analysis (FEA) (Dassault Systems, The 3DEXPERIENCE platform, 2017), allowing them to understand how a system behaves physically at any given time.

It has several advantages, including increased accuracy by examining all potential physical constraints that could affect the design and designers' ability to assess how stresses in one component affect materials in other related parts, leading to better design quality. Early testing during the development phase, where virtual prototypes replace the lengthy and costly process of physical prototyping allows designers to quickly model multiple ideas and materials. The FEA software facilitates the construction of higher-quality products in faster design cycles and with reduced material usage, increasing productivity and revenue. Modeling the interior and exterior of the design will provide more in-depth information about important design factors. This helps designers understand how key elements affect the overall structure and locate potential weak points. Models are efficiently used as one single model can be used to test multiple physical events or failure types. Calculations are fast and initial investment cost low. There is an access to previously collected experimental data that can be used to perform parametric analysis on new models based on previously tested models (Magomedov & Sebaeva, 2020).

It is important to consider the choice of bond pattern when creating a masonry wall model. The stretcher bond, English bond, Flemish bond, and header bond are four distinct bond patterns that need to be considered (see Figure 2). Rows of headers are arranged in header bond with a half-brick offset. Similar to header bond, stretcher bond uses stretchers instead of headers, with the joints in each row centered on a half-brick above and below. By alternating rows of stretchers and headers, where the joints

between the stretchers align with the headers of the lower row, English bond is achieved. In contrast, Flemish bond alternates the arrangement of stretchers and headers in each row, with the stretchers in each row centered on the headers of the lower row, giving the bond a distinctive appearance (Debnath et al, 2023).

In this simulation, the stretcher bond serves as the reference point, as indicated in reference (Abdulla et al, 2017).

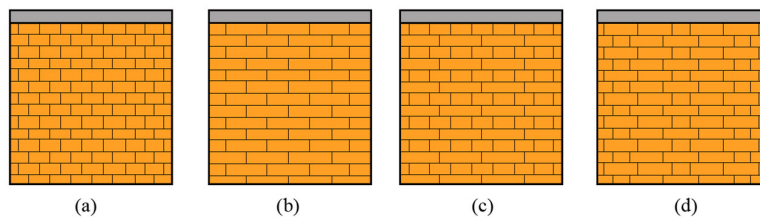


Figure 2 – Masonry bonds, (a) Stretcher bond, (b) Header bond, (c) English bond, (d) Flemish bond (Abdulla et al, 2017)

Five basic types of failure in masonry are represented in Figure 3. The first failure, as shown in Figure 3.a, is considered primarily as a tensile failure, while the second failure is considered a sliding failure by shear, as shown in Figure 3.b. Failure involves shear and diagonal cracking in Figure 3.c, besides masonry crushing failure. Last is the failure marked with cracks, as shown in Figure 3.e. This section focuses on how the computational model was undertaken, providing much detail on how to model the mortar between the two bricks precisely. The model performance is compared with earlier computations and experimental studies reported in the literature for comparison of the present results with those published (Debnath et al, 2023).

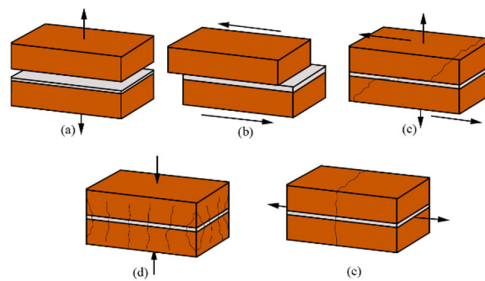


Figure 3 – Failure mechanisms a) tensile failure at the brick-mortar interface, b) shear failure by sliding at the brick-mortar interface, c) diagonal cracking of masonry, d) masonry crushing, and e) tensile cracking between the brick and mortar (Lourenço & Rots, 1997; Sarhosis & Lemos, 2018; Sarhosis et al, 2015)

Methodology description

A simplified micro-modeling technique is used in this study to approximate the three-dimensional responses of masonry specimens. These specimens undergo cyclic loading in the plane controlled by displacement as well as uniaxial compression. Both uniaxial and cyclic tests use displacement in the horizontal direction. Using the finite element modeling (FEM) analysis, the model is constructed in the commercial software Abaqus using solids and interaction surfaces. An application of the damaged plasticity (CDP) concrete model is performed to represent the behavior of masonry components. This model created with Abaqus is capable of reproducing plastic bricks and other quasi-brittle materials, such as the plastic bricks used in this case (Dassault Systems, The 3DEXPERIENCE platform, 2017). Using a surface-based cohesive property, the mortar and the interface between the mortar and masonry units are modeled. This interaction model allows for expressing cohesive connections with thin interfaces (Nela & Grajčevci, 2019).

The modeling approach employed 8-node linear brick (C3D8R) elements to represent the mortar unit, facilitating the capture of complex behaviors within the bricks. Cohesive elements (COH3D8) were utilized to model mortar layers and interfaces, enabling detailed analysis of delamination and crack propagation at brick-mortar joints. Plastic bricks were initially modeled using a linear elastic material model, transitioning to a damage plasticity model to account for post-yield behavior and plastic material characteristics. Similarly, the mortar was described with a damage plasticity model calibrated for its relatively brittle failure and lower tensile strength. Boundary conditions involved support at the base in all directions, with vertical pre-compression loads applied first to simulate self-weight and overhead loads, followed by lateral in-plane loads or cyclic lateral displacements to mimic seismic or wind forces. This sequential loading approach, starting with vertical pre-compression followed by lateral loading, reflects realistic loading conditions and facilitates accurate predictions of stress distribution and failure modes in masonry walls.

Cohesive surface based model for joints

Mathematically, this interaction is encapsulated by an elastic stiffness matrix denoted by "K". This matrix serves as a crucial representation, articulating the linkage between the tensile forces, represented by "t", and the separation vectors, denoted by " δ ". The elements within the stiffness matrix "K" are meticulously defined to govern the said relationship, thereby facilitating a precise correlation between the tensile forces exerted and the

resultant vectorial separations. This relationship is succinctly delineated through Equation (1).

Furthermore, the stiffness matrix "K" embodies a pivotal role in the predictive modeling of joint behavior under various loading conditions, offering insights into the mechanical integrity and the failure mechanisms of the joints in question. By delineating the parameters within the matrix "K", researchers and engineers are enabled to simulate and evaluate the structural response of the cohesive interfaces under scrutiny, thus providing a robust framework for the assessment and optimization of material and joint performance within a myriad of engineering applications.

$$\bar{\mathbf{t}} = \begin{Bmatrix} \bar{t}_n \\ \bar{t}_s \\ \bar{t}_t \end{Bmatrix} = \begin{bmatrix} \mathbf{K}_{nn} & \mathbf{0} & \mathbf{0} \\ \mathbf{0} & \mathbf{K}_{ss} & \mathbf{0} \\ \mathbf{0} & \mathbf{0} & \mathbf{K}_{tt} \end{bmatrix} \bar{\boldsymbol{\delta}} \quad (1)$$

In Equation (1), the terminologies "n", "s", and "t" delineate the normal and shear orientations across the two principal axes. The notation utilizes a single overbar to signify vectors, whereas a double overbar denotes matrices. The stiffness parameters can be articulated through the elastic or shear moduli pertaining to the individual elements and the dimension of the mortar layer, as elucidated in Equations (2) and (3), following the work of Lourenço (1998). Within these equations, "m" and "u" serve to identify the mortar and the unit, correspondingly.

$$\mathbf{K}_{nn} = \frac{E_u E_m}{h_m (E_u - E_m)} \quad (2)$$

$$\mathbf{K}_{ss} = \mathbf{K}_{tt} = \frac{G_u G_m}{h_m (G_u - G_m)} \quad (3)$$

The quadratic stress criterion is useful for the initiation and progression of damage as it indicates the onset of joint degradation, particularly under mixed mode loading. When the quadratic stress ratios of masonry joints reach a value of 1, this condition is considered fulfilled. Equation (4) in Abaqus illustrates the mathematical formulation of this criterion (Abdulla et al, 2017).

$$\left(\frac{\langle t_n \rangle}{t_n^{max}} \right)^2 + \left(\frac{t_s}{t_s^{max}} \right)^2 + \left(\frac{t_t}{t_t^{max}} \right)^2 = 1 \quad (4)$$

In this study, the critical shear stress for joints is regulated by the Mohr-Coulomb failure criteria, and the tensile strength of the joints determines if they undergo tensile cracking.

There are two popular methods for monitoring damage progression: one based on energy and the other on separation. The Benzeggagh-Kenane (BK) formulation is specifically used in the energy-based approach of this study for damage evolution. Equation (5) provides more information on this BK formulation and how it is implemented in Abaqus.

$$G_{IC} + (G_{IIC} - G_{IC}) \left(\frac{G_{shear}}{G_T} \right)^\eta = G_{TC} \quad (5)$$

The parameter known as the Exponent, denoted by η , delineates the behavior of the joint, with a value of 2 signifying a brittle characteristic. In essence, an elevated value of η indicates a heightened fragility of the assembly, elevating its vulnerability to abrupt and significant failure.

The energies associated with distinct failure mechanisms within the joints are categorized as G_{shear} and G_T. G_{shear} amalgamates the energies pertinent to mode III (out-of-plane shear) and mode II (in-plane shear) failure modes of the joint. Concurrently, the energy associated with mode I (tensile) failure mode is integrated with G_{shear} to constitute G_T. These parameters are instrumental in elucidating the joint's response under diverse loading conditions.

Illustrated in Figure 4 is the cohesive behavior of the joints, effectively showcasing the varied reactions of the joint under different loading scenarios and the influence of parameters such as η , G_{shear}, and G_T on such behavior.

Regarding stiffness degradation, it is observed in structural simulations that the stiffness of elements tends to diminish in response to damage or fracture, potentially leading to convergence challenges within the simulation. Convergence is achieved when an analysis yields a stable solution. However, pronounced stiffness degradation may complicate the convergence process, thereby introducing numerical difficulties in the simulation (Nela & Grajčevci, 2019).

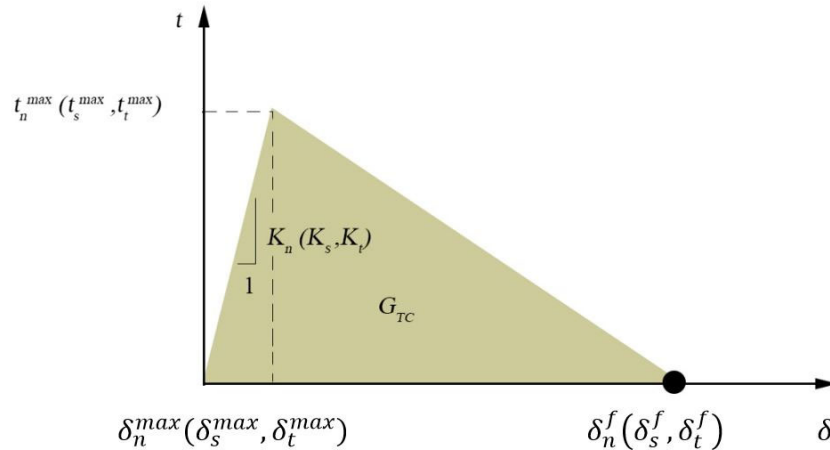


Figure 4 – Traction-separation model for joints (Abdelhak et al, 2018)

Compressive behavior

The Concrete Damage Plasticity (CDP) model uses stress-strain data for compression to characterize the material behavior under compressive pressures. The elastic strain (ϵ_{0c}^{el}), which represents the strain in the undamaged material (according to Equation 6), is subtracted from the total strain (ϵ_c) to determine the crushing strain. The model can simulate a reduction in stiffness to represent the material's response when subjected to compression and eventually reaching the crushing point by including a compression damage parameter (d_c).

$$\epsilon_c^{in} = \epsilon_c - \epsilon_{0c}^{el}; \quad (6)$$

where $\epsilon_{0c}^{el} = \frac{\sigma_c}{E_0}$,

a damage parameter that, under compression conditions, varies from 0 (indicating no weakening) to 1 (indicating total weakening or failure). Based on the relationship shown in Equation (7), Abaqus software handles this by automatically translating inelastic strain into plastic strain (ϵ_c^{pl}). Here, "c" specifically represents compression. This procedure explains the degree of damage that the material undergoes and explains how it plastically reacts to compression.

$$\epsilon_c^{pl} = \epsilon_c^{in} - \frac{d_c}{(1 - d_c)} \frac{\sigma_c}{E_0} \quad (7)$$

Tensile behavior

The Concrete Damage Plasticity (CDP) technique uses a softening curve to represent the tensile behavior. This curve illustrates how a material reacts to failure or cracking. In CDP, the deterioration of the elastic modulus (E_0) of the material is what causes this post-failure behavior.

This post-failure behavior is the result of the relationship between the post-failure stress and the crack strain (ε_t^{ck}). According to Equation (8), the crack strain is determined as the difference between the elastic strain (ε_{0t}^{el}) and the total strain (ε_t), where the elastic strain (ε_{0t}^{el}) reflects the strain in the undamaged material.

The model takes into account the decrease in stiffness that occurs when the material starts to crack under stress by including a tension damage parameter (dt). The tension damage parameter ranges from 0 (indicating no loss of strength) to 1 (indicating total loss of strength or failure). This feature helps us understand how the material reacts to tension while considering the degree of damage it has undergone.

$$\varepsilon_t^{ck} = \varepsilon_t - \varepsilon_{0t}^{el}, \quad (8)$$

where $\varepsilon_{0t}^{el} = \sigma_t / E_0$.

However, another method of modeling tensile behavior uses fracture energy (G_t) to describe the decrease in strength after cracking (as seen in Figure 5). Based on the provided fracture energy data, there is a linear loss of strength in this model upon fracture. The fracture energy and the tensile strength (σ_t) of the material are used to calculate the crack displacement (u_{t0}), which indicates the point where the material completely loses its strength. The subscript "t" specifically refers to tension in this case.

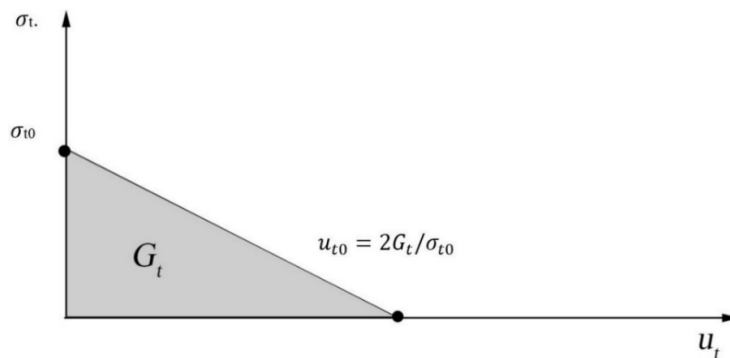


Figure 5 – Post-failure fracture energy curve (Abdelhak et al, 2018)

The effective stress concept in the CDP model relates the actual stress σ to the effective stress $\tilde{\sigma}$ through $\sigma = (1 - d)\tilde{\sigma}$ where d is dc or dt . The stress-strain relationship for the damaged material is given by $\sigma = (1 - d)E(\epsilon - \epsilon_p)$, with E as the undamaged Young's modulus, ϵ as the total strain, and ϵ_p as the plastic strain. The evolution of dc and dt can be defined as functions of equivalent plastic strains, ϵ_{pl}^c and ϵ_{pl}^t , respectively, often calibrated with experimental data, where $\epsilon_{pl}^c = \frac{\sigma}{E}(1 - d_c)$ and $\epsilon_{pl}^t = \frac{\sigma}{E}(1 - d_t)$. These relationships illustrate how damage evolves and influences the structural integrity under various loading conditions.

Masonry wall model

The units interact both linearly and nonlinearly considered in this three-dimensional finite element micromodel developed. For this, a consistent strategy based on surface modeling was adopted that would model how the joints were interacting. Discretizing nodes into surfaces and with a finite sliding formulation defined contacts between the neighboring masonry blocks. In the present model, specifically, the behavior of hard contact was implemented, wherein the pressure was transmitted between the surfaces in contact with each other in such a way that there is no penetration of tensile stress and transmission of tensile stress through the contacting surfaces. This resembles quite closely the behavior of the masonry unit surfaces in practice. They tested the validity of the proposed model by comparing its results to the experiments presented by (Mojsilović et al, 2009).

The tests were, therefore, carried out to evaluate the masonry behavior under in-plane cyclic loading (in in-seismic loading conditions) and in-plane monotonic loads. The tested walls had a nominal thickness of 110 mm, a length of 1200 mm, and a height of 1200 mm (see Figure 6). The walls were made of plastic bricks with the following dimensions: length: 230mm, height: 76mm, and thickness: 110mm. The mortar joints had a thickness of 10 mm, and the cement, lime, and sand were mixed in a ratio of 1:1:6. There were a total of 14 rows of bricks, with 5 bricks per row, arranged in a common bond pattern in each wall.

In our study, the scale ratio used for the test specimens is 1:1, meaning that the models are full-scale. The choice of full-scale specimens ensures that the results are directly applicable to real-world scenarios, providing a more accurate representation of the behavior and performance of masonry structures under various loading conditions. Utilizing full-scale

specimens eliminates the need to account for scaling effects, which can introduce additional variables and potential inaccuracies in the analysis.

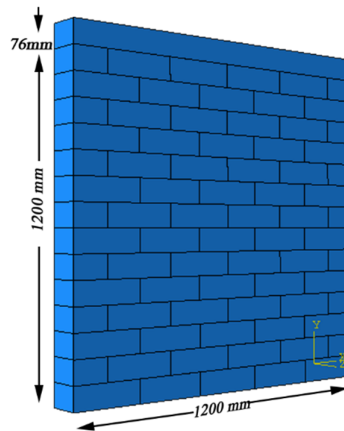


Figure 6 – Numerical model of the masonry wall.

Properties

In this illustration, the response of the wall to seismic conditions and in-plane loads reproduced above is modeled using Abaqus software, as described earlier. It had simplified brick micro-modeling assembling techniques with the mortar taken as an interaction parameter. Both cohesive behavior and damage behavior are included in these interaction characteristics.

Table 1 shows the properties of the plastic bricks. The designed geometric shapes for the plastic bricks were done in the 3D modeling environment. The bricks were represented as solid objects in order to best represent the characteristics of the designed objects. It can be obtained from the table that the characteristics of the plastic bricks are 1660 kg/m³ for density, 2771 MPa for Young's modulus, and 0.3 for Poisson's ratio (Moulai Arbi et al, 2023).

Table 1 – Properties of the plastic bricks (Moulai Arbi et al, 2023)

Density (kg/m ³)	Young's modulus (MPa)	Poisson's ratio
1660	2771	0.3

In this study, the Drucker-Prager model describes the plasticity characteristics found on the mechanical menu. In the same menu, more specifically in the plasticity zone, was the Drucker-Prager model. The model is designed with a friction angle of 36 degrees, a flow stress ratio of 1, and a dilation angle of 11.3 degrees, as shown in Table 2. It also hardens at 14.18 MPa on Drucker-Prager F. et al. (Abdulla et al, 2017) identified mortar properties, which are presented in Tables 2 and 3.

Table 2 – Properties of Drucker-Prager (Abdulla et al, 2017)

Friction angle (β)	Flow stress ratio (R)	Dilation angle (ψ)
36	1	11.3

The described construction technique delineates a masonry wall comprising 14 rows of bricks. This approach eschews the portrayal of mortar as an independent entity, opting instead for a detailed crafting and assembly of each brick. Within the Abaqus software framework, the attributes of the mortar find their representation through interaction properties.

The mechanical menu's normal behavior category specifies a friction coefficient (μ) of 0.75 (Raijmakers, 1992). Furthermore, the model incorporates cohesive behavior, encompassing the parameters Knn, Ktt, and Kss as delineated in Table 3. These parameters, Knn for the normal direction stiffness, Kss for the shear direction stiffness, and Ktt for the secondary shear direction stiffness, collectively articulate the stiffness properties of the mortar.

Table 3 – Joint interface properties (Abdulla et al, 2017)

Knn (n/mm ³)	Kss (n/mm ³)	Ktt (n/mm ³)
63	25	25

Table 4 outlines the parameters for mechanical behavior, selecting the tension damage option and assigning it a threshold of 0.2 MPa, as detailed in the literature (Abdulla et al, 2017). The chosen framework for damage analysis is the Benzagagh-Kenan model, with a specified value of 2 signifying a tendency towards brittle characteristics, in accordance with the findings in (Benzeggagh & Kenane, 1996).

For the first and second shear modes, the designated rupture energy is 0.04 N/mm (Lourenço, 2002), whereas the energy for normal rupture is established at 0.012 N/mm (Angelillo et al, 2014).

Table 4 – Properties of the masonry wall (Abdulla et al, 2017).

Friction coef (μ)	Tension t_n^{\max} (MPa)	B-K	G _{Ic} (N/mm)	G _{IIc} (N/mm)
0.75	0.2	2	0.012	0.04

In the Concrete Damage Plasticity (CDP) model used in Abaqus, the parameters ω_c and ω_t are dimensionless factors representing the reduction in stiffness due to damage under compressive and tensile loading, respectively. Specifically, ω_c is typically set to 0.9 and ω_t to 0.7, indicating that the stiffness in compression and tension is reduced by 10% and 30% respectively when the material is fully damaged. These parameters are integrated into the model through effective stress relationships: $\sigma = (1 - d_c) \tilde{\sigma}_c$ for compression and $\sigma = (1 - d_t) \tilde{\sigma}_t$ for tension, where $\tilde{\sigma}_c$ and $\tilde{\sigma}_t$ are the effective stresses. The damage parameters d_c and d_t evolve based on equivalent plastic strains, reflecting the material's degradation and ensuring accurate simulation of cyclic loading behavior.

Meshing module

Meshing, a pivotal step in the finite element analysis, entails the subdivision of a structure into myriad diminutive elements. These elements are individually computed, and aggregating their computational outcomes yields the structure's final analysis result.

This analytical process bifurcates into three principal segments: pre-processing, processing, and post-processing. During pre-processing, based on the chosen analytical framework, be it modal analysis or structural static analysis, the requisite element type is determined. This stage involves the establishment of nodes, allocation of material properties, application of boundary conditions and loads, and the fabrication of elements by linking them with nodes (Kumar, 2022).

The processing phase unfolds within the computational domain, where the software undertakes the resolution of the boundary value problem, subsequently presenting the results for user review.

In the post-processing phase, the analyst evaluates the derived results, focusing on metrics such as temperature variations, displacements, durations, stresses, strains, and natural frequencies (Magomedov & Sebaeva, 2020).

A mesh sensitivity investigation was conducted to ascertain the optimal mesh size for an accurate stress analysis in a masonry wall subjected to numerical evaluation. The initial analysis utilized a mesh

configuration of 7 X 2 X 3 elements per masonry unit, mirroring the unit's dimensions of 110 mm in thickness, 76 mm in height, and 230 mm in length, as depicted in Figure 7a. The subsequent analysis increased the mesh density by employing a 7 X 4 X 3 element arrangement for each unit, effectively augmenting the element count, as illustrated in Figure 7b. The final phase of the analysis quadrupled the element number from the initial setup by adopting a 7 X 4 X 6 element scheme for each unit, as shown in Figure 7c (Abdulla et al, 2017).

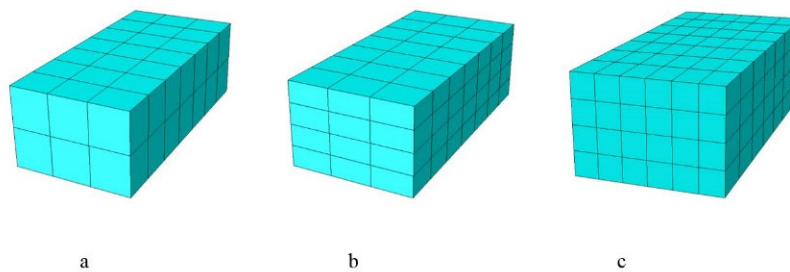


Figure 7 – Mesh sizes used in masonry units.

In the mesh module depiction of the complete masonry wall assembly, as showcased in Figure 8, the configuration with a 7 X 2 X 3 elements mesh comprises a total of 8,136 nodes and 3,600 elements. This detailed representation underscores the intricate network of computational points and structural components that constitute the analytical model of the wall.

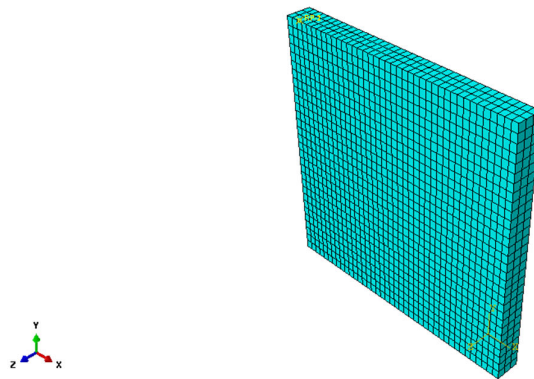


Figure 8 – Comprehensive Mesh Structure of a Masonry Wall Model: 7 X 2 X 3 Element Configuration

Figure 9 reveals that across all tested scenarios, the outcomes regarding failure modes and the elastic and plastic behaviors remained consistent. This analysis underscores the minimal sensitivity of the proposed model to variations in mesh granularity. Consequently, the adoption of coarser mesh configurations is feasible, offering the benefit of substantially decreased computational demands.

The computational time associated with each mesh configuration was a paramount consideration, given the extensive nature of our simulations. The finest mesh (7X4X6 elements) needed 110 minutes, which was the highest computational investment. On the other hand, the intermediate mesh (7X4X3 elements) required 80 minutes, and the lowest computational investment of 50 minutes was for the coarsest mesh (7X2X3 elements).

Rationale for mesh selection

The decision to opt for the coarsest mesh configuration (7X2X3 elements) was based on key findings from the sensitivity analysis. The results showed comparable accuracy across mesh densities, indicating that finer meshing would not significantly improve accuracy. Additionally, the coarsest mesh offered significant computational efficiency, with a reduction in computational time from 110 to 50 minutes, facilitating wider model utilization for large-scale parametric studies without proportional increases in computing resources.

This configuration struck an optimal balance between computational manageability and detail, ensuring sufficient capture of nuanced structural behavior, including crack initiation and propagation, critical for assessing wall strength under various loading conditions.

The applied actions, whether load or displacement, to the model during the numerical analysis were made successively. This indicates that the applied actions were actually gradually imposed actions on the model, as it may relate to the load or the displacement control.

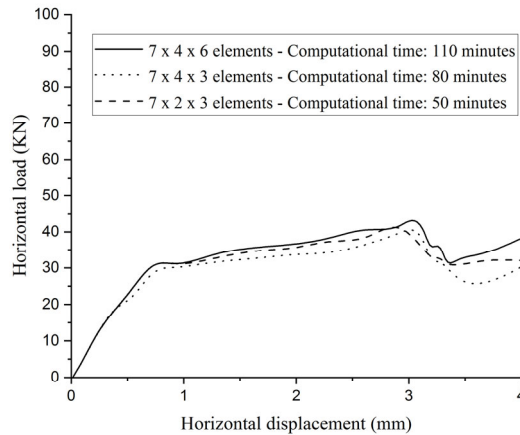


Figure 9 – Comparison between different mesh sizes.

Loads

Figure (10) shows a schematic of the experimental setup carried out in the investigation of the performance of masonry walls under horizontal cyclic loads in structural engineering. The test specimen itself, usually a masonry wall built from individual bricks or blocks, is at the heart of this system. The latter then serves to carry out a simulation of the real-life stresses, from which the wall might suffer during its service life. An actuator, a high-end device used to apply controlled loads or displacements, applies horizontal forces.

This actuator can apply the required load with not only the static, but also dynamic and cyclic loads that can be produced by environmental conditions, such as earthquakes or wind. Sensing devices are placed at strategic points on the wall and the actuator for measuring response to the loads. These sensors may be strain gauges, displacement transducers, or load cells to get real-time information of the recorded stresses, strains, and deformations at the wall.

The numerical work attempts to replicate the conditions of loading imposed on the masonry wall with realism inside the simulated environment. From the corresponding physical tests, the horizontal and cyclic loads are applied on the walls of masonry having the same characteristics (Rezapour et al, 2021).

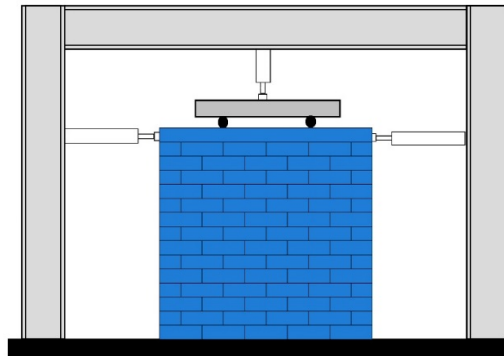


Figure 10 – Experimental masonry wall under loads

In-plane loading

The wall received a controlled vertical compressive load from the top of the beam. After setting the compressive load, it restricted the upper beam's vertical movement. Subsequently, it applied a gradual and monotonic horizontal load to the wall through the upper beam (Figure 11).

Executed in two stages, the numerical analysis first introduced the initial vertical compression load. The second phase proceeded under the identical boundary conditions as the experiment, but it added restrictions to prevent out-of-plane vertical and horizontal displacements and rotations at the top of the wall around all axes. Throughout this phase, the approach maintained the vertical compressive stress while incrementally applying the horizontal load in the plane under displacement control (Abdulla et al, 2017).

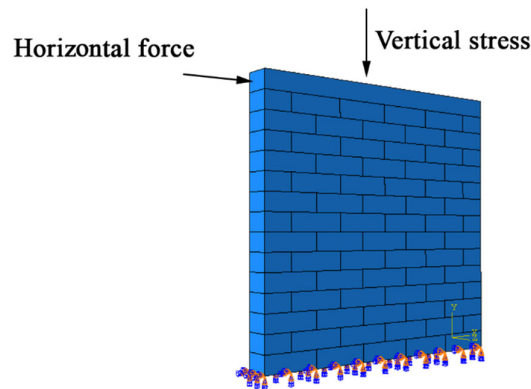


Figure 11 – Brick wall with loading in the plane

In-plane cyclic loading

In the numerical simulation detailed in Figure 12, the wall was subjected to a sequence of loading phases, beginning with a vertical compression load applied from the top, whereupon the vertical movement of the upper beam was restricted. This initial stage, termed the pre-compression phase, involved maintaining a constant vertical stress before transitioning to the second stage. During this subsequent phase, the wall, now stabilized under displacement control, was subjected to progressive cyclic horizontal loads within the plane. This methodology encapsulates a comprehensive approach to evaluating the structural response of the wall under varying load conditions, thereby enabling a detailed analysis of its behavior in a controlled numerical environment (Abdulla et al, 2017).

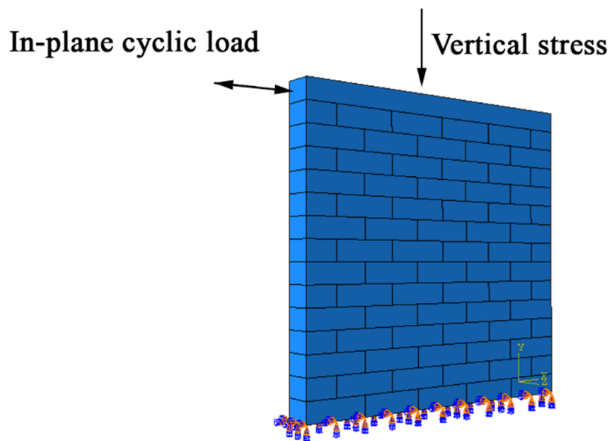


Figure 12 – Masonry wall subjected to cyclic loading in the plane

The study encompassed 19 loading cycles on a specifically selected wall, which had been subjected to an initial vertical stress of 0.7 MPa. Figure 13 illustrates the detailed load distribution patterns exerted on the wall top. This wall, uniquely identified within the experimental setup as A3-1, stood as the focal point of our investigation, offering insights into the stress response and structural behavior under the applied loading conditions (Magomedov & Sebaeva, 2020).

Data points (x, y) were collected using OriginLab (2020) and subsequently imported into Abaqus for analysis. These data, derived from cyclic loading experiments, are compiled and presented in Table 5. It displays the outcomes and patterns observed from the loading cycles.

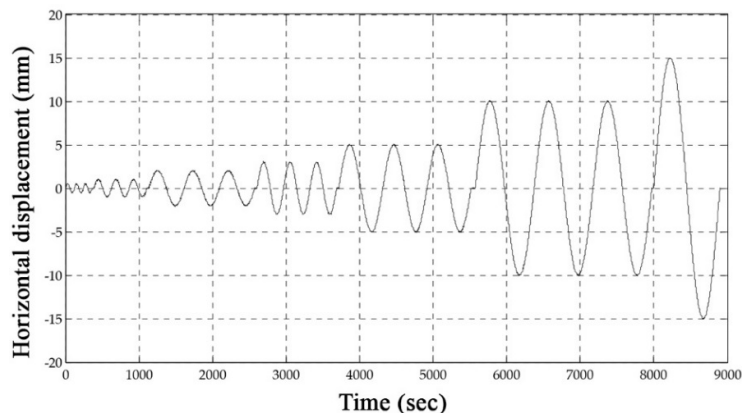


Figure 13 – Displacement loading history (Magomedov & Sebaeva, 2020)

Results

In-plane loading

The graph in Figure 14 presents a comparison of the numerical results between two types of masonry walls: one constructed with plastic bricks and another from a study by (Abdulla et al, 2017), which presumably uses traditional masonry materials.

As the horizontal displacement increases, both lines show an initial steep incline, indicating that the load capacity increases with displacement up to a certain point. This portion of the curve represents the elastic behavior of the materials where the deformation is proportional to the load and is recoverable.

However, as the displacement continues to increase, both lines plateau and exhibit peaks, representing the maximum load capacity of the walls. Beyond these peaks, the lines fluctuate and generally trend downwards, indicative of the walls experiencing damage and undergoing inelastic deformation, where the bricks are likely to have yielded or the mortar have cracked, leading to a decrease in load capacity.

The results showed consistency and good agreement in terms of failure modes. It is interesting to note that the masonry wall constructed from plastic bricks has a lower horizontal load capacity compared to the masonry wall developed by Kurdo F. et al. For example, in Kurdo F. et al.'s study, the maximum load for the masonry wall was 55.40 kilonewtons (KN), while the maximum load observed for the masonry wall using plastic bricks reached 39.10 KN (Abdulla et al, 2017).

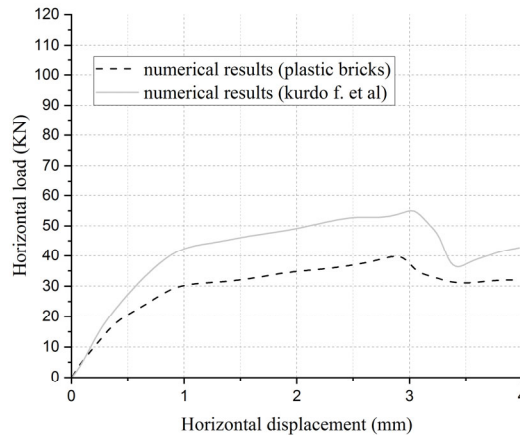


Figure 14 – Horizontal load-displacement comparison

Table 5 represents a quantitative summary of the horizontal load capacities for the two numerical models of masonry walls subjected to incremental horizontal displacements.

Table 5 – Numerical data of the wall under in-plane loading

	Horizontal displacement (mm)	0	0.5	1	1.5	2	2.5	3	3.5	4
Horizontal loads (Kn)	Plastic bricks	0	21.27	29.82	31.86	34.94	36.30	36.67	30.84	32.19
	(Abdulla et al, 2017)	0	27.75	42.81	46.24	49.33	52.75	55.40	37.35	43.15

Figure 15 depicts a comparison between the experimental results of a traditional masonry wall and the numerical simulations for plastic bricks walls, examining their behavior under horizontal loading (Vargas et al, 2023). The numerical simulation closely mirrors the trend exhibited by the experimental results, demonstrating good agreement in terms of the overall shape and peak values of the load-displacement curve. Initially, both lines ascend steeply, indicating a linear increase in load with displacement, characteristic of the elastic behavior of the wall where deformation is recoverable upon load removal. As displacement continues, both curves reach a peak point. The convergence of the two curves validates the numerical model, confirming that it is a reliable predictor of the experimental wall's behavior (Raijmakers, 1992).

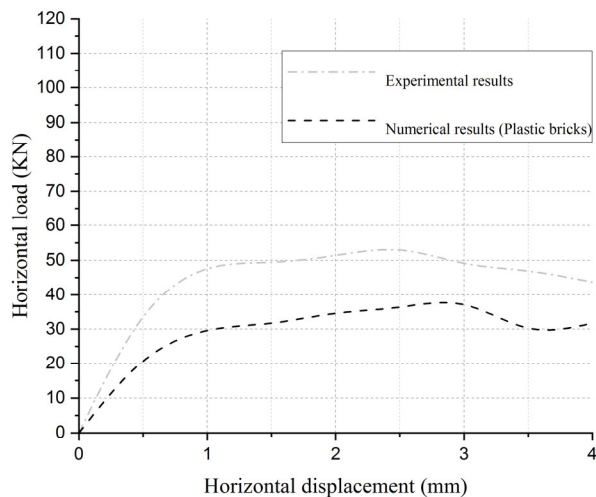


Figure 15 – Comparison between the numerical and experimental results

Table 6 presents a comparative analysis of the load capacities between a numerically modeled plastic brick masonry wall and an experimentally tested wall composed of traditional bricks across a range of horizontal displacements. The table reveals that at every displacement point, the traditional brick wall exhibits a superior load capacity compared to the plastic brick wall, with a pronounced difference at the peak load point 52.93 kN for the traditional brick wall versus 36.30 kN for the plastic brick wall at 2.5 mm displacement.

This comparison highlights the divergence in structural performance between the two materials, emphasizing the higher load-bearing efficiency of traditional bricks over their plastic counterparts.

Table 6 – Data results of the numerical and experimental work

	Horizontal displacement (mm)	0	0.5	1	1.5	2	2.5	3	3.5	4
Horizontal loads (Kn)	Plastic bricks	0	21.27	29.82	31.86	34.94	36.30	36.67	30.84	32.19
	Experimental results	0	33.51	47.53	49.42	51.36	52.93	49.14	46.89	43.70

The disparity in load capacity between the plastic brick masonry wall and a traditional masonry wall can be attributed to distinct material properties and the interaction between components within the wall system.

Plastic bricks generally exhibit a lower modulus of elasticity compared to traditional masonry materials, which contributes to a reduced capacity to withstand loads before deforming. The compressive strength of plastic bricks also tends to be less than that of traditional bricks, leading to a decrease in overall load-bearing capability (D'Altri et al, 2020). The bonding between plastic bricks and mortar is typically weaker than that of traditional brick-and-mortar joints, which can result in a lower horizontal load capacity for walls constructed with plastic bricks. Unlike traditional masonry materials, which are often brittle, plastic materials are more ductile, meaning they can undergo more extensive deformation under load, a characteristic that can lower the peak load capacity of a wall due to the material yielding at lower stress levels.

In Figure 16, "STATUSXFEM" represents the extent of fracturing within the individual elements of the masonry wall model. A full fracture within an element is indicated by a status value of 1, while a status of 0 signifies an absence of cracking. The values falling between 0 and 1 denote varying degrees of partial element fractures. The inception of tensile fractures was noted at the base of the wall as the loading commenced, which precipitated the compression and subsequent buckling of the wall lower regions. This sequence of stress response gave rise to diagonal fracturing that propagated between the blocks, leading to further cracking within the blocks themselves.

The depicted diagonal crack pattern corresponds to one of the observed failure modes in experimental settings, known as diagonal failure, which is a common mode of failure in masonry structures subjected to lateral forces (Ponte et al, 2019). Additionally, the analysis revealed both vertical and horizontal slippage occurring among the plastic brick units, contributing to the overall degradation of the wall structural integrity under stress (Ghiassi et al, 2012; Zhang et al, 2023).

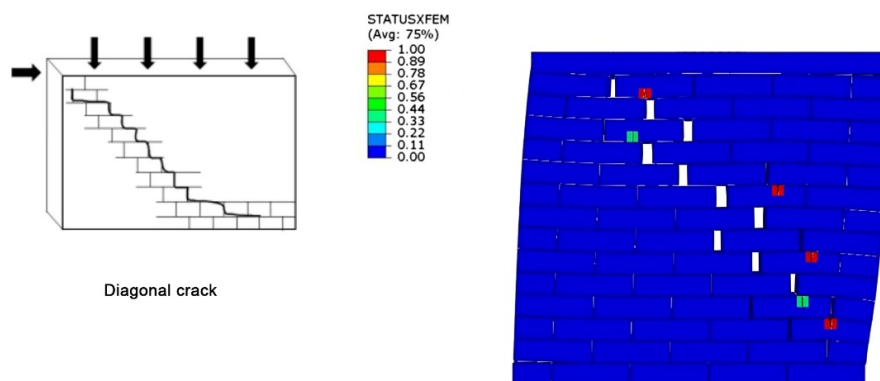


Figure 16 – Failure pattern of the masonry wall

In-plane cyclic loading

Cyclic loading graphs are instrumental in analyzing the dynamic response of structures, such as walls, during seismic events (Xia et al, 2024). The graph in Figure 17 representing force over time is derived from the numerical simulation of the plastic brick wall that subject a masonry wall to cyclical loading, mimicking the push-pull effects encountered during an earthquake. It charts the force exerted on the wall, measured in exponential units, as it oscillates over time.

By synthesizing data from the displacement loading history in Figure 12 and data from force loading history in Figure 16, a hysteresis loop can be constructed (Krtinić et al, 2023), which is a powerful tool for visualizing the energy dissipation and the cyclic stiffness degradation of the wall under seismic loading (Figure 17).

A hysteresis loop graph exhibits the relationship between load and displacement for each cycle, highlighting the wall energy dissipation capacity, an essential factor in seismic design. This capacity is crucial for quantifying how a structure absorbs and releases energy, which directly impacts its ability to withstand and recover from earthquake-induced stresses. The required computational time for the masonry wall under cyclic load is 130min.

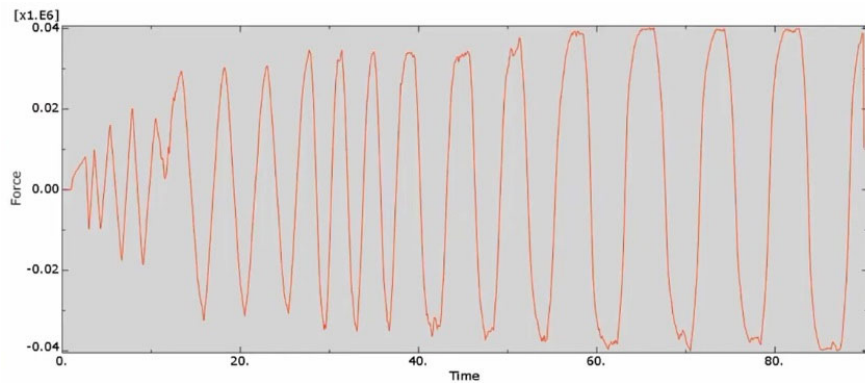


Figure 17 – Force loading history

The hysteresis graphs in Figure 18 provide a side-by-side evaluation of the experimental and computational responses of a masonry wall subjected to cyclic loading. In the comparison, it is noteworthy that the experimental model withstood a higher peak for horizontal force, reaching 45.53 kilonewtons (kN), in contrast to the numerical model, which peaked at 34.20 kN.

This discrepancy suggests that the numerical model predicted an earlier onset of horizontal slides along the lower course of the masonry units. The predominant failure mechanism in the simulation was horizontal cracking along the lower mortar joints. Furthermore, vertical slippage was a prominent feature at the base of the wall in the simulation data (Rahim et al, 2024).

The sequence from A to D in Figure 19 illustrates the escalating stress response of a masonry wall subjected to cyclic loading, as depicted by the von Mises stress distribution. The panel A shows initial stress at the wall base. As the cyclic loading progresses, the panels B and C reveal a significant increase in stress towards the center, signaling higher stress levels likely leading to material deformation. The panel D exhibits the culmination of stress throughout the wall, with the most intense stress (red areas) indicating failure.

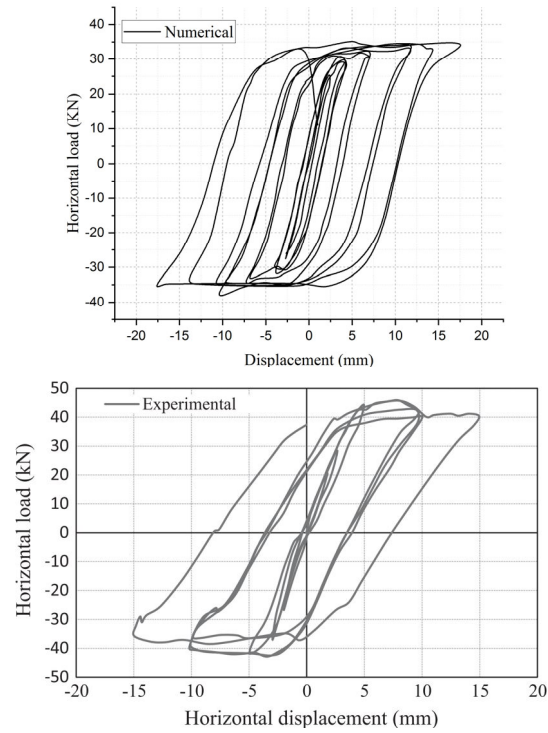


Figure 18 – Comparison between numerical and experimental cyclic loading in the plane.

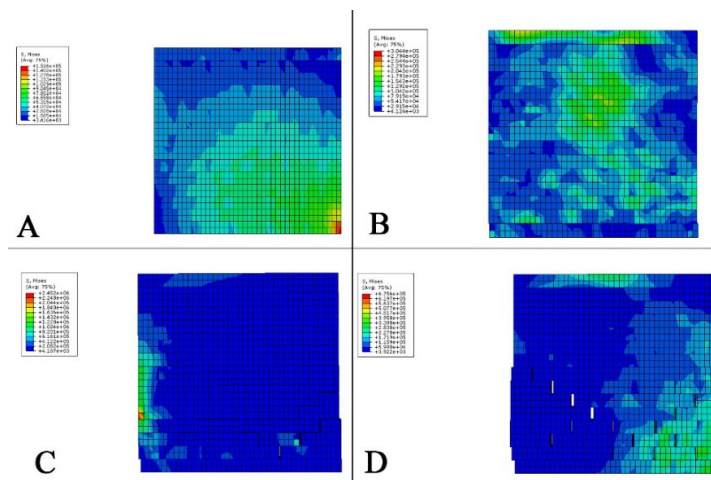


Figure 19 – Stress response of the masonry wall under cyclic loading

The four panels, labeled A to D, in Figure 20 depict the displacement progression of a masonry wall subjected to cyclic loading, revealing the deformation pattern and identifying the areas where sliding occurs between the brick units. The panel A starts with minimal displacement, and as the panels progress to D, there is a significant increase in displacement magnitude, especially evident in the lower sections of the wall.

The panel B shows the beginning of sliding in the bottom line of units, indicating a shift in the structural integrity of the wall. In the panel C, the beginning of diagonal failure occurs, suggesting increased stress concentration within the masonry structure.

The panel D shows a pronounced displacement pattern that closely resembles the diagonal tension failure observed in experimental studies (Figure 21), characterized by a distinct diagonal crack pattern within the wall. This failure mode is indicative of bricks sliding past each other, leading to a loss of cohesion in the masonry structure and the formation of cracks along the lines of maximum shear stress. The final panel D, mirroring the experimental diagonal tension failure mode, reflects a critical state where significant displacement leads to structural failure.

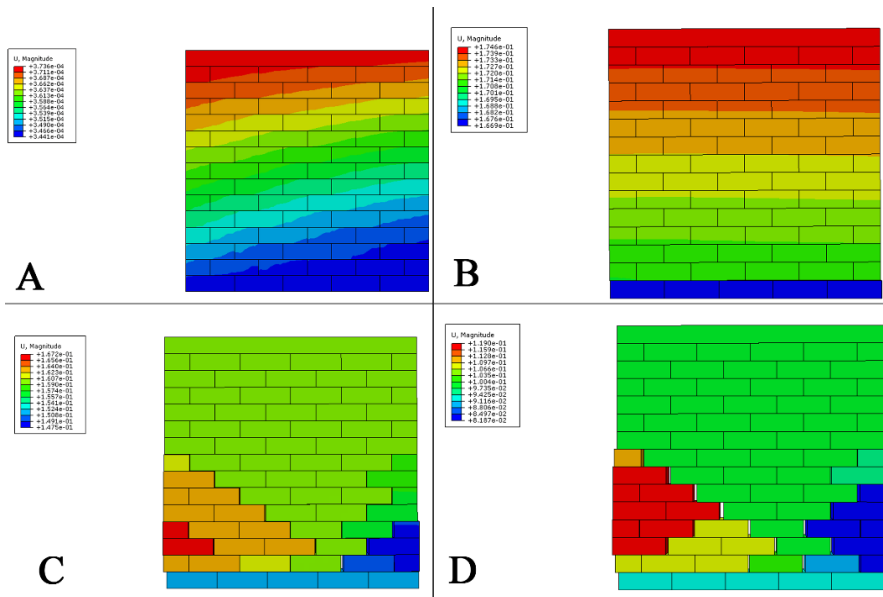


Figure 20 – Displacement progression of a masonry wall under cyclic loading

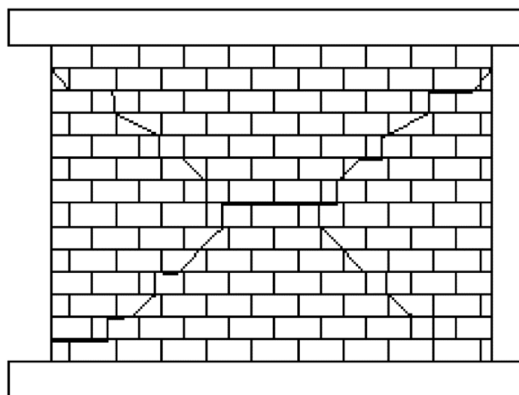


Figure 21 – Diagonal tension failure mode (Choi et al, 2023)

In addressing the comparative analysis between our numerical models and the experimental data, our investigation reveals a nuanced correlation that underscores the utility of numerical simulations in replicating the complex behaviors of masonry walls constructed with recycled plastic bricks under in-plane loading. The numerical results showcased in "Table numerical data of wall under in-plane loading" and the experimental findings presented in "Table data results of numerical and experimental work" elucidate a substantial degree of concordance, particularly in capturing the trend of load capacity against displacement. Despite the observed quantitative discrepancies, such as a lower peak load capacity in numerical predictions (36.67 kN for numerical vs. 49.14 kN experimentally at a 3 mm displacement), the numerical model effectively mirrors the overall shape of the experimental load-displacement curve. This indicates that the model adeptly captures the essential mechanical response of masonry walls, albeit with conservative estimates of peak strengths. Notably, the early onset of nonlinear behavior in numerical simulations compared to experimental observations suggests model sensitivity to material property assumptions and boundary conditions, highlighting areas for refinement. The critical examination of failure modes, where numerical analysis predicts horizontal cracking along lower mortar joints akin to experimental results, further validates the relevance of the model in simulating real-world phenomena. This qualitative agreement emphasizes the potential of the model as a predictive tool, albeit necessitating adjustments in material

characterization and enhanced detailing of the brick-mortar interface to amplify its accuracy and predictive power.

Conclusion

The numerical modeling study presented here offers a critical exploration into the structural performance of masonry walls utilizing recycled plastic bricks subjected to both in-plane and cyclic loading conditions. The analysis, conducted through a simplified micro-modeling approach in Abaqus, provides a foundational understanding of the mechanical behaviors and failure mechanisms associated with this innovative construction material. The study's findings elucidate a lower load-bearing capacity of walls constructed with plastic bricks when compared to their conventional counterparts, alongside an earlier onset of damage under cyclic loading scenarios. Notably, the emergence of horizontal cracking along lower mortar joints and the observation of diagonal failure modes and sliding, particularly at the wall base under cyclic loads, underscore the distinct structural responses of these materials under stress.

The practical significance of this research lies in its contribution to the broader field of sustainable construction practices. By demonstrating the feasibility of employing recycled plastic bricks in masonry wall construction, this study paves the way for their consideration in non-load-bearing applications and highlights their potential in contributing to waste reduction and environmental sustainability in the construction industry. Furthermore, the nuanced understanding of failure mechanisms and load-bearing behaviors garnered through this numerical modeling offers valuable insights for the development of design guidelines and the optimization of plastic brick formulations to enhance their structural performance.

In conclusion, while recycled plastic bricks present a reduction in strength compared to traditional masonry materials, their incorporation into construction projects represents a viable path toward achieving more sustainable building practices. The outcomes of this research not only advocate for the innovative use of waste materials in construction but also lay the groundwork for future investigations aimed at refining the structural capabilities and application scope of plastic bricks, thereby reinforcing the imperative of sustainability in the built environment.

References

Abdelhak, B., Mahmoudi, N. & Hacen, M. 2018. Improvement of the Interfacial Adhesion Between Fiber and Matrix. *Mechanics and Mechanical Engineering*, 22(4), pp.885-893.

Abdelmegeed, M.M.A 2015. *Damage assesement and rehabilitation of historic traditional masonry*. PhD thesis. Athens, Greece: National Technical University of Athens (NTUA), Faculty of civil engineering [online]. Available at: <https://www.fayoum.edu.eg/Arc/Restoration/pdf/MrMohamedPhd.pdf> [Accessed: 21 April 2024].

Abdulla, K.F., Cunningham, L.S. & Gillie, M. 2017. Simulating masonry wall behaviour using a simplified micro-model approach. *Engineering Structures*, 151, pp.349-365. Available at: <https://doi.org/10.1016/j.engstruct.2017.08.021>.

Angelillo, M., Lourenço, P.B., Milani, G. 2014. Masonry behaviour and modelling. In: Angelillo, M. (Eds.) *Mechanics of Masonry Structures*. CISM International Centre for Mechanical Sciences, 551, pp.1-26. Vienna: Springer. Available at: https://doi.org/10.1007/978-3-7091-1774-3_1.

Benzeggagh, M.L. & Kenane, M. 1996. Measurement of mixed-mode delamination fracture toughness of unidirectional glass/epoxy composites with mixed-mode bending apparatus. *Composites Science and Technology*, 56(4), pp.439-449. Available at: [https://doi.org/10.1016/0266-3538\(96\)00005-X](https://doi.org/10.1016/0266-3538(96)00005-X).

Bucknall, D.G. 2020. Plastics as a materials system in a circular economy. *Philosophical Transactions of the Royal Society A*, 378(2176), art.number:20190268. Available at: <https://doi.org/10.1098/rsta.2019.0268>.

Celano, T., Argiento, L.U., Ceroni, F. & Casapulla, C. 2021. In-Plane Behaviour of Masonry Walls: Numerical Analysis and Design Formulations. *Materials*, 14(19), art.number:5780. Available at: <https://doi.org/10.3390/ma14195780>.

Choi, H., Quan, C. & Jin, K. 2023. Nonlinear Performance Curve Estimation of Unreinforced Masonry Walls Subjected to In-Plane Rocking Behavior. *Applied Sciences*, 13(12), art.number:7298. Available at: <https://doi.org/10.3390/app13127298>.

Choudhury, T., Milani, G. & Kaushik, H.B. 2020. Experimental and numerical analyses of unreinforced masonry wall components and building. *Construction and Building Materials*, 257, art.number:119599. Available at: <https://doi.org/10.1016/j.conbuildmat.2020.119599>.

D'altri, A.M., Sarhosis, V., Milani, G., Rots, J., Cattari, S., Lagomarsino, S., Sacco, E., Tralli, A., Castellazzi, G. & de Miranda, S. 2020. Modeling Strategies for the Computational Analysis of Unreinforced Masonry Structures: Review and Classification. *Archives of Computational Methods in Engineering*, 27, pp.1153-1185. Available at: <https://doi.org/10.1007/s11831-019-09351-x>.

-Dassault Systems, The 3DEXPERIENCE platform. 2017. *Simulia: Abaqus Finite Element Analysis for Mechanical Engineering and Civil Engineering* [online]. Available at: <https://www.3ds.com/products/simulia/abaqus> [Accessed: 21 April 2024].

Debnath, P., Chandra Dutta, S. & Mandal, P. 2023. Lateral behaviour of masonry walls with different types of brick bonds, aspect ratio and strengthening measures by polypropylene bands and wire mesh. *Structures*, 49, pp.623-639. Available at: <https://doi.org/10.1016/j.istruc.2023.01.155>.

Desai, B.H. 2018. 14. United Nations Environment Program (UNEP). *Yearbook of International Environmental Law*, 32(1), pp.293-298. Available at: <https://doi.org/10.1093/yiel/yvac039>.

-Ellen MacArthur Foundation. 2017. The New Plastics Economy: Rethinking the future of plastics & catalysing action. *Ellenmacarthurfoundation.org* [online]. Available at: <https://www.ellenmacarthurfoundation.org/the-new-plastics-economy-rethinking-the-future-of-plastics-and-catalysing> [Accessed: 21 April 2024].

Ghiassi, B., Marcari, G., Oliveira, D.V. & Lourenço, P.B. 2012. Numerical analysis of bond behavior between masonry bricks and composite materials. *Engineering Structures*, 43, pp.210-220. Available at: <https://doi.org/10.1016/j.engstruct.2012.05.022>.

Koocheki, K. & Pietruszczak, S. 2023. Numerical analysis of large masonry structures: bridging meso and macro scales via artificial neural networks. *Computers & Structures*, 283, art.number:107042. Available at: <https://doi.org/10.1016/j.compstruc.2023.107042>.

Krtinić, N., Gams, M. & Marinković, M. 2023. Experimental and numerical investigation of the seismic response of confined masonry walls. In: Papadrakakis, M. & Fragiadakis, M. (Eds.) *ECCOMAS Proceedia COMPDYN 2023 - 9th ECCOMAS Thematic Conference on Computational Methods in Structural Dynamics and Earthquake Engineering*, Athens, Greece, pp.528-543, June 12-14. Available at: <https://doi.org/10.7712/120123.10418.20831>.

Kulkarni, P., Ravekar, V., Rao, P.R., Waigokar, S. & Hingankar, S. 2022. Recycling of waste HDPE and PP plastic in preparation of plastic brick and its mechanical properties. *Cleaner Materials*, 5, art.number:100113. Available at: <https://doi.org/10.1016/j.clema.2022.100113>.

Kumar, S. 2022. Challenge 2- Comparing the performance of three types of beams under bending load. *Skill-Lync*, 17 August [online]. Available at: <https://skill-lync.com/student-projects/challenge-2-comparing-the-performance-of-three-types-of-beams-under-bending-load-9> [Accessed: 21 April 2024].

Kurian, J.N., Mohan, C.G., Mathew, J., Moolayil, J.T. & Sreekumar, C. 2016. Fabrication of Plastic Brick Manufacturing Machine and Brick Analysis. *IJIRST – International Journal for Innovative Research in Science & Technology*, 2(11), pp.455-462 [online]. Available at: <https://ijirst.org/Article.php?manuscript=IJIRSTV2I11139> [Accessed: 21 April 2024].

Lamba, P., Kaur, D.P., Raj, S. & Sorout, J. 2022. Recycling/reuse of plastic waste as construction material for sustainable development: a review. *Environmental Science and Pollution Research*, 29, pp.86156-86179. Available at: <https://doi.org/10.1007/s11356-021-16980-y>.

Lourenço, P.B. 1998. Experimental and numerical issues in the modelling of the mechanical behaviour of masonry. In: Roca, P., Gonzáles, J.L., Onate, E. & Lourenço, P.B. (Eds.) *Structural Analysis of Historical Constructions II. Possibilities of the Numerical and Experimental*, pp.57-91. Barcelona, Spain: International Centre for Numerical Methods in Engineering (CIMNE) [online] Available at: <https://repositorium.sdum.uminho.pt/bitstream/1822/66261/1/57.pdf> [Accessed: 21 April 2024]. ISBN: 84-89925-26-7.

Lourenço, P.B. 2002. Computations on historic masonry structures. *Progress in Structural Engineering and Materials*, 4(3), pp.301-319. Available at: <https://doi.org/10.1002/pse.120>.

Lourenço, P.B. & Rots, J.G. 1997. Multisurface Interface Model for Analysis of Masonry Structures. *Journal of Engineering Mechanics*, 123(7), pp.660-668. Available at: [https://doi.org/10.1061/\(ASCE\)0733-9399\(1997\)123:7\(660\)](https://doi.org/10.1061/(ASCE)0733-9399(1997)123:7(660)).

Magomedov, I.A. & Sebaeva, Z.S. 2020. Comparative study of finite element analysis software packages. *Journal of Physics: Conference Series*, 1515, art.number:032073. Available at: <https://doi.org/10.1088/1742-6596/1515/3/032073>.

Mahmoudi, N. 2014. Effect of volume fiber and crack length on interlaminar fracture properties of glass fiber reinforced polyester composites (GF/PO composites). *Mechanica*, 20(2), pp.153-157. Available at: <https://doi.org/10.5755/j01.mech.20.2.6934>.

Mahmoudi, N. 2015. Improvement of mechanical and tribological properties of carbon fiber reinforced peek composite filled with carbon nanotubes. *Annales de Chimie - Science des Matériaux*, 39(1-2), pp.1-10.

Mojsilović, N., Simundic, G. & Page, A. 2009. Static-cyclic shear tests on masonry wallettes with a damp-proof course membrane. *IBK Bericht*, 319. Available at: <https://doi.org/10.3929/ethz-a-006068632>.

Moulai Arbi, Y., Mahmoudi, N. & Djebli, A. 2023. Manufacturing and testing of waste PET reinforced with sand bricks. *Journal of Composite Materials*, 57(16), pp.2513-2526. Available at: <https://doi.org/10.1177/00219983231175203>.

Nela, B. & Grajčevci, F. 2019. Numerical approach: FEM testing of masonry specimens with different bond configurations of units. In: *Proceedings of Congress on Numerical Methods in Engineering (CMN)*, Guimarães, Portugal, pp.962-978, July 01-03 [online]. Available at: https://www.ehu.eus/documents/13131748/23070166/17.+Thermal+modelling_CMN2019.pdf/b08ec9a0-25ee-96d1-9fe3-0b7bed78b67f?t=1602150875189 [Accessed: 21 April 2024].

-OriginLab. 2020. *OriginPro 2020*. Northampton, MA, USA: OriginLab Corporation.

Pacheco-Torgal, F., Khatib, J., Colangelo, F. & Tuladhar, R. 2018. *Use of Recycled Plastics in Eco-efficient Concrete, 1st Edition*. Woodhead Publishing. ISBN: 9780081027332.

Pandey, B.H. & Meguro, K. 2004. Simulation of brick masonry wall behavior under in-plane lateral loading using applied element method. In: *13th World Conference on Earthquake Engineering*, Vancouver, B.C., Canada, Paper No.

1664, August 1-6 [online]. Available at: https://www.iitk.ac.in/nicee/wcee/article/13_1664.pdf [Accessed: 21 April 2024].

Petracca, M., Pelà, L., Rossi, R., Zaghi, S., Camata, G. & Spacone, E. 2017. Micro-scale continuous and discrete numerical models for nonlinear analysis of masonry shear walls. *Construction and Building Materials*, 149, pp.296-314. Available at: <https://doi.org/10.1016/j.conbuildmat.2017.05.130>.

Ponte, M., Milosevic, J. & Bento, R. 2019. Parametrical study of rubble stone masonry panels through numerical modelling of the in-plane behaviour. *Bulletin of Earthquake Engineering*, 17, pp.1553-1574. Available at: <https://doi.org/10.1007/s10518-018-0511-9>.

Radnić, J., Matešan, D., Harapin, A., Smilović, M. & Grgić, N. 2012. Numerical Model for Static and Dynamic Analysis of Masonry Structures. In: Öchsner, A., da Silva, L. & Altenbach, H. (Eds.) *Mechanics and Properties of Composed Materials and Structures. Advanced Structured Materials*, 31, pp.1-33. Berlin, Heidelberg: Springer. Available at: https://doi.org/10.1007/978-3-642-31497-1_1.

Rafiee, A. & Vinches, M. 2013. Mechanical behaviour of a stone masonry bridge assessed using an implicit discrete element method. *Engineering Structures*, 48, pp.739-749. Available at: <https://doi.org/10.1016/j.engstruct.2012.11.035>.

Rahim, A.B., Noguez, C.C. & Pettit, C. 2024. Experimental Testing of Partially Grouted Masonry Shear Walls with Different Horizontal Reinforcement Types. In: Gupta, R., et al. (Eds.) *Proceedings of the Canadian Society of Civil Engineering Annual Conference CSCE 2022. Lecture Notes in Civil Engineering*, 359, pp.189-207. Cham: Springer. Available at: https://doi.org/10.1007/978-3-031-34027-7_13.

Raijmakers, T.M.J. 1992. *Deformation controlled tests in masonry shear walls: report B-92-1156*. Delft, Netherlands: TNO Bouw.

Ramos Huarachi, D.A., Gonçalves, G., de Francisco, A.C., Canteri, M.H.G. & Piekarski, C.M. 2020. Life cycle assessment of traditional and alternative bricks: A review. *Environmental Impact Assessment Review*, 80, art.number:106335. Available at: <https://doi.org/10.1016/j.eiar.2019.106335>.

Rashid, K., Ul Haq, E., Kamran, M.S., Munir, N., Shahid, A. & Hanif, I. 2019. Experimental and finite element analysis on thermal conductivity of burnt clay bricks reinforced with fibers. *Construction and Building Materials*, 221, pp.190-199. Available at: <https://doi.org/10.1016/j.conbuildmat.2019.06.055>.

Rezapour, M., Ghassemieh, M., Motavalli, M. & Shahverdi, M. 2021. Numerical Modeling of Unreinforced Masonry Walls Strengthened with Fe-Based Shape Memory Alloy Strips. *Materials*, 14(11), art.number:2961. Available at: <https://doi.org/10.3390/ma14112961>.

Roca, P., Cervera, M., Gariup, G. & Pela', L. 2010. Structural Analysis of Masonry Historical Constructions. Classical and Advanced Approaches. *Archives of Computational Methods in Engineering*, 17, pp.299-325. Available at: <https://doi.org/10.1007/s11831-010-9046-1>.

Sarhosis, V., Garrity, S.W. & Sheng, Y. 2015. Influence of brick–mortar interface on the mechanical behaviour of low bond strength masonry brickwork lintels. *Engineering Structures*, 88, pp.1-11. Available at: <https://doi.org/10.1016/j.engstruct.2014.12.014>.

Sarhosis, V. & Lemos, J.V. 2018. A detailed micro-modelling approach for the structural analysis of masonry assemblages. *Computers & Structures*, 206, pp.66-81. Available at: <https://doi.org/10.1016/j.compstruc.2018.06.003>.

Singhal, A. & Netula, O. 2018. Utilization of plastic waste in manufacturing of plastic sand bricks. *International Journal of Emerging Technologies and Innovative Research*, 5(6), pp.300-303 [online]. Available at: <https://www.jetir.org/view?paper=JETIRC006052> [Accessed: 21 April 2024].

Van Rossum, G. 1995. *Python reference manual*. Amsterdam, The Netherlands: Stichting Mathematisch Centrum - CWI [online]. Available at: <https://ir.cwi.nl/pub/5008/05008D.pdf> [Accessed: 21 April 2024].

Vargas, L., Sandoval, C., Bertolesi, E. & Calderón, S. 2023. Seismic behavior of partially grouted masonry shear walls containing openings: Experimental testing. *Engineering Structures*, 278, art.number:115549. Available at: <https://doi.org/10.1016/j.engstruct.2022.115549>.

Xia, F., Zhao, K., Zhao, J. & Cui, X. 2024. Experimental Study on the Seismic Performance of Brick Walls Strengthened by Small-Spaced Reinforced-Concrete–Masonry Composite Columns. *Buildings*, 14(1), art.number:184. Available at: <https://doi.org/10.3390/buildings14010184>.

Zhang, W., Kang, S., Liu, X., Lin, B. & Huang, Y. 2023. Experimental study of a composite beam externally bonded with a carbon fiber-reinforced plastic plate. *Journal of Building Engineering*, 71, art.number:106522. Available at: <https://doi.org/10.1016/j.jobbe.2023.106522>.

Zhai, C., Wang, X., Kong, J., Li, S. & Xie, L. 2017. Numerical Simulation of Masonry-Infilled RC Frames Using XFEM. *Journal of Structural Engineering*, 143(10). Available at: [https://doi.org/10.1061/\(ASCE\)ST.1943-541X.0001886](https://doi.org/10.1061/(ASCE)ST.1943-541X.0001886).

Evaluación del desempeño estructural de muros de mampostería que incorporan ladrillos de plástico reciclado bajo cargas monótonas y cíclicas.

Youcef Moulai Arbi^a, Noureddine Mahmoudi^b, Mohammed Bentahar^b

^a Universidad de Mustapha Stambouli, Laboratorio de Física Cuántica de Materia y Modelamiento Matemático (LPQ3M), Mascara, República Argelina Democrática y Popular, **autor de correspondencia**

^b Universidad de Saida Dr. Moulay Tahar, Facultad de Tecnología, Departamento de Ingeniería Civil e Hidráulica, Saida, República Argelina Democrática y Popular

CAMPO: ingeniería mecánica, ingeniería civil
TIPO DE ARTÍCULO: artículo científico original

Resumen:

Introducción/objetivo: Este estudio evalúa el desempeño estructural de muros de mampostería hechos de ladrillos de plástico reciclado bajo cargas monótonas y cíclicas. El propósito fue investigar la viabilidad del uso de ladrillos de plástico reciclado como alternativa para la construcción de mampostería, enfocándose en su viabilidad estructural y posibles beneficios ambientales.

Métodos: Se empleó un enfoque de micro modelado simplificado en Abaqus para simular el comportamiento de estas paredes. Los ladrillos de plástico se representaron con elementos sólidos, mientras que las juntas de mortero se modelaron mediante interacciones cohesivas. El modelo numérico fue validado mediante un análisis de sensibilidad de malla y fue sometido a compresión vertical seguida de carga horizontal.

Resultados: Los hallazgos indicaron una reducción de la resistencia en comparación con los materiales de albañilería tradicionales. Sin embargo, el estudio capturó con éxito la respuesta estructural y la evolución del daño de los muros de mampostería bajo las condiciones de carga especificadas. A pesar de la resistencia reducida, la viabilidad estructural de los ladrillos de plástico reciclado se afirmó firmemente y el comportamiento observado bajo condiciones de carga fue particularmente informativo.

Conclusión: La investigación subrayó el potencial de los ladrillos compuestos de plástico para contribuir a las prácticas de construcción sostenible. Los resultados validaron la viabilidad de incorporar ladrillos de plástico en la construcción, destacando sus beneficios ambientales e implicaciones sostenibles. Este estudio avanzó en el campo de los materiales de construcción sostenibles al demostrar la aplicación práctica y los beneficios del uso de ladrillos de plástico reciclado.

Palabras claves: análisis de elementos finitos, ladrillos plásticos, muro de mampostería, cargas en plano, cargas cíclicas en plano.

Оценка структурных характеристик кладки кирпича из переработанного пластика при монотонной и циклической нагрузке

Юсуф Мулай Арби^а, Нуредин Мамуди^б, Мухаммед Бентахар^б

^а Университет Мустафы Стамбули, лаборатория квантовой физики материи и математического моделирования (LPQ3M), Маскара, Алжирская Народная Демократическая Республика, **корреспондент**

^б Университет Саиды „Доктор Мулай Тахар“, технологический факультет, кафедра гражданского строительства и гидравлики, Саида, Алжирская Народная Демократическая Республика

РУБРИКА ГРНТИ: 67.11.00 Строительные конструкции
ВИД СТАТЬИ: оригинальная научная статья

Резюме:

Введение/цель: В данном исследовании оцениваются структурные характеристики кирпичных стен из переработанного пластика при монотонной и циклической нагрузке. Целью исследования было изучение возможности использования кирпича из переработанного пластика в качестве альтернативы кирпичной кладке. В статье особое внимание уделялось структурной устойчивости и потенциальным экологическим преимуществам пластикового кирпича.

Методы: Для моделирования поведения кирпичной стены был использован упрощенный подход к микромоделированию в Abaqus. Пластиковые кирпичи были представлены в виде монолитных элементов, в то время как швы между ними были смоделированы с помощью когезионных взаимодействий. Численная модель прошла валидацию с помощью анализа чувствительности сетки и была подвергнута вертикальному сжатию с последующей горизонтальной нагрузкой.

Результаты: Результаты исследования свидетельствуют о снижении прочности по сравнению с традиционными материалами для кладки. Тем не менее в ходе исследования была успешно зафиксирована структурная реакция и эволюция повреждений кирпичных стен при определенных условиях нагрузки. Несмотря на снижение прочности, структурная устойчивость кирпича из переработанного пластика была убедительно подтверждена, а поведение, наблюдаемое в условиях нагрузки, было особенно информативным.

Выводы: В ходе исследования выявлен потенциал пластикового кирпича из композитных материалов для содействия экологичному строительству. Результаты исследования подтвердили целесообразность использования пластикового кирпича в строительстве, подчеркнув его экологические преимущества и устойчивость. Данное исследование вносит большой вклад в область исследований об экологически чистых строительных материалах, демонстрируя практическое применение и преимущества использования кирпича из переработанного пластика.

Ключевые слова: конечно-элементный анализ, пластиковый кирпич, кирпичная кладка, нагрузка в плоскости, циклическая нагрузка в плоскости.

Процењивање понашања структуре зидова од цигли од рециклиране пластике под монотоним и цикличним оптерећењем

Јусуф Мулаи Арби^а, Нуредин Мамуди^б, Мухамад Бентахар^б

^а Универзитет „Мустафа Стамбоули“, Лабораторија за квантну физику материје и математичко моделирање (LPQ3M), Маскара, Народна Демократска Република Алжир,
аутор за преписку

^б Универзитет у Саиди „Др Мулаи Тахар“, Технолошки факултет, Департман за грађевинарство и хидраулику, Саида, Народна Демократска Република Алжир

ОБЛАСТ: машинство, грађевинарство

КАТЕГОРИЈА (ТИП) ЧЛАНКА: оригинални научни рад

Сажетак:

Увод/циљ: У раду се анализирају перформансе структуре зиданог зида од рециклираних пластичних цигала под монотоним и цикличним оптерећењем. Циљ је био да се испита могућност коришћења цигли од рециклиране пластике као замена за зидану конструкцију, с фокусом на одрживост структуре и потенцијалну корист за животну средину.

Методе: За симулацију понашања оваквих зидова коришћен је поједностављени приступ микромоделовања у Абакусу. Пластичне цигле представљене су помоћу чврстих елемената, док су спојеви од малтера моделовани путем кохезионих интеракција. Нумерички модел је валидиран помоћу анализе осетљивости мреже и подвргнут је вертикалној компресији, а затим хоризонталном оптерећењу.

Резултати: Резултати указују на смањивање чврстоће у односу на традиционалне материјале за зидање. Међутим, одговор структуре био је успешан, као и еволуција оштећења зиданих зидова под одређеним условима оптерећења. Упркос смањеној чврстоћи, структуре од цигала од рециклиране пластике показале су се као изводљиве, а њихово понашање под условима оптерећења као веома добар извор информација.

Закључак: Испитивање је показало да композитне цигле од пластике имају потенцијал да допринесу одрживој градњи. Резултати су потврдили могућност уграђивања пластичних цигли у конструкције, при чему је наглашена корист за животну средину и одрживост. Такође, унапређена је област одрживих грађевинских материјала јер је потврђена практична примена и корист од коришћења цигли од рециклиране пластике.

Кључне речи: анализа коначних елемената, цигле од пластике, зидани зид, оптерећења у равни, циклична оптерећења у равни.

Paper received on: 22.04.2024.
Manuscript corrections submitted on: 25.09.2024.
Paper accepted for publishing on: 26.09.2024.


© 2024 The Authors. Published by Vojnotehnički glasnik / Military Technical Courier (www.vtg.mod.gov.rs, втр.мо.унр.срб). This article is an open access article distributed under the terms and conditions of the Creative Commons Attribution license (<http://creativecommons.org/licenses/by/3.0/rs/>).



Optimal solution for the single-beam bridge crane girder using the Moth-Flame algorithm

Goran V. Pavlović^a, Mile M. Savković^b,
Nebojša B. Zdravković^c, Goran Đ. Marković^d,
Predrag Z. Mladenović^e

University of Kragujevac, Faculty of Mechanical and Civil Engineering in
Kraljevo, Department of Heavy Machinery, Kraljevo, Republic of Serbia


^a e-mail: gorantheopavlovic@yahoo.com, **corresponding author**,
ORCID iD:  <https://orcid.org/0000-0002-7230-1908>

^b e-mail: savkovic.m@mfkv.kg.ac.rs,
ORCID iD:  <https://orcid.org/0000-0002-4501-9149>

^c e-mail: zdravkovic.n@mfkv.kg.ac.rs,
ORCID iD:  <https://orcid.org/0000-0001-6387-2816>

^d e-mail: markovic.g@mfkv.kg.ac.rs,
ORCID iD:  <https://orcid.org/0000-0002-0957-0718>

^e e-mail: mladenovic.p@mfkv.kg.ac.rs,
ORCID iD:  <https://orcid.org/0000-0002-3315-4642>

 <https://doi.org/10.5937/vojtehg72-51953>

FIELD: mechanical engineering
ARTICLE TYPE: original scientific paper

Abstract:

Introduction/purpose: The paper analyses and optimizes the welded I-girder of the single-beam bridge crane with a U-profile as the top flange. This solution is to provide a lighter carrying structure, so the main goal is to minimize the weight of the main girder, i.e., the cross-sectional area while fulfilling the requirements defined by national standards and geometric constraints.

Methods: The Moth-Flame Optimization (MFO) algorithm was chosen for solving this single-objective multi-criteria optimization task using MATLAB. Also, the results were verified by using the Finite Element Analysis (FEA).

Results: The proposed girder shape is justified in examples of real solutions of single-beam bridge cranes and the previous research results. In this case, significant savings in the material and better results are achieved compared to the examples from the previous research.

ACKNOWLEDGMENT: This work has been supported by the Ministry of Science, Technological Development and Innovation of the Republic of Serbia, through the Contracts for the scientific research financing in 2024, 451-03-65/2024-03/200108 and 451-03-66/2024-03/200108.

Conclusion: The proposed girder shape, methodology, the optimization algorithm and the achieved savings fully justify this research. Furthermore, this algorithm enables the application of many constraint functions, whereby the optimal values of numerous variables are obtained in a relatively short period. Therefore, it would not be possible to find the solution for that engineering task by applying analytical optimization methods.

Key words: bridge crane, welded girder, FEA, optimization, metaheuristic.

Introduction

Single-beam bridge cranes are used for handling the load in industrial facilities and warehouses as well as in transport, servicing, and maintenance. They are used increasingly in practice, and, in certain cases, their application is more economical than that of double-beam bridge cranes. The main engineering task is a proper choice of equipment and lightweight design of the single-beam bridge crane carrying structure. The welded box-girder or different types of standard rolled I-profiles are most often used as the main girder of single-beam bridge cranes, depending on the span and carrying capacity. However, the applied standard I-profiles are not usually used rationally, so the main crane girder is overdimensioned. For this reason, a standard I-profile is often combined with the U-profile or L-profiles to increase global stability and achieve a lighter structure.

The analysis and optimization of crane support structures and I-girders have been the research subject in numerous publications. The optimization process can often be performed within the 3D modelling software. For example, Cvijović & Bošnjak (2016) used the 3D Finite Element Analysis (FEA) for local bending effects of the bottom flange of the monorail crane structure. Qin et al. (2015) presented the Solid Isotropic Material with Penalization (SIMP) optimization method on the example of the bridge crane's box girder, and the results were verified by using the FEA. Różyło (2016) used ABAQUS on the example of the I-girder. Finally, Ky et al. (2014) considered the problem of selecting optimal standard profiles of a steel structure by using SAP2000, where these results were compared with a heuristic optimization algorithm.

The application of various optimization algorithms is very present in engineering practice, for both single-objective and multi-objective optimization problems. For example, Qi et al. (2015) presented the Specular Reflection Algorithm application to optimize the box cross-section of the double-beam bridge crane. Wang & Diao (2012) solved a similar optimization problem using the Adaptive Genetic Algorithm.

Metaheuristic algorithms have been widely used in recent years. Pavlović et al. (2024) applied the Water Evaporation Optimization (WEO) algorithm to minimize the weight of the main girder with a non-symmetric box-like cross-section of the double-beam bridge crane. Similar to the previous, Jármay et al. (2021) optimized the cross-sectional area of the main girder of the double-beam bridge crane by applying 15 metaheuristic algorithms. Pavlović & Savković (2022) presented the application of the Moth-Flame Optimization (MFO) algorithm for the optimal design of the main girder of the double-beam bridge crane with an asymmetric box cross-section. It was concluded that the application of that method is justified. Jármay et al. (2003) considered the problem of optimizing the dimensions of the welded I-girder, where three metaheuristic algorithms were applied, as well as Rosenbrock's method.

The I-girder optimization is an actual problem in many previously cited papers. The analysis of global stability is specific to this type of structure. Ellifritt & Lue (1998) analysed the global stability of the I-girder with a channel cap (U-profile), proposing the analytical model for the calculation. The model is experimentally verified. Trahair (2009) studied the I-crane girder concerning lateral distortion buckling according to Australian Standard (AS). The design method proposed is applied to a concrete example. Mela & Heinisuo (2014) optimized the weight and cost of the high-strength steel welded I-girder by the Particle Swarm Optimization (PSO) algorithm. Gaška et al. (2017) analyzed the stresses due to the local bending of the I-girder bottom flange within the single-beam bridge crane using Eurocodes. The obtained analytical results were compared to those from the FEA conducted by ABAQUS. Pavlović et al. (2018) applied the Generalized Reduced Gradient (GRG2) algorithm to the mono-symmetric welded I-girder of the single-beam bridge crane, with significant material savings for the given examples. Sitthipong et al. (2018) considered the complex design of a crane runway beam, composed of an I-section and a U-section, using ASME standards, concerning deflection and stress. In the paper by Schaper et al. (2019), lateral torsional buckling is also considered in various welded I-girder shapes. Besides the usual checking procedure, a simplified verification according to Eurocode was made. Molnár et al. (2022) compared the analytical results to those obtained from the FEA analysis made in ANSYS on the example of the single-beam bridge crane I-girder.

The numerous publications mentioned show a broad application of metaheuristic optimization algorithms. In this paper, the MFO algorithm is applied for a single-objective multi-criteria optimization problem to reduce the weight of the single-beam bridge crane girder. MFO is highly efficient

in solving problems in mechanical and structural design, as shown in the paper by Mirjalili (2015) which presented the algorithm. Besides the good mechanical and structural design results compared to some other algorithms, it stands out in complex examples such as a marine propeller analysis. The comparison between the MFO algorithm and other algorithms was also presented in Pavlović et al. (2022), where authors studied the weight reduction of the welded cantilever beam subjected to restrained warping.

The research subject in this paper is the analysis and optimization of the welded I-cross-section with a U-profile as the top flange of the main girder of the single-beam bridge crane. A U-profile can be easily manufactured by cold-forming. Due to its geometry, the cold-formed U-profile enables a more rational material use, providing better overall resistance of the girder to the lateral instability, which is the most critical condition for that carrying structure. Furthermore, as the top part of the girder, the U-profile can be formed from a 0.5 cm thick plate, which ensures a lighter type of a carrying structure. This cross-section is simpler than the standard I-profile reinforced with a standard U-profile or a standard I-profile reinforced with two L-profiles. In this way, a light welded structure of the girder is achieved, composed mainly of thin plates (except for the bottom flange), which satisfies all necessary design and work conditions.

The trolley wheels run on the bottom flange and cause its local bending, while the top flange is compressed, so it must be stable in both vertical and horizontal planes. Using standard rolled I-profiles in single-girder bridge cranes is not rational because of the preceding reasons, so these girders are mostly overdesigned.

The objective of the proposed solution in this research is to show that, in this manner, it is possible to gain extra savings in the plate material and thus reduce the total weight of the girder. Since the upper part of the girder is exposed to compression, this solution increases the global stability of the girder and provides the most optimal structure. Finally, the results are compared to the welded girder optimization results obtained by Pavlović et al. (2018) for four examples of single-beam bridge cranes.

Optimization problem

The weight reduction of the welded main girder means to determine the optimal geometric parameters for the proposed type of the cross-section, while all constraint functions must be satisfied.

Figures 1 and 2 present the general view of a single-beam bridge crane with the accompanying equipment and the cross-section of the welded girder with the trolley, respectively.

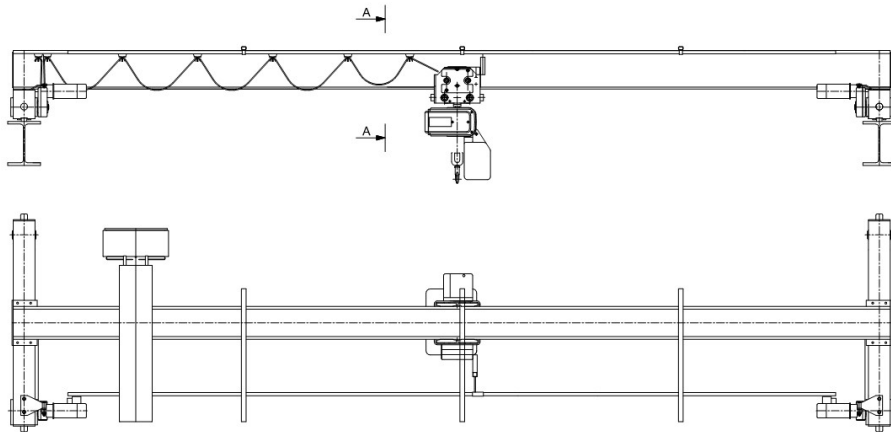


Figure 1 – General view of the structure of the single-girder bridge crane

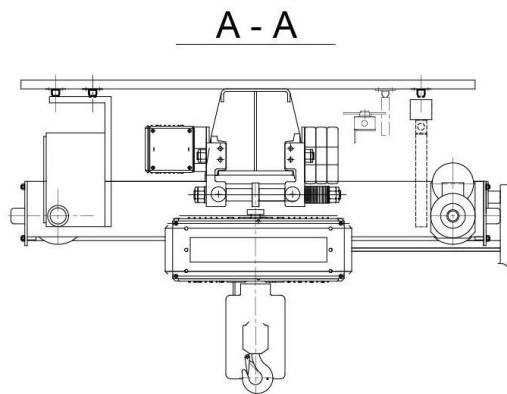


Figure 2 – Cross-section of the welded girder and the trolley (A – A section)

Figure 1 shows the crane-carrying structure which consists of the main girder and the end girders. It also shows an electrical winch with the trolley moving along the main girder.

Figure 2 shows the cross-section of the main girder with the trolley hanging on the bottom flange. This cross-sectional area is the subject of the optimization task.

Mathematical formulation of the optimization problem

This single-objective multi-criteria optimization problem can be defined as:

$$\min [f_o(X)] \text{ subject to,} \quad (1)$$

$$g_i(X) = g_{ir}(X) - g_{id}(X) \leq 0, \quad l_j \leq x_j \leq u_j, \quad (2)$$

where $f_o(X)$ is the objective function, $g_i(X)$ are the constraint functions, $g_{ir}(X)$ is the real value of the criterion, $g_{id}(X)$ is the permissible value of the criterion, $i=1, \dots, m$ is the number of constraints, $j=1, \dots, n$ is the number of design variables, and X is the design vector made of n variables.

The variables (x_j) are values that should be defined during the optimization process, and each of them is defined by its lower (l_j) and upper limit (u_j). This paper considers seven geometric variables (Figure 3):

$$X = [h \ d \ b \ t \ b_1 \ h_1 \ a_s]^T, \quad (3)$$

where h is the web height, d is the web thickness, b is the bottom flange width, t is the bottom flange thickness, b_1 is the width of the top side of the U-profile, h_1 is the inner width of the lateral side of the U-profile, and a_s is the weld thickness, (Figure 3).

The input parameters for the optimization process are, Ostrić & Tošić (2005): the Classification class, Q - the carrying capacity, L - the span, m_k - the mass of the trolley, b_k - the distance between the wheels of the trolley, e_1 - the distance between wheel 1 and the resulting force in the vertical plane (Figure 4), n_k - the number of trolley wheels (4 in all examples), $r_k=1.5$ cm - the distance from the edge of the bottom flange to the vertical load of the trolley wheel (Figure 3), γ - the coefficient which depends on the Classification class, ψ - the dynamic coefficient of the influence of load oscillation in the vertical plane, k_a - the dynamic coefficient of crane load in the horizontal plane, K_f - the coefficient of stiffness (depending on the Classification class, the purpose of the bridge crane, and the control condition), T_d - the permissible time of the damping of oscillation of the girder (depending on the purpose of the crane), v_1 - the load case 1 factored load coefficient, v_2 - the load case 2 factored load coefficient, $E=21000$ kN/cm² - Young's modulus of the plate material, and R_e - the minimum yield stress of the plate material.

In all considered examples in this research, the crane control is by an operator on the floor, using a pendant system.

Cross-sectional area (the objective function)

The cross-sectional area (Figure 3) f_o of the welded girder is given by the following equation, Eq. (4):

$$f_o = A_p + A_s, \tag{4}$$

where A_p is the area composed of the U-profile (A_U), the web (A_w), and the bottom flange (A_f), and A_s is the area of the welded joints.

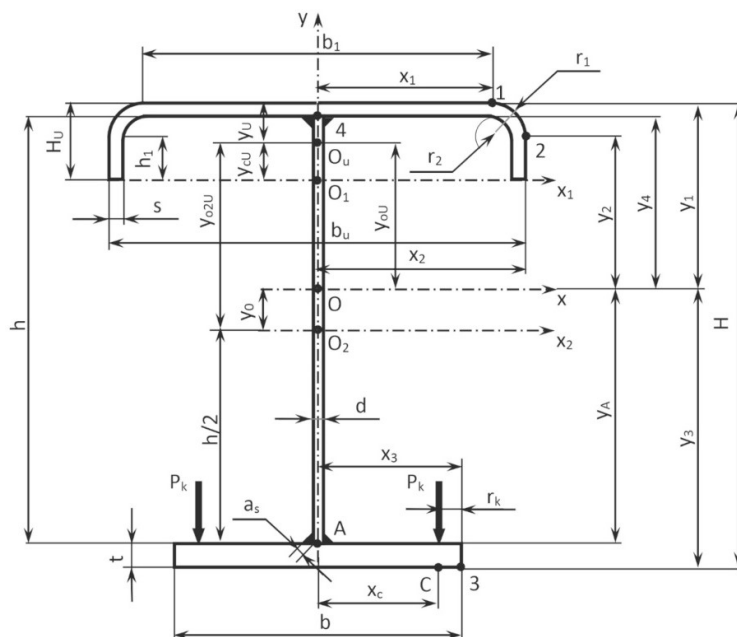


Figure 3 – Cross-section of the main girder of the single-beam bridge crane

$$A_p = A_U + A_w + A_f, \tag{5}$$

$$A_U = s(b_1 + 2h_1) + \pi(r_1^2 - r_2^2)/2, A_w = d \cdot h, A_f = t \cdot b, \tag{6}$$

$$A_s = 4a_s^2, \tag{7}$$

where A_p is the area composed of the U-profile (A_U), the web (A_w), and the bottom flange (A_f), A_s is the area of the welded joints, $r_1=r_2+s$ is the outer radius of the U-profile, r_2 is the inner radius of the U-profile ($r_2=0.6$ cm), and s is the thickness of the U-profile ($s=0.5$ cm).

Besides variables, Figure 3 depicts all other necessary geometry parameters used in this analysis.

The principal central axes' position and the geometric properties in the cross-section's characteristic points are calculated by well-known equations.

The geometric constraints for some of the dimensions are given as follows:

$$g_1 = H - H_d = h + t + s - H_d \leq 0, \quad (8)$$

$$g_2 = b_U - b_{Ud} = b_1 + 2 \cdot (r_2 + s) - b_{Ud} \leq 0, \quad (9)$$

$$g_3 = H_U - H_{Ud} = h_1 + r_2 + s - H_{Ud} \leq 0, \quad (10)$$

where H is the profile height, H_d is the permissible value of the profile height, b_U is the width of the U-profile, b_{Ud} is the permissible value of the width of the U-profile, H_U is the height of the U-profile, and H_{Ud} is the permissible value of the height of the U-profile (Figure 3).

Static model of the main girder

The following static scheme shows a model of the main girder in the form of a simple beam with loads in the vertical and horizontal planes (Figure 4). The location of forces on the beam corresponds to maximum bending moments, which are predominant for this type of structure.

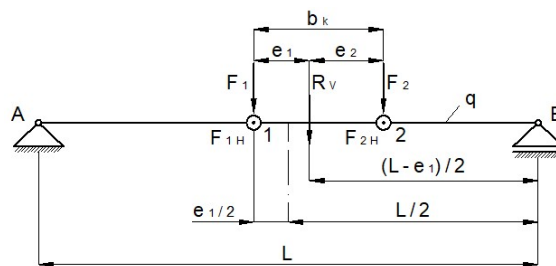


Figure 4 – Static scheme of the main girder of the single-beam bridge crane

where R_V is the resulting force in the vertical plane, F_1 , F_2 are the acting forces in the vertical plane, upon the bottom flange, from trolley wheels 1 and 2, respectively, e_2 is the distance between wheel 2 and the resulting force in the vertical plane, F_{1H} , F_{2H} are the acting forces in the horizontal plane, upon the bottom flange, from trolley wheels 1 and 2, respectively, and q is the specific weight per unit of length of the girder.

The quantities necessary for defining the optimization criteria are being calculated by using the well known expressions (Ostrić & Tošić, 2005).

The next sub-chapters introduce the criteria for analyzing and calculating the single-beam crane main girder. All conditions that have to be fulfilled related to strength, stability, stiffness and oscillation are taken into account according to Ostrić & Tošić (2005) and Serbian Standards: SRPS U.E7.121:1987, SRPS U.E7.081:1987, SRPS U.E7.086:1987, and SRPS U.E7.101:1991 (Petković & Ostrić, 1996).

Strength criterion

In this research, only normal stress components are considered. Tangential stresses are neglected, as the bending moments are predominant for this type of structure.

The maximum stresses at the observed points (Figure 3) must be lower than the permissible ones (σ_{d1} or σ_{d2}). In addition, the local stresses in the x and z directions must be lower than σ_{d1} , where σ_{d1} , σ_{d2} are the permissible stresses for the load case 1, and the load case 2, respectively.

For this criterion, the constraint functions are:

$$g_4 = \sigma_{1z} - \sigma_{d1} = \frac{M_V}{W_{1x}} + \frac{M_H}{W_{1y}} - \sigma_{d1} \leq 0, \quad (11)$$

$$g_5 = \sigma_{2z} - \sigma_{d1} = \frac{M_V}{W_{2x}} + \frac{M_H}{W_{2y}} - \sigma_{d1} \leq 0, \quad (12)$$

$$g_6 = \sigma_{3z} - \sigma_{d1} = \frac{M_V}{W_{3x}} + \frac{M_H}{W_{3y}} - \sigma_{d1} \leq 0, \quad (13)$$

$$g_7 = \sigma_{A,u} - \sigma_{d1} \leq 0, \quad (14)$$

$$g_8 = \sigma_{Az} - \sigma_{d1} = \frac{M_V}{W_{Ax}} - \sigma_{d1} \leq 0, \quad (15)$$

$$g_9 = \sigma_{A kz} - \sigma_{d1} = K_{Az} \cdot P_k / t^2 - \sigma_{d1} \leq 0, \quad (16)$$

$$g_{10} = \sigma_{A kx} - \sigma_{d1} = K_{Ax} \cdot P_k / t^2 - \sigma_{d1} \leq 0, \quad (17)$$

$$g_{11} = \sigma_{C,u} - \sigma_{d2} \leq 0, \quad (18)$$

$$g_{12} = \sigma_{Cz} - \sigma_{d1} = \frac{M_V}{W_{Cx}} + \frac{M_H}{W_{Cy}} - \sigma_{d1} \leq 0, \quad (19)$$

$$g_{13} = \sigma_{Ckz} - \sigma_{d1} = K_{Cz} \cdot P_k / t^2 - \sigma_{d1} \leq 0 \quad (20)$$

$$g_{14} = \sigma_{Ckx} - \sigma_{d1} = K_{Cx} \cdot P_k / t^2 - \sigma_{d1} \leq 0, \quad (21)$$

$$\sigma_{A,u} = \sqrt{(\sigma_{Az} + \sigma_{Akz})^2 + \sigma_{Akx}^2} - (\sigma_{Az} + \sigma_{Akz}) \sigma_{Akx}, \quad (22)$$

$$\sigma_{C,u} = \sqrt{(\sigma_{Cz} + \sigma_{Ckz})^2 + \sigma_{Ckx}^2} - (\sigma_{Cz} + \sigma_{Ckz}) \sigma_{Ckx}, \quad (23)$$

$$\sigma_{d1} = R_e / \nu_1, \quad \nu_1 = 1.5, \quad (24)$$

$$\sigma_{d2} = R_e / \nu_2, \quad \nu_2 = 1.33, \quad (25)$$

where σ_{pz} is the normal stress at the observed point p ($p=1, 2, 3, A, C$), W_{px} , W_{py} are the section moduli of the area A_p for the point p , σ_{Akz} , σ_{Akx} are the local stresses at the point A , in both directions, respectively, σ_{Ckz} , σ_{Ckx} are the local stresses at the point C , in both directions, respectively, $\sigma_{A,u}$, $\sigma_{C,u}$ are the equivalent stresses at the point A and the point C , respectively, M_V , M_H are the bending moments in the vertical and horizontal planes, respectively, P_k is the maximum pressure of the trolley wheel, K_{Az} , K_{Ax} are the corresponding coefficients for the local stresses at the point A , and K_{Cz} , K_{Cx} are the corresponding coefficients for the local stresses at the point C (Ostrić & Tošić, 2005).

Strength criterion for the welded joints

The maximum stress in the welded connection (σ_s) must be lower than the permissible one (σ_{ds}). The constraint functions for this criterion are:

$$g_{15} = \sigma_s - \sigma_{ds} = \frac{F_T \cdot S_x}{2 \cdot I_x \cdot a_s} - 0.75 \cdot \sigma_{d1} \leq 0, \quad (26)$$

$$g_{16} = a_s - 0.7 \cdot \min(s, d) \leq 0, \quad (27)$$

where F_T is the maximum shear force, S_x is the static moment of the area A_p about the x -axis, and I_x is the moment of inertia of the area A_p about the x -axis.

Local stability of the web

Checking the local stability of the web is performed according to Standard SRPS U.E7.121:1987 (Petković & Ostrić, 1996). The constraint function is:

$$g_{17} = v_1 \cdot M_V / W_{4x} - \min(R_e, c_w \cdot \chi_w \cdot R_e) \leq 0, \quad (28)$$

where W_{4x} is the section moduli of the area A_p for point 4, χ_w is a reduction factor of the web, SRPS U.E7.121:1987 (Petković & Ostrić, 1996), and c_w is a coefficient, SRPS U.E7.121:1987 (Petković & Ostrić, 1996).

Global stability of the welded girder

The verification of global stability, in this case, is performed based on Serbian Standards: SRPS U.E7.081:1987, SRPS U.E7.086:1987, and SRPS U.E7.101:1991 (Petković & Ostrić, 1996). The constraint functions for this criterion have the following form:

$$g_{18} = \max(\sigma_{1z}, \sigma_{2z}) - 1.14 \cdot \chi_p \cdot \sigma_{d1} \leq 0, \quad (29)$$

$$g_{19} = i_p - i_y = \sqrt{\frac{I_{yU}}{A_U}} - \frac{L}{40} \cdot \sqrt{\frac{R_e}{23.5}} \leq 0, \quad (30)$$

where χ_p is a non-dimensional coefficient of the global stability, SRPS U.E7.081:1987 (Petković & Ostrić, 1996), i_p is the radius of gyration of the U-profile about the y -axis, i_y is the required value of the radius of gyration, and I_{yU} is the moment of inertia of the U-profile about the y -axis.

Criterion of oscillation

With this criterion, the damping time (T) of oscillations (relaxation time) of the mass m_1 , located in the middle of the main girder, must be checked (Ostrić & Tošić, 2005). The constraint function has the following form:

$$g_{20} = T - T_d = \tau \cdot \ln(20) / \gamma_d - T_d \leq 0, \quad (31)$$

$$m_1 = Q + m_k + 17 \cdot m / 35, \quad (32)$$

$$\tau = \pi \cdot \sqrt{m_1 \cdot L^3 / (12 \cdot B_x)}, \quad (33)$$

where m is the mass of the girder, m_1 is the mass concentrated at the midspan, $B_x = E \cdot I_x$ is the flexural rigidity of the girder, τ is the period of oscillations, and γ_d is the logarithmic decrement which shows the rate of oscillation damping (depending on the ratio between the height of the welded girder, H and the span, L) (Ostrić & Tošić, 2005).

Criterion of stiffness

This criterion analyses deflection in the vertical plane. In addition to the acting of trolley wheels (f_1), the specific weight of the main girder (f_q) is also observed. The total deflection (f_u) must be lower than the permissible one (f_d):

$$f_u = f_1 + f_q \leq f_d = K_f \cdot L, \quad (34)$$

$$f_1 = \frac{F_{1,st} \cdot L^3}{48 \cdot B_x} \cdot \left\{ 1 + \frac{F_{2,st}}{F_{1,st}} \cdot \left[1 - 6 \cdot \left(\frac{b_k}{L} \right)^2 \right] \right\}, \quad (35)$$

$$f_q = \frac{5 \cdot q \cdot L^4}{384 \cdot B_x}, \quad (36)$$

where $F_{1,st}$, $F_{2,st}$ are the static forces in the vertical plane, upon the bottom flange, from trolley wheels 1 and 2, respectively (Ostrić & Tošić, 2005).

The constraint function, based on Eq. (37), is:

$$g_{21} = f_u - f_d = f_u - K_f \cdot L \leq 0. \quad (37)$$

Optimization method

The MFO algorithm is a relatively new population nature-inspired metaheuristic algorithm based on the computer simulation of the navigation of moths, introduced by Mirjalili (2015). This algorithm is widely used in science and engineering. Moths use their unique navigation methods at night. They have evolved to fly at night using the moonlight, where a moth flies by maintaining a fixed angle in relation to the moon. Since the moon is so far from a moth, a moth flies in a straight line. Moths fly spirally around the artificial lights because they are tricked by them. When moths see artificial light, they try to maintain an angle to the light

source. Since such a light source is extremely close compared to the moon, maintaining the angle to the light source causes a useless or deadly spiral flying path for moths. In this algorithm, it is presumed that the candidate solutions are moths, and variables are the positions of moths in the space. Moths and flames are both solutions. The difference between them is the way how to treat and update them in each iteration. The moths are actual search agents that move around the search space, whereas flames are the best position of moths that have been obtained so far. Therefore, each moth searches around a flame and updates it if it finds a better solution. In this way, a moth never loses its best solution.

The pseudocode for this metaheuristic optimization algorithm is shown in Mirjalili (2015).

Optimization results

The optimization process will be based on the presented MFO method, in the MATLAB software. In addition, the solutions of single-beam bridge cranes, taken from Pavlović et al. (2018), will be considered as examples to compare the results obtained (four examples of single-beam bridge cranes).

Table 1 shows the data of single-beam bridge cranes that are in exploitation. These data also represent the input parameters for the optimization process, where A_{pr} represents the cross-sectional area of the standard rolled profile and b_{min} represents the minimum value for the bottom flange width. All cranes are in Classification class 2.

Other input parameters are: $\gamma=1.05$, $\psi=1.15$, $K_f=1/500$, and $T_d=15$ s.

Table 1 – Technical parameters of single-beam cranes

Example	Q (t)	L (m)	m_k (kg)	b_k (mm)	e_1 (mm)	b_{min} (mm)	k_a (-)	Re (kN/cm ²)	A_{pr} (cm ²)
1	5	16.78	350	405	202.5	100	0.1	27.5	260
2	3.2	10.0	340	196	98	82	0.1	23.5	143
3	10	7.75	610	708	354	100	0.05	23.5	239
4	6.3	5.92	380	420	225	100	0.1	23.5	181

The control parameters of the MFO algorithm used for each example in this paper are $N_{pop}=200$ - population size and $max_it=300$ - maximum number of iterations.

The maximum values (in centrimeters) for the characteristic geometric quantities are: $H_d = 100$, $b_{Ud} = 40$, $H_{Ud} = 20$.

The boundary values (in centimeters) of the variables for all bridge cranes are: $20 \leq h \leq 100$, $0.5 \leq d \leq 2$, $b_{min} \leq b \leq 30$, $0.6 \leq t \leq 4$, $10 \leq b_1 \leq 40$, $3 \leq h_1 \leq 20$, $0.3 \leq a_s \leq 0.7$.

After applying the MFO optimization procedure, the following optimal geometric parameters, the value of the objective function and the characteristics of the optimization procedure are obtained (Table 2), where *Std* is the standard deviation of the optimization process.

Table 2 – Optimization results

Example	h (cm)	d (cm)	b (cm)	t (cm)	b ₁ (cm)	h ₁ (cm)	f _o (cm ²)	Std (-)
1	81.52	0.5	10.00	1.88	37.80	15.24	95.44	16.54
2	46.48	0.5	8.20	1.74	33.80	3.00	59.14	5.97
3	68.95	0.5	10.00	2.69	37.42	3.00	84.73	6.41
4	44.14	0.5	10.00	2.20	32.49	3.00	64.98	3.63

The optimal value for the variable a_s is 0.3 cm in all examples.

The following figures show the convergence graphs for all examples (Figures 5–8).

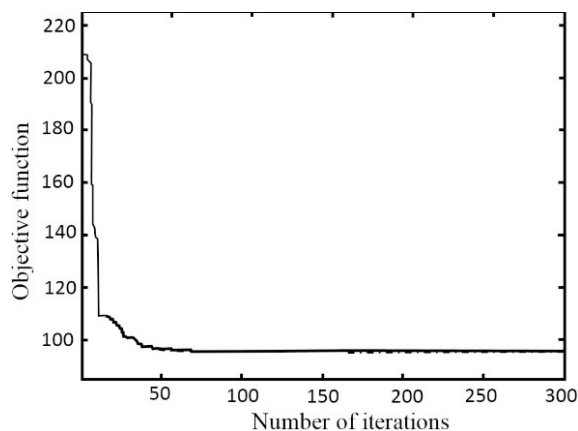


Figure 5 – Convergence graph for Example 1

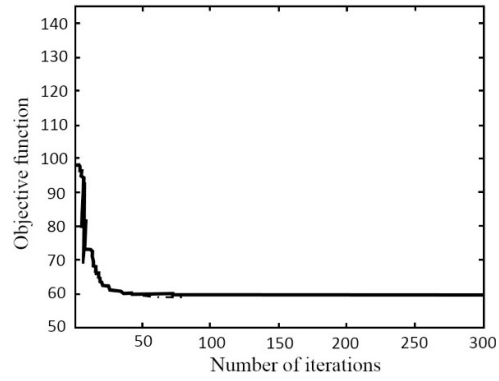


Figure 6 – Convergence graph for Example 2

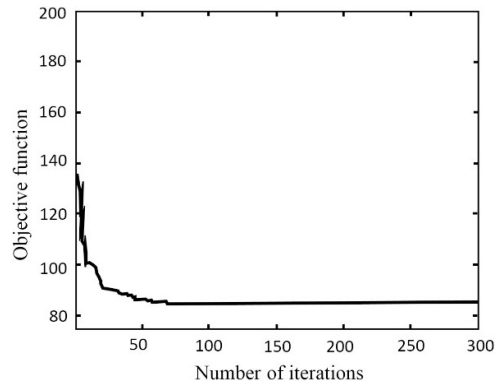


Figure 7 – Convergence graph for Example 3

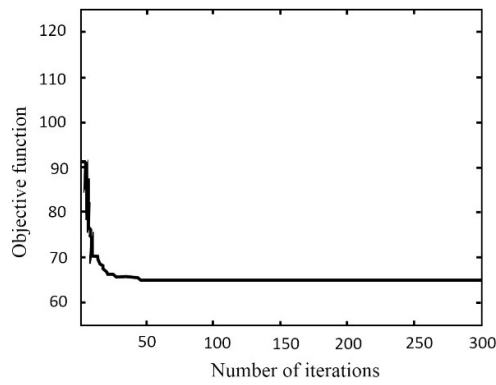


Figure 8 – Convergence graph for Example 4

Table 3 shows the rounded values of the optimal geometric parameters, the optimal areas A_{op} , and the material savings.

Table 3 – Rounded values of the optimal geometric parameters and the material savings

Example	h (cm)	d (cm)	b (cm)	t (cm)	b_1 (cm)	h_1 (cm)	A_{op} (cm ²)	Saving (%)
1	81.5	0.5	10.0	1.9	37.8	15.3	95.29	63.35
2	46.5	0.5	8.2	1.8	33.8	3.0	59.25	58.57
3	69.0	0.5	10.0	2.7	37.5	3.0	84.59	64.61
4	44.1	0.5	10.0	2.2	32.5	3.0	64.64	64.29

To determine which criteria are the most critical, Table 4 shows the values of the optimization criteria (for the obtained optimal geometric parameters, Table 2) g_{ir} and the boundary (permissible) values for two characteristic examples of optimization g_{id} . In addition, Example 1 with the largest bridge span and Example 3 with the largest carrying capacity were analysed.

For all values of $i=1, \dots, m$, $m=21$, g_{ir} is less than or equal to g_{id} , which means that the boundary conditions were not exceeded. Then, comparing two examples of bridge cranes, where the first one has a twice greater span than the second one, and the second one has a twice greater carrying capacity than the first one, it is determined which criteria are the most critical for both cases.

Table 4 – Calculated and permissible values of all criteria for Example 1 and Example 3

i	Example 1		Example 3	
	g_{ir}	g_{id}	g_{ir}	g_{id}
1 (cm)	83.90	100	72.13	100
2 (cm)	40	40	39.62	40
3 (cm)	16.34	20	4.10	20
4 (kN/cm ²)	15.25	18.33	15.67	15.67
5 (kN/cm ²)	15.26	18.33	15.61	15.67
6 (kN/cm ²)	14.81	18.33	11.77	15.67
7 (kN/cm ²)	14.14	18.33	11.80	15.67
8 (kN/cm ²)	12.86	18.33	9.74	15.67
9 (kN/cm ²)	3.21	18.33	3.14	15.67
10 (kN/cm ²)	10.51	18.33	10.27	15.67
11 (kN/cm ²)	20.68	20.68	17.67	17.67
12 (kN/cm ²)	14.38	18.33	11.40	15.67
13 (kN/cm ²)	8.72	18.33	8.52	15.67

i	Example 1		Example 3	
	g_{ir}	g_{id}	g_{ir}	g_{id}
14 (kN/cm ²)	6.31	18.33	6.17	15.67
15 (kN/cm ²)	1.25	13.75	2.27	11.75
16 (cm)	0.3	0.35	0.3	0.35
17 (kN/cm ²)	14.57	14.58	16.42	19.06
18 (kN/cm ²)	15.26	15.26	15.67	16.41
19 (cm)	15.66	45.38	12.89	19.38
20 (s)	14.03	15	4.05	15
21 (cm)	2.74	3.36	0.64	1.55

The FEA for Examples 1 and 3 were carried out in Autodesk Inventor Nastran software to check the optimization results for the stress and the stiffness (deflection) criteria. The 3D CAD models of the main girders were made in Autodesk Inventor software using the data from Tables 1 and 3. They were the basis for creating the finite element models using the shell elements. The analyses were conducted for the critical trolley position depicted in Figure 4.

Figures 9 and 10 depict the equivalent stress and the deflection for Example 1, respectively.

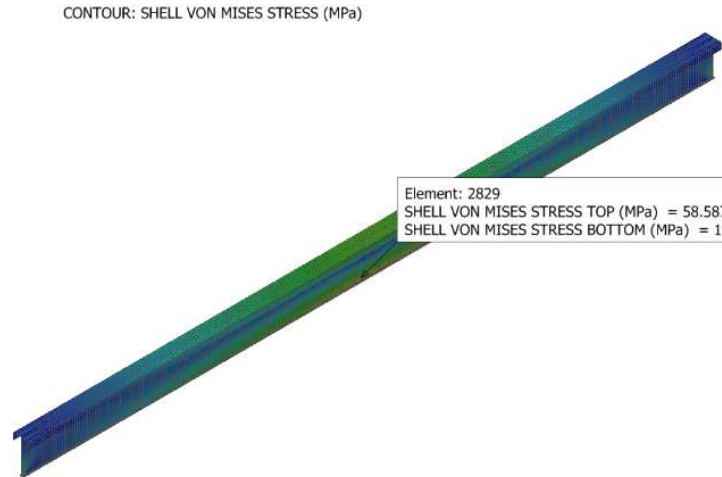


Figure 9 – Equivalent stress for Example 1

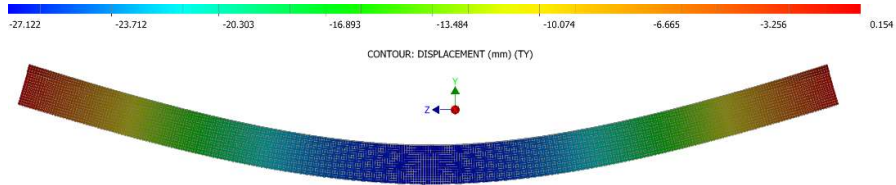


Figure 10 – Deflection for Example 1

Figures 11 and 12 depict the equivalent stress and the deflection for Example 3, respectively.

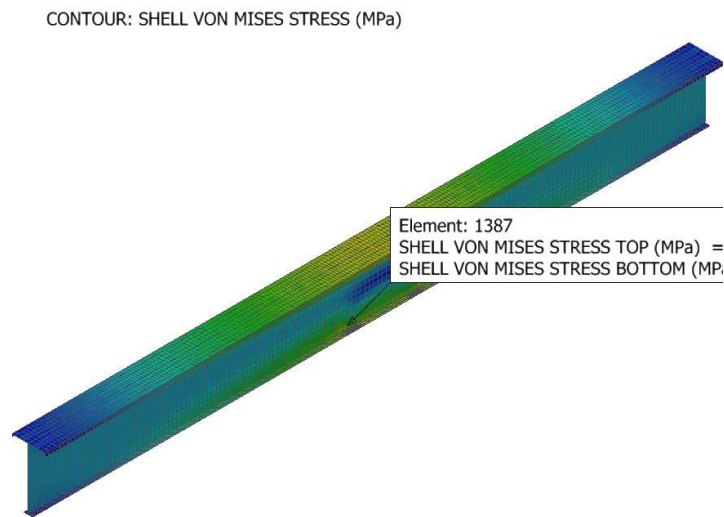


Figure 11 – Equivalent stress for Example 3

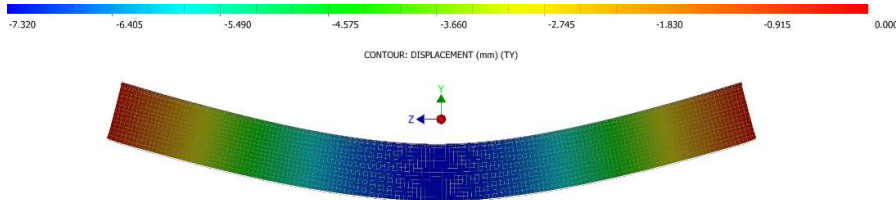


Figure 12 – Deflection for Example 3

Conclusion

This research presents the analysis and the optimization procedure for a welded I-profile with a U-profile as the top flange (the main girder) of the single-beam bridge crane, according to national standards, using the MFO optimization method. The criteria of permissible stresses in the characteristic points of the cross-section, the stress in the weld joints, the local stability of the web, the global stability of the girder, the deflection of the girder, the damping time of oscillations, and the geometric limits were applied as constraint functions. The objective function is the cross-sectional area.

The results justify the application of the presented model of the welded I-girder with a U-profile as the top flange and the applied nature-inspired optimization algorithm. This is concluded by comparing the results from Table 3 to the results in Pavlović et al. (2018).

Significant material savings within 58.57-64.61% are achieved compared to the considered examples of single-beam bridge cranes (made of standard I-profiles, Table 1). These results are better than those in Pavlović et al. (2018) (which are within 47.36-61.98%).

It should be noted that the global stability of the welded girder is of primary importance (except for the last two examples where there are smaller spans and higher carrying capacities). It is to be expected, so when designing these types of structures, one should pay attention to this condition. The local stability of the web is also essential in the analysis and optimization of these types of girders, which is specific for the examples where spans are larger than 10 m (Example 1, Table 4). Considering the strength criterion, in all examples, the stress at the point C achieved its boundary value, while in the cases of higher carrying capacities, it occurred in points 1 and 2. The stiffness criterion was not dominant in these examples. Also, the oscillation damping period did not have values close to the limit, except in the case with a larger span (Example 1). The stress in the welded joints was far lower than the limit values in all examples.

Regarding the applied metaheuristic optimization algorithm, the MFO method proved to be very efficient, which can be seen from the convergence graphs (Figures 5-8), i.e. the standard deviation (*Std*, Table 2). Furthermore, the graphs show that the minimum value of the objective function is achieved in fewer than 100 iterations, in one example in fewer than 50 iterations (Figure 8).

The FEA for Examples 1 and 3 (Figures 9-12) showed good compliance with the optimization results (Table 4). The relative deviation for the Example 1 maximum equivalent stress was 3.7% (the optimization

result was 20.68 kN/cm² while the FEA yielded 19.93 kN/cm²), and the relative deviation for the Example 1 deflection was 1.1% (the optimization result was 2.74 cm while the FEA yielded 2.71 cm). In addition, the relative deviation for the Example 3 maximum equivalent stress was 5.5% (the optimization result was 17.67 kN/cm² while the FEA yielded 18.69 kN/cm²), and the relative deviation for the Example 3 deflection was 12.5% (the optimization result was 0.64 cm while the FEA yielded 0.73 cm).

As a large number of constraint functions can be used in the presented procedure, this analysis can be further expanded. Additional conditions may be included in future research, such as manufacturability, green design, material fatigue, economic aspects, etc.

References

Cvijović G.M. & Bošnjak S.M. 2016. Calculation methods' comparative analysis of monorail hoist crane local bending effects. *Tehnika*, 71(4), pp.563-570 (in Serbian). Available at: <https://doi.org/10.5937/tehnika1604563C>.

Ellifritt, D.S. & Lue, D.M. 1998. Design of Crane Runway Beam with Channel. *Engineering Journal*, 35(2), pp.41-49. Available at: <https://doi.org/10.62913/engj.v35i2.699>.

Gaska, D., Haniszewski, T. & Margielewicz, J. 2017. I-beam girders dimensioning with numerical modelling of local stresses in wheel-supporting flanges. *Mechanika*, 23(3), pp.347-352. Available at: <https://doi.org/10.5755/j01.mech.23.3.14083>.

Jármai, K., Barcsák, C. & Marcsák, G.Z. 2021. A Box-Girder Design Using Metaheuristic Algorithms and Mathematical Test Functions for Comparison. *Applied Mechanics*, 2(4), pp.891-910. Available at: <https://doi.org/10.3390/applmech2040052>.

Jármai, K., Snyman, J.A., Farkas, J. & Gondos, G. 2003. Optimal design of a welded I-section frame using four conceptually different optimization algorithms. *Structural and Multidisciplinary Optimization*, 25, pp.54-61. Available at: <https://doi.org/10.1007/s00158-002-0272-5>.

Ky, V.S., Lenwari, A. & Thepchatri, T. 2014. Optimum Design of Steel Structures in Accordance with AISC 2010 Specification Using Heuristic Algorithm. *Engineering Journal*, 19(4), pp.71-82. Available at: <https://doi.org/10.4186/ej.2015.19.4.71>.

Mela, K. & Heinisuo, M. 2014. Weight and cost high strength steel beams. *Engineering Structures*, 79, pp.354-364. Available at: <https://doi.org/10.1016/j.engstruct.2014.08.028>.

Mirjalili, S. 2015. Moth-flame optimization algorithm: A novel nature-inspired heuristic paradigm. *Knowledge-Based Systems*, 89, pp.228-249. Available at: <https://doi.org/10.1016/j.knosys.2015.07.006>.

Molnár, D., Blatnický, M. & Dižo, J. 2022. Comparison of Analytical and Numerical Approach in Bridge Crane Solution. *Manufacturing Technology*, 22(2), pp.192-199. Available at: <https://doi.org/10.21062/mft.2022.018>.

Ostrić, D.Z. & Tošić, S.B. 2005. *Dizalice*. Belgrade: University of Belgrade, Faculty of Mechanical Engineering (in Serbian). ISBN: 978-86-7083-520-7.

Pavlović, G., Jerman, B., Savković, M., Zdravković, N. & Marković, G. 2022. Metaheuristic applications in mechanical and structural design. *Engineering Today*, 1(1), pp.19-26. Available at: <https://doi.org/10.5937/engtoday2201019P>.

Pavlović, G. & Savković, M. 2022. Analysis and optimization of the main girder of the bridge crane with an asymmetric box cross-section. *Scientific Technical Review*, 72(1), pp.03-11. Available at: <https://doi.org/10.5937/str2201003P>.

Pavlović, G., Savković, M., Zdravković, N., Bulatović, R. & Marković, G. 2018. Analysis and Optimization Design of Welded I-girder of the Single-beam Bridge Crane. In: *2018 Forth International Conference Mechanical Engineering in the XXI Century MASING 2018*, Niš, Serbia, pp.145-150, April 19-20 [online]. Available at: <https://scidar.kg.ac.rs/handle/123456789/18843> [Accessed: 02 July 2024].

Pavlović, G.V., Zdravković, N.B., Savković, M.M., Bulatović, R.R. & Marković G.Đ. 2024. Light-weight design of an overhead crane's girder with a non-symmetric box cross-section. *Proceedings of the Institution of Mechanical Engineers, Part C: Journal of Mechanical Engineering Science*, 238(3), pp.666-676. Available at: <https://doi.org/10.1177/09544062231179079>.

Petković, Z. & Ostrić, D. 1996. *Metalne konstrukcije u teškoj mašogradnji 1*. Belgrade: University of Belgrade, Faculty of Mechanical Engineering (in Serbian). ISBN: 86-70803-274-7.

Qi, Q., Xu, G., Fan, X. & Wang, J. 2015. A new specular reflection optimization algorithm. *Advances in Mechanical Engineering*, 7(10), pp.1-10. Available at: <https://doi.org/10.1177/1687814015610475>.

Qin, D., Du, P., Zhu, Q. & Yang, J. 2015. Conceptual design of box girder based on three-dimensional topology optimization. In: *2015 11th World Congress on Structural and Multidisciplinary Optimisation*, Sydney, Australia, June 07-12 [online]. Available at: https://www.aeromech.usyd.edu.au/WCSMO2015/papers/1420_paper.pdf [Accessed: 02 July 2024].

Różyło, P. 2016. Optimization of I-section profile design by the finite element method. *Advances in Science and Technology Research Journal*, 10(29), pp.52-56. Available at: <https://doi.org/10.12913/22998624/61931>.

Schaper, L., Jörg, F., Winkler, R., Kuhlmann, U. & Knobloch, M. 2019. The simplified method of the equivalent compression flange. *Steel Construction*, 12(4), pp.264-277. Available at: <https://doi.org/10.1002/stco.201900033>.

Sitthipong, S., Meengam, C., Chainarong, S. & Towatana, P. 2018. Design Analysis of Overhead Crane for Maintenance Workshop. In: *MATEC Web of Conferences: International Conference on Metal Material Processes and Manufacturing (ICMMPM 2018)*, 207, art.number:02003. Available at: <https://doi.org/10.1051/mateconf/201820702003>.

Trahair, N.S. 2009. Lateral-distortional buckling of monorails. *Engineering Structures*, 31(12), pp.2873-2879. Available at: <https://doi.org/10.1016/j.engstruct.2009.07.013>.

Wang, P.F. & Diao, X.H. 2012. Optimization Design of the Crane Girder Based on Adaptive Genetic Algorithm. *Advanced Materials Research*, 591-593, pp.123-126. Available at: <https://doi.org/10.4028/www.scientific.net/AMR.591-593.123>.

Solución óptima para la viga puente de grúa monoviga mediante el algoritmo Moth-Flame

Goran V. Pavlović, **autor de correspondencia**, Mile M. Savković, Nebojša B. Zdravković, Goran Đ. Marković, Predrag Z. Mladenović

Universidad de Kragujevac, Facultad de Ingeniería Mecánica y Civil de Kraljevo, Departamento de Maquinaria Pesada, Kraljevo, República de Serbia

CAMPO: ingeniería mecánica

TIPO DE ARTÍCULO: artículo científico original

Resumen:

Introducción/objetivo: El artículo analiza y optimiza la viga I- soldada del puente grúa monoviga con perfil en U como ala superior. Esta solución tiene como objetivo proporcionar una estructura de transporte más ligera, por lo que el objetivo principal es minimizar el peso de la viga principal, es decir, el área de la sección transversal, al tiempo que se cumplen los requisitos definidos por las normas nacionales y las limitaciones geométricas.

Métodos: Se eligió el algoritmo Moth-Flame Optimization (MFO) para resolver esta tarea de optimización multicriterio de un solo objetivo utilizando MATLAB. Además, los resultados se verificaron utilizando el análisis de elementos finitos (FEA).

Resultados: La forma de viga propuesta se justifica en ejemplos de soluciones reales de puentes grúa monoviga y en los resultados de investigaciones anteriores. En este caso, se consiguen ahorros significativos en el material y mejores resultados en comparación con los ejemplos de la investigación anterior.

Conclusión: La forma de viga propuesta, la metodología, el algoritmo de optimización y los ahorros conseguidos justifican plenamente esta investigación. Además, este algoritmo permite la aplicación de muchas funciones de restricción, con lo que se obtienen los valores óptimos de numerosas variables en un periodo relativamente corto. Por tanto, no sería posible encontrar la solución para esa tarea de ingeniería aplicando métodos de optimización analítica.

Palabras claves: puente grúa, viga soldada, FEA, optimización, metaheurística.

Оптимальное решение для однобалочной подкрановой балки моста с использованием алгоритма Moth-Flame

Горан В. Павлович, **корреспондент**, Миле М. Савкович, Небойша Б. Здравкович, Горан Д. Маркович, Предраг З. Младенович
Крагуевацкий университет, факультет механики и гражданского строительства в Кралево, кафедра тяжелого машиностроения, г. Кралево, Республика Сербия

РУБРИКА ГРНТИ: 55.51.31 Краны и крановое оборудование
ВИД СТАТЬИ: оригинальная научная статья

Резюме:

Введение/цель: В данной статье анализируется и оптимизируется сварная двутавровая балка однобалочного мостового крана с U-образным профилем в качестве верхней ламели. Это решение облегчает несущую конструкцию, так как основной целью является минимизация веса основной балки, то есть площади поперечного сечения при соблюдении требований, определенных государственными стандартами и геометрическими ограничениями.

Методы: Для решения одноцелевой задачи многокритериальной оптимизации с использованием MATLAB был выбран алгоритм оптимизации по принципу "Пламя мотылька" (MFO). Помимо того, результаты были проверены с помощью метода конечных элементов (FEA).

Результаты: Предложенная форма балки обоснована примерами реальных решений однобалочных мостовых кранов и результатами предыдущих исследований. В этом случае достигаются значительная экономия материалов и лучшие результаты по сравнению с примерами предыдущих исследований.

Выводы: Предложенная форма балки, методология, алгоритм оптимизации и достигнутая экономия полностью оправдывают данное исследование. Помимо того, этот алгоритм позволяет применять множество ограничивающих функций, благодаря чему оптимальные значения множества переменных выводятся за относительно короткий промежуток времени. Следовательно, решить эту инженерную задачу, применяя аналитические методы оптимизации, было бы невозможно.

Ключевые слова: мостовой кран, сварная балка, МКЭ, оптимизация, метаэвристика.

Оптимално решење носача једногредне мосне дизалице
применом алгоритма Мољца

Горан В. Павловић, **аутор за преписку**, Миле М. Савковић,
Небојша Б. Здравковић, Горан Ђ. Марковић, Предраг З. Младеновић
Универзитет у Крагујевцу, Факултет за машинство и грађевинарство у
Краљеву, Катедра за тешку машиноградњу, Краљево, Република Србија

ОБЛАСТ: машинство
КАТЕГОРИЈА (ТИП) ЧЛАНКА: оригинални научни рад

Сажетак:

Увод/циљ: У раду се анализира и оптимизира заварени I-носач једногредне мосне дизалице са U-профилом као горњом ламелом. Ово решење обезбеђује лакшу носећу конструкцију, тако да је главни циљ минимизирање тежине главног носача, односно површине попречног пресека, уз испуњавање услова дефинисаних националним стандардима и геометријским ограничењима.

Метод: Алгоритам Мољца (MFO) изабран је за решавање овог једноциљног вишекритеријумског задатка оптимизације применом MATLAB-а. Такође, резултати су верификовани коришћењем методе коначних елемената (МКЕ).

Резултати: Предложени облик носача је оправдан на примерима реалних решења једногредних мосних дизалица. У овом случају постижу се значајне уштеде у материјалу и бољи резултати у односу на примере из претходног истраживања.

Закључак: Предложени облик носача, методологија, алгоритам оптимизације и остварене уштеде у потпуности оправдавају ово истраживање. Поред тога, овај алгоритам омогућава примену многих функција ограничења, при чему се у релативно кратком периоду добијају оптималне вредности бројних варијабли. Због тога, применом метода аналитичке оптимизације не би било могуће наћи решење за такав инжењерски задатак.

Кључне речи: мосна дизалица, заварени носач, МКЕ, оптимизација, метахеуристика.


Paper received on: 03.02.2024.
Manuscript corrections submitted on: 25.09.2024.
Paper accepted for publishing on: 26.09.2024.

© 2024 The Authors. Published by Vojnotehnički glasnik / Military Technical Courier (www.vtg.mod.gov.rs, vtr.mo.ynp.crb). This article is an open access article distributed under the terms and conditions of the Creative Commons Attribution license (<http://creativecommons.org/licenses/by/3.0/rs/>).




Enhancing the physical and chemical characteristics of landfill leachate through a filtration system incorporating granite, iron filings, and recycled rubber waste


Benamar Balegh^a, Hamid Sellaf^b, Adda Hadj Mostefa^c, Driss Djafari^d, Ali Meksi^e


^a Adrar University, Faculty of Science and Technology, Civil Engineering Department, LGCE Laboratory, Adrar, People's Democratic Republic of Algeria, e-mail: ben.balegh@univ-adrar.edu.dz, **corresponding author**, ORCID iD:  <https://orcid.org/0000-0002-8529-7063>

^b Saida University, Faculty of Technology, Civil Engineering and Hydraulic Department, LGCE Laboratory, Saida, People's Democratic Republic of Algeria, e-mail: hamid.sellaf@univ-saida.dz, ORCID iD:  <https://orcid.org/0009-0006-3943-3024>

^c Relizane University, Faculty of Technology, Civil Engineering Department, Relizane, People's Democratic Republic of Algeria, e-mail: addahadjmostefa@yahoo.fr, ORCID iD:  <https://orcid.org/0009-0004-0086-9280>

^d Adrar University, Faculty of Science and Technology, Civil Engineering Department, LDDI Laboratory, Adrar, People's Democratic Republic of Algeria, e-mail: dr-djafari@univ-adrar.edu.dz, ORCID iD:  <https://orcid.org/0000-0002-0836-6715>

^e Mustapha Stambouli University, Faculty of Sciences and Technology, Department of Civil Engineering, Laboratory for the Study of Structures and Mechanics of Materials, Mascara, People's Democratic Republic of Algeria, e-mail: ing.meksi2009@yahoo.fr, ORCID iD:  <https://orcid.org/0009-0009-0320-3704>

 <https://doi.org/10.5937/vojtehg72-49724>

FIELD: chemical technology

ARTICLE TYPE: original scientific paper

Abstract:

Introduction/purpose: The use of composite filters made from waste such as granite powder, iron filings, and rubber granules for treating landfill leachate is an innovative approach that can help mitigate the environmental impact of landfill sites.

ACKNOWLEDGEMENT: This work was supported by PRFU project code A01L02UN010120200004 and the Civil Engineering and Environmental Laboratory of the University of Sidi Bel Abbes, Algeria.

Methods: The experiment involved assessing the performance of single-layer and three-layer filters before and after treatment. To gauge the effectiveness of each filter configuration, the permeability coefficient is calculated for every cell. Calculating the permeability coefficient for single-layer and three-layer filters is an important aspect of assessing the efficiency of the treatment process for landfill leachate. It is also essential to consider other physical and chemical parameters (e.g. color, pH, oxidation coefficient, conductivity, BOD, COD, SS, NO_4^- , NO_3^- , NH_4^+ , PO_4^- , and P) to assess the overall treatment efficiency and the removal of specific contaminants.

Results: The results demonstrated a decrease in both physical and chemical factors with the formation of each cell. Notably, cell 5, consisting of a three-layer filter, exhibited favorable outcomes across physical and chemical parameters as well as permeability. Conversely, cell 2, containing granite powder, exhibited the best physical and chemical parameters but performed poorly in terms of the transmittance factor.

Conclusion: These findings suggest that granite powder, iron filings, and rubber granules can serve as cost-effective filter layers for leachate treatment, helping alleviate its adverse environmental and groundwater impact.

Key words: leachate, granite powder, iron filings, rubber waste, permeability, physico-chemical parameters.

Introduction

Landfills are used worldwide for domestic and industrial solid waste disposal. They are greatly advantageous in terms of environmental protection and respect of sanitary and economic norms. Since landfills generally cover large areas, they are liable to rainfall. Thus, this leads to the generation of large amounts of leachate which is created at the bottom of landfills (Izumoto et al, 2019; Liu et al, 2022; Ishaq et al, 2023). This is due to the deterioration of waste resulting from a range of physical, chemical and biological processes (Azougarh et al, 2019; Gan et al, 2023). The inappropriate disposal of leachate substances induces the pollution of water bodies, groundwaters, (Chidichimo et al, 2020; Negi et al, 2020), and green spaces (Alizadeh et al, 2018; Brahmi et al, 2021).

The leachate treatment has seen a lot of interest recently due to leachate varied characteristics which include higher rates of organic and non-organic substances such as salts, ammonia, and minerals (Ahmadzadeh & Dolatabadi, 2018; Dolatabadi et al, 2021). The type of waste, the age of the storage zone, the location, and the climate in the burial zone are only a few of the factors that affect the content and

composition of leachate (Wang et al, 2021; Suknark et al, 2023; Yu et al, 2022). Generally, recently-constructed burials are characterized by higher amounts of organic compounds and non-toxic organisms, thus minimizing leachate over time. Throughout time, organic chemicals dissolve; hence, levels of their concentrations are reduced.

There are many approaches to the leachate processing. The conventional approach relies on reducing the leachate concentration through channeling it towards sanitation stations. Alternatively, the biological treatment is carried out using water pumps for oxygen stabilization, often known as aerobic and anaerobic processes. Moreover, physical and chemical treatments of leachate are supported in landfills and mines by methods such as deposition, chemical oxidation, sintering, vibration, air removal, and coagulation (Trabelsi et al, 2023; Faheem et al, 2022; Da Silva et al, 2022; Zhao et al, 2023). Some approaches, however, proved less effective in diminishing detrimental substances. From a financial perspective, some treating approaches are known to be costly; therefore, local authorities cannot manage such higher budgets. For this reason, it is highly important to introduce an economical and an environmentally-friendly plan to handle this problem.

Bougdour et al. (2022) installed a multi-layered filter of different materials, modeled in a brick-like shape; it was formed by mixing sand with sawdust, iron filings, and a fertilizer including a limited amount of coal. The current approach was promising in reducing all contaminants. The averages for BOD, COD, nitrogen, phosphorus, and ammonia were 92.8%, 88.7%, 81.6%, 72.4%, and 97%, respectively. Reddy et al. (2020) relied on the integration of four different filtration substances - calcite, zeolite, sand, and iron filings. Consequently, they were effective in removing individual contaminants such as cadmium, copper, nickel, chromium, zinc, nitrate, and phosphate in a 24-hour trial. The first-class motor model was applicable only to remove nitrates by iron filings. Sellaf et al. (2017) among others have designed a filter composed of dam deposits and rubber granules which was promising in removing organic and inorganic materials. Balegh & Sellaf (2022) installed a filter of three different layers: rubber, ceramic powder, and geotextile. This model has also demonstrated thriving potential when physical and chemical properties are reduced.

The main objective of this work is to introduce a new approach to leachate filtration by exploiting the results of previous studies. A new filter made up of monolayers (granite powder, iron filings, rubber granules) and multilayers (the same materials but repositioned) is designed to eliminate contaminants and improve the permeability and the physical and chemical

parameters of sap drainage, using composite cell filtration systems based on different residual materials. Seven filter cells were filled with layers of leftover rubber granules, iron filings and granite powder of the same thickness, changing the position of the layer each time and ensuring that the permeability of the geotextiles in the lower part of the cells was improved. They were then filled with landfill leachate. This study was designed to determine the effect of the three-layer filter element in the cells, as well as the effect of thickness stratification on various physicochemical parameters of the leachate, including permeability, color, pH, conductivity, redox potential, and carbon pollution by nitrogen and phosphorus. The economic objective is to assess the performance and suitability of the leachate treatment method at landfill sites. The study also aims to eliminate residues of rubber, iron filings, and granite and reuse them as filters for leachate treatment, thereby protecting groundwaters from pollution and preserving the environment.

Materials

Leachate

In our preliminary experiment, leachate samples were collected from the landfill site located in the city El-Keurt in the western region of Mascara in Algeria (see Figure 1): coordinates $35^{\circ} 23' 40''$ North and $0^{\circ} 08' 23''$ East. It is located at 5 km from the province of Mascara along national road N° 06 in western Algeria. The area is characterized by low hills, sparse woodlands and medium regression. The average annual rainfall is estimated at 240 and 300 mm. As for the average temperature, it is about 28°C and humidity ranges up to 60%.

Leachate is noticeably dark as a result of its complex chemical composition. Furthermore, it is stinky and liquid. In addition, its liquidity allows it to fuse into groundwaters. The samples were gathered daily at 8 a.m. for seven days. Once stabilized, they were placed in glass containers and stored in laboratories at a regular temperature and humidity. The final sample for the experiment was the resulting seven-day mixture of an equal size.

Granite waste is largely abundant in the region. It is also solid and possesses various forms. Granite powder was extracted from granite waste in construction workshops and then placed in a micro-Deval test device to be fragmented and crushed as shown in Figure 2. After that, it was sifted through a 2 mm sieve.



Figure 1 – Location map of the study area and granite waste powder



Figure 2 – Granite powder, scrap rubber, and iron filings

Granite powder underwent several laboratory identification tests based on standard procedures in accordance with international AFNOR standards. (NF P 94-051, NF P 94-054, NF 94-056, NF P 94-057, and NF P 94-068). The particle size distribution of this powder showed liquid limit 32.00%, sand 2%, silt 38%, clay 60% (see Figure 3), blue color size VB = 0.22 cm³, and specific surface SST = 4.62 m²/g. The chemical analysis of the granite powder was conducted in accordance with NF EN 1744, and the results are presented in Table 1. The results presented in Figure 4 show that the granite powder mostly contained quartz (SiO₂), some traces of orthoclase (NaKAlSi₃O₈), and albite (NaAlSi₃O₈).

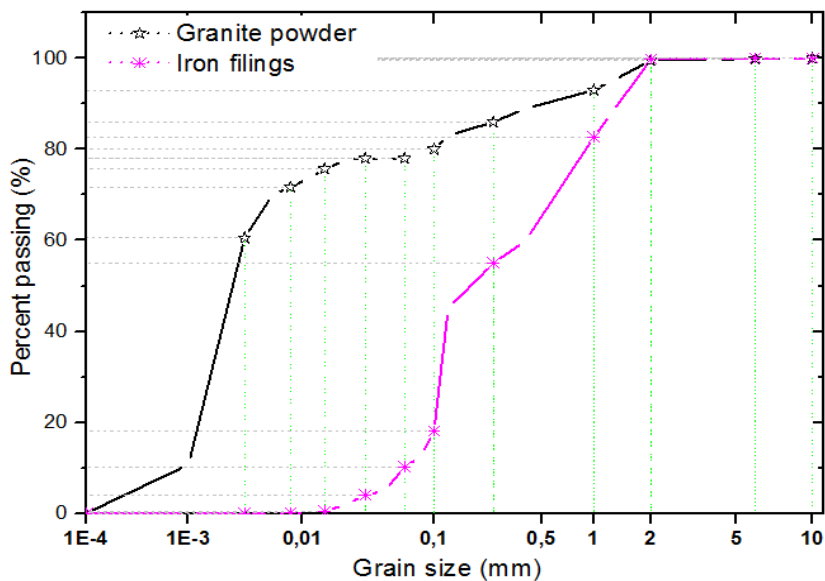


Figure 3 – Particle size distribution of granite powder and iron filings

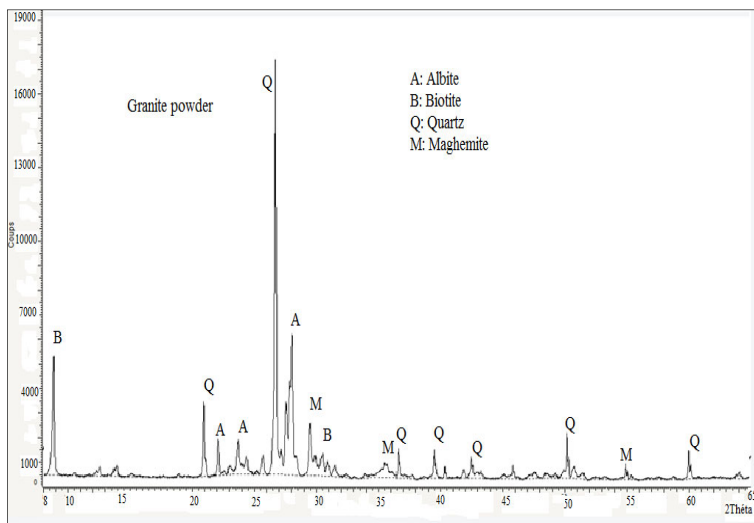


Figure 4 – XRD patterns and the identified phases of the granite powder

Table 1 – Chemical compositions of the granite powder

Property	SiO ₂ (%)	Al ₂ O ₃ (%)	Fe ₂ O ₃ (%)	CaO (%)	MgO (%)	NaOH (%)	Cl (%)	SiO ₃ (%)	P.F ₂ (%)
Granit powder	70.23	16.55	2.63	1.33	0.44	4.74	0.05	0.02	4.01

Iron waste filings

Iron filings represent a fine powder (see Figure 2) obtained from iron cutting and molding workshops, abundantly available in all construction workshops. The iron filings extracted from the construction workshop were sifted through 2 mm sieves, then washed and then dried under 50 °C. The chemical components of the iron filings were: 93.40% iron, 2.67% silicone, 0.03% phosphorus, 0.05% magnesium, 0.01% sulfur, 0.31% manganese, and 3.53% carbon (Olutoge et al, 2016; Kim et al, 2018).

Rubber waste granulate

Rubber granulate can be obtained by mechanical processing through a crush or friction machine. We exhausted the rubber and collected the scattered fragments and then sifted the output through 02 mm sieves (see Figure 2). Rubber granulate consisted of a complex mixture of elastic plastics, polyisoprene, polybutadiene, and styrene butadiene. Numerator oil (1.9%), zinc oxide (1.9%), carbon black (31.0%) and fatty acid (1.2%) are also important components in rubber scrap (Sellaf et al, 2014).

The geotextile used in the current study is non-woven. It is made of polypropylene with the estimated tensile strength of 15 kN m⁻¹, the resistance to static punching of 2700 N, the mass per unit area of 2000 gm⁻², and the permeability of 40 mms⁻¹ (Sellaf et al, 2017).

Methods

Filtration experiences

The experiment consists of seven cells of 1000 mm PVC columns, 50 mm in diameter. Figure 5 shows the scheme of the experiment. The first cell is left empty from any layer for the purpose of observing the ratio of filtration of the geotextile layer. Cells 02, 03 and 04 were filled each with one layer to a height of 600 mm (granite powder layer, iron filings layer and rubber granule layer), respectively. The remaining cells - 05, 06 and 07 - are equally filled in three layers at 200 mm height.

The position of the layers for each cell was taken into account. The positioning is depicted in Figure 5.

The cells are positioned vertically so that they flow naturally and then all cells are fed with leachate through a separate tank placed above the cells with a capacity of 4,000 ml.

The leachate flows for 30 minutes on all cells until they are saturated and then the filtration results are collected for each cell.

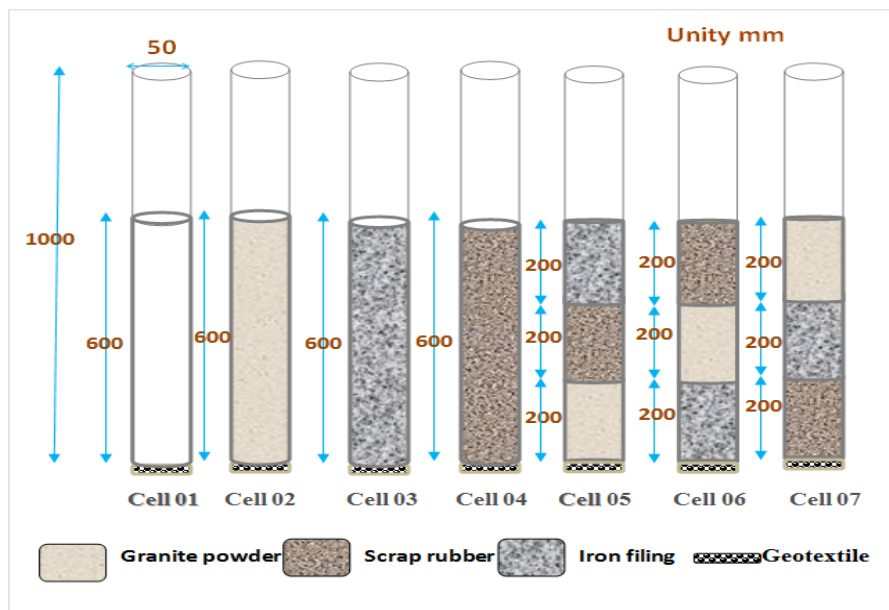


Figure 5 – Schematic representation of the apparatus for the loaded soil-geotextile filtration test

The examination and study of the cell samples are carried out for different aspects: "Color, pH, electrical conductivity (EC) and total suspended solids (SS), dissolved oxygen (DO), chemical oxygen demand (COD), biological oxygen demand (BOD), ammonia (NH_4^+) nitrate (NO_3^-), phosphate (PO_4^-), and phosphorus (P) ", based on the international standards for the analysis of water and liquid waste as shown in Table 2.

Table 2 – Parameters and methods

Parameters	Reference	Standards
pH	pH	NF T 90-008
Conductivity	EC (µs/cm)	NF EN 27888
Dissolved oxygen	DO(mg/l)	NF T 90-106
Biochemical Oxygen Demand	DBO(mg/l)	NFT 90-103-10
Suspended solids	SS(mg/l)	NFT 90-105
Phosphorus	P(mg/l)	NFT 90-042-01
Nitrite	NO ₂ ⁻ (mg/l)	NF EN ISO 13395
Nitrates	NO ₃ ⁻ (mg/l)	NF EN 26777
Ammonia	NH ₄ ⁺ (mg/l)	NF T 90-015

Results and the discussion

The major elements found in granite powder are Si, Al, Ca, Fe, and Mg in their oxidizing forms such as SiO₂, Al₂O₃, CaO, Fe₂O₃ and MgO, in addition to the metal composition of iron filing: 3.53% carbon, 2.67% silicone, 0.05% magnesium, 0.01% sulfur, 0.03% phosphorus, 0.31% manganese, and 93.40% iron as well as a complex installation of the rubber granules of elastomer (1.9%), zinc oxide (1.9%), carbon black (31.0%), and fatty acid (1.2%). All these diverse and inclusive elements result in the interconnectedness between granules, thus rendering them more effective in the leachate filtration process.

Table 3 shows the physical and chemical factors of the leachate resulting from cell number one. This cell does not contain any layer (geotextiles) and no changes in the physical and chemical factors of the leachate have been observed when compared to the leachate before filtration. This is proved by Balegh & Sellaf (2022) and Koerner & Koerner (2013).

Permeability

Water flows based on Darcy's law (Darcy, 1856) in a vertically placed porous medium: the test cell can be considered as a cylindrical tube with a size of an S. In addition, this cylindrical tube is filled with porous substances: granite powder, rubber granules and iron filings in a size of an L length. Subsequently, they are rotated with distilled water at a total height of ΔH (fixed). When the medium is saturated with water, consequently, Q is the flow (m³/s). Furthermore, k is the permeability or the hydraulic

connectivity (m/s). Moreover, A is the vertical surface of the flow (m), L is the layer length (600mm), and h marks the difference between the upstream and the downstream.

Table 3 – Filtration test results for cell 01

Property	Leachate Pre filter	Cell 01(Geotextile)
pH	7.5	7.5
EC ($\mu\text{s}/\text{cm}$ at 22C°)	3200	3200
Dissolved oxygen	4.11	4.11
COD(mg/l)	27000	27000
BOD(mg/l)	5600	5600
SS (mg/l)	820	820
P (mg/l)	1.08	1.08
PO_4 (mg/l)	3.50	3.50
NO_2 (mg/l)	1.45	1.45
NO_3 (mg/l)	7.86	7.86
NH_4^+ (mg/l)	48	48

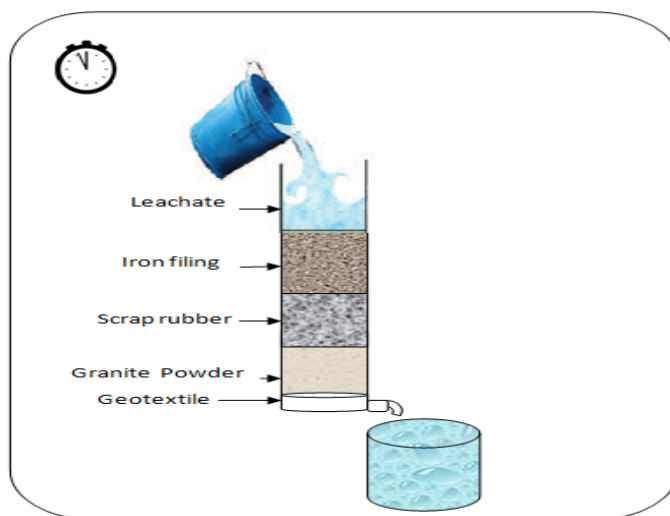


Figure 6 – Permeability test

The filter encompassing layers made up of granite powder, rubber granules, and iron filings is considered as a porous multi-layered middle barrier designed according to the Darcy permeability model (see Figure 6). The permeability coefficients were compared for all cells taking into account their composition.

As shown in Figure 7, the cell containing a single layer has the weakest permeability such as cell 02 (granite powder layer) - 1.50 mm/s, followed by cell 03 (iron filings layer) - 4.87 mm/s, contrary to cell 04 (layer of rubber granules) - 11.02 mm/s. On the other hand, the results related to the cells with three layers were correlated to the positioning of the granite powder and iron filings layers. The results were as follows: cell 05= 3.55 mm/s, cell 06= 3.07 mm/s, and cell 07= 2.89 mm/s.

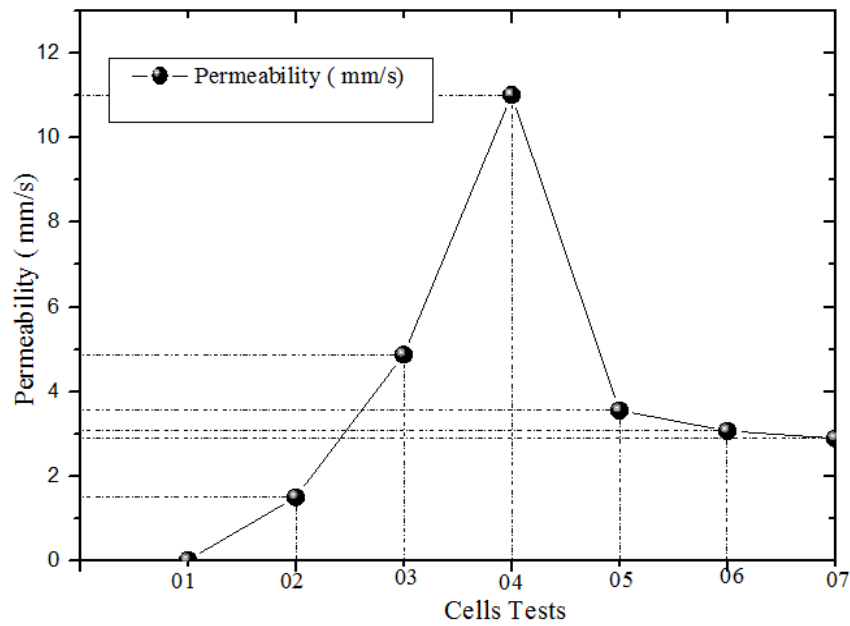


Figure 7 – Values of the permeability test (mm/s)

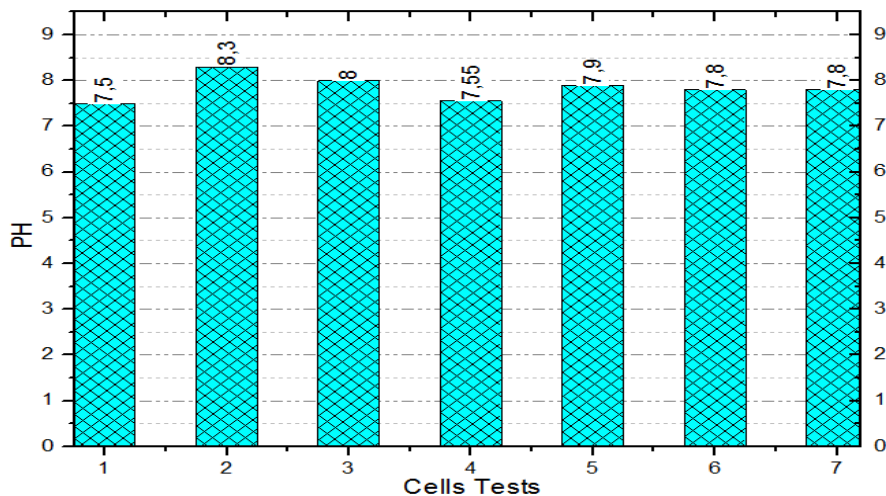


Figure 8 – Values of pH

Color

Before conducting the filtration process, the color of the leachate was dark. After flowing the leachate into the multilayer cells (granite powder layer, iron filings layer, and rubber granules layer), the color of the resulting leachate was light, though the layers were dissimilar (see cells 05, 06, and 07). Likewise, when the leachate was flown through the single layer filtration cells, there was a noticeable change in its color; it was transparent in cell 02 (granite powder layer). Yet, the color is slightly cloudy in cell 03 (iron filings layer). Similarly, it was dark brown in cell 04 (rubber granules layer).

The relevant references have demonstrated that the change in color has three main indications: the value of the hydrogen exponent, the reduction rate of COD, and ammonia. In a similar fashion, Veli et al. (2021) have proved the relationship between the pH value and the COD value besides its effect on color removal. (42% of the COD removal showed the color removal of 97% whereas removing 93% of COD demonstrated the color removal of 98%). Beyazit & Atmaca (2021) have also argued that a maximum of 83.84% COD removal resulted in removing color from the filter material of about 84.46%. Similarly, Onn et al. (2020) succeeded in removing 45.70% of the COD and in lightening the color of the filtered water to 97.30%.

pH

When pH was tested for the filtration results in all cells from 02 to 07, it was observed that the pH values were stable between 7.5 to 7.8 in the filtration of the three-layer cells containing granite powder (see Figure 8), iron filings and rubber granules despite their different position. Unlike single layer cells, different pH values were depicted. Cell 02 showed pH=8.50 while, cell 03 demonstrated pH=8.10 whereas cell 04 has demonstrated pH=7.55.

Xie et al. (2015) have confirmed the correlation between pH and concentrations in dissolved heavy metals (Zn, Cu, Ni, Pb, and Cd). The pH of leachate increases when fewer inorganic ingredients dissolve; thus the concentration of heavy metals will be reduced, Øygard et al. (2004) and Chen et al. (2020).

Potential conductivity and oxidation

According to Figures 9 and 10, variables in the conductivity potential in addition to the oxidation factor were evident in all cells, especially in single-layer cells in which values varied from 70%, 67%, and 7% (1.24, 1.34, and 3.81 mg/l, respectively) for the oxidation factor. For the conductivity factor, the results dropped to a third or a half (1250, 1850, and 3050 $\mu\text{s}/\text{cm}$).

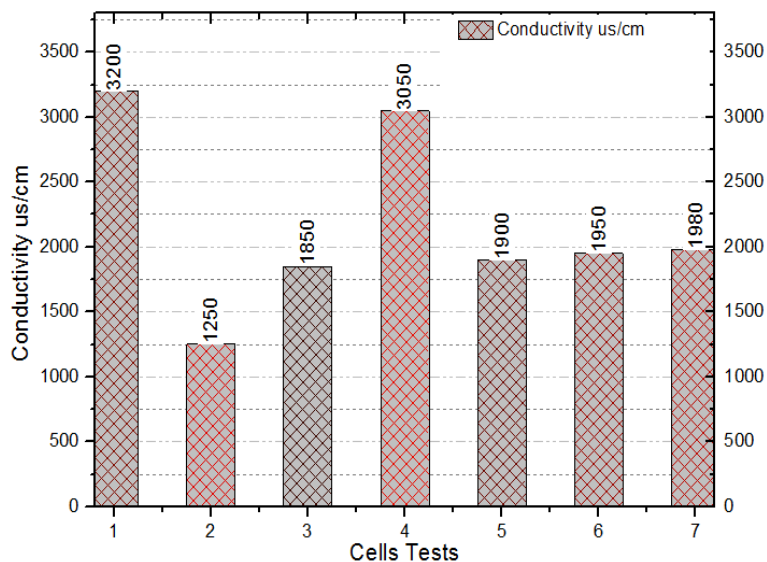


Figure 9 – Values of conductivity (mg/l)

For the three-layered cells, regardless of the positions and the arrangements of layers, the results were approximate in terms of the oxidation conductivity factor. The results of the conductivity factor were 1900, 1950, and 1980 $\mu\text{s}/\text{cm}$ in cells 05, 06 and 07, respectively. For the oxidation factor, the results were 1.42, 1.45, and 1.47 mg/l in cells 05, 06, and 07, respectively.

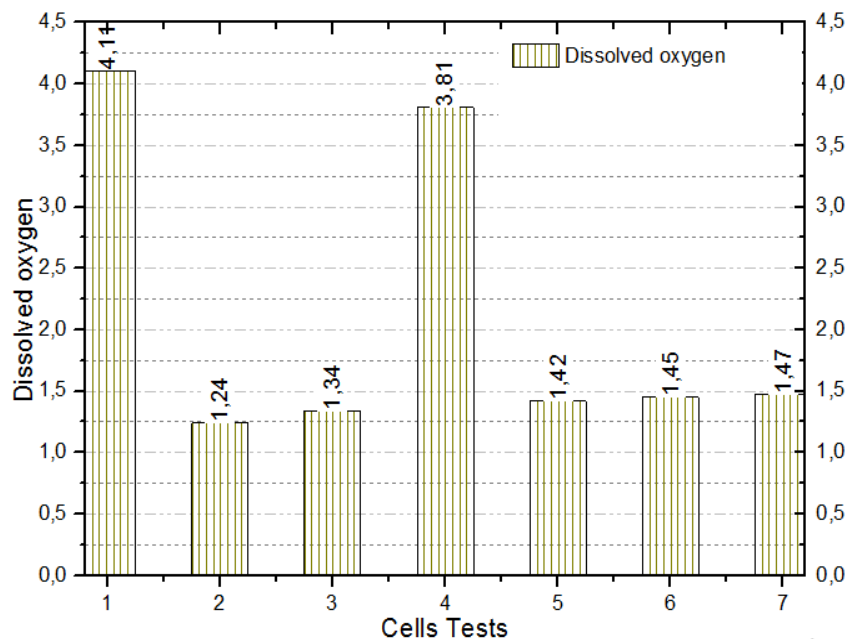


Figure 10 – Values of dissolved oxygen (mg/l)

Carbon pollution

The results presented in Figure 11 show the BOD and COD values, and the difference appears in the results depending on the cell composition, as they were close in the multilayer cells regardless of their arrangement, and were far apart in the monolayer cell results. The average BOD leachate concentrations were 1220, 2400, 5200, 2600, 2700, 2750 mg/L for cells 02, 03, 04, 05, 06 and 07, respectively.

Although the results obtained were uneven, as it was obtained that the granite powder layer achieved a 78% decrease, in contrast to the iron filings layer which achieved a 21% decrease, the decrease was estimated

at 7%. For the cells containing three layers, regardless of their order, the percentage on bioxygen demand decreased from 50% to 44%.

The chemical oxygen demand values before the filtration were estimated at 27,000 mg/L. After the intracellular filtration, the change was evident as a function of cell compositions from a monolayer to tertiary layers, and the removal curve was similar to the BOD removal curve (elimination curve), where the elimination rate amplitudes in the monolayer cells were 55%, 51%, and 48 % (cells 02, 03 and 04, respectively), while in the trilayer cells the elimination rate ranged from 55% to 49%.

The values of suspended materials ranged from 350 to 720 mg/l based on the composition of each cell. The reduction ratio in the single-layer cells was 57.4% to 10.9 % while for the three-layer cells, the reduction ratio was between 45% and 43%. These findings are in line with those found by Aziz et al. (2020).

Deng et al. (2020) have built an iron filings-filled electrochemical system (IFES) to improve the removal efficiency of total nitrogen (TN) and the chemical oxygen demand (COD). The current TN removal efficiency is significant.

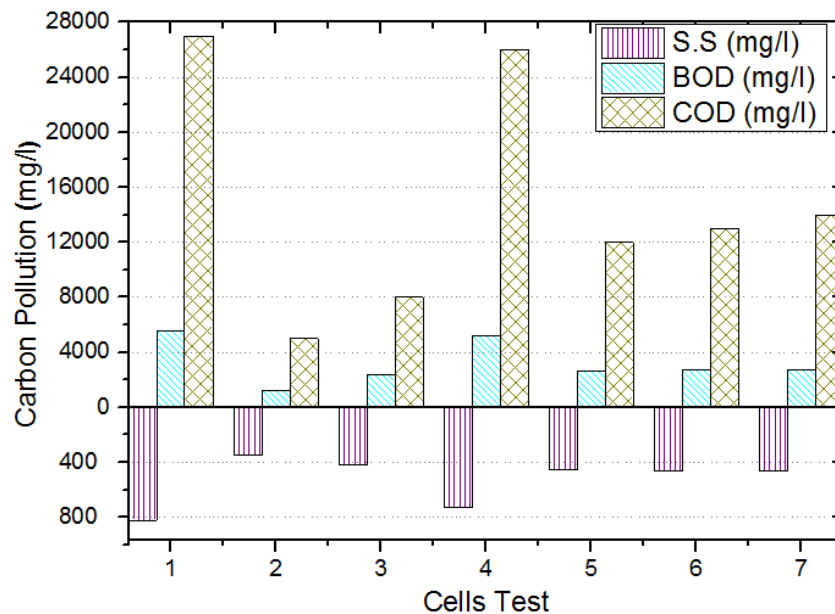


Figure 11 – Values of carbon pollution (mg/l)

Nitrogen pollution

Prior to filtration, the ammonia factor was 33 times higher (48 mg/l, and 1.45 mg/l) (see Figure 12) than the nitrate factor. The nitrite factor is normal and moderate (8.12 mg/l). After the filtration process, the reduction of the three factors in all single-layer and three-layer cells is observed. The three coefficients of the values were analogous in the three-layer cells. The ammonia values were estimated at NH_4^+ 31.51, 32.22, and 33.14 mg/l for cells 05, 06, and 07, and the nitrate values were estimated at NO_3^- 4.65, 4.71 and 4.77 for cells 05, 06, and 7. The nitrite values NO_2^- were between 0.87, 0.92, and 0.95 for cells 05, 06, and 07.

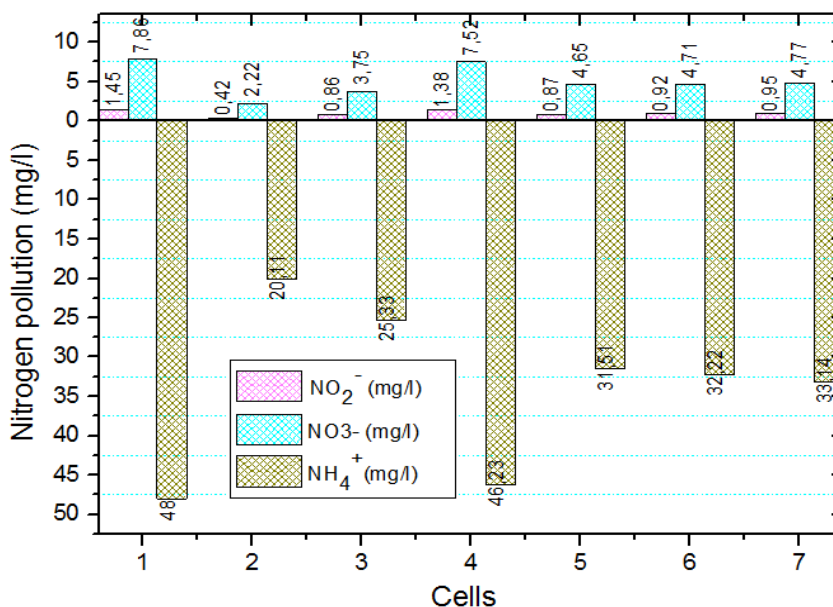


Figure 12 – Values of nitrogen pollution (mg/l)

The single-layer cells containing granite powder were promising in the removing rate for the three coefficients in which the ratio is estimated at 58% and 71%, unlike the cell containing iron filings layer where the removal ratio was estimated between 40% and 52%. Nonetheless, the cell containing the rubber granules layer had a very low removal ratio, estimated at 41% to 48%.

Sun et al. (2020) successfully removed some parameters using EC (electrocoagulation) added to iron powder to lose electrons and produce coagulants in situ, and the removal efficiency was 72.5% for total organic carbon (TOC), 98.5% for ammonia, and 98.6% for carbon and phosphorus. Some heavy metals and hardness were also removed.

Phosphorus pollution

Prior to the filtration process, the value of the phosphorus factor (P) was significantly lower than the value of the phosphate factor (PO_4^-), where the ratio made up a quarter (25%) (see Figure 13). From cell 06, the difference between the results of the single-layer cells and the three-layer cells is evident.

In the three-layer cells, the results were remarkably similar, and the variation did not surpass 0.04 for phosphate and 0.01 for phosphorus. Unlike the single layer cells, cell 02 containing granite powder layer depicted a higher removal value of 64% to 75 % for the phosphorus agent and the phosphate. Instead, cell 03 containing the iron filings layer demonstrated a weak removal value of 9% to 15 % for the phosphate and phosphorus coefficients.

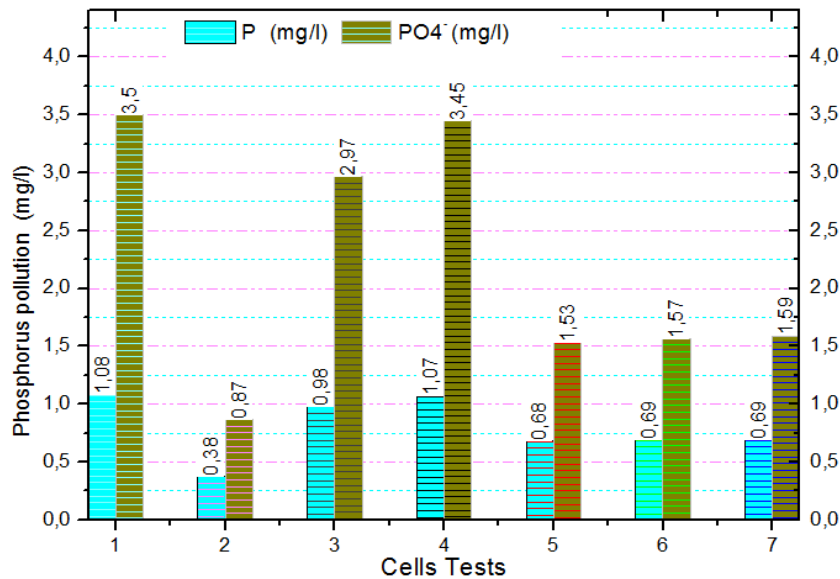


Figure 13 – Values of phosphorus pollution (mg/l)

The removal efficiency of PO_4^- , total nitrogen (TN), and total phosphorus (TP) in this study is better than the results obtained by Liang et al. (2023), where PO_4^- , TN, and TP are reduced between 89.25%, 80.64%, and 92.2%, respectively.

Conclusion

In this study, a leachate filtration system consisting of seven cells was tested and divided into two types: single-layer cells and multi-layer cells. The conclusions drawn from this experiment are limited to three branches in accordance with the permeability coefficient, the composition of the single cell, and the arrangement of layers for the permeability coefficient which is affected by the material constituting the cell in this context. Cell 04, which consists of a layer of rubber granules, has the highest permeability coefficient, while cell 02, with a layer of granite powder, has the lowest permeability coefficient. This indicates that the choice of material significantly impacts the permeability of the cell with rubber granules allowing for higher permeability compared to granite powder.

It appears that altering the arrangement or the sequence of layers within the cell had no discernible impact on the permeability coefficient. This implies that the configuration of layers in the multi-layered cell does not exert any influence on its permeability, and the permeability remains consistent irrespective of how the layers are arranged.

When using geotextile alone in the filtration of leachate, there is no change in the physicochemical parameters of the resulting water. This suggests that geotextile alone is not effective in treating leachate.

The cells with granite powder alone show better results in reducing the physicochemical parameters of leachate compared to the cells with the three layers of granite powder, iron filings, and rubber granulate. Significant improvements in various physicochemical parameters of leachate are observed in cells 02, 03, 05, and 06. For cell 04, there is almost no improvement in the physicochemical parameters of leachate.

The current study highlights the use of a three-layer filtration combination comprising granite powder, iron filings, and rubber granulate as a promising alternative to the conventional use of gravel or sand in the drainage layer of leachate collection and treatment systems. Incorporating scrap tires, iron filings, and granite waste in this manner not only offers a sustainable solution but also mitigates the challenges associated with solid waste disposal. This approach transforms waste materials into valuable resources, contributing to environmental conservation and pollution reduction.

References

- Ahmadzadeh, S. & Dolatabadi, M. 2018. Electrochemical treatment of pharmaceutical wastewater through electrosynthesis of iron hydroxides for practical removal of metronidazole. *Chemosphere*, 212, pp.533-539. Available at: <https://doi.org/10.1016/j.chemosphere.2018.08.107>.
- Alizadeh, M., Mirhoseini, S.A., Dolatabadi, M. & Ebrahimi, A.A. 2018. Evaluation the Effect of Landfill Leachate on the Surface Water Quality: A Case Study in Tonekabon Landfill. *Journal of Environmental Health and Sustainable Development*, 3(1), pp.472-480 [online]. Available at: <http://jehsd.ssu.ac.ir/article-1-102-en.html> [Accessed: 10 March 2024].
- Aziz, H.A., Noor, A.F.M, Keat, Y.W., Alazaiza, M.Y.D. & Abd Hamid, A. 2020. Heat Activated Zeolite for the Reduction of Ammoniacal Nitrogen, Colour, and COD in Landfill Leachate. *International Journal of Environmental Research*, 14, pp.463-478. Available at: <https://doi.org/10.1007/s41742-020-00270-5>.
- Azougarh, Y., Abbaz, M., Hafid, N., Benafqir, M., Ez-zahery, M. & El Alem, N. 2019. Characterization and treatment of leachate of the great agadir discharge by infiltration-percolation onto titaniferous sand. *Scientific African*, 6, e00154. Available at: <https://doi.org/10.1016/j.sciaf.2019.e00154>.
- Balegh, B. & Sellaf, H. 2022. Treatment of Leachate of Landfills Using Filters of Ceramic Waste and Scrap Rubber Waste. *Water, Air, & Soil Pollution*, 233, art.number:526. Available at: <https://doi.org/10.1007/s11270-022-06004-x>.
- Beyazit, N. & Atmaca, K. 2021. COD and Color Removal from Landfill Leachate by photo-electro-Fenton Process. *International Journal of Electrochemical Science*, 16(5), art.number:210539. Available at: <https://doi.org/10.20964/2021.05.65>.
- Bougdour, N., Radaa, C., Tajat, N., Elhayaoui, W., Zoubir, J., Hamdani, M., Qourzal, S., Nahlé, A., Assabbane, A. & Bakas, I. 2022. Treatment for landfill leachate through sequential multi-sand-layering filters coupled with sulfate radical-based advanced oxidation processes. *International Journal of Environmental Science and Technology*, 20, pp.135-148. Available at: <https://doi.org/10.1007/s13762-022-04036-8>.
- Brahmi, S., Baali, F., Hadji, R., Brahmi, S., Hamad, A., Rahal, O., Zerrouki, H., Saadali, B. & Hamed, Y. 2021. Assessment of groundwater and soil pollution by leachate using electrical resistivity and induced polarization imaging survey, case of Tebessa municipal landfill, NE Algeria. *Arabian Journal of Geosciences*, 14, art.number:249. Available at: <https://doi.org/10.1007/s12517-021-06571-z>.
- Chen, B., Han, L., Yoon, S., Lee, W., Zhang, Y., Yuan, L. & Choi, Y. 2020. Applying steel slag leachate as a reagent substantially enhances pH reduction efficiency for humidification treatment. *Environmental Science and Pollution Research*, 27, pp.18911-18923. Available at: <https://doi.org/10.1007/s11356-020-08429-5>.
- Chidichimo, F., De Biase, M. & Straface, S. 2020. Groundwater pollution assessment in landfill areas: Is it only about the leachate. *Waste Management*, 102, pp.655-666. Available at: <https://doi.org/10.1016/j.wasman.2019.11.038>.

Da Silva, V.E.P.S.G., de S. Rollemberg.S.L., da S. e Santos, S.G., Silva, T.F.C.V., Vilar, V.J.P. & Dos Santos, A.B. 2022. Landfill leachate biological treatment: perspective for the aerobic granular sludge technology. *Environmental Science and Pollution Research*, 29, pp.45150-45170. Available at: <https://doi.org/10.1007/s11356-022-20451-3>.

Darcy, H.P.G. 1856. Détermination des lois d'écoulement de l'eau á travers le sable. In: Dalmont, V. (Ed.) *Les Fontaines Publiques de la Ville de Dijon*, pp.590-594. Paris, Batignolles: Typographie Hennuyer.

Deng, Y., Chen, N., Feng, C., Chen, F., Liu, H. & Chen, Z. 2020. Enhancing electrochemical treatment of nitrogen-containing organic wastewater by iron filings: Performance, inhibition of organochlorine by-products accumulation and cost-effectiveness. *Chemical Engineering Journal*, 384, art.number:123321. Available at: <https://doi.org/10.1016/j.cej.2019.123321>.

Dolatabadi, M., Świergosz, T. & Ahmadzadeh, S. 2021. Electro-Fenton approach in oxidative degradation of dimethyl phthalate - The treatment of aqueous leachate from landfills. *Science of The Total Environment*, 772, art.number:145323. Available at: <https://doi.org/10.1016/j.scitotenv.2021.145323>.

Faheem, K., Khan, S.U., Washeem, M. & Khan, S.U. 2022. Energy efficient removal of COD from landfill leachate wastewater using electrocoagulation: parametric optimization using RSM. *International Journal of Environmental Science and Technology*, 19, pp.3625-3636. Available at: <https://doi.org/10.1007/s13762-021-03277-3>.

Gan, P., Sun, Y., Li, Y., Liu, W., Ye, J., Tong, M. & Liang, J. 2023. The degradation of municipal solid waste incineration leachate by UV/persulfate and UV/H₂O₂ processes: The different selectivity of SO₄⁻ and ·OH. *Chemosphere*, 311(1), art.number:137009. Available at: <https://doi.org/10.1016/j.chemosphere.2022.137009>.

Ishaq, A., Said, M.I.M., Azman, S.B., Abdulwahab, M.F. & Jagun, Z.T. 2023. Optimizing total ammonia–nitrogen concentration for enhanced microbial fuel cell performance in landfill leachate treatment: a bibliometric analysis and future directions. *Environmental Science and Pollution Research*, 30, pp.86498-86519. Available at: <https://doi.org/10.1007/s11356-023-28580-z>.

Izumoto, S., Hamamoto, S., Kawamoto, K., Nagamori, M. & Nishimura, T. 2019. Methane eruptions from landfill final cover soil during rainfall events in laboratory experiments. *Soils and Foundations*, 59(4), pp.1052-1062. Available at: <https://doi.org/10.1016/j.sandf.2019.05.002>.

Kim, Y., Hanif, A., Usman, M., Munir, M.J., Kazmi, S.M.S. & Kim, S. 2018. Slag waste incorporation in high early strength concrete as cement replacement: environmental impact and influence on hydration & durability attributes. *Journal of Cleaner Production*, 172, pp.3056-3065. Available at: <https://doi.org/10.1016/j.jclepro.2017.11.105>.

Koerner, R.M. & Koerner, G.R. 2013. Geotextile Filter Failures Under Challenging Field Conditions. In: Stuedlein, A.W. & Christopher, B.R. (Eds.) *Sound Geotechnical Research to Practice: Honoring Robert D. Holtz II (BOOK*

SET: Geo-Congress 2013), pp.272-289. ASCE-American Society of Civil Engineers. Available at: <https://doi.org/10.1061/9780784412770.018>.

Liang, X., Wang, D., Li, M., Liu, D., Han, J., Wei, Q., Huang, Y., Huang, H. & Feng, Q. 2023. Study on the Effect of Iron-Carbon Micro-electrolysis Process on the Removal of Nitrogen and Phosphorus from Rural Domestic Wastewater with Low Carbon to Nitrogen Ratio. *Water, Air, & Soil Pollution*, 234, art.number:113. Available at: <https://doi.org/10.1007/s11270-023-06131-z>.

Liu, M., Lu, H., Deng, Q., Ji, S., Qin, L. & Wan, Y. 2022. Shear strength, water permeability and microstructure of modified municipal sludge based on industrial solid waste containing calcium used as landfill cover materials. *Waste Management*, 145, pp.20-28. Available at: <https://doi.org/10.1016/j.wasman.2022.04.031>.

Negi, P., Mor, S. & Ravindra, K. 2020. Impact of landfill leachate on the groundwater quality in three cities of North India and health risk assessment. *Environment, Development and Sustainability*, 22, pp.1455-1474. Available at: <https://doi.org/10.1007/s10668-018-0257-1>.

Olutoge, F.A., Onugba, M.A. & Ochoi, A. 2016. Strength Properties of Concrete Produced With Iron Filings as Sand Replacement. *Current Journal of Applied Science and Technology*, 18(3), pp.1-6. Available at: <https://doi.org/10.9734/BJAST/2016/29938>.

Onn, S.W., Bashir, M.J.K., Sethupathi, S., Abu Amr, S.S. & Nguyen, T.T. 2020. Colour and COD removal from mature landfill leachate using electro-persulphate oxidation process. *Materials Today: Proceedings*, 31(1), pp.69-74. Available at: <https://doi.org/10.1016/j.matpr.2020.01.193>.

Øygaard, J.K., Måge, A. & Gjengedal, E. 2004. Estimation of the mass-balance of selected metals in four sanitary landfills in Western Norway, with emphasis on the heavy metal content of the deposited waste and the leachate. *Water Research*, 38(12), pp.2851-2858. Available at: <https://doi.org/10.1016/j.watres.2004.03.036>.

Reddy, K.R., Dastgheibi, S. & Cameselle, C. 2021. Mixed versus layered multi-media filter for simultaneous removal of nutrients and heavy metals from urban stormwater runoff. *Environmental Science and Pollution Research*, 28, pp.7574-7585. Available at: <https://doi.org/10.1007/s11356-020-11120-4>.

Sellaf, H., Trouzine, H. & Asroun, A. 2017. Assessment of the Performance of Sediments and Scrap Rubber Layers to Filter the Leachate of Landfills. *International Journal of Engineering Research in Africa*, 35, pp.162-174. Available at: <https://doi.org/10.4028/www.scientific.net/JERA.35.162>.

Sellaf, H., Trouzine, H., Hamhami, M. & Asroun, A. 2014. Geotechnical Properties of Rubber Tires and Sediments Mixtures. *Engineering, Technology & Applied Science Research (ETASR)*, 4(2), pp.618-624. Available at: <https://doi.org/10.48084/etasr.424>.

Suknark, P., Buddhawong, S. & Wangyao, K. 2023. Investigating the effect of waste age and soil covering on waste characteristics prior to landfill mining using an electrical resistivity tomography technique. *Journal of Environmental*

Management, 339, art.number:117898. Available at: <https://doi.org/10.1016/j.jenvman.2023.117898>.

Sun, D., Hong, X., Cui, Z., Du, Y., Hui, K.S, Zhu, E., Wu, K. & Hui, K.N. 2020. Treatment of landfill leachate using magnetically attracted zero-valent iron powder electrode in an electric field. *Journal of Hazardous Materials*, 388, art.number:121768. Available at: <https://doi.org/10.1016/j.jhazmat.2019.121768>.

Trabelsi, I., Salah S. & Ounaes, F. 2013. Coupling short-time sequencing batch reactor and coagulation–settling process for co-treatment of landfill leachate with raw municipal wastewater. *Arabian Journal of Geosciences*, 6, pp.2071-2079. Available at: <https://doi.org/10.1007/s12517-011-0464-7>.

Veli, S., Arslan, A., Isgoren, M., Bingol, D. & Demiral, D. 2021. Experimental design approach to COD and color removal of landfill leachate by the electrooxidation process. *Environmental Challenges*, 5, art.number:100369. Available at: <https://doi.org/10.1016/j.envc.2021.100369>.

Wang, Y.-N, Xu, R., Kai, Y., Wang, H., Sun, Y., Zhan, M. & Gong, B. 2021. Evaluating the physicochemical properties of refuse with a short-term landfill age and odorous pollutants emission during landfill mining: A case study. *Waste Management*, 121, pp.77-86. Available at: <https://doi.org/10.1016/j.wasman.2020.12.001>.

Xie, S., Ma, Y., Strong, P.J. & Clarke, W.P. 2015. Fluctuation of dissolved heavy metal concentrations in the leachate from anaerobic digestion of municipal solid waste in commercial scale landfill bioreactors: The effect of pH and associated mechanisms. *Journal of Hazardous Materials*, 299, pp.577-583. Available at: <https://doi.org/10.1016/j.jhazmat.2015.07.065>.

Yu, F., Wu, Z., Wang, J., Li, Y., Chu, R., Pei, Y. & Ma, J. 2022. Effect of landfill age on the physical and chemical characteristics of waste plastics/microplastics in a waste landfill sites. *Environmental Pollution*, 306, art.number:119366. Available at: <https://doi.org/10.1016/j.envpol.2022.119366>.

Zhao, Z., Zhang, Y., Yu, L., Hou, D., Wu, X., Li, K. & Wang, J. 2023. Fenton pretreatment to mitigate membrane distillation fouling during *treatment* of landfill leachate membrane concentrate: Performance and mechanism. *Water Research*, 244, art.number:120517. Available at: <https://doi.org/10.1016/j.watres.2023.120517>.

Mejora de las características físicas y químicas del lixiviado de vertederos mediante un sistema de filtración que incorpora granito, limaduras de hierro y residuos de caucho reciclado

Benamar Balegh^a, **autor de correspondencia**, *Hamid Sella*^b, *Adda Hadj Mostefa*^c, *Driss Djafari*^a, *Ali Meksi*^d

^a Universidad de Adrar, Facultad de Ciencias y Tecnología, Departamento de Ingeniería Civil, Laboratorio LGCE, Adrar, República Argelina Democrática y Popular

^b Universidad de Saida, Facultad de Tecnología, Departamento de Ingeniería Civil e Hidráulica, Laboratorio LGCE, Saida, República Argelina Democrática y Popular

^c Universidad de Relizane, Facultad de Tecnología,
Departamento de Ingeniería Civil,
Relizane, República Argelina Democrática y Popular

^d Universidad Mustapha Stambouli, Facultad de Ciencias y Tecnología,
Departamento de Ingeniería Civil,
Laboratorio para el Estudio de Estructuras y Mecánica de Materiales,
Mascara, República Democrática y Popular de Argelia

CAMPO: tecnología química

TIPO DE ARTÍCULO: artículo científico original

Resumen:

Introducción/objetivo: El uso de filtros compuestos hechos a partir de desechos como polvo de granito, limaduras de hierro y gránulos de caucho para tratar el lixiviado de los vertederos es un enfoque innovador que puede ayudar a mitigar el impacto ambiental de los vertederos.

Métodos: El experimento implicó evaluar el rendimiento de los filtros de una y tres capas antes y después del tratamiento. Para medir la eficacia de cada configuración de filtro, se calcula el coeficiente de permeabilidad para cada celda. Calcular el coeficiente de permeabilidad para los filtros de una y tres capas es un aspecto importante para evaluar la eficiencia del proceso de tratamiento del lixiviado de los vertederos. También es esencial considerar los demás parámetros físicos y químicos (por ejemplo, color, pH, coeficiente de oxidación, conductividad, DBO, DQO, SS, NO₄⁻, NO₃⁻, NH₄⁺, PO₄⁻ y P) para evaluar la eficiencia general del tratamiento y la eliminación de contaminantes específicos.

Resultados: Los resultados demostraron una disminución de los factores físicos y químicos con la formación de cada celda. Cabe destacar que la celda 5, que consta de un filtro de tres capas, exhibió resultados favorables en los parámetros físicos y químicos, así como en la permeabilidad. Por el contrario, la celda 2, que contiene polvo de granito, exhibió los mejores parámetros físicos y químicos, pero tuvo un desempeño deficiente en términos del factor de transmitancia

Conclusión: Estos hallazgos sugieren que el polvo de granito, las limaduras de hierro y los gránulos de caucho pueden servir como capas de filtro rentables para el tratamiento de lixiviados, ayudando a aliviar impactos ambientales y de aguas subterráneas adversos.

Palabras claves: lixiviado, polvo de granito, limaduras de hierro, desechos de caucho, permeabilidad, parámetros fisicoquímicos.

Улучшение физических и химических свойств фильтрата, образующегося на свалках, благодаря системе фильтрации, включающей гранитную пыль, металлическую стружку и переработанные резиновые отходы

*Бенамар Балех^а, корреспондент, Хамид Селлаф^б,
Адда Хадж Мостефа^в, Дрисс Джафари^а, Али Мекси^г*

^а Адрарский университет, факультет науки и технологии,
кафедра гражданского строительства,
г. Адрар, Алжирская Народная Демократическая Республика

^б Университет Саиды, технологический факультет,
Строительно-гидравлический отдел, лаборатория LGCE,
г. Саида, Алжирская Народная Демократическая Республика

^в Университет Релизана, технологический факультет,
кафедра гражданского строительства,
г. Релизана, Алжирская Народная Демократическая Республика

^г Университет Туши Мустафы Стамбули, факультет науки и технологий,
кафедра строительства,
Лаборатория исследования структуры и механики материалов,
г. Маскара, Алжирская Народная Демократическая Республика

РУБРИКА ГРНТИ: 61.13.21 Химические процессы,
61.01.94 Охрана окружающей среды

ВИД СТАТЬИ: оригинальная научная статья

Резюме:

Введение/цель: Использование композитных фильтров, изготовленных из таких отходов, как гранитная пыль, металлическая стружка и резиновая крошка для очистки фильтрата, образующегося на свалках, является инновационным подходом, который может помочь снизить воздействие свалок на окружающую среду.

Методы: В ходе эксперимента оценивались характеристики однослойных и трехслойных фильтров до и после обработки. В целях оценки эффективности каждой конфигурации фильтра для каждой ячейки был рассчитан коэффициент проницаемости. Расчет коэффициента проницаемости для однослойных и трехслойных фильтров является важным аспектом оценки эффективности процесса очистки сточных вод на свалках. Также для оценки общей эффективности очистки и удаления конкретных загрязнений важно учитывать другие физические и химические параметры: цвет, pH, коэффициент окисления, электропроводность, BOD, COD, SS, NO₄⁻, NO₃⁻, NH₄⁺, PO₄⁻, а также P.

Результаты: Результаты показали снижение как физических, так и химических факторов при формировании каждой ячейки.

Примечательно, что ячейка №5, состоящая из трехслойного фильтра, показала благоприятные результаты по физическим и химическим параметрам, а также по проницаемости. И наоборот, ячейка №2, содержащая гранитную пыль, обладала наилучшими физическими и химическими параметрами, но имела плохие показатели с точки зрения коэффициента пропускания.

Выводы: Результаты исследования свидетельствуют о том, что гранитная пыль, металлическая стружка и резиновая крошка могут использоваться как экономичные фильтрующие слои для очистки фильтра, помогая снизить его негативное воздействие на окружающую среду и грунтовые воды.

Ключевые слова: фильтр, гранитная пыль, металлическая стружка, резиновая крошка, проницаемость, физико-химические свойства.

Побољшавање физичких и хемијских карактеристика оцедних вода депонија путем филтрационог система који садржи отпад од гранита, опилџака гвожђа и рециклиране гуме

Бенамар Бали^а, аутор за преписку, Хамид Селаф^б, Ада Хаџ Мустифа^в, Дрис Џафари^а, Али Мекси^г

^а Универзитет Адрар, Факултет науке и технологије, Одељење за грађевинарство, Адрар, Народна Демократска Република Алжир

^б Универзитет Саида, Технолошки факултет, Грађевинско-хидраулични одсек, ЛГЦЕ лабораторија, Саида, Народна Демократска Република Алжир

^в Универзитет Релизана, Технолошки факултет, Одељење за грађевинарство, Релизана, Народна Демократска Република Алжир

^г Универзитет „Мустафа Стамболи“, Факултет науке и технологије, Одсек за грађевинарство, Лабораторија за испитивање структуре и механике материјала, Маскара, Народна Демократска Република Алжир

ОБЛАСТ: хемијске технологије

КАТЕГОРИЈА (ТИП) ЧЛАНКА: оригинални научни рад

Сажетак:

Увод/циљ: Коришћење композитних филтера израђених од отпада, као што су гранитни прах, опилџци гвожђа и грануле од гуме, који служе за третирање оцедних вода депонија, представља нов приступ који може да помогне у смањивању утицаја депонија на животну средину.

Метод: Експериментом су се процењивале карактеристике једнослојних и трослојних филтера пре и после третирања. За

мерење ефикасности сваке конфигурације филтера понаособ израчунат је коефицијент пермеабилности за сваку ћелију. Израчунавање коефицијента пермеабилности за једнослојне и трослојне филтере важан је аспект приликом одређивања ефикасности процеса третирања оцедних вода депонија. Такође, важно је узети у обзир остале физичке и хемијске параметре попут боје, рН фактора, коефицијента оксидације, проводљивости, BOD, COD, SS, NO₄⁻, NO₃⁻, NH₄⁺, PO₄⁻, као и P како би се одредила ефикасност процеса у целини, као и успешност уклањања специфичних загађивача.

Резултати: Резултати су показали редуковање и физичких и хемијских фактора са формирањем сваке појединачне ћелије. Нарочито је ћелија број 5, са трослојним филтером, показала пожељне резултате у погледу физичких и хемијских параметара, као и пермеабилности. Насупрот томе, ћелија број 2 са гранитним прахом имала је најбоље физичке и хемијске параметре, али се показало да је слаба у погледу фактора пропусности.

Закључак: Наведени резултати наводе на закључак да гранитни прах, опилъци гвожђа и гумени гранулат могу да буду исплативи филтрирајући слојеви при излуживању оцедних вода и да помажу да се смањи њихов утицај на животну средину и подземне воде.

Кључне речи: оцедне воде, гранитни прах, опилъци гвожђа, гумени отпад, пермеабилност, физичко-хемијски параметри.

Paper received on: 08.03.2024.

Manuscript corrections submitted on: 25.09.2024.

Paper accepted for publishing on: 26.09.2024.

© 2024 The Authors. Published by Vojnotehnički glasnik / Military Technical Courier (www.vtg.mod.gov.rs, втг.мо.унр.срб). This article is an open access article distributed under the terms and conditions of the Creative Commons Attribution license (<http://creativecommons.org/licenses/by/3.0/rs/>).



Towards the reliable chemical stability testing of the single base gunpowder using a microcalorimetry method

Milan M. Djokić^a, Zoran J. Bajić^b, Vladimir D. Ignjatović^c

^a Serbian Armed Forces, Central Logistic Base, 1st Logistic Center; University of Defence in Belgrade, Military Academy, Department for Military Chemical Engineering, Belgrade, Republic of Serbia, e-mail: milan.djokic985@gmail.com, ORCID iD: <https://orcid.org/0009-0005-4942-217X>

^b University of Defence in Belgrade, Military Academy, Department for Military Chemical Engineering, Belgrade, Republic of Serbia, e-mail: zoran.bajic@va.mod.gov.rs, **corresponding author**, ORCID iD: <https://orcid.org/0000-0002-8492-3333>

^c University of Defence in Belgrade, Military Academy, Department for Military Chemical Engineering, Belgrade, Republic of Serbia, e-mail: wlaxy@yahoo.com, ORCID iD: <https://orcid.org/0009-0009-5253-3224>

[doi https://doi.org/10.5937/vojtehg72-51113](https://doi.org/10.5937/vojtehg72-51113)

FIELD: chemical technology

ARTICLE TYPE: original scientific paper

Abstract:

Introduction/purpose: Gunpowder is a type of explosive material (EM), a mixture of chemical compounds capable of releasing their potential energy in a very fast exothermic chemical reaction. This paper investigates the single base gunpowder samples.

Methods: Microcalorimetry (MC), or heat flow calorimetry (HFC), is the only modern method that monitors the direct cause of autoignition - the rate of heat release, which is a key factor for gunpowder storage explosive safety. It is based on high-sensitivity calorimeters which allow monitoring of chemical reactions at low speeds. The microcalorimeter "TAM III" was used and the method given by the NATO standard STANAG 4582. A very reliable result was obtained on the chemical stability of the observed single base gunpowder samples, as well as an assessment of its behavior in the next 10 years.

Results: The thermal activity of gunpowder depends on several factors, the most important of which are: chemical composition, size and shape of the gunpowder grain, the degree of decomposition of the gunpowder, storage conditions, etc. Namely, it is a much more exact and consistent indicator of the chemical stability of gunpowder compared to the critical diameter.

ACKNOWLEDGMENT: The author is grateful for the financial support from University of Defence, Belgrade, VA-TT/1/22-24.

Conclusion: The MC method should be used both for monitoring the chemical stability of gunpowder during storage and for the prediction of the service life of gunpowder.

Key words: single base gunpowder, microcalorimetry, heat flow calorimetry, TAM III, STANAG 4582.

Introduction

Gunpowder is a type of explosive material (EM), a mixture of chemical compounds capable of releasing their potential energy in a very fast exothermic chemical reaction. The process of combustion (deflagration) is the basic form of explosive conversion of gunpowder (Jeremić, 2007), used to launch the projectile in the barrel of the weapon or for propulsion. At the same time, the heat required for the chemical decomposition process is transferred through EM exclusively by thermal conduction, and the burning speed is relatively low and ranges from several millimeters to several tens of centimeters per second. At these rates of explosive conversion, the released gaseous products can be used to eject projectiles from the barrel of weapons or to propel rocket projectiles, which is why gunpowders are often called propellants.

Gunpowder is divided in several ways, and the most common is the division according to the physical state of its components. In this sense, gunpowder is divided into two basic groups (Jeremić, 2007):

1. Homogeneous gunpowder created by gelatinization of nitrocellulose molecules under the influence of an organic solvent or gelatinization agent. With these powders, all components are found in the nitrocellulose molecule; together with it, they form a unit that cannot be separated mechanically.

2. Composite gunpowder is created by mixing crystals of mineral compounds rich in oxygen and a binder, which is always of organic origin, and at the same time is a carrier of combustible materials. This is a pure physical mixture and all components can be easily separated.

Homogeneous powders are further divided, according to the number of energy components in their composition, into (Jeremić, 2007):

- Single base gunpowders, which contain one energy component, nitrocellulose (NC),
- Double base gunpowders, which contain two energy components: NC and glycerin trinitrate (NG), i.e. (sometimes but less often) diethylene glycol dinitrate (DEGDN), and

- Triple base gunpowders, which contain three energy components: NC, NG, and nitroguanidine (NQ).

Composite powders include composite rocket propellants and black powder.

The basic components of homogeneous gunpowder are nitric acid esters: NC, NG (DEGDN), and NQ (Bajić, 2015). These are unstable chemical compounds which are subject to slight thermal decomposition even at ordinary temperatures. Among the products of gunpowder decomposition are nitrogen oxides which cause further autocatalytic exothermic decomposition of nitrogen esters (primarily NC), and thus change the physical-chemical and ballistic properties of gunpowder. Thermal decomposition of nitrogen esters can cause accumulation of heat and an increase in temperature in the mass of gunpowder, as a result of which self-ignition of gunpowder can occur. Historically, self-ignition of gunpowder came immediately after the conquest of the technology of low-smoke gunpowder production. Several accidents happened on warships (de Klerk, 2015).

To slow down the decomposition of nitrogen esters (primarily NC), stabilizers are added to powders. The stabilizers are substances that react very quickly with released nitrogen oxides and the acids that arise from them and absorb free radicals well, thereby preventing their further autocatalytic action. Most widely used stabilizers today are aromatic amines, and diphenylamine (DPA) is most commonly used to stabilize single base gunpowder (Stine, 1991; Grbović & Stojiljković, 2005; Jeremić & Grbović, 2006; Rusly et al, 2024). The decomposition of homogeneous gunpowder is accompanied by a series of phenomena, such as the release of gases, loss of mass, reduction of the average molecular weight of NC, consumption of stabilizers, generation of heat, etc. Regarding this, numerous methods have been developed to monitor the aforementioned changes, determine the current chemical stability, and predict the service life of gunpowder. One of the modern methods is microcalorimetry. This is the only method that measures the direct cause of self-ignition of gunpowder, i.e., the rate of heat release. It is based on calorimeters with high sensitivity, which enables the monitoring of chemical reactions at very low speeds (Grbović & Stojiljković, 2005; Jeremić & Grbović, 2006; Jelisavac et al, 2014).

Microcalorimetry method

Microcalorimetry (MS), or heat flow calorimetry (HFC), is the only modern method that monitors the direct cause of autoignition - the rate of heat release, which is a key factor for gunpowder explosive safety. It is based on high-sensitivity calorimeters, which allow monitoring of chemical reactions at low speeds.

With this method, according to the National Defense Standard (SORS 8069/91), the chemical stability of gunpowder is determined by measuring the rate of heat development in the center of the sample, which is isothermally heated at a constant temperature (SORS, 1991). The measured value of the rate of heat development (thermal activity due to the decomposition of gunpowder) is further used to calculate the critical diameter as a function of temperature. By comparing these values with the diameter of the ammunition case in which the gunpowder is stored, the state of chemical stability is evaluated, that is, the possibility of self-ignition of the gunpowder under certain storage conditions (SORS, 1991). Based on the values and the set criteria, the tested propellants are categorized (Jelisavac et al, 2014). The decision on further action about the propellant storage procedure will be made later. The standard prescribes the microcalorimetry method for determining thermal activity, which is based on the theory of thermal explosion and monitors the amount of released heat as the immediate cause of spontaneous combustion (Jelisavac et al, 2014).

According to STANAG 4582, the rate of heat development is measured at a constant temperature between 60 °C and 90 °C during the calculated time for the selected temperature (STANAG, 2004). This time is considered equivalent to isothermal storage for 10 years at 25 °C. The heat equivalent of all physical and chemical processes that take place in the system with heat exchange is measured, that is, the total heat flow is measured. The maximum permissible heat flow limit, which is also dictated by the experimental temperature represented, is used as a criterion for sufficient chemical stability (STANAG, 2004). The release of heat is of vital importance especially when large quantities of gunpowder are stored, as the heat generation from a given volume of stored gunpowder can become greater than the heat removal when self-heating begins, which can eventually cause self-ignition. This can happen even when the stabilizer is sufficiently present in the gunpowder.

Microcalorimetric measurements are performed with high-sensitivity devices, which can monitor very slow chemical reactions with low thermal activity (1 μ W/g). The microcalorimetry method is based on the thermal

theory of self-ignition of gunpowder. During the years of application, some shortcomings of this method have been identified (Jeremić & Grbović, 2006, Chelouche et al, 2020). NATO's concept of measuring the thermal activity of propellant is based on the use of far more sophisticated microcalorimetric equipment with high sensitivity for heat flow measurement (Jelisavac et al, 2014).

Experimental part

Materials

Microcalorimetric measurements were performed on several samples of naturally aged single base gunpowder taken mainly from the stored collections. A few samples were taken from the ammunition. The basic compositions of the tested gunpowder are given in Table 1, and their dimensions and shapes in Table 2.

Table 1 – Composition of the tested single base gunpowder samples

Type of gunpowder	Chemical composition %					
	NC	N content	K ₂ SO ₄	DPA	Cl	Moisture
1	2	3	4	5	6	7
NC-27	96.80±0.90	≤ 13.10		1.50±0.30		1.35±0.25
NC-29	≤ 94.30	13.05±0.10		1.20±0.30	4.00±0.80	1.25±0.25
NC-37	96.70±0.90	≤ 1.10		1.50±0.20		1.35±0.25
NC-39	93.8-96.0	≤ 13.00		1.00-2.00		1.00-1.60
NC-40		≥ 12.95		≥ 1.20		1.30
NC-44	96.70±0.70	13.20±0.05		1.45±0.15		1.30±0.20
NC-45	85.35-90.40	13.20±0.05	1.0-1.3	0.70-1.30	1.30-1.50	0.80-1.20
NC-123	96.75±0.85	≤ 13.00		1.50±0.20		1.35±0.25
NC-151	48.80±2.00	≤ 13.15	47.0±1.0	1.00±0.20		0.80±0.20
NC-281	86.65±2.55	10.00±1.50		1.55±0.25		1.25±0.25

Table 2 – Dimensions and shapes of the tested single base gunpowder samples

Type of gunpowder	Outer diameter, D (mm)	Channel diameter, d (mm)	Wall thickness, Wa (mm)	Length, L (mm)	The shape of a powder grain
1	2	3	4	5	6
NC-27	1.20±0.15	0.30±0.05	0.45±0.05	6.50±1.00	Single channel cylinder
NC-29	1.95±0.10	0.33±0.05	0.81±0.05	3.35±0.15	
NC-37	5.60±0.35	0.50±0.10	1.02±0.07	12.05±0.55	

Type of gunpowder	Outer diameter, D (mm)	Channel diameter, d (mm)	Wall thickness, Wa (mm)	Length, L (mm)	The shape of a powder grain
1	2	3	4	5	6
NC-39	3.25-3.35	0.18-0.26	0.60-0.70	5.00-6.00	
NC-40	~3.20	0.20±0.05	0.60-0.75	~6.30	
NC-44	6.00-6.90	0.50-0.70	1.12-1.22	13.50-15.50	
NC-45	1.91-2.10	0.15-0.25	0.85-0.95	3.90-4.10	Like NC-27
NC-123	4.80±0.20	2.50±0.20	1.18±0.08	705.0±0.15	Tube
NC-151	2.10±0.25	0.55±0.10	0.775±0.125	6.50±1.00	Single channel cylinder
NC-281	0.86±0.06	0.20±0.03	0.33±0.03	1.80±0.20	Single channel cylinder

Microcalorimetric measurements were performed on 10 types of single base gunpowder of different chemical compositions and different dimensions and shapes, as well as for different storage conditions.

Method

The samples are crushed as needed and each individual or group is subjected to thermal treatment, during which the data on the thermal activity of the treatment is collected for each of the samples, both to calculate the critical diameter of self-ignition according to the National Defense Standard (SORS, 1991), and to monitor the thermal activity during isothermal testing according to STANAG 4582. Microcalorimetric measurements were performed using the "TAM III" microcalorimeter. (Figure 1).



Figure 1 – Heat flow microcalorimeter TAM III

After grinding and sieving, the gunpowder samples were placed in hermetically sealed vials for sample testing. The sample volume was about 2 cm³. The vials with the samples were set into the device after its calibration. The measurement was carried out at 90 °C and the duration of the test was 3.43 days (82.5 hours) when the released heat from the sample becomes greater than 5 J/g. According to STANAG 4582, the value of the measured heat flow should be lower than the criterion prescribed for the limits of heat flow, 350.0 μW/g at 90 °C (STANAG, 2004; Jelisavac et al, 2014).

Results and the discussion

For the analysis of the previous results according to the MC method, the results of the chemical stability tests of single base gunpowder, which were obtained in the TRZ Kragujevac laboratory, were taken. Thus, all available results for single base gunpowder were analyzed (Table 3), which made it possible to observe the behavior of gunpowder with different compositions and geometric shapes and storage time.

Table 3 – The results of the chemical stability tests for the investigated gunpowder samples

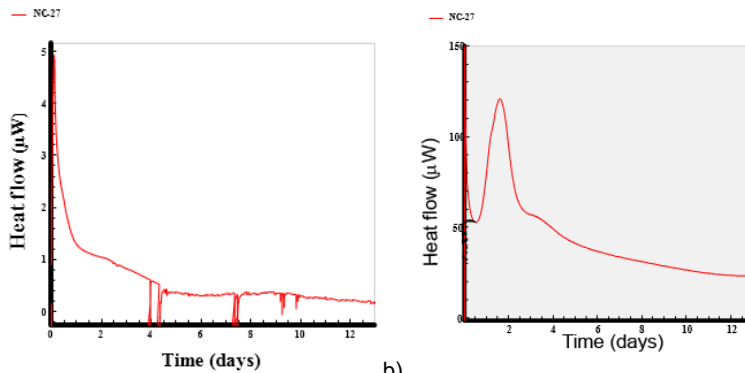
Gunpowder		t _E (y)	Stabilizer content, mas %			100 °C	D _{cr} (m)	P _{max} (μW/g)	Sample source
Type	Lot		DPA _o	DPA	DPA _{ef}				
1	2	3	4	5	6	7	8	9	10
NC-27	МБЛ 8766	15	1.62	1.2	1.46	7.00	0.48		PC-2
		18		1.13	1.47	5.00			
NC-27	МБЛ 8766	19	1.62	0.87	1.33	6.75	q(333)<0		PC-2
		20		0.24	1.11	3.75			
		22		0.06	0.66	0			
	МБЛ 0196	8	1.26	1.32	1.44	5.00	0.50	41.4	PC-1
NC-37	МБЛ 8451	17	1.50	0.22	0.86	3.75	0.71		PC-2
		18		0.16	0.92	3.50			
		19		0.18	0.76	3.75	0.53		
		20		0.11	0.86	3.50	q(333)<0		
		21		0.06	0.66	3.50	0.5		
		22		0.1	0.65	4.25			
		25		0.17	0.81	3.75	0.57		
	МБЛ 8454	17	1.66	0.24	0.77	3.75	0.55		PC-2
		18		0.12	0.86	3.75			
		19		0.18	0.80	3.75	0.52		
20		0.15		0.81	4.75	0.56			
		21		0.10	0.67	3.50			

Gunpowder		t _E (y)	Stabilizer content, mas %			100 °C	D _{cr} (m)	P _{max} (μW/g)	Sample source
Type	Lot		DPA _o	DPA	DPA _{ef}				
1	2	3	4	5	6	7	8	9	10
NC-37	МБЛ 8454	22	1.66	0.07	0.72	5.25			PC-2
		25		0.14	0.80	3.75	0.77	76.3	
	МБЛ 8464	17	1.70	0.18	1.02	4.75	q(333)<0		PC-2
		18		0.07	0.96	3.75			
		19		0.11	0.9	3.75	0.5		
		20		0.08	0.98	4.00	q(333)<0		
		21		0.03	0.74	3.75			
		22		0.04	0.77	5.25			
	МБЛ 8578	15	1.51	0.25	0.95	4.00			PC-2
		16		0.23	0.94	4.50			
		17		0.18	1.09	3.75			
		18		0.2	0.92	3.75	q(333)<0		
		19		0.16	0.69	4.00	0.53		
		20		0.13	0.74	3.75	0.5		
	МБЛ 87120	21	1.64	0.1	0.74	5.12			PC-2
		24		0.17	0.82	3.75	0.61	85.6	
15		0.44		1.3	5.00	0.5			
18		0		0.75	3.75				
МБЛ 94168	19	1.48	0	0.67	4.75			PC-2	
	22		0.03	0.48	4.50	0.62	20.3		
	МБЛ 94168		15	0.09	0.63	5.25	0.51		67.9
NC-123	МБЛ 8104	20	1.6	0.17	0.97	4.25			PC-2
		21		0.01	0.76	3.25			
		22		0.08	0.8	3.75	0.53		
		23		0	0.88	3.50	0.65		
NC-123	МБЛ 8104	24	1.6	0	0.69	3.75	0.53		PC-2
		25		0.01	0.69	5.00			
		26		0.36	0.92	4.00	0.53		
		28		0.08	0.70	4.75	0.48	79.3	
	МБЛ 8408	17	1.67	0.25	0.86	3.75	0.5		PC-2
		18		0.1	0.82	3.75			
		19		0.2	0.82	3.75	0.59		
		20		0.15	0.75	4.75	0.69		
		21		0.09	0.87	3.75	0.68		
		22		0.11	0.76	4.75			
NC-29	МБЛ 8830	23	1.25	0.20	0.79	3.75	0.68		PC-1
		25		0.22	0.79	3.75	0.55	58.9	
NC-151	МБЛ 9803	7	1.20	0.8	0.8	8.00			PC-1

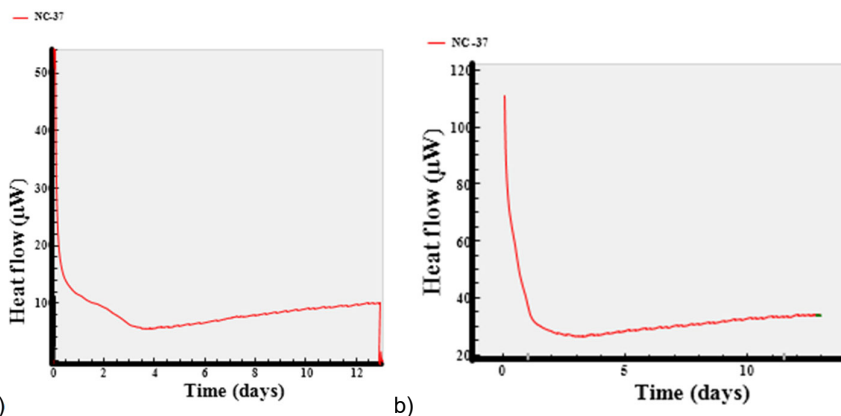
Gunpowder		t _E (y)	Stabilizer content, mas %			100 °C	D _{cr} (m)	P _{max} (μW/g)	Sample source
Type	Lot		DPA ₀	DPA	DPA _{eff}				
1	2	3	4	5	6	7	8	9	10
NC-151	МБЛ 9803	11	1.20	0.82	1.08	5.00	0.47	101.4	PC-1
NC-281	МБЛ 9715	8	1.50	1.25	1.25	8.00			PC-1
		9		1.27	1.4	7.75			
		10		1.08	1.3	8.75			
		12		1.18	1.43	7.00	7.2		
	МБЛ 0623	3	1.37	1.29	1.44	7.00	0.55	24.3	Ammo
NC-40	МБЛ 8921	15	1.41	0.94	1.17	7.75			PC-1
		17		0.58	1.06	5.75			
		18		0.18	1.05	5.75			
		20		0.26	0.77	6.00	0.46	61.3	
NC-44	МБЛ 8801	16	1.42	1.05	1.2	8.00			PC-1
		21		1.06	1.22	8.00	0.65	18.9	
NC-45	МБЛ 8801	16	0.88	2.23	2.37	10.00			PC-1
		21		0.77	0.95	8.00	0.59	15.4	
	МБЛ 9312	16	0.81	2.34	2.47	9.25	q(333)<0		Ammo
				0.83	0.98	8.00	0.48	28.1	
NC-39	МБЛ 7401	29	1.38	0.29	0.97	7.00	0.48		PC-2
		30		0.27	0.85	7.00	0.4		
		31		0.23	0.74	6.00			
		32		0.18	0.87	7.00	0.52		
		35		0.24	0.89	7.00	0.51	84.20	

In Table 3, t_E is the gunpowder service time in years, DPA₀, DPA and DPA_{eff} represent initial, measured and effective content of the stabilizer respectively, 100 °C stands for the results of 100 °C heating method, D_{cr} is the critical diameter, and P_{max} is the maximum heat flow. The sample source stands for the source of gunpowder samples, propellant collection one or two (PC-1 or PC-2) and the samples taken from the ammunition (Ammo).

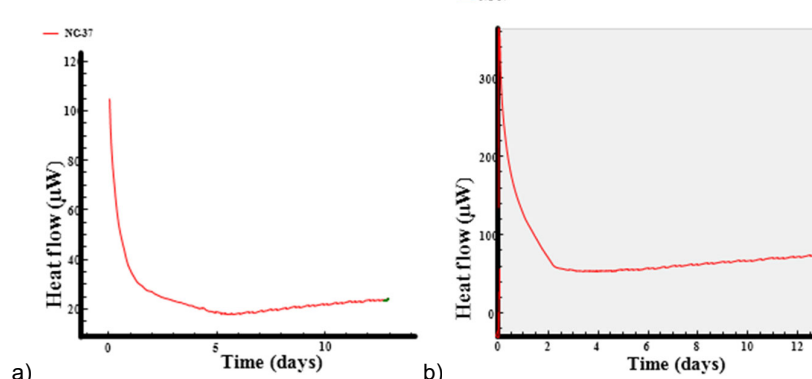
Using the "TAM III" microcalorimeter, thermal activity was measured on a total of 16 lots of 10 different types of single base gunpowder (Figures 2-10). Based on the obtained results, the maximum heat flow was determined according to STANAG 4582. In addition, for each lot of gunpowder that was tested according to the MC method, the results were compared with the results of the chemical stability data obtained according to the HPLC and 100 °C methods, as well as the analysis of all previous results of testing the chemical stability of those powders. This made it possible to comprehensively analyze the results obtained by the MC method.



a) b)
 Figure 2 – Heat flow diagrams for NC-27 a) sample 1 and b) sample 2 gunpowder



a) b)
 Figure 3 – Heat flow diagrams for NC-37 a) sample 1 and b) sample 2 gunpowder



a) b)
 Figure 4 – Heat flow diagrams for NC-37 a) sample 3 and b) sample 4 gunpowder

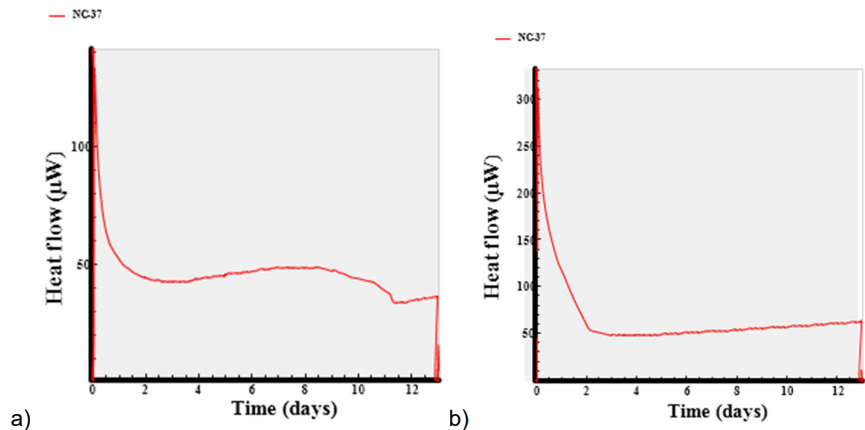


Figure 5 – Heat flow diagrams for NC-37 a) sample 5 and b) sample 6 gunpowder

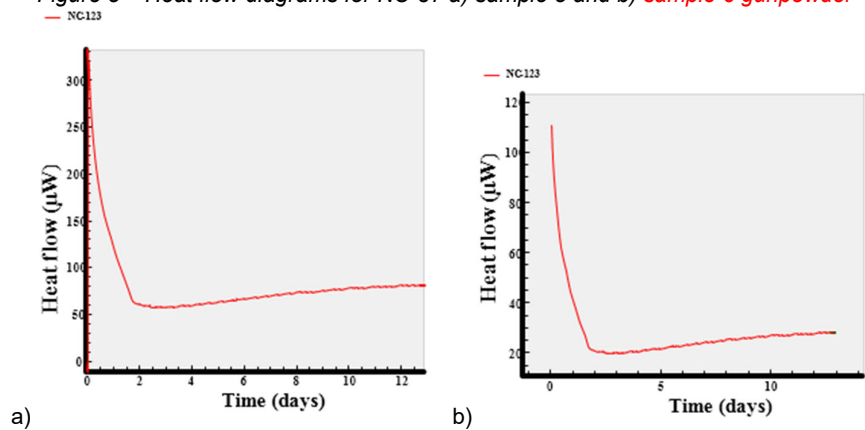


Figure 6 – Heat flow diagrams for NC-123 a) sample 1 and b) sample 2 gunpowder

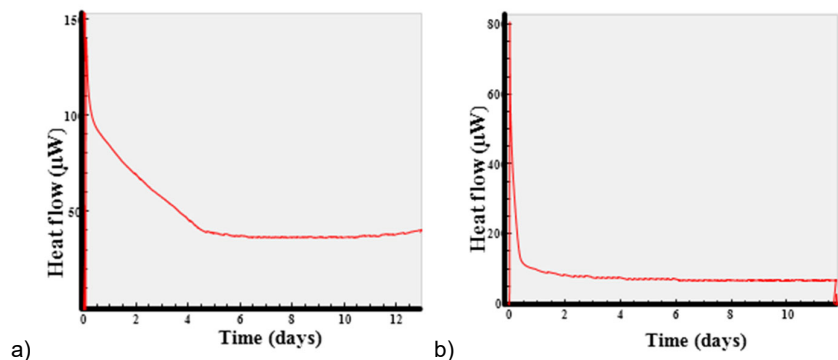


Figure 7 – Heat flow diagrams for a) NC-29 and b) NC-151 gunpowder

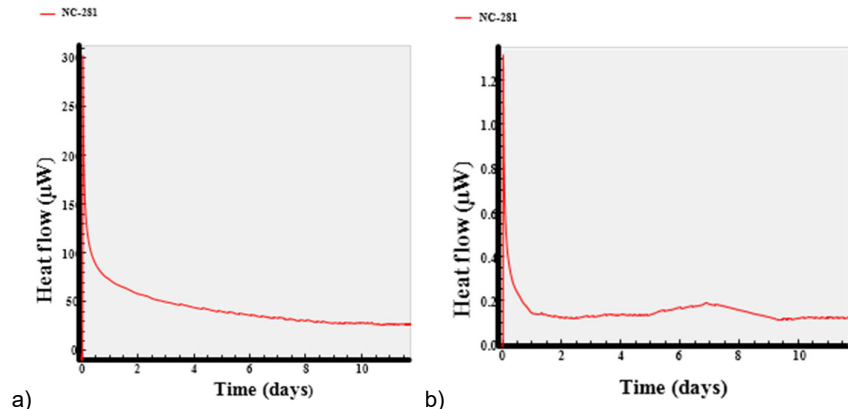


Figure 8 – Heat flow diagrams for NC-281 a) sample 1 and b) sample 2 gunpowder

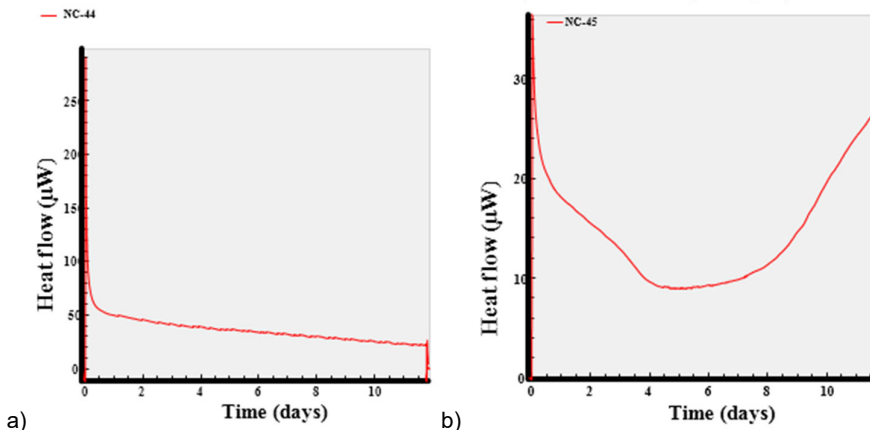


Figure 9 – Heat flow diagrams for a) NC-44 and b) NC-45 gunpowder

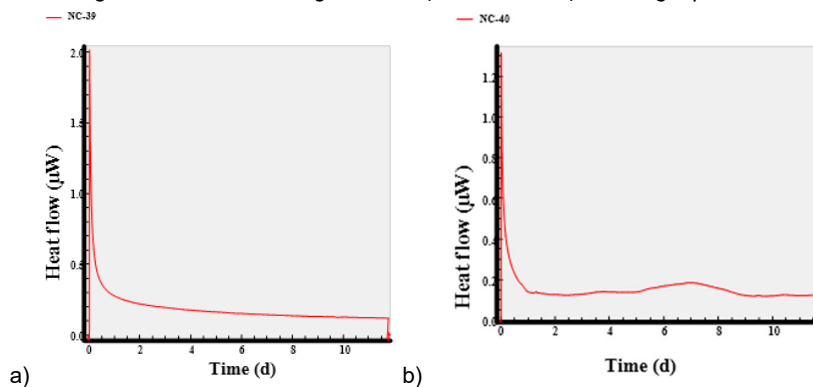


Figure 10 – Heat flow diagrams for a) NC-39 and b) NC-40 gunpowder

Microcalorimetric measurements were performed on single base gunpowders because they are the most common in Serbian Armed Forces ammunition. An analysis of the previous results of determining the critical diameter according to SORS 8069/91 was performed. These results do not correlate with the results of the HPLC method and the 100 °C heating method. It happens that with a decrease in the stabilizer content (that is, an increase in the number of days at 100 °C), the critical diameter remains unchanged or increases. In addition, the dependence of the critical diameter on other factors that significantly affect the chemical stability of gunpowder, such as the chemical composition and the dimensions and shape of the gunpowder grain, cannot be observed. It was agreed that this method is imprecise, which can be explained by several reasons (inaccuracy of the device, the short heating time of the sample about the measurement temperature, the critical diameter is recalculated with the introduction of a series of approximations, etc.) and that it would be very justified to apply the MC method prescribed by NATO standard STANAG 4582. In practice so far, not a single gunpowder has been assessed as unstable based on this criterion, while based on the results of the HPLC method and the 100 °C heating method, many lots of gunpowders have been assessed as unstable and destroyed. For example: powder NC-27, sample 1, is stable according to the MC method prescribed by standard SORS 8069/91, while according to the HPLC method as well as according to the 100 °C heating method, this powder is unstable. Given that SORS 8069/91 stipulates that the thermal activity monitoring test is in the second place of evaluation (behind the stabilizer content monitoring method), this gunpowder was assessed as unstable. At the same time, this gunpowder does not satisfy the given criterion according to the MC method prescribed by NATO standard STANAG 4582. This example confirms the shortcomings of the first method and the precision of the second MC method.

Based on the MC measurements performed using the "TAM III" device, it was concluded that the thermal activity of gunpowder depends on several factors, the most important of which are: chemical composition, size and shape of the gunpowder grain, the degree of decomposition of the gunpowder, storage conditions, etc. (the gunpowder charge was not analyzed because gunpowder samples and gunpowder collections were taken). At the same time, the maximum heat flow - Pmax (criterion according to STANAG 4582 standard) is a much more exact and consistent indicator of the chemical stability of gunpowder compared to the critical diameter - Dc (criterion according to SORS 8069/91 standard). Namely, even measurements using a modern "TAM III" microcalorimeter

cannot provide a reliable assessment of the critical diameter. The reason for this lies in a whole series of assumptions that are introduced in the assessment of the possibility of exchanging the generated heat with the environment, the conditions for heat accumulation, and the theory of self-ignition, i.e., under which critical conditions the possibility of self-ignition occurs. In this sense, the measurement of thermal activity about the determination of the critical diameter of self-ignition is a far more reliable method because it is based on the measurement and evaluation of the exact parameter of decomposition - heat flow, while when determining the critical diameter of self-ignition, the values of individual parameters are theoretically obtained and insufficiently confirmed.

The maximum heat flow depends a lot on the chemical composition of the gunpowder. The extremely good chemical stability of NC-29 and NC-45 gunpowder is the result of a favorable composition. Namely, in addition to DPA (stabilizer), these powders also contain CI (Centralite I) as a plasticizer or ballistic modifier. During long-term heating at an elevated temperature, as the DPA concentration decreases, CI is also included in the reaction with nitrogen oxides, even though it was not added to the gunpowder composition as a stabilizer. At the same time, the high thermal activity of NC-151 gunpowder can be explained by its unfavorable chemical composition. Namely, this gunpowder contains about 47% of K₂SO₄, a hygroscopic compound that releases moisture during microcalorimetric measurement, which leads to the formation of nitrous and nitric acid in the gunpowder, which autocatalytically accelerates NC decomposition and increases heat generation.

The maximum heat flow depends on the dimensions and shapes of the powder grain. Among the examined powders, from this point of view, the most characteristic is the NC-281 powder. Namely, due to its small dimensions and a favorable shape, this gunpowder exchanges the generated heat very quickly, which results in a small heat flow.

The maximum heat flow depends very much on the quality of the basic raw materials used for the production of gunpowder. The powders that were produced during the period of sanctions (e.g. NC-37 sample 6, and NC-45 sample) show a higher thermal activity compared to other younger lots of these types of powders. The fact is that many lots of NC-27 and NC-37 powders, which were produced during the 1990s, showed significantly lower chemical stability according to the HPLC method and the 100 °C heating method compared to older lots of these types of powders. This can be explained by the lower quality of the basic raw materials.

The thermal activity of gunpowder also depends on the degree of NC decomposition. However, from this aspect, the results of different lots of

the same type of gunpowder can be compared. It is observed that older lots of gunpowder with a higher degree of decomposition generate more heat than the lots with a lower degree of decomposition. This is confirmed by the results of two lots of three types of gunpowder (NC-27, NC-37, and NC-123). At the same time, this does not mean that samples of different types of gunpowder, which according to the HPLC method have approximately the same stability, will also have similar results according to the MC method. On the contrary, the results often vary widely.

Conclusion

By analyzing the results of the determination of the critical diameter of self-ignition of gunpowder according to SORS 8069/91 standard, it was concluded that they do not correlate with the results of the HPLC method and the 100 °C method. In addition, the dependence of the critical diameter on other factors that significantly influence the chemical stability of gunpowder, such as the chemical composition and the dimensions and shapes of the gunpowder grain, cannot be observed. It has been concluded that this method is imprecise, which can be explained by several reasons (inaccuracy of the device, the short heating time of the sample about the measurement temperature, the critical diameter is recalculated with the introduction of a series of approximations, etc.).

Measurements using a microcalorimeter "TAM III" and the method given by NATO standard STANAG 4582, gave reliable results on the current chemical stability of gunpowder, as well as an assessment of its behavior in the next 10 years. At the same time, the results of this MC method are in good correlation with the results of the HPLC and 100 °C methods. In addition, by applying this method, the dependence of the thermal activity of gunpowder on the factors that most significantly affect the chemical stability of gunpowder, such as chemical composition, size and shape of gunpowder grains, degree of decomposition of gunpowder, quality of basic raw materials, storage conditions, etc., can be observed.

The proposal is to apply the MC method given by NATO standard STANAG 4582 both for monitoring the chemical stability of gunpowder during storage and predicting the service life of gunpowder, as well as for the quality control of newly produced gunpowder.

References

- Bajić, Z. 2015. *Inicijalni i brizantni eksplozivi*. Belgrade: AGM knjiga. ISBN: 9788686363534.
- Chelouche, S., Trache, D., Benayachi, Z.I., Tarchoun, A.F., Khimeche, K. & Mezroua, A. 2020. A New Procedure for Stability Control of Homogeneous Solid Propellants by Combination of Vacuum Stability Test, FTIR and PCA. *Propellants, Explosives, Pyrotechnics*, 45(7), pp.1088-1102. Available at: <https://doi.org/10.1002/prop.201900424>.
- de Klerk, W.P.C. 2015. Assessment of Stability of Propellants and Safe Lifetimes. *Propellants, Explosives, Pyrotechnics*, 40(3), pp.388-393. Available at: <https://doi.org/10.1002/prop.201500040>.
- Grbović, L. & Stoiljković, S. 2005. Correlation of chemical stability estimation results of naturally and accelerated aging gun powders. *Vojnotehnički glasnik/Military Technical Courier*, 53(5), pp.442-450 (in Serbian). Available at: <https://doi.org/10.5937/vojtehg0505442G>.
- Jelisavac, Lj., Stoiljković, S., Gačić, S., Brzić S. & Bobić, N. 2014. Comparative Examination of the Chemical Stability of Powders and Double – Base Rocket Propellants by Measuring Heat Activities and Stabilizer Content. *Scientific Technical Review*, 64(1), pp.48-54 [online]. Available at: <https://scindeks.ceon.rs/article.aspx?artid=1820-02061401048J> [Accessed: 20 May 2024].
- Jeremić, R. 2007. *Eksplorzije i eksplozivi*. Belgrade: Vojnoizdavački zavod (in Serbian). ISBN: 86-335-0207-0
- Jeremić, R. & Grbović, L. 2006. The analysis of methodology for investigation of chemical stability of propellants. *Vojnotehnički glasnik/Military Technical Courier*, 54(4), pp.405-414 (in Serbian). Available at: <https://doi.org/10.5937/vojtehg0604405J>.
- Rusly, S.N.A., Jamal, S.H., Samsuri, A., Noor, S.A.M. & Rahim, K.S.A. 2024. Stabilizer selection and formulation strategies for enhanced stability of single base nitrocellulose propellants: A review. *Energetic Materials Frontiers*, 5(1), pp.52-69. Available at: <https://doi.org/10.1016/j.enmf.2024.02.007>.
- SORS. 1991. *SORS 8069/91: Praćenje hemijske stabilnosti baruta i raketnih goriva*. Belgrade: Standard odbrane Republike Srbije (in Serbian).
- STANAG. 2004. *STANAG 4582 – Explosives, Nitrocellulose Based Propellants, Stability Test Procedures and Requirements using Heat Flow Calorimetry*. Brussels: STANAG.
- Stine, G.Y. 1991. An investigation into propellant stability. *Analytical Chemistry*, 63(8), pp.475A-478A. Available at: <https://doi.org/10.1021/ac00008a742>.

Hacia la prueba fiable de estabilidad química de la pólvora de base única mediante un método de microcalorimetría

Milan M. Djokić^{ab}, Zoran J. Bajić^b, **autor de correspondencia**,
Vladimir D. Ignjatović^b

^a Fuerzas Armadas de Serbia, Base Logística Central, 1er Centro Logístico, Belgrado, República de Serbia

^b Universidad de Defensa de Belgrado, Academia Militar, Departamento de Ingeniería Química Militar, Belgrado, República de Serbia

CAMPO: tecnología química

TIPO DE ARTÍCULO: artículo científico original

Resumen:

Introducción/propósito: La pólvora es un tipo de material explosivo (EM), una mezcla de compuestos químicos capaces de liberar su energía potencial en una reacción química exotérmica muy rápida. Este artículo investiga las muestras de pólvora de base única.

Métodos: La microcalorimetría (MC), o calorimetría de flujo de calor (HFC), es el único método moderno que controla la causa directa de la autoignición- la tasa de liberación de calor, que es un factor clave para la seguridad de los explosivos en el almacenamiento de pólvora. Se basa en calorímetros de alta sensibilidad que permiten monitorear reacciones químicas a bajas velocidades. Se utilizó el microcalorímetro "TAM III" y el método dado por la norma OTAN STANAG 4582. Se obtuvo un resultado muy confiable sobre la estabilidad química de las muestras de pólvora mono-base observadas, así como una evaluación de su comportamiento en los próximos 10 años.

Resultados: La actividad térmica de la pólvora depende de varios factores, los más importantes son: composición química, tamaño y forma del grano de pólvora, grado de descomposición de la pólvora, condiciones de almacenamiento, etc. Es decir, es un indicador mucho más exacto y consistente de la estabilidad química de la pólvora en comparación con el diámetro crítico.

Conclusión: El método MC debe usarse tanto para monitorear la estabilidad química de la pólvora durante el almacenamiento como para predecir la vida útil de la pólvora.

Palabras claves: pólvora de base única, microcalorimetría, calorimetría de flujo de calor, TAM III, STANAG 4582.

Подход к надежному способу определения химической стойкости одноосновных порохов методом микрокалориметрии

Милан М. Джокич^а^б, Зоран Й. Баич^б, **корреспондент**,
Владимир Д. Игњатович^б

^а Вооружённые Силы Республики Сербия, Центральная логистическая база, 1-й центр логистики, г. Белград, Республика Сербия

^б Университет обороны в г. Белград, Военная академия, департамент военного химического инжиниринга, г. Белград, Республика Сербия

РУБРИКА ГРНТИ: 61.43.00 Технология взрывчатых веществ и средств химической защиты

ВИД СТАТЬИ: оригинальная научная статья

Резюме:

Введение/цель: Порох – это разновидность взрывчатого вещества, представляющая собой смесь химических соединений, способных высвободить свою потенциальную энергию в результате быстрой экзотермической химической реакции. В данной статье рассматриваются образцы одноосновного пороха.

Методы: Микрокалориметрия или калориметрия теплового потока является единственным современным методом, который следит за главной причиной самовоспламенения – скоростью тепловыделения. Скорость тепловыделения является ключевым фактором взрывобезопасности при хранении пороха. Метод основан на высокочувствительных калориметрах, которые позволяют отслеживать химические реакции на низких скоростях. В данном исследовании использовался микрокалориметр "TAM III", метод которого соответствует стандарту НАТО STANAG 4582. В ходе исследования получен надежный результат по химической стойкости испытуемых образцов одноосновного пороха, а также оценка его поведения в течение следующих 10 лет.

Результаты: Термическая активность пороха зависит от нескольких факторов, наиболее важными из которых являются: химический состав, размер и форма порохового зерна, степень разложения пороха, условия хранения и т.д. А это гораздо более точные и последовательные показатели химической стойкости, чем критический диаметр.

Выводы: Метод микрокалориметрии следует использовать как для контроля химической стойкости пороха при хранении, так и для прогнозирования срока хранения пороха.

Ключевые слова: одноосновный порох, микрокалориметрия, калориметрия теплового потока, TAM III, STANAG 4582.

Приступ поузданом начину одређивања хемијске стабилности једнобазних барута применом методе микрокалориметрије

Милан М. Ђокић^а, Зоран Ј. Бајић^б, аутор за преписку,
Владимир Д. Игњатовић^б

^а Војска Србије, Централна логистичка база, Први логистички центар,
Београд, Република Србија

^б Универзитет одбране у Београду, Војна академија, Катедра
војнохемијског инжењерства, Београд, Република Србија

ОБЛАСТ: хемијске технологије

КАТЕГОРИЈА (ТИП) ЧЛАНКА: оригинални научни рад

Сажетак:

Увод/циљ: Барути представљају експлозивне материје, смешу хемијских једињења способних да своју потенцијалну енергију ослободе након врло брзих егзотермних хемијских реакција. У овом раду испитују се узорци једнобазних барута.

Методе: Микрокалориметрија, или калориметрија топлотног флукса, једина је савремена метода која прати директан узрок самозапаљења – брзину ослобађања топлоте, која представља кључни фактор пиротехничке безбедности током складиштења. Заснива се на високоосетљивим калориметрима који омогућавају праћење хемијских реакција при малим брзинама. У раду је коришћен микрокалориметар „ТАМ III“ и метода која је наведена у стандарду „STANAG 4582“. Веома поуздани резултати добијени су за хемијску стабилност испитиваних узорака једнобазних барута, као и оцена њиховог понашања у наредних 10 година.

Резултати: Топлотна активност барута зависи од неколико фактора, од којих су најважнији: хемијски састав, димензије и облик барутног зрна, степен деградације барута, услови складиштења и др. Она представља егзактнији и конзистентнији индикатор хемијске стабилности него што је то критични пречник.

Закључак: Метод микрокалориметрије треба користити како при праћењу хемијске стабилности барута тако и при предвиђању животног века употребе барута.

Кључне речи: једнобазни барут, микрокалориметрија, калориметрија топлотног флукса, ТАМ III, STANAG 4582.

Paper received on: 23.05.2024.

Manuscript corrections submitted on: 25.09.2024.

Paper accepted for publishing on: 26.09.2024.

© 2024 The Authors. Published by Vojnotehnički glasnik / Military Technical Courier (www.vtg.mod.gov.rs, vtg.mo.ynp.cb). This article is an open access article distributed under the terms and conditions of the Creative Commons Attribution license (<http://creativecommons.org/licenses/by/3.0/rs/>).



Dynamic analysis of a vaulted dam

Abdelkrim Benahmed^a, Otbi Bouguenina^b, Ali Meksi^c,
Khaled Benmahdi^d, Khaled Bendahane^e, Mohamed Sadoun^f

^a University Center Nour Bachir, Department of Science and Technology, El Bayadh, People's Democratic Republic of Algeria, e-mail: a.benahmed@cu-elbayadh.dz, **corresponding author**, ORCID iD: <https://orcid.org/0009-0009-4822-2810>


^b University Center Nour Bachir, Department of Science and Technology; Advanced Materials and Instrumentation Laboratory, El Bayadh, People's Democratic Republic of Algeria, e-mail: o.bouguenina@cu-elbayadh.dz, ORCID iD: <https://orcid.org/0000-0002-5611-140X>

^c Mustapha Stambouli University, Department of Civil Engineering, Laboratory for the Study of Structures and Mechanics of Materials, Mascara, People's Democratic Republic of Algeria, e-mail: ing.meksi2009@yahoo.fr, ORCID iD: <https://orcid.org/0009-0009-0320-3704>

^d Mustapha Stambouli University, Department of Civil Engineering, Laboratory for the Study of Structures and Mechanics of Materials, Mascara, People's Democratic Republic of Algeria, e-mail: k.benmahdi@univ-mascara.dz, ORCID iD: <https://orcid.org/0000-0002-8244-5817>

^e University Center Nour Bachir, Department of Science and Technology; Advanced Materials and Instrumentation Laboratory, El Bayadh, People's Democratic Republic of Algeria, e-mail: k.bendahane@cu-elbayadh.dz, ORCID iD: <https://orcid.org/0009-0009-8408-9666>

^f Mustapha Stambouli University, Department of Civil Engineering, Laboratory for the Study of Structures and Mechanics of Materials, Mascara, People's Democratic Republic of Algeria, e-mail: m.sadoun@univ-mascara.dz, ORCID iD: <https://orcid.org/0009-0008-2314-9402>

 <https://doi.org/10.5937/vojtehg72-49173>

FIELD: mechanical engineering, materials

ARTICLE TYPE: original scientific paper

Abstract:

Introduction/purpose: The dynamic analysis of a seismic response of a concrete vault dam is a complex problem in which the representation of the behavior of the material requires some form of a nonlinear model, especially if the concrete is subjected to a significant stress load of the ground. In the case of large movements of the latter, large cracks may form in some areas

of the dam, especially at the base of the dam and near sudden changes in geometry.

Methods: This analysis was based on a numerical simulation of the dynamic effect. This work was carried out using the finite element method with the ANSYS 12.1 program. The dam was modelled in two dimensions. Four types of analysis were performed: static analysis, modal analysis, seismic analysis under excitation of two accelerograms (Asnam 1980 and Boumerdes 2003), and spectral analysis.

Results: This analysis showed the vulnerability of the Brezina dam to the Boumerdes earthquake with high stresses at the base of the structure.

Conclusions: Based on this study, it was concluded that if the Brezina dam suffers an earthquake of a greater intensity than that of Boumerdes, this will cause structural damage and cracks that will compromise the dam's watertightness as well as its durability.

Key words: dynamic behavior, finite element method, cracking, dam, spectral analysis.

Introduction

Water resources are incredibly important for promoting agricultural economic development worldwide. Hydraulic structures, such as dams, intake towers, and piles, are considered special structures that require a significant safety margin under both normal and critical conditions such as major earthquakes.

The evaluation of the seismic safety of a concrete gravity dam is one of the main subjects of design and construction, as well as other basic safety checks such as dam stability in its foundations and a high overflow velocity of a dam. The reservoir - dam interaction can be an important factor influencing the response of concrete dams. When a reservoir - dam system is subjected to a strong earthquake, its behavior is likely to be influenced.

The procedures for a seismic analysis of structures are often approached with simplifying assumptions. Among the most important is the one which assumes that the seismic signal is uniform. In the seismic analysis of structures, (Datta, 2010) explained the fundamentals of seismology that all structural engineers must know. Progress has been made (Der Kiureghian, 1981), which led to a specific application to linear structures using the response spectrum of soil motion. Different phenomena contributing to the spatio-temporal variability of the seismic signal have been grouped together, with four distinct effects (Der Kiureghian, 1996).

The first interaction model between the dam and the reservoir was developed by Westergaard (1933), who presented a solution for the two-dimensional pressure distributions on the upstream face of the dam due to seismic excitation. He assumed that the water is incompressible and the dam is rigid. Zienkiewicz & Bettles (1978) studied the problems of the dam reservoir in a coupled manner taking into account the flexibility of the dam. Fenves & Chopra (1987) presented a simplified approach for the analysis of concrete gravity dams under earthquake actions.

Jablonski & Humar (1990) explained the application of the constant boundary element method in the three-dimensional boundary element reservoir model for the seismic analysis of arch dams and gravity. A comparison of computer codes for a dam analysis was conducted by Singhal (1991) using EADG, PAS IV, as well as the ADINA software. The analysis of the severity of an earthquake on dam-reservoir systems using Eulerian and Lagrangian approaches was conducted by Calayir et al. (1996). Guan & Moore (1997) developed new techniques for modeling the reservoir-dam interaction and the dam foundation. Chopra & Gupta (1981) investigated the effects of the hydrodynamic interaction and the foundations on the seismic response of a concrete gravity dam. A hybrid numerical procedure is proposed for the dynamic frequency response of earth dams resting on a multilayered base. De Araújo & Awruch (1998) used the probabilistic finite element method for the analysis of a concrete gravity dam. Ghaemian & Ghobarah (1999) studied the nonlinear seismic response of concrete gravity dams considering the interaction between the dam and the reservoir. The dynamic analysis of the soil-structure interaction using the finite element-boundary coupling method has been studied by Yazdchi et al. (1999). The dynamic analysis of concrete arch dams by an ideal-coupled modal approach has been studied by Aftabi Sani & Lotfi (2010). A parametric study on the fluid-structure interaction problem was conducted by Maity & Bhattacharyya (2003). An evaluation of the effectiveness of the equations developed to determine the response of the fundamental mode of weight-bearing dams was carried out by Miguel & Bouaanani (2010). In their study, an iterative scheme in dynamic analysis and a complicated boundary condition were used. Küçükarslan et al. (2005) studied the transient analysis of the dam-reservoir interaction, including the effects of the reservoir bottom by coupling the finite element method in the infinite fluid domain and in the solid domain. A comparison of stochastic and deterministic dynamic responses of gravity dam-reservoir systems using finite fluid elements was conducted by Bayraktar et al. (2005). Asteris & Tzamtzis (2003) used a smeared crack analysis

model based on a non-linear fracture mechanics crack propagation criterion to study dam cracking and response.

The experimental and numerical seismic surveys of the Three Gorges Dam were conducted by Li et al. (2005). Millán et al. (2007) demonstrated the effects of the reservoir geometry on the seismic response of gravity dams. In this paper, a boundary element method (BEM) model in the frequency domain is used to study the influence of the reservoir dam geometry on the hydrodynamic response. Bayraktar et al. (2010) studied the effect of the reservoir length on the seismic performance of gravity dams to near- and far-fault ground motions. Samii & Lotfi (2007) compared coupled and decoupled modal approaches in the seismic analysis of concrete gravity dams in the time domain. Ross et al. (2008) studied the treatment of the fluid-structure acoustic interaction using localized Lagrange multipliers. Li et al. (2008) developed a semi-analytical solution for the absorption characteristics of a reservoir bottom dam retention system. Bilici et al. (2009) studied the stochastic dynamic response of the dam-reservoir-foundation system to spatial variations in earthquake ground motions. Wang et al. (2021) studied influences on the seismic response of a gravity dam with different foundation and reservoir modeling assumptions. Xu et al. (2024) studied a time series modeling approach for damage monitoring of a concrete dam under seismic effects.

The analysis aims to study the dynamic behaviour of the dam under seismic excitation and the detection of anomalies in stresses and displacements that can be harmful to the structure. Practical conclusions are also drawn from the results obtained using different numerical strategies.

Dynamic analysis has a great importance in the design of dams with respect to seismic excitations. Several mathematical concepts govern the dynamic behavior.

Fluid equation

$$\nabla^2 P = \frac{1}{C^2} \ddot{P} \tag{1}$$

where ∇^2 is the Laplacian operator in two dimensions, (C) is the speed of sound in the water, and the points represent the derivative with respect to time. Equation (1), with appropriate boundary conditions, fully defines the hydrodynamic aspects of the problem.

Finite element analysis execution

The water domain is discretised as a finite element assembly, assuming that the pressure is the nodal unknown. By using the Galerkin method, the discretised form of equation (1) is obtained as:

$$[E]\{\dot{p}\} + [A]\{p\} + \left([G] + \frac{\zeta C}{H} [A]\right)\{p\} = -\rho f[S]\{a\} \quad (2)$$

where $\{p\}$ represents the vector of nodal pressures for the water domain. The expressions for the matrices $[E]$, $[A]$, $[G]$, and $[S]$ can be found in Maity & Bhattacharyya (1999).

$$[E] = \frac{1}{c^2} \sum \int_{\Omega} [N]^T [N] d\Omega + \frac{1}{g} \sum \int_{\Gamma_f} [N]^T [N] d\Gamma \quad (3)$$

$$[A] = \frac{1}{c} \sum \int_{\Gamma_f} [N]^T [N] d\Gamma \quad (4)$$

$$[G] = \sum \int_{\omega} \left(\frac{\partial}{\partial x} [N]^T \frac{\partial}{\partial x} [N] + \frac{\partial}{\partial y} [N]^T \frac{\partial}{\partial y} [N] \right) d\Omega \quad (5)$$

$$[S] = \sum \int_{\Gamma_s} [N]^T [T] [N_s] d\Gamma \quad (6)$$

In the equations above, (3-6) Γ and Ω represent the surface and the volume of the reservoir, respectively. The indices f, s, r, and t represent the free surface, the solid-fluid interface, the bed-reservoir interface, and the truncated surface, respectively.

Differential equations governing the coupled structure of a dam

The dam-reservoir interaction is represented by two coupled second-order differential equations. The equations for the structure and the reservoir can be written in the following form:

$$[N] \{\ddot{U}\} + [C] \{\dot{U}\} + [N] \{U\} = \{f_1\} - [M] \{\ddot{U}_{gh}\} - [M] \{\ddot{U}_{gv}\} + [Q] \{P_h(t)\} \quad (7)$$

$$[G] \{P_h\} + [C^*] \{\dot{P}_h\} + [K^*] \{P_h\} = \{f_2\} - \rho [M]^T \{U\} \quad (8)$$

The point represents the time derivative. The structure of the dam is analysed using the plane deformation formulation with a side reservoir. By the analysis of the structural system using the plane deformation formulation, the elementary stiffness matrices are obtained:

$$[K^e] = \int_{\Omega} [B]^T [D][B] d\Omega \quad (9)$$

The elementary mass matrix with ρ_s is the density.

$$[M^e] = \int_{\Omega} [B^T] \rho_s [N] d\Omega \quad (10)$$

Damping matrix

The global damping matrix is calculated using the following expression since Rayleigh damping is taken into account:

$$[C] = a[M] + b[K] \quad (11)$$

According to the theory of modal analysis, the structure of the dam can be simplified as a multi-degree of freedom system, and its equation of motion control is equation (7). In free vibration analysis, we need to solve the eigenvalue equation given below:

$$([K] - \omega^2[M]) \{u\} = 0 \quad (12)$$

Dynamic analysis

The dynamic analysis method is mainly based on two methods, depending on the idealisation of the dam body, namely, the method of distributed or continuous masses and the method of discrete or grouped masses. The first method forms the dynamic stiffness matrix of the structure, which includes the elastic and inertial forces acting on the structure during vibration, and determines the natural frequency and mode of the dam by solving the frequency equation, (7) (Clough & Penzien, 1975).

The second method of calculating the static stiffness matrix of the structure reduces the natural frequencies and mode shapes using standard eigenvalue solutions (Bathe & Wilson, 1987). Chopra (1995), in his book *Dynamics of Structures*, has also developed theories and applications to seismic engineering.

Description and modeling of the dam

The Brezina Dam (El-Bayadh-Algeria) is a gravity dam, a concrete arch dam. It is built on a rocky foundation (limestone) and has a total height of 63 m. The arc length at the top is 153 m, with a maximum arc radius of 67.80 m. The maximum thickness is 41.33 m, and the thickness at the crest is 3 m as shown in Figure 1. These mechanical and physical properties are as follows: Young's modulus $E = 26.6$ GPa; Poisson's ratio $\nu = 0.2$; and density $\gamma = 2.5$ t/m³. There are also the mechanical and physical properties of the foundation (rock) and the fluid, which are, respectively, Young's modulus $E = 14$ GPa; Poisson's ratio $\nu = 0.3$; density $M_v = 2.7$ t/m³, and Young's modulus $E = 20.7 \times 10^6$ GPa; density $M_v = 1$ t/m³.

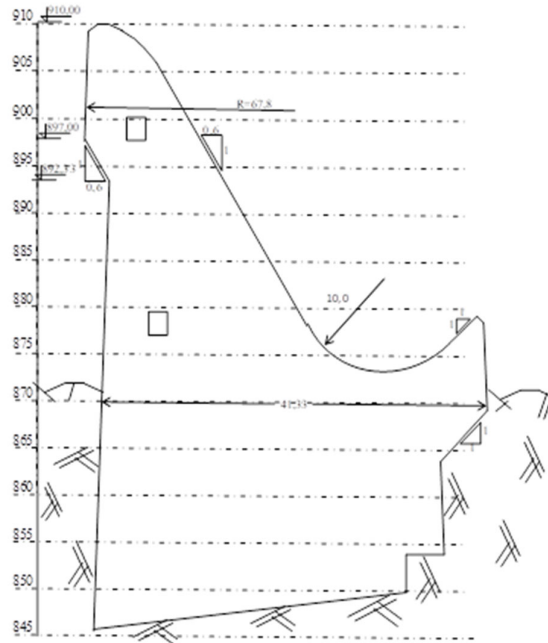


Figure 1 – Cross section and the dimensional parameters of the dam

ANSYS is a versatile finite element analysis software; it allows testing of product prototypes in a virtual environment before manufacturing them. It also identifies weaknesses and improves them. In our modeling, we used two types of finite elements: Fluid29 and Plane42; the resulting mesh included 4,790 nodes and 1,974 elements, as shown in Figure 2.

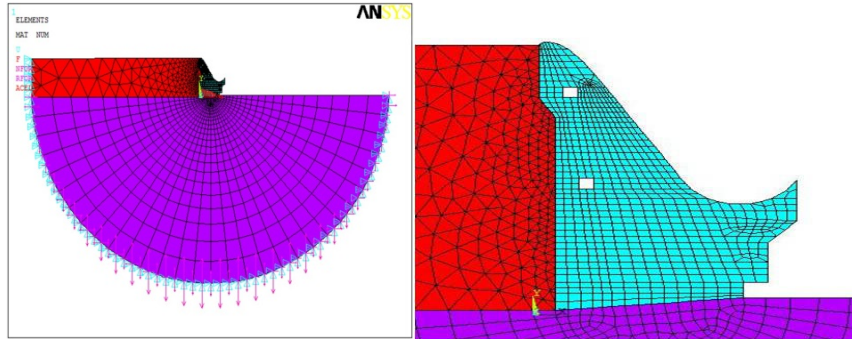


Figure 2 – Model of the Dam - Fluid - Foundation system with ANSYS

Analysis and interpretation

Static analysis

Static stresses are caused by the hydrostatic pressure and the dead weight of the dam, which is automatically distributed towards the center of gravity, while the sign convention is respected when entering the pressure and assuming that the tank is full. The results are presented in Table 1_ and Figure 3.

This shows the distribution of static stresses in the dam body. These stresses reach the maximum and minimum values in the lower part. Figures 4 and 5 show the distribution of the normal (X, Y and XY) and main (S1, S3 and Tmax) stresses in the lower part of the structure. It can be seen that these stresses vary from upstream and downstream of tension to compression.

Table 1 – Results (minimum and maximum) of the various static constraints

	Sx (MPa)	Sy (MPa)	Sxy (MPa)	S1 (MPa)	S3 (MPa)	Tmax (MPa)
MAX	0.47556	0.30071	0.90254	0.64125	0.13501	0.38813
MIN	-2.3767	-3.499	0.23755	-1.4314	-4.0006	-2.716

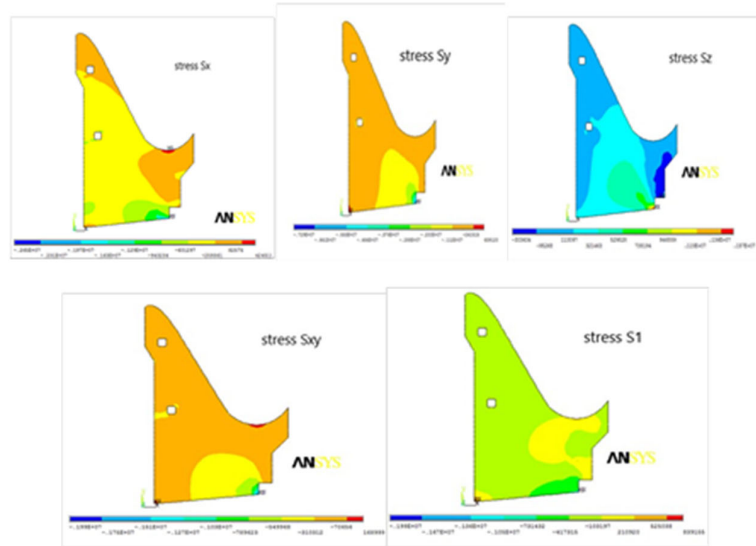


Figure 3 – Mapping the distribution of static stresses in the dam

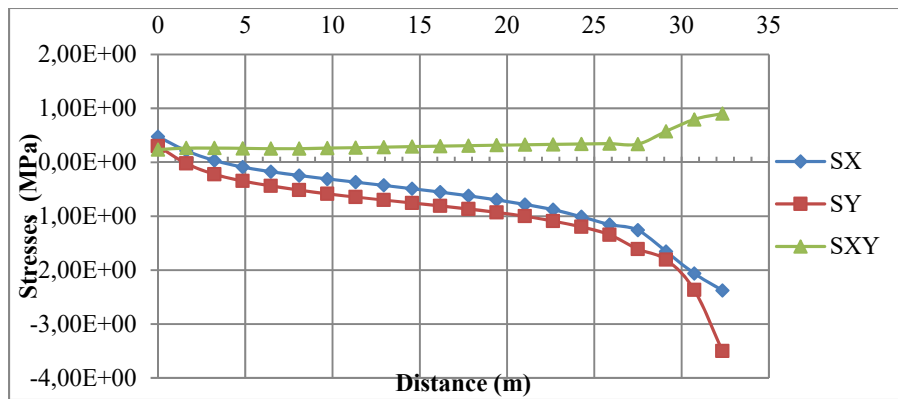


Figure 4 – Normal stresses in the directions X, Y and XY

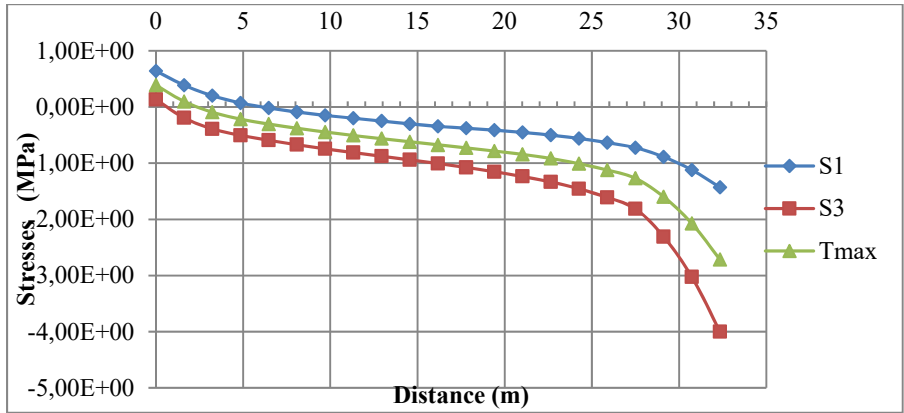


Figure 5 – Principal stresses in the directions S1, S3 and Tmax

Modal analysis

The principle of the modal method is to find, for each mode of vibration, the maximum value of the effect of seismic forces in the structure, which is represented by the calculated response spectrum. Prior to dynamic analysis, the natural frequency of the dam in the case of an empty reservoir is determined by modal analysis. The analysis is performed in the modal mode. All degrees of freedom at the base of the rock substrate and the peripheral equipment are restricted.

The value of the damping coefficient considered is 5% - the results of the analysis are shown in Table 2.

Table 2 – Results obtained for different vibration modes

Mode	Frequency [Hz]	Period [s]	Participation factor	Coefficient	Effective mass	Mass fraction	Total mass
1	4.332	0.231	1.44×10^3	1.000	2.08×10^6	0.604	0.594
2	9.729	0.103	-8.11×10^2	0.562	6.58×10^5	0.795	0.188
3	11.029	0.091	-5.81×10^2	0.403	3.38×10^5	0.892	0.096
4	18.917	0.053	6.09×10^2	0.422	3.71×10^5	1.000	0.106
5	23.073	0.043	-1.80×10^1	0.012	3.25×10^2	1.000	0.000
Sum	/	/	/	/	3.45×10^6	/	0.985

The deformations obtained for each vibration mode are presented in Figure 6.

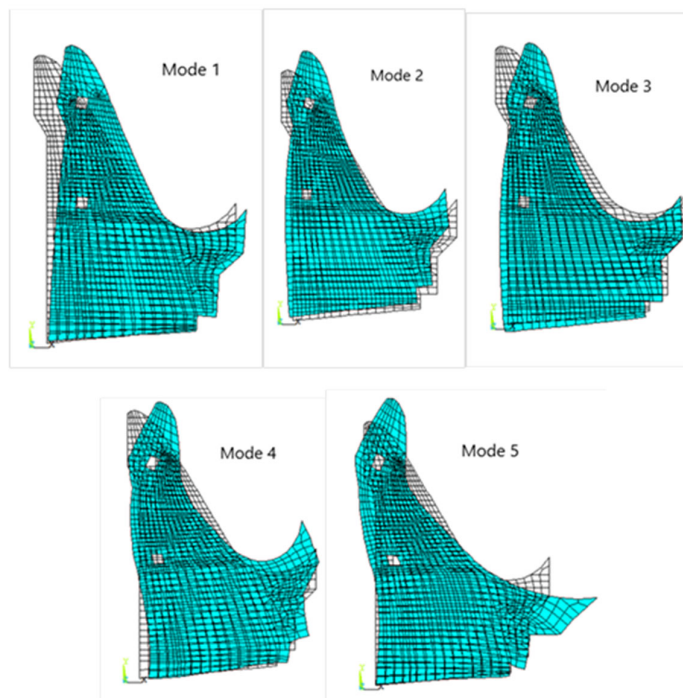


Figure 6 – Deformations of each vibration mode

Dynamic analysis by accelerograms

At this stage of the analysis, the two most destructive earthquakes recorded in Algeria have been selected, namely the Asnam earthquake and the Boumerdes earthquake. The accelerograms and the characteristics of these two earthquakes are presented in Table 3 and shown in Figure 7.

Table 3 – Characteristics of the two earthquakes

Earthquake name	Location	Date	PGA (g)	Magnitude
Asnam	15 km east of Al Asnam (CHELF) Béni Rached	10 /10/1980	0.034	7.3
Boumerdes	04 Km from the coast between Zemmouri and Boumerdes	21/05/2003	0.338	6.4

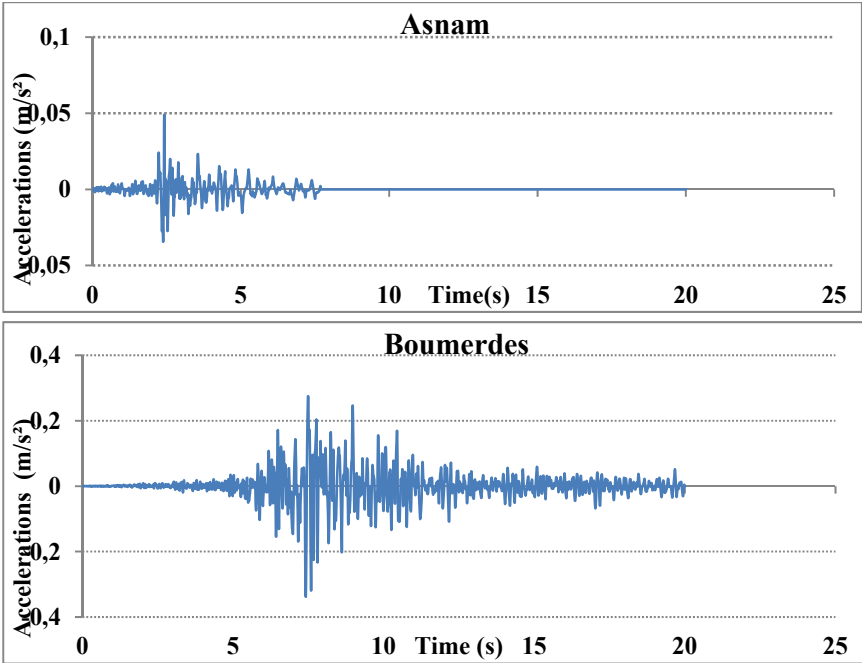


Figure 7 – Accelerograms of the two earthquakes

Results of the displacements at the top of the dam

The movement of the dam crest under the excitation of the two earthquakes is shown in Figure 8. The comparison of the two figures shows that the excitation generated by the Boumerdes earthquake has a significant effect on the movement of the dam crest.

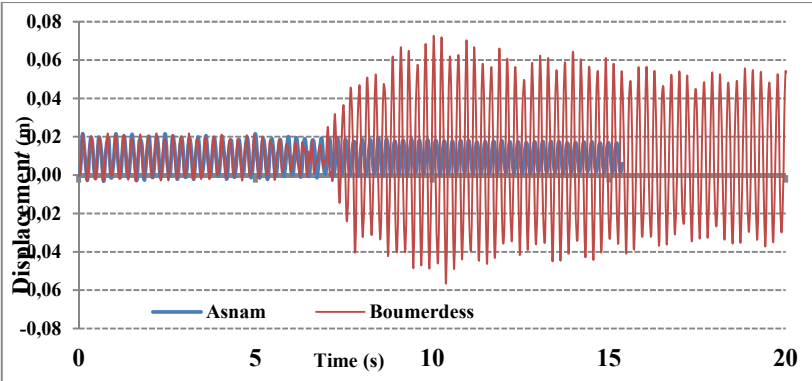


Figure 8 – Displacement to the ridge (top) of the dam under the excitation of the two earthquakes

Results of the acceleration at the top of the dam

The accelerations at the top of the dam under the excitation of the two earthquakes are illustrated in Figure 9.

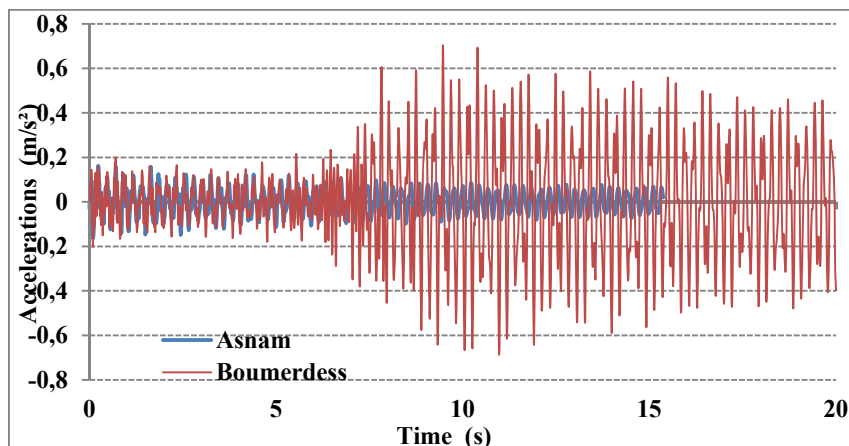


Figure 9 – Acceleration at the crest (top) of the dam under the excitation of the two earthquakes

Distribution of the principal stresses (S1) at the base as a function of time

The distributions of the main stresses at the base of the dam over time are shown in Figures 10, 11, and 12.

These figures illustrate the variation of stresses along the upstream, central, and downstream sections of the dam during two earthquakes. In particular, the tensile stresses exceed the compressive stresses in the upstream section, while both stresses decrease significantly in the central section.

Conversely, in the downstream section, compressive stresses dominate and exceed tensile stresses.

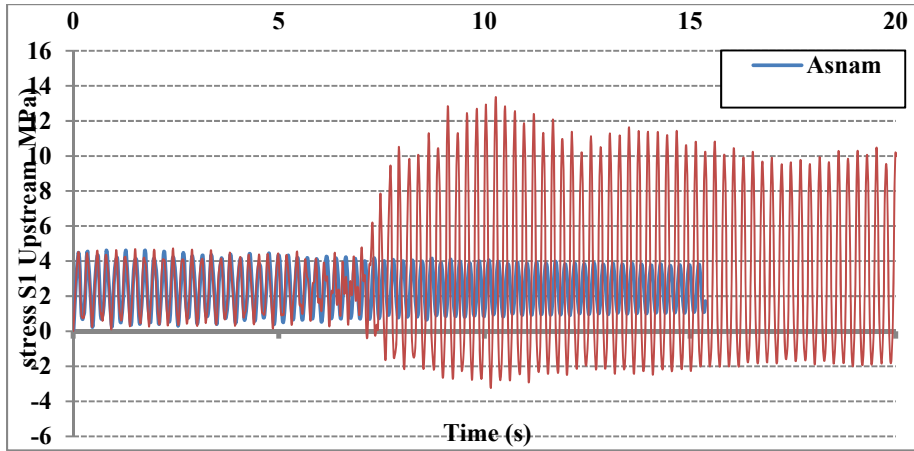


Figure 10 – Principal stresses S_1 at the basis of the dam upstream for the two earthquakes

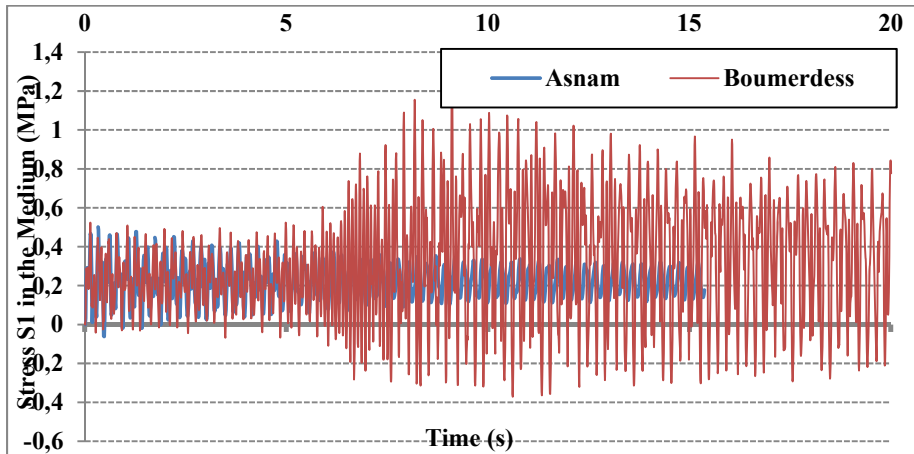


Figure 11 – Principal stresses S_1 at the basis of the dam in the middle for the two earthquakes

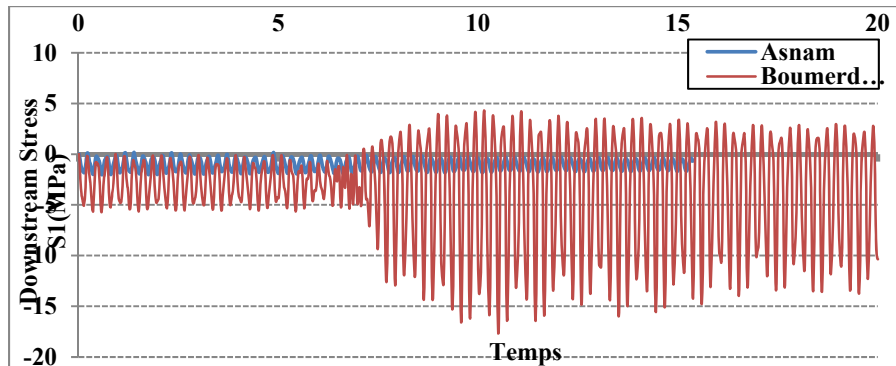


Figure 12 – Principal stresses S1 at the basis of the downstream dam for the two earthquakes

Table 4 shows the maximum displacements and accelerations at the crest and the principal stresses S1 at the base (upstream, intermediate and downstream) recorded for the two earthquakes.

Table 4 – Comparison of the results of the deferent characteristics under the effect of the excitations of the two earthquakes

	Displacement (m)	Acceleration (m/s ²)	Stresses S1 en Amant MPa	Stresses S1 au Milieu MPa	stresses S1 en Aval MPa
Asnam	2.16 X 10 ⁻⁰²	0.1617515	4.61263648	0.50066706	0.16896932
Boumerdes	7.26 X 10 ⁻⁰²	0.7032191	13.3658454	1.26142696	4.31357794

Comparing the different results in Table 4 shows that all the results obtained under the excitation of the Boumerdes earthquake are much more significant than those of the Asnam earthquake.

The tensile stresses are mainly concentrated upstream of the dam and greatly exceed the tensile strength limit of the concrete $f_t = 2.35\text{MPa}$, causing cracks at the base of the dam.

Spectral analysis

The spectral method is an approximate technique for evaluating the peak response of a structure based on the peak response of each modal oscillator read from the vibration spectrum of the excitation.

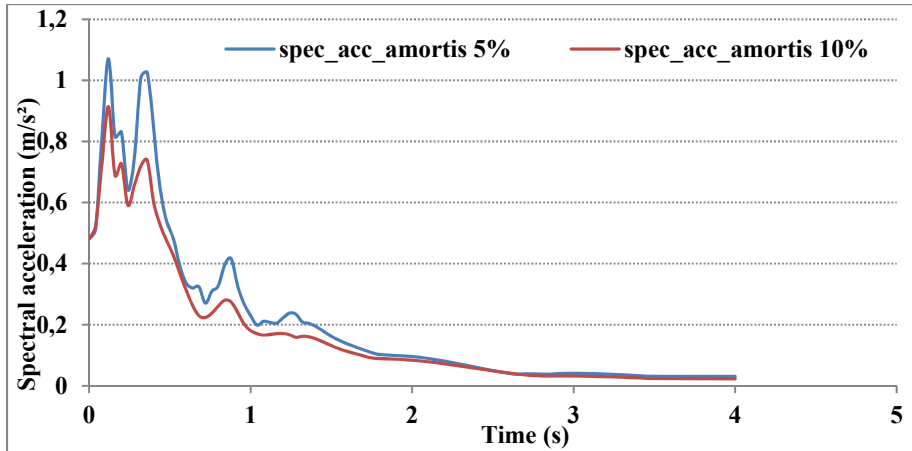


Figure 13 – Response spectra with 5% and 10% damping (Asnam earthquake)

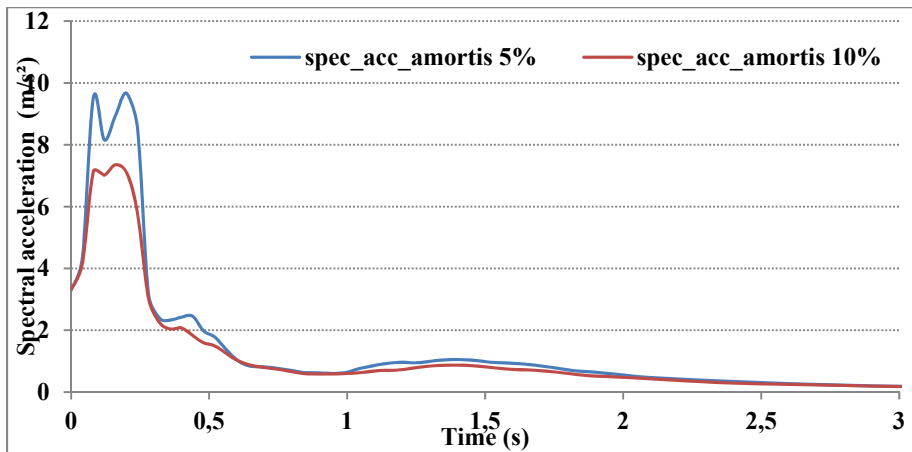


Figure 14 – Response spectra with 5% and 10% damping (Boumerdes earthquake)

The main constraints for a 5% and 10% depreciation (Asnam)

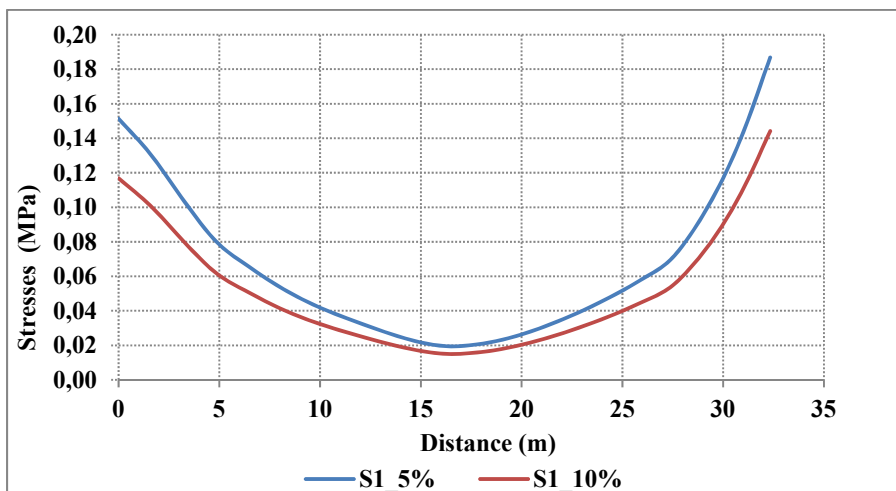


Figure 15 – Principal stresses S1 at the basis for the Asnam earthquake damped at 5% and 10%

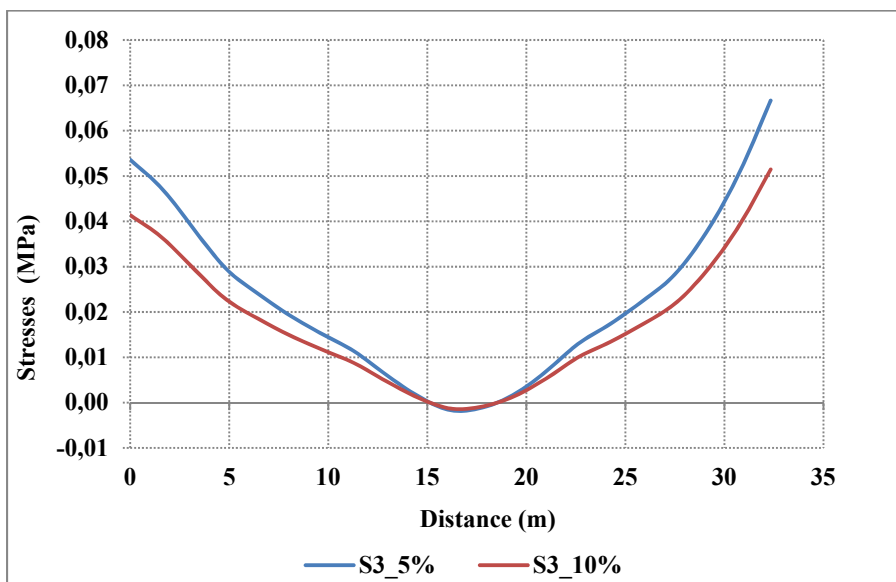


Figure 16 – Principal stresses S3 at the basis for the Asnam earthquake damped at 5% and 10%

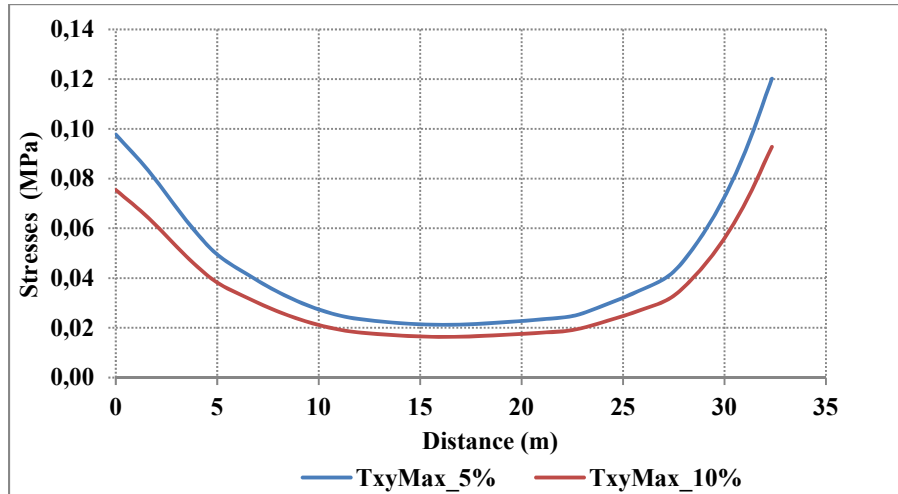


Figure 17 – Principal stresses TMax at the basis for the Asnam earthquake damped at 5% and 10%

Table 5 – Results under the excitation of the Asnam earthquake damped at 5% and 10%

	S1		S3		Tmax		Dépl max (m)	
	5%	10%	5%	10%	5%	10%	5%	10%
Max	0.18686	0.14421	0.06666	0.051446	0.1202	0.092764	8.43·10 ⁻⁰⁴	6.51·10 ⁻⁰⁴
Min	0.019478	0.01503	-0.00168	-0.00129	0.02116	0.016330		

According to Figures 15, 16, and 17, damping has an opposite effect on the principal stresses. Damping significantly reduces the stresses upstream and downstream, but in the central section, the damping effect is weak for the stresses S1 and Tmax, and negligible for the stress S3. These results are reported in Table 5.

When comparing the stress S1 with 5% and 10% damping, it can be seen that at 10% damping the stress is reduced by 0.043 MPa compared with a reduction of 5%, while for displacements the reduction is 1.92 x 10⁻⁴ m.

The main constraints for a 5% and 10% depreciation (Boumerdes)

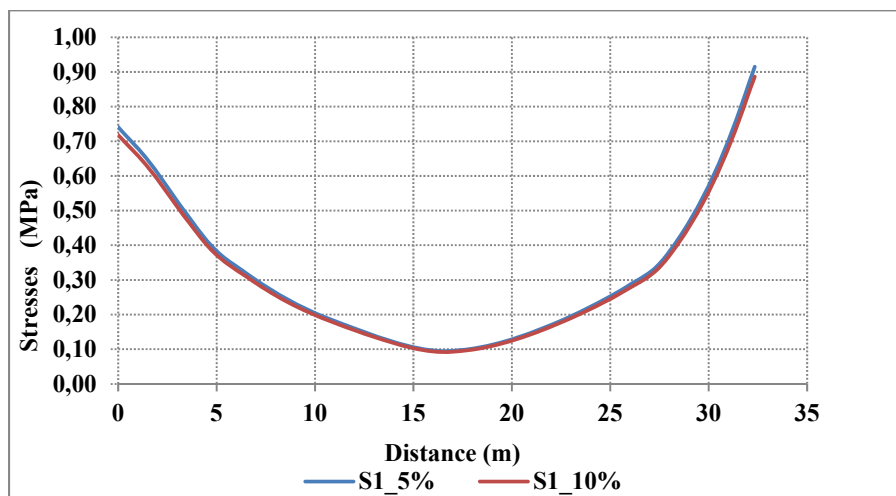


Figure 18 – Principal stresses S1 at the basis for the Boumerdes earthquake damped at 5% and 10%

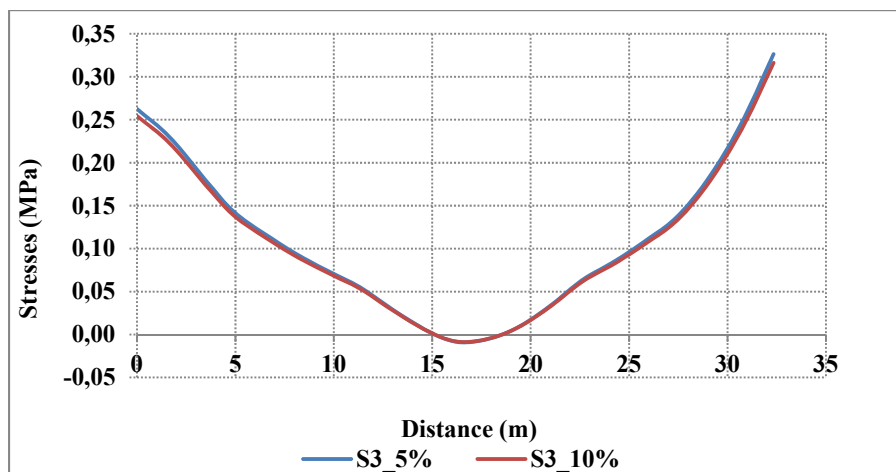


Figure 19 – Principal stresses S3 at the basis for the Boumerdes earthquake damped at 5% and 10%

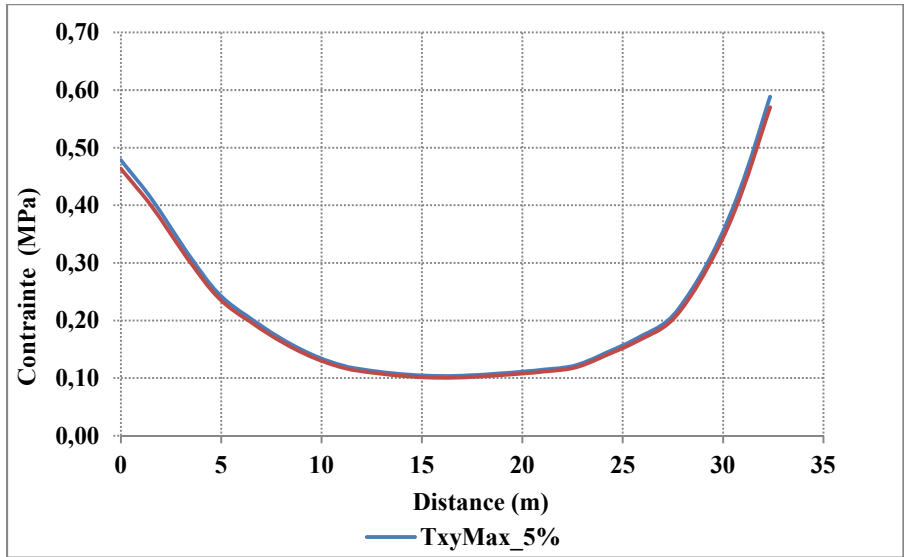


Figure 20 – Principal stresses TMax at the basis for the Boumerdes earthquake damped at 5% and 10%

Table 6 – Results under the excitation of the Boumerdes earthquake damped at 5% and 10%

	S1		S3		Tmax		Depl max (m)	
	5%	10%	5%	10%	5%	10%	5%	10%
Max	0,91489	0,8866	0,32637	0,31628	0,58852	0,57032	4,13x10 ⁻⁰³	4,00x10 ⁻⁰³
Min	0,095366	0,092417	-0,0082377	-0,007983	0,1036037	0,1004		

Similar to the Asnam earthquake and based on Figures 18, 19 and 20, it can be seen that damping has an opposite effect on the principal stress. The damping reduces the stresses in the upstream and downstream directions, but in the centre the damping effect on the three stresses is negligible. The same results are shown in Table 7. If the stresses S1 for 5% and 10% damping are compared, it can be seen that the difference is small, 0.028 MPa, whereas for displacement the reduction is still insignificant.

Conclusion

The main objective of this paper is to provide a scientific and analytical contribution on the internal constraints of arch dams, in order to better understand the complexity of the engineer's task when designing dams.

Indeed, this analysis shows that, contrary to what has been said, dams have certain displacements and no part of the superstructure is immune to the risk of failure; therefore, engineers must find feasible technical solutions.

Static analysis has shown that stresses vary from tension to compression over the entire surface of the dam. Concentrations of tension constraints are observed at the upstream base, while compression constraints are observed downstream. Whether tension or compression, the constraints remain low compared to the tolerated limits.

As for modal analysis, it allowed us to identify the natural modes of the structure. We considered the first five (5) eigenmodes, where we observed that the first two modes are the most important because their frequency is low. It is known that when the frequency is low, there is a risk of collapse.

After static and modal analyses comes dynamic analysis which is carried out under the excitation of two earthquakes, namely Boumerdes and Asnam, to get an idea of the dynamic behaviour (tension, compression and displacement) of the dam at the top.

The Boumerdes earthquake generated significant tensile stresses upstream and downstream, exceeding the ultimate tensile stress, whereas the tensile stress in the Asnam earthquake only exceeded the ultimate tensile stress upstream.

It should be noted that the values obtained under the excitation of the Boumerdes earthquake are larger than those of the Asnam earthquake. For example, the principal stress S_1 of the upstream Boumerdes earthquake is almost three (3) times greater than that of the Asnam earthquake. Although the magnitude of the Asnam earthquake was greater than that of the Boumerdes earthquake, these results are probably due to the acceleration time.

Overall, this study concludes that if the Brezina dam is affected by an earthquake of a greater intensity than that of Boumerdes, there will be structural damage and cracks that will affect the watertightness and durability of the dam.

References

- Aftabi Sani, A. & Lotfi, V. 2010. Dynamic analysis of concrete arch dams by ideal-coupled modal approach. *Engineering Structures*, 32(5), pp.1377-1383. Available at: <https://doi.org/10.1016/j.engstruct.2010.01.016>.
- Asteris, P.G. & Tzamtzis, A.D. 2003. Nonlinear Seismic Response Analysis of Realistic Gravity Dam-Reservoir Systems. *International Journal of Nonlinear Sciences and Numerical Simulation*, 4(4), pp.329-338. Available at: <https://doi.org/10.1515/IJNSNS.2003.4.4.329>.
- Bathe, K.-J. & Wilson, E.L. 1976. *Numerical methods in finite element analysis (Prentice-Hall civil engineering and engineering mechanics series)*. Prentice-Hall. ISBN: 978-0136271901.
- Bayraktar, A., Hançer, E. & Dumanoğlu, A.A. 2005. Comparison of stochastic and deterministic dynamic responses of gravity dam-reservoir systems using fluid finite elements. *Finite Elements in Analysis and Design*, 41(14), pp.1365-1376. Available at: <https://doi.org/10.1016/j.finel.2005.02.004>.
- Bayraktar, A., Türker, T., Akköse, M. & Ateş, Ş. 2010. The effect of reservoir length on seismic performance of gravity dams to near- and far-fault ground motions. *Natural Hazards*, 52, pp.257-275. Available at: <https://doi.org/10.1007/s11069-009-9368-1>.
- Bilici, Y., Bayraktar, A., Soyuluk, K., Hacıfendioğlu, K., Ateş, Ş. & Adanur, S. 2009. Stochastic dynamic response of dam-reservoir-foundation systems to spatially varying earthquake ground motions. *Soil Dynamics and Earthquake Engineering*, 29(3), pp.444-458. Available at: <https://doi.org/10.1016/j.soildyn.2008.05.001>.
- Calayir, Y., Dumanoğlu, A.A., & Bayraktar, A. 1996. Earthquake analysis of gravity dam-reservoir systems using the eulerian and lagrangian approaches. *Computers & Structures*, 59(5), pp.877-890. Available at: [https://doi.org/10.1016/0045-7949\(95\)00309-6](https://doi.org/10.1016/0045-7949(95)00309-6).
- Chopra, A.K. 1995. *Dynamics of structures: Theory and applications to earthquake engineering*. Englewood Cliffs, NJ, USA: Prentice Hall. ISBN: 0-13-855214-2.
- Chopra, A.K. & Gupta, S. 1981. Hydrodynamic and Foundation Interaction Effects in Earthquake Response of a Concrete Gravity Dam. *Journal of the Structural Division*, 107(8), pp.1399-1412. Available at: <https://doi.org/10.1061/JSDEAG.0005756>.
- Clough, R.W. & Penzien, J. 1975. *Dynamics of Structures*. McGraw-Hill College. ISBN: 978-0070113923.
- de Araújo, J.M. & Awruch, A.M. 1998. Probabilistic finite element analysis of concrete gravity dams. *Advances in Engineering Software*, 29(2), pp.97-104. Available at: [https://doi.org/10.1016/S0965-9978\(98\)00052-0](https://doi.org/10.1016/S0965-9978(98)00052-0).
- Datta, T.K. 2010. *Seismic Analysis of Structures*. Wiley. ISBN: 978-0-470-82462-7.

Der Kiureghian, A. 1981. Seismic Risk Analysis of Structural System. *Journal of Engineering Mechanics*, 107(6), pp.1133-1153. Available at: <https://doi.org/10.1061/JMCEA3.0002772>.

Der Kiureghian, A. 1996. Structural reliability methods for seismic safety assessment: a review. *Engineering Structure*, 18(6), pp.412-424. Available at: [https://doi.org/10.1016/0141-0296\(95\)00005-4](https://doi.org/10.1016/0141-0296(95)00005-4).

Fenves, G. & Chopra, A.K. 1987. Simplified Earthquake Analysis of Concrete Gravity Dams. *Journal of Structural Engineering*, 113(8), pp.1688-708. Available at: [https://doi.org/10.1061/\(ASCE\)0733-9445\(1987\)113:8\(1688\)](https://doi.org/10.1061/(ASCE)0733-9445(1987)113:8(1688)).

Ghaemian, M. & Ghobarah, A. 1999. Nonlinear seismic response of concrete gravity dams with dam-reservoir interaction. *Engineering Structures*, 21(4), pp.306-315. Available at: [https://doi.org/10.1016/S0141-0296\(97\)00208-3](https://doi.org/10.1016/S0141-0296(97)00208-3).

Guan, F. & Moore, I.D. 1997. New techniques for modelling reservoir-dam and foundation-dam interaction. *Soil Dynamics and Earthquake Engineering*, 16(4), pp.285-293. Available at: [https://doi.org/10.1016/S0267-7261\(96\)00044-9](https://doi.org/10.1016/S0267-7261(96)00044-9).

Jablonski, A.M. & Humar, J.L. 1990. Three-dimensional boundary element reservoir model for seismic analysis of arch and gravity dams. *Earthquake Engineering & Structural Dynamics*, 19(3), pp.359-376. Available at: <https://doi.org/10.1002/eqe.4290190306>.

Küçükarslan, S., Coşkun, S.B. & Taşkın, B. 2005. Transient analysis of dam-reservoir interaction including the reservoir bottom effects. *Journal of Fluids and Structures*, 20(8), pp.1073-1084. Available at: <https://doi.org/10.1016/j.jfluidstructs.2005.05.004>.

Li, S.-m., Li, H. & Li, A.-m. 2008. A Semi-Analytical Solution for Characteristics of a Dam-Reservoir System with Absorptive Reservoir Bottom. *Journal of Hydrodynamics*, 20, pp.727-734. Available at: [https://doi.org/10.1016/S1001-6058\(09\)60008-1](https://doi.org/10.1016/S1001-6058(09)60008-1).

Li, Q.S., Li, Z.N., Li, G.Q., Meng, J.F. & Tang, J. 2005. Experimental and numerical seismic investigations of the Three Gorges Dam. *Engineering Structures*, 27(4), pp.501-513. Available at: <https://doi.org/10.1016/j.engstruct.2004.11.009>.

Maitly, D. & Bhattacharyya, S.K. 1999. Time-domain analysis of infinite reservoir by finite element method using a novel far-boundary condition. *Finite Elements in Analysis and Design*, 32(2), pp.85-96. Available at: [https://doi.org/10.1016/S0168-874X\(98\)00077-8](https://doi.org/10.1016/S0168-874X(98)00077-8).

Maitly, D. & Bhattacharyya, S.K. 2003. A parametric study on fluid-structure interaction problems. *Journal of Sound and Vibration*, 263(4), pp.917-935. Available at: [https://doi.org/10.1016/S0022-460X\(02\)01079-9](https://doi.org/10.1016/S0022-460X(02)01079-9).

Miguel, B. & Bouaanani, N. 2010. Simplified evaluation of the vibration period and seismic response of gravity dam water systems. *Engineering Structures*, 32(8), pp.2488-2502. Available at: <https://doi.org/10.1016/j.engstruct.2010.04.025>

Millán, M.A., Young, Y.L. & Prévost, J.H. 2007. The effects of reservoir geometry on the seismic response of gravity dams. *Earthquake Engineering And*

Structural Dynamics, 36(11), pp.1441-1459. Available at: <https://doi.org/10.1002/eqe.688>.

Ross, M.R., Felippa, C.A., Park, K.C. & Sprague, M.A. 2008. Treatment of acoustic fluid–structure interaction by localized Lagrange multipliers: Formulation. *Computer Methods in Applied Mechanics and Engineering*, 197(33-40), pp.3057-3079. Available at: <https://doi.org/10.1016/j.cma.2008.02.017>

Samii, A. & Lotfi, V. 2007. Comparison of coupled and decoupled modal approaches in seismic analysis of concrete gravity dams in time domain. *Finite Elements in Analysis and Design*, 43(13), pp.1003-1012. Available at: <https://doi.org/10.1016/j.finel.2007.06.015>.

Singhal, A.C. 1991. Comparison of computer codes for seismic analysis of dams. *Computers & Structures*, 38(1), pp.107-112. Available at: [https://doi.org/10.1016/0045-7949\(91\)90128-9](https://doi.org/10.1016/0045-7949(91)90128-9).

Wang, C., Zhang, H., Zhang, Y., Guo, L., Wang, Y. & Thira Htun, T.T. 2021 Influences on the Seismic Response of a Gravity Dam with Different Foundation and Reservoir Modeling Assumptions. *Water*, 13(21), art.number:3072. Available at: <https://doi.org/10.3390/w13213072>.

Westergaard, H.M. 1933. Water Pressures on Dams during Earthquakes. *Transactions of the American Society of Civil Engineers*, 98(2), pp.418-472. Available at: <https://doi.org/10.1061/TACEAT.0004496>.

Xu, Y., Shao, C., Zheng, S., Li, X., Gu, H. & Zheng, D. 2024. A time series modeling approach for damage monitoring of concrete dam under seismic effects. *Structures*, 59, art.number:105656. Available at: <https://doi.org/10.1016/j.istruc.2023.105656>.

Yazdchi, M., Khalili, N. & Valliappan, S. 1999. Dynamic soil-structure interaction analysis via coupled finite-element-boundary-element method. *Soil Dynamics and Earthquake Engineering*, 18(7), pp.499-517. Available at: [https://doi.org/10.1016/S0267-7261\(99\)00019-6](https://doi.org/10.1016/S0267-7261(99)00019-6).

Zienkiewicz, O.C. & Bettles, P. 1978. Fluid-structure dynamic interaction and wave forces. An introduction to numerical treatment. *International Journal for Numerical Methods in Engineering*, 13(1), pp.1-16. Available at: <https://doi.org/10.1002/nme.1620130102>.

Análisis dinámico de una presa abovedada

Abdelkrim Benahmed^a, **autor de correspondencia**, Otbi Bouguenina^a, Ali Meksi^b, Khaled Benmahdi^b, Khaled Bendahane^a, Mohamed Sadoun^b

^a Centro Universitario Nour Bachir, Departamento de Ciencias y Tecnología, El Bayadh, República Argelina Democrática y Popular

^b Universidad Mustapha Stambouli, Facultad de Ciencias y Tecnología, Departamento de Ingeniería Civil, Laboratorio para el Estudio de Estructuras y Mecánica de Materiales, Mascara, República Democrática y Popular de Argelia

CAMPO: ingeniería mecánica, materiales
TIPO DE ARTÍCULO: artículo científico original

Resumen:

Introducción/objetivo: El análisis dinámico de la respuesta sísmica de una presa de bóveda de hormigón es un problema complejo en el que la representación del comportamiento del material requiere alguna forma de modelo no lineal, especialmente si el hormigón está sometido a una carga de tensión significativa del suelo. En el caso de grandes movimientos de estos últimos, se pueden formar grandes grietas en algunas zonas de la presa, especialmente en la base de la presa y cambios casi repentinos en la geometría

Métodos: Este análisis se basó en una simulación numérica del efecto dinámico. Este trabajo se realizó mediante el método de elementos finitos con el programa ANSYS 12.1. La presa fue modelada en dos dimensiones. Se realizaron cuatro tipos de análisis: análisis estático, análisis modal, análisis sísmico bajo excitación de dos acelerogramas (Asnam 1980 y Boumerdes 2003) y análisis espectral.

Resultados: Este análisis mostró la vulnerabilidad de la presa de Brezina al terremoto de Boumerdes con altas tensiones en la base de la estructura.

Conclusión: A partir de este estudio se concluyó que, si la presa de Brezina sufre un terremoto de mayor intensidad que el de Boumerdes, éste provocará daños estructurales y grietas que comprometerán la estanqueidad de la presa, así como su durabilidad.

Palabras claves: comportamiento dinámico, método de elementos finitos, fisuración, presa, análisis espectral.

Динамический анализ арочной плотины

Абделkrim Бенахмед^а, корреспондент, Отби Бугенина^а,
Али Мекси^б, Халед Бенмади^б, Халед Бендахане^а, Мухаммед Садоун^б

^а Университетский центр Нур Башир, департамент науки и технологии,
г. д'Эль Баяд, Алжирская Народная Демократическая Республика

^б Университет Туши Мустафы Стамбули,
факультет науки и технологий, кафедра строительства,
Лаборатория исследования структуры и механики материалов,
г. Маскара, Алжирская Народная Демократическая Республика

РУБРИКА ГРНТИ: 55.01.77 Методы исследования и моделирования.
Математические и кибернетические методы,
67.09.33 Бетоны. Железобетон. Строительные
растворы, смеси, составы,
70.17.29 Плотины водохозяйственные и
мелиоративные

ВИД СТАТЬИ: оригинальная научная статья

Резюме:

Введение/цель: Динамический анализ сейсмической реакции бетонной арочной плотины представляет сложную задачу, в которой представление поведения материала требует некоторой формы нелинейной модели, особенно если бетонный фундамент подвергается большой нагрузке. В случае массивных сдвигов грунта на плотине могут образоваться крупные трещины, особенно у ее основания, а также вблизи внезапных изменений геометрии.

Методы: В статье проведен анализ, основанный на численном моделировании динамического воздействия. С помощью программы ANSYS 12.1 применен метод конечных элементов. Плотина была смоделирована в двух измерениях. Были выполнены четыре типа анализа: статический анализ, модальный анализ, сейсмический анализ при возбуждении двух акселерограмм (Аснам, 1980 и Бумердес, 2003) и спектральный анализ.

Результаты: Анализ показал уязвимость плотины Брезина при землетрясении в Бумердесе из-за высокой нагрузки на фундамент сооружения.

Выводы: На основании данного исследования был сделан вывод, что при землетрясении большей интенсивности, чем в Бумердесе плотина Брезина могла бы сильно пострадать. Такое землетрясение могло привести к структурным повреждениям и появлению трещин, которые поставят под угрозу водонепроницаемость плотины, а также ее долговечность.

Ключевые слова: динамическое поведение, метод конечных элементов, трещинообразование, плотина, спектральный анализ.

Динамичка анализа лучне бране

Абделкрим Бенахмед^а, аутор за преписку, Отби Бугенина^а,
Али Мекси^б, Халед Бенмади^б, Халед Бендахане^а, Мохамед Садоун^б

^а Универзитетски центар „Нур Башир“, Одељење за науку и технологију,
Ел Бајад, Народна Демократска Република Алжир

^б Универзитет „Мустафа Стамболи“,
Факултет науке и технологије, Одсек за грађевинарство,
Лабораторија за испитивање структуре и механике материјала,
Маскара, Народна Демократска Република Алжир

ОБЛАСТ: машинство, материјали
КАТЕГОРИЈА (ТИП) ЧЛАНКА: оригинални научни рад

Сажетак:

Увод/циљ: Динамичка анализа сеизмичког одговора лучне бране од бетона представља сложен проблем где представљање понашања материјала захтева неки облик нелинеарног модела, нарочито ако је бетон изложен великом оптерећењу темељне површине. У случајевима када долази до масивних померања тла, велике прслине могу да се формирају на брани, нарочито у њеној основи, као и у близини изненадних промена у геометрији.

Метод: Ова анализа је заснована на нумеричкој симулацији динамичког одговора. Рад се заснива на коришћењу методе коначних елемената помоћу програма ANSYS 12.1. Брана је моделована у две димензије. Коришћене су четири врсте анализа: статичка анализа, модална анализа, сеизмичка анализа са побудом два акцелерограма (Аснам 1980 и Бумердес 2003) и спектрална анализа.

Резултати: Ова анализа указала је на рањивост бране Брезина од земљотреса јачине оног у Бумердесу са великим оптерећењима на темељ структуре.

Закључци: На основу ове студије закључено је да би земљотрес веће јачине од оног у Бумердесу изазвао структурна оштећења и прслине на брани Брезина који би угрозили њену водонепропусност и трајност.

Кључне речи: динамичко понашање, метод коначних елемената, формирање прслина, брана, спектрална анализа.

Paper received on: 14.10.2023.

Manuscript corrections submitted on: 25.09.2024.

Paper accepted for publishing on: 26.09.2024.

© 2024 The Authors. Published by Vojnotehnički glasnik / Military Technical Courier (www.vtg.mod.gov.rs, втг.мо.уип.спб). This article is an open access article distributed under the terms and conditions of the Creative Commons Attribution license (<http://creativecommons.org/licenses/by/3.0/rs/>).



REVIEW PAPERS

Dark sides of deepfake technology

Sanela Z. Veljković^a, Milica T. Ćurčić^b, Ilija P. Gavrilović^c

^a University of Belgrade, 'Vinča' Institute of Nuclear Sciences - National Institute of the Republic of Serbia, Belgrade, Republic of Serbia, e-mail: sanela.veljkovic@vin.bg.ac.rs, **corresponding author**, ORCID iD: <https://orcid.org/0009-0003-3650-290X>

^b University of Belgrade, 'Vinča' Institute of Nuclear Sciences - National Institute of the Republic of Serbia, Belgrade, Republic of Serbia, e-mail: milica.curcic@vin.bg.ac.rs, ORCID iD: <https://orcid.org/0000-0002-4326-4036>

^c University of Belgrade, Faculty of Political Sciences, Belgrade, Republic of Serbia, e-mail: gavril502323@student.fpn.bg.ac.rs, ORCID iD: <https://orcid.org/0009-0005-1348-1792>

[doi https://doi.org/10.5937/vojtehg72-49630](https://doi.org/10.5937/vojtehg72-49630)

FIELD: computer science, IT, security, artificial intelligence
ARTICLE TYPE: review paper

Abstract:

Introduction/purpose: Artificial intelligence can be used for both positive and negative purposes. In recent years, the use of deepfake technology has attracted significant attention. Deepfake technology replaces a person's face and creates events that never happened. While the use of deepfake was more noticeable in the past, the technology has advanced so rapidly that today it is impossible to determine if the content is fake or not. As a result, there is erosion of trust in the media and political institutions, manipulation of public discourse, as well as the spread of disinformation and fake news. The aim of this work is to examine the methods of creating deepfake content and explore the possibilities for detecting such content. A special focus is placed on investigating the dark side of deepfake technology, i.e., the negative purposes for which deepfake technology can be used.

ACKNOWLEDGMENT: This work was carried out within the scientific research activities of the 'Vinča' Institute of Nuclear Sciences - National Institute of the Republic of Serbia, funded by the Ministry of Science, Technology, and Innovation, grant number 451-03-66/2024-03/ 200017.

Methods: Through the use of literature review methods and content analysis, this work has provided a systematization of knowledge about deepfake technology, as well as an analysis of relevant data in this field regarding the potential misuse of deepfake technology. Deepfake technology and its use are viewed from a security perspective, i.e., how the use of these technologies can pose a social hazard. Future research should be designed to be multidisciplinary, integrating knowledge from social sciences (security, sociology, psychology) and technical sciences (information technology).

Results: The results of this research show that in a positive context, the use of deepfake is associated with medicine, the film industry, entertainment, and creative endeavors. However, deepfake is often used to create pornographic content, revenge porn, fake news, and various types of fraud.

Conclusion: Deepfake technology is neutral in the sense that the purpose of its use depends on the individual creating the content. The use of both artificial intelligence and deepfake technology raises complex legal and ethical questions. Although there is noticeable potential for societal improvement offered by these technologies, deepfake technology simultaneously poses a serious risk to human rights, democracy, and national security. Therefore, the misuse of deepfake technologies represents a social hazard for the entire population of any country. Women are particularly vulnerable due to the possibility of creating pornographic content and revenge porn using deepfake technology, although victims of this act can also be men.

Key words: deepfake, pornographic content, cyber violence, scams, fake news.

Introduction

Results of technical and technological progress often provoke certain resistance and apprehension among people, and in that regard, the development and potential application of artificial intelligence in everyday life is no exception. In society, demands for the prohibition of using artificial intelligence are increasingly heard, mostly due to the fear of losing jobs that could be replaced by this technology. In the 1990s, with the emergence of the Internet, people were concerned about the possibilities it offered. However, over time, they adapted, and many began to use the Internet not only for business but also for other purposes. The use of the Internet has facilitated people's lives by providing a lot of information that was not previously available. Today, that fear has been replaced by the fear of artificial intelligence. One of many examples is the emergence of ChatGPT, or language processing artificial intelligence models. This program is capable of understanding written and spoken human language,

as well as established rules of communication that enable it to understand posed questions and provide answers. However, the way this program will be used depends on the individual using it. The same goes for deepfake technology.

The development of deepfakes began with harmless filters on social media that allowed people to replace their friend's or family member's face with their own. These filters, although of low quality, caused immense enthusiasm among users of various social platforms. In the following years, other applications offering different possibilities emerged. The result of the development of this deepfake technology is that today it is impossible to determine whether the content is fake or not (Botha & Pieterse, 2020, p.62). This situation has led to numerous abuses of this technology, and its use is estimated to have negative consequences not only for individuals but also for the national security of states. Moreover, "products and services based on artificial intelligence technology have the potential to undermine human rights, democracy, and the rule of law" (Prlja et al, 2022, p.125). States are concerned about the spread of fake news and the creation of events that never happened, raising questions about new models of abuse of this future technology. On the other hand, the faces of many famous actresses and celebrities have been used to create deepfake pornographic video content.

The societal danger of this phenomenon stems from the fact that not only individuals in the public sphere are at risk, but anyone can become a victim of the use of this technology. Deepfake technology is easily accessible, and the costs of its use are minimal, almost conditioned solely by the motivation and knowledge of the individual abusing these technologies, while the consequences can be significant and serious. Therefore, in the first part of the paper, the development and functioning of deepfake technology will be presented, as well as the possibilities of detecting such content. In the second part of the paper, the dark sides of the use of deepfake technology will be presented in the form of creating pornographic content, revenge porn, fake news, as well as the possibilities of using this technology to carry out various types of scams.

Definition and characteristics of deepfake technology

The use of deepfake technology is conditioned by the technological advancement of information technologies, hence it does not have a long lifespan. These are new technologies, so the definitions of this type of technology date back only a few years. "Deepfake is a medium, usually video, but can also be just audio, or a combination of both - which is altered

using artificial intelligence and machine learning techniques" (Grothaus, 2021, p.1). Deepfake technology involves placing the face of one person onto the body of another (Mania, 2024, p.1). The goal of using this technology is to create events that never actually happened. Deepfake refers to "an image, sound, or other material that is entirely or partially created, or an existing image, sound, or other material that is manipulated using advanced technical means, and is difficult or impossible to distinguish from authentic material" (Van der Sloot & Wagenveld, 2022, p.4). There are two methods of creating deepfake content - autoencoders and generative adversarial networks (GANs). The development of deepfake technology has been almost fantastic over just a few years since its emergence. As Grothaus explains, when GANs were first created, it took hundreds or thousands of images of a person's face to achieve a convincing deepfake. By 2015, when the first deepfake application for smartphones, Face Swap Live, was released, face swapping could be done in real-time via the phone's camera, although the results were far from perfect. However, by 2020, deepfake technology on smartphones had advanced to the point where an application like Reface could create a realistic deepfake based on just one image of a person's face and then place that person into scenes from Hollywood movies with barely noticeable differences (Grothaus, 2021, p.26). Further development of deepfake technology raises concerns about distinguishing between fake and real content.

The compound word "deepfake" is formed by combining the English words "deeplearning" and "fake" (Vatreš, 2021, p.562). While "fake" translates as false, "deeplearning" is used in the IT world to denote deep learning, which is actually "a type of machine learning - one of the basic techniques that drives artificial intelligence. Deep learning is a key tool in the field of computer vision, where computer systems are tasked with identifying subjects in videos and photographs, and is used in everything from self-driving car systems and facial recognition systems to applications on smartphones that automatically tag owner's friends in pictures" (Grothaus, 2021, p.3). The first method of creating deepfake content relies on autoencoders. They represent a type of artificial neural network used for learning efficient data encoding, with two learning functions: an encoding function that transforms input data and a decoding function that recreates the input data from the encoded representation. In the case of generative adversarial networks, two neural networks compete against each other in a zero-sum game, where one network's gain is the other's loss. In the first technique, there is an encoder that extracts latent facial features from the image and a decoder that is used to reconstruct the facial

image, both using the same network that finds and learns similarities between two sets of facial images such as the position of eyes, nose, and mouth (Nguyen et al, 2022, p.3). In the GAN technique, there are two neural networks, a generator capable of producing images, and a discriminator whose role is to distinguish fake images from real ones (Nguyen et al, 2022, p.5). The techniques for creating deepfake content mentioned are illustrated in the following figures, where Figure 1 refers to the technique using autoencoders, while Figure 2 depicts the functioning of generative adversarial networks (GANs).

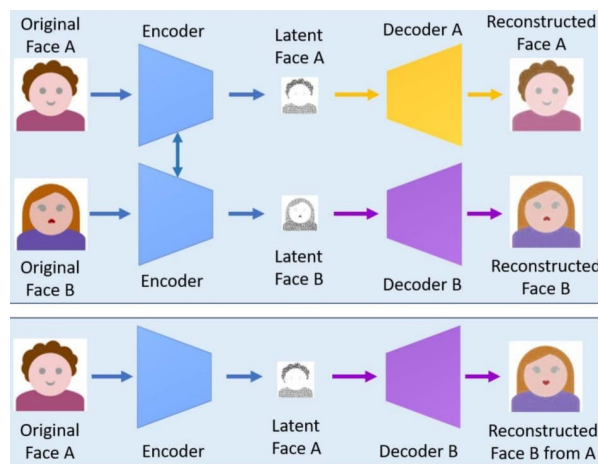


Figure 1 – Method of creating deepfake content through autoencoders (Nguyen et al, 2022, p.3)

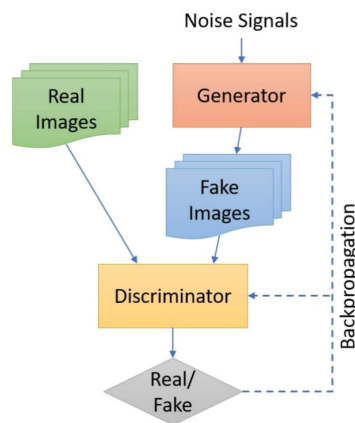


Figure 2 – Method of creating deepfake content using GANs (Nguyen et al, 2022, p.5)

Meskys et al. explain that the key idea of GANs is for the generator to try to generate images that would deceive the discriminator into believing they are real, while the central idea for autoencoders is for the encoder to try to encode the input image as a small vector, and the decoder to try to decode this small vector into the original image (Meskys et al, 2020, p.4). The GAN technique is a better version for creating deepfakes than autoencoders because its results are much more realistic. In this technique, two neural networks play the roles of a forger and an inspector, where "each time the AI inspector labels a fake photo as fake, the AI forger inspects aspects of that forgery, which naturally were not good enough to fool the AI inspector, analyzes a set of authentic photos, identifies what is different about them, and then tries again to fool the AI inspector with another, improved forgery" (Grothaus, 2021, p.4). Despite the possibilities offered by using GAN technology to create deepfake content, what is particularly concerning from a security perspective is that with the development of the technology, the number of photos needed to create fake content has decreased over time. This further indicates that not only politicians and celebrities are at risk but also every individual, given that almost everyone readily shares their photos on social media today. Moreover, the accessibility of deepfake technology is alarming, as extensive knowledge of information technology is not necessary to create fake content. This raises the question of who can create deepfake content, and the answer is that anyone with motivation and a smartphone can do so. In the literature, four groups of actors are usually distinguished: communities composed of individuals for whom this is a hobby; political players such as foreign governments and various activists; malicious actors aiming to carry out various types of scams; and legitimate actors such as television companies (Westerlund, 2019, p.41).

Despite the presence of various legitimate actors and many positive purposes, the use of deepfakes is most commonly perceived as a threat to state security and the stability of the political system. The reasons are numerous, among which stand out: pressure on journalists struggling to distinguish real news from fake; national security is compromised by the spread of propaganda and interference in elections; citizens' trust in information coming from authorities is undermined; and questions about internet security for individuals and organizations arise (Westerlund, 2019, p.42). However, it should be borne in mind that the purpose of using any technology, including deepfake technology, is determined by the individual using that technology. The fact that tools, as well as technology in general, do not inherently carry essence or value is especially evident when Grothaus emphasizes that moral judgment can only be made about the

person who used the technology in a certain way. As an example, he cites the use of an airplane, which can be used as a tool for evacuating civilians from areas affected by natural disasters or as a tool for demolishing buildings. This confirms the hypothesis that the airplane as a form of technology is neutral in both cases, and it is the human who determines its purpose according to the given situation of use (Grothaus, 2021, p.25). Such perception can also be applied in the case of using deepfake technology. However, since there will always be individuals who will use this technology for negative purposes, the next section of the paper presents certain possibilities for detecting deepfake content.

Possibility of detecting deepfake content

For a short period, deepfake technology has evolved and been able to correct earlier flaws, which makes detecting fake content more difficult. There are numerous artificial intelligence tools used for detecting deepfake content. However, the problem with this approach lies in establishing a feedback loop between two groups of artificial intelligence. Namely, when a detection deepfake finds a new indicator revealing that content is fake, the deepfake creating that content learns how to correct the flaws and deceive the detection deepfake (Grothaus, 2021, p.223). In the literature, examples of different methods for detecting deepfake content can be found. According to one group of authors, detection methods include facial recognition such as tracking eye blinks, eye color, and dental flaws; multimedia forensics that interpret parameters such as pixel correlation, image continuity, and lighting; applying watermarks that allow identification of alterations; as well as convolutional neural networks working on machine learning principles enabling the detection of fake content through powerful image analysis functions (Albahar & Almalki, J, 2019, pp.3247-3248). On the other hand, some authors have classified methods for detecting fake content into general network-based methods; methods based on temporal consistency; methods based on visual artifacts; methods based on camera fingerprints; and methods based on biological signals. These methods are illustrated in Table 1.

Considering the variety of methods for detecting deepfake content proposed by different authors, it seems that there is no problem with their detection. However, given the short period in which deepfake technology has managed to overcome previous shortcomings, there remains a fear that in the future it will not be possible to distinguish deepfake content from genuine content. Today, "although you may be able to prove that a video is a deepfake, you can never prove with absolute certainty that the video

is not a deepfake" (Grothaus, 2021, p.2017). In this regard, new scientific research on deepfake technology mainly focuses on two levels of harm, specifically on: "individual harm to the dignity and emotional well-being of subjects of deepfake recordings, and broader societal harm that includes threats to national security and democratic institutions" (Kugler & Pace, 2021, p.623). Deepfake technology does not possess essence; rather, its manner of use is determined by the individual employing it. In a positive context, the use of deepfake technology is associated with medicine, the film industry, entertainment, and creative expression. However, it is essential to emphasize the impact that deepfake technology can have on each individual as well as on the state if used for negative purposes.

Table 1 – Methods of detecting deepfake content (Marković, 2022, pp.33-34).

Methods	Description
General network-based methods	In this method, detection is considered a frame-level classification task ending with a Convolutional Neural Networks.
Methods based on temporal consistency	It has been determined that there are inconsistencies between adjacent frames in deepfake videos due to flaws in the falsification algorithm. Therefore, Recurrent neural network is applied to detect such inconsistencies.
Methods based on visual artifacts	Mixing operations in the generation process would cause substantial deviations in the image within the blending boundaries. Methods based on Convolutional Neural Networks are used to identify these artifacts.
Methods based on camera fingerprints	Due to the specific generation process, devices leave different traces on captured images. At the same time, it is acknowledged that faces and background images come from different devices. Therefore, the detection task can be completed using these traces.
Methods based on biological signals	GANs find it difficult to understand the hidden biological signals of faces, which complicates the synthesis of human faces with reasonable behavior. Based on this observation, biological signals are extracted to detect fake video clips.

Possibilities of abusing deepfake technology

The availability and ease of use of deepfake technology results in every individual possibly discovering that their face has been exploited to create deepfake pornographic content. Moreover, every individual may find themselves in a situation where they receive a deepfake video via email, featuring their face, showing actions that never actually occurred, potentially intended for blackmailing the person depicted. This raises questions about human perception, questioning whether one can trust their eyes and ears when watching a video of a politician discussing important international, regional, and national issues. Lastly, each of us could fall victim to identity theft and various other scams that are now feasible due to the advancement of deepfake technology. In the following section, the dark side of deepfake technology is presented, namely the potential for its misuse by individuals who employ it. Primarily, the use of deepfakes to create pornographic content is highlighted, as well as how the development of this technology has resulted in any woman becoming a potential victim of deepfake technology. Additionally, as a result of the development of this technology and the inability to distinguish between fake and authentic content, various forms of cyberbullying and the spread of fake news are possible. Thanks to deepfakes and their widespread availability, identity theft is now possible not only in the form of stealing someone's face but also their voice.

Pornographic content

The use of deepfakes to create pornographic content featuring famous and well-known personalities is often cited as one of the primary negative uses of this technology. The integrity of numerous actresses, singers, and other famous women became compromised when the first pornographic deepfake video content was created. In the early years, it was not possible to prove the misuse of the technology and thus demonstrate the falsehood of such posts, and the videos were further distributed over the Internet, creating the illusion that they depicted real events. The creation of deepfake pornography using the face of a famous individual poses several problems. Firstly, neither the famous personality whose face is used in the video nor the person whose body is used has given consent for the creation of this type of content (Grothaus, 2021, p.70). On the other hand, even though these videos feature famous personalities and are widespread on the Internet, the creators of such content fail to consider the consequences it may have on the individual. It seems that despite crossing many ethical boundaries, the creators of such

content have certain rules when making fake pornographic videos. These rules are as follows: there are no fake images or videos of any famous personality under the age of 18, and there are no fake images or videos of any famous personality over the age of 18 using their face or body from images or videos taken when they or the donor body were under 18 years old (Grothaus, 2021, p.86). Of course, this does not justify the creation of fake pornographic content using the face of a famous personality over 18 years old. Research indicates that pornographic deepfake content mainly elicits negative emotions among online users. Anger, disgust, and contempt are typically reported as responses to this type of content (Wang & Kim, 2022, p.7). However, in the following years, the development of deepfake technology has resulted in not only famous and prominent individuals but also any person worldwide being potentially subjected to victimization.

DeepNude was the first software specifically aimed at any female individual, not just famous and well-known women, by enabling the removal of clothing from images and creating fake content that could then be shared via the internet and social media (Grothaus, 2021, p.97). This software provided the opportunity for one individual to easily harm another person, facilitated by the fact that people willingly share their pictures on various social media platforms today. Nowadays, the availability of photographs is not a problem because we all readily share our pictures on numerous social media platforms. However, DeepNude was not the only weapon against women. In 2020, the company Sensity released a shocking report revealing that "all it took for anyone who wanted to create 'deepfake' women was to send a photo of the victim to a chatbot in the popular Telegram messaging application. The bot would then undress the woman and send a fake nude photo to the person who requested it" (Grothaus, 2021, p.98). A vast number of women fell victim to this situation, with their faces being used on naked bodies generated by artificial intelligence. Many of them were unaware that their faces were being used in this way by colleagues, friends, or acquaintances. Moreover, there was the possibility of paying a fee to remove the watermarks from the fake nude images created by the bot (Grothaus, 2021, p.99). This is particularly concerning because if a victim's photo were to surface, they would not be able to prove that the image resulted from the use of deepfake technology. Although the integrity of every individual can be compromised through the use of artificial intelligence, practice has shown that women are a more vulnerable category, given the societal danger posed by this threat. Despite the stated use of DeepNude, today the software is used from images of men and women to images of animals and even objects.

The importance of a watermark lies in the fact that it indicates that the content is fake. However, the problem arises with the possibility of removing the watermark before sharing the image with other users via the Internet (Grothaus, 2021, p.101). The possibility of removing watermarks puts the victim of this technology's use in a particularly difficult position, making it challenging to prove that the content is false. Additionally, removing watermarks from images or videos produced by artificial intelligence is problematic in the context of revenge porn. An individual wishing to harm another can easily do so using deepfake technology. The ease of abusing deepfake technologies for pornographic purposes, as well as the significant, often irreparable consequences of publishing such content on the Internet, make these technologies particularly dangerous. Furthermore, most people are unaware of the existence of such technologies, so they interpret such content as authentic, further stigmatizing the victims. Such a situation can "erode trust, leading individuals to question the legitimacy of visual and auditory content, which further results in increased skepticism and confusion" (Wazid et al, 2024, p.2). This not only compromises the victim's privacy but also their mental health, deepening this negative social phenomenon.

Cyber violence

With the development and further refinement of deepfake technology, the possibility has emerged for fake content to be used as a means of extortion. "The most obvious example of this is the scenario in which someone creates 'deepfake' targets but does not publish the 'deepfake' publicly. Instead, the 'deepfaker' sends the target themselves in 'deepfake.' They might show the target physically or sexually assaulting someone or engaging in taboo sexual acts. The goal here is not to deceive the target into thinking it is real—because they know it is not. Instead, the aim is to induce anxiety, fear, and concern in the target that others might believe it is real if the 'deepfake' were publicly released" (Grothaus, 2021, p.115). These activities can leave serious negative consequences for the victim, and such behavior represents a form of cyber violence. Deepfake videos may not only contain sexual scenes that never occurred; today, there is a "threat that people will be implicated in 'deepfakes' showing them committing crimes they did not commit" (Grothaus, 2021, p.113). The impact this would have on the potential victim depends on numerous factors, but the consequences are immense in any case. Given the increasingly common cases of malicious software (ransomware) being used to block access to data on a computer until a ransom is paid, there is now the possibility of using deepfake ransomware. This software

operates as follows: instead of encrypting an individual's data to restrict access, it first analyzes the data on the computer to learn the user's identity. It then searches for publicly available images or videos of the person on the Internet or the computer itself and uses those media files to create a "deepfake" version of that person in an embarrassing situation. The ransomware would then display this "deepfake" version of the individual on the screen with a visible countdown timer. If the timer expires before the ransom is paid, the "deepfake" version of that person will be publicly released (Grothaus, 2021, p.117). The current development of technology has also enabled discussions about deepfake resurrections, referring to content featuring a deceased individual who appears to be alive and speaks or acts as the content creator desires (Lu & Chu, 2023).

Adults engage in creating deepfake content for various reasons, with women being a particularly vulnerable group. The question arises as to what the situation would look like if children and young people used this technology for cyberbullying. Children quickly adopt new technologies, having access to the Internet and various applications on their mobile phones. The use of deepfake technology does not seem complicated; on the contrary, it is widely available and easy to use because the software does most of the work for the user. It can be concluded that while in the 1990s, peer violence usually ended at the end of the school day, today, with the Internet, smartphones, and social media, victims of peer violence often have no respite from abuse. Peer violence has become digital in the 21st century and can be relentless, following people at all times, and attacking them anytime. Now, thanks to deepfake technology, it can be even more drastic than ever before (Grothaus, 2021, p.19). Although such events have not yet occurred, it is necessary to avoid such scenarios in the future because it cannot be assumed how detrimental they could be to the development of children and young people. Moreover, considering the short time in which deepfake technology has significantly advanced in eliminating previous shortcomings, we can speculate about what the future may hold.

Fake news

Creating fake content on the Internet is not a novelty. The faces of politicians have been previously used to create entertaining content. Today, with the development of deepfake technology, we find ourselves in a situation where we are not sure if the content is fake or not. In this regard, it is necessary to differentiate between shallowfake and deepfake content. Although they have the same goal, unlike deepfakes, which rely on deep machine learning techniques, shallowfakes rely on traditional editing tools

and manual work to alter existing media. They are often called 'cheapfakes' because, due to the required manual editing and human editing skills, some of them may look cheaply made if the creator lacks the necessary expertise in graphics and video editing (Grothaus, 2021, pp.39-40). Therefore, due to the numerous shortcomings of shallowfake content, it is much easier to conclude that it is fake. As Marković and Dimovski emphasize, given the advancement of deepfake technology, "governments worldwide are concerned that material obtained using these applications could be used to undermine national security, spread political propaganda, and disrupt electoral campaigns" (Marković & Dimovski, 2023, p.299). In earlier deepfake videos, there were flaws based on which the observer could conclude that it was fake, which is not the case today. Today, "deepfake video technology - AI techniques for creating real video footage of fake events, often with real people saying things they never actually said - is being used for political purposes" (Schneier, 2021, p.16). This can result in enormous consequences for society and state institutions. "Deepfake videos can have deep negative consequences for democracies: fake news created by deepfake videos may aim to tarnish the reputation of certain individuals, portray false events (e.g., fake terrorist attacks), or influence democratic processes such as election campaigns or other socially significant events" (Meskys et al, 2020, p.8). Faces of many politicians worldwide have been used to create deepfake content, causing concern for many governments. Precisely because of the quality of today's deepfake videos featuring certain influential politicians saying things they never actually said, some countries fear the potential consequences of fake content.

Some political leaders around the world have started using deepfake technology for propaganda purposes, both among the population of their own country and among the populations of other countries. The dangers of propaganda are numerous, as the consequences of using deepfake technology as a geopolitical tool are immeasurable (Grothaus, 2021, p.206). Deepfake technology can be a powerful weapon for causing instability in certain states and regions. Moreover, this technology can be used during international conflicts to: legitimize war; fabricate orders; create confusion; divide armies; undermine support; polarize society; divide allies; and discredit leaders (Byman et al, 2023, pp.6-8). It seems that it has never been easier to disseminate false information and content than it is today. All of this leads us to question whether we can trust our eyes and ears. "We will soon live in a world where we have to wonder 'is it real?' about everything because we will no longer be able to believe that the photos we see, the videos we watch, and the sound we hear are

authentic representations of facts. Even now, with every passing month - just months - deepfake algorithms are becoming increasingly polished and powerful" (Grothaus, 2021, pp.214-215). In the coming years, there is a possibility that deepfake technology will advance to the point where it will be impossible to determine whether the content is fake by any detection method. Research shows that people are overly confident in their ability to detect fake and deepfake content, yet in practice, this is often not the case (Köbis et al, 2021). The availability of deepfake technology, as well as the simple process of creating fake content, already has enormous negative consequences for human rights, democracy, society, state institutions, and national security. From this perspective, what awaits in the future seems daunting considering the speed of deepfake technology development.

Frauds

In the world, there have already been cases of using deepfake technology to carry out certain types of fraud. Due to the possibilities offered by this technology, identity theft is no longer an unexpected phenomenon. Today, there is a significant shift toward biometric authentication for security verifications, and the goal of deepfake content creators is to appear as somebody else to deceive biometric systems (Grothaus, 2021, p.117). With the development of deepfake technology, the creator of deepfake content does not necessarily have to use only someone's face but also their voice. This is not an unexpected occurrence in today's world. The creator of deepfake content can perpetrate numerous scams by using someone else's face or voice. Many applications today require verification in the form of your picture or a recording of your voice. Images are usually available on numerous social media platforms and can easily be abused for these purposes. However, although faking someone else's voice may seem like a slightly bigger problem, that is not the case. Every recording of your voice or the potential availability of your video recordings on social media is what the deepfake content creator needs. After successfully cloning your voice, based on a minute or less of recording, the deepfake creator will be able to create a fake recording of you saying whatever they want you to say (Grothaus, 2021, p.120). There are two main methods for creating deepfake speech: text-to-speech synthesis (which uses written text to produce synthesized speech that sounds like a specific person) and voice conversion (which uses the original voice uttering the desired phrase and a target voice, and the output is the original phrase spoken by the target voice) (Firc et al, 2023, p.14). Identity theft in the form of stealing your face and voice is not the only type of fraud that deepfake content creators can carry out in today's world.

Frauds can be directed toward both individuals and various companies, financial markets, central banks, and financial regulators (Bateman, 2020). Certain attacks that have used deepfake technology and were carried out in the past few years with the aim of gaining huge financial gains are presented in Table 2.

Table 2 – Deepfake attacks launched for financial gain (Kshetri, 2023, p.91).

Year	Victim and location	Type of attack	Amount scammed
2019	Californian women	Deepfake videos	About US \$300,000
2019	United Kingdom-based energy company	Vishing	US \$234,000
2020	A United Arab Emirates bank	Deepfake voice technology	>US \$35 million
2018-2021	Japanese Manga artist	Deepfake videos	>US \$500,000

In a comparative perspective, there is a noticeable disproportion between different types of attacks and the targets that have been subjected to these attacks. Vishing, the technique of using fake phone calls to deceive victims and obtain sensitive information, was used during 2019, with the target being an energy company based in the United Kingdom. On that occasion, the perpetrators gained a profit of \$234,000. On the other hand, the target of the fraud, with a total profit exceeding \$35 million, was a bank in the United Arab Emirates, and the means used to achieve the goal was deepfake voice technology. The use of deepfake technology may not necessarily be aimed at gaining financial profit but can result in reputational damage and loss of trust among stakeholders (Mustak et al, 2023, p.12). Often, malicious software (ransomware) is used to block access to data on a computer until a ransom is paid. Numerous hospitals and healthcare facilities worldwide have been targeted by hackers using this software. This prevents healthcare workers from accessing medical records and other vital patient health-related data. In addition to the potential use of malicious software for various types of extortion and forms of cyber violence, there is also the possibility of using deepfake technology to manipulate CT (computerized tomography) scans. 'Researchers have found that deepfake technology can be used to generate CT-quality images of internal organs that a hacker can then insert into a patient's medical records - replacing authentic CT scans with

deepfaked CT scans' (Grothaus, 2021, p.125). There are several reasons for such types of fraud: the hacker wants to inflict psychological or emotional stress on a specific individual; the hacker does this to gain money and a competitive advantage; and finally, the hacker may compel the doctors of a particular patient to perform a risky operation to try to alleviate the problem, thereby endangering the patient's life (Grothaus, 2021, p.126). Although these cases may seem extreme, they are not impossible today precisely because of the development and availability of deepfake technology. The technology, while neutral in itself, can be abused in various ways depending solely on the individual using it. However, assuming that the development of this technology will continue in the future, with further refinement, there remains a fear of the various other ways malicious individuals worldwide may exploit it.

Conclusion

As an integral part of artificial intelligence, deepfake technology is causing concern among individuals and states worldwide. Despite its positive applications, deepfake technology is often used for negative purposes. The creation of deepfake content impacts the human rights of individuals, national security, and the political systems of countries. Fake videos can cause instability in certain countries and regions. The faces of politicians are used to create fake content and events that never actually happened. Likewise, the faces of famous actresses and celebrities have been used to create pornographic video content that circulates widely on the Internet. With the development of deepfake technology, every person is at risk because this technology allows faces to be used on artificially generated nude bodies. Although every individual is at risk, based on previous practice, it can be concluded that women are a particularly vulnerable and endangered category. Privacy is seriously compromised, and the consequences for victims are immeasurable from various perspectives. Everyone's photos are publicly available on social media and other platforms, resulting in anyone potentially becoming a victim. While it once required a vast number of photos to create fake content, today only one is needed. People's safety is compromised as the development of deepfake technology has provided opportunities for numerous scams. Identity theft is now more possible than ever in history.

A deepfake creator can not only steal someone's face but also someone's voice. It is not just individuals at risk on an individual level, but also countries, various companies, and financial institutions. In recent years, scams have occurred worldwide due to the development of

deepfake technology, targeting both individuals and companies. Furthermore, the use of malicious software and deepfake technology can result in various forms of extortion representing a form of cyberattack. Although there are different methods of detecting deepfake content, it is difficult to prove that a video was created using this technology. It is challenging to trust our eyes and ears in a world where manipulation of public discourse is widespread. Previously, it was possible to detect certain irregularities in a video and realize that the content was fake. Since 2014 and the development of GAN techniques, deepfakes have become more realistic, making it difficult to determine whether the content is true or not. The technique works by improving itself and eliminating flaws, resulting in fantastic results. What should always be kept in mind is that deepfake technology is neither inherently good nor bad. Its usage depends on the individual employing it. However, given that deepfakes are now being used for various negative purposes, the question arises: what can be expected in the future? Therefore, for a comprehensive approach to this researched problem, it is recommended that future research be of a multidisciplinary nature, incorporating not only security but also an information technology approach.

References

Albahar, M. & Almalki, J. 2019. Deepfakes: Threats and countermeasures systematic review. *Journal of Theoretical and Applied Information Technology*, 97(22), pp.3242-3250 [online]. Available at: <https://www.jatit.org/volumes/Vol97No22/7Vol97No22.pdf> [Accessed: 02 March 2024].

Bateman, J. 2020. *Deepfakes and synthetic media in the financial system: Assessing threat scenarios* [e-book]. Washington: Carnegie Endowment for International Peace. Available at: https://carnegieendowment.org/files/Bateman_FinCyber_Deepfakes_final.pdf [Accessed: 21 January 2024].

Botha, J. & Pieterse, H. 2020. Fake News and Deepfakes: A Dangerous Threat for 21st Century Information Security. In: *Proceedings of the 15th International Conference on Cyber Warfare and Security*, Norfolk, Virginia, USA, pp.57-67, March 12-13.

Byman, D.L., Gao, C., Meserole, C. & Subrahmanian, V.S. 2023. *Deepfakes and international conflict* [e-book]. Washington: Brookings Institution. Available at: https://www.brookings.edu/wp-content/uploads/2023/01/FP_20230105_deepfakes_international_conflict.pdf [Accessed: 21 January 2024].

Firc, A., Malinka, K. & Hanáček, P. 2023. Deepfakes as a threat to a speaker and facial recognition: An overview of tools and attack vectors. *Heliyon*, 9(4), e15090. Available at: <https://doi.org/10.1016/j.heliyon.2023.e15090>.

Grothaus, M. 2021. *Trust No One: Inside the World of Deepfakes*. London, UK: Hodder Studio. ISBN: 9781529347982.

Köbis, N.C., Doležalová, B. & Soraperra, I. 2021. Fooled twice: People cannot detect deepfakes but think they can. *iScience*, 24(11), art.number:103364. Available at: <https://doi.org/10.1016/j.isci.2021.103364>.

Kshetri, N. 2023. The Economics of Deepfakes. *Computer*, 56(8), pp.89-94. Available at: <https://doi.org/10.1109/MC.2023.3276068>.

Kugler, M.B. & Pace, C. 2021. Deepfake Privacy: Attitudes and Regulation. *Northwestern University Law Review* 611, *Northwestern Public Law Research Paper No. 21-04*. Available at: <https://doi.org/10.2139/ssrn.3781968>.

Lu, H. & Chu, H. 2023. Let the dead talk: How deepfake resurrection narratives influence audience response in prosocial contexts. *Computers in Human Behavior*, 145, art.number:107761. Available at: <https://doi.org/10.1016/j.chb.2023.107761>.

Mania, K. 2024. Legal Protection of Revenge and Deepfake Porn Victims in the European Union: Findings From a Comparative Legal Study. *Trauma, Violence, & Abuse*, 25(1), pp.117-129. Available at: <https://doi.org/10.1177/15248380221143772>.

Marković, D. 2022. *Detektovanje manipulacije u video snimcima stvorenih „deepfake“ tehnikom sistemom učenja prostorno vremenskih karakteristika*. PhD thesis. Belgrade: Singidunum University [online]. Available at: <https://nardus.mpn.gov.rs/handle/123456789/20763> (in Serbian) [Accessed: 02 March 2024].

Marković, E. & Dimovski, D. 2023. Deepfake as a new form of crime. In: *XII International conference on social and technological development*, Trebinje, Republic of Srpska, Bosnia & Herzegovina, pp.296-308, June 15-18 [online]. Available at: https://stedconference.com/wp-content/uploads/2024/02/Book-of-Proceedings_STEDC_2023-sa-DOI-brojevima_compressed.pdf (in Serbian) [Accessed: 02 March 2024].

Meskys, E., Liaudanskas, A., Kalpokiene, J. & Jurcys, P. & 2020. Regulating deep fakes: legal and ethical considerations. *Journal of Intellectual Property Law & Practice*, 15(1), pp.24-31. Available at: <https://doi.org/10.1093/jiplp/jpz167>.

Mustak, M., Salminen, J., Mäntymäki, M., Rahman, A. & Dwivedi, Y.K. 2023. Deepfakes: Deceptions, mitigations, and opportunities. *Journal of Business Research*, 154, art.number:113368. Available at: <https://doi.org/10.1016/j.jbusres.2022.113368>.

Nguyen, T.T., Nguyen, Q.V.H., Nguyen, D.Ti., Nguyen, D.Th., Nuynh-The, T., Nahavandi, S., Nygen, T.T., Pham, Q.- V. & Nygen, C.M. 2022. Deep learning for deepfakes creation and detection: A survey. *Computer Vision and Image Understanding*, 223, art.number:103525. Available at: <https://doi.org/10.1016/j.cviu.2022.103525>.

Prija, D., Gasmi, G. & Korać, V. 2022. *Human rights and artificial intelligence* [e-book]. Belgrade: Institute of Comparative Law (in Serbian). Available at: <http://ricl.iup.rs/1295/1/Ljudska%20prava%20i%20ve%C5%A1ta%C4%8Dka%20inteligencija-Prija-Gasmi-Korac.pdf> (in Serbian). [Accessed: 21 January 2024]. ISBN: 978-86-80186-82-5.

Schneier, B. 2021. *The Coming AI Hackers* [e-book]. United States: Harvard Kennedy School, Belfer Center for Science and International Affairs. Available at: <https://www.belfercenter.org/sites/default/files/2021-04/HackingAI.pdf> [Accessed: 21 January 2024].

Vatreš, A. 2021. Deepfake Phenomenon: An Advanced Form of Fake News and Its Implications on Reliable Journalism. *Društvene i humanističke studije DHS (Social Sciences and Humanities Studies)*, 6(3), pp.561-576 (in Serbian). Available at: <https://doi.org/10.51558/2490-3647.2021.6.3.561>.

Van der Sloot, B. & Wagenveld, Y. 2022. Deepfakes: regulatory challenges for the synthetic society. *Computer Law & Security Review*, 46, art.number:105716. Available at: <https://doi.org/10.1016/j.clsr.2022.105716>.

Wang, S. & Kim, S. 2022. Users' emotional and behavioral responses to deepfake videos of K-pop idols. *Computers in Human Behavior*, 134, art.number:107305. Available at: <https://doi.org/10.1016/j.chb.2022.107305>.

Westerlund, M. 2019. The Emergence of Deepfake Technology: A Review. *Technology Innovation Management Review*, 9(11), pp.39-52. Available at: <https://doi.org/10.22215/timreview/1282>.

Wazid, M., Mishra, A.K., Mohd, N. & Das, A.K. 2024. A Secure Deepfake Mitigation Framework: Architecture, Issues, Challenges, and Societal Impact. *Cyber Security and Applications*, 2, art.number:100040. Available at: <https://doi.org/10.1016/j.csa.2024.100040>.

El lado oscuro de la tecnología deepfake

Sanela Z. Veljković^a, **autor de correspondencia**,
Milica T. Ćurčić^a, Ilija P. Gavrilović^b

^a Universidad de Belgrado, Instituto de Ciencias Nucleares 'Vinča' - Instituto Nacional de la República de Serbia, Belgrado, República de Serbia

^b Universidad de Belgrado, Facultad de Ciencias Políticas, Belgrado, República de Serbia

CAMPO: ciencias de la computación, TI, seguridad, inteligencia artificial
TIPO DE ARTÍCULO: artículo de revisión

Resumen:

Introducción/objetivo: La inteligencia artificial puede utilizarse tanto con fines positivos como negativos. En los últimos años, el uso de la tecnología deepfake ha atraído una atención significativa. La tecnología deepfake reemplaza el rostro de una persona y crea eventos que nunca sucedieron. Si bien el uso de deepfake era más notorio en el pasado, la tecnología ha

avanzado tan rápidamente que hoy es imposible determinar si el contenido es falso o no. Como resultado, hay erosión de la confianza en los medios y las instituciones políticas, manipulación del discurso público, así como la difusión de desinformación y noticias falsas. El objetivo de este trabajo es examinar los métodos de creación de contenido deepfake y explorar las posibilidades de detectar dicho contenido. Se pone atención especial en investigar el lado oscuro de la tecnología deepfake, es decir, los fines negativos para los que se puede utilizar la tecnología deepfake.

Métodos: Mediante el uso de métodos de revisión de bibliografía y análisis de contenido, este trabajo ha proporcionado una sistematización del conocimiento sobre la tecnología deepfake, así como un análisis de datos relevantes en este campo con respecto al posible mal uso de la tecnología deepfake. La tecnología deepfake y su uso se analizan desde una perspectiva de seguridad, es decir, cómo el uso de estas tecnologías puede representar un peligro social. Las investigaciones futuras deben diseñarse para ser multidisciplinarias, integrando el conocimiento de las ciencias sociales (seguridad, sociología, psicología) y las ciencias técnicas (tecnología de la información).

Resultados: Los resultados de esta investigación muestran que, en un contexto positivo, el uso de deepfake se asocia con la medicina, la industria cinematográfica, el entretenimiento y los esfuerzos creativos. Sin embargo, deepfake se utiliza a menudo para crear contenido pornográfico, pornografía de venganza, noticias falsas y varios tipos de fraude.

Conclusión: La tecnología deepfake es neutral en el sentido de que el propósito de su uso depende del individuo que crea el contenido. El uso tanto de inteligencia artificial como de tecnología deepfake plantea cuestiones legales y éticas complejas. Aunque estas tecnologías ofrecen un potencial notable de mejora social, la tecnología deepfake supone al mismo tiempo un grave riesgo para los derechos humanos, la democracia y la seguridad nacional. Por tanto, el uso indebido de las tecnologías deepfake representa un peligro social para toda la población de cualquier país. Las mujeres son especialmente vulnerables debido a la posibilidad de crear contenido pornográfico y pornografía vengativa mediante la tecnología deepfake, aunque las víctimas de este acto también pueden ser hombres.

Palabras claves: deepfake, contenido pornográfico, ciberviolencia, estafas, noticias falsas.

Темные стороны дипфейк технологии

Санела З. Велькович^а, **корреспондент**,
Милица Т. Чурчич^а, Илья П. Гаврилович^б

^а Белградский университет, Институт ядерных исследований
«Винча» – Институт государственного значения для Республики Сербия,
г. Белград, Республика Сербия

^б Белградский университет, факультет политических наук,
г. Белград, Республика Сербия

РУБРИКА ГРНТИ: 28.23.00 Искусственный интеллект

ВИД СТАТЬИ: обзорная статья

Резюме:

Введение/цель: Искусственный интеллект можно использовать как в положительных, так и в отрицательных целях. В последнее время использование технологии дипфейк привлекает большое внимание. С помощью технологии дипфейк можно заменить лицо определенного человека и создавать события, которых никогда не было. Раньше использование дипфейков было гораздо заметнее, но технологии за короткий промежуток времени настолько прогрессировали, что на сегодняшний день практически невозможно отличить фейковый контент от настоящего. В результате образовались: эрозия доверия к средствам массовой информации и политическим институтам, возможность манипулирования общественным дискурсом, а также распространение дезинформации и фейковых новостей. Целью данной статьи является изучение способов создания дипфейкового контента, а также исследование возможностей обнаружения такого контента. Особое внимание уделено исследованию темной стороны технологии дипфейк и негативным целям, в которых ее можно использовать.

Методы: На основании тщательного обзора литературы и контент-анализа в данной статье представлена систематизация знаний о технологии дипфейк, а также анализ соответствующих данных в этой области относительно возможности злоупотребления технологии дипфейк. Технологии дипфейк и их использование рассматриваются с точки зрения безопасности, то есть исследуется, насколько они опасны и какую социальную угрозу может представлять использование этих технологий. Рекомендуется, чтобы будущие исследования имели мультидисциплинарный характер, интегрируя знания социальных наук (безопасность, социология, психология) и технических наук (информационные технологии).

Результаты: Результаты данного исследования показывают, что в положительном контексте использование дипфейка

связано с медициной, киноиндустрией, развлечениями и творчеством. Однако дипфейки часто используются для создания порнографического контента, порномести, фейковых новостей, а также для осуществления разных видов мошенничества.

Выводы: Технология дипфейк сама по себе нейтральна в том смысле, что цель ее использования зависит от человека, создающего конкретный контент. Однако использование как искусственного интеллекта, так и технологии дипфейк поднимает сложные юридические и этические вопросы. Хотя потенциал, который эти технологии обеспечивают для улучшения общества, заметен, технология дипфейк одновременно представляет собой серьезный риск для прав человека, демократии и национальной безопасности стран. Ввиду вышеизложенного, недобросовестное использование дипфейковых технологий представляет социальную опасность населения каждой страны в целом. Женщины являются особо уязвимой категорией населения из-за возможности создания порнографического контента и порномести с использованием технологии дипфейк, однако жертвами могут стать и мужчины.

Ключевые слова: дипфейк, порнографический контент, кибернасилие, мошенничество, ложные новости.

Тамне стране дипфејк технологије

Санела З. Вельковић^а, аутор за преписку,
Милица Т. Ђурчић^а, Илија П. Гавриловић^б

^а Универзитет у Београду, Институт за нуклеарне науке „Винча“ –
Национални институт Републике Србије, Београд, Република Србија

^б Универзитет у Београду, Факултет политичких наука,
Београд, Република Србија

ОБЛАСТ: рачунарске науке, ИТ, безбедност, вештачка интелигенција
КАТЕГОРИЈА (ТИП) ЧЛАНКА: прегледни рад

Сажетак:

Увод/циљ: Последњих година употреба дипфејк технологије привлачи огромну пажњу. Њоме се могу креирати лажни ликови као и догађаји који се никада нису десили. Ранијих година била је препознатљива, али је у последње време толико напредовала да је данас немогуће проценити да ли је неки садржај лажан или не. Резултат тога јесте недостатак поверења у медије и политичке институције, могућност манипулесања јавним дискурсом, као и ширење дезинформација и лажних вести. Циљ овог рада јесте

испитивање начина креирања дипфејк садржаја, као и истраживање могућности за његово откривање. Посебно су истраживане могућности злоупотребе дипфејк технологије.

Методе: Посредством коришћења литературе и анализе садржаја, у раду су систематизована знања о дипфејк технологији и анализирани релевантни подаци у овој области у вези са могућностима злоупотребе. Дипфејк технологија и њена употреба сагледане су и са безбедносног аспекта, односно показано је на који начин она може представљати друштвену опасност. Препорука је да будућа истраживања буду мултидисциплинарна – да интегришу знања друштвених наука (безбедност, социологија, психологија) и техничких наука (информационе технологије).

Резултати: Резултати овог истраживања показују да се дипфејк технологија примењује медицини, филмској индустрији, забави и креативном стваралаштву. Међутим, неретко се користи како би се креирали порнографски садржаји, лажне вести и извеле одређене врсте превара.

Закључак: Дипфејк технологија јесте неутрална, што значи да сврха њене употребе зависи од појединца који креира одређени садржај. Употреба како вештачке интелигенције, тако и дипфејк технологијенамеће сложена правна и етичка питања. Иако је уочљив потенцијал који ове технологије пружају унапређењу друштва, дипфејк технологија истовремено представља озбиљан ризик по људска права, демократију и националну безбедност држава. Посебно угрожену категорију становништва представљају жене због могућности креирања порнографских садржаја и осветничке порнографије употребом дипфејк технологије, иако жртве могу бити и мушкарци.

Кључне речи: дипфејк, порнографски садржај, сајбер насиље, преваре, лажне вести.

Paper received on: 04.03.2024.

Manuscript corrections submitted on: 25.09.2024.

Paper accepted for publishing on: 26.09.2024.

© 2024 The Authors. Published by Vojnotehnički glasnik / Military Technical Courier (www.vtg.mod.gov.rs, втг.мо.унр.срб). This article is an open access article distributed under the terms and conditions of the Creative Commons Attribution license (<http://creativecommons.org/licenses/by/3.0/rs/>).



САВРЕМЕНО НАОРУЖАЊЕ И ВОЈНА ОПРЕМА
 СОВРЕМЕННОЕ ВООРУЖЕНИЕ И ВОЕННОЕ ОБОРУДОВАНИЕ
 MODERN WEAPONS AND MILITARY EQUIPMENT

Ракета AIM-174 – нова варијанта ракете SM-6¹



F/A-18E из Strike Fighter Squadron 192 (VFA-192), the „Golden Dragons” (Златни змајеви), са пројектилима XAIM-174B испод сваког крила, виђени у војној бази у Перл Харбору

Већ дуже време се знало за ракете AIM-174 које поседују велики потенцијало и наносе огромне тактичке последице, иако је америчка морнарица упорно игнорисала њихово постојање. Сада је позната и њихова званична ознака.

Ваздушна верзија изузетно разноврсне ракете SM-6, такође познате као RIM-174, појавила се на борбеним авионима америчке морнарице F/A-18E/F Super Hornet на вежби „Руб Пацифика” (RIMPAC), која се одвија једном у две године и представља највећу светску међународну поморску вежбу. Ракете јасно носе ознаку AIM-174, што указује на ракету ваздух-ваздух (веома дугог домета), иако она има потенцијал да погоди копнене циљеве високог приоритета, као што су локације противваздухопловне одбране и ратни бродови, који дејствују као квазибалистичке ракете.

Саме ракете, које имају ознаку NAIM-174Bs истакнуту на предњем крају, обојене су сивом бојом, за разлику од претходних примерака

¹ <https://www.twz.com/> July 3, 2024

наранцасте боје које су виђене у прошлости. Ракете су означене као инертне (што значи да није уграђена бојева глава) и такође носе плаве траке које то потврђују и немају мотор под напоном. Црно-жута ознака близу центра тела ракете изгледа као ознака за калибрацију, што олакшава проучавање понашања пројектила након што је пуштен или за тестове подвесног качења.

Чињеница да су се ове ракете појавиле током вежбе RIMPAC је, у најмању руку, интригантна. То може бити индикативно за тестирање тактике, али такође може сугерисати да се бојеви AIM-174В може користити као део вежбе гађања. Ракета би могла бити у варијанти ваздух-ваздух, али је такође могуће да ће брод USS Tarawa, амфибијски јуришни брод америчке морнарице који је повучен из употребе, вероватно бити потопљен код обале Хаваја током вежбе. То би било прилично неувобичајено, јер би било први пут у више од деценије да се амфибијски јуришни брод било које врсте потопи у вежби SINKEX коју предводе САД.



Снимак из априла 2024. године, Super Hornet са ракетом AIM-174В

Ако AIM-174В задржи способност површинског удара коју поседује ракета SM-6, а бојеве ракете сада постоје, прилика да се ракета тестира против мете ове величине током велике мултинационалне вежбе представљала би снажну поруку противницима.

Комбинација F/A-18E/F и SM-6/AIM-174В први пут је примећена пре три године, али, као што је раније поменуто, америчка морнарица је никада није званично признала.

Ове године појавило се више фотографија ракете коју је, 17. априла 2024. године, носио F/A-18E/F северно од поморске станице ваздушног

оружја Чајна Лејк у Калифорнији. Том приликом, летелица је припадала ескадрили за ваздушно тестирање и процену (VX) 9, или евентуално VX-31.

Јасно је да је пројектил већ дуже време на тестирању или бар у концептуалној процени. Чињеница да се сада види да их авиони флоте носе, иако се вероватно ради о пробним пилотима за командама, такође указује на то да ова способност сазрева у оперативну.

Ипак, још увек се не зна за које врсте циљева је AIM-174B првенствено намењен, иако његова ознака говори да се ради о ракети ваздух-ваздух, али је питање какве су друге секундарне способности SM-6?

Ракета SM-6 са површинским лансирањем првобитно је дизајнирана да се бори са ваздушним претњама на великим дometима, као и са балистичким пројектиlima у њиховим завршним фазама лета. Сада, такође, има способност пресретања хиперсоничног оружја, под одређеним околностима.



Лансирање ракете SM-6 са америчког разарача класе Arleigh Burke

Могућност да се стандардна ракета SM-6 користи против копнених и морских циљева високог приоритета представља огромну додатну вредност. Ова способност би се, такође, могла проширити на AIM-174B, што би га сврстало у класу квазибалистичких пројектила, категорију оружја које постаје све релевантније у области ваздушних лансирања.

Ракета SM-6 је, такође, „умрежена” са могућношћу примања критичних података са низа платформи које могу да обезбеде даљинско гађање. У том смислу, могла би да искористи различите предности концепта Naval Integrated Fire Control-Counter Air concept (интегрисани концепт система за ваздушно управљање ватром) или NIFC-CA, који све више обједињује комплементарне могућности платформи као што је „невидљиви” ловац-бомбардер F-35, авион за рано упозоравање E-2D Advanced Hawkeye, ратне бродове опремљене радарским системом Aegis и ракете попут SM-6. На пример, оваква архитектура требало би да омогући ловцу бомбардеру Super Hornet да користи ракету AIM-174B за гађање циљева који су изван домета његовог сопственог радара, као и скупова циљева које иначе не може да детектује, попут балистичких пројектила.

Као оружје ваздух-ваздух, AIM-174B би обезбедио летелици Super Hornet могућност да обухвати различите ваздушне претње на удаљеностима од преко стотина миља, односно преко 150 км, што је значајна предност у односу на постојећу ракету ваздух-ваздух AIM-120 AMRAAM. Ова ракета би вероватно надмашила и домет ракете AIM-260 JATM која је још увек у развоју. Лансирање ракете из ваздушног простора, с обзиром на брзину и надморску висину, значи да ће она имати знатно већи домет и побољшану маневарабилност у односу на варијанту која се лансира са површине, иако нема ракетни бустер који користи стандардна ракета SM-6. Тренутно се сматра да домет ракете SM-6 која се лансира са површине износи око 230 миља, односно преко 300 км, али то зависи од многих фактора, укључујући начин на који се користи.

Таква ракета дугог домета имала би огромну предност с обзиром на то да Кина уводи у наоружање своје ракете ваздух-ваздух веома великог домета. Коришћење ракете AIM-174B против авиона за рано упозоравање, извиђање, поморско патролирање, пуњење горивом у ваздушном простору и авиона бомбардера-носача крстарећих ракете на екстремним дометима представљало би велико побољшање у ваздушним борбеним способностима морнарице и огромну претњу за гломазне непријатељске авионе. То би био један од кључних начина на који би САД могле да се супротставе кинеском систему забране приступа области.

Против копнених или поморских површинских циљева ракета AIM-174B би, такође, омогућила ловцу-бомбардеру Super Hornet средство за напад на значајним удаљеностима, односно оружјем које је изузетно тешко пресрести. Достижање брзине близу хиперсоничне брзине или веће од ње током завршне фазе лета чини ракету главним изазовом за одбрану. Та брзина значи да ракета може погађати и великим убојним дејством и користити се против неких утврђених мета.

Такође, треба поменути да би ова ракета могла да се користи као сурогат за обуку и тестирање, да опонаша способности противника, као што је балистичка ракета која се лансира из ваздушног простора. Иако је то сасвим могуће, ознака не мора да указује на такву улогу, нити тајност која је пратила програм. Ракета SM-6 која се лансира из ваздушног простора могла би да послужи и као сурогат мета потенцијалне претње, као и оперативно оружје.

Јасно је да би ове врсте способности биле изузетно релевантне за будући потенцијални сукоб са Кином на Пацифику, за који америчка војска сматра да би у њему доминирали „ланци убијања” веома дугог домета, нешто што ће сигурно бити демонстрирано током итерације RIMPAC.

Суштина је да овај најновији развој снажно сугерише да је верзија SM-6 лансирана из ваздушног простора или оперативна реалност или је близу тога да то постане. Ако се то догоди, морнарица ће ускоро остварити велики скок у способностима. На тај начин америчка војска се враћа на домете које је некада имала, а које Русија већ неко време оперативно користи.



Ракета AIM-54 Phoenix на ловцу пресретачу типа Grumman F-14 Tomcat

Наиме, америчко ваздухопловство је у јеку хладног рата са Совјетским Савезом имало у наоружању ракету ваздух-ваздух великог домета. Ради се о пројектилу AIM-54 Phoenix, радарски вођеној ракети пројектованој за гађање циљева ван визуелног домета. Била је предвиђена искључиво за ловце пресретаче типа Grumman F-14 Tomcat, а пројектована је за нападе на совјетске бомбардере Tu-16 Badger и Tu-22M Backfire који су били наоружани ракетама ваздух-море великог домета и, као такви, предвиђени за напад на америчке групе носача авиона.

Предвиђено је да се ракета користи са радаром AWG-9 у америчком пресретачу F-14 Tomcat. Сам радар могао је да прати истовремено 24

циља и да наводи до шест ракета. Ловац F-14 могао је да носи до четири овакве ракете на подвесним тачкама испод крила.

Док америчка морнарица која је користила поменуте авионе није никада имала прилику да употреби ове пројектиле против Совјетског Савеза, то није био случај са Ираном. Иран је за време владавине Шаха Резе Пахлавија, поред осталог наоружања, набавио и већи број ловаца пресретача F-14, чак 80 од којих је испоручено 79, као и већи број ракета AIM-54 Phoenix. Током Ирачко-иранског рата ловци F-14 су оборили око 160 ирачких летелица и то углавном коришћењем поменутих ракета ваздух-ваздух,

У међувремену је америчко министарство одустало од даљег развоја ракета ваздух-ваздух великог домета, док је Русија наставила са њиховим развојем и увела их у оперативну употребу.

Руске ракете ваздух-ваздух великог домета



Руска ракета ваздух-ваздух великог домета Vympel R-37 на пресретачу MiG-31BM

Руска хиперсонична ракета ваздух-ваздух Vympel R-37 (НАТО назив: AA-13 Achehead) великог домета има веома велики домет. Ракета и њене варијанте су и K-37, izdeliye 610 и RVV-BD (Ракета Воздух-Воздух Большой Дальности – ракета ваздух-ваздух дугог домета), са НАТО називима Achehead и Andi, а развијена је на основу ракете R-33.

Ракета је пројектована да обара авионе за рано упозоравање AWACS и друге авионе типа C41STAR, а истовремено да напада циљеве ван визуелног домета.

Према стручном војном часопису „Janes”, постоје две варијанте R-37 и R-37M. Ракета ваздух-ваздух 37M је опремљена ракетним бустером који се

може одбацили, па захваљујући њему добија домет на „300–400 км” (160–220 нм). Компанија „Рособоронекспорт” је, 2023. године, представила извозну верзију R-37М, означену као РВВ-БД, која има домет лансирања до 200 км (120 миља; 110 нми) и максималну висину од 25 км (82.000 стопа) са бојевом главом од 60 кг (130 лб). Ракета је компатибилна са авионима Sukhoi Su-57, Sukhoi Su-30, Sukhoi Su-35, Mikoyan MiG-31BM и Mikoyan MiG-35.

Од октобра 2022. године, ракета R-37М представља главну претњу украјинском ратном ваздухопловству. Током руске инвазије на Украјину, 2022. године, авиони MiG-31 су наводно оборили неколико украјинских авиона, углавном коришћењем ове ракете великог домета. Задржавајући велику брзину и велику висину, пресретачи MiG-31 су били у стању да дејствују практично без отпора због тога што украјинским ловцима недостаје домет, брзина или висина која је неопходна за долазак у домет лансирања својих пројектила ваздух-ваздух. Украјинском ратном ваздухопловству, такође, недостају ракете типа испали и заборави, па су се ослонили на ракете R-27, односно R-27R и R-27ER. Украјински пилоти морају да осветле руску летелицу својим радаром и да је прате радаром до циља, што значи да су руски пилоти у великом преимућству јер су њихови авиони опремљени радаром са активном фазном решетком. Ракете ваздух-ваздух R-77 пружају руским пилотима могућност да лансирају своје ракете, а затим да предузму акцију избегавања, док су украјински пилоти приморани да лете врло ниско и користе маскирање у односу на терен како би се довољно приближили да могу испалити ракете пре него што буду откривени и оборени.

У извештају Краљевског института уједињених служби (Royal United Services Institute) наводи се да је, у октобру 2023. године, на украјинско ваздухопловство дневно испаливано око шест ракета R-37М. Авион Su-35 се такође користи као носач за ове ракете.

Током 2022. године, руске снаге су имале борбену ваздушну патролу коју је чинио пар ловаца бомбардера Su-35S или ловаца пресретача MiG-31 на дежурству ради обарања украјинских авиона. Краљевски институт навео је да су руске ВКС у том периоду лансирале и до шест ракета R-37М дневно. Изузетно велика брзина ове ракете, заједно са веома великим ефективним дометом и трагачем пројектованим за гађање циљева на малим висинама, смртоносна је комбинација коју је ретко који нападнути непријатељски авион могао избећи.

Америка је након краја хладног рата успорила развој новог наоружања. Међутим, како је Русија у неким областима, као што је развој ракета ваздух-ваздух великог домета, наставила са развојем и предњачила, САД се сада труди да достигне и престигне Русију по сваку цену. Рат у Украјини је поново подстакао нову трку у наоружању која се све више убрзава. Овог пута је питање да ли ће остати ограничења из хладног рата.

Руски ракетни систем Rubezh-M²

Према наводима неколико руских медија, руска фабрика за израду инструмената „Тајфун” у Калуги, као део концерна Morinformsystems-Agat, завршила је развој обалског ракетног система Rubezh-M 6. јула 2024. године. Овај систем сада је у припреми за усвајање од стране руске морнарице, заједно са његовом извозном верзијом Rubezh-ME. Rubezh-M интегрише контролни центар, радар и лансере на шасији, а КАМАЗ укључује све неопходне компоненте, као што су четири пројектила, локатор, контролни системи, напајање и комуникације.



Обалски ракетни систем Rubezh-M, који користи противбродске ракете Kh-35U Uran, може да гађа површинске циљеве као што су бродови до 5.000 т

Развој ракетног система Rubezh-M почео је средином 2010-их година и завршио се до краја деценије. До почетка 2019. године фабрика „Тајфун” је представила рекламне материјале система, откривајући његове главне карактеристике и параметре. У јулу 2019. године, експериментална верзија Rubezh-M/ME је први пут приказана јавности на Међународном сајму поморске одбране (IMDS-2019) у Санкт Петербургу, представивши његов самоходни лансер и контролни пункт. Од тада је систем приказан на разним домаћим изложбама, укључујући и најновији IMDS у Санкт Петербургу, где су представљене његове карактеристике и предности.

Упоредо са овим изложбама, спроведена су и испитивања система. Иницијални тестови су обављени крајем 2010-их, а до септембра 2020. произвођач је најавио да ће се тестирање завршити до краја 2021. године. Специфична природа ових тестова, било фабричких, државних или

² Naval News Navy 2024, 23 Jul, 2024

заједничких, није откривена, али је фабрика „Тајфун“ наводно завршила све неопходне евалуације. Систем је сада позициониран за промоцију на тржишту.

Концерн Morinformsystem-Agat, заједно са компанијом „Rosoboronexport“, промовише извозну верзију Rubezh-M на међународном тржишту, очекујући ускоро поруџбине из неколико земаља. Представници ратне морнарице сматрају да је систем Rubezh-M постигао задовољавајуће резултате током тестирања и да ће ускоро бити у употреби и серијски се производити. Намењен је да допуни већи и скупљи обалски ракетни систем Bal, који може да прими до осам пројектила по лансеру.



Систем Rubezh-M намењен је да допуни већи и скупљи обалски ракетни систем Bal, који може да прими до осам пројектила по лансеру.

Имајући у виду поморске границе Русије са 12 земаља, које се протежу на преко 39.000 км (приближно дужине екватора), и тренутну међународну ситуацију, обалски ракетни систем Rubezh-M употпуњава способности руске обалске артиљерије. Очекује се да ће ускоро и званично бити у употреби. Rubezh-M/ME је дизајниран да заштити територијалне воде и ексклузивне економске зоне од непријатељских бродова и пловила; способан је да открије и нападне различите површинске и потенцијално копнене циљеве. За разлику од свог претходника из 1970-их, систем 4K51 Rubezh Rubezh-M/ME укључује модерне технологије и системе, засноване на решењима из пројекта 3K60 Bal, али знатно редизајниране.

Посебност обалског ракетног система Rubezh-M/ME је његова интеграција свих битних компоненти на једној шасији, укључујући радар, контролну кабину и лансер са ракетама, што му омогућава да самостално извршава борбене задатке. Овај концепт, који се у Русији назива „брод на

точковима”, наглашава мобилност и управљивост система, слично ракетним чамцима руске морнарице који су базирани на копну. Ракетни систем Rubezh-M користи или радар SPU-A или пасивну радарску станицу SPU-P за независно откривање циљева. Активни радар детектује површинске циљеве удаљене до 250 км, док пасивни радар може открити циљеве удаљене до 500 км. Уграђена опрема обрађује примљене информације и преноси их на ракету пре лансирања на циљ. Систем борбене контроле, такође, може да обрађује податке из сопствених система радарског извиђања и система за детекцију трећих страна.

Аутоматизација система омогућава да се све информације и подаци о лету пошаљу на ракету уз минимално учешће оператера, омогућавајући контролу само једном члану посаде. Потребно је мање од једног минута да се Rubezh-M припреми за лансирање ракете. Систем Rubezh-M је завршио тестирање и тренутно се разматра његово увођење у употребу, јер, према неким изворима, способан је да гађа и земаљске радарске циљеве. Овај систем са лансером за четири ракете може да открије и нападне различите површинске циљеве помоћу противбродских ракета Kh-35U Uran у било које доба дана, у свим временским условима, па чак и под дејством електронског ратовања и противваздухопловне одбране.



Ракета Kh-35UE, примарно наоружање система Rubezh-ME, има турбомлазни мотор мале величине, који постиже брзину од 0,8 до 0,85 Маха и домет лета до 260 километара за извозне верзије и до 450-500 км за домаће верзије.

Ракета Kh-35UE, дужине 4.400 мм, пречника 420 мм, распона крила 1.330 мм, дизајнирана је за уништавање површинских циљева као што су бродови до 5.000 т. Ова противбродска ракета лети на висини од око 10 м изнад врхова таласа током фазе крстарења и око 3-4 м током терминалне фазе, што, у комбинацији са ниским радарским пресеком, отежава откривање и пресретање. Подзвучна крстарећа брзина ракете је 265-280 м/с, приближно 1.000 км/х, са дометом од 7 до 260 км за извозне верзије и

до 500 км за модернизovanу верзију намењену руској морнарици. Удаљеност од обале за лансирање износи до 15 км, са интервалом лансирања од око 3 с између пројектила, пошто ракета користи инерцијалну и сателитску навигацију уз своју радарску главу за навођење.

Ракета Kh-35U, као примарно наоружање система Rubezh-ME, има турбомлазни мотор мале величине, који постиже брзину од 0,8 до 0,85 Маха и домет лета до 260 км за извозне верзије и до 450-500 км за домаће верзије. Радарска глава за навођење ракете активира се близу мете, способна је да ради и у активном и у пасивном режиму, и носи високоексплозивну бојеву главу од 145 кг, ефикасну против малих и средњих површинских циљева. Занимљиво је да ракете серије Kh-35, опремљене појачивачем на чврсто гориво и пробојном високоексплозивном запаљивом бојевом главом од 145 кг, користи и обалски ракетни систем Val који је развио Московски конструкторски биро за машинство.



Систем Rubezh-ME обухвата самоходни командно-контролни и комуникациони пункт (SKPUS), израђен на сличној шасији, али са другачијом надградњом и опремљен радаром Monolith-B.

Типична батерија Rubezh-ME садржи до осам лансера са пројектиlima и мобилно командно место опремљено радаром Monolith-B. Ова поставка такође је заснована на шасији војног камиона КАМАЗ 8к8. Свако лансирно возило је подржано припадајућим возилом за претовар, опремљено краном, и носи ракете за поновно пуњење. Батерија Rubezh-ME може да лансира до 32 противвродске крстареће ракете, довољне да

поремете операције велике непријатељске борбене групе. Након лансирања, потребно је 30-40 мин за поновно пуњење возила лансера.

Систем Rubezh-ME обухвата и самоходни командно-контролни и комуникациони пункт (SKPUS), изграђен на сличној шасији, али са другачијом надградњом, и опремљен радаром Monolith-B. Овај радар побољшава системске могућности праћења циљева и укупни оперативни домет.



Посебност обалског ракетног система Rubezh-M/ME чини интеграција свих битних компоненти на једној шасији, укључујући радар, контролну кабину и лансер са ракетама, што му омогућава да самостално обавља борбене задатке.

Драган М. Вучковић (*Dragan M. Vučković*),
e-mail: draganvuckovic64@gmail.com,
ORCID iD: <https://orcid.org/0000-0003-1620-5601>

ПОЗИВ И УПУТСТВО АУТОРИМА
ПРИГЛАШЕНИЕ И ИНСТРУКЦИЈА ДЛЈ АВТОРОВ РАБОТ
CALL FOR PAPERS AND INSTRUCTIONS FOR AUTHORS

ПОЗИВ И УПУТСТВО АУТОРИМА О НАЧИНУ ПРИПРЕМЕ ЧЛАНКА

Упутство ауторима о начину припреме чланка за објављивање у *Војнотехничком гласнику* урађено је на основу Правилника о категоризацији и рангирању научних часописа Министарства просвете, науке и технолошког развоја Републике Србије ("Службени гласник РС", број 159/20). Примена овог Правилника првенствено служи унапређењу квалитета домаћих часописа и њиховог потпунијег укључивања у међународни систем размене научних информација.

Војнотехнички гласник / Vojnotehnički glasnik / Military Technical Courier (втг.мо.упр.срб, www.vtg.mod.gov.rs, ISSN 0042-8469 – штампано издање, e-ISSN 2217-4753 – online, UDC 623+355/359, DOI: 10.5937/VojnotehnickiGlasnik; <https://doi.org/10.5937/VojnotehnickiGlasnik>), јесте рецензирани научни часопис.

Власници часописа су Министарство одбране Републике Србије и Војска Србије. Издавач и финансијер часописа је Универзитет одбране у Београду (Војна академија).

Програмска оријентација часописа заснива се на годишњој категоризацији часописа, коју врши надлежно државно министарство у одређеним областима, као и на његовом индексирању у међународним индексним базама.

Часопис обухвата научне, односно стручне области у оквиру образовно-научног поља **природно-математичких наука**, као и у оквиру образовно-научног поља **техничко-технолошких наука**, а нарочито области **одбрамбених наука и технологија**. Објављује теоријска и практична достигнућа која доприносе усавршавању свих припадника српске, регионалне и међународне академске заједнице, а посебно припадника војски и министарстава одбране. Публикује радове са уравнотеженим извештавањем о аналитичким, експерименталним и примењеним истраживањима, као и нумеричким симулацијама, обухватајући различите дисциплине. Објављени материјали су високог квалитета и релевантности, написани на начин који их чини доступним широкој читалачкој публици. Сви радови који извештавају о оригиналним теоријским и/или практично оријентисаним истраживањима или проширеним верзијама већ објављених радова са конференција су добродошли. Радови за објављивање одабирају се двоструко слепим поступком рецензије како би се осигурала оригиналност, релевантност и читљивост. Притом циљ није само да се квалитет објављених радова одржи високим већ и да се обезбеди правовремени, темељни и уравнотежени поступак рецензије.

Уређивачка политика *Војнотехничког гласника* заснива се на препорукама Одбора за етичност у издаваштву (COPE Core Practices) и заједничким принципима транспарентности и најбоље праксе у издаваштву COPE, DOAJ, OASPA и WAME, као и на најбољим прихваћеним праксама у научном издаваштву. *Војнотехнички гласник* је члан COPE (Committee on Publication Ethics) од 2. маја 2018. године и члан OASPA (Open Access Scholarly Publishers Association) од од 27. новембра 2015. године.

Министарство просвете, науке и технолошког развоја Републике Србије утврдило је дана 27. 12. 2023. године категоризацију *Војнотехничког гласника*, за 2023. годину:

- на листи часописа за рачунарске науке:
категирија врхунски часопис националног значаја (M51),
- на листи часописа за електронику, телекомуникације и информационе технологије:
категирија врхунски часопис националног значаја (M51),
- на листи часописа за машинство:
категирија национални часопис међународног значаја (M24),
- на листи часописа за материјале и хемијске технологије:
категирија национални часопис међународног значаја (M24).

Усвојене листе домаћих часописа за 2023. годину могу се видети на сајту *Војнотехничког гласника*, страница *Категоризација часописа*.

Детаљније информације могу се пронаћи и на сајту Министарства просвете, науке и технолошког развоја Републике Србије.

Подаци о категоризацији могу се пратити и на сајту КОБСОН-а (Конзорцијум библиотека Србије за обједињену набавку).

Категоризација часописа извршена је према Правилнику о категоризацији и рангирању научних часописа Министарства просвете, науке и технолошког развоја Републике Србије ("Службени гласник РС", број 159/20).

Часопис се прати у контексту Српског цитатног индекса – СЦИндекс (база података домаћих научних часописа), Научно-информационог система Redalyc и Руског индекса научног цитирања (РИНЦ). Подвргнут је сталном вредновању (мониторингу) у зависности од утицајности (импакта) у самим базама. Детаљи о индексирању могу се видети на сајту *Војнотехничког гласника*, страница *Индексирање часописа*.

Војнотехнички гласник, у погледу свог садржаја, пружа могућност отвореног приступа (DIAMOND OPEN ACCESS) и примењује Creative Commons (CC BY) одредбе о ауторским правима. Детаљи о ауторским правима могу се видети на сајту часописа, страница *Ауторска права и политика самоархивирања*.

Радови се предају путем онлајн система за електронско уређивање АСИСТЕНТ, који је развио Центар за евалуацију у образовању и науци (ЦЕОН).

Приступ и регистрација за сервис врше се на сајту www.vtg.mod.gov.rs, преко странице АСИСТЕНТ или СЦИНДЕКС, односно директно на линку aseestant.ceon.rs/index.php/vtg.

Детаљно упутство о регистрацији и пријави за сервис налази се на сајту www.vtg.mod.gov.rs, страница *Упутство за АСИСТЕНТ*.

Потребно је да се сви аутори који подносе рукопис за објављивање у *Војнотехничком гласнику* региструју у регистар ORCID (Open Researcher and Contributor ID), према упутству на страници сајта *Регистрација за добијање ORCID идентификационе шифре*.

Војнотехнички гласник објављује чланке на енглеском језику (arial, величина слова 11 pt, проред Single).

Поступак припреме, писања и уређивања чланка треба да буде у сагласности са *Изјавом о етичком поступању* (<http://www.vtg.mod.gov.rs/izjava-o-etickom-postupanju.html>).

Чланак треба да садржи сажетак са кључним речима, увод (мотивацију за рад), разраду (адекватан преглед репрезентативности рада у његовој области, јасну изјаву о новини у представљеном истраживању, одговарајућу теоријску

позадину, један или више примера за демонстрирање и дискусију о представљеним идејама), закључак и литературу (без нумерације наслова и поднаслова). Обим чланка треба да буде до једног ауторског табака (16 страница формата А4 са проредом Single), а највише 24 странице.

Чланак треба да буде написан на обрасцу за писање чланка, који се у електронској форми може преузети са сајта на страници *Образац за писање чланка*.

Наслов

Наслов треба да одражава тему чланка. У интересу је часописа и аутора да се користе речи прикладне за индексирање и претраживање. Ако таквих речи нема у наслову, пожељно је да се придода и поднаслов.

Текући наслов

Текући наслов се исписује са стране сваке странице чланка ради лакше идентификације, посебно копија чланака у електронском облику. Садржи презиме и иницијал имена аутора (ако аутора има више, преостали се означавају са „et al.“ или „и др.“), наслове рада и часописа и колацију (година, волумен, свеска, почетна и завршна страница). Наслови часописа и чланка могу се дати у скраћеном облику.

Име аутора

Наводи се пуно име и презиме (свих) аутора. Веома је пожељно да се наведу и средња слова аутора. Имена и презимена домаћих аутора увек се исписују у оригиналном облику (са српским дијакритичким знаковима), независно од језика на којем је написан рад.

Назив установе аутора (афилијација)

Наводи се пун (званични) назив и седиште установе у којој је аутор запослен, а евентуално и назив установе у којој је аутор обавио истраживање. У сложеним организацијама наводи се укупна хијерархија (нпр. Универзитет одбране у Београду, Војна академија, Катедра природно-математичких наука). Бар једна организација у хијерархији мора бити правно лице. Ако аутора има више, а неки потичу из исте установе, мора се, посебним ознакама или на други начин, назначити из које од наведених установа потиче сваки од наведених аутора. Афилијација се исписује непосредно након имена аутора. Функција и звање аутора се не наводе.

Контакт подаци

Адреса или е-адреса свих аутора даје се поред имена и презимена аутора.

Категорија (тип) чланка

Категоризација чланака обавеза је уредништва и од посебне је важности. Категорију чланка могу предлагати рецензенти и чланови уредништва, односно уредници рубрика, али одговорност за категоризацију сноси искључиво главни уредник.

Војнотехнички гласник објављује научне чланке.

Научни чланак је:

– оригиналан научни рад (рад у којем се износе претходно необјављени резултати сопствених истраживања научним методом);

– прегледни рад (рад који садржи оригиналан, детаљан и критички приказ истраживачког проблема или подручја у којем је аутор остварио одређени допринос, видљив на основу аутоцитата);

– кратко или претходно саопштење (оригинални научни рад пуног формата, али мањег обима или прелиминарног карактера);

– научна критика, односно полемика (расправа на одређену научну тему, заснована искључиво на научној аргументацији) и осврти.

Изузетно, у неким областима, научни рад у часопису може имати облик монографске студије, као и критичког издања научне грађе (историјско-архивске, лексикографске, библиографске, прегледа података и сл.), дотад непознате или недовољно приступачне за научна истраживања.

Радови класификовани као научни морају имати бар две позитивне рецензије.

Ако се у часопису објављују и прилози ваннаучног карактера, научни чланци треба да буду груписани и јасно издвојени у првом делу свеске.

Пожељно је да обим кратких саопштења буде 4 до 7 страница, научних чланака и студија случаја 10 до 14 страница, док прегледни радови могу бити и дужи. Број страница није строго ограничен и, уз одговарајуће образложење, пријављени чланци такође могу бити дужи или краћи.

Ако су радови који су претходно објављени на конференцији проширени, уредници ће проверити да ли је додато довољно новог материјала који испуњава стандарде часописа и квалификује поднесак за поступак рецензије. Додати материјал не сме бити претходно објављен. Нови резултати нису нужно потребни, али су пожељни. Међутим, поднесак треба да садржи проширене кључне идеје, примере, разраде, итд., који су претходно били садржани у поднеску са конференције.

Језик рада

Језик рада треба да буде енглески.

Текст мора бити језички и стилски дотеран, систематизован, без скраћеница (осим стандардних). Све физичке величине морају бити изражене у Међународном систему мерних јединица – SI. Редослед образаца (формула) означава се редним бројевима, са десне стране у округлим заградама.

Сажетак

Сажетак јесте кратак информативан приказ садржаја чланка који читаоцу омогућава да брзо и тачно оцени његову релевантност. У интересу је уредништава и аутора да сажетак садржи термине који се често користе за индексирање и претрагу чланака. Саставни делови сажетка су увод/циљ истраживања, методи, резултати и закључак. Сажетак треба да има од 100 до 250 речи и треба да се налази између заглавља (наслов, имена аутора и др.) и кључних речи, након којих следи текст чланка.

Кључне речи

Кључне речи су термини или фразе које адекватно представљају садржај чланка за потребе индексирања и претраживања. Треба их додељивати ослањајући се на неки међународни извор (попис, речник или тезаурус) који је најшире прихваћен или унутар дате научне области. За нпр. науку уопште, то је листа кључних речи Web of Science. Број кључних речи не може бити већи од 10, а у интересу је уредништва и аутора да учесталост њихове употребе буде што већа. У чланку се пишу непосредно након сажетка.

Систем АСИСТЕНТ у ту сврху користи специјалну алатку KWASS: аутоматско екстраховање кључних речи из дисциплинарних тезауруса/речника по избору и рутине за њихов одабир, тј. прихватање односно одбацивање од стране аутора и/или уредника.

Датум прихватања чланка

Датум када је уредништво примило чланак, датум када је уредништво коначно прихватило чланак за објављивање, као и датуми када су у међувремену достављене евентуалне исправке рукописа наводе се хронолошким редоследом, на сталном месту, по правилу на крају чланка.

Захвалница

Назив и број пројекта, односно назив програма у оквиру којег је чланак настао, као и назив институције која је финансирала пројекат или програм, наводи се у посебној напомени на сталном месту, по правилу при дну прве стране чланка.

Претходне верзије рада

Ако је чланак у претходној верзији био изложен на скупу у виду усменог саопштења (под истим или сличним насловом), податак о томе треба да буде наведен у посебној напомени, по правилу при дну прве стране чланка. Рад који је већ објављен у неком часопису не може се објавити у *Војнотехничком гласнику* (прештампати), ни под сличним насловом и измењеном облику.

Табеларни и графички прикази

Пожељно је да наслови свих приказа, а по могућству и текстуални садржај, буду дати двојезично, на језику рада и на енглеском језику.

Табеле се пишу на исти начин као и текст, а означавају се редним бројевима са горње стране. Фотографије и цртежи треба да буду јасни, прегледни и погодни за репродукцију. Цртеже треба радити у програму word или corel. Фотографије и цртеже треба поставити на жељено место у тексту.

За слике и графиконе не сме се користити снимак са екрана рачунара програма за прикупљање података. У самом тексту чланка препоручује се употреба слика и графикана непосредно из програма за анализу података (као што су Excel, Matlab, Origin, SigmaPlot и други).

Навођење (цитирање) у тексту

Начин позивања на изворе у оквиру чланка мора бити једнообразан.

Војнотехнички гласник за референцирање (цитирање и навођење литературе) примењује Харвардски систем референци, односно Харвардски приручник за стил (Harvard Referencing System, Harvard Style Manual). У самом тексту, у обичним заградама, на месту на којем се врши позивање, односно цитирање литературе набројане на крају чланка, обавезно у обичној загради написати презиме цитираног аутора, годину издања публикације из које цитирате и, евентуално, број страница. Нпр. (Petrović, 2012, pp.10–12).

Детаљно упутство о начину цитирања, са примерима, дато је на страници сајта *Упутство за Харвардски приручник за стил*. Потребно је да се позивање на литературу у тексту уради у складу са поменутиим упутством.

Систем АСИСТЕНТ у сврху контроле навођења (цитирања) у тексту користи специјалну алатку CiteMatcher: откривање изостављених цитата у тексту рада и у попису референци.

Напомене (фусноте)

Напомене се дају при дну стране на којој се налази текст на који се односе. Могу садржати мање важне детаље, допунска објашњења, назнаке о коришћеним

изворима (на пример, научној грађи, приручницима), али не могу бити замена за цитирану литературу.

Листа референци (литература)

Цитирана литература обухвата, по правилу, библиографске изворе (чланке, монографије и сл.) и даје се искључиво у засебном одељку чланка, у виду листе референци. Референце се не преводe на језик рада и набрајају се у посебном одељку на крају чланка.

Војнотехнички гласник, као начин исписа литературе, примењује Харвардски систем референци, односно Харвардски приручник за стил (Harvard Referencing System, Harvard Style Manual).

Литература се обавезно пише на латиничном писму и набраја по алфавитном редоследу, наводећи најпре презимена аутора, без нумерације.

Детаљно упутство о начину пописа референци, са примерима, дато је на страници сајта *Упутство за Харвардски приручник за стил*. Потребно је да се попис литературе на крају чланка уради у складу са поменутиим упутством.

Нестандардно, непотпуно или недоследно навођење литературе у системима вредновања часописа сматра се довољним разлогом за оспоравање научног статуса часописа.

Систем АСИСТЕНТ у сврху контроле правилног исписа листе референци користи специјалну алатку RefFormatter: контрола обликовања референци у складу са Харвардским приручником за стил.

Изјава о ауторству

Поред чланка доставља се *Изјава о ауторству* у којој аутори наводе свој појединачни допринос у изради чланка. Такође, у тој изјави потврђују да су чланак урадили у складу са *Позивом и упутством ауторима* и *Изјавом о етичком поступању часописа*.

Сви радови подлежу стручној рецензији.

Списак рецензената *Војнотехничког гласника* може се видети на страници сајта *Списак рецензената*. Процес рецензирања објашњен је на страници сајта *Рецензентски поступак*.

Уредништво

Адреса редакције:
Војнотехнички гласник
Вељка Лукића Курјака 33
11042 Београд
e-mail: vojnotehnicki.glasnik@mod.gov.rs.
тел: војни 40-260 (011/3603-260), 066/8700-123

ПРИГЛАШЕНИЕ И ИНСТРУКЦИЯ ДЛЯ АВТОРОВ О ПОРЯДКЕ ПОДГОТОВКИ СТАТЬИ

Инструкция для авторов о порядке подготовки статьи к опубликованию в журнале «Военно-технический вестник» разработана согласно Регламенту о категоризации и ранжировании научных журналов Министерства образования, науки и технологического развития Республики Сербия («Службени гласник РС», № 159/20). Применение этого Регламента способствует повышению качества отечественных журналов и их более полному вовлечению в международную систему обмена научной информацией.

Военно-технический вестник (Vojnotehnički glasnik / Military Technical Courier), втг.мо.упр.срб, www.vtg.mod.gov.rs/index-ru.html, ISSN 0042-8469 – печатное издание, e-ISSN 2217-4753 – online, UDK 623+355/359, DOI: 10.5937/VojnotehnickiGlasnik; <https://doi.org/10.5937/VojnotehnickiGlasnik>, является рецензируемым научным журналом.

Собственники журнала: Министерство обороны и Вооруженные силы Республики Сербия.

Издатель журнала: Университет обороны в г. Белград (Военная академия).

Программная ориентация журнала основана на ежегодной категоризации журнала, которая производится соответствующим отраслевым министерством, в зависимости от области исследований, а также на его индексировании в международных наукометрических базах данных.

Журнал охватывает научные и профессиональные сферы в рамках учебно-научной области **естественно-математических наук**, а также в рамках учебно-научной области **техничко-технологических наук**, особенно в области **оборонных наук и технологий**. В журнале публикуются теоретические и практические достижения, которые способствуют повышению квалификации представителей сербского, регионального и международного академического сообщества, особенно служащих Министерств Обороны и Вооружённых сил. В журнале публикуются статьи со соответствующими обзорами об аналитических, экспериментальных и прикладных исследованиях, а также о численном моделировании, охватывая различные дисциплины. Публикуемые материалы отличаются высоким качеством и актуальностью. Они написаны научным, но понятным и доступным для широкого круга читателей языком. Приветствуются все статьи, сообщающие об оригинальных теоретических и/или практических исследованиях и/или расширенные версии ранее опубликованных статей, представленных на конференциях. Статьи для публикации отбираются путем двойного слепого рецензирования, которое гарантирует оригинальность, актуальность и удобочитаемость. Цель состоит не только в поддержании высокого качества публикуемых статей, но и в обеспечении своевременного, тщательного и соответствующего процесса рецензирования.

Редакционная политика журнала «Военно-технический вестник» основана на рекомендациях Комитета по этике научных публикаций (COPE Core Practices), общих принципах прозрачности и лучшей практике издательской деятельности COPE, DOAJ, OASPA и WAME, а также на лучшей практике научно-издательской деятельности. Журнал «Военно-технический вестник» является членом COPE (Комитет по этике научных публикаций) со 2 мая 2018 года и членом OASPA (Ассоциация научных издателей открытого доступа) с 27 ноября 2015 года.

Министерством образования, науки и технологического развития Республики Сербия утверждена 27 декабря 2023 г. категоризация журнала «Военно-технический вестник» за 2023 год:

- **Область компьютерные науки:**
ведущий журнал государственного значения (M51),
- **Область электроники, телекоммуникаций и информационных технологий:**
ведущий журнал государственного значения (M51),
- **Область машиностроения:**
национальный журнал международного значения (M24),
- **Область материалов и химической технологии:**
национальный журнал международного значения (M24).

С информацией относительно категоризации за 2023 год можно ознакомиться на странице сайта «Военно-технического вестника» *Категоризация Вестника*.

Более подробную информацию можно найти на сайте Министерства образования, науки и технологического развития Республики Сербия.

С информацией о категоризации можно ознакомиться и на сайте КОБСОН (Консорциум библиотек Республики Сербия по вопросам объединения закупок).

Категоризация Вестника проведена согласно Регламенту о категоризации и ранжировании научных журналов Министерства образования, науки и технологического развития Республики Сербия («Службени гласник РС», № 159/20)

Журнал соответствует стандартам Сербского индекса научного цитирования (СЦИИндекс/SCИндекс) - наукометрической базы данных научных журналов Республики Сербия, Научно-информационного система Redalys, а также Российского индекса научного цитирования (РИНЦ). Журнал постоянно подвергается мониторингу и оценивается количественными наукометрическими показателями отражающими его научную ценность.

С информацией об индексировании можно ознакомиться на странице сайта журнала *Индексирование Вестника*.

«Военно-технический вестник» относительно своего содержания предоставляет пользователям возможность открытого доступа (DIAMOND OPEN ACCESS) и положениями об авторских правах, утвержденными Creative Commons (CC BY). С инструкцией об авторских правах можно ознакомиться на странице сайта журнала *Авторские права и политика самоархивирования*.

Рукописи статей направляются в редакцию журнала с использованием online системы ASSISTANT, запущенной Центром поддержки развития образования и науки (ЦПРОН). Регистрация в системе и оформление прав доступа выполняется по адресу <http://www.vtg.mod.gov.rs/index-ru.html>, через страницу ASSISTANT или СЦИИНДЕКС (aseestant.ceon.rs/index.php/vtg). С инструкцией по регистрации и правам доступа можно ознакомиться по адресу <http://www.vtg.mod.gov.rs/index-ru.html>, на странице *Инструкция по ASSISTANT*.

Все авторы, предоставляющие свои рукописи для публикации в редакцию журнала «Военно-технический вестник» должны пройти предварительную регистрацию в реестре ORCID (Open Researcher and Contributor ID). Эта процедура осуществляется в соответствии с инструкцией, размещенной на странице сайта *Регистрация в реестре ORCID для присвоения идентификационного кода*.

«Военно-технический вестник» публикует статьи на английском языке (Arial, шрифт 11 pt, пробел Single). Процесс подготовки, написания и редактирования статьи

должен осуществляться в соответствии с принципами *Этического кодекса* (<http://www.vtg.mod.gov.rs/eticheskiy-kodyeks.html>). Статья должна содержать резюме с ключевыми словами, введение (цель исследования), основную часть (соответствующий обзор представительного исследования в данной области, четкое изложение научной новизны в представленном исследовании, соответствующую теоретическую основу, один или несколько примеров для демонстрации и обсуждения представленных тезисов), заключение и список литературы (без нумерации заголовков и подзаголовков). Объем статьи не должен превышать один авторский лист (16 страниц формата A4 с одинарным интервалом, максимум до 24 страниц, включая ссылки и приложения). Статья должна быть набрана на компьютере с использованием специально подготовленного редакцией макета, который можно скачать на странице сайта *Правила и образец составления статьи*.

Заголовок

Заголовок должен отражать тему статьи. В интересах журнала и автора необходимо использовать слова и словосочетания, удобные для индексации и поиска. Если такие слова не содержатся в заголовке, то желательно их добавить в подзаголовок.

Текущий заголовок

Текущий заголовок пишется в титуле каждой страницы статьи с целью упрощения процесса идентификации, в первую очередь копий статьей в электронном виде. Заголовок содержит в себе фамилию и инициал имени автора (в случае если авторов несколько, остальные обозначаются с «et al.» или «и др.»), название работы и журнала (год, том, выпуск, начальная и заключительная страница). Заголовок статьи и название журнала могут быть приведены в сокращенном виде.

ФИО автора

Приводятся полная фамилия и полное имя (всех) авторов. Желательно, чтобы были указаны инициалы отчеств авторов. Фамилия и имя авторов из Республики Сербия всегда пишутся в оригинальном виде (с сербскими диакритическими знаками), независимо от языка, на котором написана работа.

Наименование учреждения автора (аффилиация)

Приводится полное (официальное) наименование и местонахождение учреждения, в котором работает автор, а также наименование учреждения, в котором автор провёл исследование. В случае организаций со сложной структурой приводится их иерархическая соподчинённость (напр. Военная академия, кафедра военных электронных систем, г. Белград). По крайней мере, одна из организаций в иерархии должна иметь статус юридического лица. В случае если указано несколько авторов, и если некоторые из них работают в одном учреждении, нужно отдельными обозначениями или каким-либо другим способом указать в каком из приведённых учреждений работает каждый из авторов. Аффилиация пишется непосредственно после ФИО автора. Должность и специальность по диплому не указываются.

Контактные данные

Электронный адрес автора указываются рядом с его именем на первой странице статьи.

Категория (тип) статьи

Категоризация статей является обязанностью редакции и имеет особое значение. Категорию статьи могут предлагать рецензенты и члены редакции, т.е.

редакторы рубрик, но ответственность за категоризацию несет исключительно главный редактор.

Журнал «Военно-технический вестник» публикует научные статьи.

Научные статьи:

– оригинальная научная статья (работа, в которой приводятся ранее неопубликованные результаты собственных исследований, полученных научным методом);

– обзорная статья (работа, содержащая оригинальный, детальный и критический обзор исследуемой проблемы или области, в который автор внёс определённый вклад, видимый на основе автоцитат);

– краткое сообщение (оригинальная научная работа полного формата, но меньшего объёма или имеющая предварительный характер);

– научная критическая статья (дискуссия-полемика на определённую научную тему, основанная исключительно на научной аргументации) и научный комментарий.

Однако, в некоторых областях знаний научная работа в журнале может иметь форму монографического исследования, а также критического обсуждения научного материала (историко-архивного, лексикографического, библиографического, обзора данных и т.п.) – до сих пор неизвестного или недостаточно доступного для научных исследований. Работы, классифицированные в качестве научных, должны иметь, по меньшей мере, две положительные рецензии. В случае если в журнале объявляются и приложения, не имеющие научный характер, научные статьи должны быть сгруппированы и четко выделены в первой части номера.

Объем кратких сообщений составляет 4-7 страниц, исследовательские статьи и тематические исследования с проблемно-ситуационным анализом – 10-14 страниц, однако объем обзорных статей может быть больше. Ограничения по количеству страниц не являются строгими, следовательно при соответствующем обосновании предоставленные работы могут быть длиннее или короче. В случае подачи расширенных версий ранее опубликованных докладов, представленных на конференции, редакция проверит было ли добавлено достаточно новых материалов для того, чтобы статья соответствовала стандартам журнала и условиям рецензирования. Добавленный материал должен быть новым, неопубликованным ранее. Новые результаты приветствуются, но не являются обязательным условием; однако ключевые тезисы, примеры, разработки и пр. должны быть более подробно представлены в статье по сравнению с первичным докладом на конференции.

Язык работы

Статья должна быть написана на английском языке. Текст должен быть в лингвистическом и стилистическом смысле упорядочен, систематизирован, без сокращений (за исключением стандартных). Все физические величины должны соответствовать Международной системе единиц измерения – СИ. Очередность формул обозначается порядковыми номерами, проставляемыми с правой стороны в круглых скобках.

Резюме

Резюме является кратким информативным обзором содержания статьи, обеспечивающим читателю быстроту и точность оценки её релевантности. В интересах редакции и авторов, чтобы резюме содержало термины, часто используемые для индексирования и поиска статьей. Составными частями резюме

являются введение/цель исследования, методы, результаты и выводы. В резюме должно быть от 100 до 250 слов, и оно должно находиться между титулами (заголовков, ФИО авторов и др.) и ключевыми словами, за которыми следует текст статьи.

Ключевые слова

Ключевыми словами являются термины или фразы, адекватно представляющие содержание статьи, необходимые для индексирования и поиска. Ключевые слова необходимо выбирать, опираясь при этом на какой-либо международный источник (регистр, словарь, тезаурус), наиболее используемый внутри данной научной области. Число ключевых слов не может превышать 10. В интересах редакции и авторов, чтобы частота их встречи в статье была как можно большей. В статье они пишутся непосредственно после резюме.

Программа ASSISTANT предоставляет возможность использования сервиса KWASS, автоматически фиксирующего ключевые слова из источников/словарей по выбору автора/редактора.

Дата получения статьи

Дата, когда редакция получила статью; дата, когда редакция окончательно приняла статью к публикации; а также дата, когда были предоставлены необходимые исправления рукописи, приводятся в хронологическом порядке, как правило, в конце статьи.

Выражение благодарности

Наименование и номер проекта, т.е. название программы благодаря которой статья возникла, совместно с наименованием учреждения, которое финансировало проект или программу, приводятся в отдельном примечании, как правило, внизу первой страницы статьи.

Предыдущие версии работы

В случае если статья в предыдущей версии была изложена устно (под одинаковым или похожим названием, например, в виде доклада на научной конференции), сведения об этом должны быть указаны в отдельном примечании, как правило, внизу первой страницы статьи. Работа, которая уже была опубликована в каком-либо из журналов, не может быть напечатана в «Военно-техническом вестнике» ни под похожим названием, ни в изменённом виде.

Нумерация и название таблиц и графиков

Желательно, чтобы нумерация и название таблиц и графиков были исполнены на двух языках (на языке оригинала и на английском). Таблицы подписываются таким же способом как и текст и обозначаются порядковым номером с верхней стороны. Фотографии и рисунки должны быть понятны, наглядны и удобны для репродукции. Рисунки необходимо делать в программах Word или Corel. Фотографии и рисунки надо поставить на желаемое место в тексте. Для создания изображений и графиков использование функции снимка с экрана (скриншота) не допускается. В самом тексте статьи рекомендуется применение изображений и графиков, обработанных такими компьютерными программами, как: Excel, Matlab, Origin, SigmaPlot и др.

Ссылки (цитирование) в тексте

Оформление ссылок на источники в рамках статьи должно быть однообразным. «Военно-технический вестник» для оформления ссылок, цитат и списка использованной литературы применяет Гарвардскую систему (Harvard Referencing System, Harvard Style Manual). В тексте в скобках приводится фамилия цитируемого автора (или фамилия первого автора, если авторов несколько), год издания и по

необходимости номер страницы. Например: (Petrović, 2010, pp.10-20). Рекомендации о способе цитирования размещены на странице сайта *Инструкция по использованию Гарвардского стиля*. При оформлении ссылок, цитат и списка использованной литературы необходимо придерживаться установленных норм. Программа ASSISTANT предоставляет при цитировании возможность использования сервиса CiteMatcher, фиксирующего пропущенные цитаты в работе и в списке литературы.

Примечания (сноски)

Примечания (сноски) к тексту указываются внизу страницы, к которой они относятся. Примечания могут содержать менее важные детали, дополнительные объяснения, указания об использованных источниках (напр. научном материале, справочниках), но не могут быть заменой процедуры цитирования литературы.

Литература (референции)

Цитированной литературой охватываются, как правило, такие библиографические источники как статьи, монографии и т.п. Вся используемая литература в виде референций размещается в отдельном разделе статьи. Названия литературных источников не переводятся на язык работы. *«Военно-технический вестник»* для оформления списка использованной литературы применяет Гарвардскую систему (Harvard Style Manual). В списке литературы источники указываются в алфавитном порядке фамилий авторов или редакторов. Рекомендации о способе цитирования размещены на странице сайта *Инструкция по использованию Гарвардского стиля*. При оформлении списка использованной литературы необходимо придерживаться установленных норм. При оформлении списка литературы программа ASSISTANT предоставляет возможность использования сервиса RefFormatter, осуществляющего контроль оформления списка литературы в соответствии со стандартами Гарвардского стиля. Нестандартное, неполное и непоследовательное приведение литературы в системах оценки журнала считается достаточной причиной для оспаривания научного статуса журнала.

Авторское заявление

Авторское заявление предоставляется вместе со статьей, в нем авторы заявляют о своем личном вкладе в написание статьи. В заявлении авторы подтверждают, что статья написана в соответствии с *Приглашением и инструкциями для авторов*, а также с *Кодексом профессиональной этики журнала*.

Все рукописи статей подлежат профессиональному рецензированию.

Список рецензентов журнала *«Военно-технический вестник»* размещён на странице сайта *Список рецензентов*. Процесс рецензирования описан в разделе *Правила рецензирования*.

Редакция

Почтовый адрес редакции:

«Војнотехнички гласник»

ул. Велька Лукича Куряка 33, 11042 Белград, Республика Сербия

e-mail: vojnotehnicki.glasnik@mod.gov.rs,

тел: +381 11 3603 260, +381 66 8700 123

CALL FOR PAPERS AND ARTICLE FORMATTING INSTRUCTIONS

The instructions to authors about the article preparation for publication in the *Military Technical Courier* are based on the Regulations on categorization and ranking of scientific journals of the Ministry of Education, Science and Technological Development of the Republic of Serbia (Official Gazette of the Republic of Serbia, No 159/20). This Regulations aims at improving the quality of national journals and raising the level of their compliance with the international system of scientific information exchange.

The Military Technical Courier / Vojnotehnički glasnik (www.vtg.mod.gov.rs/index-e.html, vtg.mo.yrp.cpb, ISSN 0042-8469 – print issue, e-ISSN 2217-4753 – online, UDC 623+355/359, DOI: 10.5937/VojnotehnickiGlasnik; <https://doi.org/10.5937/VojnotehnickiGlasnik>), is an peer-reviewed scientific journal.

The owners of the journal are the Ministry of Defence of the Republic of Serbia and the Serbian Armed Forces. The publisher and financier of the *Military Technical Courier* is the University of Defence in Belgrade (Military Academy).

The program of the journal is based on the annual classification of journals performed by a relevant Ministry as well as on its indexing in international indexing databases.

The journal covers scientific and professional fields within the educational-scientific field of **Natural-Mathematical Sciences**, as well as within the educational-scientific field of **Technical-Technological Sciences**, and especially the field of **defense sciences and technologies**. It publishes theoretical and practical achievements leading to professional development of all members of Serbian, regional and international academic communities as well as members of the military and ministries of defence in particular. It publishes papers with balanced coverage of analytical, experimental, and applied research as well as numerical simulations from various disciplines. The material published is of high quality and relevance, written in a manner that makes it accessible to a wider readership. The journal welcomes papers reporting original theoretical and/or practice-oriented research as well as extended versions of already published conference papers. Manuscripts for publication are selected through a double-blind peer-review process to validate their originality, relevance, and readability. This being so, the objective is not only to keep the quality of published papers high but also to provide a timely, thorough, and balanced review process.

The editorial policy of the *Military Technical Courier* is based on the COPE Core Practices, common COPE, DOAJ, OASPA and WAME Principles of Transparency and Best Practice in Scholarly Publishing as well as on the best accepted practices in scientific publishing. The Military Technical Courier has been a COPE (Committee on Publication Ethics) member since 2nd May 2018 and a member of OASPA (Open Access Scholarly Publishers Association) since 27th November 2015.

The Ministry of Education, Science and Technological Development of the Republic of Serbia classified the *Military Technical Courier* for the year 2023, on December 27, 2023

- on the list of periodicals for computer sciences,
category: reputed national journal (M51),
- on the list of periodicals for electronics, telecommunications and IT,
category: reputed national journal (M51),
- on the list of periodicals for mechanical engineering,
category: national journal of international importance (M24),
- on the list of periodicals for materials and chemical technology,
category: national journal of international importance (M24).

The approved lists of national periodicals for the year 2023 can be viewed on the website of the *Military Technical Courier*, page *Journal categorization*.

More detailed information can be found on the website of the Ministry of Education, Science and Technological Development of the Republic of Serbia.

The information on the categorization can be also found on the website of KOBSON (Consortium of Libraries of Serbia for Unified Acquisition).

The periodical is categorized in compliance with the Regulations on categorization and ranking of scientific journals of the Ministry of Education, Science and Technological Development of the Republic of Serbia (Official Gazette of the Republic of Serbia, No 159/20). More detailed information can be found on the website of the Ministry of Education, Science and Technological Development.

The journal is in the Serbian Citation Index – SCIndex (data base of national scientific journals), in the Scientific Information System Redalyc, and in the Russian Index of Science Citation/Российский индекс научного цитирования (RINC/РИНЦ) and is constantly monitored depending on the impact within the bases themselves. More detailed information can be viewed on the website of the *Military Technical Courier*, page *Journal indexing*.

The *Military Technical Courier*, in terms of its content, offers the possibility of open access (DIAMOND OPEN ACCESS) and applies the Creative Commons Attribution (CC BY) licence on copyright. The copyright details can be found on the *Copyright notice and Self-archiving policy* page of the journal's website.

Manuscripts are submitted online, through the electronic editing system ASSISTANT, developed by the Center for Evaluation in Education and Science – CEON.

The access and the registration are through the *Military Technical Courier* site <http://www.vtg.mod.gov.rs/index-e.html>, on the page *ASSISTANT* or the page *SCINDEKS* or directly through the link (aseestant.ceon.rs/index.php/vtg).

The detailed instructions about the registration for the service are on the website <http://www.vtg.mod.gov.rs/index-e.html>, on the page *Instructions for ASSISTANT*.

All authors submitting a manuscript for publishing in the *Military Technical Courier* should register for an ORCID ID following the instructions on the web page *Registration for an ORCID identifier*.

The *Military Technical Courier* publishes articles in English, using Arial and a font size of 11pt with Single Spacing.

The procedures of article preparation, writing and editing should be in accordance with the *Publication ethics statement* (<http://www.vtg.mod.gov.rs/publication-ethics-statement.html>).

The article should contain an abstract with keywords, introduction (motivation for the work), body (adequate overview of the representative work in the field, a clear statement of the novelty in the presented research, suitable theoretical background, one or more examples to demonstrate and discuss the presented ideas), conclusion, and references (without heading and subheading enumeration). The article length should not normally exceed 16 pages of the A4 paper format with single spacing, up to a maximum of 24 pages with references and supplementary material included.

The article should be formatted following the instructions in the Article Form which can be downloaded from website page *Article form*.

Title

The title should be informative. It is in both Journal's and author's best interest to use terms suitable for indexing and word search. If there are no such terms in the title, the author is strongly advised to add a subtitle.

Letterhead title

The letterhead title is given at a top of each page for easier identification of article copies in an electronic form in particular. It contains the author's surname and first name initial (for multiple authors add "et al"), article title, journal title and collation (year, volume, issue, first and last page). The journal and article titles can be given in a shortened form.

Author's name

Full name(s) of author(s) should be used. It is advisable to give the middle initial. Names are given in their original form (with diacritic signs if in Serbian).

Author's affiliation

The full official name and seat of the author's affiliation is given, possibly with the name of the institution where the research was carried out. For organizations with complex structures, give the whole hierarchy (for example, University of Defence in Belgrade, Military Academy, Department for Military Electronic Systems). At least one organization in the hierarchy must be a legal entity. When some of multiple authors have the same affiliation, it must be clearly stated, by special signs or in other way, which department exactly they are affiliated with. The affiliation follows the author's name. The function and title are not given.

Contact details

The postal addresses or the e-mail addresses of the authors are given in the first page.

Type of articles

Classification of articles is a duty of the editorial staff and is of special importance. Referees and the members of the editorial staff, or section editors, can propose a category, but the editor-in-chief has the sole responsibility for their classification.

The *Military Technical Courier* publishes scientific articles.

Scientific articles:

- Original scientific papers (giving the previously unpublished results of the author's own research based on scientific methods);
- Review papers (giving an original, detailed and critical view of a research problem or an area to which the author has made a contribution demonstrated by self-citation);
- Short communications or Preliminary communications (original scientific full papers but shorter or of a preliminary character);
- Scientific commentaries or discussions (discussions on a particular scientific topic, based exclusively on scientific argumentation) and opinion pieces.

Exceptionally, in particular areas, a scientific paper in the Journal can be in a form of a monograph or a critical edition of scientific data (historical, archival, lexicographic, bibliographic, data survey, etc.) which were unknown or hardly accessible for scientific research.

Papers classified as scientific must have at least two positive reviews.

If the journal contains non-scientific contributions as well, the section with scientific papers should be clearly denoted in the first part of the Journal.

Short communications are usually 4-7 pages long, research articles and case studies 10-14 pages, while reviews can be longer. Page number limits are not strict and, with

appropriate reasoning, submitted manuscripts can also be longer or shorter. If extended versions of previously published conference papers are submitted, Editors will check if sufficient new material has been added to meet the journal standards and to qualify such manuscripts for the review process. The added material must not have been previously published. New results are desired but not necessarily required; however, submissions should contain expansions of key ideas, examples, elaborations, etc. of conference papers.

Language

The language of the article should be in English. The grammar and style of the article should be of good quality. The systematized text should be without abbreviations (except standard ones). All measurements must be in SI units. The sequence of formulae is denoted in Arabic numerals in parentheses on the right-hand side.

Abstract and summary

An abstract is a concise informative presentation of the article content for fast and accurate evaluation of its relevance. It contains the terms often used for indexing and article search. A 100- to 250-word abstract has the following parts: introduction/purpose of the research, methods, results and conclusion.

Keywords

Keywords are terms or phrases showing adequately the article content for indexing and search purposes. They should be allocated heaving in mind widely accepted international sources (index, dictionary or thesaurus), such as the Web of Science keyword list for science in general. The higher their usage frequency is, the better. Up to 10 keywords immediately follow the abstract and the summary, in respective languages. For this purpose, the ASSISTANT system uses a special tool KWASS for the automatic extraction of key words from disciplinary thesauruses/dictionaries by choice and the routine for their selection, i.e. acceptance or rejection by author and/or editor.

Article acceptance date

The date of the reception of the article, the dates of submitted corrections in the manuscript (optional) and the date when the Editorial Board accepted the article for publication are all given in a chronological order at the end of the article.

Acknowledgements

The name and the number of the project or programme within which the article was realised is given in a separate note at the bottom of the first page together with the name of the institution which financially supported the project or programme.

Article preliminary version

If an article preliminary version has appeared previously at a meeting in a form of an oral presentation (under the same or similar title), this should be stated in a separate note at the bottom of the first page. An article published previously cannot be published in the *Military Technical Courier* even under a similar title or in a changed form.

Tables and illustrations

All the captions should be in the original language as well as in English, together with the texts in illustrations if possible. Tables are typed in the same style as the text and are denoted by Arabic numerals at the top. Photographs and drawings, placed appropriately in the text, should be clear, precise and suitable for reproduction. Drawings should be created in Word or Corel.

For figures and graphs, proper data plot is recommended i.e. using a data analysis program such as Excel, Matlab, Origin, SigmaPlot, etc. It is not recommended to use a screen capture of a data acquisition program as a figure or a graph.

Citation in the text

Citation in the text must be uniform. The *Military Technical Courier* applies the Harvard Referencing System given in the Harvard Style Manual. When citing sources within your paper, i.e. for in-text references of the works listed at the end of the paper, place the year of publication of the work in parentheses and optionally the number of the page(s) after the author's name, e.g. (Petrovic, 2012, pp.10-12). A detailed guide on citing, with examples, can be found on *Military Technical Courier* website on the page *Instructions for Harvard Style Manual*. In-text citations should follow its guidelines. For checking in-text citations, the ASSISTANT system uses a special tool CiteMatcher to find out quotes left out within papers and in reference lists.

Footnotes

Footnotes are given at the bottom of the page with the text they refer to. They can contain less relevant details, additional explanations or used sources (e.g. scientific material, manuals). They cannot replace the cited literature.

Reference list (Literature)

The cited literature encompasses bibliographic sources such as articles and monographs and is given in a separate section in a form of a reference list. References are not translated to the language of the article.

In compiling the reference list and bibliography, the *Military Technical Courier* applies the Harvard System – Harvard Style Manual. All bibliography items should be listed alphabetically by author's name, without numeration. A detailed guide for listing references, with examples, can be found on *Military Technical Courier* website on the page *Instructions for Harvard Style Manual*. Reference lists at the end of papers should follow its guidelines. In journal evaluation systems, non-standard, insufficient or inconsequent citation is considered to be a sufficient cause for denying the scientific status to a journal.

Authorship Statement

The Authorship statement, submitted together with the paper, states authors' individual contributions to the creation of the paper. In this statement, the authors also confirm that they followed the guidelines given in *the Call for papers* and the *Publication ethics and malpractice statement of the journal*.

All articles are peer reviewed.

The list of referees of the *Military Technical Courier* can be viewed at website page *List of referees*. The article review process is described on the *Peer Review Process* page of the website.

Editorial Team

Address of the Editorial Office:
Vojnotehnički glasnik / Military Technical Courier
Veljka Lukića Kurjaka 33
11042 Belgrade, Republic of Serbia
e-mail: vojnotehnicki.glasnik@mod.gov.rs, tel.: +381 11 3603 260, +381 66 8700 123

Ликовно-графички уредник
Марија Марић, е-mail: marija.maric@mod.gov.rs

Лектор
Добрила Милетић, е-mail: miletic.dobрила@gmail.com

Превод на енглески
Јасна Вишњић, е-mail: jasnavisnjic@yahoo.com

Превод на шпански
Јована Јовановић, е-mail: jovana.jov92@gmail.com

Превод на руски
Др Карина Авагјан, е-mail: karinka2576@mail.ru

CIP – Каталогизација у публикацији
Народна библиотека Србије, Београд

623+355/359

ВОЈНОТЕХНИЧКИ гласник : научни часопис Министарства одбране
и Војске Србије = Военно-технический вестник : научный журнал
Министерства обороны и Вооружённых сил Республики Сербия =
Military Technical Courier : scientific Journal of the Ministry of Defence and the Serbian
Armed Forces / главни и одговорни уредник Драган Памучар. -
Год. 1, бр. 1 (1. јан. 1953) - . - Београд : Универзитет одбране у Београду,
Војна академија, 1953- (Београд : Војна штампарија). - 23 cm

Тромесечно. - Текст на срп., рус. и енгл. језику. - Друго издање
на другом медијуму: Војнотехнички гласник (Online) = ISSN 2217-4753
ISSN 0042-8469 = Војнотехнички гласник
COBISS.SR-ID 4423938

Цена: 600,00 динара

Тираж: 100 примерака

На основу мишљења Министарства за науку, технологију и развој Републике
Србије, број 413-00-1201/2001-01 од 12. 9. 2001. године,
часопис „Војнотехнички гласник“ је публикација од посебног интереса за науку.

УДК: Народна библиотека Србије, Београд

Адреса редакције: Војнотехнички гласник,
Велка Лукића Курјака 33, 11042 Београд

<https://www.scopus.com/sourceid/21101207440>

<http://www.vtg.mod.gov.rs>

<http://aseestant.ceon.rs/index.php/vtg/issue/current>

<http://scindeks.nb.rs/journaldetails.aspx?issn=0042-8469>

<https://www.redalyc.org/revista.oa?id=6617>

http://elibrary.ru/title_about.asp?id=53280

<https://doaj.org/toc/2217-4753>

Војнотехнички гласник је лиценциран код EBSCO Publishing-a.

Комплетан текст Војнотехничког гласника доступан је у базама података EBSCO Publishing-a.

е-mail: vojnotehnicki.glasnik@mod.gov.rs; X: @MilTechCourier

Претплата на штампано издање: е-mail: vojnotehnicki.glasnik@mod.gov.rs; тел. 066/87-00-123.

Часопис излази тромесечно.

Први штампани број Војнотехничког гласника објављен је 1. 1. 1953. године.

Прво електронско издање Војнотехничког гласника на Интернету објављено је 1. 1. 2011. г.

Штампа: Војна штампарија – Београд, Ресавска 40б, е-mail: vojna.stamparija@mod.gov.rs

Художественный редактор
Мария Марич, e-mail: marija.maric@mod.gov.rs

Корректор
Добрила Милетич, e-mail: miletic.dobрила@gmail.com

Перевод на английский язык
Ясна Вишнич, e-mail: jasnavisnjic@yahoo.com

Перевод на испанский язык
Йована Йованович, e-mail: jovana.jov92@gmail.com

Перевод на русский язык
Д.филол.н. Карина Кареновна Авагян, e-mail: karinka2576@mail.ru

CIP – Каталогизация в публикации
Национальная библиотека Сербии, г. Белград

623+355/359

ВОЈНОТЕХНИЧКИ гласник : научни часопис Министарства одбране
и Војске Србије = Военно-технический вестник : научный журнал
Министерства обороны и Вооружённых сил Республики Сербия =
Military Technical Courier : scientific Journal of the Ministry of Defence and the Serbian
Armed Forces / главни и одговорни уредник Драган Памучар. -
Год. 1, бр. 1 (1. јан. 1953)- . - Београд : Универзитет одбране у Београду,
Војна академија, 1953- (Београд : Војна штампарија). - 23 cm

Тромесечно. - Текст на срп., рус. и енгл. језику. - Друго издање
на другом медијуму: Vojnotehnički glasnik (Online) = ISSN 2217-4753
ISSN 0042-8469 = Војнотехнички гласник
COBISS.SR-ID 4423938

Цена: 600,00 динаров

Тираж: 100 екземпляров

На основании решения Министерства науки и технологий Республики Сербия,
№ 413-00-1201/2001-01 от 12. 9. 2001 года, журнал «Военно-технический вестник»
объявлен изданием, имеющим особое значение для науки.

УДК: Национальная библиотека Сербии, г. Белград

Адрес редакции: Војнотехнички гласник,

Ул. Велька Лукича Куряка 33, 11042 Белград, Република Сербия

<https://www.scopus.com/sourceid/21101207440>

<http://www.vtg.mod.gov.rs>

<http://aseestant.ceon.rs/index.php/vtg/issue/current>

<http://scindeks.nb.rs/journaldetails.aspx?issn=0042-8469>

<https://www.redalyc.org/revista.oa?id=6617>

http://elibrary.ru/title_about.asp?id=53280

<https://doaj.org/toc/2217-4753>

«Военно-технический вестник» включен в систему EBSCO. Полный текст журнала
«Военно-технический вестник» можно найти в базах данных EBSCO Publishing.

e-mail: vojnotehnicki.glasnik@mod.gov.rs, X: @MilTechCourier

Подписка на печатную версию журнала: e-mail: vojnotehnicki.glasnik@mod.gov.rs;

тел. +381 66 87 00 123.

Журнал выпускается ежеквартально.

Первый номер журнала «Военно-технический вестник» выпущен 1.1.1953 года.

Первая электронная версия журнала размещена на интернет странице 1.1.2011 года.

Типография: Војна штампарија – Белград, Ресавска 40б, e-mail: vojna.stamparija@mod.gov.rs

Graphic design editor

Marija Marić, e-mail: marija.maric@mod.gov.rs

Proofreader

Dobrila Miletić, e-mail: miletic.dobrila@gmail.com

English translation and polishing

Jasna Višnjić, e-mail: jasnavisnjic@yahoo.com

Spanish translation and polishing

Jovana Jovanović, e-mail: jovana.jov92@gmail.com

Russian translation and polishing

Dr. Karina Avagyan, e-mail: karinka2576@mail.ru

CIP – Catalogisation in the publication

National Library of Serbia, Belgrade

623+355/359

ВОЈНОТЕХНИЧКИ гласник : научни часопис Министарства одбране и Војске Србије = Военно-технический вестник : научный журнал Министарства обороны и Вооружённых сил Республики Сербия = Military Technical Courier : scientific Journal of the Ministry of Defence and the Serbian Armed Forces / главни и одговорни уредник Драган Памучар. - Год. 1, бр. 1 (1. јан. 1953)- . - Београд : Универзитет одбране у Београду, Војна академија, 1953- (Београд : Војна штампарија). - 23 cm

Тромесечно. - Текст на срп., рус. и енгл. језику. - Друго издање на другом медијуму: Vojnotehnički glasnik (Online) = ISSN 2217-4753
ISSN 0042-8469 = Војнотехнички гласник
COBISS.SR-ID 4423938

Price: 600.00 RSD

Printed in 100 copies

According to the Opinion of the Ministry of Science and Technological Development No 413-00-1201/2001-01 of 12th September 2001, the *Military Technical Courier* is a publication of special interest for science.

UDC: National Library of Serbia, Belgrade

Address: Vojnotehnički glasnik/Military Technical Courier,
Veljka Lukića Kurjaka 33, 11042 Belgrade, Republic of Serbia

<https://www.scopus.com/sourceid/21101207440>

<http://www.vtg.mod.gov.rs/index-e.html>

<http://aseestant.ceon.rs/index.php/vtg/issue/current>

<http://scindeks.nb.rs/journaldetails.aspx?issn=0042-8469>

<https://www.redalyc.org/revista.oa?id=6617>

http://elibrary.ru/title_about.asp?id=53280

<https://doaj.org/toc/2217-4753>

Military Technical Courier has entered into an electronic licensing relationship with EBSCO Publishing. The full text of *Military Technical Courier* can be found on EBSCO Publishing's databases.

e-mail: vojnotehnicki.glasnik@mod.gov.rs, X: @MilTechCourier

Subscription to print edition: e-mail: vojnotehnicki.glasnik@mod.gov.rs; Tel. +381 66 87 00 123.

The journal is published quarterly.

The first printed issue of the *Military Technical Courier* appeared on 1st January 1953.

The first electronic edition of the *Military Technical Courier* on the Internet appeared on 1st January 2011.

Printed by Voјna štampariја – Belgrade, Resavska 40b, e-mail: vojna.stamparija@mod.gov.rs

